ARF regulating proteins as novel drug targets in *Trypanosoma brucei*

Jaksha Piraveen Chandrathas

Thesis submitted to Keele University for the degree of Doctor of Philosophy

June 2020

Abstract

Human African Trypanosomiasis (HAT) and Animal African Trypanosomiasis (AAT) are neglected tropical diseases that pose a huge socioeconomic and health burden in poorer countries in sub-Saharan Africa. The causative agents of these diseases are the *Trypanosoma brucei* (*T. brucei*) *spp.*, kinetoplastid parasites that is transmitted by tsetse flies (*Diptera Glossina*). Drugs against HAT and nagana are toxic, species and in nagana, host specific. With reports of emerging resistance to current drugs, it is essential to identify novel drug targets against *T. brucei*. This thesis focuses on identifying and characterising regulating proteins of ADP-ribosylation factors (ARFs) in *T. brucei*. ARFs are small GTPase binding proteins that have been shown to be essential in bloodstream form *T. brucei*. However the *T. brucei* ARFs share a high level of sequence identity with human ARFs, thus making them unsuitable as drug targets. Guanine nucleotide exchange factors (GEFs) and GTPase activating proteins (GAPs) regulate the activity of ARFs and have been shown to have highly diverse protein sequences. A total of 3 putative ARF GEFs and 4 putative ARF GAPs were identified in bloodstream form *T. brucei* by bioinformatics RNA interference (RNAi) cell lines were successfully generated for two GEFs and two GAPs in Lister 427 bloodstream form *T. brucei*. Tetracycline-induced knockdown was used to demonstrate that TbGEF3 is essential for viability of bloodstream form *T. brucei*. A decrease in cell growth was observed from 24 hours post RNAi, correlating with a decrease in cell cycle progression and an increase in cell death. The ‘BigEye’ phenotype could also be seen from 24 hours post RNAi, and cells were identified to have an endocytosis defect. These results combined with low level of sequence similarities at the essential ARF binding regions of TbGEF3 demonstrated that TbGEF3 may be a potential drug target. The TbGEF3 RNAi cells were used to assess the sensitivity of suramin, a drug taken up via endocytosis, in the presence of a partial endocytosis defect. Cells incubated in tetracycline for 24 hours prior to drug treatment had a reduced sensitivity to suramin compared to cells grown in the absence of tetracycline. The Pathogen Box set of compounds was screened for molecules with activity against *T. brucei* parasites. Identified hit compounds were

used in preliminary studies to initiate development of an assay to distinguish compounds that are taken up via endocytosis. In summary, the putative ARF-regulating protein TbGEF3 has been shown to be essential for viability in *T. brucei* and has promise as a potential drug target. Further work is required in order to validate the use of the TbGEF3 RNAi line as a drug screening tool.

Table of Contents

List of Figures i

List of Tables vi

Abbreviations vii

Acknowledgements ix

Chapter 1 – Introduction 1

1.1 Neglected tropical diseases and Trypanosomatidae 2

1.1.1 African Trypanosomiasis 3

1.1.2 Life cycle 10

1.1.3 Immune evasion 15

1.1.4 Host immune response 19

1.1.5 Diagnosis 26

1.1.6 Treatments for HAT 28

1.1.7 Treatments for nagana 34

1.2 ADP-ribosylation factors 35

1.2.1 ADP-ribosylation factor and ARF-like proteins 35

1.2.2 ARF functions 39

1.3 ARF regulators 45

1.3.1 Guanine nucleotide exchange factors 45

1.3.2 GTPase activating proteins 49

1.4 ARF regulating proteins as potential drug targets 53

1.5 Aims 57

Chapter 2 – Materials and Methods 58

2.1 Materials 59
2.1.1 Laboratory equipment 59
2.1.2 Chemicals and reagents 60
2.1.3 Kits 61
2.1.4 Media 61
2.1.5 Oligonucleotides 62
2.2 Methods 63
2.2.1 Bioinformatics 63
2.2.2 General Methods 65
2.2.3 Molecular cloning 66
2.2.4 Transfection of T. brucei 69
2.2.5 Induction of RNAi 71
2.2.6 Quantification of gene expression following RNAi 71
2.2.7 Microscopy 73
2.2.8 Flow cytometry 74
2.2.9 Concanavalin A endocytosis assay 75
2.2.10 Drug Screening 76
Chapter 3 – Identification and functional prediction of ARF regulators in *Trypanosoma brucei* using bioinformatics 79
3.1 Introduction 80
3.1.1 Aims 81
3.2 Methods 81
3.2.1 Protein BLAST 81

3.2.2 Sequence alignment....82
3.2.3 Domain analysis....82
3.2.4 Structural analysis....82
3.2.5 Protein localisation....82
3.2.6 Putative orthologues of *T. brucei* ARF regulators in other kinetoplastids....83
3.3 Results....83
3.3.1 Identification of *T. brucei* GEFs and GAPs....83
3.3.2 Structural and sequence similarities....85
3.3.3 Prediction of protein localisation....101
3.3.4. Putative orthologues of *T. brucei* ARF regulators in other Kinetoplastids....111
3.4. Discussion....114
3.4.1 TbGEFs and TbGAPs are highly conserved at the catalytic domains on amino acid and structural level....114
3.4.3 Predicted protein localisation of TbGEFs and TbGAPs may not be accurate in bloodstream form *T. brucei*....123
3.4.5 Putative orthologues of *T. brucei* ARF regulators in other Kinetoplastids may have similar functions....125
3.5. Conclusions....127
Chapter 4 – Identification of essential ARF regulators in bloodstream form *T. brucei*....128
4.1 Introduction....129
4.1.1 Aims....130
4.2 Methods....131
4.2.1 Selection and amplification of RNAi regions....131
4.2.2 Generation of RNAi constructs....131

4.2.3 Transfection....131
4.2.4 Induction of RNAi....131
4.2.5 Propidium Iodide flow cytometry....132
4.2.6 Live/Dead flow cytometry....132
4.2.7 Quantitative polymerase chain reaction (qPCR)....132
4.2.8 Indirect immunofluorescent microscopy....132
4.2.9 Transmission Electron Microscopy (TEM)....132
4.2.10 Concanavalin A (Con A) endocytosis assay....133
4.3 Results....133
4.3.1 Identification and amplification of RNAi regions....133
4.3.2 Generation of RNAi constructs and transfection....134
4.3.3 Effects of RNAi on parasite growth....140
4.3.4 Quantification of gene expression....145
4.3.5 Flow cytometry....149
4.3.6. Microscopy....161
4.3.7 Concanavalin A endocytosis assay....173
4.4 Discussion....178
4.4.1 Unsuccessful transfections may be due to a leaky inducible expression system....178
4.4.2 Identification of essential ARF regulators in bloodstream form *T. brucei*....181
4.4.3 TbGEF3 may be involved in endocytic pathways....185
4.5 Conclusions....187
Chapter 5 – Exploring the use of *T. brucei* GEF3 RNAi cell line in drug discovery....189
5.1 Introduction....190

5.1.1 Aims 192
5.2 Methods 192
5.2.1 Determination of IC_{50} of tetracycline 192
5.2.2 Determination of IC_{50} of suramin 192
5.2.3 Determination of IC_{50} of diminazene aceturate 193
5.2.4 MMV Pathogen Box 193
5.2.5 Determination of IC_{50} of Pathogen Box compounds 193
5.3 Results 194
5.3.1 Identifying the IC_{50} of tetracycline, suramin and diminazene aceturate in transgenic lines of *T. brucei* 194
5.3.2. Identifying the potency of suramin on transgenic *T. brucei* in the presence of tetracycline 200
5.3.3 Pathogen Box (MMV) screening 207
5.4 Discussion 227
5.4.1 Inducing a partial endocytosis defect in a TbGEF3 RNAi cell line 227
5.4.2 Measuring parasite viability 230
5.4.3 Pathogen Box screening 231
5.5 Conclusions 234
Chapter 6 – Discussion 235
6.1 General Discussion 236
6.1.1 Why study *T. brucei* drug targets? 236
6.1.2 ARF GEFs and GAPs are conserved at the catalytic domains 239
6.1.3 TbGEF3 is essential for viability in *T. brucei* 241

6.2 Future work 242

6.2.1 Identification of ARF regulator structures 243

6.2.2 Identifying ARF and ARF-regulator interactions 244

6.2.3 Different systems of gene targeting 245

6.2.4 Effects of TbGEF3 RNAi on *T. brucei* in a mouse infection model 246

6.2.5 Screening inhibitors against TbGEF3 using compound libraries 247

6.3 Conclusion 248

References 249

Appendix 1 299

Appendix 2 308

Appendix 3 313

Appendix 4 315

Appendix 5 317

Appendix 6 319

Appendix 7 326

Appendix 8 333

Appendix 9 338

List of Figures

Figure 1.1. Distribution of Human African Trypanosomiasis in Africa. 4

Figure 1.2. Total number of new cases of HAT reported to the World Health Organisation from 1940-2013. 6

Figure 1.3. Number of reported HAT cases per year from 2000-2016. 8

Figure 1.4 Geographical distribution of* T. vivax *and* T. congolense *infection. 9

Figure 1.5.* Trypanosoma brucei *life cycle. 11

Figure 1.6. Illustration of procyclic form* T. brucei *cell structure and replication process. 15

Figure 1.7. VSG and the structure of GPI anchor from bloodstream form* T. brucei*. 17

Figure 1.8. Schematic representation of EP and GPEET procyclin expressed in procyclic* T. brucei *trypomastigotes. 18

Figure 1.9. TLF1 and TLF2 pathways of entry into* T. brucei*. 20

Figure 1.10. Drugs against Human African Trypanosomiasis (HAT). 31

Figure 1.11. Activation and inactivation of ARFs. 36

Figure 1.12. Crystal structure of ARF1. 38

Figure 1.13. COPI coat assembly model. 41

Figure 1.14. Structure of Cytohesin-2 Sec7 domain. 47

Figure 1.15. Domains present in ARF GAPs. 50

Figure 2.1. Percentage viability formula. 77

Figure 3.1. Multiple sequence alignment of* T. brucei *and human GEFs. 87

Figure 3.2. Multiple sequence alignment of* T. brucei *and human GAPs. 88

Figure 3.3. Schematic representation of domains present in human ARF GEF subfamilies. 90

Figure 3.4. Schematic representation of domains present in human ARF GAP subfamilies. 91

Figure 3.5. Schematic representation of identified* T. brucei *ARF regulators. 93

Figure 3.6. Predicted structure of **T. brucei** *GAPs*. 95

Figure 3.7. Predicted structure of **T. brucei** *GEFs*. 96

Figure 3.8. Structural alignment of **T. brucei** *GEFs and GAPs with human CYTH and ARFGAP subfamily.* 97

Figure 3.9. Predicted localisation of TbGEFs and TbGAPs in **T. brucei.** 102

Figure 3.10. Predicted localisation of ARF/ARLs in **T. brucei.**. 108

Figure 3.11. Predicted localisation of ARF/ARLs, TbGEFs and TbGAPs in **T. brucei.**.110

Figure 3.12. Multiple sequence alignment of orthologues......113

Figure 4.1. Amplification of **T. brucei** *GEFs and GAPs RNAi regions.*.....134

Figure 4.2. Schematic representation of the P2T7^{Ti} vector and the function of the vector. 135

Figure 4.3. P2T7^{Ti} vector digest.. 136

Figure 4.4. Visualisation of TbGEF RNAi inserts in P2T7^{Ti} plasmid DNA. 138

Figure 4.5. Visualisation of TbGAP RNAi inserts in P2T7^{Ti} plasmid DNA.. 139

Figure 4.6. RNAi effect on the growth of wild type and transgenic P2T7-TbGAP1 cell line. 141

Figure 4.7. RNAi effect on the growth of transgenic P2T7-TbGAP4 cell line......142

Figure 4.8. RNAi effect on the growth of transgenic P2T7-TbGEF2 cell line. 143

Figure 4.9. RNAi effect on the growth of transgenic P2T7-TbGEF3 cell line. 144

Figure 4.10. **TbGEF3** *Standard curve.* 146

Figure 4.11. **α-tubulin** *Standard curve.*.....147

Figure 4.12. Relative expression change of **TbGEF3** *following RNAi.* 148

Figure 4.13. Propidium iodide flow cytometry of wild type bloodstream form **T. brucei.** 150

Figure 4.14. GEF RNAi effect on cell cycle progression in **T. brucei.** 152

Figure 4.15. GAP RNAi effect on cell cycle progression in **T. brucei.**.....153

Figure 4.16. Live/Dead flow cytometry of P2T7-TbGAP1 post RNAi at different time points. 155

Figure 4.17. Live/Dead flow cytometry of P2T7-TbGAP4 post RNAi at different time points. 157

Figure 4.18. Live/Dead flow cytometry of P2T7-TbGEF2 post RNAi at different time points. 158

Figure 4.19. Live/Dead flow cytometry of P2T7-TbGEF3 post RNAi at different time points. 159

Figure 4.20. Live/Dead cell percentage at different time points post RNAi. 160

Figure 4.21. Indirect immunofluorescent microscopy of wild type bloodstream form* T. brucei *and PT27-TbGAP1. 163

Figure 4.22. Indirect immunofluorescent microscopy of bloodstream form* T. brucei *post RNAi of TbGAP4. 164

Figure 4.23. Indirect immunofluorescent microscopy of bloodstream form* T. brucei *post RNAi of TbGEF2. 165

Figure 4.24. Indirect immunofluorescent microscopy of bloodstream form* T. brucei*. 167

Figure 4.25. Number of BigEye and slender* T. brucei *cells at different time points post RNAi. 168

Figure 4.26. Transmission Electron Microscopy of wild type bloodstream form* T. brucei*. 170

Figure 4.27. Transmission Electron Microscopy RNAi induced bloodstream form* T. brucei*. 171

Figure 4.28. Transmission Electron Microscopy RNAi induced bloodstream form* T. brucei*. 172

Figure 4.29. Endocytosis of Con A at 4°C. 174

Figure 4.30. Endocytosis of Con A at 12°C. 175

Figure 4.31. Endocytosis of Con A at 37°C. 177

Figure 5.1. IC_{50} for suramin in transgenic* T. brucei *cell lines. 195

Figure 5.2. IC_{50} of diminazene aceturate in transgenic cell lines. 197

Figure 5.3. IC_{50} of tetracycline for the transgenic TbGEF3 cell lines. 199

Figure 5.4. Identifying the tetracycline concentration that affects the growth of transgenic* T. brucei *cells in the presence of suramin. 202

Figure 5.5. Comparison of IC_{50} for suramin in transgenic P2T7-TbGEF3 cell line incubated +/- tetracycline. 203

Figure 5.6. Effects of TbGEF3 RNAi on parasite sensitivity to suramin. 205

Figure 5.7. Effect of diminazene aceturate on cells before and after induction of TbGEF3 RNAi. 206

***Figure 5.8. Plate 1 of the Pathogen Box compounds screened at 10 μM Lister 427 bloodstream form* T. brucei.** 208

***Figure 5.9. Plate 2 of the Pathogen Box compounds screened at 10 μM on Lister 427 bloodstream form* T. brucei.** 209

***Figure 5.10. Plate 3 of the Pathogen Box compounds screened at 10 μM on Lister 427 bloodstream form* T. brucei.** 210

***Figure 5.11. Plate 4 of the Pathogen Box compounds screened at 10 μM on Lister 427 bloodstream form* T. brucei.** 211

***Figure 5.12. Plate 5 of the Pathogen Box compounds screened at 10 μM on Lister 427 bloodstream form* T. brucei.** 212

***Figure 5.13. Plate 1 of Pathogen Box compounds screened at 1 μM on Lister 427 bloodstream form* T. brucei.** 213

***Figure 5.14. Plate 2 of Pathogen Box compounds screened at 1 μM on Lister 427 bloodstream form* T. brucei.** 214

***Figure 5.15. Plate 3 of Pathogen Box compounds screened at 1 μM on Lister 427 bloodstream form* T. brucei.** 215

***Figure 5.16. Plate 4 of Pathogen Box compounds screened at 1 μM on Lister 427 bloodstream form* T. brucei.** 216

***Figure 5.17. Plate 5 of Pathogen Box compounds screened at 1 μM on Lister 427 bloodstream form* T. brucei.** 217

Figure 5.18. IC_{50} of positive hit compounds from Pathogen Box. 219

Figure 5.19. IC_{50} of positive hit compounds from Pathogen Box. 220

Figure 5.20. Determining the activity of selected compounds in transgenic P2T7-TbGEF3 cells. 226

***Figure 6.1. Electron Micrograph of lethal phenotype in bloodstream form* T. brucei.** . 238

Figure 6.2. The CRISPR/Cas-9 gene editing system. 246

List of Tables

Table 1.1. Localisation and function of class I, II and III ARFs. 42

Table 1.2. ARF/ARLs in* T. brucei *and their homologue to human ARF/ARLs. 56

Table 2.1. Gradient PCR cycle. 67

Table 2.2. qPCR cycle and dissociation curve steps. 73

Table 3.1. Homologues of ARF GEFs and GAPs in* T. brucei*. 85

Table 3.2. RMS values of the three identified* T. brucei *GEFs. 99

Table 3.3. RMS values of the four identified* T. brucei *GAPs. 100

Table 3.4. Localisation of* T. brucei *ARF regulators determined through TrypTag. 104

Table 3.5. Localisation of* T. brucei *ARF/ARLs were determined through TrypTag. 106

Table 5.1. IC_{50} of suramin in transgenic* T. brucei *lines. 196

Table 5.2. IC_{50} values for diminazene aceturate in transgenic* T. brucei *cell line. 197

Table 5.3. IC_{50} of tetracycline in transgenic* T. brucei *cell line. 199

Table 5.4. IC_{50} of suramin with and without tetracycline in transgenic P2T7-TbGEF3 cell line. 204

Table 5.5. IC_{50} and 95% confidence interval for all positive hits. 221

Table 5.6. Chemical structure and pathogen screens of the positive hits. 223

Abbreviations

AAT	Animal African Trypanosomiasis
ARF	ADP-ribosylation factor
ARL	ARF-Like proteins
bp	Base pairs
BSA	Bovine serum albumin
cDNA	Complementary DNA
CO_2	Carbon dioxide
DALYs	Disability adjusted life years
DAPI	4′,6-diamidino-2-phenylindole
DMSO	Dimethyl sulfoxide
DNA	Deoxyribonucleic acid
DNDi	Drugs for Neglected Diseases initiative
dNTP	Deoxynucleotide
dsRNA	Double stranded RNA
EDTA	Ethylenediaminetetraacetic acid
FBS	Foetal bovine serum
GAP	GTPase activating proteins
GDP	Guanosine diphosphate
GEF	Guanine nucleotide exchange factors
gRNA	Guide RNA
GTP	Guanosine triphosphate
HAT	Human African Trypanosomiasis
IC_{50}	Half maximal inhibitory concentration
kb	Kilo bases
mg	Milligram
mL	Millilitre

mM	Millimolar
MMV	Medicines for Malaria Venture
miRNA	Micro RNA
mRNA	Messenger RNA
NECT	Nifurtimox-Eflornithine combination therapy
NTDs	Neglected Tropical Diseases
PBS	Phosphate buffered saline
PCR	Polymerase chain reaction
PFR	Paraflagellar rod
qPCR	Quantitative polymerase chain reaction
RISC	RNA induced silencing complex
RNA	Ribonucleic acid
RNAi	RNA interference
siRNA	Small interfering RNA
SRA	Serum resistance associated proteins
TAE	Tris, acetic acid and EDTA
Taq	Thermus aquaticus
TAT1	Alpha tubulin
TEM	Transmission Electron Microscopy
TetOP	Tet operator
TetR	Tet repressor
UV	Ultra-violet
vPBS	Voorheis' modified PBS
WHO	World Health Organisation

Acknowledgements

I would like to first express my sincere gratitude to my supervisor, Dr Helen Price, for providing me with the opportunity to study for my PhD. Words cannot describe how grateful I am for all the support, advice and guidance you have given me throughout my PhD. You have been a great supervisor, being patient with me whilst also encouraging me to never give up. I appreciate all the help, advice and comments on my work and my thesis.

I would like also to thank Dr Sarah Berry. You have been with me since day one of my PhD, supporting me and guiding me in the right direction. You have always been there when I needed academic and non-academic advice, pointing me in the right direction.

To the members of Haldane laboratory and Life Sciences Department, Huxley; I cannot thank you all enough for your help and entertainment. Especially Dr Florian Noulin, you are the laboratory entertainer and a great source of help.

I would like to thank my parents and my siblings for supporting me emotionally and financially. To my mum and dad, you have had to work two jobs each to support our family and provide us with everything we had asked for. Both of you have been my inspiration to keep working hard and never give up on what I desire the most. It is now my turn to look after you, and I hope I will make you proud. To my brother and sister, words cannot describe how grateful I am to be able to talk to you when I'm feeling down. Both of you have encouraged me and pushed me to keep going, now it will be my turn to encourage you both academically and non-academically.

To Sanaa Tabassum Ejaz, meeting you was probably God's way of encouraging me to keep pushing through. Words cannot express how thankful I am for your emotional support, you have been my motivation and my goal, as your namesake, you have also been my light in my darkest hours.

Chapter 1 – Introduction

1.1 Neglected tropical diseases and Trypanosomatidae

Neglected tropical diseases (NTDs) are defined as diseases affecting tropical and subtropical countries that are associated with poverty and limited health services (Molyneux *et al*., 2017). More than one billion people suffer from the burden of NTDs, with 500,000 deaths and 57 million disability adjusted life years (DALYs) per year (Garchitorena *et al*., 2017). Parasites, eukaryotic organisms that complete part or all of their life cycles within a host organism, are causative agents of many of the NTDs (Goater *et al*., 2013). Parasitic diseases often present non-specific symptoms and commonly affect the most marginalised populations in developing countries, leading to high morbidity and mortality (Piperaki and Tassios, 2016).

The Trypanosomatidae family are a diverse family of protozoan parasites that contribute to considerable morbidity and mortality (Malvy and Chappuis, 2011, de Clare Bronsvoort *et al*., 2010, Kaufer *et al*., 2017). Since the discovery and documentation of trypanosomatids in insects by Burnett in 1851 and the establishment of the first genera by Kent in 1880, trypanosomatids were further redefined into their genera during the mid-1960s by Hoare and Wallace. These latter definitions were based on specific morphotypes and life cycles, establishing the taxonomic system of Trypanosomatidae with which we are familiar (Maslov *et al*., 2013).

Trypanosomatidae are a family of flagellated parasites that belong to the class Kinetoplastida, which are identified by the presence of a DNA-containing region known as the kinetoplast in their single large mitochondrion. Although Trypanosomatidae are predominantly monoxenous parasites, those that are restricted to one host; several genera of Trypanosomatidae, such as *Leishmania*, *Trypanosoma* and *Phytomonas* require two hosts for their lifecycle (dixenous). The dixenous Trypanosomatidae, particularly those with a vertebrate host, are of huge medical and economic importance as causative agents of important human and animal diseases. These Trypanosomatidae are from the genus *Trypanosoma* and *Leishmania* and account for more than 900 vertebrate-infecting species, with *Trypanosoma* totalling about 600 of these

species (Stuart *et al*., 2008, Molinari and Moreno, 2018, Maslov *et al*., 2013, Kaufer *et al*., 2017, Podlipaev, 2001).

Parasites from the *Trypanosoma* genera include *Trypanosoma brucei* (*T. brucei*) and *Trypanosoma cruzi* (*T. cruzi*) which cause African Trypanosomiasis and American Trypanosomiasis (Chagas disease) respectively; whilst infection from parasites of the *Leishmania* genera results in various clinical forms of leishmaniasis (Smith *et al*., 2007, Simpson *et al*., 2006, Simpson *et al*., 2004, De Gaudenzi *et al*., 2011, Kaufer *et al*., 2017). This work will primarily focus on the dixenous parasite *T. brucei*.

1.1.1 African Trypanosomiasis

1.1.1.1 Human African Trypanosomiasis

Human African Trypanosomiasis (HAT) is a neglected tropical disease (NTD) that is also commonly known as sleeping sickness (Njamnshi *et al*., 2017, Cordon-Obras *et al*., 2015). Two subspecies of *T. brucei* are causative agents of HAT: *T. b. gambiense* and *T. b. rhodesiense* (Kennedy, 2019). These two subspecies of *T. brucei* are genetically and morphologically related, however they differ in clinical features, including epidemiology, transmission and geographical distribution (Keating *et al*., 2015, Büscher *et al*., 2017). HAT affects 36 countries in sub-Saharan Africa from the latitude of 14° north to 29° south of the equator, this geographical distribution is known as the tsetse belt due to their transmission being influenced by their primary host and vectors, the tsetse flies (*Diptera Glossina*) (Cayla *et al*., 2019, Kennedy, 2019).

T. b. gambiense is endemic to West and Central Africa, with the highest prevalence found in poor rural populations of the least developed countries in these regions (Figure 1.1). The parasite is responsible for causing the chronic form of HAT, which can last months or even years. *T. b. gambiense* has been traditionally considered as an anthroponosis, meaning that humans are the single main reservoir for this parasite. However recent studies have identified

T. b. gambiense infections in domestic animals such as dogs, pigs and cattle (N'Djetchi *et al*., 2017, Büscher *et al*., 2017, Umeakuana *et al*., 2019).

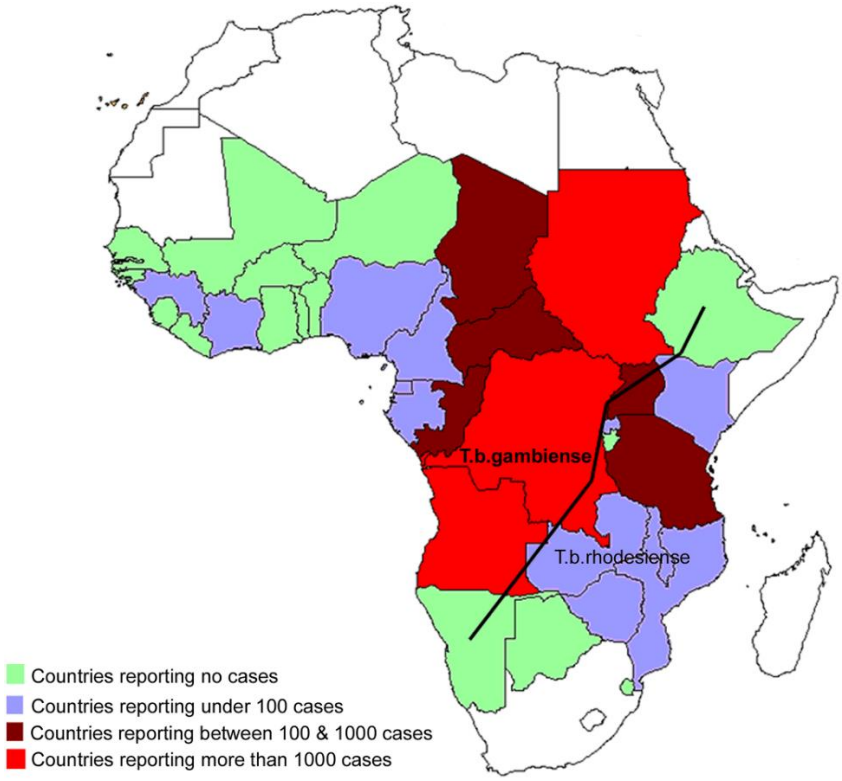

Figure 1.1. Distribution of Human African Trypanosomiasis in Africa. *Map showing the countries affected by* T. b. gambiense *and* T. b. rhodesiense *(Fevre et al., 2008).*

In contrast, the zoonotic subspecies *T. b. rhodesiense* is responsible for the acute form of HAT which is more common in Eastern and Southern Africa, where infected wild reservoir hosts such as warthogs and buffaloes as well as cattle are found. HAT caused by *T. b. rhodesiense* can be fatal within a year or less if left untreated (Muchiri *et al*., 2015, Kennedy, 2019). Although both of these parasites are found in the same continent, it should be noted that there is currently little to no overlap between the endemic areas, *T. b. gambiense* affecting around 24 out of the 37 countries that are affected by HAT (Figure 1.1); with Uganda being the only country that is endemic to both *T. b. gambiense* and *T. b. rhodesiense*, albeit in geographically

distinct areas (Franco *et al*., 2018, Keating *et al*., 2015, Kimuda *et al*., 2018). Approximately 98% of HAT cases occur in West and Central Africa due to infection with *T. b. gambiense*; compared to the 2% of cases caused by *T. b. rhodesiense* that are found in both domestic and wilderness areas (Cordon-Obras *et al*., 2015, Rock *et al*., 2015, Capewell *et al*., 2011).

Human African Trypanosomiasis (HAT) is characterised by a chronic disease caused by *T. b. gambiense* and an acute disease caused by *T. b. rhodesiense*, with both forms of the disease having two clinical stages (Muchiri *et al*., 2015, Checchi *et al*., 2015). The haemolymphatic or first stage corresponds to the proliferation of the trypanosomes within the host's blood and lymphatic systems, and is often undiagnosed (Büscher *et al*., 2017). HAT caused by *T. b. gambiense* presents with irregular symptoms such as fever, fatigue, headaches, pruritus and arthralgia; since these symptoms are nonspecific the patients could often be misdiagnosed for other tropical diseases such as malaria and filariasis (Simarro *et al*., 2008, Chappuis *et al*., 2005). In contrast to this, HAT caused by *T. b. rhodesiense* presents with feverish illness from 1 to 3 weeks post infection and the illness progresses more rapidly than the *T. b. gambiense* illness (Chappuis *et al*., 2005, Kennedy and Rodgers, 2019). In some cases the presence of symptoms often goes largely unobserved, for instance the visibility of skin rashes are more prominent on European patients than those with darker skin. The presence of a chancre is also more commonly identified in European patients, particularly those infected with *T. b. rhodesiense*, than in African patients with the same infection (Chappuis *et al*., 2005).

The final stage of HAT is known as the late or second stage, in which the parasites have successfully penetrated the blood-brain barrier and invaded the central nervous system (CNS) (Checchi *et al*., 2015, Kennedy and Rodgers, 2019). In this stage the patient experiences neurological symptoms such as sleep, sensory and motor abnormalities and body wasting, eventually leading to coma and even death if left untreated (Muchiri *et al*., 2015, Chappuis *et al*., 2005, Kennedy, 2008). The time taken to develop into the clinical second stage of the disease is dependent on the *Trypanosoma brucei* subspecies; in *T. b. gambiense* this can take

from several months to several years whilst in *T. b. rhodesiense* this can occur within 6 months of infection (Chappuis *et al*., 2005).

The importance of disease control and the negative impact of HAT were largely recognised in the 1930s during the colonial administration (Simarro *et al*., 2008). Routine screening and treatment as well as the follow-up of individuals led to a large decrease in HAT transmission in the 1960s (Figure 1.2) (Legros *et al*., 2002, Simarro *et al*., 2008, Gubler, 1998). Conflicts and emergence of independence in many of the HAT-endemic countries resulted in a reduction in human and financial resources to combat the disease (Legros *et al*., 2002, Simarro *et al*., 2008, Gubler, 1998), leading to a re-emergence of HAT cases in the 1980s. It was estimated that 57 million people lived in high *T. b. gambiense* risk areas in 1998. This figure rises to around 60 million people at high risk of HAT when combined with *T. b. rhodesiense* (Chappuis *et al*., 2005, Kennedy, 2019).

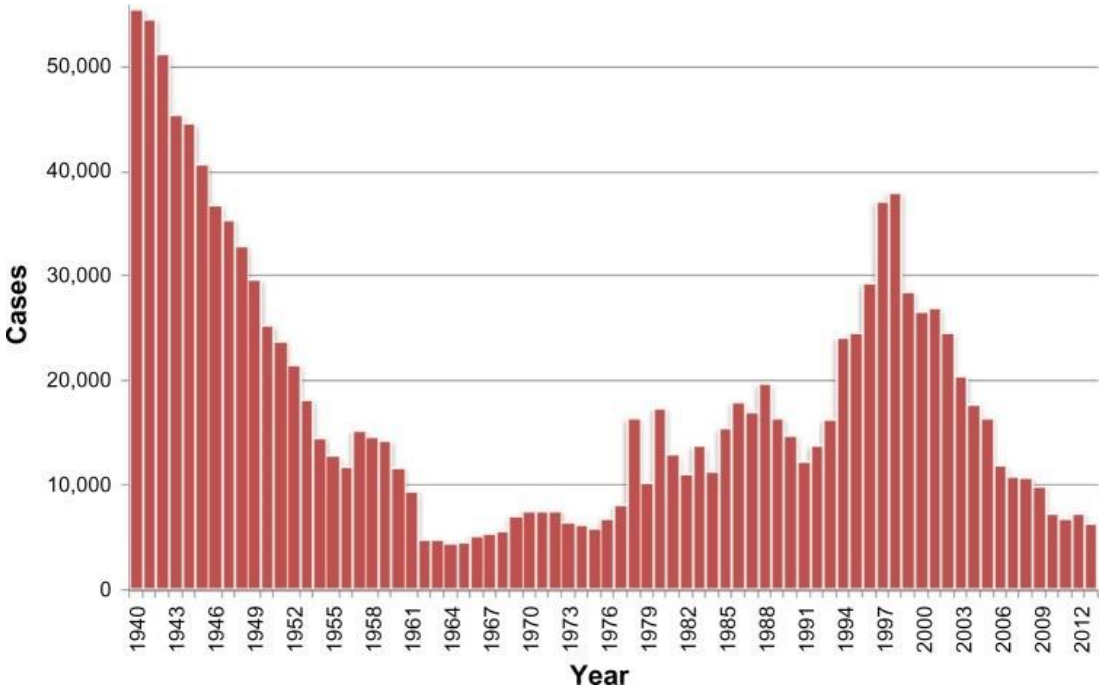

Figure 1.2. Total number of new cases of HAT reported to the World Health Organisation from 1940-2013. *Through routine screening and treatments the number of HAT cases reported was significantly reduced in the 1960s and late 2000s. (Franco et al., 2014).*

The World Health Organisation (WHO) report from 1998 suggested that around 20,000 to 25,000 people have been infected with HAT in that year, however there is a possibility that these figures may have been significantly higher than 300,000 considering that only 3 to 4 million people were actually under surveillance (Legros *et al*., 2002, Chappuis *et al*., 2005, Smith *et al*., 1998). Through concern expressed by WHO in 1995, outreach activities, production and distribution of free drugs, a 68% decrease in HAT cases from 1995 to 2006 was reported (Simarro *et al*., 2008). With continued effort from WHO outreach activities and pharmaceutical companies, the number of cases dropped below 10,000 in 2009 and below 6,228 in 2013 (Holmes, 2014, Simarro *et al*., 2011). HAT was also highlighted in The London Declaration on Neglected Tropical Diseases, with a target set to reduce the number of *T. b. gambiense* case to less than 1 new case/10,000 population at risk globally by 2020 and to zero incidences by 2030 through the use of frequent screening and outreach activities. The number of HAT cases in 2016 had dropped to 2,184, suggesting that the initiative to eliminate the HAT cases by 2030 may be within reach (Figure 1.3) (Rock *et al*., 2015, Kennedy, 2019, Franco *et al*., 2018).

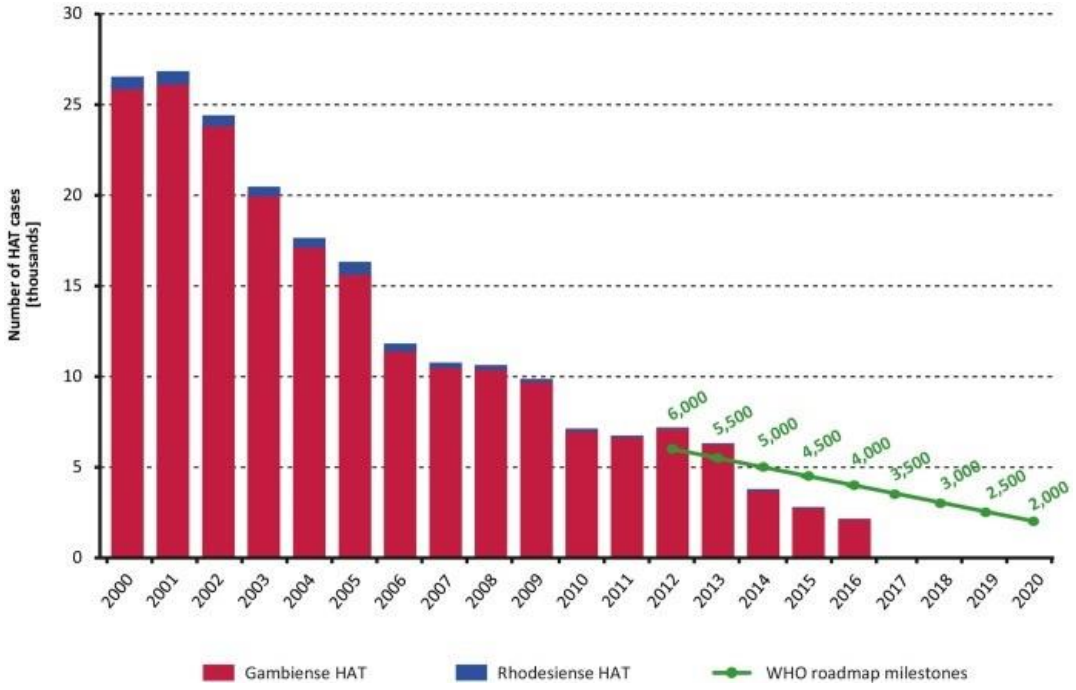

Figure 1.3. Number of reported HAT cases per year from 2000-2016. *Through outreach activities and frequent screening the number reported HAT cases dropped to 2,184 per year. The green lines show the WHO Roadmap to HAT elimination milestones, highlighting that elimination of HAT by 2030 is within reach (Franco et al., 2018).*

1.1.1.2 Animal African Trypanosomiasis

Although initiatives to eliminate HAT have led to significant reduction in the number of reported cases in sub-Saharan Africa since 1995, Animal African Trypanosomiasis or nagana as it is commonly known is still a prevalent infectious disease that threatens livestock such as cattle, sheep and goats (Morrison *et al*., 2016). The economic impact of nagana remains very high. Nagana contributes to the death of three million animals per year, leading to loss of meat and milk production as well as rendering a quarter of Africa unsuitable for livestock farming. The total loss due to nagana and its vector is estimated to be around billions of US dollars annually. This places a huge socioeconomic burden for poorer countries in sub-Saharan Africa (Giordani *et al*., 2019, Meyer *et al*., 2018, Morrison *et al*., 2016).

Nagana infection is characterised by chronic anaemia, anorexia, lethargy and overall decline in production and condition; resulting in lower yield of milk and stillborn offspring (Batista *et al*., 2011, de Clare Bronsvoort *et al*., 2010). This infection is caused by the third subspecies of *T. brucei*, *T. b. brucei* as well as *Trypanosoma congolense* (*T. congolense*) and *Trypanosoma vivax* (*T. vivax*) (de Clare Bronsvoort *et al*., 2010, Majekodunmi *et al*., 2013). As with HAT infections, *T. b. brucei*, *T. congolense* and *T. vivax* are transmitted by tsetse flies, making nagana endemic to sub-Saharan Africa. However the ability of *T. vivax* to develop directly into epimastigotes within insect proboscis means that *T. vivax* is also able to be transmitted by other insects. As a result of this, *T. vivax* has been able to spread outside of the 'tsetse belt' in sub-Saharan Africa and into Northern Africa and South America (Figure 1.4) (Jackson *et al*., 2015, Morrison *et al*., 2016).

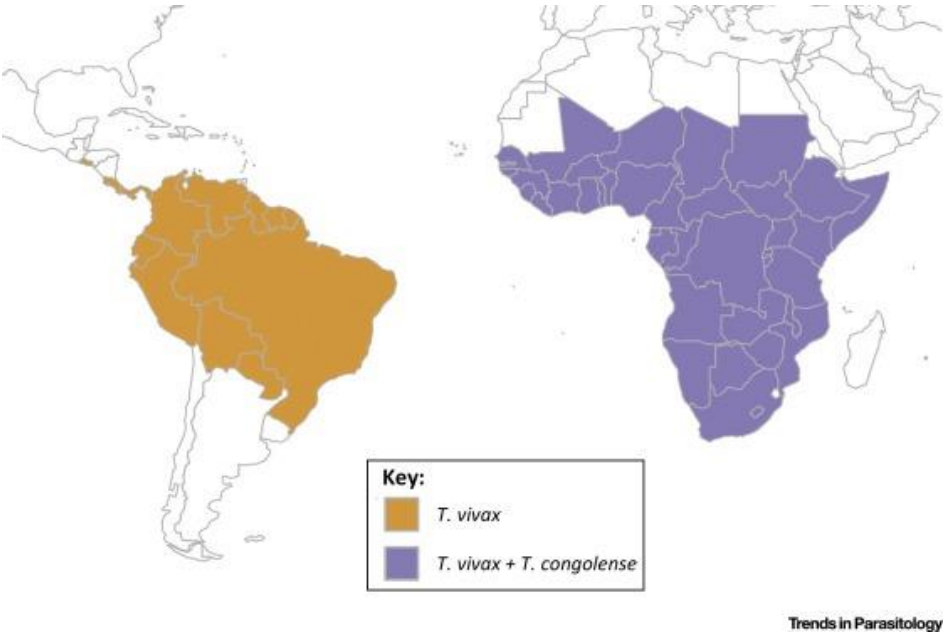

Figure 1.4 Geographical distribution of* T. vivax *and* T. congolense *infection. T. congolense *infections are endemic to sub-Saharan Africa (tsetse belt) whilst* T. vivax *infections are endemic to sub-Saharan Africa, Northern Africa and South America (Morrison et al., 2016)*

1.1.2 Life cycle

1.1.2.1 Establishing infection in host

In order to develop novel control methods for *Trypanosoma brucei*, it is important to understand the life cycle of these parasites. As dixenous parasites, all three subspecies of *Trypanosoma brucei* share a life cycle between two different hosts (Figure 1.5). The parasites have an insect vector, the tsetse fly (*Diptera Glossina*) which is required for the transmission of these parasites (Rock *et al*., 2015, Muchiri *et al*., 2015, Cordon-Obras *et al*., 2015, Ahmed *et al*., 2015, Siegel *et al*., 2010). Insect borne parasites undergo life cycle stage differentiation due to changes in temperature, pH and other factors (Dean *et al*., 2009). This is also true for trypanosomes: undergoing differentiation during their life cycle within mammalian host and tsetse flies as an immune evasion mechanism. The *Trypanosoma brucei* parasites are transmitted to mammals from tsetse flies during a blood meal, during this stage the infective metacyclic trypomastigotes present in the tsetse salivary glands are transferred to the mammalian host via dermal connective tissue (Figure 1.5.A) (Mitashi *et al*., 2015, Albisetti *et al*., 2015, Keating *et al*., 2015).

During the transmission of the parasites to the host tissues, a local immune reaction occurs which result in the development of a 'chancre'. The appearance of this painful skin ulceration usually occurs between 5 to 15 days after the first bite by tsetse flies and is more common in *T. b. rhodesiense* infections than *T. b. gambiense* (Kennedy, 2013, Caljon *et al*., 2016). From the dermal connective tissues, the metacyclic trypomastigotes transform into the bloodstream form trypomastigotes (Figure 1.5.B). These parasites are able to travel to other target sites within the body, such as blood capillaries, tissue fluids and cerebrospinal fluids (Kennedy, 2013, Fenn and Matthews, 2007, Vickerman, 1985, Breidbach *et al*., 2002). Interestingly, Capewell *et al* (2016) identified the presence of *T. brucei* in skin in undiagnosed patients, suggesting that the skin may represent an anatomical reservoir for *T. brucei* infections (Capewell *et al*., 2016).

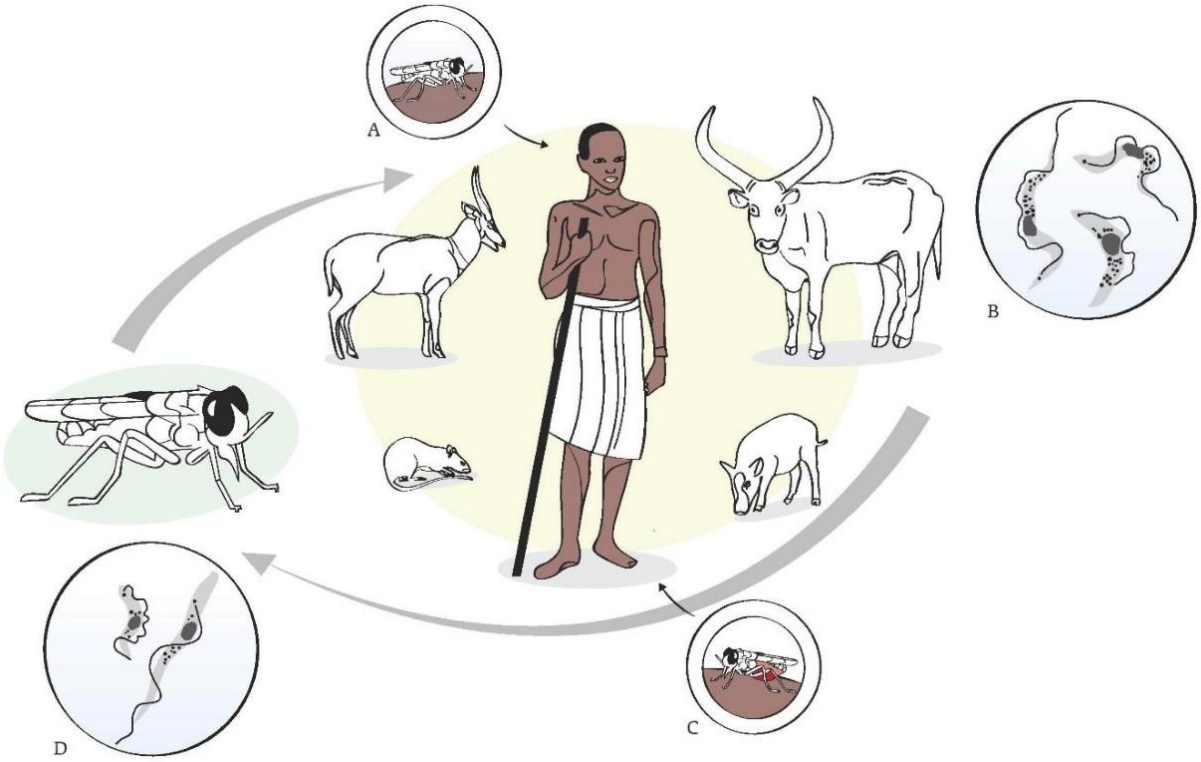

Figure 1.5. **Trypanosoma brucei *life cycle.*** *(A) Ingestion of blood by tsetse initiates the infection in host. (B) Metacyclic trypomastigotes differentiate into bloodstream form trypomastigotes. (C) Another blood meal re-establishes infection in tsetse flies. (D) The stumpy trypomastigotes differentiate into procyclic trypomastigotes in tsetse midgut.* T. b. rhodesiense *and* T. b. gambiense *causes infect humans whilst* T. b. brucei *infect livestock and wild animals. (Büscher et al., 2017).*

1.1.2.2 Parasite stages within the mammalian host

Once the trypomastigotes have reached their target sites, they start to multiply. Single copy organelles such as kinetoplast, nucleus, flagellum, basal body and Golgi that are present in trypomastigotes are duplicated and segregated in a precise order in order to produce viable progeny (Hammarton, 2007, Jones *et al*., 2014). This process of duplication and segregation of single copy organelles is referred to as binary fission and is tightly regulated by specific protein kinases (Hammarton, 2007, Jones *et al*., 2014). Similar to the mammalian cell cycles

which are regulated by cyclin-dependent kinases (CDKs) and their cyclins, *Trypanosoma brucei* cells also contain 11 CDKs known as cdc2-related kinases (CRKs) and 10 cyclins (CYCs). A number of CRKs have been shown to be involved in specific stages of cell cycle; for example RNA interference (RNAi) of CYC2 resulted in the arrest of preparation stage of cell division (G1/G0) (Hammarton, 2007, Hu *et al*., 2016). Another example of CRKs involvement in *Trypanosoma brucei* was demonstrated by Hammarton *et al.* (2003); RNAi of CYC6 showed the absence of mitotic process in the parasite and growth arrest in not only the bloodstream form but also in the procyclic trypomastigotes, the insect infective form of *Trypanosoma brucei* (Hammarton *et al*., 2003).

Bloodstream form trypomastigotes are characterised as elongated cells with post-nuclear kinetoplast and flagellum along the side of the cell, a form which is commonly termed as the 'slender' form (Figure 1.5.B). Upon increased parasitaemia, the slender form trypomastigotes undergo a morphological change into the 'stumpy' form. These cells have characteristic shortened flagellum, a large digestive vacuole, elaborated mitochondrion and the kinetoplast positioned at the posterior end of the cell (Zimmermann *et al*., 2017, Jones *et al*., 2014).

The mechanism by which morphological changes occur in trypomastigotes has been investigated by Vasella *et al.* (1997). They identified that an increase in parasite density in the host triggers the stumpy inducing factor, a density sensing mechanism that triggers the arrest of G0/G1 phase of cell cycle (Vassella *et al*., 1997, Rojas and Matthews, 2019). It should be noted that the slender to stumpy form transition does not occur due to the host immune response. This was highlighted by studies with irradiated mice which were unable to produce antibodies against *T. brucei* infection but still showed the presence of stumpy form trypomastigotes, rather the transition of slender to stumpy form may be triggered as a means to establish a stable host-parasite relationship (Vassella *et al*., 1997).

Stumpy forms are unable to proliferate due to the G0/G1 arrest or to undergo antigenic variation. This means that the parasite will either be transmitted back into the tsetse flies during their next blood meal or be cleared by macrophage phagocytosis (Fenn and Matthews, 2007,

Silvester *et al*., 2017). The stumpy form expresses enzymes associated with the citric acid cycle and electron transport system, which are not needed in the slender form since the abundance of glucose present in mammalian host means that the protozoan parasites are able to generate ATP with the aid of glycolysis, whereas amino acids are the principle energy source in tsetse flies (Brems *et al*., 2005, Breidbach *et al*., 2002, Milne *et al*., 1998).

1.1.2.3 Parasite stages within the insect vector

Stumpy form trypomastigotes are ingested by tsetse flies during their blood meal from an infected mammalian host, thus initiating an infection in the vector (Figure 1.5.C). Once these parasites have entered the tsetse fly midgut, they undergo differentiation into procyclic trypomastigotes around two to three days after infection (Figure 1.5.D). This differentiation is characterised by morphological changes; cells becoming elongated and the expansion and branching of the mitochondrion is observed. Metabolic and antigenic changes are also observed in these cells. The kinetoplast that was in the posterior position of the cell in stumpy form trypomastigotes is relocated to the anterior position of the nucleus (Silvester *et al*., 2018, Crozier *et al*., 2018). In a similar manner to metacyclic trypomastigotes, procyclic trypomastigotes are also able to multiply via binary fission in order to produce epimastigotes (Brems *et al*., 2005, Kennedy, 2013, Breidbach *et al*., 2002, Urwyler *et al*., 2007). Approximately 1-2 weeks after the initial infection in the tsetse fly midgut, procyclic trypomastigotes migrate to the salivary glands of the fly and differentiate into epimastigotes which contains a prenuclear kinetoplast and can also undergo asymmetric division (Kennedy, 2013, Urwyler *et al*., 2007, Rotureau *et al*., 2012). These epimastigotes attach themselves tightly to the epithelial cells that are lined along the salivary gland lumen (Vickerman, 1985, Tetley *et al*., 1987, Urwyler *et al*., 2007). This attachment arises due to the branching dendritic outgrowths in the flagellum (flagellipodia) that wrap around the microvilli present in the epithelial cells and form junctional complexes (Vickerman, 1985, Tetley *et al*., 1987).

The epimastigotes undergo differentiation into metacyclic trypomastigotes through binary fission, a differentiation process which occurs in several stages (Zhang *et al*., 2019). Firstly the epimastigotes differentiate into the premetacyclic trypomastigotes. In this stage the trypomastigotes are still attached to the epithelial cells, however a reduction of size in the flagellipodia is observed. The premetacyclic form still retains the branched mitochondrion and has the capacity to undergo binary fission like the epimastigotes, however this binary fission is assumed to be brief (Tetley *et al*., 1987, Sharma *et al*., 2009). At a specific point, the premetacyclic trypomastigotes cease binary fission and start developing into the coated metacyclic trypomastigotes that are unattached to the epithelial cells, with the kinetoplast back in the posterior position of the cell. These metacyclic trypomastigotes in the salivary glands of the tsetse fly are ready to be transmitted to the host, thus starting the human stage lifecycle of *Trypanosoma brucei*. This process of procyclic trypomastigotes to the infective metacyclic trypomastigotes maturation in tsetse flies takes approximately 20-30 days (Urwyler *et al*., 2007, Kennedy, 2013, Fenn and Matthews, 2007, Tetley and Vickerman, 1985). The arrest of binary fission at the G0/G1 phase of stumpy form trypomastigotes in mammals and metacyclic trypomastigotes in the tsetse salivary glands is a way of pre-adapting the parasite to life in a new host (Figure 1.6), whilst the slender form trypomastigotes and the procyclic trypomastigotes in tsetse flies are the infective phase of the parasite (Hammarton *et al*., 2003, Hammarton, 2007).

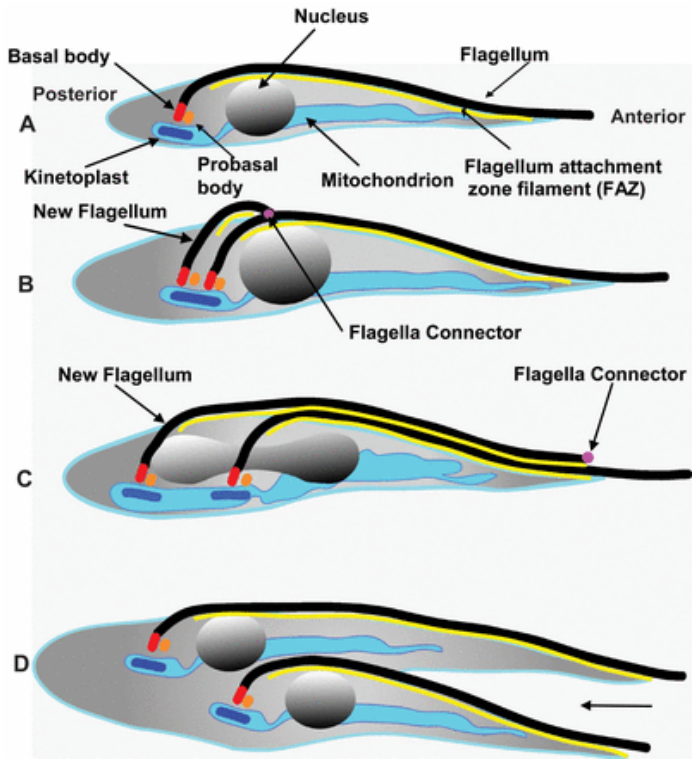

Figure 1.6. Illustration of procyclic form* T. brucei *cell structure and replication process. *(A) The G1 phase cell with a single copy of key organelles. (B) Probasal body maturation takes place, a new flagellum extends and attaches to the old flagellum by flagella connector. (C) New flagellum extends to roughly full length of the old flagellum and kinetoplast segregates, marking the start of mitosis. (D) Cytokinesis is initiated from the anterior end of the cell to the posterior end, resulting in two new cells*

1.1.3 Immune evasion

1.1.3.1 Surface coat proteins in the bloodstream form

T. brucei are extracellular in nature, not entering host cells at any point of their life cycles, which means that the parasites are continually exposed to the host's immune responses (Pays and Vanhollebeke, 2009, Quintana *et al*., 2018). The long-lasting chronic infection caused by *Trypanosoma brucei* is due to their ability to evade the host's immune response with the aid of variant surface glycoprotein (VSG). These 55 kDa homodimeric glycoproteins are the major component of the dense coat that covers the entire cell. With around 10^7 copies of VSGs

present, only one VSG is expressed at the surface of the cell at a time and are replaced as the host immune system produces antibodies against them; ensuring that a small percentage of the parasite survive and re-establish the population (Quintana *et al*., 2018, Shimogawa *et al*., 2015, Tiengwe *et al*., 2016). *T. brucei* also internalises and recycles VSGs from the surface via the flagellar pocket, recycling the entire surface VSGs in approximately 12 minutes (Engstler *et al*., 2007). This clearance of VSGs from the cell surface enables *T. brucei* to maintain chronic infection in host by also clearing anti-VSG immunoglobulins (Engstler *et al*., 2007, Engstler *et al*., 2004).

The VSGs are dimeric with each monomer consisting of a 350-400 residue N terminal domain that is hypervariable and one or two 30-70 residue C terminal domains that are conserved and buried within the coat. The covalent link of the C terminus domain to a glycophosphatidylinositol (GPI) anchor ensures that the VSGs are stable on the outer surface of the coat of trypanosomes (Figure 1.7) (Berriman *et al*., 2005, Chattopadhyay *et al*., 2005, Moreno *et al*., 2019). The location of the expressed VSG gene is found in the metacyclic expression site (MES) or the bloodstream expression site (BES) depending on whether the parasite is located in the salivary glands of tsetse flies or in mammalian host respectively (Vanhamme *et al*., 2001, Stanne and Rudenko, 2010). VSG gene switching in *T. brucei* occurs due to coding gene expression changes. The long polycistronic units of BES contain around a dozen of expression site associated genes (ESAGs) and end with telomeric repeats, with the last gene of BES being the VSG (Berriman *et al*., 2005, Vanhamme *et al*., 2001). Since there are about 20 to 30 BESs depending on the subspecies and 1000 VSGs found in trypanosomes, they can either switch between the BESs by *in situ* activation/inactivation or replace the VSG by homologous recombination (Hertz-Fowler *et al*., 2008, Becker *et al*., 2004).

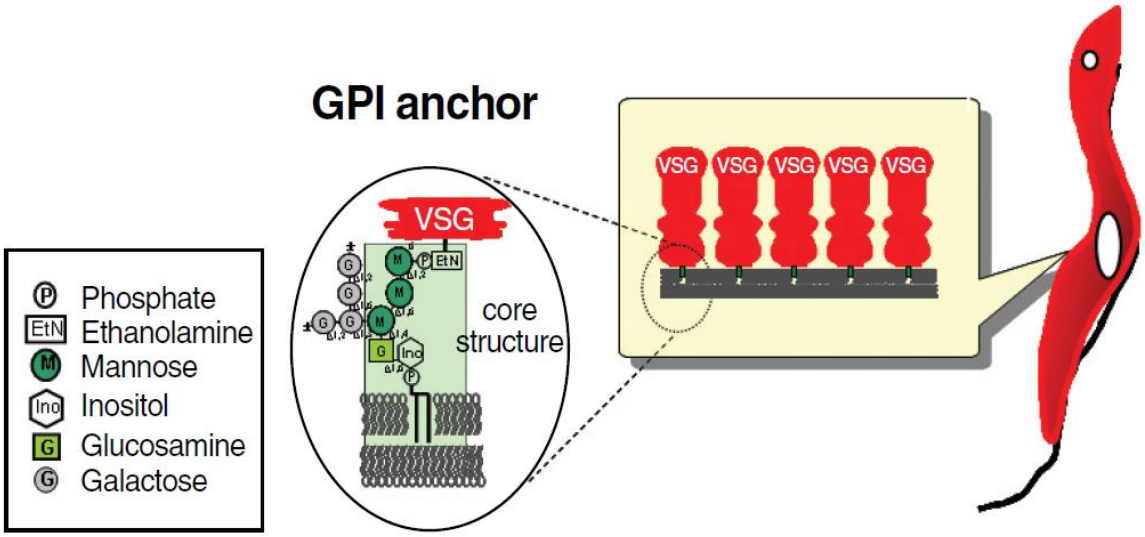

***Figure 1.7. VSG and the structure of GPI anchor from bloodstream form* T. brucei.** *The covalent link of the conserved C domain to GPI ensures that VSGs are stable on the surface of* T. brucei *coat. (Hong and Kinoshita, 2009)*

1.1.3.2 Surface coat proteins in the procyclic form

The surface coat of *Trypanosoma brucei* undergoes changes depending on the stage of the life cycle. Unlike bloodstream form trypomastigotes that express VSGs in order to avoid the host immune response, procyclic trypomastigotes in tsetse flies express a different cell surface glycoprotein coat called procyclins, also known as procyclic acidic repetitive protein (PARP) (Milne *et al*., 1998, Acosta-Serrano *et al*., 2001). Shedding of VSGs takes around 4 hours after the parasites have been ingested by tsetse fly and to reach maximum level of procyclin expression in a single cell takes 12-16 hours post ingestion by the tsetse flies (Roditi *et al*., 1989). The shedding of VSGs in procyclic form occurs due to the activity of two identified enzymes, the GPI-phospholipase C (GPI-PLC) and a metalloprotease *T. brucei* major surface protease B (TbMSP-B). These enzymes cleave the VSGs close to its GPI anchor, by the C terminal domain. MSP-B expression is induced once the differentiation to procyclic form commences and this enzyme continues to be expressed in procyclic form trypomastigotes. In contrast to this, GPI-PLC expression is downregulated during the differentiation into procyclic

form that induces MSP-B expression, but is accessible to the parasite surface (Fenn and Matthews, 2007, Urwyler *et al*., 2007, Grandgenett *et al*., 2007).

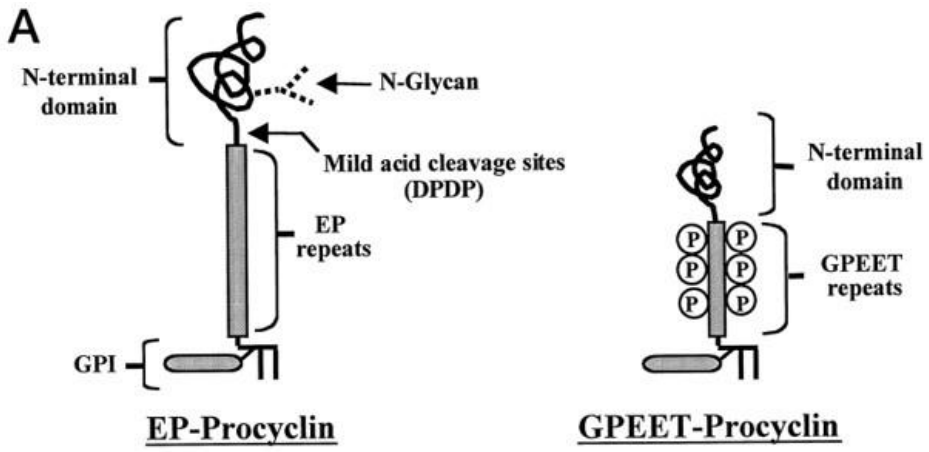

Figure 1.8. Schematic representation of EP and GPEET procyclin expressed in procyclic* T. brucei *trypomastigotes. *EP and GPEET procyclins vary in amino acid repeats at the C-terminal. (Acosta-Serrano et al., 1999)*

Two major forms of procyclins are expressed in procyclic trypomastigotes, with each form varying in the type of amino acid repeats present in their C-terminal (Figure 1.8). The EP procyclins consist of Glu-Pro repeats whilst the GPEET procyclins consist of Gly-Pro-Glu-Glu-Thr repeats. These procyclins serve as a barrier against proteases and other immune defences in the tsetse fly (Urwyler *et al*., 2007, Acosta-Serrano *et al*., 2001, Vassella *et al*., 2009). Each of the EP and GPEET procyclins are expressed at different periods of the infection establishment in tsetse fly midgut. During the early phases of procyclic infection (within 24 hours), GPEET are mainly expressed whilst traces of EP are found. This however changes 7 days post infection as GPEET expression halts and EP1 and EP3 expression is detected (Urwyler *et al*., 2007, Liniger *et al*., 2004). Like the VSGs, the procyclins are also attached to the surface coat via GPI anchors at the C terminal domain and they also have a basic lysine rich N-terminal domain and a highly conserved signal peptide (Liniger *et al*., 2004, Shimogawa

et al., 2015). VSGs that are downregulated in the procyclic form trypomastigotes are reacquired during the metacyclic phase in the tsetse salivary glands (Tetley *et al*., 1987, Barry *et al*., 1998); however the VSGs expressed by the metacyclic trypomastigotes are of a limited repertoire (Pays *et al*., 1989). There are 27 repertoires of VSGs known as the metacyclic VSGs (M-VSGs) that are differentially expressed by each metacyclic trypomastigotes in the salivary glands in order to prepare for mammalian immune response (Casas-Sánchez *et al*., 2018). Activation of the M-VSGs follows the same basic principles as the bloodstream form VSGs. However unlike the bloodstream form VSGs that are activated by the polycistronic BESs, the metacyclic VSGs are activated by the monocistronic MESs (Ramey-Butler *et al*., 2015).

1.1.4 Host immune response

1.1.4.1 Trypanosome lytic factors

As an innate defence against *T. brucei* infections, humans and several primates express trypanosome lytic factors (TLFs) in serum (Capewell *et al*., 2011, Symula *et al*., 2012). Laveran and Mesnil (1912) first noted that normal human serum had the capacity to lyse *T. brucei* (Vanhamme and Pays, 2004), while the presence of two types of TLFs was later described by Hawkings *et al.* (1973) (Tetley and Vickerman, 1985). Two types of TLFs have now been identified in humans. The first TLF (TLF1) is a 500 kDa subset of high density lipoprotein (HDL) that consists of apolipoprotein A-I (apoA-I), haptoglobin-related protein (Hpr), apolipoprotein L-I (Apol1), human cathelicidin antimicrobial peptide (hCAP18), glycosylphosphatidylinositol-specific phospholipase D (GPI-PLD), apolipoprotein A-II and paraoxonase (Molina-Portela *et al*., 2008, Drain *et al*., 2001). Intriguingly Hpr, a heterodimeric protein with over 90% amino acid sequence identity to Haptoglobin and consisting of an α-subunit and a β-subunit bound by disulfide bond, is not found in any other HDLs, being exclusive to trypanolytic HDLs only (Drain *et al*., 2001, Raper *et al*., 2001). The second TLF identified is the TLF2, which is a 1000 kDa protein complex that is not rich in lipid and consists of apoA-I, Hpr, Apol1, hCAP18, GPI-

PLD and immunoglobulin M (Molina-Portela Mdel *et al*., 2005, Drain *et al*., 2001, Raper *et al*., 2001).

Lysis of *T. brucei* by TLF1 is achieved by binding onto the receptors found on the cell surface of trypanosomes; TLF1 is then endocytosed through the aid of coated pits where it is then targeted to the trypanosome lysosome (Drain *et al*., 2001). Binding of TLF1 to the flagellar pocket of trypanosomes occur with the help of ligands, which have been identified as ApoA-I and Hpr; Hpr binding to the haptoglobin-haemoglobin receptor (Figure 1.9). This means that there are two potential routes for TLF1 to enter the trypanosomes (Capewell *et al*., 2011, Raper *et al*., 2001, Currier *et al*., 2018). Although little is known about TLF2 uptake and mode of action, it has been suggested that TLF2 may be endocytosed by an uncharacterised potent mechanism or could also use ApoA-I as a mechanism of entry into *T. brucei* cellular pathway (Figure 1.9); this is mainly due to the fact that haptoglobin-haemoglobin complex competitively inhibits the uptake of TLF1 whilst the uptake of TLF2 is not hindered (Capewell *et al*., 2011, Uzureau *et al*., 2013, Currier *et al*., 2018).

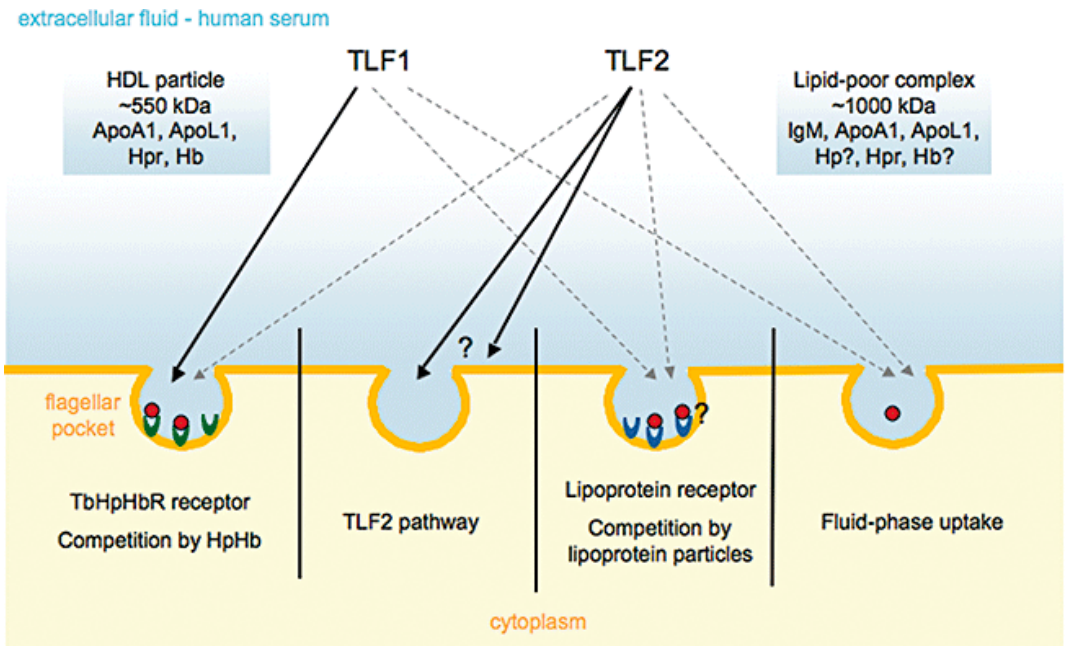

***Figure 1.9. TLF1 and TLF2 pathways of entry into* T. brucei.** *The composition of TLF1 and TLF2 are also highlighted (Vanhollebeke and Pays, 2010)*

1.1.4.2 Mechanism of T. brucei lysis in host

Initially it was assumed that after the uptake of TLF1 to the lysosome, the difference in pH triggers peroxidase activity and causes membrane destruction, ultimately leading to trypanosome auto-digestion (Molina Portela *et al*., 2000, Smith *et al*., 1995). However del Pilar Molina-Portela *et al.* (2000) found this to be inconclusive since their investigation on both TLF1 and TLF2 found that no peroxidative mechanism appears to be involved in TLF mediated lysis of trypanosomes (Molina Portela *et al*., 2000). Instead del Pilar Molina-Portela *et al.* (2005) demonstrated in their study that TLF1 induces formation of cation permeable pores in *T. brucei* membranes, thus resulting in the disruption of membrane potential and leading to osmotically driven swelling, which eventually results in the lysis of trypanosomes (Molina-Portela Mdel *et al*., 2005).

Primarily it was assumed that the lytic component of HDLs is the ApoA-I, but this was discounted since patients with Tangier disease (where levels of HDLs and ApoA-I are undetectable) still retained the trypanolytic activity (Pays and Vanhollebeke, 2009, Raper *et al*., 2001). One possible explanation to this may be due to the fact that patients with Tangier disease also exhibited low levels of haptoglobin. As a natural TLF1 inhibitor, the level of haptoglobin found in normal human serum correlates to the variation of trypanolytic activity in an individual (Drain *et al*., 2001, Raper *et al*., 2001). This would mean that patients with Tangier disease will have limited TLF1 inhibitory effect as opposed to normal human serum due to the low levels of haptoglobin present in the serum. The inhibitory effect of haptoglobin however appears to be only limited to TLF1, since Raper *et al.* (1996) identified that TLF2 activity was not inhibited in the presence of haptoglobin (Raper *et al*., 1996). This may suggest that TLF2 might actually be the predominant trypanolytic factor in normal human serum. Immunodepletion studies with anti- immunoglobulin M in normal human serum revealed an 80% decrease in trypanolytic activity, further supporting the hypothesis that TLF2 might be the main trypanolysis factor (Raper *et al*., 2001). This may suggest that TLF2 might actually be the predominant trypanolytic factor in normal human serum.

Immunodepletion studies with anti- immunoglobulin M in normal human serum revealed an 80% decrease in trypanolytic activity, further supporting the hypothesis that TLF2 might be the main trypanolysis factor (Raper *et al*., 2001). Haptoglobins are known to bind to haemoglobins with high affinity in order to form haptoglobin-haemoglobin (Hp-Hb) complexes (Molina Portela *et al*., 2000).The VSGs of *Trypanosoma brucei* exhibit receptors for Hp-Hb termed TbHpHbR. Trypanosomes are able to incorporate heme to hemoproteins via endocytosis of Hp-Hb, which is necessary for their survival (Pays and Vanhollebeke, 2009, Hardwick *et al*., 2014). Hpr is also capable of binding to haemoglobin to form Hpr-Hb complex, which in turn can also bind to the TbHpHbR on *Trypanosoma brucei*. Binding of Hpr-Hb complex that is also part of the TLF1 complex allows TLF1 to be endocytosed into the parasite. Once inside the parasite, the Bcl2-like protein – Apol1 is trafficked to the lysosome compartments. The change in pH triggers a pH mediated conformational change in Apol1, which in turn causes lysis of the parasite through swelling and rupture. Apol1 has been shown to be involved in selective ion movement via interaction with the lysosome membrane (Hardwick *et al*., 2014, Higgins *et al*., 2013).

1.1.4.3 Trypanolysis evasion by T. b. rhodesiense

Trypanolysis is the mechanism which prevents *T. b. brucei* from being infective to humans, enabling effective lysis of *T. b. brucei*. However, *T. b. gambiense* and *T. b. rhodesiense* are able to avoid lysis induced by normal human serum and thus effectively infect humans (Capewell *et al*., 2011, Hardwick *et al*., 2014). *T. b. rhodesiense* is able to evade lysis by TLF1 through the serum-resistance associated (SRA) proteins. These SRA proteins are members of the VSGs, sharing several structural and sequence homologies, such as the similarity in the carboxy-terminal domain structure except for two substitutions at the second subdomain. VSGs and SRAs share similar amino-terminal domain, except for the deletion of approximately 100 amino acids in SRAs (Oli *et al*., 2006, Stephens and Hajduk, 2011, Stijlemans *et al*., 2016). The localisation of SRAs and the location of interaction with TLFs within *T. b. rhodesiense* have been extensively studied. Initially it was assumed that the localisation of SRAs was

exclusively at the lysosome, where it would interact with the Apol1 and inhibit its pH mediates trypanolytic activity. However a study by Bart *et al.* (2015) using monoclonal antibodies as markers has identified that approximately 50% of SRA proteins are localised at the trypanosome lysosome, whilst the other SRA proteins are distributed to other parts of the parasite via the endocytic pathway (Bart *et al*., 2015). Interestingly Bart *et al*. (2015) found that SRAs were absent from the flagellar pocket (Bart *et al*., 2015).

Co-localisation of SRA proteins and TLFs was reported to occur at the small cytosolic vesicles, and it could be speculated that the interaction between SRAs and TLFs would likely occur at these small vesicles (Oli *et al*., 2006). Lecordier *et al.* (2009) speculated that the mechanism of SRA interacting with Apol1 in order to inhibit trypanolysis seem to involve coiled-coil binding of SRA to a C-terminal α-helical region of Apol1. Mutation and deletion of the Apol1 C-terminal resulted in the reduced interaction of SRA with Apol1 whilst the Apol1 still maintained its pore forming activity *in vitro* and in transgenic mice (Lecordier *et al*., 2009).

The importance of SRA in resistance to trypanolytic factors was highlighted by several studies involving *T. b. brucei*, which lacked the SRA gene. Xong *et al.* (1998) transfected the insect specific procyclic *T. b. brucei* with SRA and then measured the generated bloodstream form transformants both *in vitro* and in mice. They identified that the lysis of the control group occurred after 10 hours whilst the transfected group was unaffected, even 22 hours post exposure to normal human serum (Xong *et al*., 1998). This was further supported by Oli *et al.* (2006), where similar transfection of SRA into bloodstream form *T. b. brucei* was sufficient to induce resistance to TLFs in parasite lines (Oli *et al*., 2006). A study by Szempruch *et al* (2016) has highlighted the possibility that SRA can be transferred from *T. b. rhodesiense* to T*. b. brucei* via membranous nanotubes originating from flagellar membrane. This could mean that resistance in *T. b. brucei* can be established, thus enabling them to infect humans (Szempruch *et al*., 2016).

1.1.4.4 Trypanolysis evasion by T. b. gambiense

While there is strong evidence of *T. b. rhodesiense* resistance to trypanolytic HDLs being conferred via SRA proteins, this is not the case for *T. b. gambiense*, in which SRA genes have not been found. Little is known about the mechanism of *T. b. gambiense* resistance to TLF1 (Kieft *et al*., 2010, Capewell *et al*., 2011). *T. b. gambiense* is divided into two genetically distinct groups: the dominant group 1 form which is different to *T. b. brucei* and *T. b. rhodesiense*, and the less common group 2 which resembles *T. b. brucei* and has the capacity to lose resistance to normal human serum during serial passage in rodents (Kieft *et al*., 2010, Barrett *et al*., 2003).

The group 1 *T. b. gambiense* is distinguishable from the group 2 *T. b. gambiense* by the conserved single nucleotide polymorphism of the *T. brucei* haptoglobin-haemoglobin receptor (TbHpHbR), causing a reduction of TLF1 uptake (Kieft *et al*., 2010, Capewell *et al*., 2011, Capewell *et al*., 2013). Kieft *et al.* (2010) demonstrated that by reducing the expression of *T. b. brucei* haptoglobin-haemoglobin receptor genes, a resistance to TLF1 was induced that corresponded to the resistance that was observed in group 1 *T. b. gambiense*. Thus Kieft *et al*. (2010) highlighted the significance of reduced TbHpHbR expression in *T. b. gambiense* as a mechanism of resistance to normal human serum (Kieft *et al*., 2010). Although this may explain the resistance to trypanolytic event in human serum by TLF1, it does not clearly explain as to why *T. b. gambiense* is still able to resist trypanolysis by TLF2. This gives rise to the question on whether group 1 *T. b. gambiense* interacts with Apol1 in both TLF1 and TLF2 (Capewell *et al*., 2011).

The discovery of a 47 kDa VSG like protein termed *T. gambiense-specific glycoprotein* (TgsGP) in 2001 by Berberof *et al.* (Berberof *et al*., 2001) brought forward a possibility of resistance mechanism of group 1 *T. b. gambiense*. To demonstrate the possibility of the involvement of TgsGP in trypanolysis resistance, Berberof *et al.* conducted a transfection of *T. b. brucei* with TgsGP. This however did not demonstrate a resistance in the transfected parasites, implying that other mechanisms might be working alongside TgsGP in group 1 *T. b. gambiense* (Berberof *et al*., 2001). At the time of the study, despite their attempts Berberof *et*

al. were not able to demonstrate TgsGP involvement in group 1 *T. b. gambiense* resistance, due both to the unsuccessful efforts to delete the gene and the failure to induce resistance in the transfected *T. b. brucei* expressing TgsGP (Capewell *et al*., 2013, Berberof *et al*., 2001). In 2013 this study was revisited by Capewell *et al.* (2013), who successfully deleted TgsGP in group 1 *T. b. gambiense*, resulting in sensitivity to TLF1, Apol1 and human serum. TgsGP complementation lines, i.e. knockout parasites in which TgsGP was reintroduced, also showed resistance; concluding that TgsGP may be an essential component to normal human serum resistance by *T. b. gambiense* (Capewell *et al*., 2013).

The importance of TgsGp N-terminal domain structure in normal human serum resistance was identified by Uzureau *et al*. (2013); they identified the presence of α-helical and β-sheet hydrophobic linker between the two N-terminal domain helices in TgsGP (Uzureau *et al*., 2013). Disruption of the β-sheet hydrophobicity was observed to have affected the function and localisation of TgsGP, whilst a change in the α-helix hydrophobicity does not appear to have an effect since the disruption of the hydrophobic character of α-helix in TgsGP did not affect TgsGP's activity (Uzureau *et al*., 2013). Although little is known about the mechanism of resistance of the least common group 2 *T. b. gambiense*, it has been identified that the group 2 *T. b. gambiense* are superficially similar to *T. b. rhodesiense* in exhibition of a variable human serum resistance phenotype (Capewell *et al*., 2011). Unlike the group 1 *T. b. gambiense*, group 2 does not exhibit avoidance to TLF uptake, instead being dependent on a separate mechanism to neutralise the lysis effect of the internalised Apol1 (Capewell *et al*., 2011, Symula *et al*., 2012). Initially it was speculated that the mechanism of neutralising Apol1 in group 2 *T. b. gambiense* occurs with the aid of TgsGP, however the presence of TgsGP in group 2 *T. b. gambiense* as well as the other two Trypanosome brucei subspecies have not been identified, implying that the TgsGP may be exclusive to only group 1 *T. b. gambiense* (Capewell *et al*., 2013). The complex mechanism of host immune evasion by *T. brucei* spp. makes targeting these parasites and eradicating them a complicated process.

1.1.5 Diagnosis

Diagnosis of HAT is critical in order to identify infected individuals and properly administer the necessary treatment in order to minimise transmission. Diagnosis is usually based on a combination of clinical and investigative data (Kennedy, 2019). Key to diagnosis is the geographical location of the infection, as *T. b. gambiense* and *T. b. rhodesiense* endemic regions do not overlap except in some regions of Uganda (Figure 1.1) (Keating *et al*., 2015, Kennedy, 2008). However, since non-specific symptoms such as fever can easily be mistaken for other tropical diseases such as malaria, it is crucial to perform clinical testing to establish the type of infection in patients before administrating drugs (Kennedy, 2019, Büscher *et al*., 2017). Diagnosis of haemolymphatic stage *T. brucei* often involves testing patient samples by microscopy, demonstrating the presence of the parasite in the peripheral blood using stained thick or thin films. Although this method could be used to diagnose *T. b. rhodesiense* infection due to their permanent presence in the blood, this method is not ideal to use to detect the presence of *T. b. gambiense* infection as few parasites are present in the blood in this latter subspecies, varying around 100 trypanosomes/mL to 10,000 trypanosomes/mL (Kennedy, 2019, Bonnet *et al*., 2015). Microscopy can also be used to detect the presence of parasites in fluid taken from the cervical lymph nodes (CLNs) (Bonnet *et al*., 2015).

Card agglutination trypanosomiasis test (CATT) is used to diagnose *T. b. gambiense*. This serological test is cheap, practical and relatively quick to perform and has been used widely since its development in 1978 (Kennedy, 2019, Bonnet *et al*., 2015). CATT involves the detection of *T. b. gambiense* specific antibodies (LiTAT 1.3 antigen) in the patient's blood. A drop of blood is mixed with a drop of reagent and shaken for 5 minutes and the result can be visualised easily with the naked eye (Bonnet *et al*., 2015). Although this test has good specificity, there is a risk of false negatives, especially amongst patients that are infected with trypanosomes that do not express the LiTAT 1.3 genes (Bonnet *et al*., 2015, Büscher *et al*., 2017). In order to accurately determine the stage of the infection and avoid inappropriate treatment, it is important to identify the presence of trypanosomes in the CNS (Kennedy, 2004,

Kennedy, 2008). This is achieved by lumbar puncture and examination of the cerebrospinal fluid (CSF) and by determining pleocytosis, analysis of white blood cell (WBC) and protein concentration (Bonnet *et al*., 2015, Kennedy, 2019).

An additional method of diagnosing trypanosome infection is the detection of chancre formation; however the formation of chancre is more common in *T. b. rhodesiense* infection than that of *T. b. gambiense*, therefore any infection by *T. b. gambiense* is likely to be ignored using this method. To further complicate this, European patients are more likely to exhibit chancre than African patients (Kennedy, 2013). Biological markers could also be considered as a method of diagnosing different *T. brucei* subspecies infection. It is already known that CATT test incorporates the *T. b. gambiense* LiTAT 1.3 antigen, however there are other strain specific markers that could be used as a biomarker. In the case of *T. b. rhodesiense*, identification of SRA proteins in *T. b. gambiense* and *T. b. brucei* by Gibson *et al.* (2002) yielded negative results, suggesting that this protein is exclusive to only *T. b. rhodesiense* (Gibson *et al*., 2002). In the same manner, Gibson *et al.* (2010) studied the presence of TgsGP in group 1 and 2 *T. b. gambiense* as well as the other *Trypanosoma brucei* subspecies and noted that TgsGP is conserved in group 1 throughout all of its endemic regions, whereas TgsGP-like genes were present in some group 2 and other Trypanosoma brucei subspecies (Gibson *et al*., 2010).

Other rapid diagnosis tests (RDTs) have been developed for *T. b. gambiense*. These RDTs partly test for the same antigens that are tested in CATT. The SD Bioline HAT (Standard Diagnostics, Yongin, South Korea); a lateral flow immunochromatography introduced in 2012, the HAT Sero-Strip; a dipstick test, and the HAT Sero-K-SeT test (Coris BioConcept, Gembloux, Belgium); a lateral flow device introduced in 2013 all test for the presence of *T. b. gambiense* antigens LiTAT 1.3 and LiTAT 1.5. All three of these RDTs have shown *T. b. gambiense* antigens (Boelaert *et al*., 2018, Bisser *et al*., 2016, Büscher *et al*., 2017). These RDTs fully comply with the ASSURED criteria (Affordable, Sensitive, Specific, User-friendly, Rapid and robust, Equipment free and Deliverable to end-users). This means that they can be

used in countries with lack of electricity or laboratory infrastructure (Büscher *et al*., 2017). However the use of CATT and RDTs are not always 100% specific, especially when disease prevalence is low. For example, with a specificity of 98% and prevalence of 0.1%; the predicted positive value is 4.5% (Büscher *et al*., 2017).

DNA amplification can be used to stage HAT disease. The loop-mediated isothermal amplification (LAMP) technique amplifies specific parasite DNA sequence from blood, CSF, saliva or urine samples. This technique has high specificity and sensitivity, and can be used in countries with minimal laboratory equipment (Bonnet *et al*., 2015, Njiru *et al*., 2017).

1.1.6 Treatments for HAT

Antigenic variation of the Variable Surface Glycoproteins (VSGs) of the human infective *T. b. gambiense* and *T. b. rhodesiense* means that creating an effective vaccine for these parasites is very challenging (Baker and Welburn, 2018, Jones and Avery, 2015). There are currently five clinically approved drugs available to combat African trypanosomiasis, of which three of these were developed over 50 years ago and the newest one was recently registered for use against *T. b. gambiense*. These five drugs are both species and stage specific, administered after the diagnosis of the *T. brucei* infection (Baker and Welburn, 2018).

1.1.6.1 Suramin

The first clinically approved drug to be used against trypanosome infection was suramin (Figure 1.10.2), manufactured by Bayer; this colourless drug is a sulfonated naphthylamine that was first used in 1922 to treat trypanosomiasis cases in field (Babokhov *et al*., 2013). This drug has been used to successfully treat the early phase of *T. b. rhodesiense* infection and remains the drug of choice against early phase *T. b. rhodesiense* infection (Baker and Welburn, 2018). Being a highly soluble drug, suramin can be administered intravenously via injection but since it is unable to cross the blood-brain barrier, it is not effective against the late phase

infection (Wiedemar *et al*., 2018). Suramin has the capability to bind strongly to serum proteins including LDLs; this gives suramin a very long half-life of 44-54 days in humans (Bacchi, 2009). Since suramin is bound to LDLs, it is endocytosed within the flagella pocket of the parasite; once inside the parasite, suramin is shown to inhibit glycolytic enzymes as well as other enzymes involved in a range of pathways such as pyruvate kinase (Wiedemar *et al*., 2018, Thomas *et al*., 2018, Baker and Welburn, 2018). Although suramin inhibits glycolytic enzymes, this inhibition is assumed to be slow since the trypanocidal action of the drug has been observed to be slow (Bacchi, 2009, Fairlamb, 2003). The activity of suramin is enhanced by ornithine (Thomas *et al*., 2018).

The pleotropic effect of suramin might explain why cases of suramin resistance in human pathogenic trypanosomes are rare. However resistance to suramin has been described in animal pathogenic trypanosomes (Wiedemar *et al*., 2018, Barrett *et al*., 2007). The side effects of suramin administration range from mild to life-threatening, these can be divided into immediate side effects such as vomiting, shock and nausea; or delayed reactions such as kidney damage, exfoliative dermatitis, haemolytic anaemia, jaundice, agranulocytosis and severe diarrhoea (Fairlamb, 2003, Thomas *et al*., 2018).

1.1.6.2 Pentamidine

Pentamidine (Figure 1.10.1) is a water soluble aromatic diamidine manufactured by Aventis, which has been used against trypanosomes since the 1930s (Baker and Welburn, 2018). Since this drug is found to be very effective against early phase *T. b. gambiense* infection as opposed to *T. b. rhodesiense* infection, it is considered as a drug of choice against early phase *T. b. gambiense* infection (Schmidt *et al*., 2018, Thomas *et al*., 2018). The current dosing of this drug requires 7-10 intramuscular injections, however alternative dosing for this drug is also being considered (Bacchi, 2009, Barrett *et al*., 2007). Pentamidine is taken up by the adenine/adenosine P2 transporter as well as high-affinity pentamidine transporter 1 (HAPT1) and low-affinity pentamidine transporter 1 (LAPT1) (Munday *et al*., 2014, Song *et al*., 2016).

Once within the parasite, pentamidine promotes cleavage of kinetoplast DNA by binding to the minor groove, which leads to the development of dyskinetoplastic cells (Bacchi, 2009, Thomas *et al*., 2018). Resistance to this drug occurs due to the deletion and loss-of-function mutation to the *TbAT1* gene that is responsible for encoding the P2 transporter. However trypanosomes are still able to take up the drug with the aid of the HAPT1 and LAPT1 transporters (Barrett *et al*., 2007, Baker and Welburn, 2018). The loss of both P2 and HAPT1 has been associated with greatly reduced uptake of pentamidine and potential resistance (Baker and Welburn, 2018). *T. brucei* aquaglyceroporin 2 (TbAQP2), a major intrinsic protein, has been shown to increase the affinity of pentamidine uptake. Munday *et al* (2014) examined melarsoprol and pentamidine cross resistance *T. brucei* strains and identified deletion or rearrangements of TbAQP2 (Munday *et al*., 2014). Interestingly reintroduction of TbAQP2 into melarsoprol-pentamidine cross resistant *T. brucei* strains reinstated HAPT1 functions but not P2 transporters (Munday *et al*., 2014). Intravenous administration of pentamidine causes hypotensive reaction, therefore the drug is administered intramuscularly, but even then the side effects of this drug can be fatal. Side effects include kidney, liver and pancreas damage, with pancreatic damage having the potential to lead to diabetes (Babokhov *et al*., 2013).

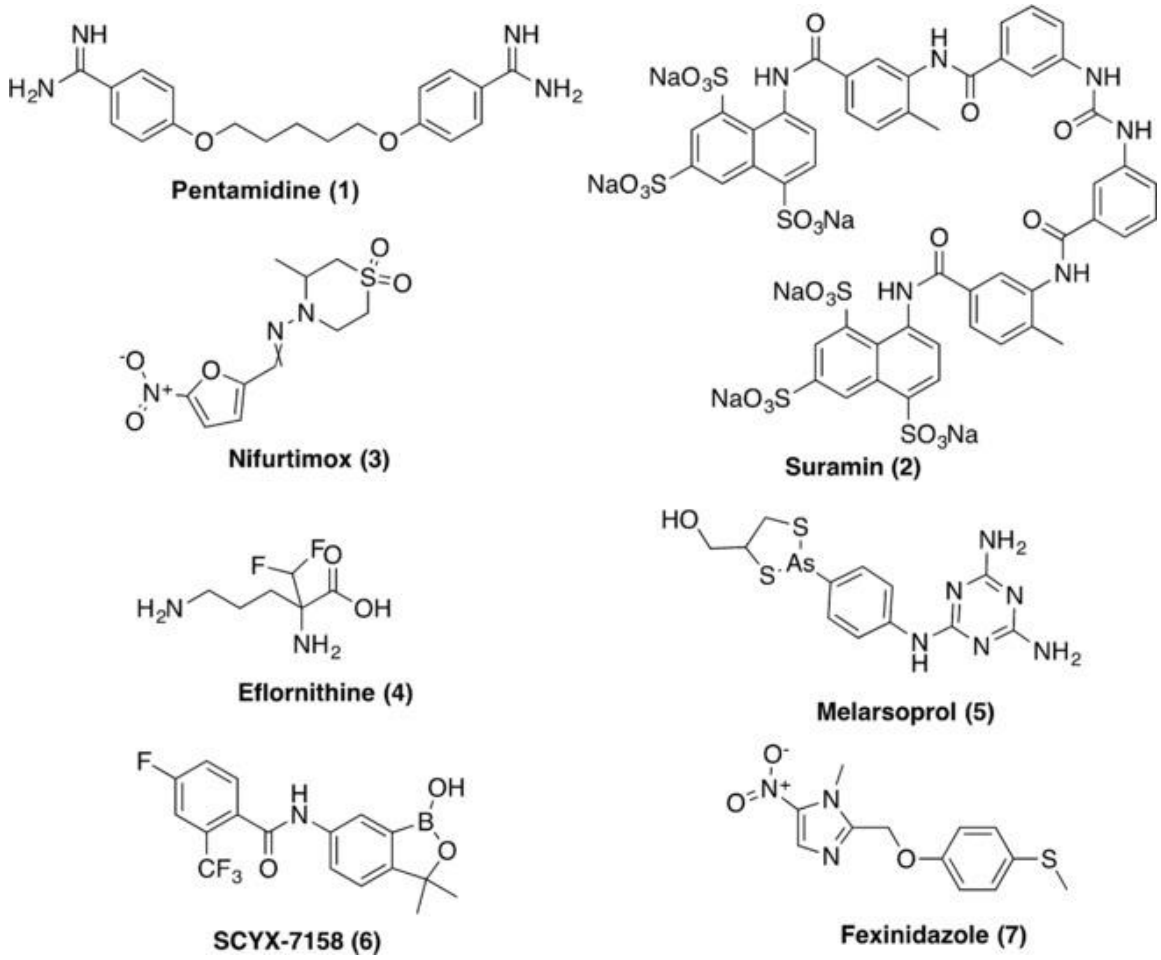

Figure 1.10. Drugs against Human African Trypanosomiasis (HAT). *Current (1-5) and new (6 and 7) drugs used to treat HAT.*

1.1.6.3 Melarsoprol

Melarsoprol is an arsenical drug manufactured by Aventis (Figure 1.10.5), and was introduced in 1949 (Babokhov *et al*., 2013, Baker and Welburn, 2018). This drug is used to treat the late stage *T. b. gambiense* and *T. b. rhodesiense* infection and is often administered as 2-4 series of three intravenous injections daily or as a single daily injection for 10 days (Fairlamb and Horn, 2018). Although the mechanism of melarsoprol action is not fully understood, it was noted that trypanosomes undergo rapid lysis after the administration of this drug. The inhibition of pyruvate kinase and other pathways involved in glycolysis has been attributed to this rapid lysis of trypanosomes (Thomas *et al*., 2018, Fairlamb and Horn, 2018). As with pentamidine,

Melarsoprol is also taken up by the trypanosomes via the P2 transporter, therefore exposing the parasite to cross-resistance (Nok, 2003, Baker *et al*., 2013) and identification of trypanosomes resistant to melarsoprol identified nine mutations in the *TbAT1* gene (Nok, 2003, Munday *et al*., 2014). As melarsoprol is insoluble in water, it needs to be dissolved in propylene glycol before being administered intravenously. Administration by this route is very painful and often destroys veins after several doses (Fairlamb and Horn, 2018, Baker and Welburn, 2018). Side effects include vomiting, peripheral neuropathy, arthralgia, abdominal colic and thrombophlebitis. 5-10% of cases involving melarsoprol administration to patients developed serious reactive encephalopathy, of which 50% will die. (Babokhov *et al*., 2013, Fairlamb and Horn, 2018).

1.1.6.4 Eflornithine

The fourth clinically approved drug for HAT is eflornithine (Figure 1.10.4); this drug is manufactured by Aventis and is the drug of choice for late stage *T. b. gambiense* infection (Kansiime *et al*., 2018, Baker and Welburn, 2018). Although not a trypanocidal drug, eflornithine is known to irreversibly inhibit ornithine carboxylase, an enzyme involved in the polyamine biosynthetic pathway (Thomas *et al*., 2018, Kansiime *et al*., 2018). In 2009 the use of eflornithine with another drug called nifurtimox (Figure 1.10.3) as a combination therapy (Nifurtimox-Eflornithine combination therapy; NECT) was introduced to the WHO Essential Medicines List to target late stage *T. b. gambiense* infection. This new treatment option is cheaper and easier to administer to patients compared eflornithine monotherapy, requiring only 14 intravenous infusions over 7 days as opposed to 56 infusions over 14 days (Yun *et al*., 2010, Bacchi, 2009, Kansiime *et al*., 2018). Bloodstream form trypanosomes exposed to Eflornithine show arrested proliferation and transform into the stumpy form, which are then killed by the host immune system (Baker and Welburn, 2018, Thomas *et al*., 2018). The disadvantages of this drug are cost of production and difficulty in administration; patients are

given four daily infusions for 7-14 days and each infusion requires 400mg kg^{-1} of eflornithine (Babokhov *et al*., 2013).

1.1.6.5 Fexinidazole

Due to the increased cost of production, serious side effects and emerging resistance to existing clinically approved drugs against HAT, there has been a rise in research for alternative treatment against HAT that are easy to use and effective (Mesu *et al*., 2018). This has recently led to the discovery of fexinidazole (Figure 1.10.7), a nitroimidazole that was discovered during a proactive compound mining approach (Torreele *et al*., 2010). Fexinidazole is a drug that can be used to treat the haemolymphatic and meningoencephalitic stages of HAT and is administered orally. Phase II and phase III clinical trial on patients with late stage *T. b. gambiense* HAT demonstrated 91% success rate 18 months post treatment with fexinidazole versus 98% success rate with NECT. The overall results demonstrate that fexinidazole is an effective and safe oral drug for treatment against HAT compared to NECT and has now been registered for use (Mesu *et al*., 2018, Pollastri, 2018, Chappuis, 2018).

1.1.6.6 New treatments

Research into other potential drugs against HAT has led to the development of Benzoxaborole (SCYX-7158). SCYX-7158 showed potency in curing mice infected with late stage *T. brucei* infection 7 days post oral administration at a dose of 25 mg/kg. SCYX-7158 is currently awaiting phase III clinical trials (Figure 1.10.6) (Jacobs *et al*., 2011, Mäser *et al*., 2012, Steketee *et al*., 2018). Other possible drugs that can be used to treat HAT are microtubule stabilising drugs; these drugs are primarily used for cancer chemotherapy, however the potential to treat other diseases such as diseases of CNS have been highlighted in several studies. One such study demonstrated the use of Paclitaxel, a microtubule stabilising drug to inhibit the replication of *T. brucei* (Monti *et al*., 2018, Lama *et al*., 2012).

1.1.7 Treatments for nagana

Animal African Trypanosomiasis (nagana) contributes to considerable loss of livestock and profit, rendering approximately 25% of arable land mass unsuitable for farming livestock and costing Africa billions of US dollars annually. The current drugs against nagana are diminazene aceturate (Berenil); an aromatic diamidine, homidium (Ethidium); a phenanthridine and isometamidium (Samorin); a phenanthridine-aromatic amidine (Giordani *et al*., 2019, Büscher *et al*., 2019, Delespaux and de Koning, 2007).

1.1.7.1 Diminazene aceturate

Diminazene aceturate is administered to cattle as a therapeutic agent and is the first-line treatment against nagana due to its low relative cost, availability and trypanocidal effect. Diminazene aceturate binds to kinetoplast DNA via interacting with adenine-thymine base pairs rather than intercalating, this interaction inhibits RNA primer synthesis, resulting in inhibition of kDNA replication due to accumulation of replicating intermediates (Tsegaye *et al*., 2015, Delespaux and de Koning, 2007). Due to diminazene aceturate being cleared rapidly post administration, it has been assumed that resistance to this drug may not been widespread. However since this drug is taken up by the P2 transporter in *T. brucei*, resistant to diminazene aceturate due to loss of activity in P2 transporter have been documented (Tsegaye *et al*., 2015, Delespaux and de Koning, 2007).

1.1.7.2 Isometamidium and homidium

Isometamidium was first synthesised by coupling homidium and diminazene aceturate. This drug alongside Homidium are administered to cattle as a prophylactic and therapeutic drug. Although homidium and isometamidium are localised differently inside trypanosomes; Isometamidium being concentrated in the kinetoplast whilst homidium is spread throughout the cell, both of these drugs interact by intercalating between DNA base pairs and inhibiting nucleic acid synthesis as well as causing the inhibition of RNA and DNA polymerases (Tsegaye *et al*., 2015, Delespaux and de Koning, 2007, Anene *et al*., 2001). As with diminazene aceturate,

both homidium and isometamidium are taken up by trypanosomes through the P2 transporters; thus deletion or loss-of function mutation to the P2 transporter gene *TbAT1* results in cross resistance to both of these drugs (Anene *et al*., 2001, Delespaux and de Koning, 2007, Tsegaye *et al*., 2015, Geerts *et al*., 2001, Gysin *et al*., 2018).

Although there has been great success due to the introduction of fexinidazole as a new treatment for HAT, there is always the threat of parasites developing resistance. This issue coupled with the rising resistance to drugs against nagana means that research into new methods of Human African Trypanosomiasis and Animal African Trypanosomiasis treatment should remain a priority. The ADP-ribosylation factors (ARFs) are known to have important roles in *T. brucei* and may be promising targets, either directly or indirectly, for new therapeutics against *T. brucei spp.* infection.

1.2 ADP-ribosylation factors

1.2.1 ADP-ribosylation factor and ARF-like proteins

1.2.1.1 What are ADP-ribosylation factors?

ADP-ribosylation factors (ARFs) are small guanine nucleotide binding proteins (approximately 20kDa) that belong to the Ras superfamily of GTPases. However ARFs lack the C-terminal isoprenylation and carboxymethylation regions that are present in other members of the Ras GTPase superfamily (Morgan *et al*., 2015, Guadalupe *et al*., 2018, Muthamilarasan *et al*., 2016). These proteins were originally identified due to their ability to act as cofactors to stimulate cholera toxin ADP-ribosyltransferase activity (Kahn and Gilman, 1984). ARFS have been found in all studied eukaryotic organisms to date and are highly conserved at the amino acid level (Nie *et al*., 2003).

Six ARF isoforms have been identified in mammals; these isoforms are divided into three classes depending on their gene organisation and primary sequence (Nie *et al*., 2003, Chun

et al., 2008). The class I ARFs consist of ARFs that are localised mainly in the Golgi apparatus (Yorimitsu *et al*., 2014, Myers and Casanova, 2008). Although little is known about Class II ARFs, it was generally concluded that class I and class II ARFs are localised in the same area, Golgi apparatus (Hosoi *et al*., 2018). Live cell imaging techniques by Chun *et al.* (2008) identified that class I ARFs and class II ARFs also localised at the ER-Golgi intermediate compartment (ERGIC) (Chun *et al*., 2008). ARF6 is the only member of class III ARF; unlike class I and II ARFs, ARF6 does not localise at the Golgi complex but instead is found primarily in the endosomes and plasma membrane (Nie *et al*., 2003, Chun *et al*., 2008, Myers and Casanova, 2008). As small guanine nucleotide binding proteins, ARFs exist as either the active GTP bound form or as the inactive GDP bound form, depending on the type of g-phosphate nucleotide bound. Cycling between the active and inactive forms is regulated by ARF regulators (Figure 1.11) (Kötting and Gerwert, 2004, Scheffzek and Ahmadian, 2005).

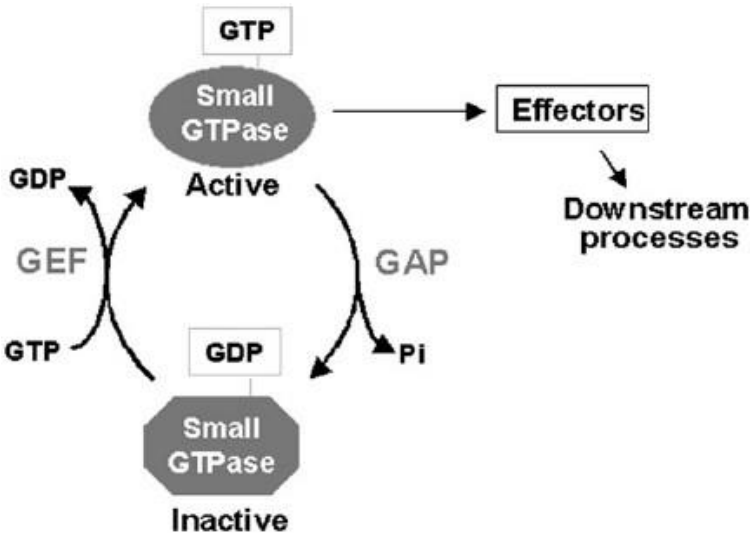

Figure 1.11. Activation and inactivation of ARFs. *ARFs are activated by guanine nucleotide exchange factors (GEFs) and GTPase activating proteins (GAPs) (Nielsen et al., 2008).*

1.2.1.2 ARF structure

Although ARFs are members of the Ras superfamily, structurally they are more similar to heterotrimeric G protein α subunits than they are to other Ras like proteins, with the same size of approximately 20 kDa (Muthamilarasan *et al*., 2016, Moss and Vaughan, 1995). ARFs are made up of five α-helices, six β-strands and five highly conserved polypeptide (G) loops (Figure 1.12). The functional activities of the small G-proteins occurs due to the G loops, making them an essential part of the ARFs (Serbzhinskiy *et al*., 2015, Paduch *et al*., 2001, Vetter and Wittinghofer, 2001). The nucleotide binding occurs due to the G1 loop (also referred to as the P loop) that is located between the β1 strand and the α2 helix (Serbzhinskiy *et al*., 2015, Paduch *et al*., 2001). The G2 loop that connects α1 helix and β2 strand contains a conserved threonine (Thr27) residue that is known to play a key role in Mg^{2+} ion binding. This region is more commonly referred to as the switch I region (Serbzhinskiy *et al*., 2015, Paduch *et al*., 2001, Amor *et al*., 2001).

In addition to the switch I region, ARFs also contain a switch II region that is made up of the G3 loop located at the N-terminus of the α2 helix; which provides residues for Mg^{2+} and γ-phosphate binding (Figure 1.12.B) (Paduch *et al*., 2001, Amor *et al*., 2001). The interaction of ARFs with guanine nucleotides occurs due to the G4 and G5 loops, each of the G loops share a particular role in order to bind effectively (Serbzhinskiy *et al*., 2015). The lysine and aspartate residues present in G4 loops interact with the nucleotides whilst the G5 loop has a partial responsibility for guanine base recognition (Serbzhinskiy *et al*., 2015).

The N-terminus of ARFs consists of an *N*-myristoylation site that is unique to this group of the small GTPase superfamily, followed by an amphipathic helix (Munro, 2005, Pasqualato *et al*., 2002, Peurois *et al*., 2019). The *N*-myristoylation allows ARF to bind to the membrane depending on the nucleotide conformation. Thus in the GDP bound form the ARF is water soluble and in the GTP bound form the ARF becomes lipid soluble and is able to be inserted into membranes (Anders and Jurgens, 2008, Muthamilarasan *et al*., 2016).

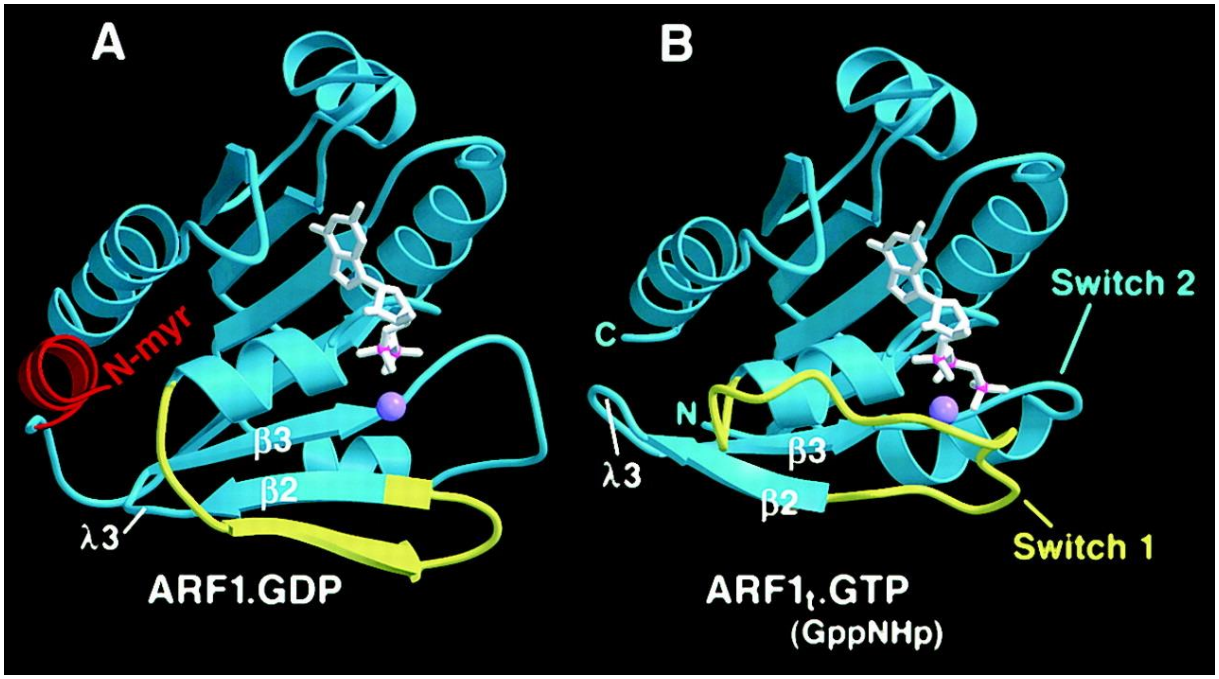

Figure 1.12. Crystal structure of ARF1. *Crystal structure shows 5 a-helices, 6 b-sheets and 5 loops. (A) shows ARF1 in GDP bound conformation whilst (B) shows ARF1 in GTP bound conformation (Mossessova et al., 2003).*

1.2.1.3 ARF-like proteins

The accidental discovery of an adjacent gene to *Brahma* gene in *Drosophila melanogaster* that encoded a protein related to mammalian ARFs led to the identification of ARF-like proteins (ARLs) (Munro, 2005, Tamkun *et al*., 1991). More than 20 ARLs have been identified in humans, leading to the conclusion that there are significantly more ARLs than ARFs in humans (Amor *et al*., 2001, Burd *et al*., 2004, Sharma *et al*., 2019). The contrast between sequence similarity and function of ARFs and ARLs helps to define the two groups of proteins (Amor *et al*., 2001), with ARLs sharing 40-60% of sequence homology with each other and the ARFs whilst lacking GTPase activity (Amor *et al*., 2001, Munro, 2005, Hanzal-Bayer *et al*., 2005). Structurally ARLs and ARFs are very similar, consisting of six β-strands and five α-helices (Burd *et al*., 2004); however x-ray crystallography of *S. cerevisiae* ARF2 and ARL1 by Amor

et al. (2001) revealed structural differences in the N terminus and its surrounding regions between the two proteins (Amor *et al*., 2001).

1.2.1.4 Switch regions

ARF consists of two highly conserved switch regions that are involved in the activation and inactivation of ARFs through binding to their respective regulators (Khan and Ménétrey, 2013). Binding of ARF regulators to the switch regions causes conformational changes to the switch regions. For examples the binding of guanine nucleotide exchange factors (GEFs) to the two switch regions contributes to structural changes in the ARF, this result in the inhibition of phosphate and metal ion binding (Vetter and Wittinghofer, 2001). Implication of the switch regions has also been demonstrated in several studies, the invariant glutamine found in the switch II region is shown to be involved in GTP hydrolysis; mutation of this glutamine to any other amino acids results in 50-fold reduction in GTP hydrolysis (Scheffzek and Ahmadian, 2005, Geyer and Wittinghofer, 1997, Gideon *et al*., 1992).

1.2.2 ARF functions

1.2.2.1 Class I and class II ARFs

Table 1.1 shows the localisation of different classes of ARFs in mammalian cell. The localisation of the ARFs may give an indication of their function within the cell. Of the three classes of ARFs, ARF1 and ARF6 have been most extensively characterised (Xie *et al*., 2016). Class I ARFs are implicated in a number of roles involving regulation of intracellular vesicular trafficking in the ER-Golgi and endosomal systems; this occurs at multiple stages of the secretory and lysosomal/vacuolar transport pathways (Xu and Scheres, 2005, Lee *et al*., 2002, Takeuchi *et al*., 2002). Through a series of *in vitro* ARF inhibition and assay studies conducted by Balch *et al.* in 1992 and Dascher and Balch in 1994, the significance of ARFs in vesicular trafficking between the endoplasmic reticulum and cis-Golgi was demonstrated (Balch *et al*.,

1992, Dascher and Balch, 1994). Class I ARFs are involved in the formation of transport vesicles as well as the selection of transmembrane protein cargo from donor compartments in mammalian cells (Xu and Scheres, 2005, Donaldson and Jackson, 2000). Although less is known about class II ARF function it has been speculated that like class I ARFs, the class II ARFs are involved primarily in regulating vesicular trafficking between the Golgi and ER (Hsu *et al*., 2015).

A number of studies have elucidated the functions of ARF1, a key member of class I ARFs, in eukaryotes. One of the functions of ARF1 is the recruitment of cytoplasmic coatomers to COPI-coated vesicles (Arakel and Schwappach, 2018). Vesicle coated proteins such as COPI and COPII are 'molecular machines' that enable vesicle formation and selection of proteins and lipid cargo to be packaged (Arakel and Schwappach, 2018). The coats of non-clathrin-coated (COPI-coated) vesicles contain the protein complex: coatomers, which are membrane bound transport vesicle coating protein complex, and ARFs. Presley *et al.* (2002) identified that activated ARF1 recruits coatomers to the membrane and the coatomers remain associated with the membranes even when ARF1 is disassociated (Figure 1.13) (Stamnes and Rothman, 1993, Presley *et al*., 2002). Within the Golgi stacks, these COPI-coated vesicles are involved in transport. In their study, Gu and Gruenberg (2000) showed that the endosomal pH is involved in the regulation of ARF1 binding to endosomal membranes, thus explaining the pH dependence of COPI binding to endosomes (Gu and Gruenberg, 2000).

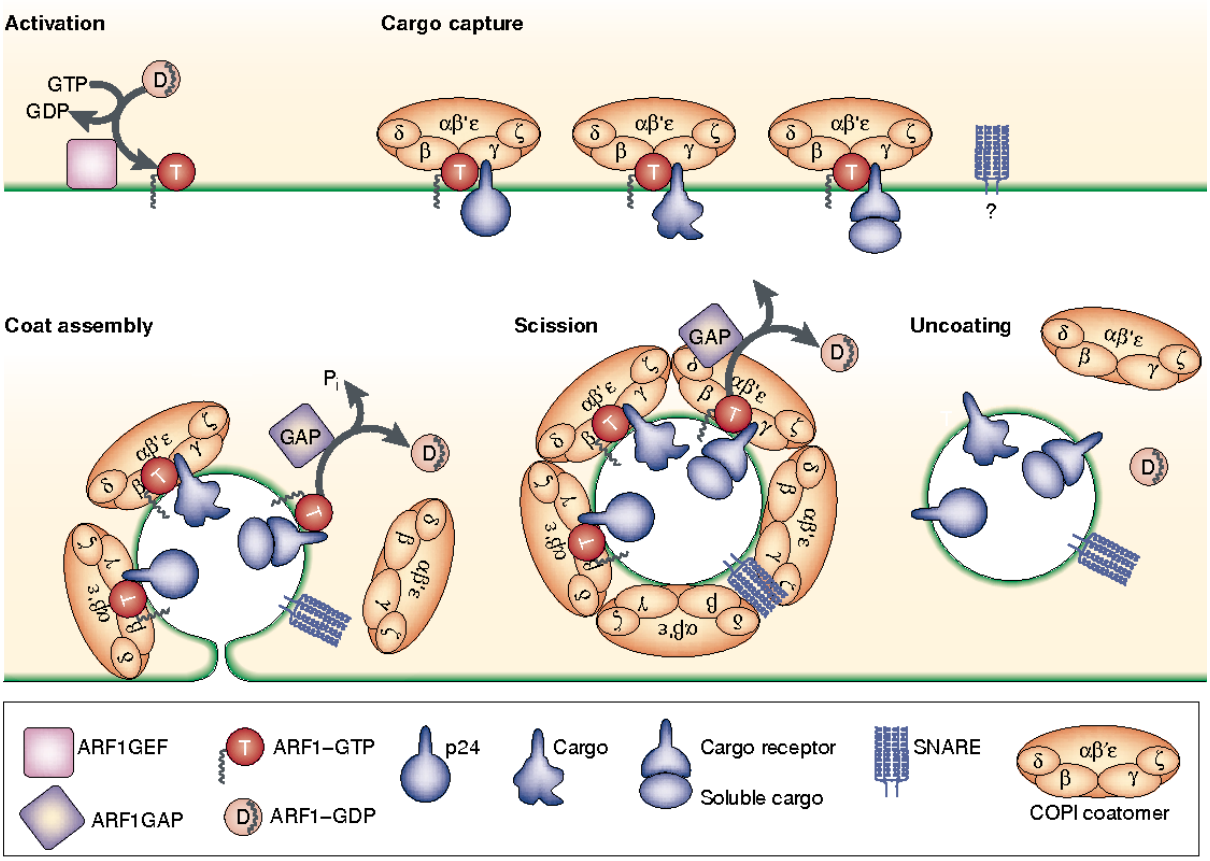

Figure 1.13. COPI coat assembly model. *The activation of ARF1 by ARF1GEF results in the recruitment of COPI coatomer by the activated ARF1. Vesicle buds once the formation of coat is complete. Hydrolysis of GTP bound ARF1 by ARF1GAP allows the ARF1 to dissociate from the complex. Adapted from (Kirchhausen, 2000).*

Class	Name	Localisation	Function	References
Class I	ARF1 ARF2 ARF3	Mainly in the Golgi apparatus and ERGIC	Intracellular vesicle trafficking in ER-Golgi and endosomal systems. Coatomer recruitment	Xu and Scheres (2005) Lee *et al*. (2002) Presley *et al*. (2002)
Class II	ARF4 ARF5	ERGIC and Golgi apparatus	Regulating vesicle trafficking between ER and Golgi	Hsu *et al*. (2015) Donaldson and Jackson (2000)
Class III	ARF6	Plasma membrane and endosome	Actin cytoskeleton remodelling. Regulating secretion. Plasma membrane protein and endosomal recycling. Cell polarity. Cell migration	Altschuler *et al.* (1999) Morgan *et al*. (2015) Zhang *et al*. (1999) Zhang *et al*. (1998)

Table 1.1. Localisation and function of class I, II and III ARFs.

1.2.2.2 Class III ARFs

ARF6 is found exclusively in the endosomal system and plasma membrane of mammalian cells (Table 1.1). The protein has been implicated in a number of diverse functional roles such as actin cytoskeletal remodelling, regulating secretion, plasma membrane protein and endosomal recycling, cell polarity and finally cell migration (Morgan *et al*., 2015, Hsu *et al*., 2015, Donaldson and Jackson, 2000). The implication of ARF6 in macrophage phagocytosis was highlighted by Zhang *et al.* in 1998. They identified that expression in macrophages of mutant ARF6s that were defective in GTP hydrolysis caused inhibition of phagocytosis of erythrocytes that are coated with IgG. Interestingly, in this study Zhang *et al.* demonstrated that ARF6 mutants that were defective in binding to GTP also contributed to inhibition of phagocytosis, suggesting that FcγR mediated phagocytosis in macrophages requires guanine nucleotide cycling by ARF6 (Donaldson and Jackson, 2000, Zhang *et al*., 1999, Zhang *et al*., 1998).

1.2.2.3 ARLs

The importance of ARL1 in regulating Golgi structure and function was highlighted in a study conducted by Lu *et al.* in 2001; overexpression of ARL1 mutant that is restricted to the GDP bound form resulted in the disassembly of the Golgi apparatus, whilst the overexpression of a mutant GTP-locked form of ARL1 caused the expansion of Golgi apparatus (Lu *et al*., 2001). ARL1 is also shown to be involved in various other cellular functions ranging from secretory trafficking, lipid droplet and salivary granule formation, and innate immunity and neuronal development (Yu and Lee, 2017).

ARL2 involvement in native tubulin folding by interacting with tubulin folding Cofactor D has been highlighted by Bhamidipati *et al.* (2000). The destruction of tubulin and microtubules by overexpressed Cofactor D is averted by the expression of GDP-bound ARL2, which causes the down-regulation of GTPase activating protein activity in Cofactor D (Pasqualato *et al*., 2002, Hanzal-Bayer *et al*., 2005, Bhamidipati *et al*., 2000). Sharer and Kahn (1999) identified

that ARL2 binds to a novel 19 kDa protein termed Binder of ARL Two (BART) (Sharer and Kahn, 1999). Both ARL2 and BART were later identified by Sharer *et al.* (2002) to be able to enter mitochondria, and together bind to adenine nucleotide transporter (Sharer *et al*., 2002).

The function of ARL4 that are localised in the nucleus may be implicated during development; Lin *et al.* (2000) identified that mouse ARL4 is developmentally regulated during mouse embryogenesis (Pasqualato *et al*., 2002, Lin *et al*., 2000).

Mutations in BBS3, the gene which encodes ARL6, has been implicated in Bardet-Biedl Syndrome (BBS), a heterogeneous human disorder characterised by the dysfunction of basal body and/or cilia (Wiens *et al*., 2010). The BBSome is an octameric complex of proteins of BBS, consisting of eight BBS proteins (Jin and Nachury, 2009, Jin *et al*., 2010, Kahn *et al*., 2005). *BBS3*, one of the genes that are implicated in BBSome complex has also been identified to encode ARL6. This ARL6/BBS3 is absent in plants and fungi but highly conserved in ciliated organisms, thus suggesting a potential role in cilium biogenesis (Jin and Nachury, 2009, Jin *et al*., 2010, Price *et al*., 2012). Jin *et al*. (2010) identified that GTP-bound ARL6 is involved in the recruitment of BBSome onto the membranes, forming an electron dense coat. This recruited BBSome coat complex is involved in sorting membrane proteins to cilia, thus it could be speculated that the absence of ARL6/BBS3 could result in inhibited BBSome recruitment to the membrane, therefore leading to cilium biogenesis inhibition (Jin *et al*., 2010). The sorting of membrane proteins into cilia occurs via intraflagellar transport (IFT). Recruitment of BBSome acts as an adapter for membrane proteins and uses IFT to cycle through cilia (Wingfield *et al*., 2018).

1.3 ARF regulators

1.3.1 Guanine nucleotide exchange factors

ARFs exist as either the active GTP bound form or the inactive GDP bound form (Serbzhinskiy *et al*., 2015, Kötting and Gerwert, 2004). The cycling between the active and inactive forms of ARFs is regulated by guanine nucleotide exchange factors (GEFs) and GTPase-activating proteins (GAPs) respectively (Jackson and Casanova, 2000). Under physiological conditions the exchange of GDP for GTP occurs very slowly (Jackson and Casanova, 2000); however the rate of GDP to GTP exchange is increased with the aid of GEFs, proteins that catalyse the dissociation of the GDP on ARFs, thus allowing GTP to associate with ARFs and become activated (Jackson and Casanova, 2000, Anders and Jurgens, 2008, Schmidt and Hall, 2002, Bhatt et al., 2016).

Since their first discovery in 1992, the importance of GEFs and their diversity has been demonstrated in a number of studies that have been reviewed by Jackson and Casanova (Jackson and Casanova, 2000). Although the GEFs identified to date are very divergent to each other at the amino acid level, they share a region that is more highly conserved. This 200 amino acid sequence is known as the Sec7 domain, due to a high degree of homology with the yeast Sec7p protein (Jackson and Casanova, 2000, Mansour et al., 1999). 14 human ARF GEFs were identified. These identified GEFs can be divided by their size and organisation into the low molecular weight and high molecular weight GEFs. The small molecular weight GEFs (<100 kDa) consist of CYTH, IQSEC and PSD subfamilies. These family of GEFs are the encoded by the pleckstrin-Sec7 domain genes (Mouratou *et al*., 2005, Sztul *et al*., 2019).

The high molecular weight GEFs (>100 kDa) consists of GBF1; a GEF that is closely related to the yeast Gea1 and Gea2 proteins, and the Brefeldin A (BFA) sensitive ARFGEF subfamilies. These GEFs are closely related to yeast Sec7 (Le *et al*., 2013, Sztul *et al*., 2019).

1.3.1.1 ARF GEF structure

Crystal structures of Cytohesin-1 and Cytohesis-2 helped determine the structure of GEFs. Both of these GEFs consist of an N terminal coiled-coil region, a C-terminal consisting of pleckstrin homology domain and a Sec7 domain (Mayer *et al*., 2001, Mossessova *et al*., 1998). The crystal structure Cytohesin-2 Sec7 region by Mossessova *et al.* (1998) at 2.2 Å resolutions identified the presence elongated 10 α-helices with a distinctive hydrophobic groove (Beraud-Dufour *et al*., 1998, Mossessova *et al*., 1998). To easier understand the structure of the Sec7 domain, each of the 10 α-helices is designated a letter (from A-J) (Beraud-Dufour *et al*., 1998). The distinct hydrophobic groove is made up of the hydrophobic residue present on F and G helices, making up the bottom of the groove. The two facing sides of the groove consist of the hydrophobic residue present on the H helix and the hydrophilic residue present on the F and G helices, forming a loop.

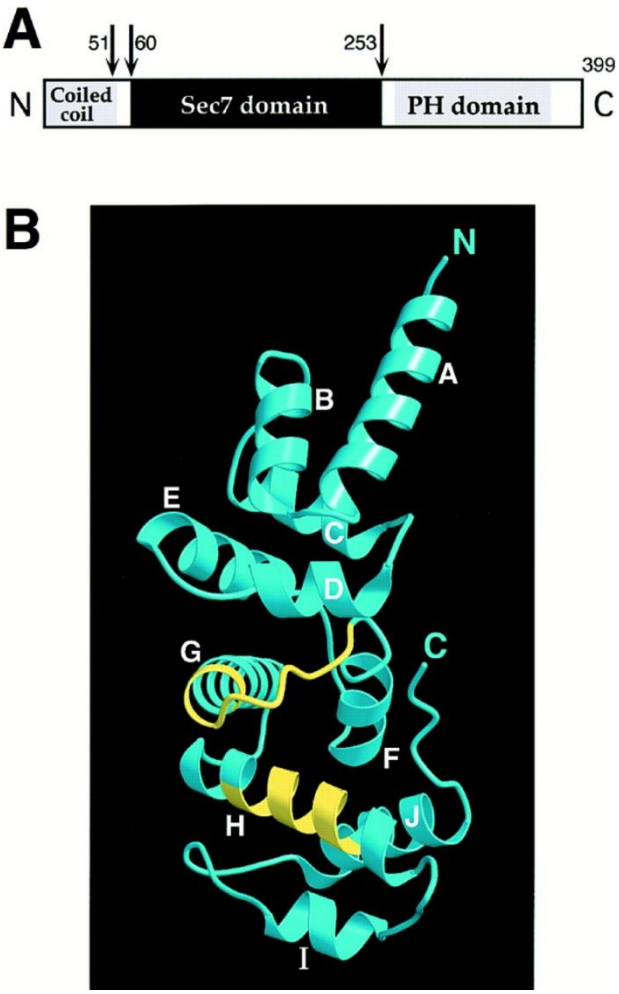

Figure 1.14. Structure of Cytohesin-2 Sec7 domain. *(A) Schematic diagram of domains that are present in human Cytohesin-2. (B) Ribbon representation of human Cytohesin-2 Sec7 domain. The seven α-helices from the N-terminus are right-handed superhelix (A-G) against three C-terminal α-helices. Areas in yellow represent the active site regions (Mossessova et al., 1998)*

The Sec7 domain grooves of the GEFs interact with the switch I and II regions present in ARFs. Béraud-Dufour *et al.* (1998) identified the presence of a glutamic finger (Glu156) in the hydrophilic F-G loop of the Cytohesin-2 Sec7; they proposed that the Glu156 carboxyl group may interact with Mg^{2+}(found in the switch regions), destabilising its co-ordinations with the β-phosphate of GDP and a strong steric and repulsive effect on the bound GDP, thus causing

the dissociation of GDP from ARF (Beraud-Dufour et al., 1998, Donaldson and Jackson, 2000, Jackson and Casanova, 2000, Goldberg, 1998). The F-G loop and the H helix are conserved in all members of the Sec7 family, suggesting that its mechanism of GDP dissociation may be similar in all GEFs. Through site directed mutagenesis studies, this region has been identified as the ARF interacting site has been demonstrated (Beraud-Dufour *et al*., 1998, Mossessova *et al*., 1998).

1.3.1.2 GEF interaction with ARFs

The activation of ARF1 by Sec7 through a positive feedback mechanism was demonstrated by Richardson *et al.* in 2012 (Richardson *et al*., 2012). Conformational changes in ARF is induced during the binding of GTP that are present in the cell, the conformational change of ARF was demonstrated by intrinsic fluorescent coincident changes (Kahn *et al*., 1991, Kahn and Gilman, 1986). This conformational change allows the *N*-myristoylated terminal of ARFs to be inserted into cellular membranes (Jackson and Casanova, 2000, Roth, 1999). Conformational changes also occur at the ARF switch regions, mediating the binding of GTP and GDP by tightly binding to γ-phosphate of GTP and weakly to GDP nucleotides (Pasqualato *et al*., 2001, Pasqualato *et al*., 2002).

1.3.1.3 ARF GEF and Brefeldin A

Brefeldin A (BFA) is a small hydrophobic lactone compound produced as a metabolite in toxic fungi. Addition of BFA to cells has dramatic effects on mammalian cells, causing rapid dissociation of protein from the Golgi complex as well as Golgi complex disassembly and redistribution of Golgi proteins to the endoplasmic reticulum, making it a potent secretion inhibitor (Myers and Casanova, 2008, Xu and Scheres, 2005, Ohashi *et al*., 2012). BFA selectively inhibits Golgi-associated ARF-GEF action in mammalian, plant and fungal cells, thereby inhibiting the activation of ARFs (Myers and Casanova, 2008, Yorimitsu *et al*., 2014,

Xu and Scheres, 2005, Ohashi *et al*., 2012). For instance the ARF1 function of COPI coat recruitment is inhibited when the ARF-GEF rate is inhibited by BFA (Xu and Scheres, 2005). BFA in particular targets the ARF-GDP-GEF intermediate, thus causing it to stabilise and in turn block the activation of the ARF cycle (Donaldson and Jackson, 2000). Mossessova *et al.* (2003) concluded from the crystal structure of GDP bound ARF1 with Sec7 and BFA complex that binding of BFA occurs at the protein-protein interface, inhibiting ARF1 conformational changes that are required for Sec7 domain to dislodge GDP molecule (Xu and Scheres, 2005, Peyroche *et al*., 1999, Mossessova *et al*., 2003). Although BFA inhibits ARF GEF function of large ARF GEFs, BFA has little effect on the small molecular weight GEFs (Donaldson and Jackson, 2000). An example of this is when the function of ARF6 in membrane association is not affected by addition of BFA. This is because the GEF that activates the function of ARF6 is PSD, a member of low molecular weight GEFs (Zhang *et al*., 1998). Similarly Cytohesin-2 is also not that sensitive to BFA, however it is interesting to note that the Sec7 domain of Cytohesin-2 is structurally similar to Gea2 (Chardin and McCormick, 1999, Goldberg, 1998).

1.3.2 GTPase activating proteins

The activated ARFs by GEFs are inactivated by GAPs, thus resulting in the cycling of ARFs within cells. Intrinsically the GTPase activity of ARFs are slow, however GAPs accelerate the GTPase activity; causing the hydrolysis of GTP to GDP and inorganic phosphate (Donaldson, 2000, Scheffzek *et al*., 1997, Scheffzek and Ahmadian, 2005). 26 GAPs have been identified in humans, these identified GAPs all have ARFGAP domain in common, which is roughly 130 amino acids in length. Besides this domain, the GAP family can be divided into 10 subgroups based on their domain structure and phylogenetic analysis. The 10 subgroups can be further classified into two groups depending on the position of the ARFGAP domains (Figure 1.15) (Campa and Randazzo, 2008, Kahn *et al*., 2008, Sztul *et al*., 2019).

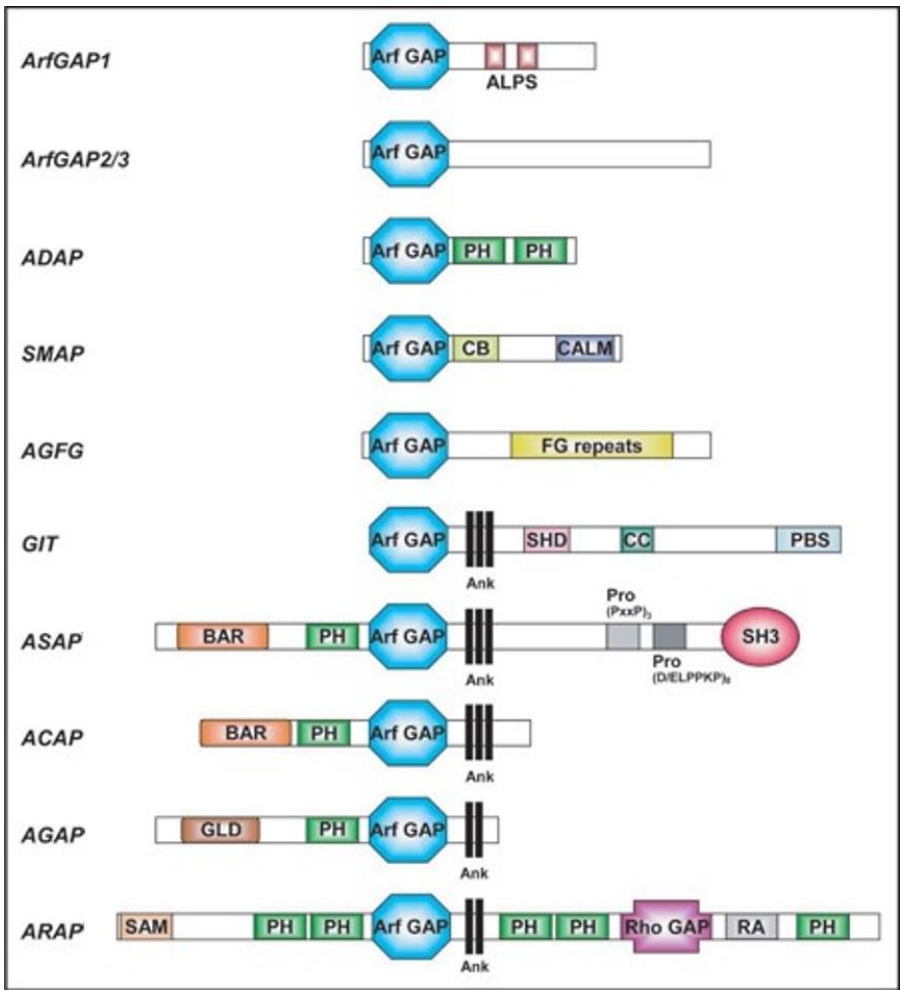

Figure 1.15. Domains present in ARF GAPs. *ARF GAPs can be divided into 10 subgroups based on their structure and domains; however all of the 10 subgroups have highly conserved ARF GAP domain. Adapted from (Campa and Randazzo, 2008).*

Through a series of *in vitro* analysis it was demonstrated that ARFGAP1, ASAP1 and ASAP2 interacted with ARF1 and ARF5 more effectively than ARF6 whilst GIT1 showed no preference within these three ARFs (Donaldson, 2000, Jackson and Casanova, 2000, Randazzo et al., 2000). Jackson *et al.* (2000) identified ACAP1 and ACAP2, two ARF6 GAPs. These two GAPs were found to be widely expressed in various cell lines and behaved in a similar manner to ASAP1, in the sense that overexpression lead to the inhibition of the formation of platelet-derived growth factor (PDGF)-induced dorsal membrane ruffles in NIH 3T3 fibroblasts. Just as how ARFGAP1, ASAP1 and ASAP2 had greater affinity for interacting with ARF1 and ARF5,

in vitro study has shown that ACAP1 and ACAP2 had greater affinity to ARF6 than with ARF1 or ARF5 (Jackson and Casanova, 2000).

1.3.2.1 ARF GAP structure

The crystal structure of human ARF1 and rat ARFGAP complex was determined at 1.95 Å by Goldberg (1999), from this crystal structure it was identified that the ARFGAP domain resembled a clenched fist; the "fingertips" consisting of β-strands whilst the "palm" consisting of α-helices, together these two regions forms a groove that serves as ARF1 binding site. The presence of Cys_4 zinc finger with a characteristic $CX_2CX_{16}CX_2C$ motif was also observed, this region is nestled in an array of α-helices and a β-sheet and form the "knuckle" region that faces away from the protein-protein interface (Goldberg, 1999). Goldberg observed that the ARFGAP molecule binds to and stabilises the switch II region as well as the α3 helix in order to direct the ARF1 residues for catalysis. ARFGAP does not provide a catalytic arginine finger or any other amino acid side chains to the GTPase active site for GTP hydrolysis (Scheffzek and Ahmadian, 2005, Goldberg, 1999); instead Goldberg noted that the addition of coatomer to the reaction in *in vitro* GTPase assays increased the hydrolysis of GTP by almost 1000-fold (Goldberg, 1999). ARFGAP1 binding to ARF1 does not involve the switch I region, instead the switch I regions appears to bind to coatomer (Scheffzek and Ahmadian, 2005). It can be concluded that binding of coatomer to switch I region provides a catalytic residue such as arginine finger that aids in the hydrolysis of GTP (Scheffzek and Ahmadian, 2005, Goldberg, 1999).

Although the structure of ARFGAP1 with ARF1-GDP complex and interaction determined by Goldberg (1999) is invaluable in order to understand more about ARF GAP interactions, it should be noted that ARFGAP1 lacks the Ankyrin repeats at the C terminal as well as several other domains such as PH domains and SH3 domains that are present in several other subgroups of ARF GAPs (Campa and Randazzo, 2008, Goldberg, 1999, Sztul *et al*., 2019).

The PH domains bind to phosphatidylinositol (4,5)-bisphosphate and/or phosphatidylinositol (3,4,5)-trisphosphate which causes the activation of the catalytic ARFGAP domain (Robinson and Kanamarlapudi, 2017, Kahn and Lambright, 2015). The SH3 domain is involved in the binding of focal adhesion tyrosine kinase (Randazzo *et al*., 2000). The Ankyrin repeats are involved in protein-protein interactions and cargo binding (Chan *et al*., 2017, Bai *et al*., 2012). The lack of additional domains means that ARFGAP1 utilises a different interaction mechanism to the other ARF GAP subfamilies.

To resolve this issue, Mandiyan *et al.* (1999) studied the crystal structure of PYK2-associated protein β (PAPβ) ARFGAP domain and the Ankyrin repeats at 2.1 Å resolutions. PAPβ (ASAP2) is one of the ARF GAPs that consists of the PH domain, Ankyrin repeats, SH3 domain and ARFGAP domain (Mandiyan *et al*., 1999, Sztul *et al*., 2019). Mandiyan *et al.* identified the presence of 3 β-sheets flanked by 5 α-helices, a Zn^{2+} ion coordinated by the $CX_2CX_{16-17}CX_2C$ sequence motifs and four Ankyrin repeats; it should be noticed that the structure of the ARFGAP domain is similar to that described by Goldberg (1999) (Goldberg, 1999, Mandiyan *et al*., 1999).

Taking this into consideration, it can be assumed that all of the ARFGAP domains of the identified GAPs consists of zinc finger motif with the specific spacing of four Cysteines motifs (East and Kahn, 2011, Cukierman *et al*., 1995, Huber *et al*., 2002). In their study, Mandiyan *et al.* found that there is an overlap between the ARF1 and the third and fourth Ankyrin repeats. They concluded that either these Ankyrin repeats are dislodged or PAPβ undergoes extensive rearrangements before binding (Scheffzek and Ahmadian, 2005, Mandiyan *et al*., 1999). As opposed to the conclusions by Goldberg (1999), mutation studies on PAPβ revealed that mutation of Arg292 to lysine resulted in 10,000 fold decrease in GTP hydrolysis, suggesting that the invariant arginine maybe required for GTP hydrolysis by ARF GAPs in the other subfamilies (Scheffzek and Ahmadian, 2005, Goldberg, 1999, Mandiyan *et al*., 1999).

1.3.2.2 ARF GAP functions

The cycling of GEFs and GAPs are important in regulating the function of ARF/ARLs. Previous studies had highlighted the functions of ARF GAPs and their importance for cellular functions. For example, Randazzo *et al.* (2000) demonstrated that the overexpression of ASAP1 caused focal adhesion morphology alteration and inhibited cell spreading of NIH 3T3 fibroblasts *in vitro* (Randazzo *et al*., 2000). The hydrolysis of ARF1-GTP by GAP causes the uncoating of coated vesicles; this is an important step before the vesicles fuse with the acceptor compartment (Mandiyan *et al*., 1999, Antonny *et al*., 1997). However, overexpression of ARFGAP1 causes redistribution of the entire Golgi complex to the endoplasmic reticulum and the release of COPI from Golgi membranes to cytosol (Mandiyan *et al*., 1999). The activity of GAPs have been demonstrated to be affected by several molecules within the cell, for example ARF GAP is highly dependent on Phosphatidylinositol 4,5-bisphosphate (PIP_2) and are sensitive to phosphatidic acid (PA) and phosphatidylcholine (PC), stimulating and inhibiting ARF GAP activity respectively (East and Kahn, 2011, Randazzo and Kahn, 1994). The dependence of ARF GAP to PIP_2 was further identified by Kam *et al.* (2000), they identified that activation of ASAP1 required PIP_2 binding to the PH domain (Kam *et al*., 2000); minimum GAP activity can be observed in the presence of GAP mutants that lacked PH domain (Mandiyan *et al*., 1999).

1.4 ARF regulating proteins as potential drug targets

ARFs and their regulators have been the targets of interest for several diseases, most notably as a potential target for cancer (Ohashi *et al*., 2012). Ohashi *et al* (2012) identified BFA like inhibitor of ARF1-ARFGEF termed AMF-26. AMF-26 inhibited ARF1 activation and oral administration of AMF-26 saw complete regression of human breast cancer BSY-1 xenografts *in vivo* (Ohashi *et al*., 2012). ARFs and their regulators have also been connected to several genetic diseases. Mutations of IQSEC2 has been shown to cause nonsyndromic X-linked intellectual disability (Shoubridge *et al*., 2010). Similarly mutation of ARFGEF2 has been linked

to autosomal recessive periventricular heterotopia, a disorder that leads to severe malformation of the cerebral cortex (Jackson and Bouvet, 2014).

There may be potential to target ARFs or their regulators in order to develop new therapeutics for African trypanosomiasis.

1.4.1 RNA interference of T. brucei ARF/ARLs

Several studies have been carried out on RNA interference (RNAi) of *T. brucei* ARFs and ARLs which have demonstrated the functions of ARFs and ARLs in bloodstream form *T. brucei*. Nine ARF/ARLs have previously been identified in *T. brucei* (Price *et al*., 2005b, Price *et al*., 2005a). Several tetracycline-inducible RNAi studies of the identified ARF/ARLs were carried out on bloodstream form *T. brucei*. The importance of ARL6 has been discussed in section 1.2.2.3. Mutation of BBS3/ARL6 is characterised by the dysfunction of basal body and/or cilia (Wiens *et al*., 2010). The flagellum in *T. brucei* is important for cell division, survival within the tsetse fly and immune evasion. However Price *et al.* (2012) demonstrated through RNAi of ARL6 that although RNAi of ARL6 leads to significant shortening of flagellum, the RNAi did not affect the viability of the bloodstream form *T. brucei* (Hemsworth *et al*., 2013, Price *et al*., 2012).

In contrast to this however, RNAi of ARL1 and ARF1 lead to significant levels of *T. brucei* cell death. ARL1 in *T. brucei* is only expressed during the mammalian bloodstream form stage, where it localises to the Golgi apparatus of the parasite; RNAi of ARL1 in this stage of *T. brucei* life cycle resulted in parasite cell death between 24 and 48 hours post RNAi. Prior to cell death, the depletion of ARL1 caused Golgi structure disintegration and delay in exocytosis of GPI anchored VSGs, presence of multiple flagella, nuclei and vesicles; this demonstrated the importance of ARL1 in *T. brucei* viability (Price *et al*., 2005b, Price *et al*., 2005a).

ARF1 in *T. brucei* is localised to the Golgi apparatus, inhibition of the ARF by RNAi has demonstrated increased cell death in *T. brucei*. RNAi of ARF1 in bloodstream form *T. brucei* resulted in lethal phenotypes and cell division decreasing by 24 hours post induction, the

phenotypes included development of cells with multiple nuclei and abnormal morphology such as the “BigEye” large vacuole morphology. Although the morphology of the parasite was affected, electron microscopy and immunofluorescence assay of the Golgi matrix marker showed that the Golgi was intact (Price *et al*., 2007b). Interestingly overexpression of ARF1 in bloodstream form *T. brucei* proved to be lethal to the parasite, contributing to Golgi to lysosome transport defect (Price *et al*., 2007b). In contrast to what was observed in the knockdown of ARF1 in bloodstream form *T. brucei*; knockdown of ARF1 in the procyclic form *T. brucei* does not affect endocytosis, particularly the fluid phase endocytosis of dextran. However RNAi of ARF1 in procyclic form *T. brucei* did affect the lysosome, resulting in an enlarged lysosome without any significant impairment in protein degradation (Price *et al*., 2007a).

The involvement of ARL2 in *T. brucei* cytokinesis function was demonstrated by RNAi and overexpression study in bloodstream form *T. brucei*. RNAi of ARL2 in *T. brucei* resulted in a severe cytokinesis defect due to the inhibition of formation and ingression of cleavage furrows, the overexpression of C-terminally myc-tagged ARL2 also showed the same results as the RNAi but overexpression of untagged ARL2 did not affect the parasite. Although inhibited cell division was observed by 24 hours post induction; the parasites themselves were still viable, demonstrating a cytostatic effect rather than a cytotoxic effect (Price *et al*., 2010b).

These studies have demonstrated that ARFs and ARLs found in *T. brucei* are important in essential cellular functions and targeting these proteins as a novel therapeutic target could lead to parasite death. However a major problem with targeting ARF/ARLs is the fact that they share a high level of protein sequence identity with ARF/ARL sequences from other species, particularly humans (Table 1.2). Multiple sequence alignment showed that identified *T. brucei* ARF/ARLs and human ARF/ARLs have high level of sequence identity at the GDP/GTP α- and β- phosphate binding site, which is also essential for GEF binding. Other sites that had high level of sequence identity include the switch II region that interacts with GTP, and the NKXD region where GTP magnesium and β- phosphate binding occurs (Price *et al*., 2007b, Price *et al*., 2005b).

Inhibiting the function of ARF/ARLs would likely require inhibitors to bind to one of these highly conserved site. However this may lead to complications since drugs inhibiting *T. brucei* ARF/ARLs functions by binding to the highly conserved regions could also potentially target human ARF/ARLs as well. Alternative potential therapeutic targets that could be exploited are the ARF regulators. Considering the overall sequence divergence of both GEFs and GAPs and the complications of overexpression or mutation of these regulators (Xu and Scheres, 2005, Mandiyan *et al*., 1999, Antonny *et al*., 1997), targeting ARF regulating proteins as novel drug targets against *T. brucei* and potentially other kinetoplastids could prove to be effective.

Gene	Human homologue	Similarity (%)	Size (kDa)
TbARL1	ARL1	53%	20.7
TbARL2	ARL2	63%	20.7
TbARL3A	ARL3	48%	19.9
TbARL3B	ARL3	59%	21.9
TbARL3C	ARL3	42%	20.0
TbARL6	ARL6	43%	20.0
TbARLX	ARL1	45%	21.0
TbARF1	ARF1	75%	20.6
TbARF2	ARF4	57%	21.2

Table 1.2. ARF/ARLs in* T. brucei *and their homologue to human ARF/ARLs. *The high percentage of similarity between* T. brucei *ARF/ARLs and human ARF/ARLs makes finding a suitable drug target complicated. Adapted from: (Price et al., 2005b).*

1.5 Aims

The overall aim of this study is to determine whether regulating proteins of ARFs are suitable as drug targets against *T. brucei*. To achieve this aim, the following objectives will be addressed:

1. Identify ARF regulator protein orthologues in *T. brucei*

Bioinformatics will be used to identify the orthologues of ARF GEFs and GAPs in the *T. brucei* genome.

2. Generate RNAi expressing cell lines

Tetracycline inducible RNAi constructs will be generated and transfected into bloodstream form *T. brucei* to generate stable cell lines.

3. Determine whether regulating proteins are essential

The effect of knockdown of specific ARF regulators on cell growth will be determined by counting the number of cells at a range of time points. Changes in morphology will be assessed using immunofluorescent and electron microscopy. Extraction of RNA at different time points post-induction of RNAi will be carried out and the change in gene expression will be determined using real-time PCR.

4. In addition to studying ARF regulators as drug targets, transgenic cell lines exhibiting endocytosis defect will be evaluated as research tools to investigate drug uptake

Transgenic cell lines that can be induced to express endocytosis defect will be used to identify if compounds from open-access libraries that are effective against *T. brucei* are taken up via endocytosis.

Chapter 2 – Materials and Methods

2.1 Materials

Unless specified, all plasticware and glassware were purchased from the following companies: Greiner Bio-One (Solingen, Germany), Star Lab (Milton Keynes, UK), Eppendorf (Cambridge, UK) and VWR International (Lutterworth, UK). Pathogen Box compound library was provided by Medicines for Malaria Ventures (MMV) (https://www.mmv.org/mmv-open/pathogen-box - accessed: Feb 2020). Parasite culture was carried out in a Health and Safety Executive approved Category III cell culture facility under a Specified Animal Pathogens Order (SAPO) licence.

2.1.1 Laboratory equipment

The following list of equipment were used during experimental work described in this thesis:

3520 Advance bench pH meter	Jenway (Cole-Palmer) (Stone, UK)
AMAXA® Nucleofector®	Lonza (Basel, Switzerland)
Discovery Comfort Pipettes	HTL Lab Solutions (Warszawa, Poland)
EVOS FL Cell Imaging System	Thermo Fisher Scientific (Loughborough, UK)
G:BOX F3	Syngene (Cambridge, UK)
GloMax® Multi Detection System	Promega Corporation (Southampton, UK)
Guava EasyCyte 6-2L flow cytometer	Merck Millipore (Watford, UK)
Magnetic Stirrers	VWR International (Lutterworth, UK)
NanoDrop™ 1000 Spectrophotometer	Thermo Fisher Scientific (Loughborough, UK)
PowerPac™ Basic Power Supply	Bio-Rad Laboratories (Watford, UK)
PTC-2000 Gradient Thermal Cycler	Bio-Rad Laboratories (Watford, UK)
StepOne Plus Real-Time System	Thermo Fisher Scientific (Loughborough, UK)

2.1.2 Chemicals and reagents

Chemicals and reagents were sourced as follows:

Thermo Fisher Scientific (Gibco®) (Loughborough, UK)	Heat inactivated Foetal Bovine Serum; HMI-9 powder; L-glutamine (4 mM); PrestoBlue®; Concanavalin A; dNTPs; KOD Hot Start DNA polymerase; $MgSO_4$; PowerUp™ SYBR® Green; RNAseOUT Recombinant Ribonuclease inhibitor; Image-iT™ FX Signal enhancer; 1X PBS; Loading buffer (X5); ProLong™ Diamond Antifade Mountant; SOC medium; Voorheis' modified PBS (vPBS) – PBS supplemented with 10 mM glucose and 46mM sucrose
Sigma-Aldrich (Merck) (Watford, UK)	2-mercaptoethanol; Ethidium bromide; LB Broth (Miller); LB Broth with Agar (Lennox); Sodium bicarbonate; Tris-Acetate-EDTA; Methylene blue (0.01% in 1X TAE); Paraformaldehyde; Propidium Iodide
VWR International (Lutterworth, UK)	Chloroform; Methanol; Triton™ X-100; Ethanol
Lonza (Basel, Switzerland)	SeaKem® Agarose; Sodium acetate (3M)
Bioline (London, UK)	TRIsure™; 1kb+ Hyperladder
New England BioLabs (Hitchin, UK)	Taq Polymerase; Quick-Load® 2-Log DNA Ladder;

2.1.3 Kits

Ambion™ DNAse Kit	Thermo Fisher Scientific (Invitrogen™) (Loughborough, UK)
Omniscript® RT kit	Qiagen (Hilden, Germany)
QIAprep® Spin Miniprep kit	Qiagen (Hilden, Germany)
QIAquick® Gel Extraction kit	Qiagen (Hilden, Germany)
T4 DNA ligase kit	New England BioLabs (Hitchin, UK)
TOPO® TA Cloning® kit	Thermo Fisher Scientific (Invitrogen™) (Loughborough, UK)

2.1.4 Media

HMI-9 medium	1.8 g/L HMI-9 powder, 0.036 M $NaHCO_3$, 10% heat inactivated tetracycline free Foetal Bovine Serum, 100 U/mL Penicillin & 100 μg/mL Streptomycin, 4 mM L-glutamine, 5.72 mM 2-Mercaptoethanol,
LB medium	25 g/L LB Broth (Miller), 1 L dH_2O, autoclaved for sterilisation and antibiotics added once LB medium has cooled down to 50°C
LB-Agar with ampicillin medium	35 g/L LB Broth (Lennox), 1 L dH_2O Autoclaved for sterilisation, 100 μg/mL ampicillin added once LB-Agar has cooled down to 50°C
Cryo medium for *T. brucei*	20% glycerol in HMI-9 medium

2.1.5 Oligonucleotides

Name	Sequence
TbGAP1 (For)	5’-CCGCCGATCTAGACGCGTGGAAGC-3’
TbGAP1 (Rev)	5’-CCGAACCCCTTTTTCTCTAGACCACCACC-3’
TbGAP2 (For)	5’-CCGGTCTAGATCGGTCAGCAGGTA-3’
TbGAP2 (Rev)	5’-GCATTGGGTGTCTAGAAGAGATCATCTATG-3’
TbGAP3 (For)	5’-GGATGCCCGTCTAGACCGTG-3’
TbGAP3 (Rev)	5’-CGTACCACTCTAGAGGTGTCCAC-3’
TbGAP4 (For)	5’-GGAACTTCTAGACAATCAACGGGC-3’
TbGAP4 (Rev)	5’-CTGCTCTAGAAGTGTCTTGCGCC-3’
TbGEF1 (For)	5’-GGTCCGAGAGACCTTCTAGAGGTGATGAAG-3’
TbGEF1 (Rev)	5’-CAACTACGCACATGTTGTTGCTCTAGAGGG-3’
TbGEF2 (For)	5’-TGAGAGCAGTAGCCGTCTAGATGCCCC-3’
TbGEF2 (Rev)	5’-CCTGCATCCTGGACGACTCTAGAGCAC-3’
TbGEF3 (For)	5’-GCAGGGAGTCTAGAGACGCTGG-3’
TbGEF3 (Rev)	5’-CCAGCTCTAGAGTTAGCATCATCAGG-3’
TbGEF3 ORF (For)	5’-ATGGAGGCTCTCCTGCGGTC-3’
TbGEF3 ORF (Rev)	5’-CTACAGCCACATGCATTCCGGTG-3’
TbGEF3 qPCR (For)	5’-ATGTGTCGCAGTACCGTTTC-3’
TbGEF3 qPCR (Rev)	5’-AACTCCATTTCAGCCTGTCG-3’
TbGAP1 sequencing	5’-GTCAAAACGGCTCCACTGG-3’
TbGAP4 sequencing	5’-TACGAGGCGCATCTTCCTAA-3’
TbGEF1 sequencing	5’-CCAAAGGTCGTGAAGCAACA-3’
TbGEF2 sequencing	5’-CTCCCGCGAGTTTTGACTTC-3’
TbGEF3 sequencing	5’-GGAGTGTTGGTTACCACTGGA-3’

2.2 Methods

2.2.1 Bioinformatics

2.2.1.1 Identification of T. brucei regulator genes

Literature and NCBI database searches (http://www.ncbi.nlm.nih.gov/ - accessed: Oct 2015) were used to identify ARF GEFs and GAPs that are present in humans. Known names and accession numbers as well as the presence of the Sec7 and ARFGAP domains were used to identify human ARF GEFs and GAPs. Protein sequences for the identified GEFs and GAPs were acquired from NCBI database. BLAST search using the human GEFs and GAPs protein sequences were carried out on TriTrypDB website (Aslett *et al*., 2010) to identify possible orthologues in *T. brucei* Lister 427 strain. Possible orthologues in *T. brucei* genome with the lowest e-values were selected. Catalytic domain search on TriTrypDB was then carried out on the selected *T. brucei* orthologues to support the possibility that the selected genes were those of the ARF regulators. The presence of Sec7 domain and ARFGAP domain in the identified *T. brucei* orthologues confirmed the validity of the genes. Reverse BLAST search on the identified *T. brucei* orthologues was carried out on the NCBI database to further ensure the identified orthologues were ARF regulators.

2.2.1.2 Sequence alignment

Identified human and *T. brucei* ARF GEF and GAP amino acid sequences were aligned using Uniprot Align software tool (http://www.uniprot.org/align/ - accessed: Oct 2015). The percentage identity between pairs of human and *T. brucei* ARF regulators was also determined using this software tool. Sequence alignments on the *T. brucei* GEFs and GAPs was carried out against each subfamily of their respective human ARF regulators and the average percentage identity for each subfamily was obtained.

2.2.1.3 Domain and Structural analysis

Domains present in each of the identified human and *T. brucei* ARF GEF and GAP amino acid sequences were determined using the online software SMART: sequence analysis (Schultz *et al*., 1998, Letunic *et al*., 2015). Schematic representation of the domains were obtained for each of the human ARF regulator subfamilies and for each of the *T. brucei* GEFs and GAPs. In order to carry out structural analysis the *T. brucei* GEFs and GAPs were analysed on Phyre2 (http://www.sbg.bio.ic.ac.uk/~phyre2/html/page.cgi?id=index – accessed: May 2018) (Kelley *et al*., 2015) software to generate PDB files on predicted structures. The generated PDB files were opened on PyMOL Molecular Graphics System, Version 2.0 supplied by Schrödinger, LLC and the predicted structures for each of the *T. brucei* GEFs and GAPs were analysed. Structural similarities were also determined on PyMOL.

2.2.1.4 Prediction of protein localisation

Localisation of the identified *T. brucei* GEFs and GAPs were predicted using TrypTag resource (http://tryptag.org/ - accessed: March 2018) (Dean *et al*., 2017). BLASTP of the identified *T. brucei* GEFs and GAPs protein sequence on TriTrypDB identified closest homologues in TREU927 cell lines. Accession numbers obtained from the TREU927 cell lines were used to identify localisation of *T. brucei* GEFs and GAPs in *T. brucei*.

2.2.1.5 Identification of putative orthologues in other kinetoplastids

Presence of identified *T. brucei* GEF and GAP orthologues in other kinetoplastids was determined for each *T. brucei* GEFs and GAPs. Accession number search for each *T. brucei* GEFs and GAPs on TriTrypDB identified orthologue group number for each gene. The identified orthologue group numbers were searched on OrthoMCL to identified parasites with the same orthologue groups. Kinetoplastid group was selected as a search criteria and respective orthologues of *T. brucei* GEFs and GAPs were identified in other kinetoplastids.

2.2.2 General Methods

2.2.2.1 Gel electrophoresis

2.2.2.1.1 Ethidium bromide gel

Separation of DNA based on their size was carried out using 1.5% (w/v) Agarose gel, unless otherwise stated. Powdered SeaKem® LE Agarose (Lonza) was dissolved in Tris-Acetate-EDTA running buffer (40 mM Tris-Acetate, 1 mM EDTA, pH 8.0) containing 12.5 pg/mL ethidium bromide, and allowed to set at room temperature. The gel was transferred to electrophoresis tank containing Tris-Acetate-EDTA buffer and DNA samples mixed with loading dye were loaded onto the gel. 2 log ladder (New England BioLabs) was also loaded onto the gel as markers. The loaded gel was run for 60 minutes at 90V on (PowerPac™ Basic Power Supply, Bio-Rad Laboratory). The finished gel was viewed under ultra violet (UV) light on G:BOX F3 (Syngene) using the GENEsys (v1.2.8.0) software and images were captured.

2.2.2.1.2 Methylene blue gel

A 1.5% (w/v) Agarose gel was prepared for gel extraction of DNA. Powdered SeaKem® LE Agarose (Lonza) was dissolved in Tris-Acetate-EDTA running buffer (40 mM Tris-Acetate, 1 mM EDTA, pH 8.0) without ethidium bromide, and allowed to set at room temperature. The gel was transferred to an electrophoresis tank containing Tris-Acetate-EDTA buffer and DNA samples mixed with loading dye were loaded onto the gel. Quick-Load® Purple 2-log ladder (New England Biolabs) was also loaded onto the gel as markers. The loaded gel was run for 60 minutes at 90V on (PowerPac™ Basic Power Supply, Bio-Rad Laboratories). The finished gel was incubated overnight at 4°C in 0.01% methylene blue/1X TAE as described previously (Soto and Draper, 2012).

2.2.2.2 Gel extraction and DNA purification

Gel extraction was carried out using the QIAquick® Gel Extraction kit (Qiagen) on methylene blue stained Agarose gel. All extraction steps were performed as stated in the manufacturer's handbook (QIAquick® Spin handbook). DNA enzymatic purification was carried out following the same kit and handbook as the gel extraction. All steps for the enzymatic purification were followed as stated in the handbook.

2.2.2.3 NanoDrop™ Spectrophotometry

DNA concentration was determined using NanoDrop™ 1000 Spectrophotometer (Thermo Scientific). Loading of the samples and concentration measurement was carried out as stated in the user's manual and all results were analysed using the NanoDrop™ 1000 (v3.7) software.

2.2.3 Molecular cloning

2.2.3.1 Generation of RNAi constructs

2.2.3.1.1 Amplification of GEFs and GAPs for RNAi cloning

A suitable RNAi region from nucleic acid sequences for each of the *T. brucei* GEFs and GAPs were selected using the software RNAit – RNAi target selection for Trypanosome genomes (https://dag.compbio.dundee.ac.uk/RNAit/ - accessed: Nov 2018). Primers were designed for *TbGAP1*, *TbGAP2*, *TbGAP3*, *TbGAP4*, *TbGEF1*, *TbGEF2* and *TbGEF3* (see section 2.1.5) with *Xba*I restriction site on the 5' and 3' ends of the RNAi region to enable cloning into P2T7^{Ti} RNAi vector. The designed primers were generated by Eurofins MWG Operon (Ebersberg, Germany). Gradient PCR was used to amplify the RNAi region of *T. brucei* GEFs and GAPs from *T. brucei* genomic DNA. 20 μL reaction consisting of 1X KOD Hot Start DNA polymerase buffer (Novagen), 0.04 units KOD Hot Start DNA polymerase (Novagen), 0.4 mM dNTPs, 3 mM $MgSO_4$, 0.6 μM forward and reverse primers, and water was prepared for each of the genes. The PCR cycle was initiated on a Peltier Thermal Cycler PTC-200 (Bio-Rad

Laboratories) for 35 cycles (Table 2.1). A restriction digest was carried out with *Xba*I enzyme (Thermo Fisher Scientific FastDigest) on the P2T7TbARL6 vector (Price *et al*., 2012) and purified amplified PCR products. The digested plasmid vectors were treated with Alkaline Phosphatase (Thermo Scientific FastAP). The reaction was set up as stated in the manufacturer's handbook and 1 μg vector DNA was used per reaction (Thermosensitive Alkaline Phosphatase). The reagents were incubated at 37°C for 10 minutes followed by termination of the reaction at 75°C for 5 minutes. Alkaline Phosphatase treated vector and *Xba*I digested inserts were ligated using T4 DNA ligase kit (New England Biolabs). The protocol for ligation was adapted from the manufacturer's handbook (NEB Ligation Protocol with T4 DNA Ligase). Approximately 97.85 ng vector and 73.5 ng insert was added to 1.5 μL 10X T4 DNA ligase buffer with 10 mM ATP and 1 μL T4 DNA ligase enzyme, water was added to make a final volume of 15 μL. The reaction was left at room temperature for 10 minutes.

Gradient PCR cycle			
Step	**Temperature**	**Time**	**Repeats**
Initialisation	95°C	2 minutes	34
Denaturation	95°C	20 seconds	
Annealing	55-65°C	20 seconds	
Elongation	70°C	1 minute	
Final elongation	70°C	10 minutes	N/A
Cycle end	4°C	∞	N/A

Table 2.1. Gradient PCR cycle. *Table detailing the steps and number of cycles used for gradient PCR*

2.2.3.1.2 Transformation

Ligated products were transformed into One Shot® TOP10 Chemically Competent *E. coli* (Invitrogen). 3 μL of ligated product was added to the competent cells and kept in ice for 30 minutes. This was then heat shocked at 42°C for 45 seconds and then placed in ice immediately for 2 to 3 minutes. 200 μL of SOC medium was added to the cells and incubated at 37°C for 1 hour. 150 μL of SOC-competent cells were plated onto LB-ampicillin (ampicillin concentration of 100 μg/mL) agar plates and incubated at 37°C overnight. 6 colonies were transferred into 5ml LB-ampicillin liquid medium and incubated at 37°C overnight with shaking.

2.2.3.1.3 Plasmid miniprep preparation

Plasmid DNA was isolated and purified from selected colonies grown overnight in LB-ampicillin liquid medium using QIAprep® Spin Miniprep kit (Qiagen). All miniprep steps were carried out as recommended by the manufacturer. The purified plasmid DNAs were subjected to restriction digest using *Xba*I and the products were then separated on a gel electrophoresis in order to validate the presence of inserts. Successfully ligated and transformed plasmid DNAs were selected and sent for sequencing by Eurofins MWG Operon (Ebersberg, Germany). List of primers used for sequencing are provided in section 2.1.5.

2.2.3.2 TOPO® cloning

2.2.3.2.1 Design of Oligonucleotides for TOPO® cloning

The open reading frame (ORF) for *T. brucei* GEF3 was amplified from *T. brucei* genomic DNA using KOD DNA polymerase (Novagen). Specific primers were designed for *TbGEF3* (section 2.1.5) and gradient PCR was used to amplify the ORF following the same procedure as described in section 2.2.3.1.1.

2.2.3.2.2 3’ A-overhangs addition

Addition of 3’ A-overhangs reaction was conducted as follows: 100 ng/μL PCR products, 5 μL Taq Polymerase buffer (New England BioLabs), 1 μL 10 mM dNTPs, 0.5 U/μL Taq Polymerase (New England BioLabs) and 3 μL water was added together and incubated at 72°C for 10 minutes.

2.2.3.2.3 TOPO® TA® Cloning®

TOPO® cloning reaction was set up using the TOPO® TA® Cloning® kit (Invitrogen). All steps were carried out as stated by the manufacturer (Invitrogen) and 0.5 μg PCR products were used for this reaction. The products of the TOPO cloning reaction was transformed into One Shot® TOP10 Chemically Competent *E. coli*. (Invitrogen) as stated above and grown in LB-ampicillin (100 μg/mL) overnight. A restriction digest was carried out with *Eco*RI enzyme (Thermo Scientific FastDigest) on 1 μg purified plasmid DNA samples extracted from individual clones. Reaction mixes were incubated for 10 minutes at 37°C and then viewed by gel electrophoresis.

2.2.4 Transfection of T. brucei

2.2.4.1 Parasite culture

T. brucei bloodstream form (BSF) strain Lister 427 (Single Marker) was maintained as described (Wirtz *et al*., 1999) in HMI-9 media with 2 μg/mL Geneticin™ (Gibco, Thermo Fisher Scientific) and incubated at 37°C with 5% CO_2. This strain stably expresses a phage derived T7 RNA polymerase and tetracycline repressor. HMI-9 media consisted of 1.8 g/L HMI-9 powder (custom made by Gibco, Thermo Fisher Scientific), 0.036 M $NaHCO_3$ (Sigma-Aldrich), 10% heat inactivated tetracycline free Foetal Bovine Serum (Gibco, Thermo Fisher Scientific), 100 U/mL Penicillin & 100 μg/mL Streptomycin (Gibco, Thermo Fisher Scientific), 4 mM L-glutamine (Gibco, Thermo Fisher Scientific) and 5.72 mM 2-Mercaptoethanol (Sigma-Aldrich).

2.2.4.2 Preparation of DNA for Transfection

RNAi constructs were subjected to restriction digest by *Not*I enzyme (Thermo Scientific FastDigest). The digested products were purified using enzymatic purification kit (Qiagen). *Not*I digested plasmid DNA was further purified and concentrated via ethanol precipitation. A 1/10 volume of 3M sodium acetate (AccuGene®, Lonza) and 2 volumes of 100% ethanol were added to the plasmid DNA samples. The solution was then incubated at -20°C for 30 minutes and then centrifuged at 14,500 *g* for 10 minutes. Supernatant was discarded and the plasmid DNA samples were washed with 1 mL 70% ethanol. This was then centrifuged 14,500 *g* for 10 minutes and most of the supernatant was removed.

2.2.4.3 Transfection

Mid-log phase *T. brucei* BSF strain parasites were transfected with the *Not*I digested P2T7^{Ti}-TbGAP/GEF plasmid as described (Price *et al*., 2005b). AMAXA® Human T cell Nucleofector kit (Lonza) was used to perform the transfection. 2X10^7 mid log-phase *T. brucei* BSF strain parasites were centrifuged at 800 *g* for 10 minutes and supernatant was discarded. The parasites were re-suspended in 10 mL 1X PBS and centrifuged at 800 *g* for 10 minutes and the majority of the supernatant was discarded. Parasites were transferred to a 1.5 mL microtube. The microtube was centrifuged at 1,990 *g* for 5 minutes and all supernatant was removed. Parasites were resuspended in T-cell nucleofection solution (Lonza) (100 μL per transfection). The suspension was transferred to the *Not*I digested DNA sample, then transferred to AMAXA® cuvettes and nucleofection was performed using an AMAXA® nucleofector device (programme X-001) (Lonza). The nucleofected parasites were transferred to HMI-9 media and incubated at 37°C with 5% CO_2.

2.2.5 Induction of RNAi

RNAi of the transfected bloodstream form Lister 427 *T. brucei* was induced by adding 1 μg/mL tetracycline (Sigma-Aldrich). The density of the parasites was determined by counting the number of parasites using a haemocytometer. The phenotype of the induced parasites were also observed every 24 hours post addition of the tetracycline using light microscopy. Parasites with a density of $5X10^4$/mL were grown in 10 mL HMI-9 medium (with neomycin) in two sets of triplicates. Tetracycline was added to one set of the experimental triplicates.

2.2.6 Quantification of gene expression following RNAi

2.2.6.1 Design of Oligonucleotides for qPCR

Primers for qPCR (section 2.1.5) were designed utilising the Primer 3 software (http://frodo.wi.mit.edu/ - accessed: May 2019) and the Beacon Designer Free Edition software (http://free.premierbiosoft.com/ - accessed: May 2019) and all standard parameters were used as stated (Thornton and Basu, 2011).

2.2.6.2 RNA extraction

Total RNA was extracted from mid-log phase BSF *T. brucei* following incubation in 1 μg/mL tetracycline for a range of time points. The extraction of RNA was performed using TRIsure™ (Bioline) and all steps were followed as stated in the manufacturer's handbook. The parasites were centrifuged at 800 *g* for 10 minutes and the supernatant was discarded. The parasites were then re-suspended in 45 mL PBS and centrifuged at 800 *g* for 10 minutes and the supernatant was then discarded. Parasites were resuspended in 100 μL PBS and transferred to a nuclease-free microtube. 1 mL TRIsure™ (Bioline) was added to the suspension and incubated at room temperature for 5 minutes. 200 μL chloroform was added to the microtube, mixed vigorously for 15 seconds and incubated at room temperature for 3 minutes. The samples were centrifuged at 12,000 *g* for 15 minutes at 4°C. The aqueous upper phase was

transferred to new microtube, 500 μL isopropanol was added and mixed. The samples were then incubated at room temperature for 10 minutes, followed by centrifugation at 12,000 *g* for 15 minutes at 4°C. The supernatant was removed and the pellet was washed by adding 75% ethanol and vortexing briefly. The solution was then centrifuged at 7500 *g* for 5 minutes at 4°C and the supernatant was removed. The pellet was air-dried and then re-suspended in 30 μL nuclease free water.

2.2.6.3 DNAse treatment

The extracted RNA samples were subjected to DNase treatment using the DNase kit (Ambion), using 4 μg RNA, 5 μL 1X DNase buffer, 0.04 U/μL DNase I enzyme and 5 μL inactivation buffer. All procedures were carried out as stated in the manufacturer's handbook.

2.2.6.4 Reverse transcription

Reverse transcription was carried out on the DNase treated samples using the Omniscript® RT kit (Qiagen), Oligo dT (Qiagen) and RNaseOUT™ Recombinant Ribonuclease Inhibitor (Invitrogen). A 40 μL reaction containing 4 μg of RNA was set up following the procedures stated in the manufacturer's handbook.

2.2.6.5 Quantitative Polymerase Chain Reaction

qPCR reactions were set up as stated in the Universal SYBR® Green Quantitative PCR Protocol (Sigma-Aldrich). A master mix consisting of PowerUP™ SYBR® Green master mix (Applied Biosystems), DNA template, 0.3 μM forward and 0.3 μM reverse primers were prepared with nuclease-free water to make 25 μL reagent per well. 25 μl reagents were aliquoted into each well and the qPCR run was performed using StepOne Plus Real-Time

System (Thermo Fisher Scientific) (programme detailed in Table 2.2). Results were analysed with StepOne Software v2.3 (Thermo Fisher Scientific) and Excel.

qPCR cycle			
Step	**Temperature**	**Time**	**Repeats**
UDG activation	50°C	2 minutes	Hold
Dual-Lock DNA Polymerase	95°C	2 minutes	Hold
Denature	95°C	15 seconds	40
Anneal/Extend	60°C	1 minute	
Dissociation curve			
Step	**Ramp rate**	**Temperature**	**Time**
1	1.6°C/second	95°C	15 seconds
2	1.6°C/second	60°C	1 minute
3	0.15°C/second	95°C	15 seconds

Table 2.2. qPCR cycle and dissociation curve steps. *Table detailing the steps, number of cycles and temperature used for qPCR. A dissociation curve was used to determine the specificity of the qPCR.*

2.2.7 Microscopy

2.2.7.1 Indirect immunofluorescence

Log-phase BSF parasites (1x10^7/mL) were harvested by centrifugation at 800 *g* for 10 minutes. BSF cells were washed in Voorheis' modified PBS (vPBS; PBS supplemented with 10mM glucose and 46mM sucrose) and fixed for 1 hour on ice in 4% (w/v) paraformaldehyde. Fixed cells were washed and adhered to poly-lysine microscope slides for 20 minutes at room

temperature in humid chamber. The cells were then permeabilised with 0.1% (w/v) Triton-X 100 in PBS for 10 minutes (Allen *et al*., 2003). Image-iT™ FX Signal Enhancer (Invitrogen) signal enhancer was added to the slides and incubated at room temperature for 1 hour. A primary mouse monoclonal antibody 1 (TAT1) against *T. brucei* α-tubulin (1:200, a gift from Keith Gull) and a primary anti-rabbit monoclonal antibody against paraflagellar rod protein 1 (PFR1) (1:200) (Hemsworth *et al*., 2013) were added to the slides and incubated for 1 hour at room temperature. Unbound primary antibodies were washed off with PBS. Alexa Fluor 488 and 594 conjugated secondary antibodies (1:250, Invitrogen) were added to the slides and incubated at room temperature for 1 hour. Unbound secondary antibodies were washed off with PBS and 5 μg/mL DAPI was added to all cells. Cells were incubated at room temperature for 5 minutes and washed with PBS. ProLong™ Diamond Antifade Mounting (Invitrogen) medium was added to the slides and sealed with coverslips. All samples were visualised by fluorescence microscopy using EVOS FL Cell Imaging System (Life Technologies).

2.2.7.2 Transmission Electron Microscopy (TEM)

Log-phase BSF parasites ($2x10^7$ cells/mL) were washed three times in serum free HMI9 media and once in PBS. Samples were then processed for TEM by Meg Stark (Technology Facility, Department of Biology, University of York) using methods described previously (Price *et al*., 2007a). Images were viewed with a Tecnai 12 BioTwin (FEI) at 120 kV and images were acquired using SIS MegaView III digital camera.

2.2.8 Flow cytometry

2.2.8.1 Propidium iodide flow cytometry

Mid-log phase BSF parasites were incubated for 0 to 72 hours in the presence of 1 μg/mL tetracycline. $1x10^7$ cells were harvested by centrifugation at 1000 *g* for 10 minutes at 4°C and washed in PBS and prepared for propidium iodide flow cytometry as described previously

(Ibrahim *et al*., 2011). 10 ng/mL RNase A (Thermo Fisher Scientific) was added to each samples and tubes were incubated in 37°C for 2 hours. 10 ng/mL propidium iodide (Sigma-Aldrich) was then added to the samples and the tubes were further incubated for 45 minutes at 37°C. Samples were processed on a Guava EasyCyte 6-2L flow cytometer (Merck Millipore) and 20,000 events were counted per sample. The flow cytometer was calibrated before each use as described in the manufacturer's protocol. InCyte software (Merck Millipore) was used to analyse the data.

2.2.8.2 Live/Dead flow cytometry

Mid-log phase BSF parasites ($1x10^7$ cells) induced at different time points with 1 μg/mL tetracycline were harvested by centrifugation for 10 minutes at 800 *g*, washed with PBS and resuspended in 1 mL PBS. 1 μL of Live/Dead Fixable Red Dead Stain (Thermo Fisher Scientific) was added to the samples and incubated for 30 minutes at 20°C in dark. The samples were centrifuged at top speed for 20 seconds (Labnet Prism™ Microcentrifuge) and resuspended in 1 mL 4% (w/v) paraformaldehyde, these were then incubated at room temperature in dark for 15 minutes. The samples were washed in PBS by centrifugation at 800 *g* for 10 minutes and resuspended in 1 mL PBS. Flow cytometry was carried out using Guava EasyCyte 6-2L flow cytometer (Merck Millipore) and 20,000 events were counted per sample, InCyte software (Merck Millipore) was used to analyse the data.

2.2.9 Concanavalin A endocytosis assay

Log-phase BSF parasites ($1x10^7$ cells) were harvested by centrifugation at 800 *g* for 10 minutes and resuspended in 1 mL serum free HMI9/1% BSA. Samples were incubated at 4°C, 12°C or 37°C for 45 minutes. 25 μg/mL Concanavalin A (Alexa Fluor™ 488 Conjugate, Thermo Fisher Scientific) was added to each samples and the samples were further incubated for 1 hour at temperatures as before. The samples were washed in Voorheis' modified PBS (vPBS;

PBS supplemented with 10 mM glucose and 46 mM sucrose) and resuspended in 0.5 mL vPBS. 0.5 mL 6% (w/v) paraformaldehyde was added and the samples were incubated at 4°C for 1 hour. The samples were washed and resuspended in 1 mL PBS. The samples were then prepared for an indirect immunofluorescence assay as previously described in section 2.7.1. Rabbit anti-TbRab5A against *T. brucei* early endosomes (1:100, a gift from Mark Field, Department of Pathology, University of Cambridge, UK) and mouse anti-P67 against *T. brucei* lysosomes (1:100, a gift from Jay Bangs, Department of Medical Microbiology and Immunology, Madison, WI, USA) were used on samples incubated at 12°C and 37°C respectively. The primary antibodies were detected using Alexa Fluor 488 and 594 conjugated secondary antibodies (1:250, Invitrogen). All samples were visualised by fluorescence microscopy using EVOS FL Cell Imaging System (Life Technologies).

2.2.10 Drug Screening

2.2.10.1 Determination of IC_{50} of tetracycline in T. brucei *lines*

The IC_{50} of tetracycline in P2T7-GEF3 cell lines was identified in order to determine a suitable concentration of tetracycline for inducing a non-lethal defect in endocytosis. 2-fold dilutions of tetracycline with concentrations ranging from 1 μg/mL to 7.63 pg/mL were prepared in HMI-9 media. 100 μL of the prepared dilutions were dispensed into each well of the 96 well plate in triplicates, 100 μL of log-phase BSF P2T7-GEF3 *T. brucei* ($1x10^5$ cells) were added to each dilutions. Positive (Amphotericin B) and negative (water) controls were also included in all plates. The plates were incubated for 48 hours in 37°C with 5% CO_2. PrestoBlue® (Thermo Fisher Scientific) was added to a dilution of 1:10 per well and plates were incubated in the dark for 3 hours in 37°C with 5% CO_2. Plates were read on a Promega GloMax® Multi Detection System ($\lambda_{ex}/\lambda_{em}$ = 525/580-640 nm). Percentage viability was calculated as described previously (Berry *et al*., 2018). The data were analysed using GraphPad Prism7 to determine the half maximal inhibitory concentration (IC_{50}) of tetracycline.

Percentage viability for all drug screening experiments were calculated as described by Berry *et al*. 2018:

$$Viability\left(\%\right) = 100\ x\ \frac{[\mu(s) - \mu(-)]}{[\mu(+) - \mu(-)]}$$

Figure 2.1. Percentage viability formula. *μs = mean value for samples, μ(+) = mean of negative control, μ(-) = mean of positive control (Amphotericin B) (Berry et al., 2018).*

2.2.10.2 Determination of IC_{50} of suramin in T. brucei *lines*

2-fold dilutions of suramin were prepared in HMI-9 medium with concentrations ranging from 1mM to 1.95μM as described previously (Bruhn *et al*., 2015). 100 μL of the dilutions were dispensed into each well of the 96 well plate in triplicates. 100 μL of log-phase BSF P2T7-GEF3 *T. brucei* ($1x10^5$ cells) were added to each well containing the dilutions. Positive (Amphotericin B) and negative (water) controls were also included in all plates. The plates were incubated for 48 hours in 37°C with 5% CO_2. PrestoBlue® (Thermo Fisher Scientific) was added to a dilution of 1:10 per well and plates were incubated in the dark for 3 hours in 37°C with 5% CO_2. Plates were read on a Promega GloMax® Multi Detection System ($\lambda_{ex}/\lambda_{em}$ = 525/580-640 nm). Percentage viability was calculated as described previously (Berry *et al*., 2018). The data were analysed using GraphPad Prism7 to determine the half maximal inhibitory concentration (IC_{50}) of suramin.

2.2.10.3 MMV Pathogen Box

The Pathogen Box consisting of 400 drug like compounds against neglected tropical diseases was obtained from Medicines for Malaria Venture (MMV). The compounds were dissolved in

dimethyl sulfoxide (DMSO) at a concentration of 10 μM and further diluted to a concentration of 1 μM in HMI-9 media. Each compound was added to the well at a final concentration of 1 μM and 10 μM in duplicates. 100 μL of log-phase wild type BSF *T. brucei* ($1x10^5$ cells) was added to each well. Positive (Amphotericin B) and negative (DMSO) controls were also included in all plates. The plates were incubated for 48 hours in 37°C with 5% CO_2. PrestoBlue® (Thermo Fisher Scientific) was added to a dilution of 1:10 per well and plates were incubated in dark for 3 hours in 37°C with 5% CO_2. Plates were read on a Promega GloMax® Multi Detection System ($\lambda_{ex}/\lambda_{em}$ = 525/580-640 nm). The percentage viability was calculated as described previously (Berry *et al*., 2018) and data was analysed using GraphPad Prism7. Percentage viability of 5% or below compared to the diluent only control (DMSO) was identified as a positive hit. IC_{50} of the positive hits was carried out as described in section 2.2.10.2.

Chapter 3 – Identification and functional prediction of ARF regulators in *T. brucei* using bioinformatics

3.1 Introduction

Since the discovery of ADP-ribosylation factors (ARFs) in the 1980s for their ability to act as cofactors to stimulate cholera toxin ADP-ribosyltransferase activity (Kahn and Gilman, 1984, Enomoto and Gill, 1980), ARFs have been extensively studied and documented, resulting in the identification of these proteins in all studied eukaryotic organisms to date (Nie *et al*., 2003). The identified ARFs have been shown to be highly conserved throughout eukaryotic evolution (Nie *et al*., 2003, Li *et al*., 2004, Muthamilarasan *et al*., 2016, Serbzhinskiy *et al*., 2015). This was further shown by Price *et al.* through amino acid sequence analysis of the 9 identified *T. brucei* ARF/ARLs against closest homologues of human ARF/ARLs, finding the level of similarities to range from 43% to 75% (Price *et al*., 2005b, Price *et al*., 2005a).

Knockdown studies on *T. brucei* ARF/ARLs using a tetracycline inducible RNAi system have demonstrated the potential roles of ARF/ARLs in bloodstream form *T. brucei*. Previous studies have demonstrated that ARL6 may be involved in maintaining flagellum length since RNAi of ARL6 led to shortening of the flagellum length (Price *et al*., 2012). Price *et al* demonstrated the potential roles of ARF1 and ARL1 in *T. brucei* endocytosis and trafficking. RNAi of ARF1 and ARL1 in bloodstream form *T. brucei* led to increase in lethal phenotypes and cell death (Price *et al*., 2007b, Price *et al*., 2005a, Price *et al*., 2005b). These studies have highlighted that many of these proteins are essential for *T. brucei* viability. However the high level of amino acid similarity between *T. brucei* and human ARF/ARLs suggest that targeting *T. brucei* ARF/ARLs may inadvertently target human ARF/ARLs; thus possibly leading to adverse side effects for the host (Müller and Hemphill, 2016).

Guanine nucleotide exchange factors (GEFs) and GTPase activating proteins (GAPs) regulate the activity of ARF/ARLs. GEFs aid in the dissociation of GDP and association of GTP to ARF/ARLs, resulting in their activation. GAPs on the other hand aid in the hydrolysis of GTP into GDP that are bound to ARF/ARLs, thus leading to their inactivation (Scheffzek and Ahmadian, 2005, Jackson and Casanova, 2000). Previous studies have demonstrated that the overexpression or mutation of these regulators affects the function of ARFs, thus disrupting

cellular functions; highlighting the essential nature of these regulating proteins. Unlike ARF/ARLs, GEFs and GAPs are highly diverse at the amino acid level, with the highly conserved regions being the Sec7 and ARFGAP catalytic domains respectively (Jackson and Casanova, 2000, Pocognoni et al., 2018, Kahn et al., 2008). Therefore this high level of diversity found in these ARF/ARL regulating proteins could possibly make them drug targets against *T. brucei*.

3.1.1 Aims

The aim of this chapter is to use bioinformatics tools to identify *T. brucei* GEFs and GAPs, to find the level of homology with human GEFs and GAPs at both the sequence and structural level, and to explore protein localisation using existing datasets.

Additionally this chapter also aims to identify orthologues in other kinetoplastids. While *T. brucei* are extracellular parasites, not entering host cells at any point of their life cycles, the related kinetoplastids *T. cruzi* and *Leishmania spp*. have intracellular stages in the host. This difference in localisation environment may lead to alteration in functions of GEFs and GAPs or the absence of members of these groups of regulating proteins.

3.2 Methods

Bioinformatics tools were used to identify *T. brucei* ARF GEFs and GAPs, as well as to analyse the structure and see if it would be possible to determine their interactions and functions.

The methods used in this chapter are as follows:

3.2.1 Protein BLAST

Literature and NCBI database searches were used to identify human GEFs and GAPs (https://www.ncbi.nlm.nih.gov/ - accessed: Oct 2015). BLAST searches (BLASTP) using the

protein sequences of human GEFs and GAPs were used to identify possible homologues in the *T. brucei* genome database (https://tritrypdb.org/tritrypdb/ - accessed: Oct 2015).

3.2.2 Sequence alignment

Amino acid sequence alignment was used to determine regions of sequence similarity between human and *T. brucei* GEFs and GAPs. The amino acid sequences for *T. brucei* and human GEFs and GAPs were aligned using UniProt sequence alignment (Clustal Omega) (www.https://uniprot.org/align/ - Oct 2015).

3.2.3 Domain analysis

Visualisation and analysis of the domains present in *T. brucei* GEFs and GAPs was carried out using Simple Modular Architecture Research Tool (SMART) (http://smart.embl-heidelberg.de/ - accessed: June 2017). The same was done for all human GEFs and GAPs, and the domain composition was compared between the two species.

3.2.4 Structural analysis

The structure of identified *T. brucei* GEFs and GAPs was determined with the aid of structure prediction tool; Phyre2 (http://www.sbg.bio.ic.ac.uk/phyre2/html/page.cgi?id=index – accessed: May 2018). The predicted structures for both human and *T. brucei* ARF regulators were analysed on PyMOL Molecular Graphics System, Version 2.0 supplied by Schrödinger, LLC.

3.2.5 Protein localisation

Subcellular localisation of the identified *T. brucei* GEFs and GAPs was searched using TrypTag (http://tryptag.org/ - accessed: March 2018), a protein localisation resource (Dean *et*

al., 2017). The same was done for previously identified *T. brucei* ARF/ARLs. The Human Protein Atlas (www.proteinatlas.org – accessed: April 2019) was used to the search for existing datasets to explore subcellular localisation of human GEFs and GAPs.

3.2.6 Putative orthologues of *T. brucei* ARF regulators in other kinetoplastids

Putative orthologues of *T. brucei* GEFs and GAPs in other kinetoplastids was determined with the aid of OrthoMCL (https://orthomcl.org/orthomcl/ - accessed: April 2019). Orthologue groups for the *T. brucei* GEFs and GAPs were identified and searched for in other kinetoplastids such as *Trypanosoma cruzi* and *Leishmania* spp.

3.3 Results

3.3.1 Identification of *T. brucei* GEFs and GAPs

Literature and gene sequence searches were carried out using the National Center for Biotechnology Information (NCBI) protein database (https://www.ncbi.nlm.nih.gov/protein/ - accessed: Oct 2015) to identify human ARF regulators and their protein sequences. 26 human ARF GAP genes were identified. The 26 human ARF GAPs were classified according to their subfamilies (Appendix 1): ARFGAP, ADAP, SMAP, GIT, ASAP, ACAP and ARAP; based on their protein-protein interaction domains (Sztul *et al*., 2019). 14 human ARF GEF genes were also identified (Appendix 2). The GEF genes were also classified into their subfamilies according to their protein-protein interacting domains and size. These are: CYTH, GBF, ARFGEF, PSD and IQSEC (Sztul *et al*., 2019).

Protein sequences for each human GEFs and GAPs were obtained. BLASTP was carried out using the protein sequences on TriTrypDB (release 42), a collective genomic database on Trypanosomatidae (Aslett *et al*., 2010), to identify similar proteins in *T. brucei* Lister 427 strain. BLASTP results identified 9 *T. brucei* genes which are potential orthologues to more than one human ARF GAP genes. Four *T. brucei* GAP genes that had the lowest e-values (no higher

than $1e^{-5}$) were selected for further analysis (Table 3.1). Similarly BLASTP results identified three *T. brucei* genes which are potential orthologues to more than one human ARF GEF genes. The three identified *T. brucei* GEF genes had e-values that were no higher than e^{-5} (Table 3.1).

To check that the identified *T. brucei* genes are orthologues to human ARF regulators, a reverse BLAST was executed. Reverse BLAST results confirmed that the identified *T. brucei* genes did correspond to their correct orthologues in humans. The *T. brucei* genes that came up on BLAST searches but were not selected were also subjected to reverse BLAST search. Results showed that these genes did not correspond to any ARF orthologues in humans.

The four *T. brucei* ARF GAPs were assigned names: TbGAP1 (Tb427tmp.244.2540), TbGAP2 (Tb427tmp.01.0920), TbGAP3 (Tb427tmp.01.6060). The same was done to the three *T. brucei* ARF GEFs: TbGEF1 (Tb427.08.1840), TbGEF2 (Tb427.04.2200) and TbGEF3 (Tb427tmp.01.7610).

Accession number	Assigned name	Size (amino acids)/ kDa	Highest similarities (%)	Regulator similar to
Tb427tmp.244.2540	TbGAP1	417/46.16	19	ARFGAP3
Tb427tmp.01.0920	TbGAP2	291/31.68	20	ADAP1
Tb427tmp.01.6060	TbGAP3	306/33.98	20	ARFGAP1
Tb427.03.5300	TbGAP4	275/31.24	14	SMAP2
Tb427.08.1840	TbGEF1	2054/225.09	15	GBF1
Tb427.04.2200	TbGEF2	1666/183.63	15	ARFGEF2
Tb427tmp.01.7610	TbGEF3	1046/117.05	14	IQSEC1

***Table 3.1. Homologues of ARF GEFs and GAPs in* T. brucei.** *BLASTP was performed on amino acid sequences of human ARF GAPs to identify homologs in* T. brucei*. BLASTP results yielding e-values lower than $1e^{-5}$ were selected, and four putative* T. brucei *GAPs and three putative* T. brucei *GEFs with the lowest e-values were selected for further analysis. Amino acid sequence analysis was carried out on the identified* T. brucei *GEFs and GAPs against all known human GEFs and GAPs. The highest percentage of similarities for each of the putative* T. brucei *ARF regulators are shown.*

3.3.2 Structural and sequence similarities

3.3.2.1 Amino acid sequence alignment

In order to use ARF regulators as novel drug targets against *T. brucei*, a low level of sequence identity between the human and *T. brucei* ARF regulators would be preferable. UniProt sequence alignment (Clustal Omega) tool was used to determine the level of amino acid sequence identity between the identified human ARF regulators and *T. brucei* ARF regulators, as well as to identify regions of similarity between the two regulators.

Amino acid sequences of the 26 identified human ARF GAPs were aligned with each of the amino acid sequences of the 4 identified *T. brucei* GAPs. Percentage of similarities was obtained from UniProt sequence alignment (Clustal Omega) tool for each of the 4 *T. brucei* GAPs against the 26 human ARF GAPs. The same was done with the amino acid sequences of the 14 identified human ARF GEFs and the amino acid sequences of each of the 3 identified *T. brucei* GEFs. Percentage of similarities of amino acid sequences between human and *T. brucei* ARF regulators demonstrated the high level of diversity of these regulators between the two species.

BoxShade was used to highlight regions of amino acid sequence similarity between identified *T. brucei* GEFs and human GEFs post multiple sequence alignment (Figure 3.1). Further analysis of the similar amino acid sequences showed that the identical regions were the highly conserved Sec7 catalytic domains present in all GEFs. The regions marked by red and blue lines above and below the sequences are the ARF binding sites that are formed from the hydrophobic and hydrophilic residues present on F and G helices (red lines), and the hydrophobic residue present on the H helix (blue lines); forming a loop (Pai, 1998).

The same was done for *T. brucei* GAPs and human GAPs using BoxShade (Figure 3.2). Analysis of the identical amino acid regions revealed them to be the highly conserved ARFGAP catalytic domains that are present in GAPs. The characteristic Cys_4 zinc finger present in ARFGAP domains are highlighted by the red lines above and below the sequences.

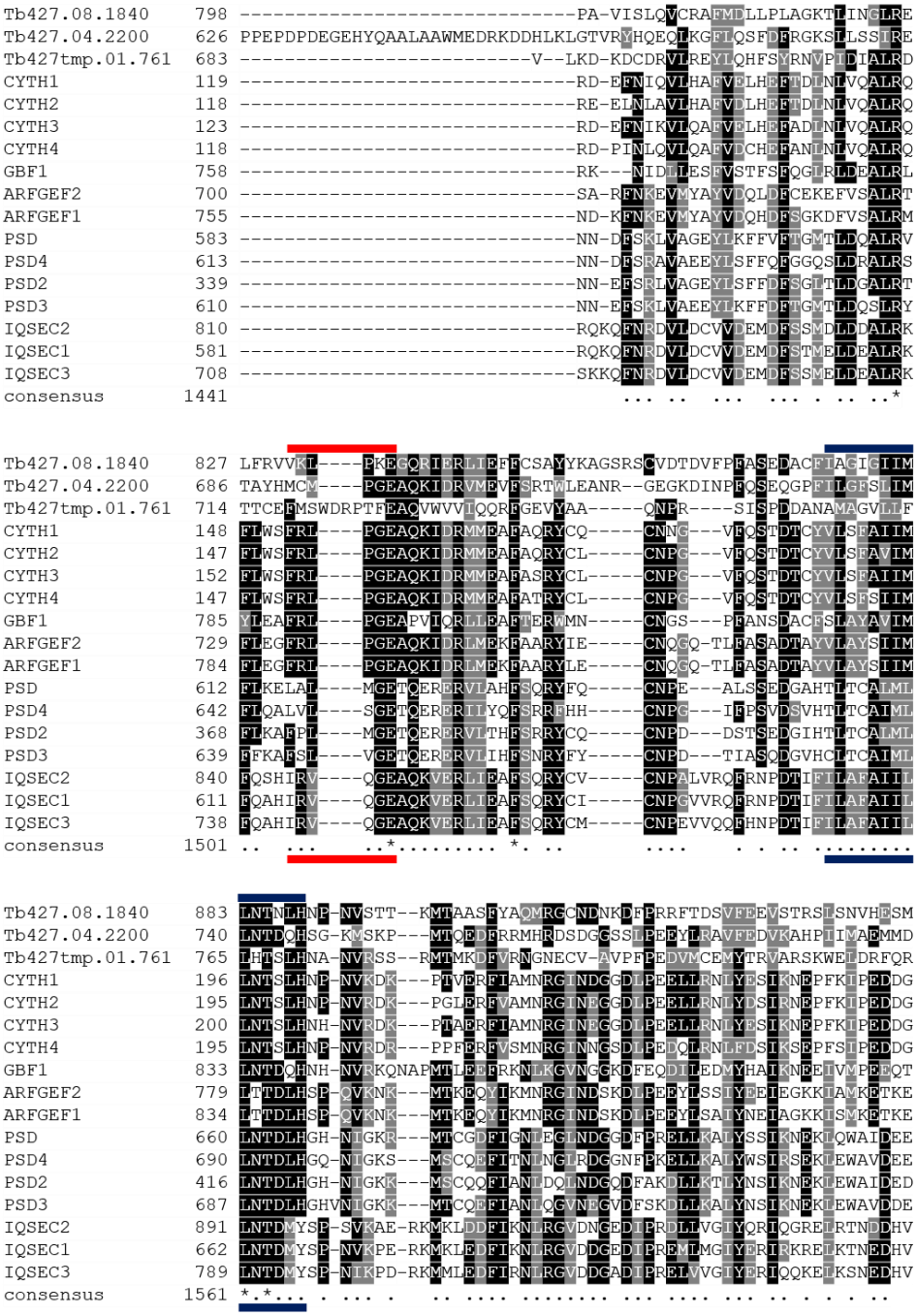

Figure 3.1. Multiple sequence alignment of* T. brucei *and human GEFs. *Partial sequence from multiple sequence alignment of human and* T. brucei *GEFs. Regions of similarities were depicted using BoxShade. Amino acids shaded black are identical, whilst amino acids shaded grey display similar properties. Regions highlighted by red and blue lines represent the ARF binding sites of GEFs. The asterisks (*) and dots (.) under the sequence indicate completely conserved and highly conserved amino acids.*

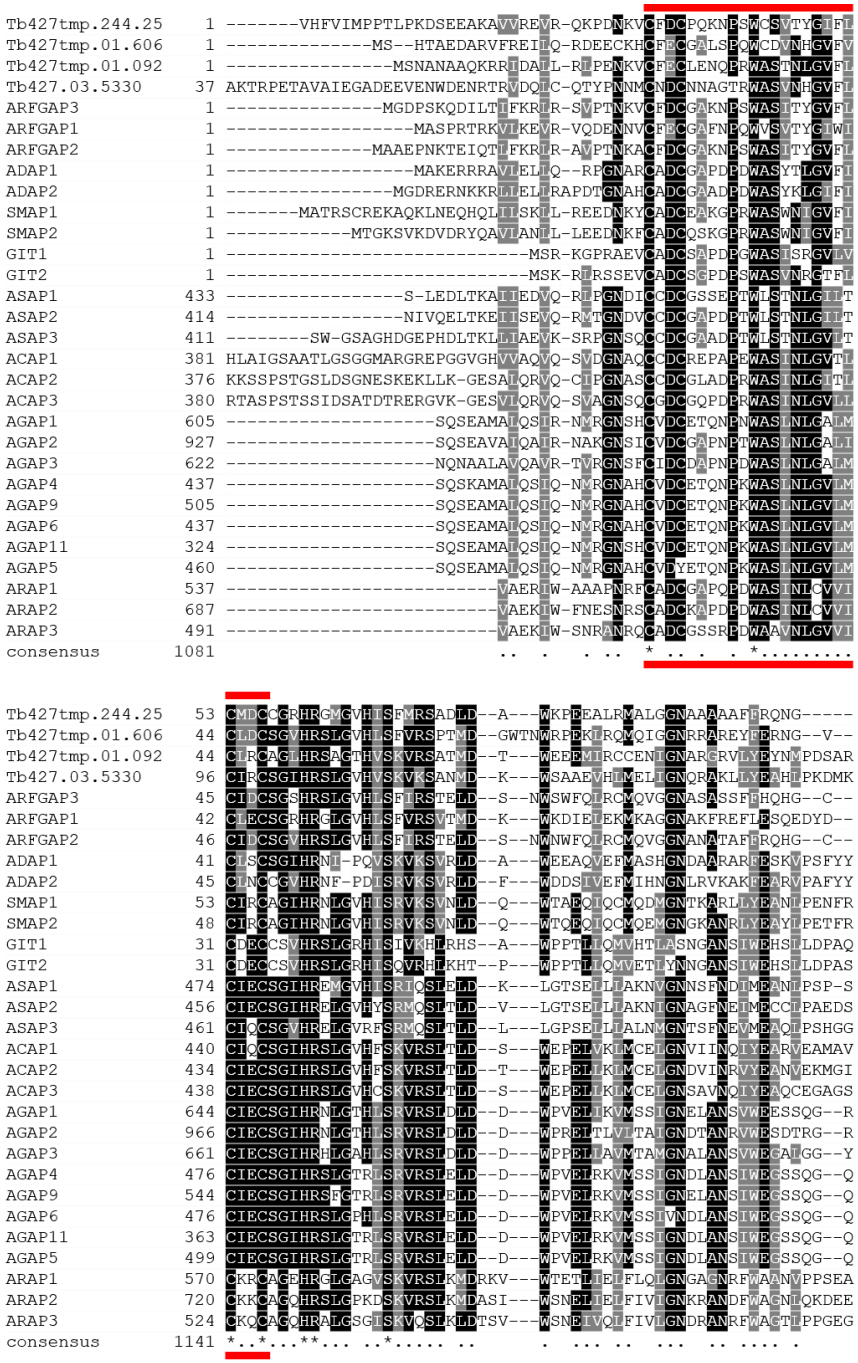

Figure 3.2. Multiple sequence alignment of* T. brucei *and human GAPs. *Partial sequence from multiple sequence alignment of human and* T. brucei *GAPs. Regions of similarities were depicted using BoxShade. Amino acids shaded black are identical, whilst amino acids shaded grey display similar properties. The region highlighted by red lines represent the* Cys_4 *Zinc finger motif that is characteristic of ARFGAP domain. The asterisks (*) and dots (.) under the sequence indicate completely conserved and highly conserved amino acids.*

3.3.2.2 Domain prediction

The Simple Modular Architecture Research Tool (SMART) was used to identify and analyse domains that are present in identified human and *T. brucei* ARF regulators. SMART is a web resource that allows the identification and analysis of protein domains once a protein sequence has been inputted (Letunic and Bork, 2017, Letunic *et al*., 2015). Schematic representation of protein domains were generated for all subfamilies of human ARF GEFs and GAPs using obtained protein sequences (Figure 3.3 & 3.4), and for all identified *T. brucei* GEFs and GAPs (Figure 3.5).

SMART analysis identified the presence of pleckstrin homology (PH) domain in CYTH, PSD and IQSEC subfamilies of human GEFs (Figure 3.3), PH domains are involved in binding of phosphatidylinositol to membranes and other proteins such as βγ subunits of trimeric G-proteins (Wang *et al*., 1994). Interestingly the human ARFGEF and GBF subfamilies lacked the PH domain (Figure 3.3). SMART analysis also revealed the presence of the Sec7 catalytic domain in all human GEFs as expected.

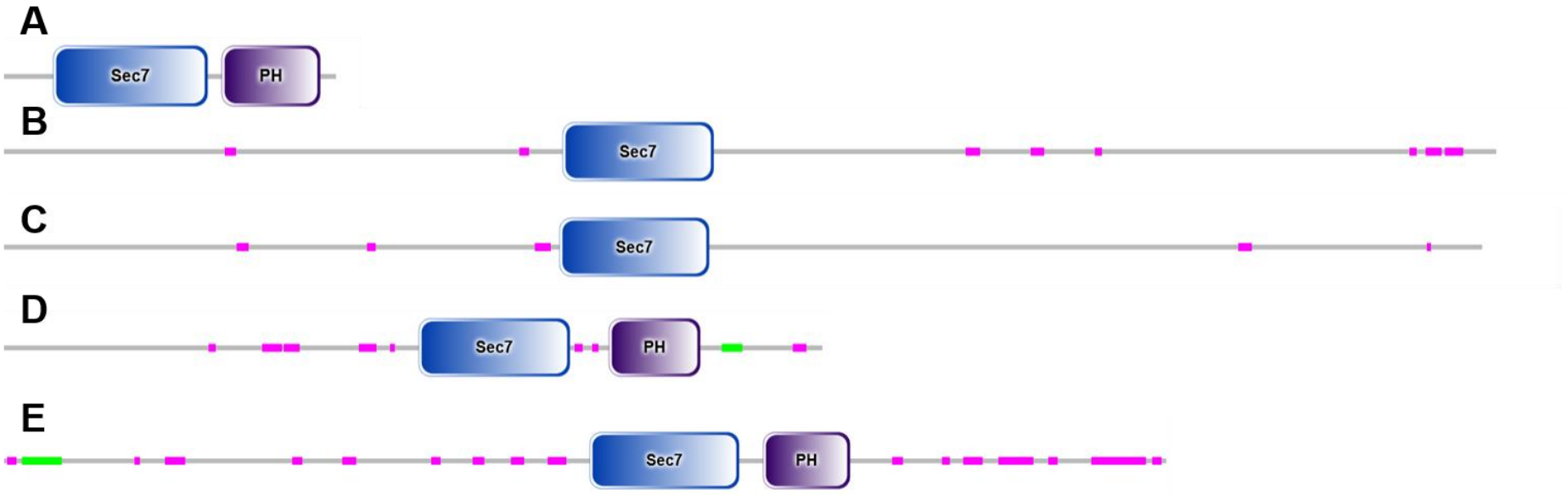

Figure 3.3. Schematic representation of domains present in human ARF GEF subfamilies. *Simple Modular Architecture Research Tools (SMART) analysis was used to get schematic representation of CYTH (A), GBF (B), ARFGEF (C), PSD (D) and IQSEC (E) subfamilies of ARF GEFs. All of the ARF GEF subfamilies except for ARFGEF and GBF contained a pleckstrin homology (PH) domain. The pink regions depict low complexity regions, and the green regions depict coiled coil regions.*

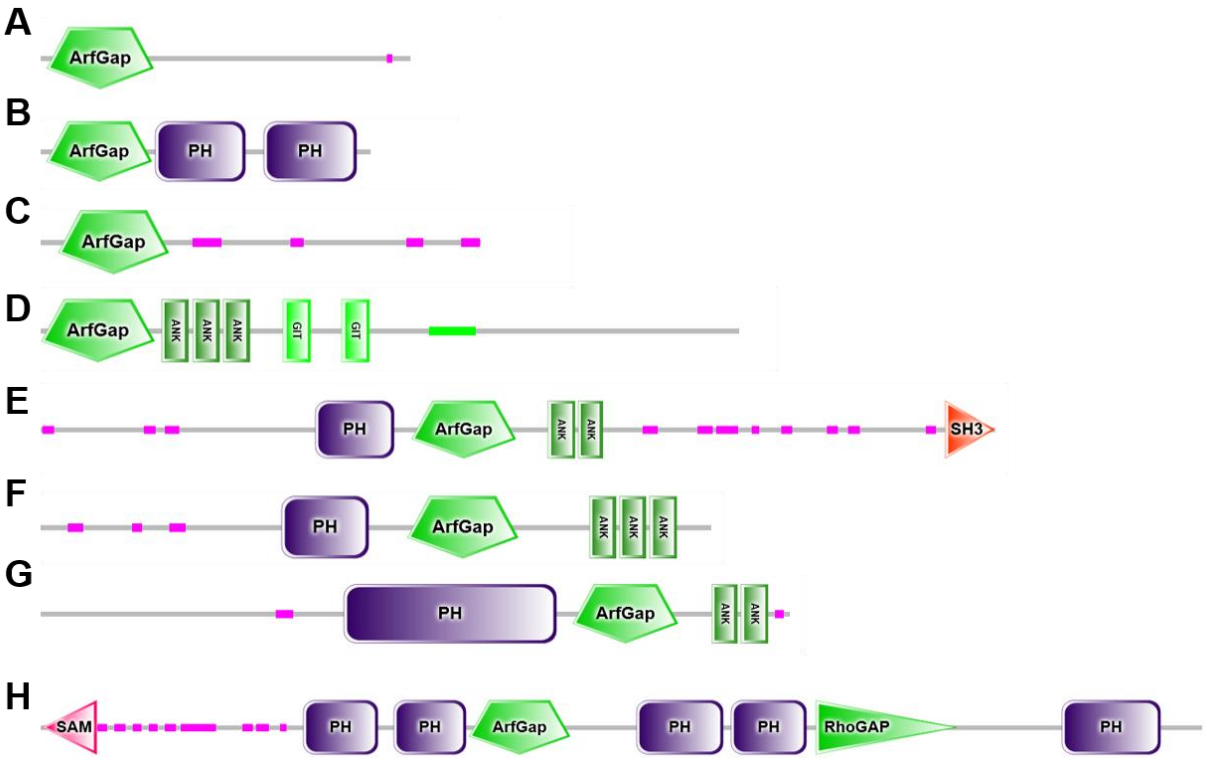

Figure 3.4. Schematic representation of domains present in human ARF GAP subfamilies. *Simple Modular Architecture Research Tools (SMART) analysis was used to get schematic representation of ARFGAP (A), ADAP (B), SMAP (C), GIT (D), ASAP (E), ACAP (F), AGAP (G) and ARAP (H) subfamilies. The presence of pleckstrin homology (PH) domains, ankyrin repeats (ANK), Spa2 homology domains (GIT), Scr homology 3 (SH3) domains, sterile alpha motif (SAM) and RhoGAP domains are also depicted. The pink regions depict low complexity regions, and the green regions depict coiled coil regions.*

SMART analysis of human GAPs revealed the presence of ARFGAP catalytic domain in all of the identified ARF GAPs. The schematic representation in Figure 3.4 showed that the ADAP, ASAP, ACAP, AGAP and ARAP subfamilies had PH domains similarly to the GEFs. Additionally to the PH domains, the human ARF GAPs also contained other functional domains. Ankyrin repeat (ANK) domains are present in the GIT, ASAP, ACAP and AGAP subfamilies. Scr homology 3 (SH3) domains, sterile alpha motif (SAM) were only present in ASAP and ARAP subfamilies respectively. Ankyrin repeat (ANK) domains and Scr homology 3 (SH3) domains are domains that are required for protein-protein interactions and protein bindings respectively (Bork, 1993, Mayer, 2001), whereas the sterile alpha motif (SAM) is involved in cell-cell initiated signal transduction mediation (Schultz *et al*., 1997). The GIT domains are Spa2 homology domains that interact with binding proteins (Kim *et al*., 2003). The ARFGAP and SMAP subfamilies of the human GAPs only consisted of the ARFGAP catalytic domain (Figure 3.4).

Analysis of identified *T. brucei* GEFs and GAPs using SMART tool revealed the presence of Sec7 and ARFGAP domains respectively (Figure 3.5), confirming the possibility that the identified *T. brucei* GEFs and GAPs could be homologues to human ARF regulators. Domain analysis also showed that the identified *T. brucei* GEFs and GAPs are similar to ARFGEF and GBF subfamilies, and ARFGAP and SMAP subfamilies respectively.

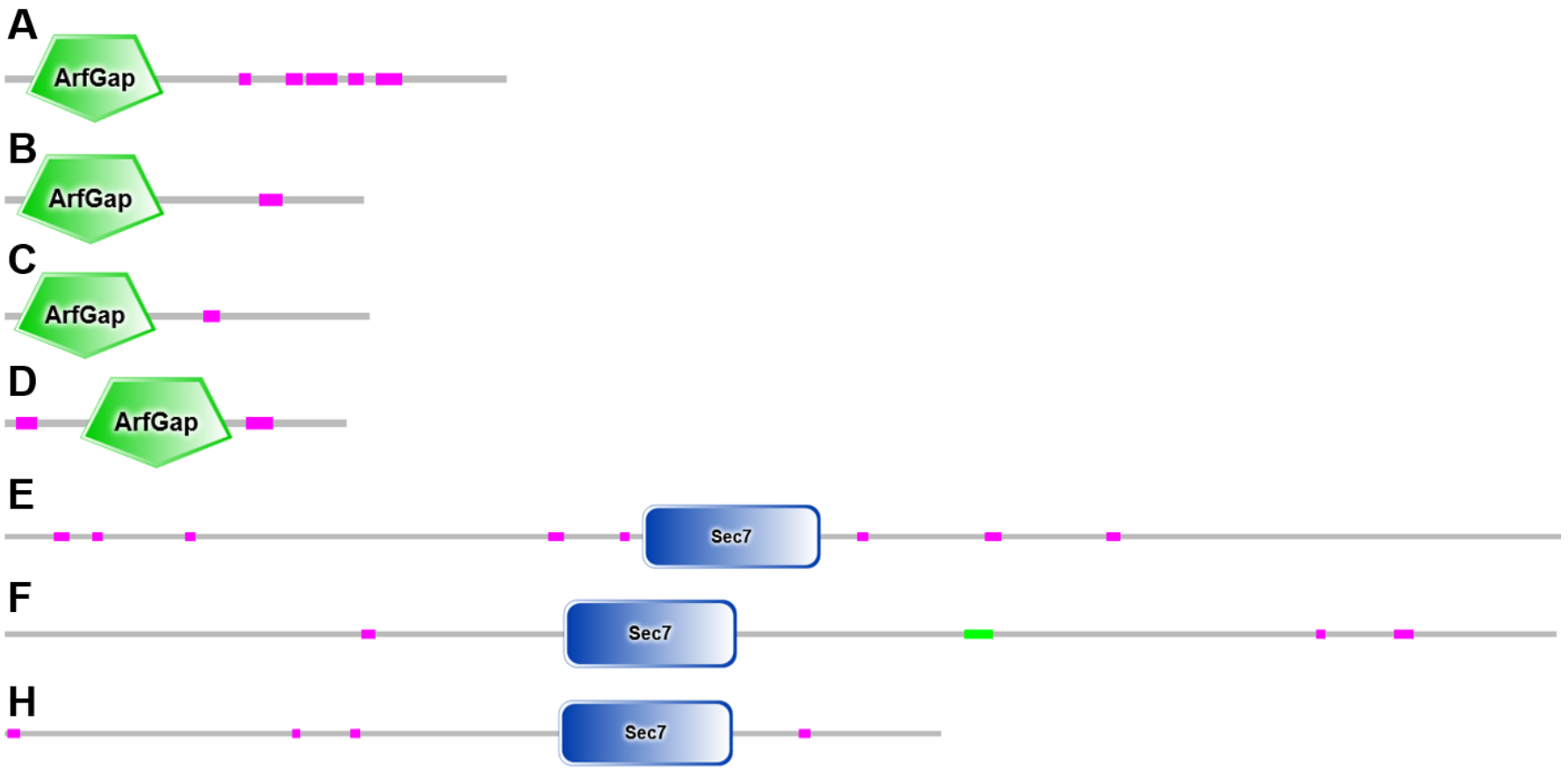

Figure 3.5. Schematic representation of identified* T. brucei *ARF regulators. *Simple Modular Architecture Research Tools (SMART) analysis was used to identify the domains present in TbGAP1 (A), TbGAP2 (B), TbGAP3 (C), TbGAP4 (D), TbGEF1 (E), TbGEF2 (F) and TbGEF3 (G). The pink regions depict low complexity regions, and the green regions depict coiled coil regions.*

3.3.2.3 Structure prediction and analysis

Amino acid sequence analysis in section 3.3.2.1 showed the diversity between identified human and *T. brucei* ARF regulators at the amino acid sequence level. Section 3.3.2.2 conversely highlighted the similarities between domains in human ARF regulators and *T. brucei* ARF regulators. Therefore, structural analysis was carried out in order to identify structural similarities between human and identified *T. brucei* ARF regulators.

The structures of identified *T. brucei* GEFs and GAPs were predicted by analysis of amino acid sequences on Phyre2, a web-based protein structure prediction service (Kelley *et al*., 2015). Phyre2 structural prediction results revealed that 30% - 45% of the whole sequence was covered at 100% confidence for *T. brucei* GAPs, whilst only 10% - 18% of the whole sequence was covered at 100% confidence for *T. brucei* GEFs. This means that 30% - 45% of *T. brucei* GAPs, and 10% - 18% of *T. brucei* GEFs had true homology to the template used by Phyre2 software.

Phyre2 generated Protein Data Bank (PDB) files for the identified *T. brucei* GEFs and GAPs. The PDB files were used to predict 3D structures using PyMOL Molecular Graphics System, Version 2.0 Schrödinger, LLC. Predicted 3D structures for *T. brucei* GAPs identified the presence of α-helices and β-sheets for TbGAP1, TbGAP3 and TbGAP4 (Figure 3.6). TbGAP2 however only consisted of α-helices, lacking the β-sheets that could be seen in the other *T. brucei* GAPs (Figure 3.6). The overall structure of TbGAP1, TbGAP3 and TbGAP4 also differed in the number of α-helices and β-sheets. TbGAP1 consisted of 5 α-helices and 3 β-sheets, TbGAP3 consisted of 5 α-helices and 2 β-sheets, whilst TbGAP4 consisted of 6 α-helices and 3 β-sheets.

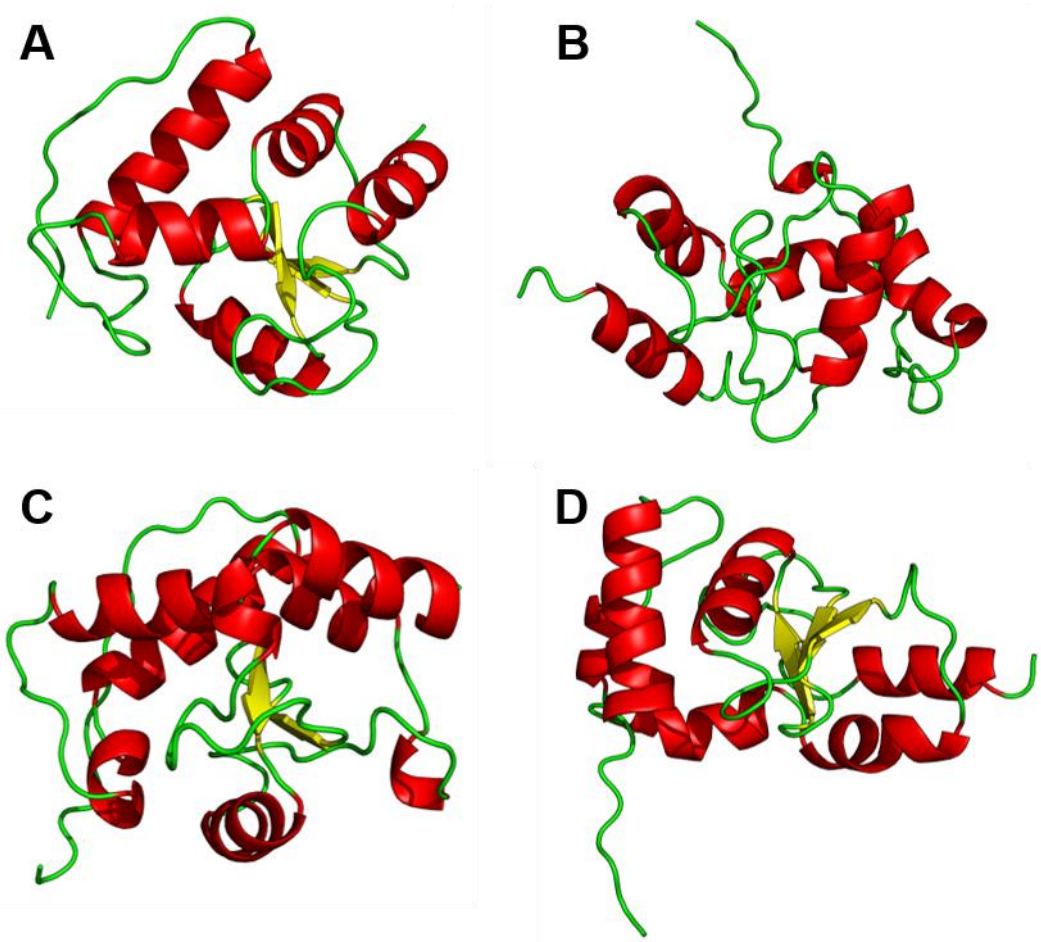

Figure 3.6. Predicted structure of* T. brucei *GAPs*. Phyre2 was used to predict the structure of identified* T. brucei *GAPs and 3D structural analysis was carried out on PyMOL Molecular Graphics System. The predicted structures of TbGAP1 (A), TbGAP3 (C) and TbGAP4 (D) revealed the presence of α-helices and β-sheets characteristic of the ARFGAP domain. TbGAP2 (B) is predicted to only consists of α-helices.*

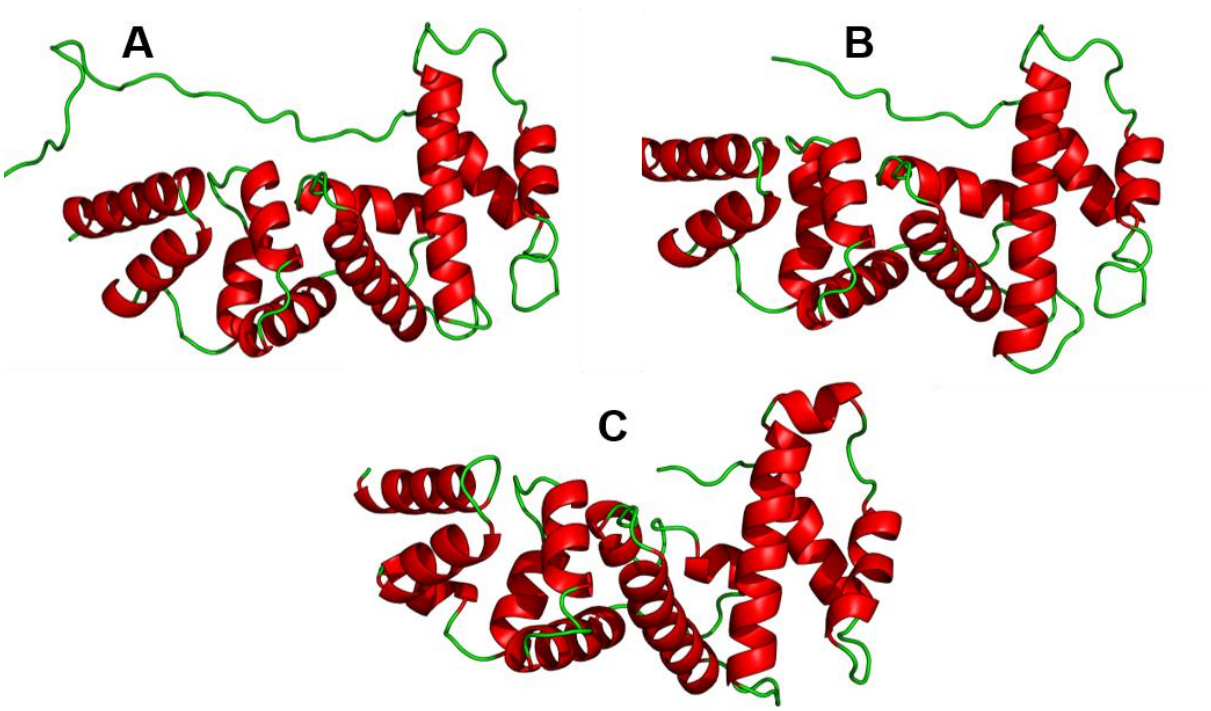

Figure 3.7. Predicted structure of* T. brucei *GEFs. *Phyre2 was used to predict the structure of identified* T. brucei *GEFs and 3D structural analysis was carried out on PyMOL Molecular Graphics System. The predicted structure of TbGEF1 (A), TbGEF2 (B) and TbGEF3 (C) demonstrates the presence of 10 α-helices that correlates to the Sec7 domain in GEFs. TbGEF3 however consists of two additional small α-helices.*

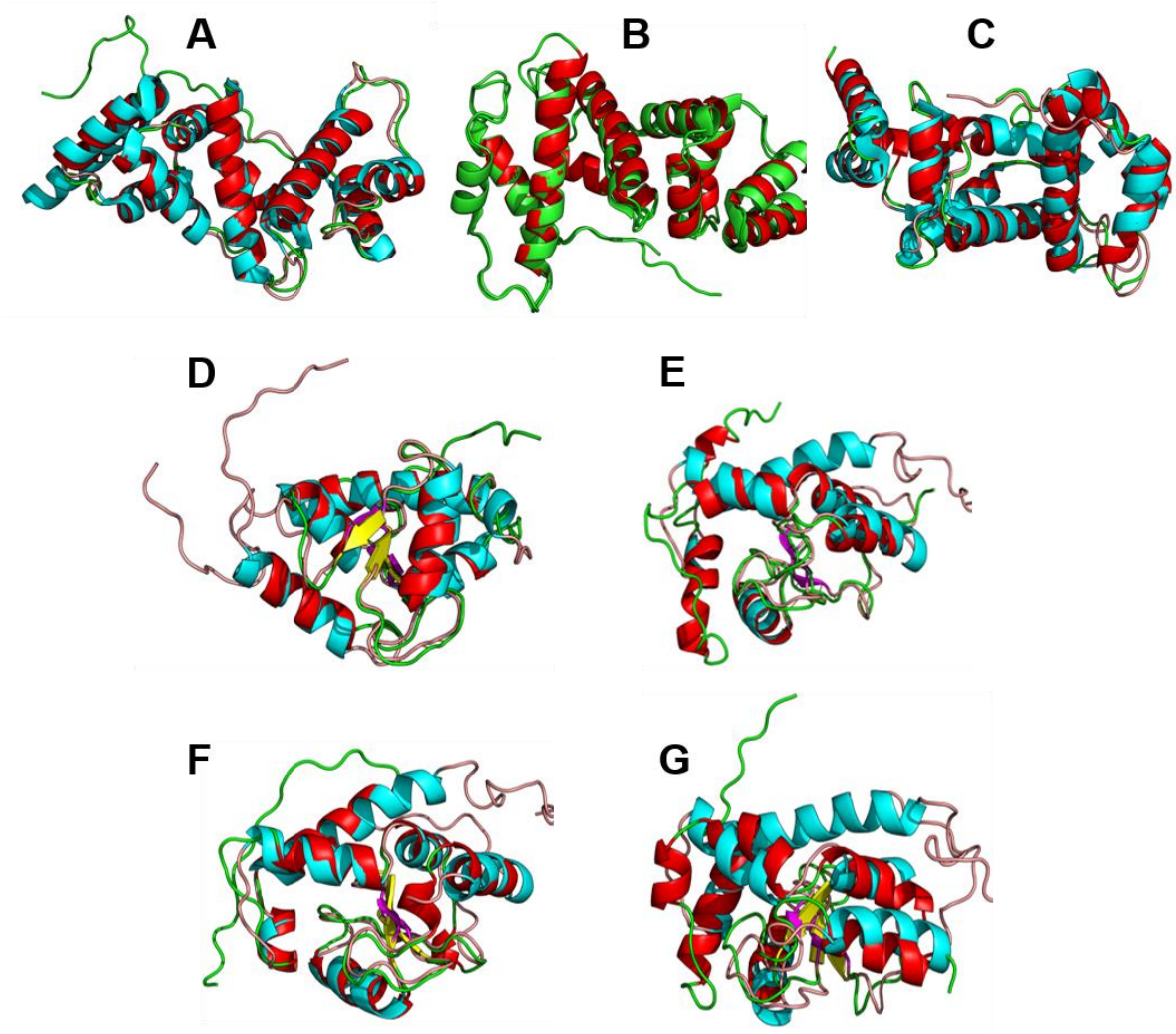

Figure 3.8. Structural alignment of* T. brucei *GEFs and GAPs with human CYTH and ARFGAP subfamily. *Structural alignment was carried out on PyMOL Molecular Graphics System to identify structural homology of TbGEF1 (A), TbGEF2 (B) and TbGEF3 (C) against CYTH1. The same was done for TbGAP1 (D), TbGAP2 (E), TbGAP3 (F) and TbGAP4 (G) against ARFGAP3. RMS values obtained from structural alignment signified the level of homology between the structures. Structures depicted in red are predicted* T. brucei *structures.*

Predicted 3D structures of identified *T. brucei* GEFs on PyMOL Molecular Graphics System showed the presence of α-helices for all of the *T. brucei* GEFs. The predicted structure of TbGEF1 and TbGEF2 consisted of 10 α-helices whilst TbGEF3 consisted of 12 α-helices (Figure 3.7). Unlike the predicted structures of *T. brucei* GAPs, the *T. brucei* GEFs lacked β-sheets.

Structural alignments on all of the predicted structures for *T. brucei* GEFs against all available structure of human GEFs from RCSB Protein Data Bank was carried out on PyMOL Molecular Graphics System (Figure 3.8.A-C). The same was done for the predicted structures of all *T. brucei* GAPs against all available structures of human GAPs (Figure 3.8.D-G). The structural alignment for each *T. brucei* ARF regulator against their respective human ARF regulators gave a Root Mean Square (RMS) value. A RMS value closest to 0 suggests the two protein structures are similar, whilst a larger RMS value suggest that the two protein structure are not similar.

RMS values from structural alignment for each *T. brucei* GEFs and GAPs against all available human GEFs and GAPs showed high level of structural similarities between the identified *T. brucei* GEFs and human CYTH1 and CYTH2 (Table 3.2). Human CYTH3 had the least level of structural similarities with *T. brucei* GEFs, despite being part of the CYTH subfamily. This may be due to CYTH3 being a protein structure in solution whilst CYTH1 and CYTH2 were crystal protein structures.

Human GEF	TbGEF1	TbGEF2	TbGEF3
CYTH1	0.900	0.860	0.918
CYTH2	0.763	0.827	0.625
CYTH3	6.258	9.786	14.078
ARFGEF2	1.171	1.167	1.729
ARFGEF1	1.845	1.796	2.106
IQSEC2	1.881	1.926	3.244
IQSEC1	1.622	1.539	1.692

Table 3.2. RMS values of the three identified* T. brucei *GEFs. *Structural alignment of the three identified* T. brucei *GEFs against identified human GEFs was carried out on PyMOL Molecular Graphics System. RMS values closer to zero signified the similarities of the compared structures (coloured in green).*

In contrast to the RMS values for GEFs above, the RMS values for each *T. brucei* GAP against all available human GAPs showed a varying level of structural similarities (Table 3.3). All of the *T. brucei* GAPs were structural similar to SMAP2. TbGAP1 and TbGAP3 were structurally similar to ARFGAP subfamily and ADAP1, with TbGAP1 also being structural similar to ACAP1 whilst TbGAP3 being structurally similar to AGAP3. TbGAP2 is structurally similar to ADAP1 and SMAP1, whilst TbGAP4 is structurally similar to ASAP3 and ACAP1.

Human GAP	TbGAP1	TbGAP2	TbGAP3	TbGAP4
ARFGAP3	0.854	1.070	0.777	4.218
ARFGAP1	0.327	1.093	0.338	1.006
ARFGAP2	0.802	1.392	0.751	2.858
ASAP3	1.015	1.133	7.604	0.328
ACAP1	0.815	1.188	1.391	0.681
AGAP3	11.145	9.145	0.537	12.703
ARAP1	4.406	2.836	3.401	4.504
ADAP1	0.718	0.968	0.889	1.279
SMAP1	1.042	0.203	1.070	1.283
SMAP2	0.683	0.839	0.718	0.783

Table 3.3. RMS values of the four identified* T. brucei *GAPs. *Structural alignment of the four identified* T. brucei *GAPs against identified human GAPs was carried out on PyMOL Molecular Graphics System. RMS values closer to zero signified the similarities of the compared structures (coloured in green).*

3.3.3 Prediction of protein localisation

The interactions and functions of GEFs and GAPs are influenced by their subcellular localisation (Donaldson and Jackson, 2011). Therefore, determining the localisation of the *T. brucei* GEFs and GAPs using available resources could give indications about their functions within *T. brucei*. The subcellular localisation of the identified *T. brucei* ARF regulators was predicted with the aid of TrypTag, a *T. brucei* protein localisation resource with data on proteins in the *T. brucei* genome tagged with mNeonGreen tag at N and/or C terminals (Dean *et al*., 2017). TrypTag resources are currently only available for the procyclic form pleomorphic TREU927 *T. brucei* cell lines; as opposed to the bloodstream form Lister 427 *T. brucei* cell lines used in this research. In order to obtain localisation data on the identified *T. brucei* ARF regulators from TrypTag, TREU927 homologues were identified through BLASTP and accession numbers were used to obtain data on localisation of *T. brucei* GEF and GAP homologues (Table 3.4). Localisation results gave data for N terminal tagging and C terminal tagging for the identified *T. brucei* ARF regulators (Figure 3.9). The localisation data of identified *T. brucei* ARF GEFs and GAPs were compared to the known localisation data of human ARF GEFs and GAPs (Appendix 1 and 2) with the aid of The Human Protein Atlas (www.proteinatlas.org – accessed: April 2019), a spatial map of human proteome (Thul *et al*., 2017, Uhlen *et al*., 2010).

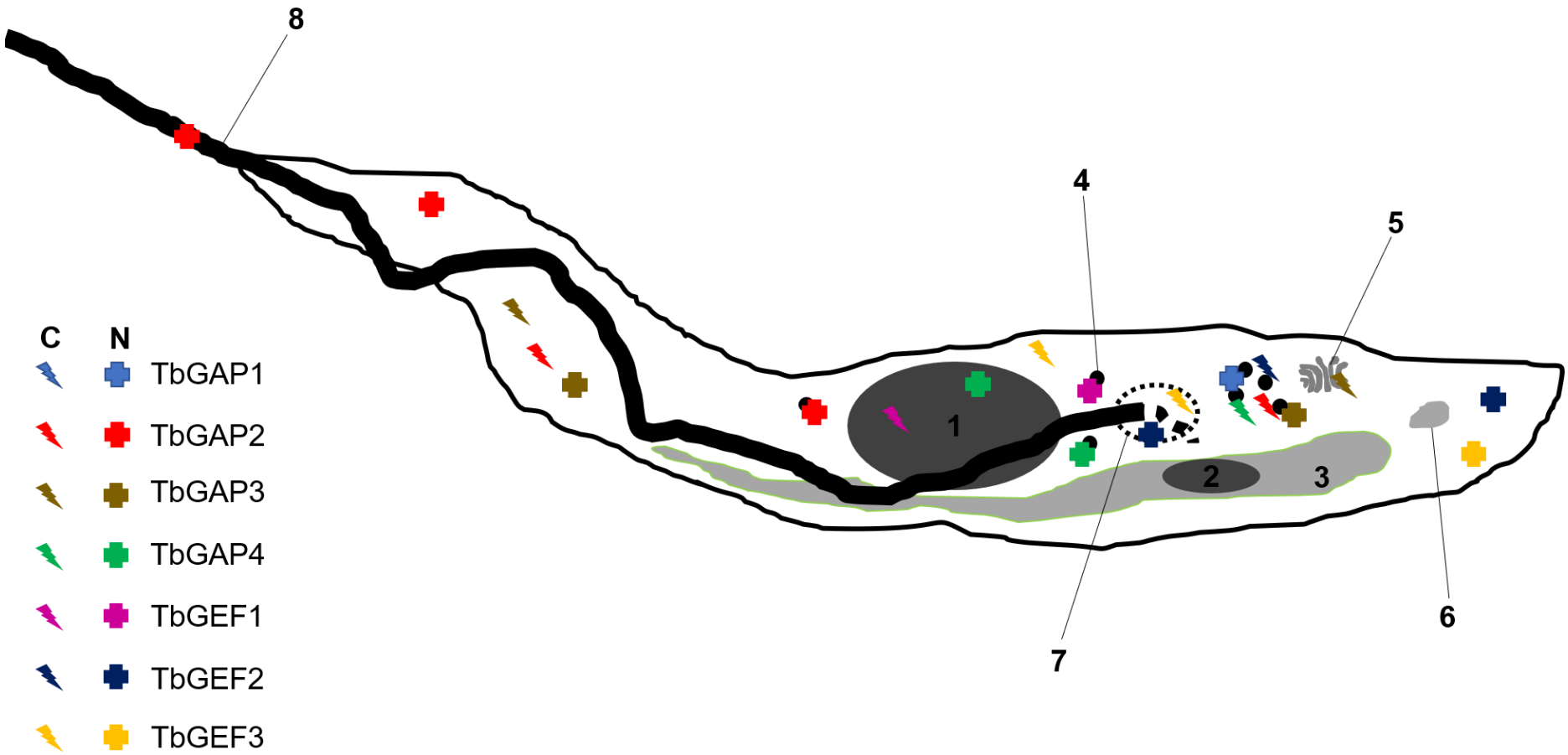

***Figure 3.9. Predicted localisation of TbGEFs and TbGAPs in* T. brucei.** *Simplified schematic representation of* T. brucei *showing (1) nucleus, (2) kinetoplast, (3) mitochondria, (4) endosomes, (5) Golgi, (6) lysosomes, (7) flagellar pocket and (8) flagellum. The predicted localisation of TbGEFs and TbGAPs are represented as stars for C terminal tagged data and crosses for N terminal tagged data.*

Localisation data for the TREU927 homologues of the identified *T. brucei* GEFs showed that TbGEF1 was localised to the nucleolus and endosomes. TbGEF2 was localised to the endosomes, cytoplasm and hook complex, and TbGEF3 to the cytoplasm and flagellar pocket (Table 3.4). This data suggests that the homologues of the identified *T. brucei* GEFs may be implicated in endocytic pathways. The hook complex is a cytoskeletal structure located at the flagellar pocket neck and is thought to be involved in endocytosis at the flagellar pocket; the subcellular localisation of TbGEF3 (Perry *et al*., 2018, Albisetti *et al*., 2017). The similarities of the subcellular localisation of TbGEF2 and TbGEF3 may suggest that these two GEFs may be involved in a similar function or could be interacting with the same ARF/ARLs present in *T. brucei*. Comparison of the subcellular localisation of human GEFs against identified *T. brucei* GEFs showed that the human ARFGEF, GBF and IQSEC subfamilies shared the same subcellular localisation as TbGEF2 and TbGEF3; at the cytoplasm (Yamaji *et al*., 2000, Mazaki *et al*., 2012, Someya *et al*., 2001). These similarities in localisation could mean that TbGEF2 and TbGEF3 may be implicated in a similar function as well. Interestingly TbGEF1 is shown to be localised at the nucleolus as well. This subcellular localisation is also shared by ARFGEF1 (Padilla *et al*., 2004), suggesting that TbGEF1 and ARFGEF1 may have a similar function or could be interacting with similar ARF/ARL homologues.

Accession number (Lister 427)	Accession number (TREU927)	Assigned name	N terminus tagging	C terminus tagging
Tb427tmp.244.2540	Tb927.9.15490	TbGAP1	N/A	Endosome
Tb427tmp.01.0920	Tb927.11.9180	TbGAP2	Endosome Cytoplasm	Flagellum Cytoplasm Endosome
Tb427tmp.01.6060	Tb927.11.14460	TbGAP3	Golgi Cytoplasm	Endosome Cytoplasm
Tb427.03.5330	Tb927.3.5330	TbGAP4	Endosome	Endosome Nucleolus
Tb427.08.1840	Tb927.8.1840	TbGEF1	Nucleolus	Endosome
Tb427.04.2200	Tb927.4.2200	TbGEF2	Endosome	Hook complex Cytoplasm
Tb427tmp.01.7610	Tb927.11.15970	TbGEF3	Cytoplasm Flagellar pocket	Cytoplasm

Table 3.4. Localisation of* T. brucei *ARF regulators determined through TrypTag*. Homologs of the Lister 427* T. brucei *ARF regulators were identified in TREU927 cell lines and accession numbers were used to identify localisation with the aid of TrypTag Trypanosome protein localisation resource.*

Similar to *T. brucei* GEFs, the localisation data for the TREU927 homologues of the identified *T. brucei* GAPs highlighted the different subcellular localisation for each *T. brucei* GAP. TbGAP1 was localised to the endosomes; TbGAP2 was localised to cytoplasm, flagellum and endosomes; TbGAP3 was localised to endosomes, cytoplasm and Golgi apparatus; whilst TbGAP4 was localised to endosomes and nucleolus (Table 3.4). All of the *T. brucei* GAPs were localised to the endosomes; suggesting that they are implicated in the endocytic pathway similar to *T. brucei* GEFs. TbGAP2 and TbGAP3 were localised to the cytoplasm, a subcellular localisation that is also shared by the human ADAP, SMAP, GIT, ASAP, AGAP and ARAP subfamilies (Hanck *et al*., 2004, Kon *et al*., 2008, Hasegawa *et al*., 2012). TbGAP3 is also localised at the Golgi apparatus, similar to the ARFGAP and ARAP subfamilies (Santy and Casanova, 2002, Parnis *et al*., 2006). The similarities in subcellular localisation between *T. brucei* GAPs and human GAP subfamilies may suggest that they share similar functions and interactions. Interestingly TbGAP2 was the only identified *T. brucei* GAP that was shown to be localised to the flagellum. This may suggest that TbGAP2 could be interacting with the same ARF/ARLs that TbGEF2 and TbGEF3 might be interacting with.

Accession number	Assigned name	N terminus tagging	C terminus tagging
Tb927.9.13680	ARF1	Cytoplasm, Flagellum, Nuclear lumen	Flagellar pocket, Endosome
Tb927.9.7650	ARF2	Cytoplasm, Flagellum, Nuclear lumen	N/A
Tb927.7.6230	ARF3	Cytoplasm, Flagellum, Nuclear lumen	N/A
Tb927.9.7230	ARL1B	Cytoplasm, Flagellum, Nuclear lumen	Cytoplasm, Flagellum, Nuclear lumen, Endosome
Tb927.10.4250	ARL2	N/A	Cytoplasm
Tb927.3.3450	ARL3A	N/A	Axoneme, Basal body, Cytoplasm, Nucleus
Tb927.10.8580	ARL3B	N/A	Cytoplasm
Tb927.6.3650	ARL3C	Cytoplasm, Basal body, Flagellum, Nuclear lumen	Cytoplasm, Nucleus, Flagellum, Basal body
Tb927.8.5060	ARL6	Cytoplasm, Flagellum, Nucleoplasm	Cytoplasm, Flagellum, Nucleoplasm, Basal body

Table 3.5. Localisation of* T. brucei *ARF/ARLs were determined through TrypTag*. Homologs of the ARF/ARLs identified by Price et al. (2005) were identified in TREU927 cell lines and accession numbers were used to identify localisation with the aid of TrypTag Trypanosome protein localisation resource.*

The function of ARF/ARLs are tightly regulated by GEFs and GAPs, initiating and terminating ARF/ARL activities respectively (Jackson and Casanova, 2000). Extensive studies on human ARF/ARLs and their regulators have identified the relationship and localisation of these proteins. Price *et al.* had identified 9 ARF/ARLs in *T. brucei* in their previous work (Price *et al*., 2005b). In order to understand the relationship between the identified *T. brucei* ARF regulators and the identified ARF/ARLs by Price *et al.* (2005), the subcellular localisation of the 9 *T. brucei* ARF/ARLs were identified with the use of TrypTag (Figure 3.10). Accession numbers of the 9 *T. brucei* ARF/ARLs were used to obtain protein sequences. BLASTP was then executed to find TREU927 homologues of the 9 ARF/ARLs. Accession numbers of the TREU927 homologues were used to determine the localisation of the ARF/ARLs on TrypTag database. Localisation data for N terminus and C terminus tagging was obtained (Table 3.5).

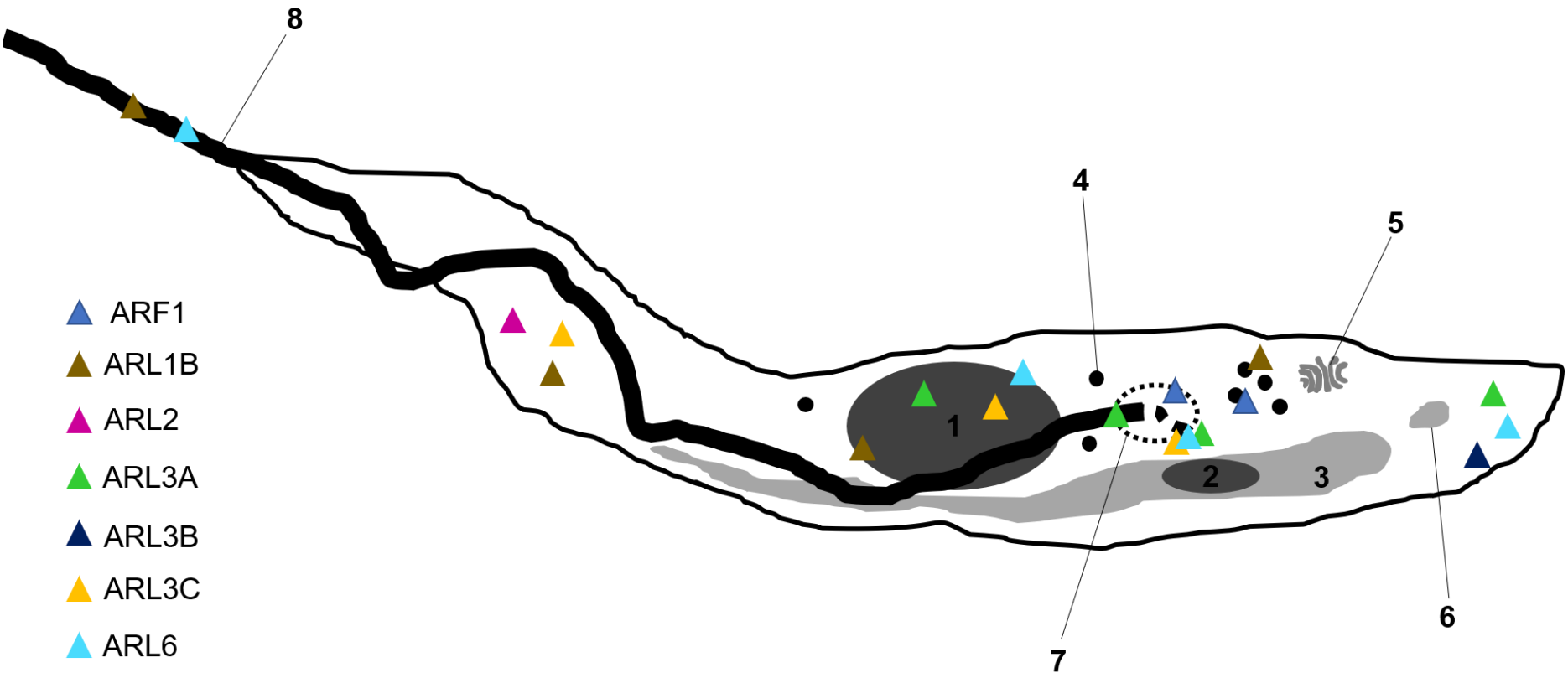

***Figure 3.10. Predicted localisation of ARF/ARLs in* T. brucei.** *Simplified schematic representation of* T. brucei *showing (1) nucleus, (2) kinetoplast, (3) mitochondria, (4) endosomes, (5) Golgi, (6) lysosomes, (7) flagger pocket and (8) flagellum. Triangles represent ARF/ARLs. The predicted localisation of ARF/ARLs based on C terminus tagging is shown.*

N terminus and C terminus tagging of the proteins showed that the ARF/ARLs are localised mainly to the cytoplasm, flagellum/components of the flagellum and nucleus (Table 3.5). All of the identified ARF/ARLs shared a subcellular localisation with TbGEF2, TbGEF3, TbGAP2 and TbGAP3 at the cytoplasm. 7 out of the 9 *T. brucei* ARF/ARLs were shown to be localised to the flagellum or components of the flagellum (Table 3.5). These ARF/ARLs may be regulated by TbGEF2, TbGEF3 and TbGAP3 due to their subcellular localisation being components of the flagellum as well. Similarly 7 out of the 9 *T. brucei* ARF/ARLs were also localised to components of the nucleus, a subcellular localisation that is shared by TbGEF1 and TbGAP4. Figure 3.11 shows a simplified schematic representation of ARF/ARL and identified *T. brucei* regulators and their predicted subcellular localisation.

The researchers who performed the TrypTag project recognise the limitations of using mutant forms of the proteins to determine their localisation. They used gene ontology and localisation modifiers to determine locations of proteins when necessary (Dean *et al*., 2017). Additionally, the N terminus tagging of *T. brucei* ARF/ARLs shown in Table 3.5 may not represent an accurate localisation data since N terminal myristoylation is required for ARF/ARL functions (Padovani *et al*., 2013, Liu *et al*., 2009).

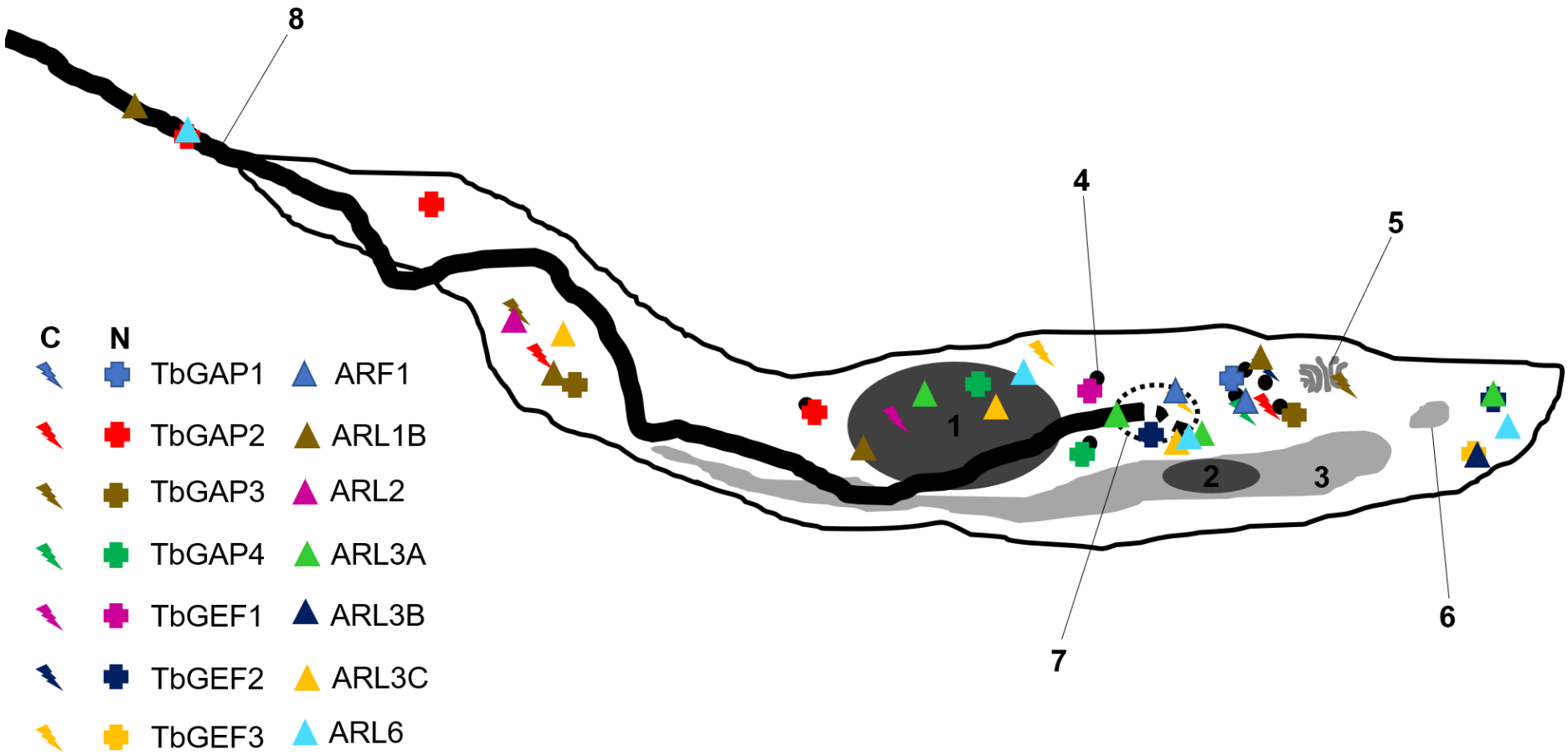

***Figure 3.11. Predicted localisation of ARF/ARLs, TbGEFs and TbGAPs in* T. brucei.** *Simplified schematic representation of* T. brucei *showing (1) nucleus, (2) kinetoplast, (3) mitochondria, (4) endosomes, (5) Golgi, (6) lysosomes, (7) flagger pocket and (8) flagellum. Triangles represent ARF/ARLs. Lightning and crosses represent TbGEF/TbGAPs according to C terminal and N terminal tagging data respectively.*

3.3.4. Putative orthologues of *T. brucei* ARF regulators in other Kinetoplastids

Unlike *T. cruzi* or *Leishmania* spp., *T. brucei* are extracellular in all stages of their life cycle (Pays and Vanhollebeke, 2009), being constantly exposed to host's immune response. The differences in pH, availability of nutrients and composition in extracellular and intracellular environment as well as exposure to host immune response means that parasites have to adapt differently depending on their environment (Dean *et al*., 2009, Quintana *et al*., 2018). This difference in localisation and therefore adaptation in *T. brucei* and other kinetoplastids may results in changes in protein functions or lack of a particular protein. Presence of ARF/ARLs and their regulators have been identified previously by Price *et al*. (Price *et al*., 2005b) and in section 3.3.1, the identified *T. brucei* GEFs and GAPs amino acid sequences will be used to identify orthologues of these proteins in other intracellular kinetoplastids.

Accession number searches were carried out on each of the identified *T. brucei* ARF GEFs and GAPs on TriTrypDB. Orthologue group (OG) numbers were obtained from the database search for each of the gene. A search on the obtained OG numbers for each of the ARF regulators was carried out on OrthoMCLDB, a public database containing orthologue groups based on the OrthoMCL algorithm (Chen *et al*., 2006). OrthoMCLDB identified orthologues of *T. brucei* GEFs and GAPs in *L. braziliense*, *L. infantum*, *L. major*, *L. mexicana*, *T. b. gambiense*, *T. congolense*, *T. cruzi* and *T. vivax* (Table 3.6). However TbGEF3 and TbGAP3 did not generate orthologues in *T. cruzi* (marked as red on the table), suggesting that the functions of these proteins may not be implicated in *T. cruzi* cellular pathways. There is also a possibility that orthologues of the TbGEF3 and TbGAP3 are significantly different on amino acid sequence level in *T. cruzi*, thus not identified in the searches on TriTrypDB.

Multiple amino acid sequence alignment was carried out for each orthologue groups in order to identify any regions of similarities the ARF regulators share between the kinetoplastid species (Appendix 3 - 8). Sequence alignment showed that the ARF regulators for each orthologue groups were highly conserved at the catalytic Sec7 and ARFGAP domains (Figure 3.12). Other than the catalytic domains, the sequence alignment showed that many of the orthologues consisted of highly conserved regions (Appendix 3 - 8); suggesting that the ARF regulators might function similarly in other kinetoplastid species.

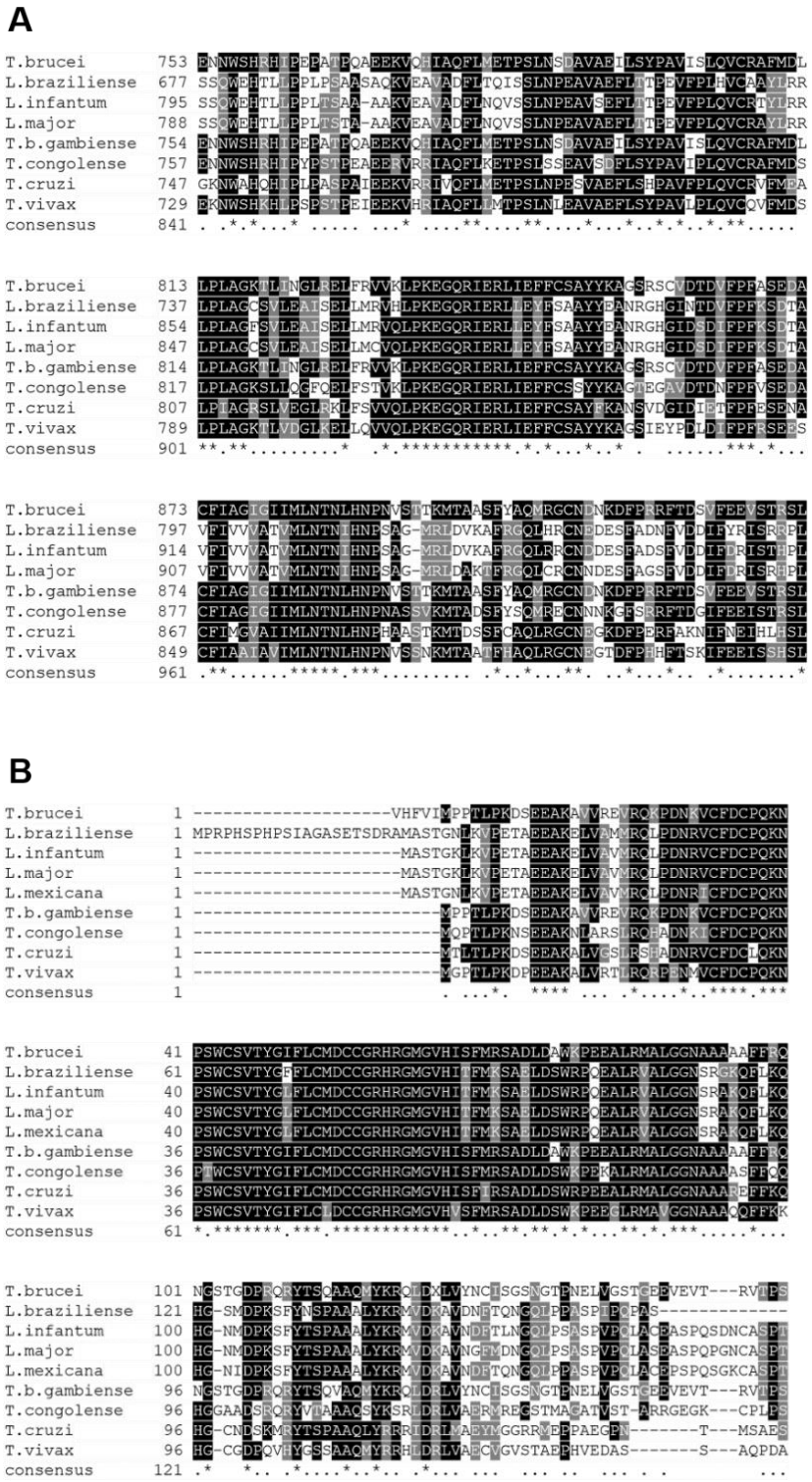

Figure 3.12. Multiple sequence alignment of orthologues. *Partial multiple sequence of (A) TbGEF1 and (B) TbGAP1. The highly conserved regions shown are the Sec7 and ARFGAP catalytic domains in GEFs and GAPs respectively. Regions of similarities were depicted using BoxShade. Amino acids shaded black are identical, whilst amino acids shaded grey display similar properties.*

3.4. Discussion

This chapter aimed to identify *T. brucei* GEFs and GAPs using literature searches and bioinformatics tools. 26 human ARF GAPs and 14 human ARF GEFs were identified with the aid of literature searches and gene searches on NCBI database. BLASTP of the identified human ARF regulator protein sequences identified orthologues in *T. brucei*, 4 ARF GAPs and 3 ARF GEFs with the lowest e-values were selected for further analysis.

3.4.1 TbGEFs and TbGAPs are highly conserved at the catalytic domains on amino acid and structural level

In order to use ARF regulators as novel drug targets against *T. brucei*, a low level of sequence identity between human and *T. brucei* ARF regulators would be ideal. This is so that inhibitors binding to essential functional regions of *T. brucei* ARF regulators would not be able to bind to and affect human ARF regulators with as great affinity. UniProt sequence alignment (Clustal Omega) of the identified *T. brucei* GEFs and GAPs against humans ARF GEFs and GAPs in section 3.3.2.1 revealed overall low levels of sequence identity. This result is a contrast to the results observed by Price *et al.*, who identified high levels of sequence identity between the 9 *T. brucei* ARF/ARLs and their closest human homologues that was identified by them (Price *et al*., 2005b). This suggests that there is a high level of diversity amongst human and *T. brucei* ARF regulators compared to the ARF/ARLs identified by Price *et al*. (2005).

Multiple protein sequence alignment showed that the Sec7 and ARFGAP domains in *T. brucei* ARF regulators and human ARF regulators were very similar at the amino acid sequence level. The Sec7 and ARFGAP catalytic domains are highly conserved and present in ARF GEFs and GAPs in all studied eukaryotes to date (Pocognoni *et al*., 2018, Arakel *et al*., 2020). Figure 3.1 showed that the ARF binding site present in GEFs are very conserved at amino acid level in two of the three identified *T. brucei* GEFs. Although TbGEF3 appears to have the ARF binding motifs, the amino acid sequence of that region does not appear to share high levels of identity

with the other GEFs. This would mean that targeting the ARF binding region in TbGEF3 via inhibitors may not inadvertently target ARF binding regions in human GEFs. Although the catalytic domains in the other *T. brucei* GEFs and GAPs appear to be conserved at the amino acid level, there is a possibility for these domains to have ARF/ARL binding specificity (Panethymitaki *et al*., 2006). It may also be possible to exploit selectivity pockets and any possible secondary structure differences to specifically target *T. brucei* ARF regulators (Spinks *et al*., 2015). Domain and structural analysis were carried out in order to identify any differences that can be exploited.

Domain analysis on human and identified *T. brucei* GEFs using SMART resource in section 3.3.2.2 highlighted the lack of PH domains in all *T. brucei* GEFs. Out of the five human ARF GEF subfamilies that was analysed in section 3.3.2.2, only CYTH, PSD and IQSEC subfamilies contained PH domains. Like the identified *T. brucei* GEFs, the ARFGEF and GBF subfamilies also lacked PH domains. This correlates with previous studies that highlighted the differences between small molecular weight GEFs and high molecular weight GEFs. Small molecular weight GEFs such as CYTH, PSD and IQSEC subfamilies contain PH domains whilst the high molecular weight GEFs such as ARFGEF and GBF subfamilies lacked the PH domains (Meissner et al., 2018, Jackson and Casanova, 2000).

The PH domains are involved in binding of specific phosphatidylinositol to membranes and other proteins such as $\beta\gamma$ subunits of trimeric G-proteins (Wang *et al*., 1994, Roy *et al*., 2016). In small molecular weight GEFs, the PH domains are required for regulating GEF activity. For example the PH domain in CYTH subfamily inhibit the association of Sec7 domain to ARF-GDP, however the binding of phosphatidylinositol (3,4,5)-trisphosphate and ARF6-GTP to the PH domain confers PH domain rearrangement and recruitment of CYTH subfamilies to the plasma membrane. This recruitment and release of autoinhibition allows CYTH to associate with ARF1/6-GDP, thus enabling the GEF activity (Roy *et al*., 2016, Lee *et al*., 2015). In contrast to the PH domain activity in CYTH subfamilies, the PH domain in PSD subfamilies act as a negative feedback loop for the association of ARF-GDP to Sec7 domain. Binding of ARF6-

GTP to the PH domain caused the inhibition of PSD Sec7 catalytic activity with ARF1 and ARF6 (Padovani *et al*., 2014). Unlike the PH domain functions in CYTH and PSD subfamilies, the PH domain in IQSEC subfamilies bind to phosphatidylinositol (4,5)-bisphosphate and increase the association of ARF-GDP to the Sec7 catalytic domain by forming part of the catalytic interface with IQSEC (Roy *et al*., 2016, Jian *et al*., 2012).

Although the high molecular weight GEFs lack PH domains, they are still able to interact with ARFs through different mechanisms, albeit not fully understood. Functional studies on yeast SEC7, closest homology to human ARFGEF subfamily, identified the Homology Downstream of Sec7 (HDS1) domain that is involved in regulating the activation and membrane recruitment of yeast SEC7 similarly to the PH domains. HDS1 domains act as an inhibitor to SEC7, preventing the association of yeast SEC7 with ARF-GDP. However in the presence of ARF1-GTP, the HDS1 domain activates the catalytic Sec7 domain in yeast SEC7 as well as the recruitment of yeast SEC7 to Trans Golgi Network (TGN); thus enabling the yeast SEC7 to associate with ARF-GTP found in the TGN (Richardson *et al*., 2012, Richardson and Fromme, 2012). The GBF subfamily also contain the HDS1 domain, however unlike the yeast SEC7/ARFGEF interaction of HDS1 domain, the GBF HDS1 domain is implicated in GBF recruitment to Golgi through binding of phosphatidylinositol (4,5)-bisphosphate, phosphatidylinositol 3-phosphate or phosphatidylinositol 4-phosphate (Meissner *et al*., 2018).

BLAST search on TriTrypDB identified the presence of PH domains in other proteins in *T. brucei*, suggesting that the lack of PH domains seen in section 3.3.2.2 may have been due to the absence of PH domains in *T. brucei* genome. The lack of PH domains in section 3.3.2.2 may also indicate that the identified GEFs are close homologues to high molecular weight GEFs such as ARFGEF and GBF subfamilies. High molecular weight GEFs are classified as GEFs that are above 100 kDa (Shinotsuka *et al*., 2002b). The calculated molecular weight of the identified *T. brucei* GEFs in Table 3.1 are shown to be above 100 kDa, further supporting the possibility of the identified GEFs to be close homologues to human ARFGEFs and GBF.

ARFGEF1, ARFGEF2, ARFGEF3 and GBF1 regulate the activities of ARF1, ARF2, ARF5 and ARF6; being involved in vesicle trafficking and coating (Boal and Stephens, 2010, Li *et al*., 2003, Shinotsuka *et al*., 2002a, Zhao *et al*., 2006, Szul *et al*., 2007). The domain similarities between these human GEFs and identified *T. brucei* GEFs may suggest that *T. brucei* GEFs could have a similar function, implicated in vesicle trafficking.

Similar to *T. brucei* ARF GEFs, the *T. brucei* ARF GAPs only consisted of the catalytic ARFGAP domains; lacking the PH domains, ANK domains, SH3 domains, SAM and GIT domains. This trait is also shared by ARFGAP and SMAP subfamilies of human GAPs. Domain analysis of the other 6 human GAP subfamilies in section 3.3.2.2 revealed the presence of a variety of domains in different subfamilies.

Similar to the human small molecular weight GEFs, the PH domain in GAPs are involved in the activation of catalytic ARFGAP domain through binding of specific phosphatidylinositol. The PH domain in ASAP subfamily initiates the catalytic activity of ARFGAP domain through the binding of phosphatidylinositol (4,5)-bisphosphate, however this activation mechanism has yet to be established (Kahn and Lambright, 2015, Luo *et al*., 2008). The binding of phosphatidylinositol (3,4)-bisphosphate and/or phosphatidylinositol (3,4,5)-trisphosphate by the C terminal PH domain in ADAP subfamily triggers the recruitment of ADAP to the plasma membrane. The other PH domain present in ADAP only binds to phosphatidylinositol (3,4,5)-trisphosphate (Stricker and Reiser, 2014, Robinson and Kanamarlapudi, 2017). Similar to the ASAP subfamily, the binding of phosphatidylinositol (4,5)-bisphosphate to the PH domains present in ACAP subfamilies activates the catalytic ARFGAP domain. However the PH domain in ACAP is also implicated in oligomerization and bending of membrane (Shi *et al*., 2012, Chan *et al*., 2017). PH domain present in AGAP subfamily are very similar to PH domains present in ADAP subfamily, initiating the activation of the catalytic ARFGAP domain in AGAP by binding to phosphatidylinositol (3,4)-bisphosphate and/or phosphatidylinositol (3,4,5)-trisphosphate, however AGAP2 GAP activity is stimulated more strongly by the binding of phosphatidylinositol (3,4,5)-trisphosphate to the PH domain (Nie *et al*., 2002, Nie *et al*., 2005). The PH domain in

AGAP1 and AGAP2 are also involved in the binding of adapter protein 3 (AP3) and adapter protein 1 (AP1) respectively. These adapter proteins are clathrin associated complexes that are required for ARF vesicle formation (Nie *et al*., 2005, Park and Guo, 2014). A unique feature of the ARAP subfamily is the presence of 5 PH domains. These PH domains bind to specific phosphatidylinositol in order to activate the catalytic ARFGAP domain (Segeletz *et al*., 2018, Campa *et al*., 2009).

The ANK domains in GAPs do not activate the ARFGAP catalytic activity directly, however they are important for the function of GAPs through interacting with other proteins and molecules. The ANK domains that are present in ASAP has been hypothesised to aid in lipid binding to PH domain (Luo *et al*., 2008), whilst the three ANK domains present in ACAP are involved in cargo binding to ACAP (Chan *et al*., 2017, Bai *et al*., 2012). AGAP ANK domains are hypothesised to function similarly to the ASAP subfamily ANK domains. The ANK domains present in GIT subfamily are involved in binding to endosomes (Hoefen and Berk, 2006).

The other domains present in human GAPs are also involved in various functions that indirectly aid in GAP activities. The SH3 domain present near the C terminal of ASAP is involved in the binding of focal adhesion tyrosine kinase (Randazzo *et al*., 2000). The SAM domain in ARAP subfamily interacts with SHIP2, a SH2 containing inositol 5-phosphatase. The binding of phosphatidylinositol initiates GAP activity in ARAP GAPs, however the binding of SHIP2 via SAM domain is hypothesised to induce a negative feedback in ARAP through dephosphorylation of specific phosphatidylinositol, thus deactivating the GAP functions of ARAP (Raaijmakers *et al*., 2007, Leone *et al*., 2009). Another unique feature of ARAP subfamily is the presence of RhoGAP domain as well as the ARFGAP domain. This means that ARAP subfamily can regulate ARF proteins and Rho GTP-binding proteins. However the RhoGAP domain in ARAP2 is inactive, suggesting that ARAP1 and ARAP3 might be the only members of the ARAP subfamily that can regulate ARF and Rho GTP-binding proteins (Miura *et al*., 2002). The GIT domains (also known as Spa2 homology domain) present in GIT

subfamily of ARF GAPs bind to p21 activated kinase interacting exchange factors (Hoefen and Berk, 2006, Webb *et al*., 2006).

The ARFGAP and SMAP subfamilies of human GAPs lacked the PH, ANK, GIT, SAM and SH3 domains that were described above. Instead these GAP subfamilies are hypothesised to initiate the ARFGAP activity through a mechanism that is not fully understood. Previous studies have identified the SMAP subfamily role in clathrin dependent endocytosis (Tanabe *et al*., 2005) whilst ARFGAP2 and ARFGAP3 initiate uncoating via binding to coatomer (Shiba *et al*., 2011, Beck *et al*., 2009). ARFGAP1 on the other hand is implicated in the COPI complex (Bai *et al*., 2011). The lack of additional domains in identified *T. brucei* GAPs may suggest that the *T. brucei* GAPs may also be implicated in similar functions as ARFGAP and SMAP subfamilies.

The results of domain similarities observed in section 3.3.2.2 may suggest that the *T. brucei* GEFs may function similarly to the human ARFGEF and GBF subfamilies. The same can be hypothesised for *T. brucei* GAPs and the human ARFGAP and SMAP subfamilies. However, protein functional studies and domain interaction studies need to be carried out in order to confirm this hypothesis since a generalisation could not be made with the available data. An example of experiment that can be used to identify domains in the *T. brucei* GEFs and GAPs would be analysis of crystal structures. Mossessova *et al.* (1998), Goldberg (1999) and Mandiyan *et al.* (1999) all studied crystal structures of GEFs and GAPs in order to identify domains that are present (Mossessova *et al*., 1998, Mandiyan *et al*., 1999, Goldberg, 1999). Other techniques that can be used include NMR and mass spectrometry.

As no previous data were available on *T. brucei* ARF regulators or their structures, Phyre2 was utilised to predict the structure of the identified ARF regulators (Kelley *et al*., 2015). However Phyre2 predicted 30% - 45% of the whole sequence at 100% confidence for *T. brucei* GAPs and 10% - 18% of the whole sequence at 100% confidence for *T. brucei* GEFs. Phyre2 protein structure prediction occurs with the aid of pre-existing templates of homologous proteins structures. The lack of structural data available on *T. brucei* ARF regulators may have resulted

in Phyre2 software predicting the highly conserved catalytic Sec7 and ARFGAP domains with 100% confidence.

Visualisation and analysis of the Phyre2 predicted structure on PyMOL Molecular Graphics System, Version 2.0 in section 3.3.2.3 highlighted the structural differences between *T. brucei* GEFs and GAPs. All of the identified *T. brucei* GEFs were predicted to have α-helices structure, with TbGEF1 and TbGEF2 consisting of 10 α-helices and TbGEF3 consisting of 12 α-helices (Figure 3.7). The identified *T. brucei* GAPs on the other hand were predicted to have α-helices and β-sheets structures, albeit with differences in the number of α-helices and β-sheets present in each identified *T. brucei* GAP (Figure 3.6).

Mandiyan *et al.* (1999) described the crystal structure of PAPβ ARFGAP domain in their study. They identified the presence of 3 β-sheets flanked by 5 α-helices and a Zn^{2+} ion coordinated by the $CX_2CX_{16\text{-}17}CX_2C$ sequence motifs. This structure was similar to the structure observed by Goldberg (1999) in rat ARFGAP (Mandiyan *et al*., 1999, Goldberg, 1999), suggesting that the ARFGAP domain has a conserved structure. The β-sheets flanked by α-helices motif can also be observed in the predicted structures for the identified *T. brucei* GAPs: TbGAP1, TbGAP3 and TbGAP4 as described above. The predicted structure of TbGAP1 is very similar to the ARFGAP structure observed by Mandiyan *et al.* (1999). Although TbGAP3 and TbGAP4 consisted of the β-sheets flanked by α-helices motif, TbGAP3 consisted of 2 β-sheets flanked by 5 α-helices whilst TbGAP4 consisted of 3 β-sheets flanked by 6 α-helices. The similarities between the predicted structures of *T. brucei* GAP and the PAPβ ARFGAP domain observed by Mandiyan *et al.* suggests that the predicted structure of the *T. brucei* GAPs by Phyre2 could have been the ARFGAP domain. This may also explain the 30% - 45% of the whole sequence being predicted at 100% confidence since the ARFGAP domain is made up of 130 amino acids and are highly conserved (Frigerio *et al*., 2007, Schlacht *et al*., 2013).

Structural alignment of predicted *T. brucei* GAP structures with all available human GAP structures from RCSB Protein Data Bank identified various degrees of structural similarities

amongst the *T. brucei* GAPs. TbGAP1 was identified to be structurally similar to ARFGAP1, SMAP2 and ADAP1. TbGAP3 was structurally similar to ARFGAP1, AGAP3, ADAP1 and SMAP2. TbGAP4 was structurally similar to ASAP3 and ACAP1. Despite TbGAP2 not consisting of the β-sheets flanked by α-helices motif, structural alignment showed that TbGAP2 was structurally similar to ADAP1, SMAP1 and SMAP2. The protein structure of human ARFGAP1, SMAP2, ASAP3, ACAP1 and ADAP1 showed the crystal structure ARFGAP domain, whilst the protein structure of SMAP1 is shown to be the ARFGAP domain in solution. The high level of structural similarities of these ARFGAP domain structure to predicted structure of identified *T. brucei* GAPs highlights the possibility of the predicted structure of *T. brucei* GAPs being the conserved ARFGAP domain. An interesting observation to be made is the structural similarity of TbGAP3 to AGAP3 crystal structure of Ras like domain. This structural similarity is not shared by the other identified *T. brucei* GAPs, suggesting that TbGAP3 may also exhibit regulatory effect on Ras-like GTPase proteins in a similar mechanism to human ARAP subfamilies. Despite the presence of Ras-like GTPase proteins, *T. brucei* does not express true members of the Ras GTPases (Field, 2005).

Similar to the ARFGAP domains, the Sec7 catalytic domain present in ARF GEFs are also highly conserved with a 200 amino acid sequence (Jackson and Casanova, 2000, Mansour et al., 1999). The structure of ARNO (Cytohesin-2) Sec7 domain was determined at 2.2 Å resolution by Mossessova *et al.* (1998) who showed that the Sec7 domain is made up 10 α-helices, 7 N-terminal α-helices that form a right handed superhelix and 3 C-terminal α-helices (Mossessova *et al*., 1998). The Sec7 domain also consisted of a distinctive hydrophobic groove, which was later identified to contain a glutamic finger by Béraud-Dufour *et al*. (1998). Béraud-Dufour *et al.* proposed that this glutamic finger in the hydrophobic groove may interact with the Mg^{2+} found in the switch regions of the ARFs (Beraud-Dufour *et al*., 1998). Similar structure was observed for the predicted structures of the three identified *T. brucei* GEFs as describes above. The predicted structures for TbGEF1 and TbGEF2 were identical to the structure studied by Mossessova *et al.* (1998), consisting of 10 α-helices. Although the

predicted structure for TbGEF3 consists of the α-helices motif as described by Mossessova *et al*. (1998) and Béraud-Dufour *et al*. (1998), TbGEF3 also contains additional 2 α-helices. The similarities between the predicted *T. brucei* GEF structures by Phyre2 and the Sec7 domain of ARNO described by Mossessova *et al*. (1998) suggest that Phyre2 successfully predicted the Sec7 domain that are present in the identified *T. brucei* GEFs. This is further supported by the percentage of sequence covered by Phyre2. Phyre2 predicted 10% - 18% of the whole sequence at 100% confidence for *T. brucei* GEFs. The Sec7 domain is 200 amino acids long whilst the whole *T. brucei* GEF sequences are 1046 – 2054 amino acids long, correlating to the percentage covered at 100% confidence by Phyre2.

The structural alignment of predicted *T. brucei* GEFs against all available human GEFs on PyMOL Molecular Graphics System, Version 2.0 showed that all three of the identified *T. brucei* GEFs were structurally more similar to CYTH1 and CYTH2 than the other GEF protein structures. However the proteins structures of CYTH1 and CYTH2 on the RCSB Protein Data Bank are crystal structures of the Sec7 domain, suggesting that the high level of structural similarities was due to the highly conserved Sec7 domain. An interesting observation that can be made from the RMS values for structural alignment in section 3.3.2.3 is the low level of structural similarities between ARFGEF1 crystal structure of Sec7 domain and the identified *T. brucei* GEFs. The ARFGEF subfamily were shown to have similar domain composition as the identified *T. brucei* GEFs, lacking the PH domain. The low level of structural similarities may suggest that despite *T. brucei* GEFs not having the PH domain, they could function similarly to the CYTH subfamily. However further functional studies and protein interaction studies need to be carried out in order to give a conclusive answer.

3.4.3 Predicted protein localisation of TbGEFs and TbGAPs may not be accurate in bloodstream form *T. brucei*

The prediction of subcellular localisation of proteins using bioinformatics can aid in the understanding of their relationship and function (Pang *et al*., 2019). Previous studies on human ARFs and their regulators have identified their subcellular localisation, the relationships between the ARF and their regulators, as well as their functions. Although Price *et al.* identified 9 ARF/ARLs in *T. brucei*, there is a lack of information available on the relationship between ARF/ARLs and their regulators as well as the subcellular localisation of the regulators. TrypTag was used in order to identify the subcellular localisation of the identified *T. brucei* GEFs and GAPs.

TrypTag is a *T. brucei* protein localisation resource that has data on proteins that are tagged with mNeonGreen tag at N and/or C terminals (Dean *et al*., 2017). The current data available on TrypTag is based on the procyclic form of *T. brucei* that are found in the tsetse midgut as opposed to the mammalian infectious bloodstream form *T. brucei* on which this thesis will be focusing. The difference in environment during trypanosome life cycle results in *T. brucei* adapting accordingly. For example the bloodstream form *T. brucei* relies on glucose that are present in the mammalian blood in order for metabolism to occur, whilst the procyclic form *T. brucei* adapts to use amino acids such as proline and threonine for metabolism (Millerioux *et al*., 2018). The rate of endocytosis has also been shown to be different, with bloodstream form *T. brucei* having a higher rate of metabolism than compared to the procyclic form *T. brucei* (Natesan *et al*., 2011). The procyclic and bloodstream form *T. brucei* express proteins differentially. Procyclic form *T. brucei* express surface glycoproteins called procyclic acidic repetitive proteins (PARPs) that aids in the immune evasion (Castillo-Acosta *et al*., 2017). The bloodstream form *T. brucei* on the other hand expresses antigenic variant surface glycoproteins (VSGs) that enable the parasite to evade host immune response and establish a chronic infection (Castillo-Acosta *et al*., 2017, Kolev *et al*., 2018).

Endocytosis occurs at the flagellar pocket via coated vesicles in bloodstream for *T. brucei*. Interestingly these coated vesicles are absent in procyclic form *T. brucei*, instead relying on cysteine-rich acidic transmembrane proteins (CRAM). The absence of coated vesicles suggests that the functions of ARF/ARLs and their regulators may also differ in the procyclic form (Liu *et al*., 2000, Qiao *et al*., 2006). This could mean that the localisation data obtained from TrypTag on *T. brucei* ARF/ARLs and their regulators in section 3.3.3 may not always be applicable to protein localisation in bloodstream form *T. brucei*. Tagging identified *T. brucei* GEFs and GAPs as well as the 9 ARF/ARLs using fluorescent marker proteins in bloodstream form *T. brucei* may aid in accurate identification of localisation in bloodstream form *T. brucei*.

TrypTag tags proteins using mNeonGreen, a monomeric 26 kDa fluorescent protein (Stockmar *et al*., 2018). mNeonGreen is tagged at the N terminus and C terminus of the protein. ARF/ARLs are small GTPases (~22 kDa) that are myristoylated at the N terminus, this N-myristoylation allows the ARF/ARLs to associate to the membrane during activation (Padovani *et al*., 2013, Liu *et al*., 2009). Tagging of mNeonGreen at the N terminus would inhibit myristoylation at the N terminus, thus affecting the function and localisation of the ARFs. With this in mind, I focused primarily on the localisation data for C terminus tagged proteins. The large size of mNeonGreen in comparison to ARF/ARLs may also affect the function of ARF/ARLs as well as their interactions with GEFs and GAPs in *T. brucei*.

Localisation data in section 3.3.3 highlighted the localisation of TREU927 homologues of *T. brucei* GEFs and GAPs, as well as the 9 identified ARF/ARLs. TrypTag data showed that some of the ARF/ARLs and identified regulators were localised at the same place in *T. brucei*. However this localisation data does not provide information on which ARF/ARLs interact with the identified *T. brucei* GEFs and GAPs. To overcome this disadvantage, protein-protein interaction studies using biotin identification (BioID) could be used. The identified *T. brucei* GEFs and GAPs can be fused with mutated version of *E. coli* biotin ligase (BirA*). Reactive bioAMP are readily released by BirA*, these bioAMP covalently interact with primary amines

present in proximity to BirA* fused proteins. The biotinylated proteins can then be isolated via streptavidin affinity purification and identified through mass spectrometry (Khan *et al*., 2018).

3.4.5 Putative orthologues of *T. brucei* ARF regulators in other Kinetoplastids may have similar functions

Kinetoplastids are parasites that are distinguished by the presence of kDNA. These parasites include *Trypanosoma brucei*, *Trypanosoma cruzi* and *Leishmania spp*. All three parasites have a lifecycle that takes place in both invertebrate host and vertebrate host (Filardy *et al*., 2018). However *T. cruzi* and *Leishmania spp*. are intracellular, infecting a wide range of cells and phagolysosomes of macrophages respectively (Salassa and Romano, 2018, Kohl *et al*., 2018), whilst *T. brucei* are exclusively extracellular (Pays and Vanhollebeke, 2009).

OrthoMCL was used to check if orthologues of the identified *T. brucei* GEFs and GAPs are present in other kinetoplastids. Results in section 3.3.4 highlighted the presence of GEFs and GAPs orthologues in other kinetoplastids. Multiple sequence alignment of the *T. brucei* GEFs and GAPs and their orthologs in other kinetoplastids showed that majority of the sequences were similar on the amino acid level (Appendix 3 - 8). This suggests that the orthologues may function similarly. Orthologues of TbGEF3 and TbGAP3 were absent in *T. cruzi*, a possible explanation for this could be due to how *T. cruzi* undergoes endocytosis.

The flagellar pocket, an invagination of the cell surface located where the flagellum exits is the site where endocytosis primarily occurs in kinetoplastids. Endocytosis in *T. brucei* is mediated by *T. brucei* clathrin heavy chain (TbCLH), with Morgan *et al.* (2001) identifying the correlation between TbCLH and endocytosis (Morgan et al., 2001). Clathrin dependent endocytosis in *T. brucei* was further proven by Allen *et al.* (2003) through RNAi studies. Showing that RNAi of TbCLH disrupted endocytosis and became lethal to bloodstream form *T. brucei* (Allen et al., 2003). Similarly *Leishmania* utilises clathrin dependent endocytosis. Agarwal *et al*. (2013) identified that overexpression of *Leishmania* clathrin heavy chain (Ld-CHC) lead to enhanced

uptake of haemoglobin, whilst expression of clathrin hub fragment in *Leishmania* proved to be fatal (Agarwal *et al*., 2013, Rastogi *et al*., 2016). Interestingly *T. cruzi* exhibits clathrin dependent and independent endocytosis. Kalb *et al.* (2014) demonstrated that *T. cruzi* clathrin heavy chain (TcCHC) and light chain (TcCLC) were localised to the flagellar pocket and were utilised in endocytosis of albumin. However endocytosis of transferrin was cholesterol dependent and occurred at the cytostome/cytopharynx complex (Kalb *et al*., 2014). The cytostome/cytopharynx complex is located near the flagellar pocket, this complex consists of an opening in the membrane referred to as cytostome and a deep membrane invagination referred to as cytopharynx (Alcantara *et al*., 2017). Alcantara *et al*. (2014) stated that although *T. cruzi* utilises flagellar pocket for clathrin dependent endocytosis, the main site of endocytosis in *T. cruzi* is at the cytostome/cytopharynx complex via clathrin independent (Alcantara *et al*., 2014).

This difference in endocytosis in *T. cruzi* may explain the absence of TbGEF3 and TbGAP3 orthologues. Section 3.3.3 identified the subcellular localisation of TREU927 homologues of TbGEF3 and TbGAP3 to be in flagellar pocket and flagellum respectively. The subcellular localisation of TbGEF3 and TbGAP3 could possibly mean that these two ARF regulators may be implicated in endocytic functions at the flagellar pocket. The preference of *T. cruzi* utilising cytostome/cytopharynx complex as the main site of endocytosis could have meant that *T. cruzi* may have adapted to avoid utilising the functions of TbGEF3 and TbGAP3 in the flagellar pocket and flagellum respectively. However the function of TbGEF3 and TbGAP3 could not be confirmed with the available data in this chapter. Protein-protein interactions studies described in section 3.4.3 and protein functional studies could give more insight into the function of TbGEF3 and TbGAP3. Likewise, assumptions could not be made for the orthologues of *T. brucei* GEFs and GAPs in other kinetoplastids. Further studies need to be carried in order to understand the specific functions of *T. brucei* GEFs and GAPs and their orthologues in other kinetoplastids.

3.5. Conclusions

The main findings of this chapter are as follows:

- Homologues of human ARF regulators were identified in *T. brucei* – BLASTP was used to identify 3 *T. brucei* GEFs and 4 *T. brucei* GAPs that were followed up for further analysis.
- There is a high level of diversity between human and *T. brucei* ARF regulators on the amino acid level.
- *T. brucei* GEFs and GAPs lacked additional protein-protein interaction domains that are present in many human GEFs and GAPs.
- *T. brucei* GEFs and GAPs appear structurally similar to some human ARF regulator subfamilies.
- *T. brucei* ARF regulators are predicted to be localised in the cytoplasm and endocytic pathways
- Orthologues of TbGEF3 and TbGAP3 were absent in *T. cruzi* but present in *Leishmania* and *Trypanosoma spp*.

In order to understand the function of the identified *T. brucei* GEFs and GAPs within bloodstream form *T. brucei*, the next stage of the investigation was to knockdown the expression of the identified *T. brucei* GEFs and GAPs using an inducible RNAi system. The observation of the effect of RNAi for each *T. brucei* GEFs and GAPs in bloodstream form *T. brucei* should highlight the essential GEFs and GAPs and their possible functions within bloodstream form *T. brucei*.

Chapter 4 – Identification of essential ARF regulators in bloodstream form *T. brucei*

4.1 Introduction

Currently eight registered drugs are used to treat African Trypanosomiasis; suramin, pentamidine, melarsoprol, eflornithine and fexinidazole for Human African Trypanosomiasis (HAT); and diminazene aceturate, homidium and isometamidium against Animal African Trypanosomiasis i.e. nagana. These drugs are disease stage and *T. brucei* subspecies specific. As mentioned in Chapter 1 Section 1.1.7, the emergence of drug resistance, adverse side effects and low efficacy of these drugs means that research into alternative drug targets is essential (Moreno *et al*., 2019, Giordani *et al*., 2016, Baker and Welburn, 2018). An ideal drug target is defined by several rules including:: 1) absent in host or sufficiently different in order for specific targeting; 2) essential for survival of the host-stage parasite; and 3) 'druggable' (Ilari *et al*., 2018, Kandoi *et al*., 2015).

A 'druggable' biological target is a molecule (usually a nucleic acid, peptides or proteins) that has the potential to bind to drugs which alter its biological functions (Hussein *et al*., 2017). A 'druggable' target should also be able to have the capacity to change disease progression whilst having low impact on the modulation of physical conditions of the host (Kandoi *et al*., 2015, Gashaw *et al*., 2011, Ilari *et al*., 2018). Previous studies on ARF/ARLs have identified inhibitors that can alter or inhibit their functions, demonstrating that ARF/ARLs could be used as a 'druggable' target (Benabdi *et al*., 2017). Moreover, RNAi induced knockdown of *T. brucei* ARF/ARLs has demonstrated that several of these ARF/ARLs are essential for *T. brucei* viability (Price *et al*., 2005b, Price *et al*., 2010b, Price *et al*., 2007b). However sequence alignment showed a high percentage of sequence similarity with *T. brucei* and human ARF/ARLs, especially at the essential binding sites (Price *et al*., 2005b, Price *et al*., 2005a). This high level of similarity between human and *T. brucei* ARF/ARLs may mean that inhibitors to the parasite proteins could also bind to human ARFs, contradicting the first rule for an ideal drug target. Therefore, ARF/ARLs may not be ideal drug targets against HAT.

ARF/ARLs are regulated by guanine nucleotide exchange factors (GEFs) and GTPase activating proteins (GAPs), activating and inactivating the ARF/ARLs respectively. In the

previous chapter, I identified three GEFs and four GAPs in *T. brucei* through BLASTP searches on known human ARF regulator protein sequences. However, amino acid sequence alignment to compare identified *T. brucei* and human ARF regulators showed a low level of overall sequence similarity, but the catalytic domains that regulate ARF functions were highly conserved; with the exception of *TbGEF3*.

Bioinformatics analysis in the previous chapter identified the domain and structural similarities of *T. brucei* GEFs and GAPs to human GEFs and GAPs, as well as the possible localisation of these proteins in *T. brucei*. However due to lack of available data, bioinformatics analysis alone could not determine the functions of the GEFs and GAPs in *T. brucei* or identify which of these regulators are essential for bloodstream form *T. brucei* viability.

Previous studies highlighting essential genes in *T. brucei* used tetracycline inducible RNAi systems to knock down the function of a particular gene (Alibu *et al*., 2005). RNAi is a gene expression knockdown mechanism that utilises small interfering RNAs (siRNAs) and microRNAs (miRNA) which are incorporated into the RNA-induced silencing complex (RISC), causing mRNA translation interference and knockdown of target gene (Fire *et al*., 1998, Ding *et al*., 2018). The same RNAi system was used to highlight the essential ARF/ARLs in bloodstream form *T. brucei* (Price *et al*., 2007b, Price *et al*., 2005b, Price *et al*., 2012).

4.1.1 Aims

The aim of the work described in this chapter was to identify which of the Tb*GEF*s and Tb*GAP*s are essential for the viability of bloodstream form *T. brucei* and to identify the effects of RNAi on these genes.

4.2 Methods

Molecular laboratory techniques were used in order to generate and transfect RNAi constructs into bloodstream form *T. brucei* and then to identify the effect of GEF/GAP knockdowns on bloodstream form *T. brucei* viability and morphology. The methods used in this chapter are as follows:

4.2.1 Selection and amplification of RNAi regions

RNAi regions for each *T. brucei* GEFs and GAPs were selected and amplified using PCR with suitable *Xba*I restriction sites.

4.2.2 Generation of RNAi constructs

Amplified RNAi regions were ligated to the P2T7^{Ti} vector and transformed into One Shot® TOP10 Chemically Competent *E. coli*. Plasmid DNA were then isolated and purified.

4.2.3 Transfection

RNAi constructs were subjected to restriction digest by *Not*I restriction enzyme and then purified via enzymatic purification. The linearised RNAi constructs were prepared for transfection and transfected into mid-log phase bloodstream form *T. brucei*. Transfected cells were incubated at 37°C with 5% CO_2.

4.2.4 Induction of RNAi

RNAi of the transfected bloodstream form Lister 427 *T. brucei* was induced by adding tetracycline. The density of the parasites was determined by counting the number of parasites using a haemocytometer.

4.2.5 Propidium Iodide flow cytometry

Mid-log phase bloodstream form Lister 427 *T. brucei* incubated in tetracycline at different time points were harvested and a propidium iodide flow cytometry was carried out.

4.2.6 Live/Dead flow cytometry

Mid-log phase bloodstream form Lister 427 *T. brucei* incubated in tetracycline at different time points were harvested and stained with Live/Dead Fixable Red Dead Stain. The sample were then processed using flow cytometry.

4.2.7 Quantitative polymerase chain reaction (qPCR)

Total RNA was extracted from mid-log phase bloodstream form *T. brucei* following induction of RNAi at different time points. cDNAs were generated from the RNA samples and a qPCR reaction was set up.

4.2.8 Indirect immunofluorescent microscopy

Log-phase bloodstream form *T. brucei* were harvested and processed for indirect immunofluorescent microscopy. Primary mouse monoclonal antibody 1 (TAT1) against *T. brucei* α-tubulin and primary anti-rabbit monoclonal antibody against paraflagellar rod protein 1 (PFR1) were used.

4.2.9 Transmission Electron Microscopy (TEM)

Log-phase bloodstream form *T. brucei* were harvested and processed for TEM.

4.2.10 Concanavalin A (Con A) endocytosis assay

Log-phase bloodstream form *T. brucei* samples incubated at different time points in tetracycline were harvested and prepared for endocytosis assay. Concanavalin A was used to determine defects in endocytosis.

4.3 Results

4.3.1 Identification and amplification of RNAi regions

In order to carry out RNAi of the identified *T. brucei* GEFs and GAP, a suitable RNAi region was identified for each of the genes using RNAit – target selection for Trypanosoma genomes (http://dag.compbio.dundee.ac.uk/RNAit/ - accessed: Nov 2018), a web-based tool for the identification of RNAi regions and primers in kinetoplastids. This was done to ensure that the possibility of cross or co-suppression was avoided between closely related genes (Redmond *et al*., 2003). The RNAi regions were then checked for possible presence of *Xba*I restriction sites using Webcutter 2.0 (http://www.firstmarket.com/cutter/cut2.html - accessed: Nov 2015).

The selected regions for RNAi were amplified using Polymerase Chain Reaction (PCR) and visualised by agarose gel electrophoresis. Figure 4.1 shows the successful amplification of the RNAi regions from genes encoding six putative *T. brucei* ARF regulators. The seventh ARF regulator (TbGAP3) was not successfully amplified. New primers were designed but the amplification of GAP3 was still unsuccessful, therefore no further work was carried out on this putative regulator.

The known size of the RNAi regions for each *T. brucei* GEFs and GAPs are as follows: TbGAP1 – 397bp; TbGAP2 – 457bp; TbGAP3 – 398bp; TbGAP4 – 427bp; TbGEF1 – 469bp; TbGEF2 – 503bp; and TbGEF3 – 483bp. These sizes were compared to the gel electrophoresis image of the amplified PCR products. The close proximity of the size of the PCR products to the known size of the RNAi region suggest that the amplification of the region was successful (Figure 4.1).

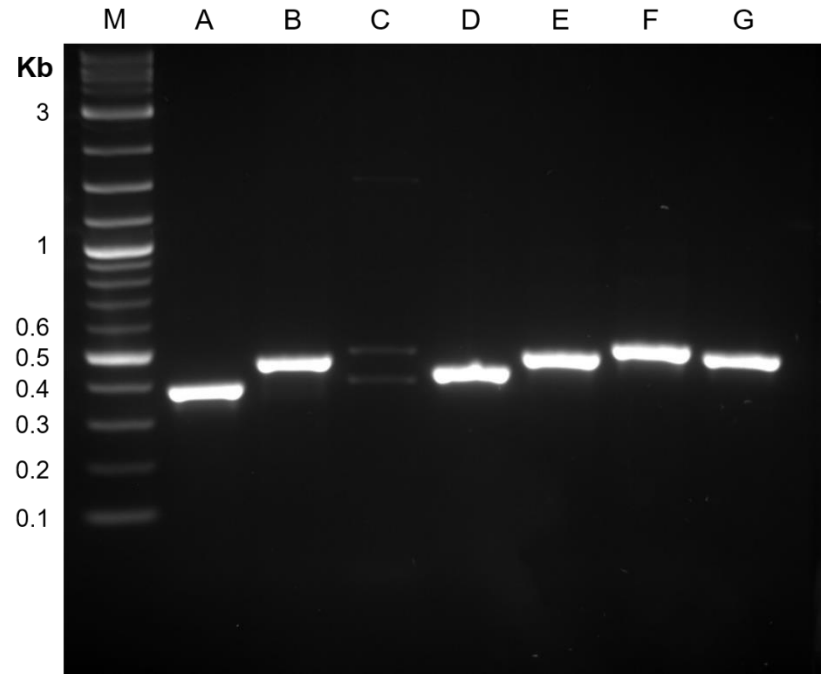

Figure 4.1. Amplification of* T. brucei *GEFs and GAPs RNAi regions. *RNAi regions of (A) TbGAP1, (B) TbGAP2, (D) TbGAP4, (E) TbGEF1, (F) TbGEF2 and (G) TbGEF3 were amplified using PCR technique and visualised by agarose gel electrophoresis (1.5% agarose). Despite several attempts, amplification of (C) TbGAP3 was not successful. Quick-Load® 2-log DNA ladder (M) was used as marker.*

4.3.2 Generation of RNAi constructs and transfection

The amplified RNAi regions of *T. brucei* ARF regulators were ligated into the P2T7^{Ti} vector. The P2T7^{Ti} RNAi system was used in this thesis to induce knockdown of identified *T. brucei* ARF regulators, since this system overcame the transient effect of other RNAi systems (Ngô *et al*., 1998). The P2T7^{Ti} vector consists of two inverted repeat T7 promoters with a downstream Tet Operator (TetOP) (LaCount and Donelson, 2001). The transgenic bloodstream form *T. brucei* strain Lister 427 expresses Tet repressor (TetR) and T7 RNA Polymerase (Poon *et al*., 2012). The TetR binds to TetOP (Figure 4.2.B), which prevents the transcription of the RNAi region by T7 RNA Polymerase from the T7 promoter site (LaCount *et al*., 2000, Alibu *et al*., 2005). However addition of tetracycline prevents the binding of TetR

to TetOP (Figure 4.2.C), thus enabling transcription of the target RNAi region to occur. Transcription of the RNAi region produces dsRNAs that are then cleaved by TbDCL1 and TbDCL2 into small interfering RNAs (siRNAs). These siRNAs are incorporated into the RISC complex which induces gene knockdown (Shi *et al*., 2009).

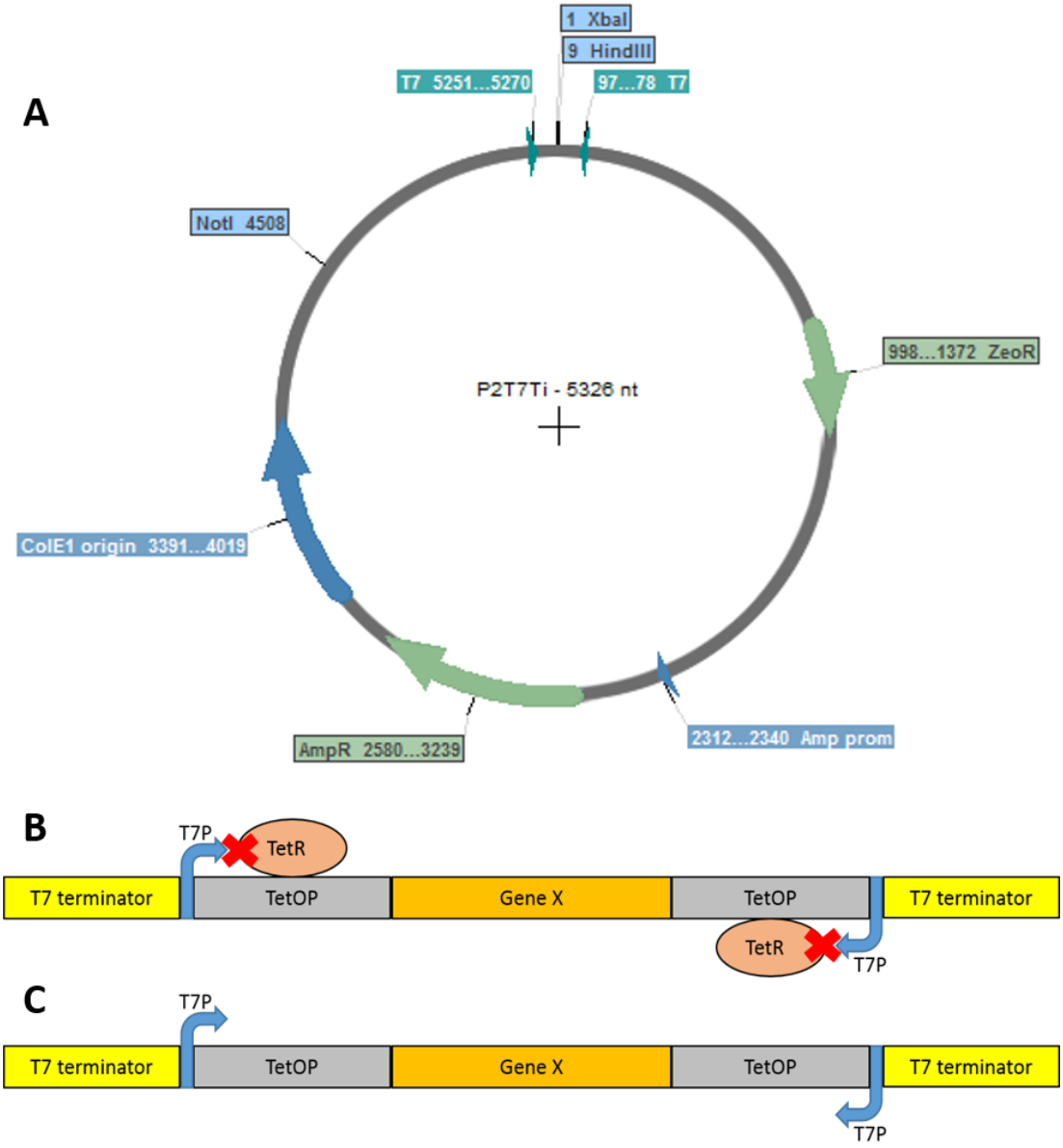

Figure 4.2. Schematic representation of the P2T7^{Ti} vector and the function of the vector. *The P2T7^{Ti} vector consists of T7 promoters and Tet Operators (TetOP). Tet Repressors (TetR) present in the transgenic cell lines bind to TetOP preventing transcription of the target RNAi region (B). Addition of tetracycline prevents the binding of TetR to TetOP (C), thus allowing transcription to occur.*

The available P2T7^{Ti} vector was already ligated to TbARL6. Therefore a restriction digest using *Xba*I restriction enzyme was carried out in order to isolate the P2T7^{Ti} vector. Successful digestion and isolation of the P2T7^{Ti} vector was visualised using gel electrophoresis (Figure 4.3). Amplified RNAi regions were also subjected to *Xba*I restriction digest prior to ligation in order to facilitate easier ligation.

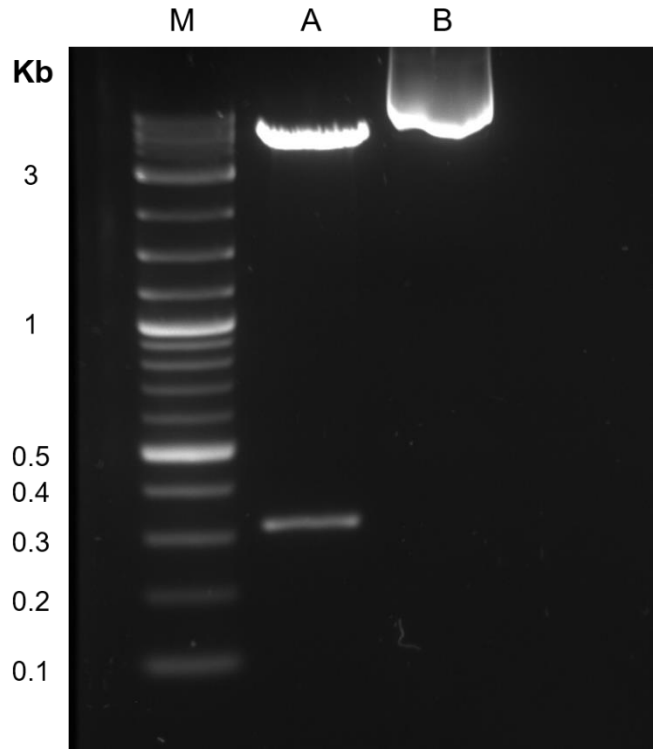

Figure 4.3. P2T7^{Ti} vector digest. *Visualisation of (A) restriction and (B) undigested P2T7-ARL6 vector on 1.5% Agarose gel. Restriction digest was performed using* Xba*I restriction digest. Quick-Load® 2-Log DNA Ladder (M) was used as a marker.*

The ligated P2T7^{Ti}-*TbGEF*/*GAP* plasmid was transformed into chemically competent *E. coli* in order to generate large quantities of recombinant DNA for transfection. Transformed *E. coli* cells were grown on agar with ampicillin. Recombinant plasmid DNA was purified from successfully grown *E. coli* colonies. In order to check the presence of RNAi inserts in the eluted recombinant DNA, the DNA samples were subjected to restriction digest with *Xba*I and then visualised on gel electrophoresis (Figure 4.4 and Figure 4.5).

Figures 4.4 and 4.5 showed that transformation of *TbGAP1*, *TbGAP4*, *TbGEF1*, *TbGEF2* and *TbGEF3* were successful due to the presence of large bands (>5000bp) indicating the P2T7^{Ti} vector, and small bands (300bp to 5000bp) which indicates the presence of the inserts. Despite transformation of *TbGAP2* producing ampicillin resistant *E. coli* colonies, the eluted recombinant DNA did not show presence of the TbGAP2 RNAi insert (Figure 4.5).

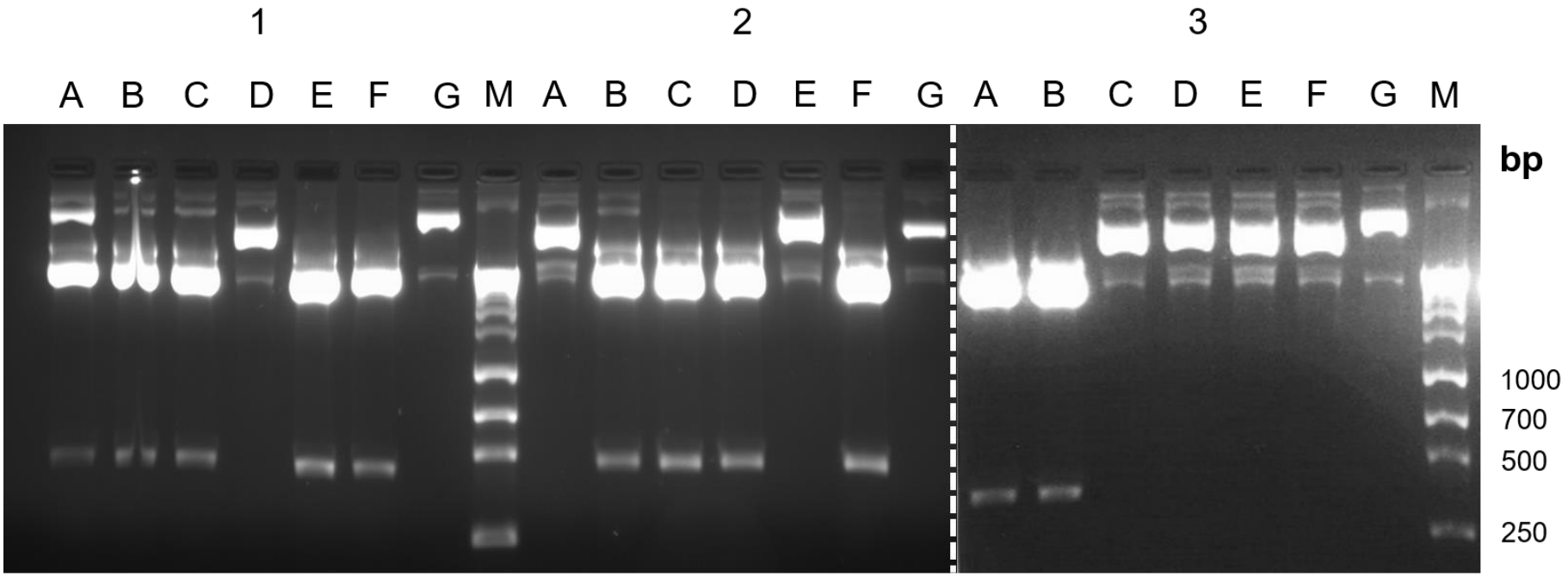

Figure 4.4. Visualisation of TbGEF RNAi inserts in P2T7^{Ti} plasmid DNA. *Plasmid DNAs were purified from transformed colonies and subjected to restriction digest using* XbaI *restriction enzyme. Digested products were visualised on 1.5% Agarose gels. Two separate bands in some colonies confirmed the presence of RNAi inserts for (1) TbGEF3, (2) TbGEF2 and (3) TbGEF1. 1kb+ Hyperladder (M) was used as a marker.*

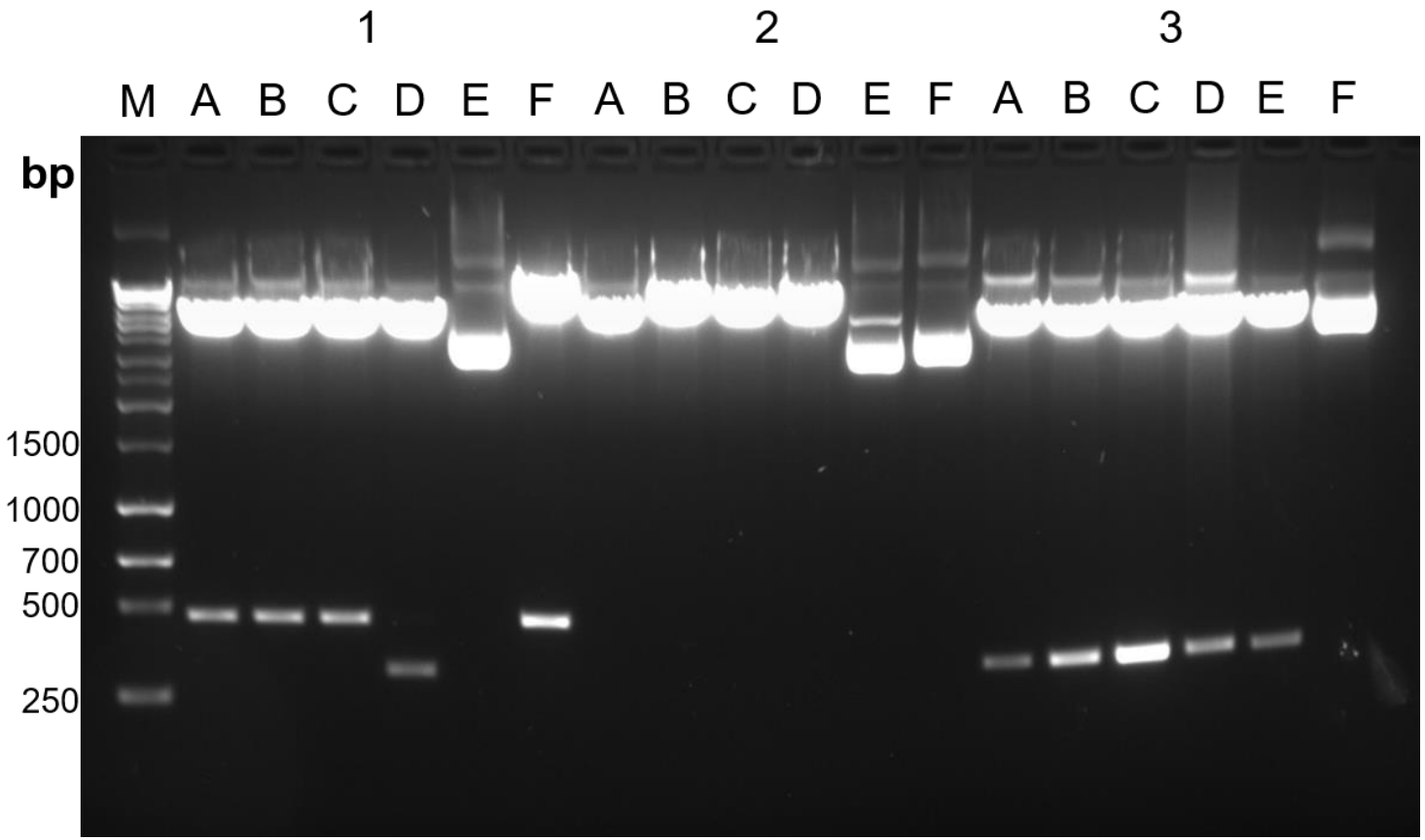

Figure 4.5. Visualisation of TbGAP RNAi inserts in P2T7^{Ti} plasmid DNA. *Plasmid DNAs were purified from transformed colonies and subjected to restriction digest using XbaI restriction enzyme. Digested products were visualised on 1.5% Agarose gels. Two separate bands in some colonies confirmed the presence of RNAi inserts for (1) TbGAP1 and (3) TbGAP4. No inserts were detected in colonies transfected with (2) TbGAP2. 1kb+ Hyperladder (M) was used as a marker.*

The eluted recombinant DNA samples were subjected to restriction digest by *Not*I restriction enzyme in order to linearise the recombinant DNA. The samples were prepared for transfection and transfected into Lister 427 bloodstream form *T. brucei*. Transfected bloodstream form *T. brucei* were grown in HMI-9 media with the presence of phleomycin and neomycin at 37°C and 5% CO_2.

Transfected cell lines will be referred to by their respective RNAi genes. Transfection of P2T7-*TbGAP1*, P2T7-*TbGAP4*, P2T7-*TbGEF2* and P2T7-*TbGEF3* RNAi genes generated stable bloodstream form Lister 427 *T. brucei* cell lines that were taken forward for further studies. Three attempts were made at transfection of P2T7-*TbGEF1* gene into bloodstream form Lister 427 *T. brucei*, but despite attempts at growing 72 wells of transgenic cells, no wells generated stable cell lines from 24 hours post transfection.

4.3.3 Effects of RNAi on parasite growth

Three transfected cell lines from each TbGEFs and TbGAPs were randomly selected to identify the effect of RNAi of each gene on bloodstream form *T. brucei* growth. Transfected parasite cell lines were grown in selective HMI-9 media and RNAi was induced with the addition of tetracycline. The number of parasites were counted at 24 hours intervals for 72 hours. The same was done for control cultures for each of the TbGEF and TbGAP cell lines, which were grown in the absence of tetracycline. The effect of addition of tetracycline on wild type Lister 427 bloodstream form *T. brucei* was also determined as a control to ensure that no effects were due to presence of the antibiotic alone.

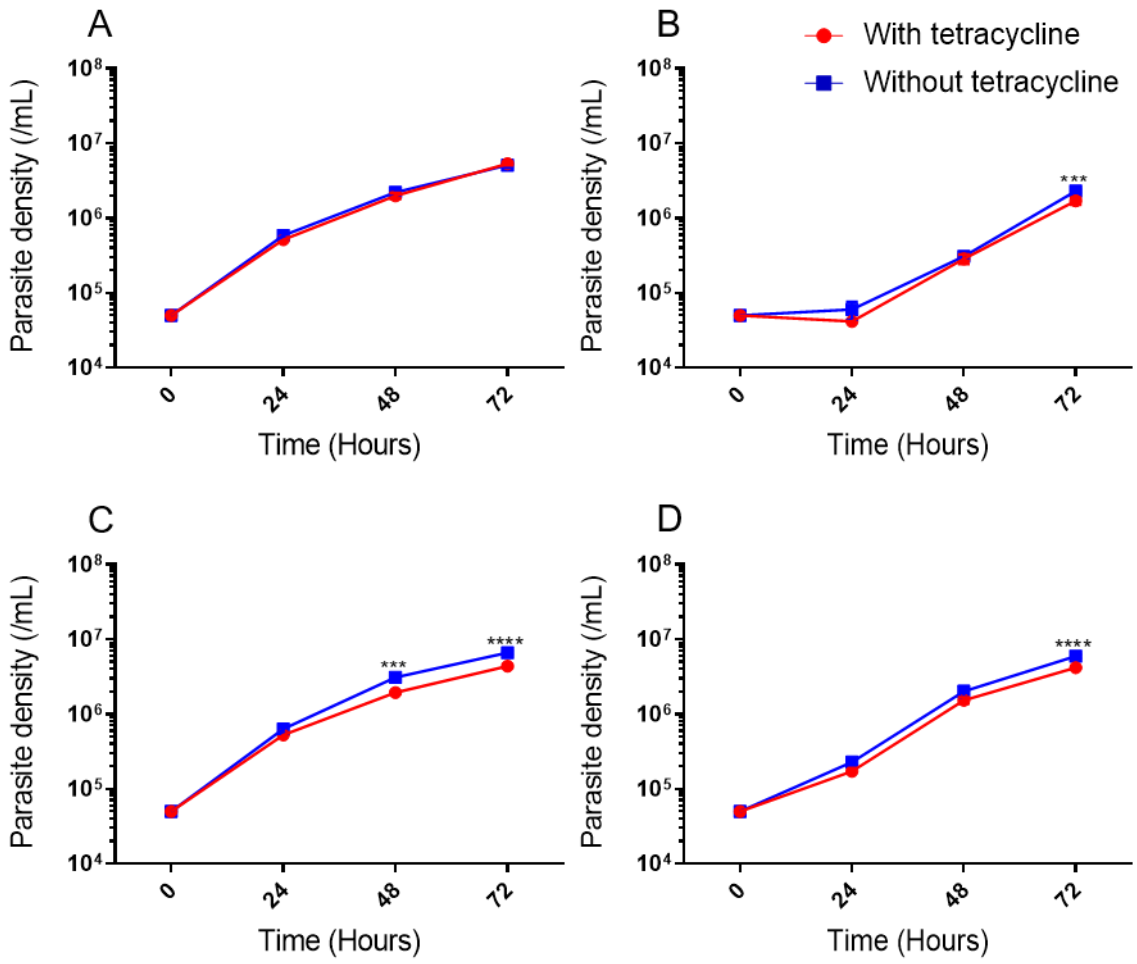

Figure 4.6. RNAi effect on the growth of wild type and transgenic P2T7-TbGAP1 cell line. *The effect of RNAi on (B) clone 1, (C) clone 2 and (D) clone 3 of the P2T7-TbGAP1 transgenic cell lines was studied at 24 hours interval. The effect of tetracycline on (A) wild type was also studied at 24 hours interval. *** = P ≤ 0.001; **** = P ≤ 0.0001.*

Parasite growth for clones from P2T7-TbGAP1 cell line shows that there were no significant differences in growth between the RNAi induced (red) and control group (blue) up until 72 hours post RNAi (P ≤ 0.0001) (Figure 4.6). However clone 2 shows that there were slightly less parasite growth form 48 hours post RNAi (P ≤ 0.001). Tetracycline did not affect the growth of wild type bloodstream form *T. brucei* (Figure 4.6.A), therefore any results observed from addition of tetracycline could be considered as due to RNAi taking place.

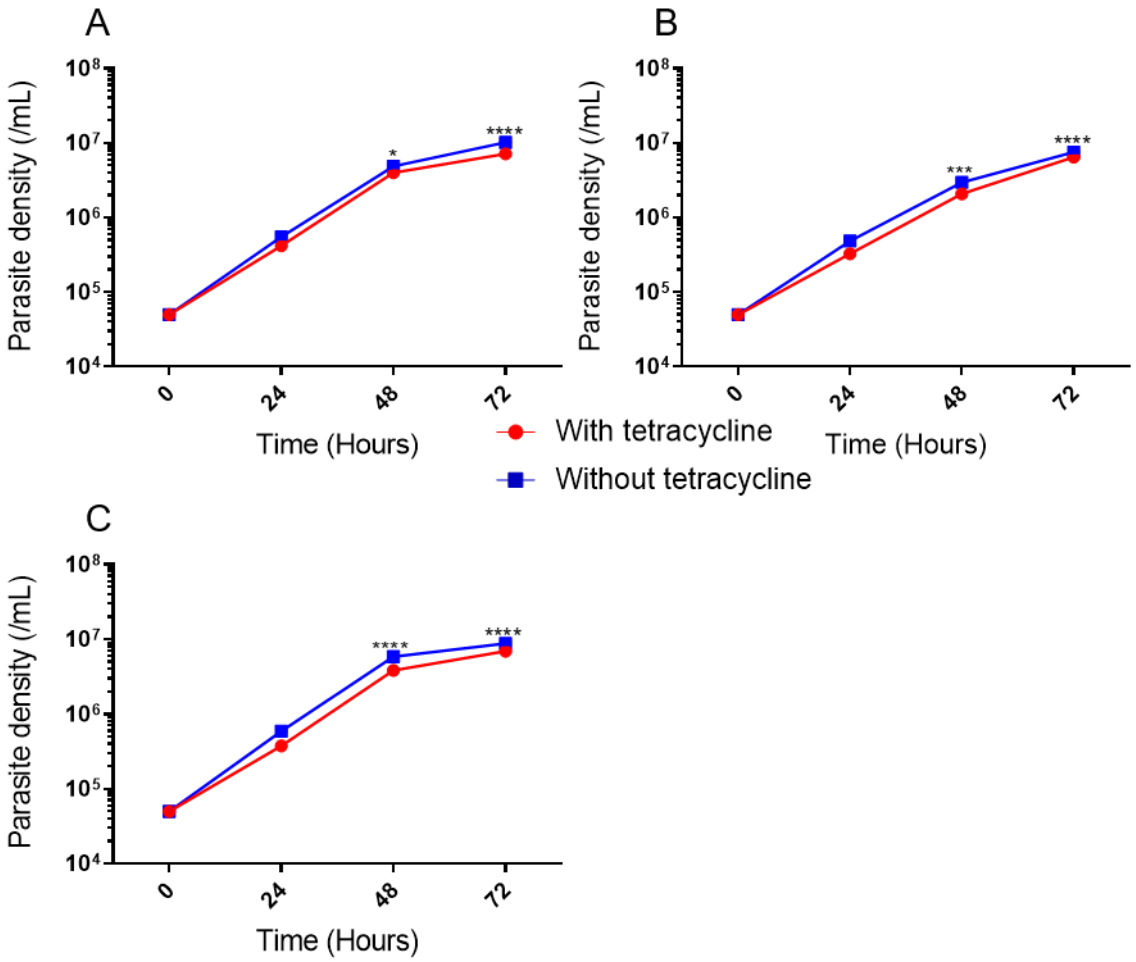

Figure 4.7. RNAi effect on the growth of transgenic P2T7-TbGAP4 cell line. *The effect of RNAi was studied in (A) clone 2, (B) clone 4 and (C) clone 6 of the transgenic P2T7-TbGAP4 cell line at 24 hours interval. * = P ≤ 0.05; *** = P ≤ 0.001; **** = P ≤ 0.0001.*

As with the clones from P2T7-TbGAP1 cell line, the RNAi of clones from the P2T7-TbGAP4 cell line did not appear affect the growth of bloodstream form *T. brucei* greatly until 72 hours post RNAi (Figure 4.7). However the growth of bloodstream form *T. brucei* from 48 hours post RNAi of TbGAP4 appears to significantly affect, albeit differently for each clone (P ≤ 0.05 – P ≤ 0.0001).

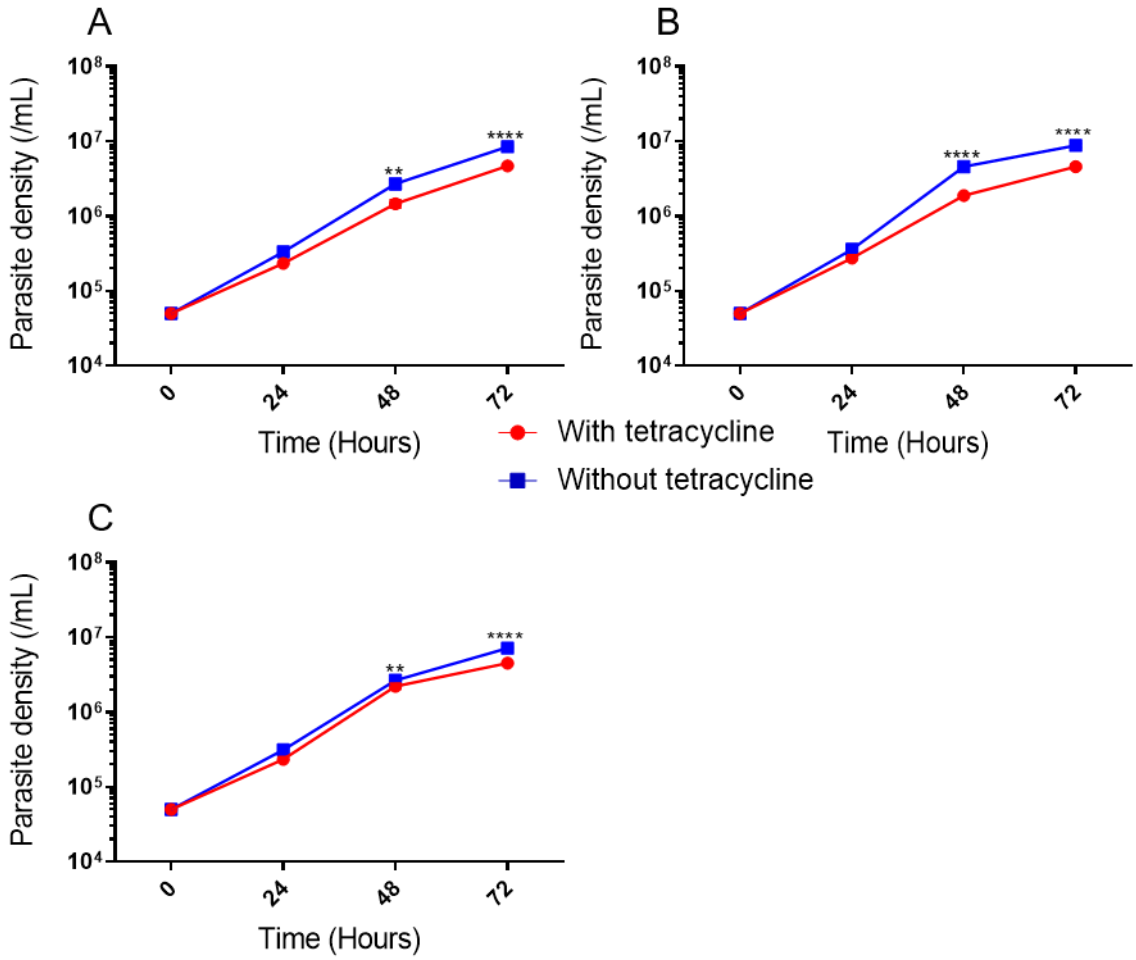

Figure 4.8. RNAi effect on the growth of transgenic P2T7-TbGEF2 cell line. *The RNAi effect in (A) clone 1, (B) clone 2 and (C) clone 3 from the transgenic P2T7-TbGEF3 cell line was studied at 24 hours interval. ** = P ≤ 0.01; **** = P ≤ 0.0001.*

The growth of different clones from the P2T7-TbGEF2 cell lines appear to be affected differently post RNAi (Figure 4.8). All clones appear to have significantly lower parasite growth from 48 hours post RNAi of TbGEF2. However, the RNAi effect on the growth of clone 2 appears to be greater than in clone 1 and 3; P ≤ 0.0001 from 48 hours for clone 2 whilst clone 1 and 3 had a P value of P ≤ 0.01 from 4 8 hours.

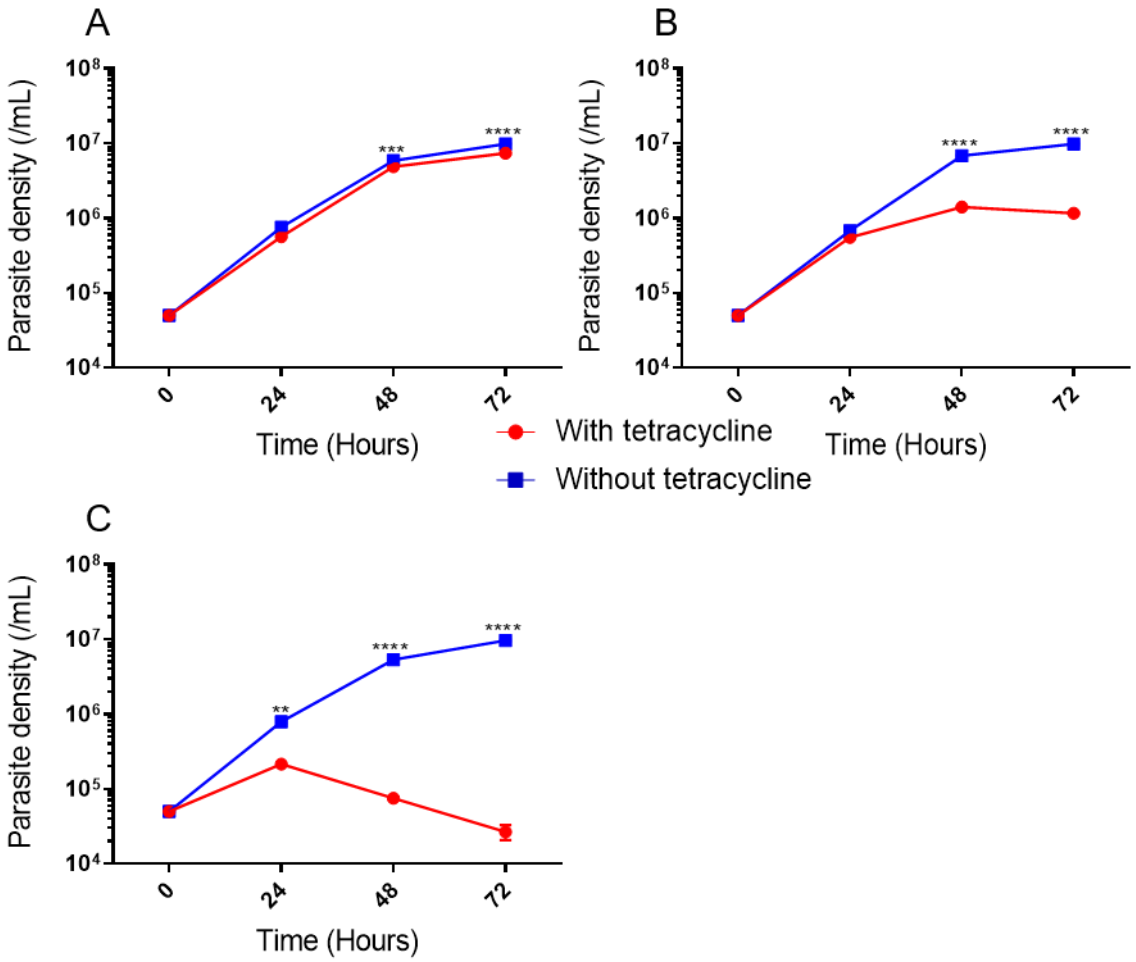

Figure 4.9. RNAi effect on the growth of transgenic P2T7-TbGEF3 cell line. *The effect of RNAi on (A) clone 1, (B) clone 3 and (C) clone 6 of the P2T7-TbGEF3 transgenic cell line was studied at 24 hours interval. ** = P ≤ 0.01; *** = P ≤ 0.001; **** = P ≤ 0.0001.*

Parasite growth in the clones 3 and 6 from P2T7-TbGEF3 cell lines are shown to be greatly affected by the RNAi of TbGEF3 (Figure 4.9.B-C), with significantly lower parasite growth from 48 hours post RNAi in clone 3 (P ≤ 0.0001) and from 24 hours post RNAi in clone 6 (P ≤ 0.01). Clone 1 from P2T7-TbGEF3 cell line did not appear to have been affected by the RNAi of TbGEF3 to a greater extent than the other two clones. However there was still a significant difference in the growth from 48 hours post RNAi (P ≤ 0.001).

4.3.4 Quantification of gene expression

The expression of clone 6 from P2T7-TbGEF3 was quantified at different time points post RNAi using qPCR. This is to ensure that the effect of TbGEF3 RNAi on bloodstream form *T. brucei* that can be observed from section 4.3.3 was due to reduced expression of *TbGEF3*.

qPCR is a sensitive technique that is used to identify changes in gene expression (Panina *et al*., 2018). SYBR Green was used in this thesis to determine the changes in the expression of TbGEF3 post RNAi at 0, 4, 24 and 48 hour time points via qPCR. SYBR Green is an intercalating dye that binds to double stranded DNA to produce fluorescence. The intensity of the fluorescence can be used to determine the relative fold changes of the gene of interest's expression (Cao and Shockey, 2012). Expression changes of the gene of interest is normalised against a housekeeping gene that is constituently expressed in the cells (Panina *et al*., 2018, Cao and Shockey, 2012). In this thesis α*-tubulin* was used as a housekeeping gene in order to normalise the results obtained for *TbGEF3*. A standard curve was generated for *TbGEF3* and α*-tubulin* templates in order to assess the efficiency of the qPCR reaction (Svec *et al*., 2015). The R^2 value generated from the standard curve gave a value closer 1 (0.986 and 0.952 for *TbGEF3* and α*-tubulin* respectively) and qPCR efficiency of 90.198% - 101.608%, confirming that the results observed were obtained at the best qPCR efficiency and the primers used for each gene worked optimally (Kuang *et al*., 2018).

The differences in *TbGEF3* relative expression across all time points was determined using $2^{-\Delta\Delta ct}$ method (Livak and Schmittgen, 2001), with the wild type as the control group. One-way ANOVA was used to determine the statistical significance of fold change of 4, 24 and 48 hours post RNAi compared to the 0 hour time point.

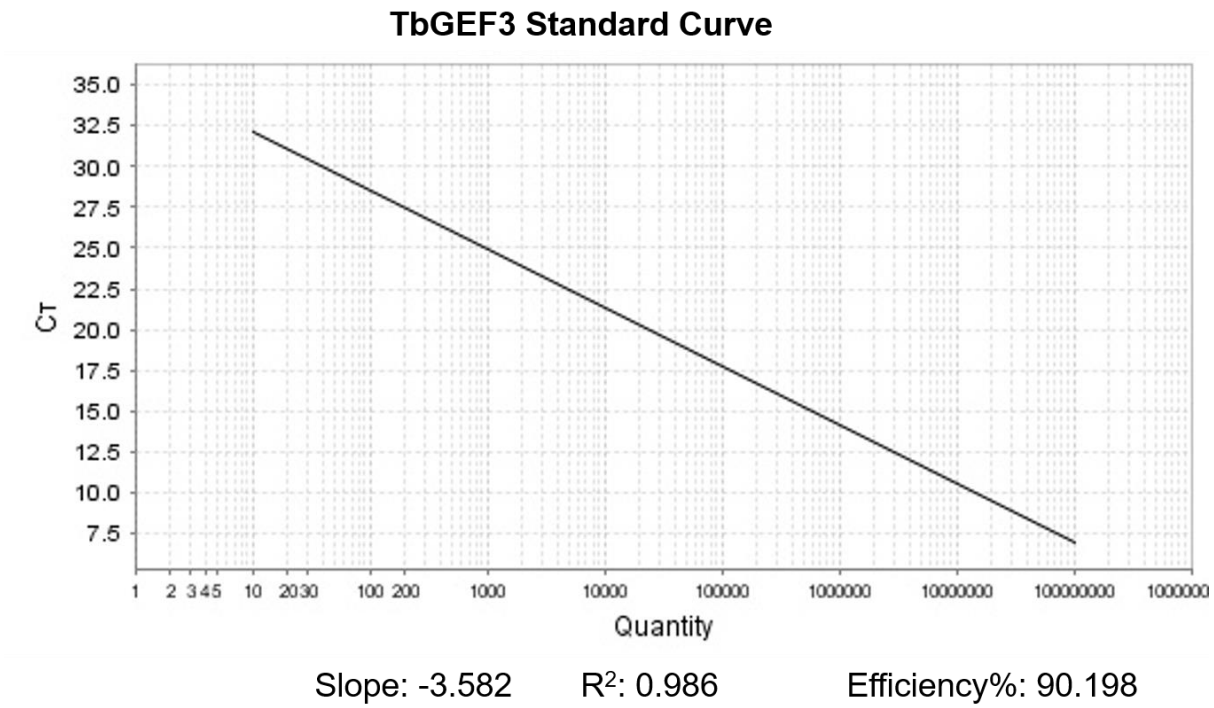

Figure 4.10. **TbGEF3** ***Standard curve.*** *Standard curve for* TbGEF3 *template was generated after preparing a series of templates with 10-fold dilution. StepOne Software Version 2.3 was used to analyse the* R^2 *value, slope and efficiency percentage.*

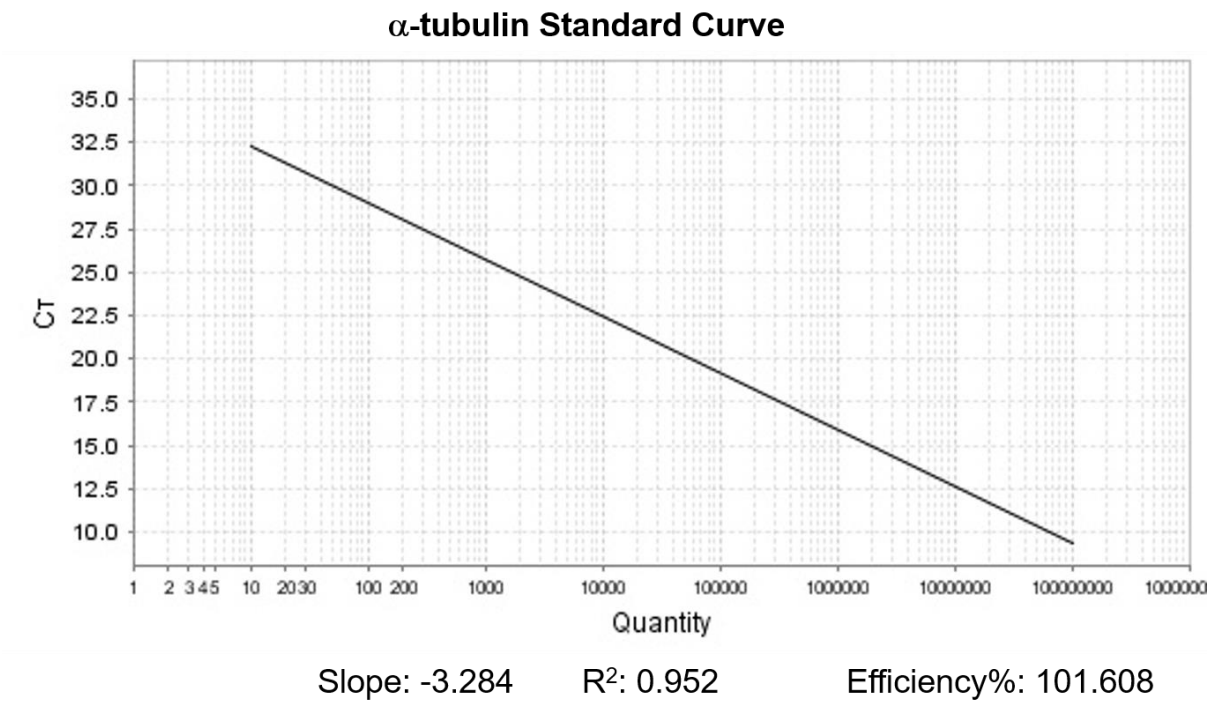

Figure 4.11. **α-tubulin** ***Standard curve.*** *Standard curve for α-tubulin template was generated after preparing a series of templates with 10-fold dilution. StepOne Software Version 2.3 was used to analyse the R^2 value, slope and efficiency percentage.*

Figure 4.12 shows that compared to 0 hour time point, the expression of TbGEF3 was reduced from 4 hours post RNAi. The expression of TbGEF3 continued to be further reduced up until 48 hours post RNAi. Although there was a reduced expression of TbGEF3 from 0 to 4 hour time point, the expression change was not big enough to be statistically significant. However the expression changes of TbGEF3 in 24 and 48 hour time points compared to 0 hours were statistically significant ($P \leq 0.05$). This result confirms that the RNAi system used targeted the TbGEF3 gene in bloodstream form *T. brucei*. Therefore, this suggests that the reduced expression of TbGEF3 may have resulted in the observed changes in bloodstream form *T. brucei* growth in section 4.3.3.

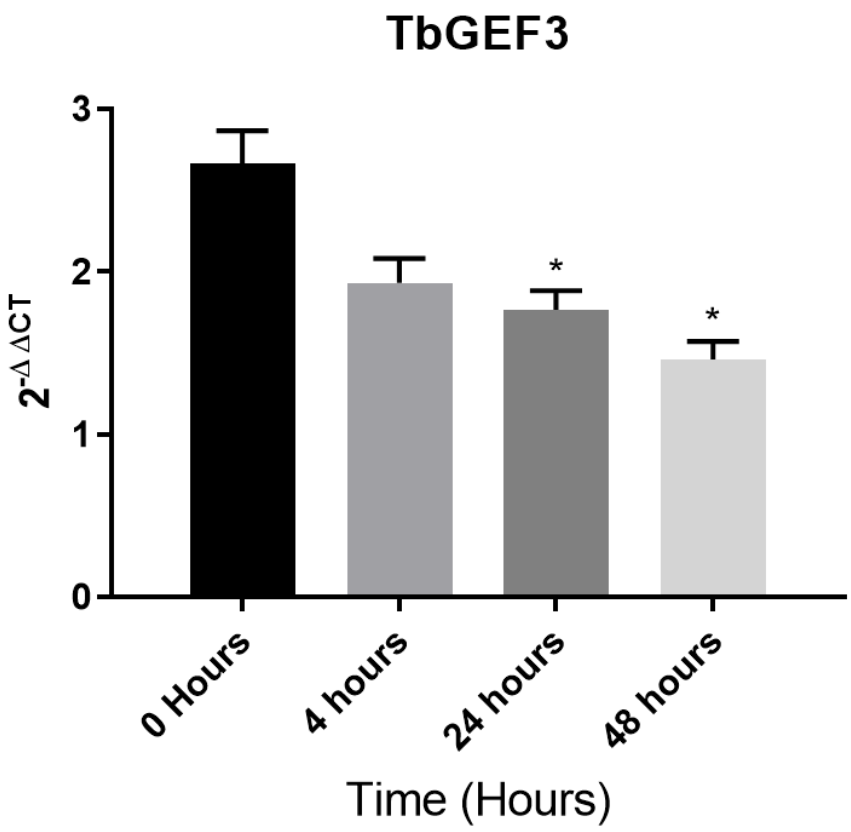

Figure 4.12. Relative expression change of* TbGEF3 *following RNAi. *Expression change of* TbGEF3 *at 0, 4, 24 and 48 hours post RNAi was identified using qPCR. Fold changes were calculated using* $2^{-\Delta\Delta CT}$ *method. Graph depicts results from TbGEF3 clone 6.*

4.3.5 Flow cytometry

4.3.5.1 Propidium iodide flow cytometry

Propidium iodide flow cytometry was used to determine whether knockdown of the TbGEFs and TbGAPs caused any defects in bloodstream form *T. brucei* cell cycle progression. Mid-log phase bloodstream form *T. brucei* were harvested at 0, 4, 24 and 48 hours post RNAi and treated with RNAse A prior to staining with propidium iodide. The samples were processed and analysed on InCyte software (Merck Millipore).

Propidium iodide is a small fluorescent intercalating agent that binds to DNA (Crowley *et al*., 2016, de Silva Rodrigues *et al*., 2016). Cells with multiple nuclei or undergoing cell cycle will fluorescence differently compared to healthy cells with single nuclei due to the difference in propidium iodide binding to DNA. The number of nucleus present in a cell can be determined using flow cytometry. Samples stained with propidium iodide are rapidly passed in front of a laser and the changes in wavelength emitted by each cell is detected in flow cytometry (Dey, 2018). *T. brucei* cells with defect in cytokinesis and containing multiple nuclei emit light at a different wavelength compared to healthy cells containing single nucleus. These results are collated and visualised in histograms. The number of peaks represents the number of nuclei present in each cell. A single peak corresponds to a single diploid nucleus (2C) whilst the subsequent peaks corresponding to the number of nuclei post mitosis (Price *et al*., 2010b).

Wild-type bloodstream form *T. brucei* was used as a control sample to identify cell cycle progression using propidium iodide flow cytometry in normal cells prior to transfection of P2T7-TbGEF/TbGAP plasmids. Data was collected from unstained wild type samples in order to eliminate false positives. Flow cytometry settings were adjusted so that unstained cells and background readings were avoided (Figure 4.13.A). As an intercalating agent, propidium iodide is able to bind to both DNA and dsRNA, this could lead to misleading data on cell cycle progression (Rieger *et al*., 2010). Two wild type samples were prepared in order to identify if samples with RNA present were significantly different to samples that were treated with RNAse A (Figure 4.13.B and C).

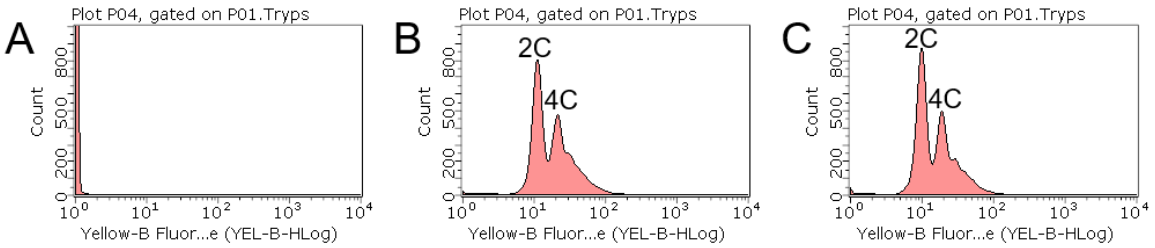

***Figure 4.13. Propidium iodide flow cytometry of wild type bloodstream form* T. brucei.** *Cell cycle progression in wild type bloodstream form* T. brucei *was determined using (A) no stain, (B) propidium iodide only and (C) propidium iodide with RNAse A.*

Figure 4.13. shows that samples that were not treated with RNAse A were not significantly different to samples treated with RNAse A. However the peaks indicating the number of DNA content present were more prominent in samples that had undergone RNAse A treatment. Two peaks can be observed that corresponds to a DNA content of 2C and 4C (Figure 4.13)

The settings used for wild type samples were kept the same for transfected bloodstream form cell lines. The effect of cell cycle progression at different time points post RNAi was determined for the two TbGEFs and TbGAPs. The results show that all of the transfected cell lines had a DNA content similar to wild types: 2C and 4C, at 0 and 4 hours post RNAi (Figure 4.14 and Figure 4.15). This suggests that RNAi of TbGEFs and TbGAPs did not affect cell cycle progression during those time points.

As expected from the growth curves, RNAi of TbGAP1 and TbGAP4 from 24 hour time points did not show any difference in the number of DNA content present in the cell population (Figure 4.15). Similar results can be observed from RNAi of TbGEF2 (Figure 4.14.A). This suggests that RNAi of the TbGAPs and TbGEF2 does not affect bloodstream form *T. brucei* cell cycle progression, correlating with data from the growth curves.

Flow cytometry data for TbGEF3 from 24 hours post RNAi showed that the cell population had a decrease in 2C cells, with significant decrease of 2C cell population observed in 48 hours post RNAi time point. The number of 4C population remained approximately the same at 24 hours post RNAi of TbGEF3. However the 4C cell population decreased as well in the 48 hours post RNAi samples. A new cell population with a DNA content of 8C was observed from 24 hours post RNAi. This population size increased in the 48 hours post RNAi samples. A rise in a new population containing DNA content of 16C can also be observed in the 48 hours post RNAi samples (Figure 4.14.B).

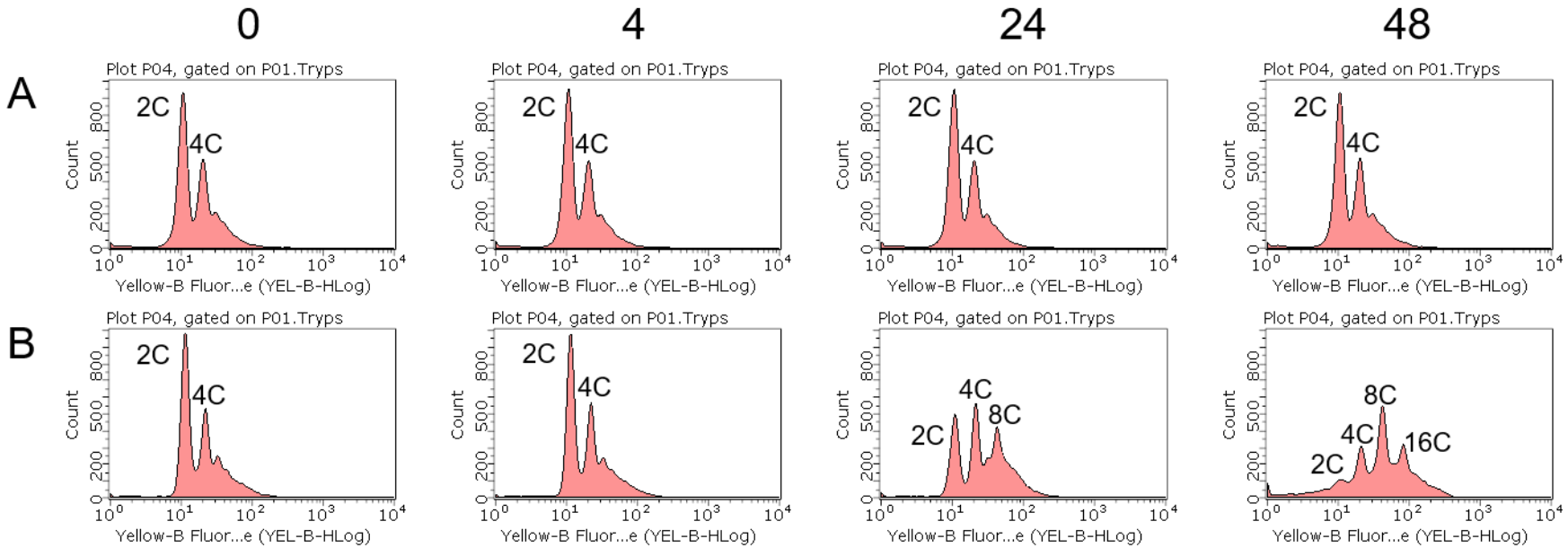

***Figure 4.14. GEF RNAi effect on cell cycle progression in* T. brucei.** *The effect of RNAi on cell cycle progression was identified in (A) P2T7-TbGEF2 and (B) P2T7-TbGEF3 at 0, 4, 24 and 48 hour time points. The peaks were labelled according to their DNA content.*

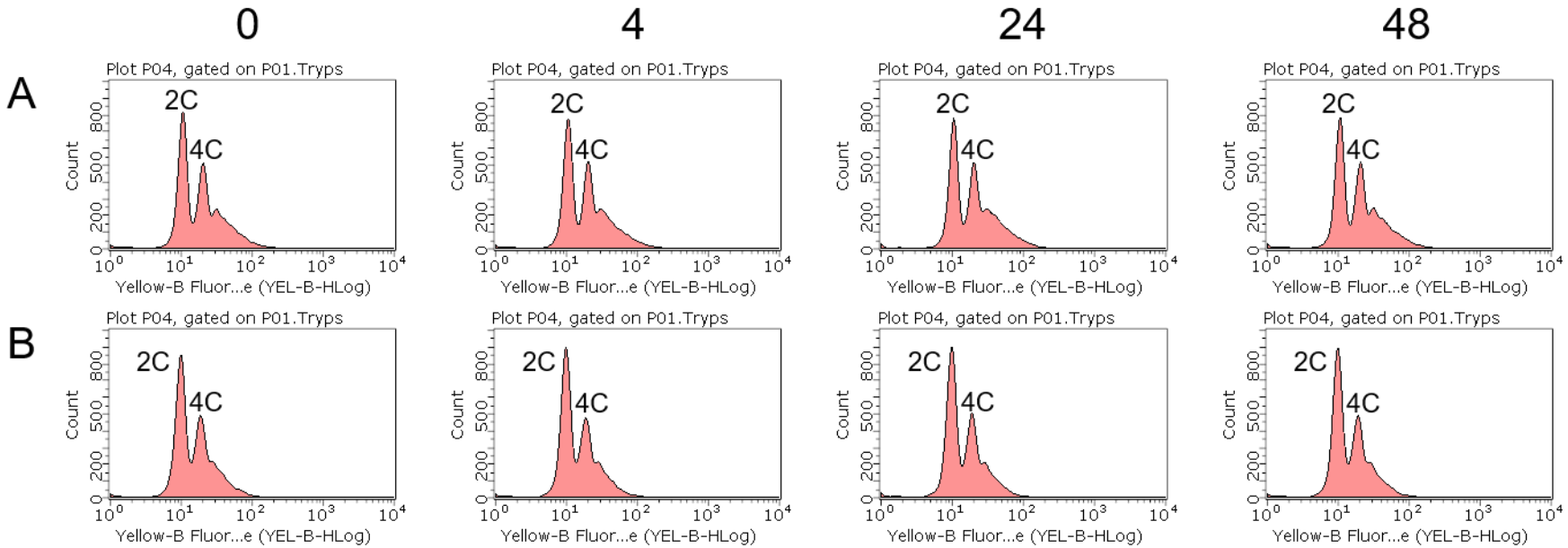

***Figure 4.15. GAP RNAi effect on cell cycle progression in* T. brucei.** *The effect of RNAi on cell cycle progression in (A) P2T7-TbGAP1 and (B) P2T7-TbGAP4 was identified at 0, 4, 24 and 48 hour time points. The peaks were labelled according to their DNA content.*

4.3.5.2 Live/Dead flow cytometry

Propidium iodide flow cytometry data in section 4.3.5.1 showed that RNAi of TbGAPs and TbGEF2 did not affect cell cycle progression, whilst RNAi of TbGEF3 led to an increase in a cell population with a DNA content of 8C and more. This suggested that RNAi against TbGEF3 possibly had a cytostatic effect on bloodstream form *T. brucei*. However in order to asses if RNAi of TbGEF3 does have a cytostatic effect or if the results observed are caused by cell death (cytocidal), a Live/Dead flow cytometry was carried out. Live/Dead flow cytometry was carried out on TbGAP1, TbGAP4 and TbGEF2 to see if RNAi of these regulators have a cytocidal effect as well.

Mid-log phase bloodstream form *T. brucei* were harvested at 0, 4, 24 and 48 hours post RNAi. The harvested cells were stained with Live/Dead Fixable Red Dead dye and the effect or RNAi was observed using Guava EasyCyte 6-2L flow cytometer (Merck Millipore) and on InCyte software (Merck Millipore). Live/Dead flow cytometry results for RNAi of TbGEFs and TbGAPs showed two distinct populations that were identified as live and dead cells. The two different populations were differentiated using gates and data for each population was analysed. One-way ANOVA test was used to determine the statistical significance of population change at different time points post RNAi compared to 0 hours.

Live/Dead flow cytometry results for TbGAP1 at different time points post RNAi showed that there was an increase in live cell population than compared to the dead cell population across the different time points (Figure 4.16). 97% of the cell population were live cells at all time points compared to 0.5 – 0.6% of the cell population being dead cells. Although there was a slight increase in dead cells at 48 hours post RNAi, the increase was not statistically significant and could not be concluded to be an effect of RNAi of TbGAP1 (Figure 4.20).

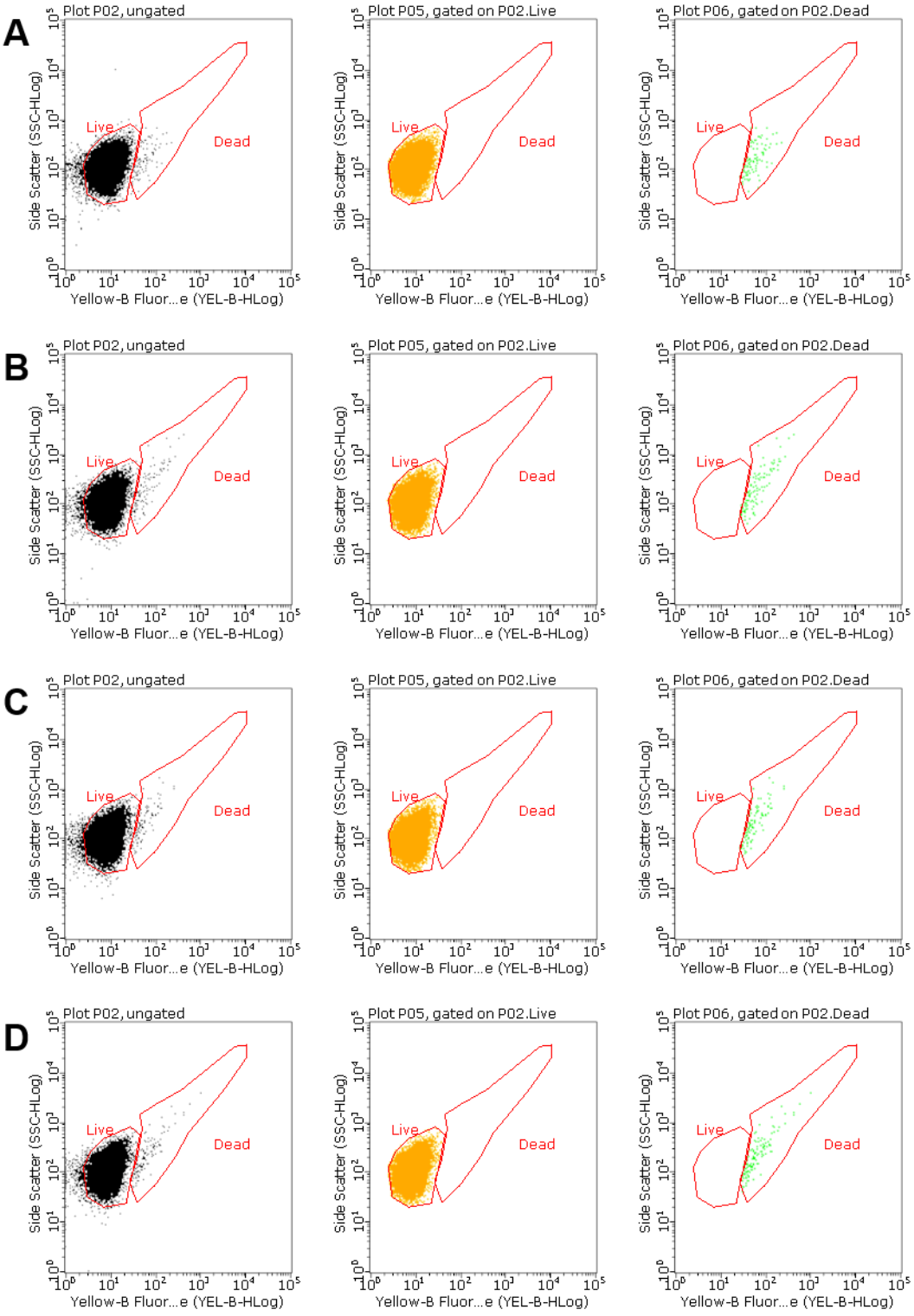

Figure 4.16. Live/Dead flow cytometry of P2T7-TbGAP1 post RNAi at different time points. *P2T7-TbGAP1 cells were harvested at (A) 0 hours, (B) 4 hours, (C) 24 hours and (D) 48 hours post RNAi of TbGAP1 and stained with Live/Dead Fixable Red Dead dye. Samples were processed by flow cytometry to differentiate between live and dead cells.*

Live/Dead flow cytometry results showed that RNAi of TbGAP4 did not cause a significant increase in cell death ($P > 0.05$) similarly to the RNAi of TbGAP1. 94 – 97% of the cell population consisted of live cells whilst only 1 – 2% of the cell population consisted of dead cells at all of the time points post RNAi (Figure 4.17 and Figure 4.20). The same was observed for samples at different time points post RNAi of TbGEF2 (Figure 4.18). A high percentage of the cell population consisted of live cells (95 – 97%) at all time points post RNAi. Similarly to TbGAPs, RNAi of TbGEF2 resulted in only 1% dead cells in the population counted (Figure 4.20).

Live/Dead flow cytometry results for TbGEF3 at different time points post RNAi showed that changes in the live and dead cell population sizes from 48 hours post RNAi was clearly observable (Figure 4.19). The results show that RNAi of TbGEF3 did not cause immediate cell death since 93 – 94% of the cell population consisted of live cells from 0 to 24 hours post RNAi. A significant increase in dead cell population ($P \leq 0.0001$) can be observed from 48 hours post RNAi (Figure 4.20).

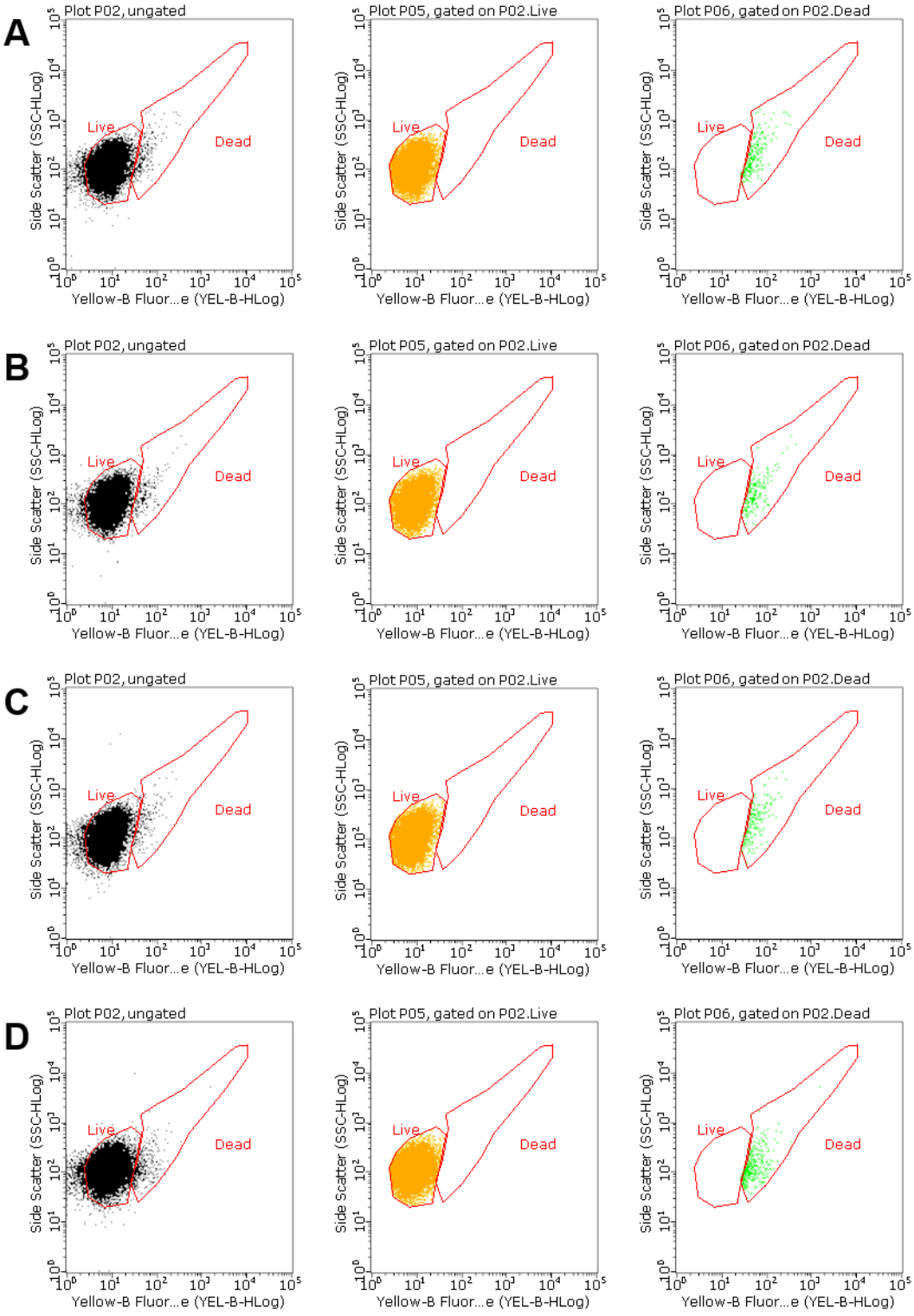

Figure 4.17. Live/Dead flow cytometry of P2T7-TbGAP4 post RNAi at different time points. *P2T7-TbGAP4 cells were harvested at (A) 0 hours, (B) 4 hours, (C) 24 hours and (D) 48 hours post RNAi of TbGAP4 and stained with Live/Dead Fixable Red Dead dye. Samples were processed by flow cytometry to differentiate between live and dead cells.*

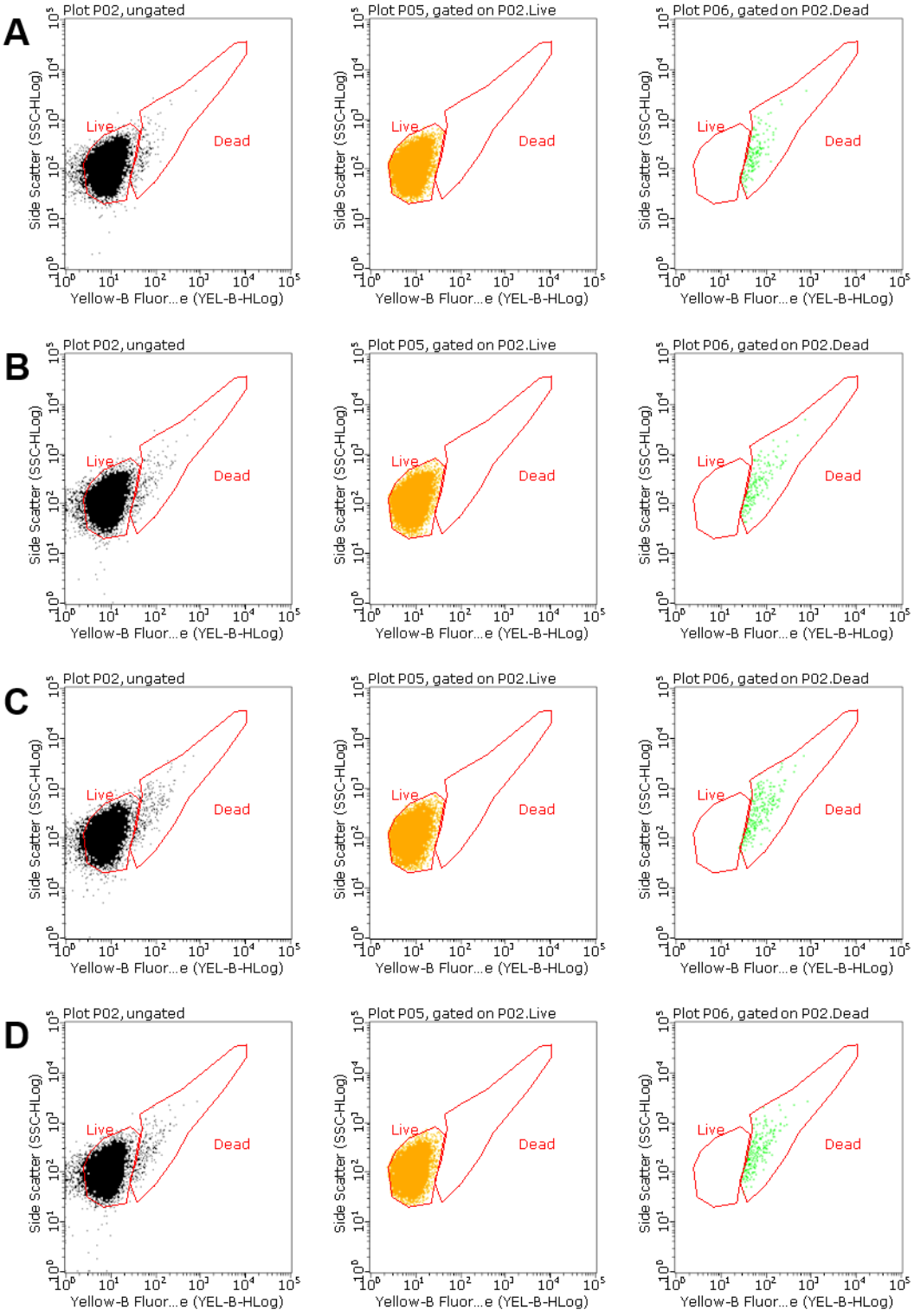

Figure 4.18. Live/Dead flow cytometry of P2T7-TbGEF2 post RNAi at different time points. *P2T7-TbGEF2 cells were harvested at (A) 0 hours, (B) 4 hours, (C) 24 hours and (D) 48 hours post RNAi of TbGEF2 and stained with Live/Dead Fixable Red Dead dye. Samples were processed by flow cytometry to differentiate between live and dead cells.*

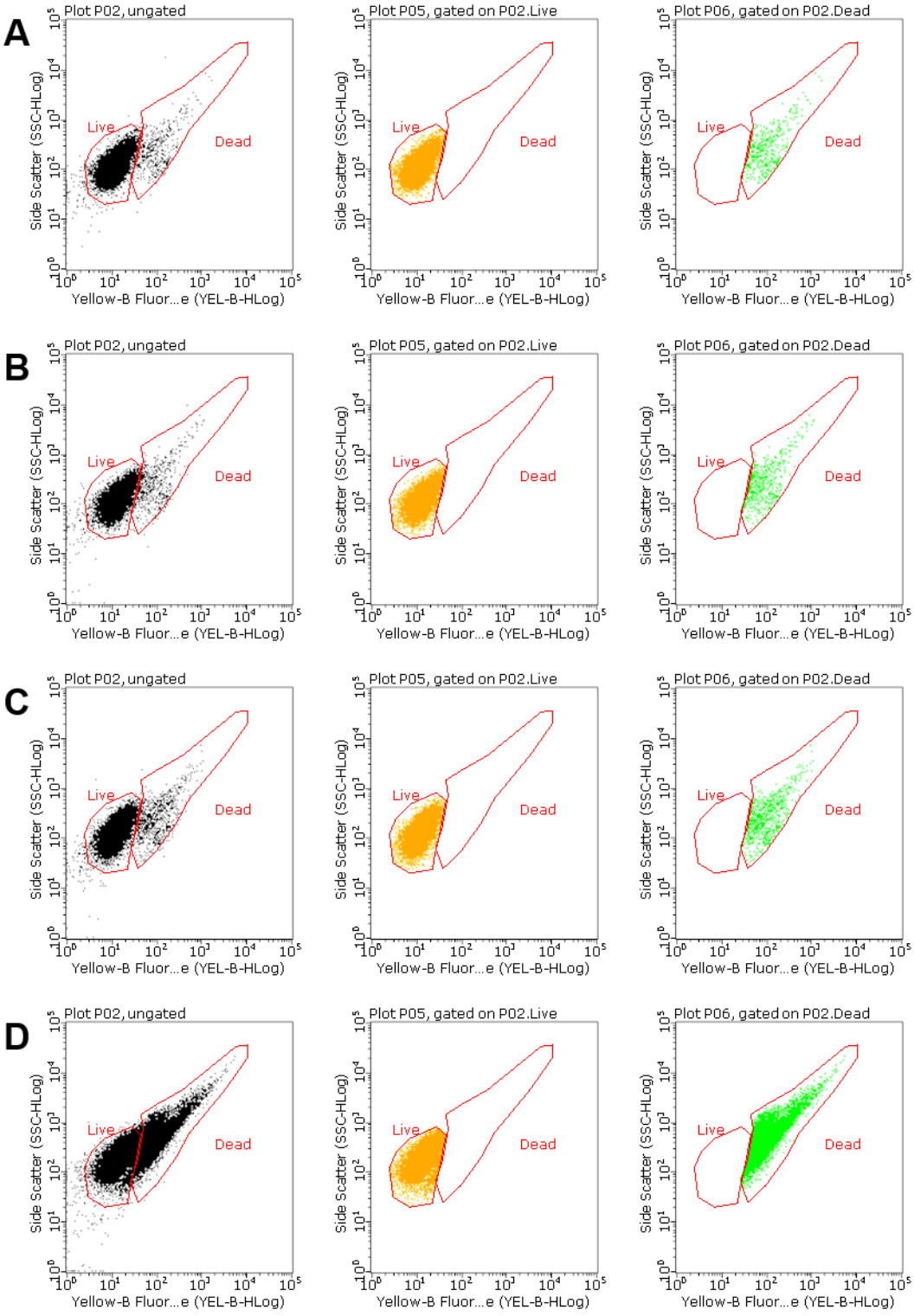

Figure 4.19. Live/Dead flow cytometry of P2T7-TbGEF3 post RNAi at different time points. *P2T7-TbGEF3 cells were harvested at (A) 0 hours, (B) 4 hours, (C) 24 hours and (D) 48 hours post RNAi of TbGEF3 and stained with Live/Dead Fixable Red Dead dye. Samples were processed by flow cytometry to differentiate between live and dead cells.*

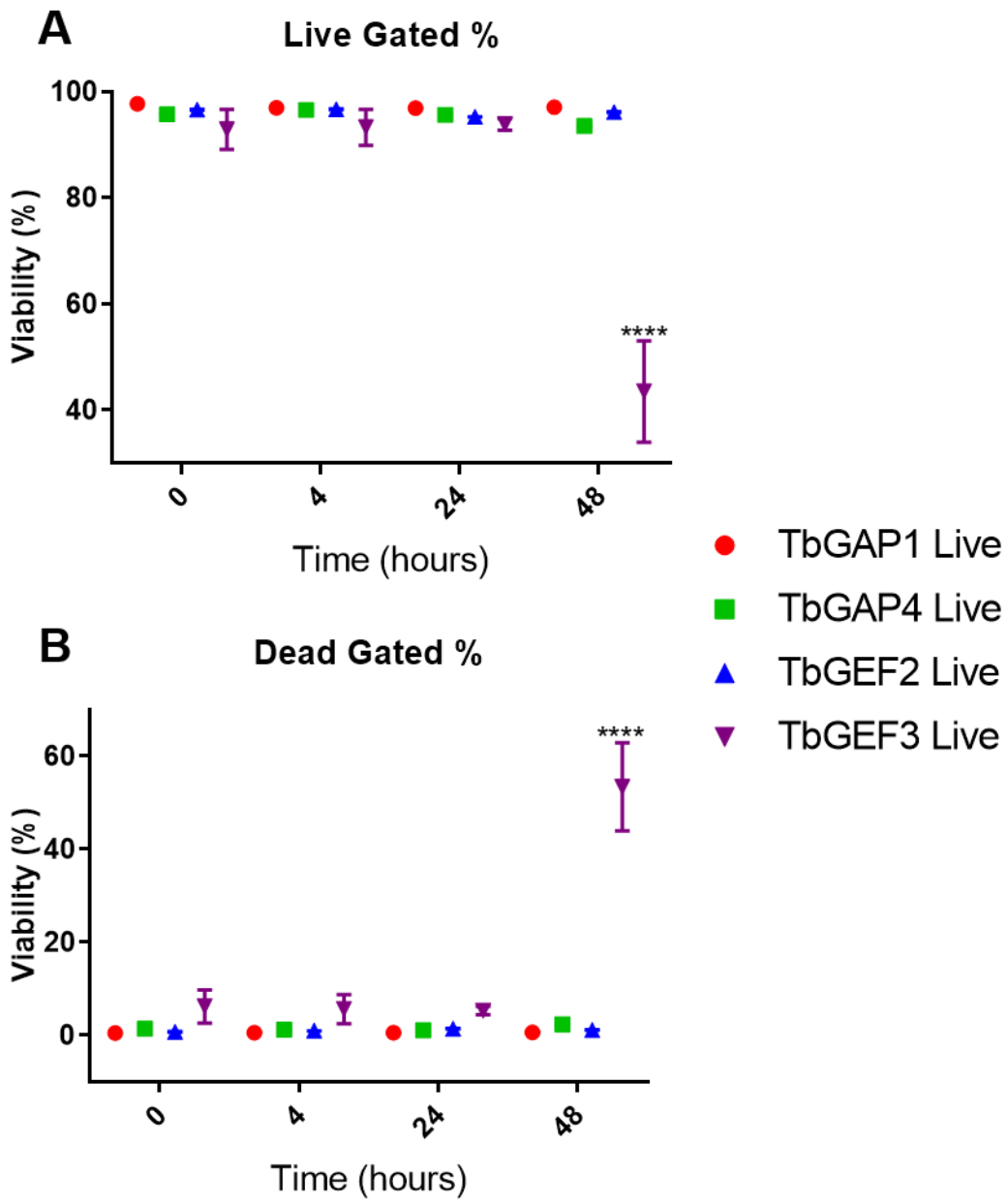

Figure 4.20. Live/Dead cell percentage at different time points post RNAi. *The percentage of (A) Dead and (B) Live cells for each time point post RNAi of their respective GEFs and GAPs was analysed to determine the statistical significance between the two populations. **** = P ≤ 0.0001.*

4.3.6. Microscopy

4.3.6.1 Indirect immunofluorescent microscopy

Immunofluorescent microscopy is a cell imaging technique that utilises fluorescent labelled antibodies to detect specific antigens in order to visualise target proteins or cell structures (Odell and Cook, 2013). This technique is further divided into two classes depending on the fluorophore tagged antibodies used. Direct immunofluorescent microscopy is a one-step staining procedure where the fluorophore tagged antibody binds directly to the antigen. In contrast to this, fluorophore tagged secondary antibodies and primary antibodies are utilised in indirect immunofluorescent microscopy. Primary antibodies bind to surface antigens, fluorophore tagged secondary antibodies then bind to the primary antibodies; enabling visualisation of target proteins or structures of the cell (Becheva *et al*., 2018, Mohan *et al*., 2008).

Indirect immunofluorescent microscopy was utilised in this project to visualise the cell structure of bloodstream form *T. brucei* at 0, 4, 24 and 48 hours post RNAi of TbGEFs and TbGAPs. Primary mouse monoclonal antibody 1 (TAT1) and primary anti-rabbit monoclonal antibody was used against *T. brucei* α-tubulin and paraflagellar rod protein 1 (PFR1) respectively. Alexa Fluor 488 and 594 conjugated secondary antibodies were used to detect primary antibodies. The cell structure of bloodstream form *T. brucei* was visualised using EVOS FL Cell Imaging System (Life Technologies).

The cellular structure of *T. brucei* transfected with P2T7-TbGAP1 plasmid prior to RNAi (0 hours) were similar to those of the infective wild type bloodstream form (Figure 4.21.A-B). This is characterised by the vermiform shape with tapered ends (highlighted by α-tubulin in green) with a single flagellum along the length of *T. brucei* body (highlighted by PFR1 in red) (Ralston *et al*., 2009). The vermiform shape in transfected *T. brucei* was maintained across all time points post RNAi (Figure 4.21.C-E). This suggests that RNAi of TbGAP1 did not grossly affect the cellular structure of bloodstream form *T. brucei*. The same was observed for bloodstream form *T. brucei* transfected with P2T7-TbGAP4 and P2T7-TbGEF2 plasmids, following incubation in tetracycline (Figure 4.22 and Figure 4.23).

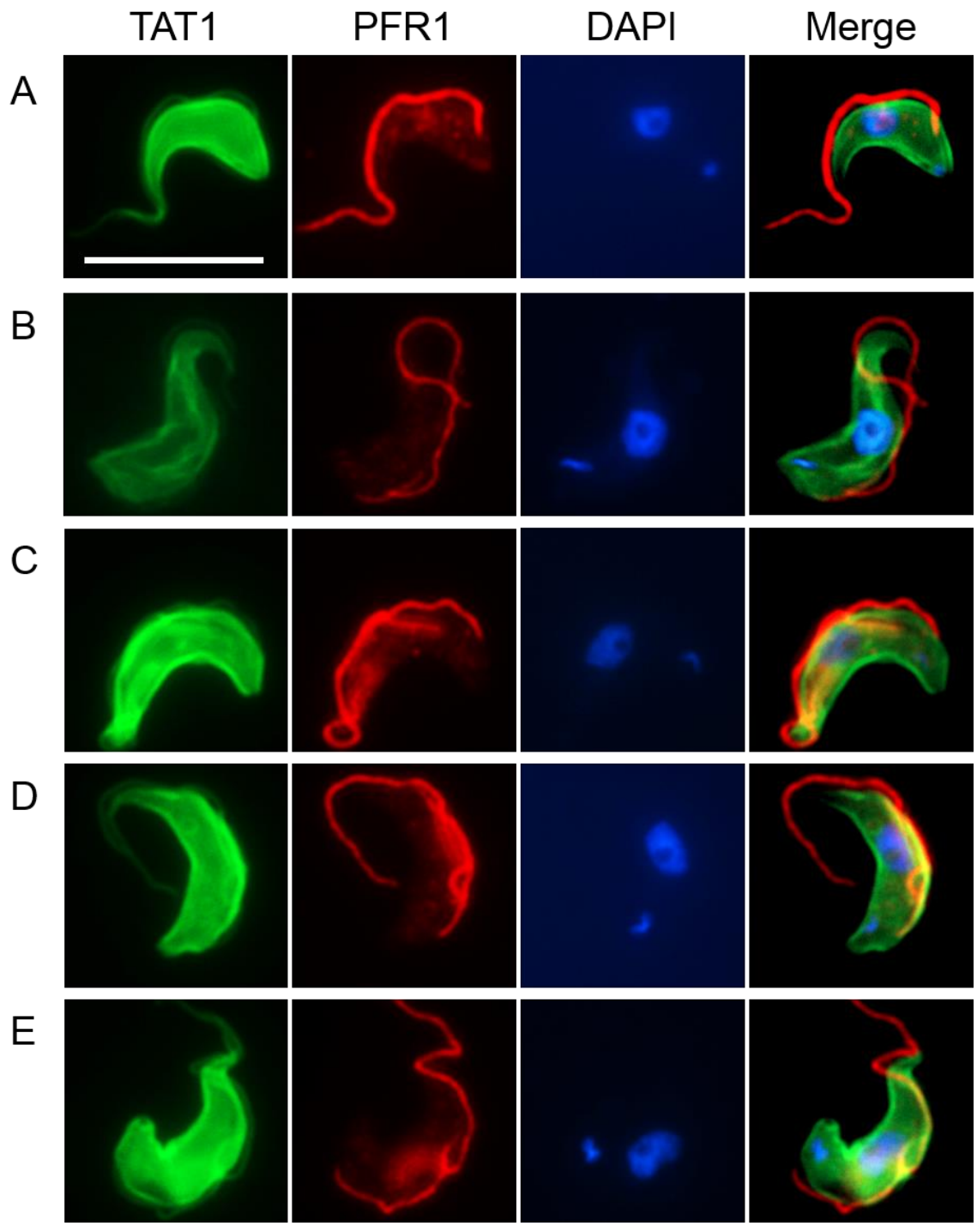

Figure 4.21. Indirect immunofluorescent microscopy of wild type bloodstream form* T. brucei *and PT27-TbGAP1. *The cellular structure of (A) wild type, (B) 0 hours, (C) 4 hours, (D) 24 hours and (E) 48 hours post RNAi of TbGAP1 was studied. α-tubulin is shown in (green), paraflagellar rod is shown in red, nucleus and kinetoplast is shown in blue. Scale bar = 10 μm.*

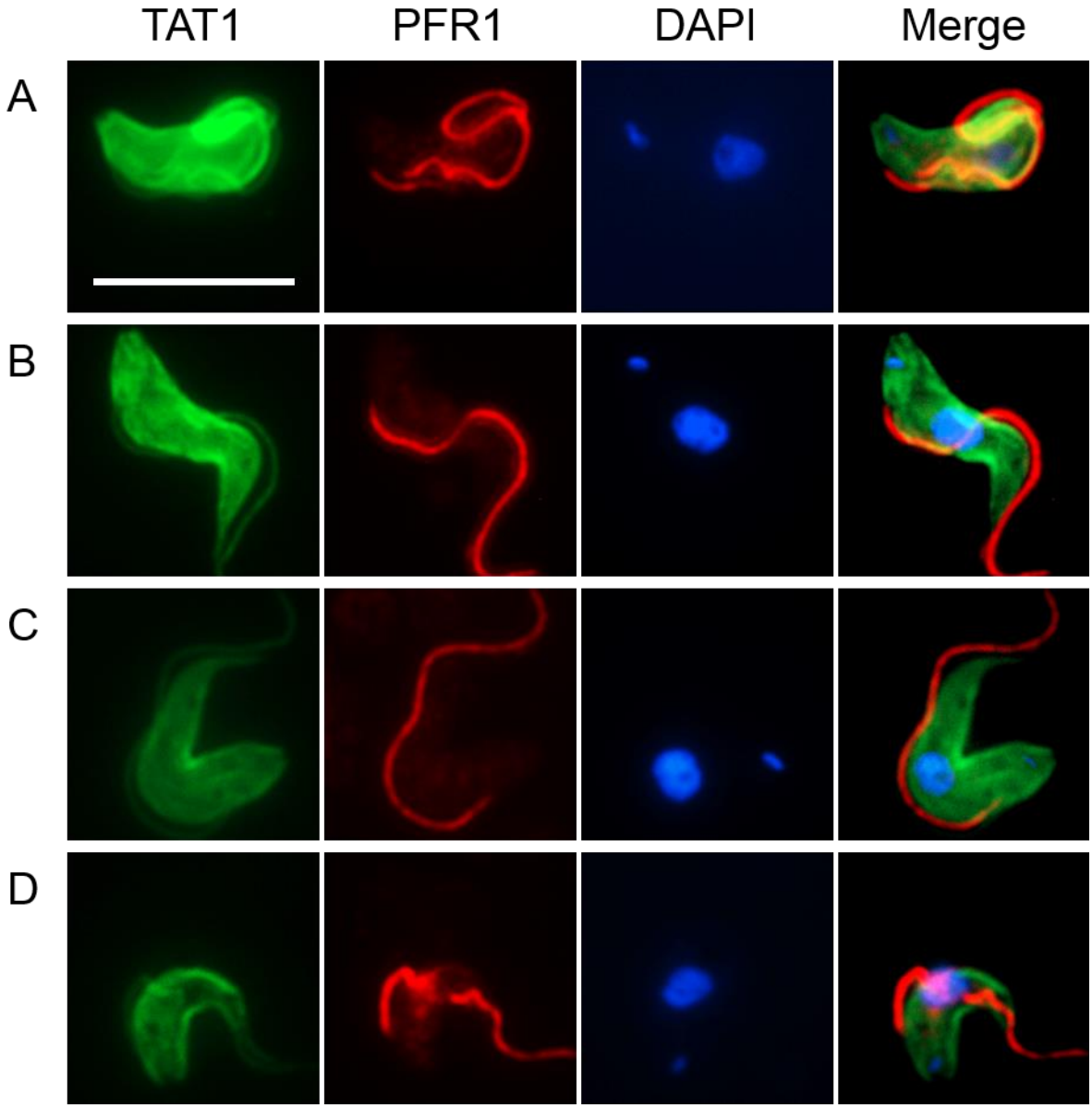

Figure 4.22. Indirect immunofluorescent microscopy of bloodstream form* T. brucei *post RNAi of TbGAP4. *The cellular structure of (A) wild type, (B) 0 hours, (C) 4 hours, (D) 24 hours and (E) 48 hours post RNAi of TbGAP4 was studied. α-tubulin is shown in (green), paraflagellar rod is shown in red, nucleus and kinetoplast is shown in blue. Scale bar = 10 μm*

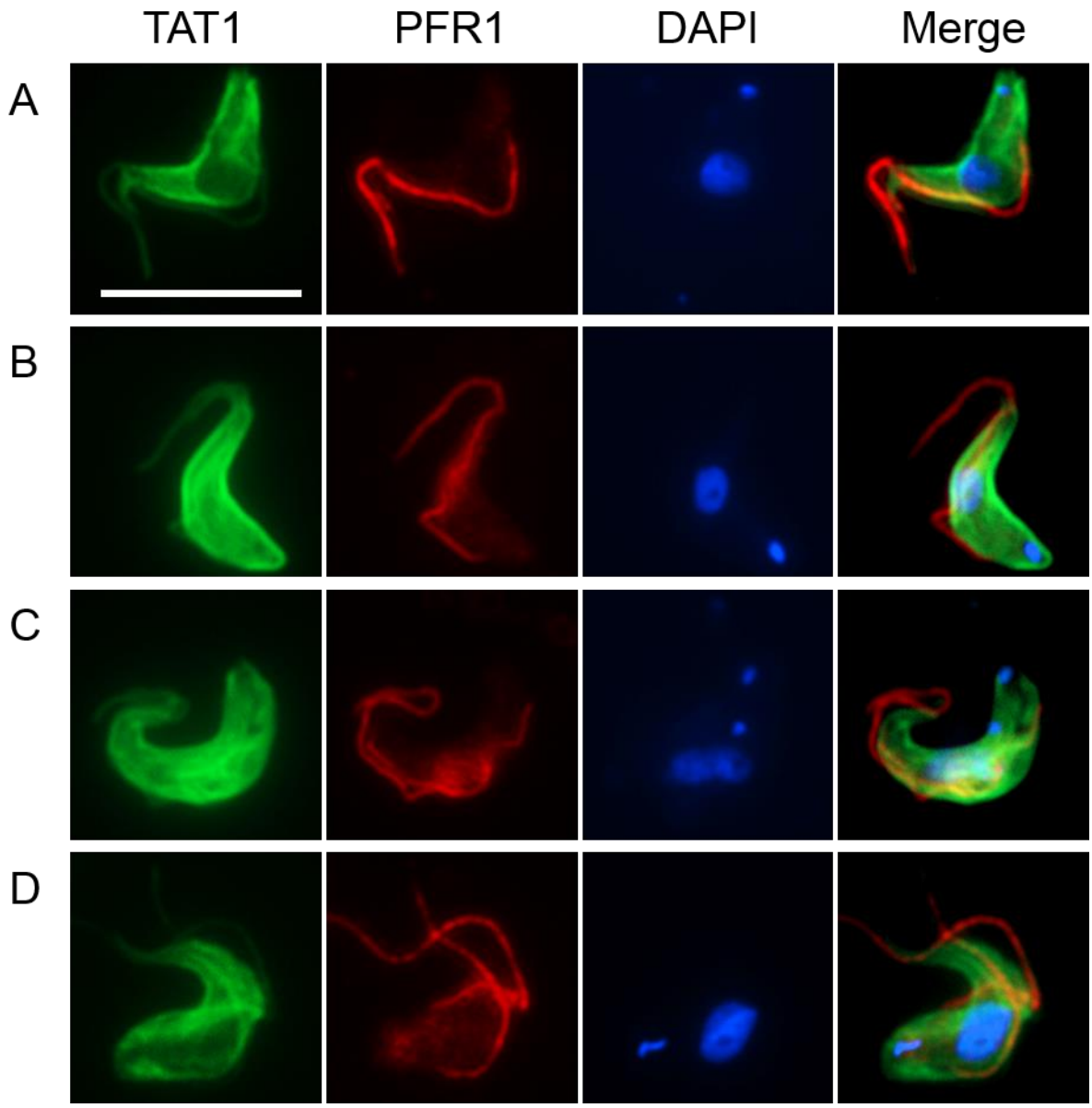

Figure 4.23. Indirect immunofluorescent microscopy of bloodstream form* T. brucei *post RNAi of TbGEF2. *The cellular structure of (A) wild type, (B) 0 hours, (C) 4 hours, (D) 24 hours and (E) 48 hours post RNAi of TbGEF2 was studied. α-tubulin is shown in (green), paraflagellar rod is shown in red, nucleus and kinetoplast is shown in blue. Scale bar = 10 μm.*

Similar to the other *T. brucei* ARF regulators that were transfected into bloodstream form *T. brucei*, the cellular structure of *T. brucei* transfected with P2T7-TbGEF3 plasmid at 0 hours (before RNAi was induced) had a vermiform shape that is characteristic of the wild type bloodstream form *T. brucei*. This shape was retained up until 4 hours post RNAi of TbGEF3 (Figure 4.24.A-B). However from 24 hours post RNAi, the shape of the bloodstream form *T. brucei* became circular (Figure 4.24.C-D) and resembled the BigEye phenotype that was described previously by Allen *et al*. (Allen *et al*., 2003).

Since bloodstream form *T. brucei* transfected with P2T7-TbGEF3 demonstrated changes in cellular structure from 24 hours post RNAi. The numbers of circular and vermiform (slender) morphology present in the indirect immunofluorescent slides were counted for all time points post RNAi of TbGEF3. 100 cells were counted in total for each sample and the percentage was calculated for each morphology type across the different time points (Figure 4.25). The circular morphology present in the samples were assumed to be caused by an enlarged flagellar pocket and is termed as BigEye phenotype (Allen *et al*., 2003). However enlargement of the flagellar pocket could not be confirmed with the use of indirect immunofluorescent microscopy.

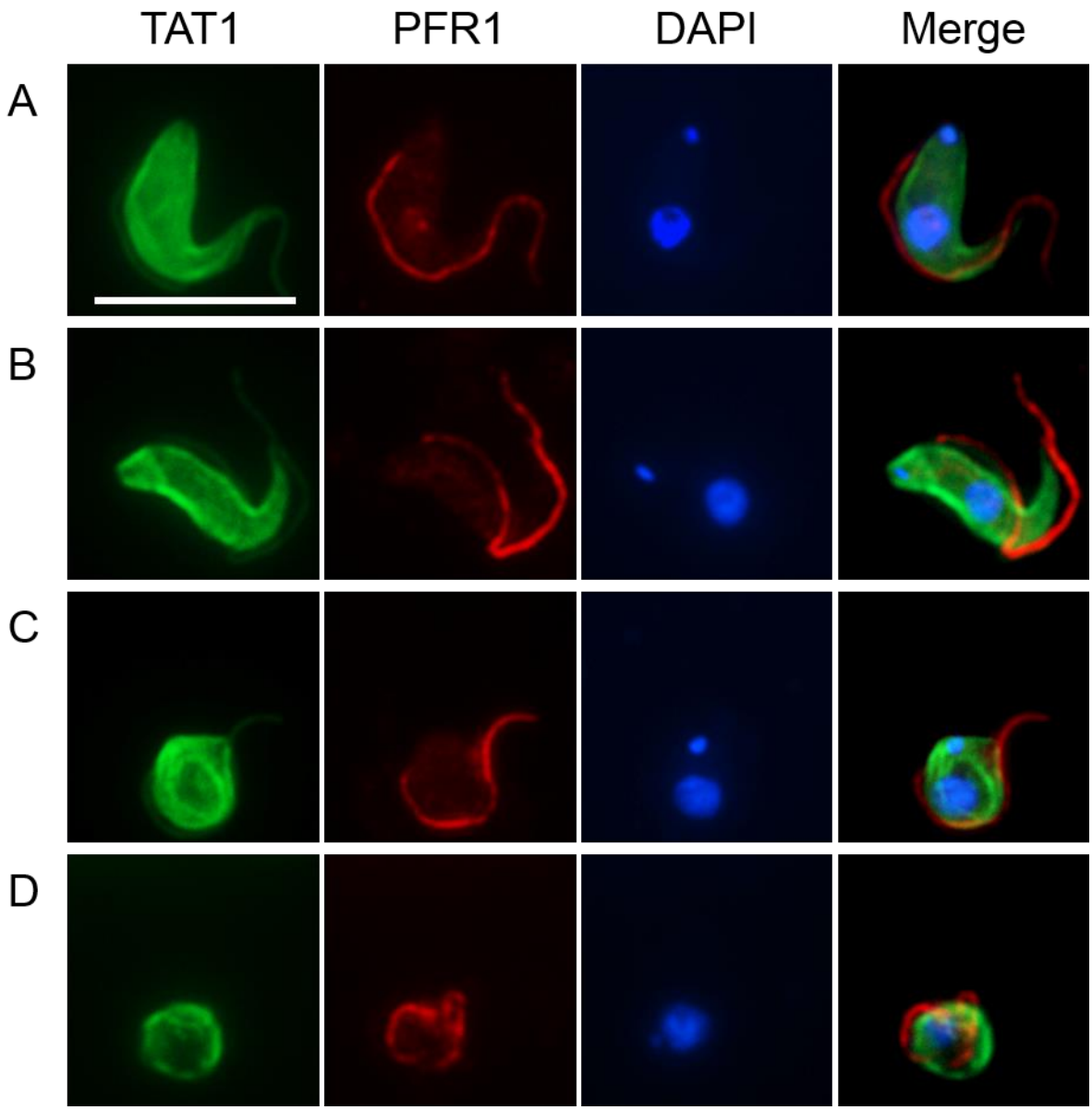

***Figure 4.24. Indirect immunofluorescent microscopy of bloodstream form* T. brucei.** *The cellular structure of (A) wild type, (B) 0 hours, (C) 4 hours, (D) 24 hours and (E) 48 hours post RNAi of TbGEF3 was studied. α-tubulin is shown in (green), paraflagellar rod is shown in red, nucleus and kinetoplast is shown in blue. Scale bar = 10 μm.*

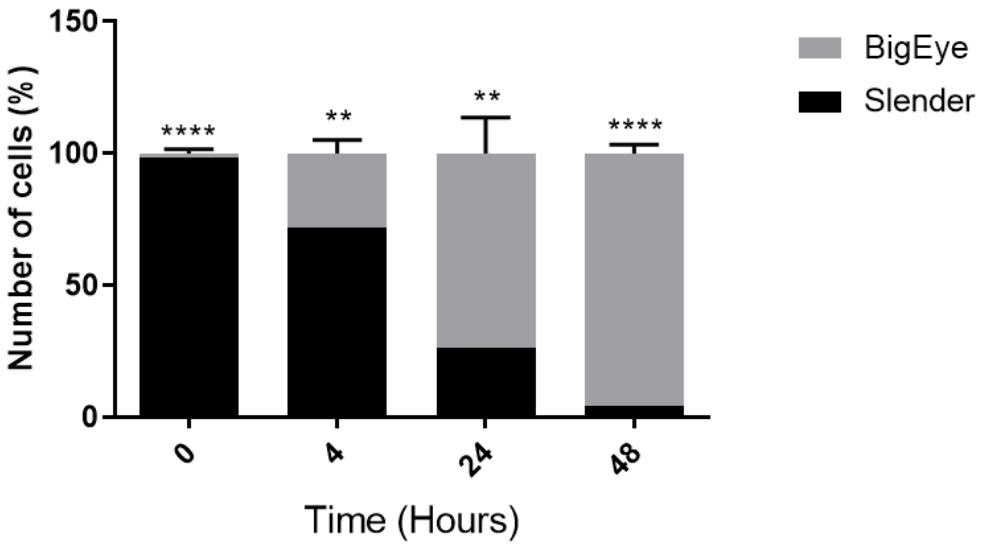

Figure 4.25. Number of BigEye and slender* T. brucei *cells at different time points post RNAi. *The number of BigEye Vs slender morphology observed at different time points post RNAi of TbGEF3 was counted. 100 cells were counted for each time point sample and a percentage was calculated. ** = P ≤ 0.01, **** = P ≤ 0.0001.*

4.3.6.2 Transmission Electron Microscopy

The circular morphology that was observed at different time points post RNAi of TbGEF3 in section 4.3.6.1 resembled the BigEye morphology. The BigEye morphology is characterised by the presence of enlarged flagellar pocket (Allen *et al*., 2003). However the presence of an enlarged flagellar pocket could not be determined clearly by indirect immunofluorescent microscopy. Transmission Electron Microscopy (TEM) was used in order to characterise changes in morphology in greater detail.

Electron microscopy enables high resolution imaging of cellular structures and proteins (Schorb *et al*., 2017). This is achieved by utilising a beam of electrons instead of light to illuminate and record the image (McIntosh *et al*., 2017). There are two subclasses of electron microscopy, Scanning Electron Microscopy (SEM) and Transmission Electron Microscopy (TEM). SEM looks at the surface of the sample, identifying structural abnormalities and shapes

of the sample. In contrast TEM provides informative two dimensional details on cellular ultrastructure (McIntosh *et al*., 2017).

Bloodstream form *T. brucei* at 0, 24 and 48 hours post RNAi of TbGEF3 were harvested and prepared for TEM. The prepared samples were kindly processed for TEM at Technology Facility, Department of Biology, University of York by Meg Stark.

TEM enabled the visualisation of *T. brucei* ultrastructure at different time points post RNAi, and these results were compared to the wild type *T. brucei* ultrastructure. The cellular ultrastructure of wild type and 0 hours post RNAi samples were similar. Regular morphology of subpellicular microtubules, nucleus, paraflagellar rod and flagellum can be observed in both samples (Figure 4.26 and Figure 4.27). The cellular ultrastructure for samples that were subjected to RNAi for 24 hours were different to the wild type ultrastructure (Figure 4.28). The presence of nucleus and paraflagellar rod could not be visualised clearly in the 24 hours RNAi samples. Presence of a large vacuole can be observed and this was identified by TEM as the enlarged flagellar pocket. The vacuole was designated as the flagellar pocket due to the presence of an electron dense VSG coat on the membrane and the presence of flagellum bound to the membrane via flagellum attachment zone (Allen *et al*., 2003). Unfortunately cells in the 48 hours post RNAi samples lysed during processing and therefore TEM images could not be obtained.

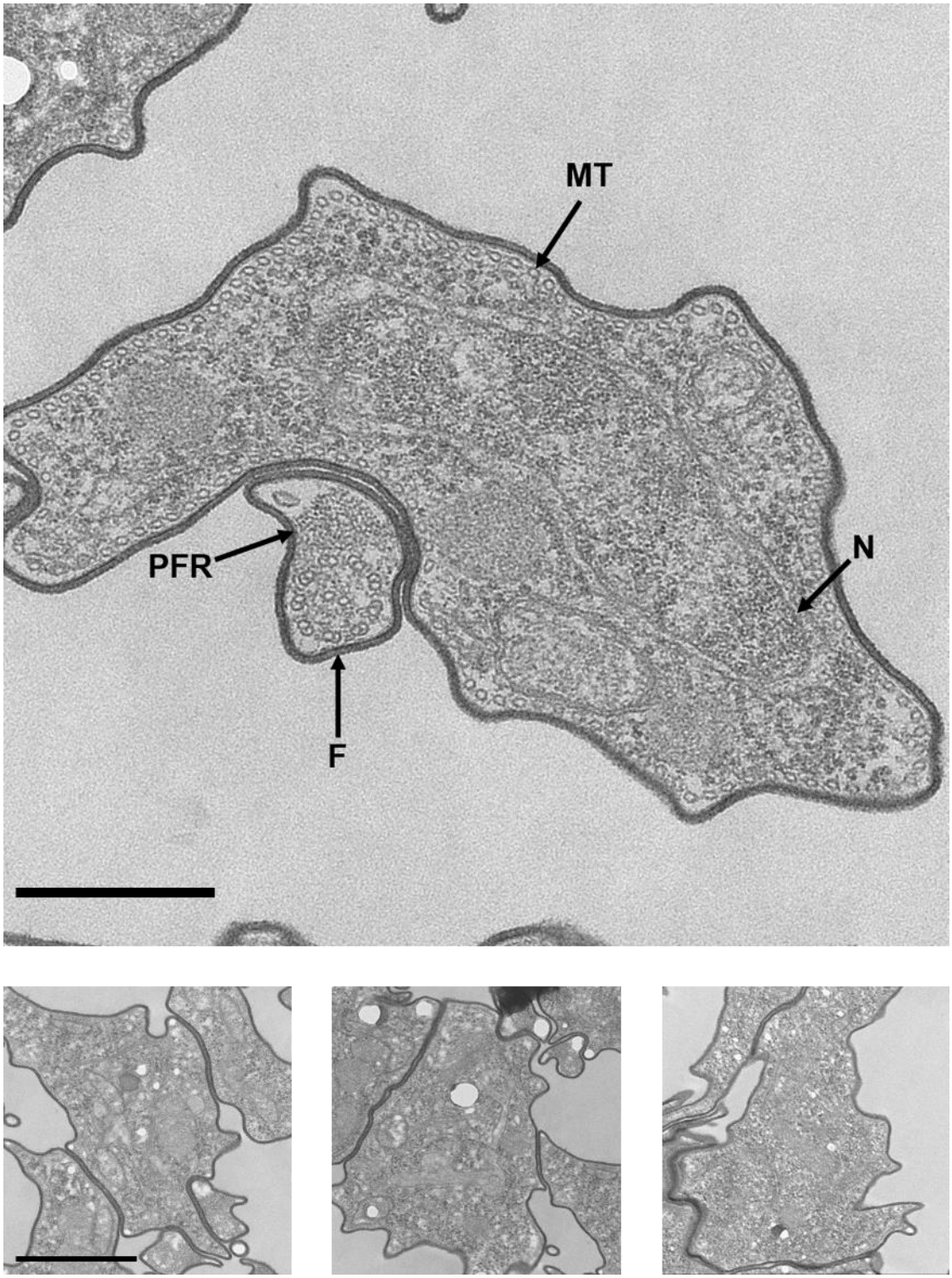

***Figure 4.26. Transmission Electron Microscopy of wild type bloodstream form* T. brucei.**

The cellular ultrastructure of wild type bloodstream form T. brucei *was determined. Visible components of the cells were labelled. MT; microtubules, PFR; paraflagellar rod, F; flagellum, and N; nucleus. Scale bars: Large image – 500 nm, small image – 1 μm.*

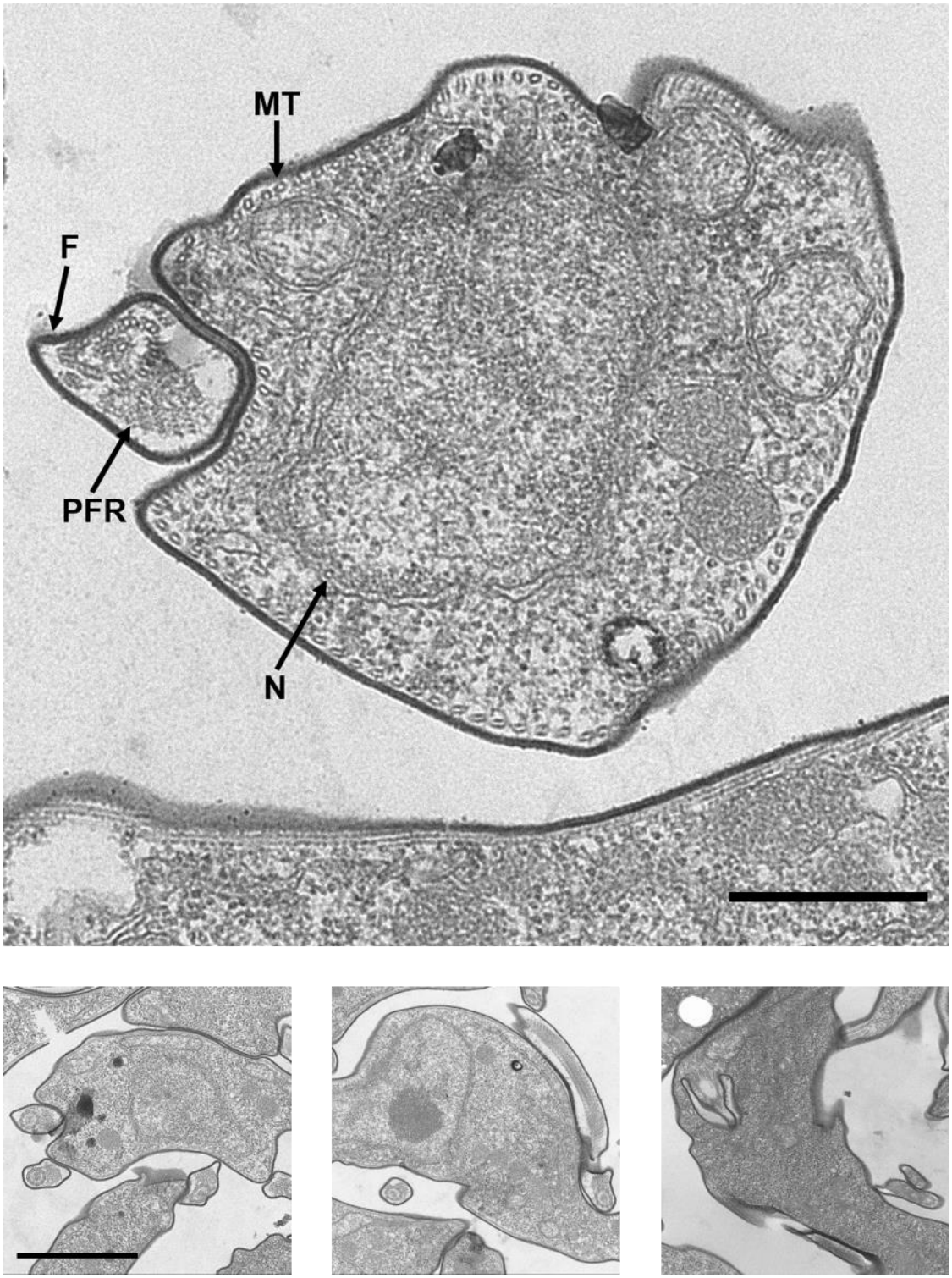

***Figure 4.27. Transmission Electron Microscopy RNAi induced bloodstream form* T. brucei.** *Samples from 0 hours post RNAi of TbGEF3 were analysed using TEM. Visible components of the cells were labelled. MT; microtubules, PFR; paraflagellar rod, F; flagellum, and N; nucleus. Scale bars: Large image – 500 nm, small image – 1 μm.*

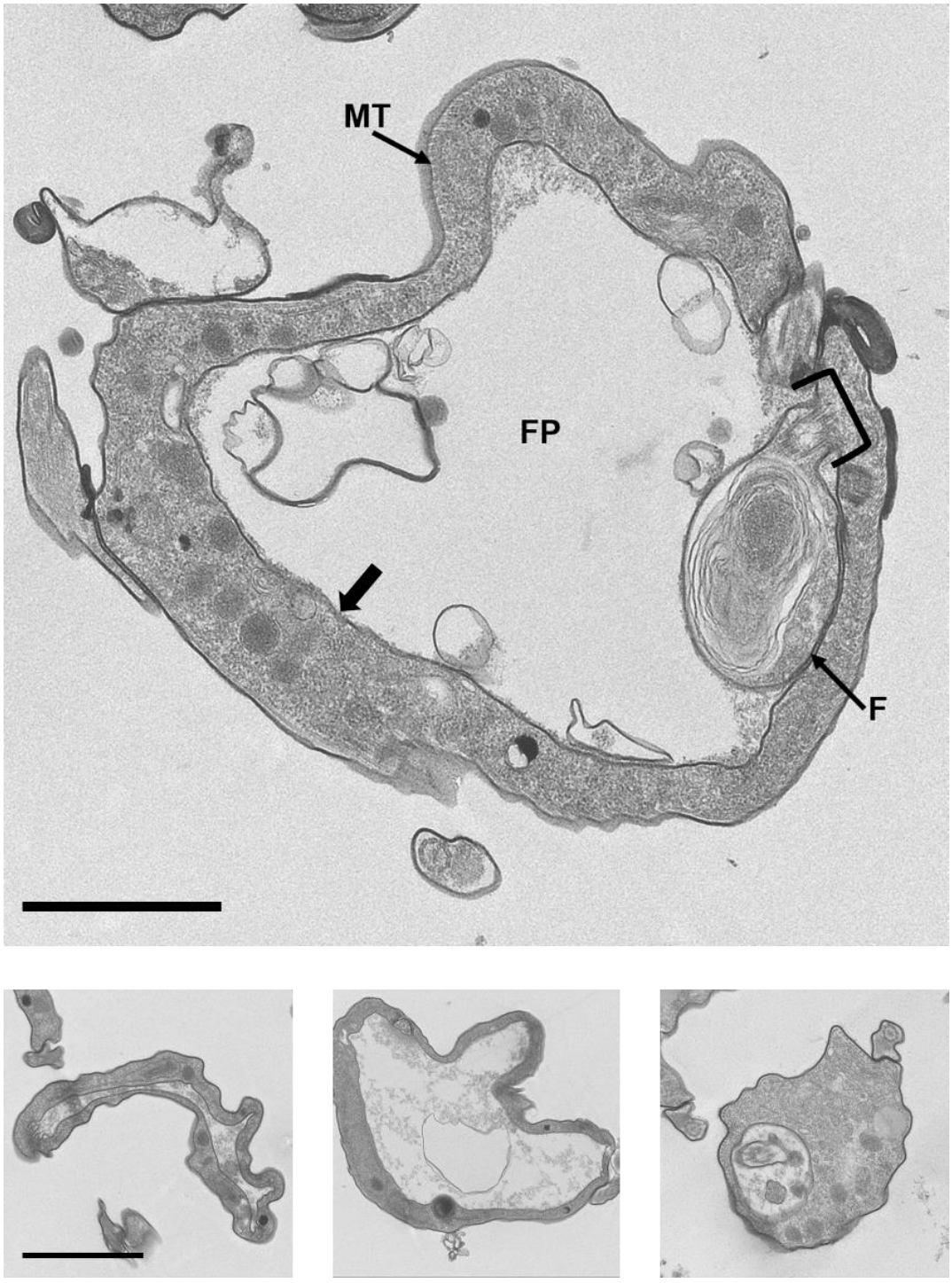

***Figure 4.28. Transmission Electron Microscopy RNAi induced bloodstream form* T. brucei.** *Samples from 24 hours post RNAi of TbGEF3 were analysed using TEM. MT; microtubules, FP; flagellar pocket, F; flagellum; arrow indicate the electron dense VSG coat; and open bracket indicates the flagellar attachment zone. Scale bars: Large image – 500 nm, small image – 1 μm.*

4.3.7 Concanavalin A endocytosis assay

Allen *et al*. (2003) demonstrated the correlation between endocytosis defect and the presence of BigEye morphology in bloodstream form *T. brucei* post RNAi of TbCLH (Allen *et al*., 2003). Price *et al*. (2007) also observed similar results post RNAi of TbARF1 (Price *et al*., 2007b). This suggests that the BigEye morphology observed in microscopy images post RNAi of TbGEF3 in section 4.3.6 may also hint to possible endocytosis defect. Receptor mediated and fluid phase endocytosis occurs at the flagellar pocket in *T. brucei*. Endocytosed components such as antibody bound VSGs are delivered to early endosomes (TbRab5A/B) and recycled to either recycling endosomes (TbRab11) or late endosomes (TbRab7). The VSG is then trafficked to the single lysosome where it is degraded (Umaer *et al*., 2018, Engstler *et al*., 2004, Overath and Engstler, 2004). A defect in endocytosis would mean that lipids, solutes and receptor bound ligands would not be delivered to the endosomes; and would accumulate in the flagellar pocket instead.

An endocytosis defect in Lister 427 bloodstream form *T. brucei* was identified by Allen *et al*. (2003) and Price *et al*. (2007) with the use of FITC-labelled Concanavalin A (Con A). Con A is a legume lectin that is readily taken up by bloodstream form *T. brucei* via endocytosis (Allen *et al*., 2003). At different temperatures Con A will be localised at different endocytic pathway components. At 4°C Con A is localised at the flagellar pocket where endocytosis occurs. At 12°C Con A is taken deeper into the cell via endocytic pathways and localised to TbRab5A early endosomes. At 37°C Con A is further taken up to the lysosomes (Allen *et al*., 2003, Jeffries *et al*., 2001). TbRab5A endosomes and lysosomes (P67) were labelled with Rabbit anti-TbRab5A and mouse anti-P67 primary antibodies respectively, and Alexa Fluor 594 secondary antibodies were used to detect the primary antibodies. This is to ensure that the localisation of Con A can be visualised and determined if they are in close proximity to the organelles.

Figure 4.29 shows that Con A is present next to the kinetoplast, where the flagellar pocket is located. This suggests that Con A was taken up into the flagellar pocket and it remained

localised to the flagellar pocket for all time points post RNAi of TbGEF3 at 4°C as expected. There was an increase in number of cells from 48 hours post RNAi that did not have Con A present in their cells. This may suggest that there is an increase in the number of dead cells from 48 hours post RNAi.

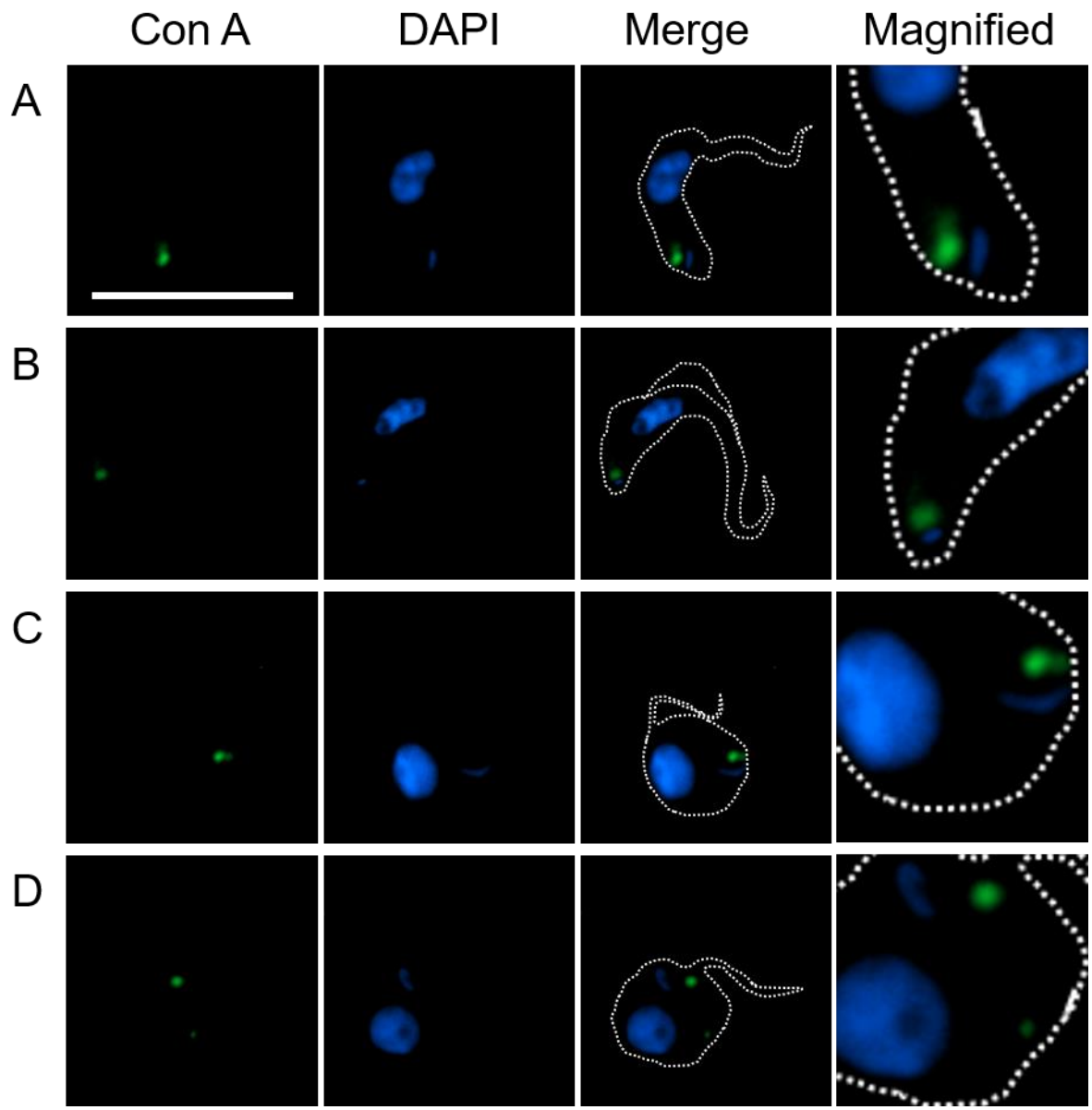

Figure 4.29. Endocytosis of Con A at 4°C. *Endocytosis disruption was examined in* T. brucei *samples from (A) 0 hours, (B) 4 hours, (C) 24 hours and (D) 48 hours post RNAi of TbGEF3. FITC-labelled Con A (green) was used to detect endocytosis. Nucleus and kinetoplast are labelled in blue. Scale bar = 10 μm. Images in the last column were magnified by 2.5 fold.*

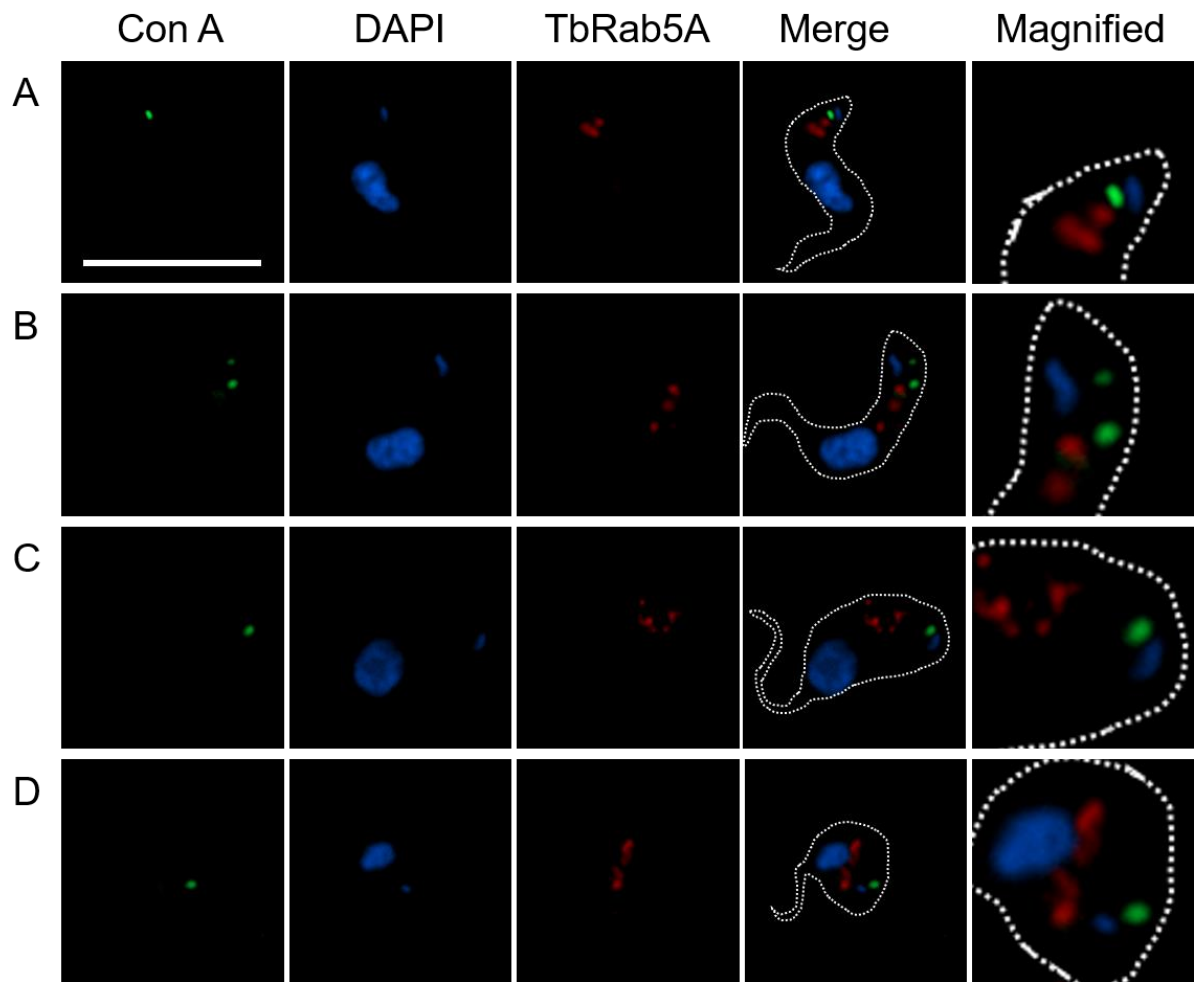

Figure 4.30. Endocytosis of Con A at 12°C. *Endocytosis disruption was examined in* T. brucei *samples from (A) 0 hours, (B) 4 hours, (C) 24 hours and (D) 48 hours post RNAi of TbGEF3. FITC-labelled Con A (green) was used to detect endocytosis, TbRab5A are shown in red. Nucleus and kinetoplast are shown in blue. Scale bar = 10 μm. Images in the last column were magnified by 2.5 fold.*

At 12°C Con A is transported to the early endosomes (labelled here by TbRab5A) (Allen *et al*., 2003). The localisation of TbRab5A was visualised by using rabbit anti-TbRab5A primary antibody and Alexa Fluor 594 secondary antibody. Figure 4.26 shows that TbRab5A can be visualised in multiple puncta in the cells at all time points post RNAi. However endocytosed Con A only partially co-localises with TbRab5A from 0 hours post RNAi to 4 hours post RNAi (Figure 4.30.A-B). Although Con A was present in the flagellar pocket of cells with BigEye morphology from 24 hours post RNAi, the Con A were not taken up further into TbRab5A (Figure 4.30.C-D). This shows endocytosis being compromised in cells from 24 hours post RNAi.

Similar results were observed in cells incubated at 37°C with Con A. At 37°C, Con A is transported to the terminal endosomal compartment, the lysosome, a single organelle in trypanosomes (Allen *et al*., 2003). The localisation of the lysosome was visualised using mouse anti-P67 primary antibodies and Alexa Fluor 594 secondary antibodies. The cells from 0 hours to 4 hours post RNAi showed that Con A was transported to compartments adjacent to the p67-stained lysosome (Figure 4.31.A-B). However, from 24 hours post RNAi, the cells started to exhibit BigEye morphology. This was accompanied by the lack of transport of Con A away from the flagellar pocket (Figure 4.31.C-D). This further suggests that an endocytosis defect is present in bloodstream form *T. brucei* cells that had undergone RNAi of TbGEF3 for 24 hours or more. Interestingly around 60% of cells from 48 hours post RNAi of TbGEF3 showed no presence of Con A signal (Figure 4.31.D). This may suggest that uptake into the flagellar pocket is compromised or that the cells from 48 hours post RNAi have died or lysed during the preparation of the endocytosis assay. This finding coincides with the live/dead flow cytometry data from section 4.3.5.2; where increase in cell death was observable from 48 hours post RNAi of TbGEF3.

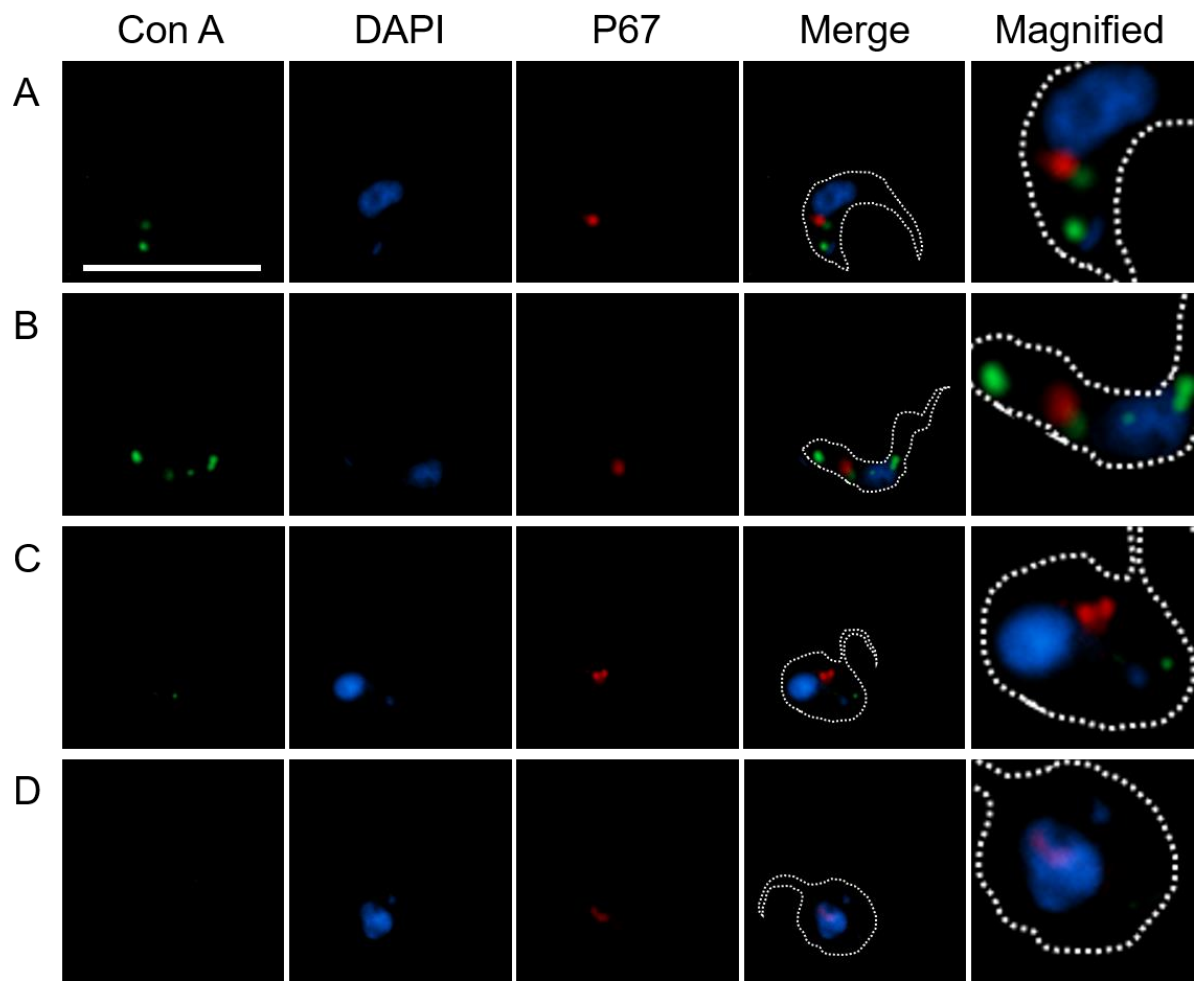

Figure 4.31. Endocytosis of Con A at 37°C. *Endocytosis disruption was examined in* T. brucei *samples from (A) 0 hours, (B) 4 hours, (C) 24 hours and (D) 48 hours post RNAi of TbGEF3. FITC-labelled Con A (green) was used to detect endocytosis, P67 lysosomes are shown in red. Nucleus and kinetoplast are shown in blue. Scale bar = 10 μm. Images in the last column were magnified by 2.5 fold.*

4.4 Discussion

This chapter aimed to identify which of the TbGEFs and TbGAPs were essential for bloodstream form *T. brucei* viability. This chapter also aimed to identify the effects of RNAi of TbGEFs and/or TbGAPs on growth and morphology of bloodstream form *T. brucei*, as well as identify any differences can be observed between the RNAi of TbGEFs and TbGAPs. Suitable RNAi regions were identified and amplified by PCR. RNAi constructs were generated and transfected into bloodstream form *T. brucei* for further analysis in order to analyse the effects of RNAi on bloodstream form *T. brucei*.

4.4.1 Unsuccessful transfections may be due to a leaky inducible expression system

RNAi is an ancient and ubiquitous mechanism of antiviral defence that utilises small interfering RNAs (siRNAs) and microRNAs (miRNA) produced from the cleavage of double stranded RNAs (dsRNA) by DICER, a ribonuclease (Saurabh *et al*., 2014, Fire *et al*., 1998, Ding *et al*., 2018). The siRNAs and miRNAs are incorporated into the RNA-induced silencing complex (RISC). This results in the interference of mRNA translation, thus leading to gene expression knockdown (Saurabh *et al*., 2014, Fire *et al*., 1998, Ding *et al*., 2018). A functioning RNAi system was first demonstrated in *T. brucei* in 1998, making *T. brucei* the first protozoan parasites with an identified operational RNAi system (Kolev *et al*., 2011). The RNAi system in *T. brucei* utilises two DICER like homologues (TbDCL1 and TbDCL2) that synthesise siRNAs (Shi *et al*., 2006, Patrick *et al*., 2009). The synthesised siRNAs associates with the single argonaute protein present in *T. brucei* (TbAGO1), which is then incorporated into the RISC complex and induces gene knockdown via mRNA translation interference (Durand-Dubief and Bastin, 2003, Shi *et al*., 2004, Shi *et al*., 2009).

Original RNAi studies in *T. brucei* involved transfection of dsRNA to induce knockdown of target mRNAs, however the effect of this knockdown was short and only present for one cell cycle (Ngô *et al*., 1998). To overcome the temporary effect of RNAi post transfection of dsRNA

in *T. brucei*, a tetracycline inducible RNAi system was introduced (discussed in detail in section 4.3.2). RNAi regions of the identified *T. brucei* GEFs and GAPs were ligated to the tetracycline inducible RNAi system, transformed and grown on selective agar plates in order to generate large quantities of recombinant DNA (Rahimzadeh *et al*., 2016). The purified recombinant DNA were transfected into bloodstream form *T. brucei*.

Transfection can be broadly categorised into three types of techniques that can be used to introduce foreign nuclei acids into a cell; biological, chemical and physical transfection (Chow *et al*., 2016). Delivery of linear recombinant DNA into bloodstream form *T. brucei* was achieved by electroporation, a physical transfection technique, in this chapter. Electroporation technique was first demonstrated by Neumann *et al.* (1982) on mouse lyoma cells, who showed that electric impulses greatly increased intake of DNA into cells (Neumann *et al*., 1982). The duration, intensity and frequency of the electric impulse affected the efficiency of gene delivery into a cell (Heller *et al*., 2005). The electric impulse generates temporary permeability in the cell membrane, allowing DNA to enter the cell without damaging the cell (Kamimura *et al*., 2011, Sugar and Neumann, 1984).

Stable cell lines were grown post transfection of P2T7-TbGEF/GAP into Lister 427 bloodstream form *T. brucei*. However transfection of P2T7-TbGEF1 into bloodstream form *T. brucei* did not yield stable transgenic cell lines from 24 hours post transfection despite numerous attempts. Previous studies have highlighted that transfection of the P2T7^{Ti} vector sometimes caused 'leaky' expression in uninduced cells (LaCount *et al*., 2002). This leaky expression coupled with knockdown of an essential gene may have caused the rapid killing of bloodstream form *T. brucei* from 24 hours post transfection of P2T7-TbGEF1. Further evidence of leaky expression in transfected bloodstream form *T. brucei* was observed during light microscopy visualisation of the cells after transfection of TbGEF1. Uninduced transfected bloodstream form *T. brucei* exhibited phenotypes with large vacuole and sometimes multiple flagellum. The presence of large vacuoles in bloodstream form *T. brucei* is known as BigEye morphology, and has been known to be caused by enlarged flagellar pocket (Allen *et al*.,

2003). Previous RNAi studies on *T. brucei* have identified the presence of BigEye morphology when RNAi was induced. An example of this is the study by Price *et al*. (2007), who demonstrated that inducing RNAi of ARF1 resulted in BigEye morphology in bloodstream form *T. brucei* (Price *et al*., 2007b).

Alternative methods of gene knockdown systems in bloodstream form *T. brucei* are available for tightly controlled inducible expression of dsRNA for essential genes. The p*Tb*FIX vectors consists of two transcription units. The RNAi of target gene is driven by inducible rRNA promoter containing two TetOPs and a downstream dicistronic unit that encodes TetR. The p*Tb*FIX vector contains the sequence of interest and regulatory elements for gene silencing; thus this vector eliminates the need for pre-existing transgenic cell lines that can be transfected with the RNAi sequence (Niemirowicz *et al*., 2018). Niemirowicz *et al* (2018) successfully knocked down the expression of clathrin heavy genes in bloodstream form *T. brucei* using the p*Tb*FIX vector (Niemirowicz *et al*., 2018).

Another alternative inducible system is the *glmS* ribozyme based inducible gene expression system. The *glmS* ribozyme is inserted into the C-terminal of the gene of interest allele. The *glmS* acts as a self-cleaving riboswitch, which when inserted into the 5'-UTR or 3'-UTR of the gene of interest causes gene silencing in the presence of glucosamine 6-phosphate (Cruz-Bustos *et al*., 2018). Cruz-Bustos *et al*. had noted that the *glmS* ribozyme inducible system worked as effectively as the conventional RNAi system, minus the drawback from leaky expression (Cruz-Bustos *et al*., 2018). The *glmS* ribozyme inducible system was used to knockdown the expression of TbVPS41 and compare the knockdown effect to RNAi knockdown system. Results showed that whilst knockdown of TbVPS41 was only effective for 2 days, the knockdown of TbVPS41 using the *glmS* ribozyme inducible system remained stable (Cruz-Bustos *et al*., 2018).

Future work involving one of these gene knockdown techniques on TbGEF1 may provide a stable transfected cell line that can be further studied.

4.4.2 Identification of essential ARF regulators in bloodstream form *T. brucei*

A tetracycline induced RNAi system has been used in this thesis to inhibit the expression of *T. brucei* GEFs and GAPs in bloodstream form *T. brucei*. Three clones were randomly selected from transgenic cell lines that were successfully transfected with TbGAP1, TbGAP4, TbGEF2 and TbGEF3; and the effect of RNAi on bloodstream form *T. brucei* growth was studied. RNAi of TbGEF3 was shown to have greatly affected the growth of bloodstream form *T. brucei*. Especially in clone 6 where the effect of RNAi of bloodstream form *T. brucei* growth can be observed from 24 hours post addition of tetracycline. This could possibly mean that TbGEF3 is essential for the viability of bloodstream form *T. brucei*. There was also a significant difference in parasite growth from 48 hours post RNAi of TbGEF2, suggesting that TbGEF2 may also be essential in bloodstream form *T. brucei*. Although there was a significant difference in bloodstream form *T. brucei* growth post RNAi of TbGAP1 and TbGAP4, the differences were not as great as the effect of TbGEF3 RNAi.

The effect of RNAi on parasite growth was not uniform in all clones of P2T7-TbGEF3 cell lines, with the same trend being observed in the P2T7-TbGAP1, P2T7-TbGAP4 and P2T7-TbGEF2 cell lines. There is a possibility that the lack of difference in bloodstream form *T. brucei* growth observed in section 4.3.3 in some clones of the P2T7-TbGAP1, P2T7-TbGAP4, P2T7-TbGEF2 and P2T7-TbGEF3 cell lines may be due to incomplete knockdown or lack of RNAi taking place. A qPCR can be used to analyse the expression of the TbGEF and TbGAP genes in order to determine if there was a partial knockdown or no RNAi taking place in some of the clones.

Successful qPCR data was only obtained for clone 6 of TbGEF3 cell line. The data in section 4.3.4 showed that the expression of TbGEF3 had reduced from 0 to 48 hours post RNAi. The change in TbGEF3 expression from 0 hour to 4 hours was not statistically significant. However, the expression of TbGEF3 in 24 hours and 48 hours post RNAi samples were significantly reduced compared to 0 hours post RNAi sample. qPCR on all clones for TbGEFs and TbGAPs

should be carried out in the future to determine if the differences in parasite growth observed was due to incomplete knockdown or no RNAi taking place.

In order to determine if the lack of parasite growth observed in section 4.3.3 was due to increase in parasite death from 24 hours post RNAi of TbGEF3, a Live/Dead flow cytometry analysis was carried out using Live/Dead Fixable Red Dead Stain on clone 6 from P2T7-TbGEF3 cell line. The same was done for clone 2 from P2T7-TbGAP1, clone 6 from P2T7-TbGAP1 and clone 2 from P2T7-TbGEF2 cell lines. These clones showed the most significant differences in bloodstream form *T. brucei*, therefore they chosen for further analysis.

All eukaryotic cell surfaces are covered by lipids and proteins, making up the plasma membrane. Cell death due to either apoptosis, necrosis or other factors lead to compromised plasma membrane (Zhang *et al*., 2018, Bridges *et al*., 2008). Live/Dead Fixable Red Dead dye reacts with amines present on the cell surface. The dye also reacts with free amines present inside membrane compromised dead cells. Thus the intensity of the fluorescent dye increases in plasma membrane compromised cells than compared to viable cells. Similar to propidium iodide flow cytometry, the samples stained with Live/Dead Fixable Red Dead dye are rapidly passed in front of a laser. Dead cells will emit stronger fluorescence than live cells. This difference in fluorescence data is collated and visualised in Dot plot graphs (Dey, 2018).

Live/Dead flow cytometry data from section 4.3.5.2 showed that the RNAi of TbGAP1, TbGAP4 and TbGEF2 had similar results. Around 97% of the cell population were live for all three cell lines at all time points post RNAi. This suggests TbGAP1, TbGAP4 and TbGEF2 may not be essential for the viability of bloodstream form *T. brucei*. Hence no effects were seen on the growth of bloodstream form *T. brucei* following the RNAi of their respective regulators.

Similarly, RNAi of TbGEF3 data showed that there were no significant differences between live and dead cells from 0 to 24 hours post RNAi of TbGEF3. High percentage of the cell population (90-93%) consisted of live cells whilst 6-9% of the cell population were dead.

However an increase in dead cells was observed at 48 hours post RNAi, with 54% of the cell population being dead and 43% of the population being alive. This data suggests that RNAi of TbGEF3 does not cause rapid cell death, but cell death occurs slowly.

Propidium iodide flow cytometry was then used in order to identify if the differences in parasite growth for each ARF regulator gene was due to defect in cell cycle progression, since RNAi of TbGEFS and TbGAPs did not cause cell death (or rapid cell death) that may explain the growth curve data seen in section 4.3.3.

Like other eukaryotic cells, *T. brucei* undergoes a tightly regulated cell cycle. Broadly following the G_0/G_1, S, G_2 and M phases of the cell cycle. However *T. brucei* consists of single copies of nucleus and kinetoplast (mitochondrial DNA), as well as other organelles and structures. These single copy organelles and structures are duplicated and segregated at particular phases of the cell cycle (Hammarton, 2007, Benz *et al*., 2017, Jakob *et al*., 2016). Kinetoplast replication and segregation occurs prior to nuclear replication and segregation, enabling *T. brucei* cells to progress from 1K1N (K refers to kinetoplast whilst N refers to nucleus) to 2K1N configuration. Nuclear division during mitosis progresses *T. brucei* cells to 2K2N configuration. Mitosis is followed by cytokinesis, leading to the formation of two daughter cells (Hammarton, 2007, Benz *et al*., 2017). Previous studies have shown that cell cycle arrest and defect in cytokinesis in *T. brucei* is characterised by the presence of multiple nuclei, flagellar and abnormal morphology (Mudogo *et al*., 2018, Price *et al*., 2010b). The presence of multiple nucleus was examined in section 4.3.5.1 to determine if RNAi of TbGEFs and TbGAPs caused a cell cycle defect.

Results in section 4.3.5.1 showed that all transfected cells lines prior to RNAi (0 hours) and wild type samples consisted of cells with DNA content of 2C and 4C. Normal bloodstream form *T. brucei* undergo cell division that lasts for approximately 8 hours in order to produces viable progeny. During the cell division the parasite transitions from G_0/G_1 phase of the cell cycle, where DNA content of 2C is present, to the G_2 phase where DNA content of 4C is present (Hammarton, 2007, Peacock *et al*., 2014, Benz *et al*., 2017). This controlled cell division may

explain the presence of 2C and 4C DNA content in the 0 hours post RNAi and wild type samples. However defect in cytokinesis leads to *T. brucei* cells replicating without forming daughter cells, thus leading to multiple nucleus present in the cell and a DNA content of 8C or more (Jones *et al*., 2014).

A normal cell population with DNA content of 2C and 4C was observed in all time points post RNAi of TbGAP1, TbGAP4 and TbGEF2. This suggests that RNAi of these genes has not affected the cell cycle progression in bloodstream form *T. brucei*. Although the 0 and 4 hours post RNAi of TbGEF3 samples showed that the cell population consisted of healthy cells with DNA content of 2C and 4C. The DNA content of TbGEF3 samples from 24 and 48 hours post RNAi showed a significant decrease in populations with DNA content of 2C. An increase in new populations with DNA contents of 8C and 16C can be observed in 24 and 48 hours post RNAi samples respectively. This suggest that a defect in cytokinesis is present in bloodstream form *T. brucei* from 24 hours post RNAi of TbGEF3. This may also suggest that TbGEF3 may be implicated in the function of cytokinesis and cell cycle progression in bloodstream form *T. brucei*, albeit at a lower level since RNAi did not affect cell cycle progression immediately.

Propidium iodide flow cytometry result for TbGEF3 also coincides with the results observed in section 4.3.3, suggesting that defect in cell cycle progression contributed to lack of bloodstream form *T. brucei* growth; since cell cycle defect results in lack of healthy daughter cells being produced, thus leading to decrease in parasite growth. There is also a possibility that the high percentage of dead cells in 48 hours post RNAi may have been caused by accumulation of cells with cytokinesis defect dying from 48 hours post RNAi of TbGEF3. The gene expression change results observed in section 4.3.4 may also explain the morphological and physiological changes observed in bloodstream form *T. brucei* post RNAi of TbGEF3. The absence of significant expression changes in TbGEF3 at 4 hours post RNAi could mean that the function of TbGEF3 could have resumed without causing any effect on bloodstream form *T. brucei*, hence no changes in cell cycle progression or cell death was observed until 24 hours post RNAi.

GEFs and GAPs are known to interact with more than one ARF/ARLs in order to regulate their functions (Sztul *et al*., 2019). The lack of significant effect on bloodstream form *T. brucei* growth seen post RNAi of TbGAP1 and TbGAP4 may mean that more than one *T. brucei* GAPs may be interacting with the ARF/ARLs that are regulated by TbGAP1 and TbGAP4. Identification of the ARF/ARLs that interact with TbGAP1 and TbGAP4 using protein-protein interaction studies may identify other *T. brucei* GAPs or GEFs that interacts with their respective ARF/ARLs. Following this, a pairwise knockdown (Tu and Wang, 2005) of TbGAP1/4 and another regulator that interacts with the target ARF/ARLs may provide with additional information on the effect of multiple ARF regulators at the same time.

4.4.3 TbGEF3 may be involved in endocytic pathways

Propidium iodide and Live/Dead flow cytometry data in section 4.3.5 showed that RNAi of TbGEF3 causes a cell cycle defect in bloodstream form *T. brucei* as opposed to rapid parasite killing. Defect in cell cycle is characterised by the presence of multiple nucleus, flagellum and abnormal morphology in bloodstream form *T. brucei* (Mudogo *et al*., 2018, Price *et al*., 2010b). Mudogo *et al*. (2018) identified the presence of BigEye morphology in bloodstream form *T. brucei* that had partial cell cycle arrest (Mudogo *et al*., 2018). Indirect immunofluorescent microscopy was used to visualise the cell structure of bloodstream form *T. brucei* at different times points post RNAi of TbGEF3 in section 4.3.6.1 and to identify the presence of abnormal morphology. Indirect immunofluorescent microscopy was also used to visualise the cellular structures of bloodstream form *T. brucei* post RNAi of TbGAP1, TbGAP4 and TbGEF2.

Microscopy images showed bloodstream form *T. brucei* having slender morphology termed vermiform from 0 to 4 hours post RNAi of TbGEF3 and in all time points for TbGAP1, TbGAP4 and TbGEF2. This cell structure was similar to the wild type cell structure observed in section 4.7.1 as well as the cell structure described in literature for wild type bloodstream form *T. brucei* (Pineda *et al*., 2018). Formation of bloodstream form *T. brucei* with circular morphology was observed from 24 hours to 48 hours post RNAi of TbGEF3. Previous studies on

bloodstream form *T. brucei* with circular morphology has been identified as the 'BigEye' morphology caused by enlarged flagellar pocket (Allen *et al*., 2003, Price *et al*., 2007b). However indirect immunofluorescent microscopy images did not clearly show the presence of a vacuole caused by enlarged flagellar pocket. TEM was used in order to identify if the cells with circular morphology that was observed in the indirect immunofluorescent microscopy.

RNAi was induced at 0, 24 and 48 hour time points in bloodstream form *T. brucei*. However only 0 and 24 hours samples were successfully processed for TEM. Unfortunately 48 hour time point RNAi sample did not survive transportation for TEM processing. TEM images in section 4.3.6.2 showed that wild type and 0 hours post RNAi *T. brucei* cells had similar cellular structure with visible microtubules, flagellum, paraflagellar rod and nucleus. This suggest that transfection of P2T7-TbGEF3 did not cause any cellular changes in *T. brucei*.

The presence of an enlarged vacuole in *T. brucei* cellular structure from 24 hours post RNAi can be observed in section 4.3.6.2. The enlarged structure was identified as the flagellar pocket. The flagellar pocket is a small invagination in the plasma membrane from where the proximal end of the flagellum emerges. Flagellar pocket is also the site where endocytosis and exocytosis takes place in bloodstream form *T. brucei* (Field and Carrington, 2009, Langousis and Hill, 2014). Enlarged flagellar pocket was first described by Allen *et al*. (2003), who identified the presence of BigEye morphology post RNAi of TbCLH (*T. brucei* clathrin heavy chain) in bloodstream form *T. brucei* (Allen *et al*., 2003). Allen *et al*. also noted a severe defect in endocytosis in cells with an enlarged flagellar pocket, suggesting that BigEye morphology is characterised by absence of endocytosis in bloodstream form *T. brucei* (Allen *et al*., 2003). Price *et al*. (2007) also identified a decrease in endocytosis post RNAi of TbARF1 in bloodstream form *T. brucei* (Price *et al*., 2007b). This may mean that the *T. brucei* cells exhibiting BigEye morphology post RNAi of TbGEF3 may also have an endocytosis defect.

Endocytosis was investigated in the cell lines using FITC-labelled Concanavalin A (Con A), a legume lectin that is readily taken up by bloodstream form *T. brucei* via receptor-mediated endocytosis (Allen *et al*., 2003). Data in section 4.3.7 shows that Con A was further

endocytosed into TbRab5A and P67 lysosomes at 12°C and 37°C respectively at 0 and 4 hours post RNAi of TbGEF3. Interestingly Con A did not localise to TbRab5A and P67 lysosomes at their respective temperatures from 24 hours post RNAi of TbGEF3. This demonstrates defect in endocytosis in samples with BigEye morphology.

Around 60% of *T. brucei* cells in the 48 hours post RNAi of TbGEF3 samples consisted of cells with no visible presence of Con A in the flagellar pocket or other organelles. This may be due to the severity of endocytosis and cell cycle defect. Live/Dead flow cytometry data from section 4.3.5.2 showed that there was an increase in cell death at 48 hours post RNAi of TbGEF3. There is also a possibility that the stress of preparation of samples for the endocytosis assay may have killed cells that had severe endocytosis defects. Endocytosis assay on the 48 hours post RNAi time point was carried out four time and the same results was seen across all samples at that particular time point. Further investigation needs to be carried out in order to determine if lack of Con A presence in cells is due to endocytosis defect or cell death.

4.5 Conclusions

The main findings of this chapter are as follows:

- TbGEF3 is essential for bloodstream form *T. brucei* viability. RNAi of TbGEF3 negatively affects the growth, morphology and cell cycle of bloodstream form *T. brucei*.
- RNAi of TbGEF3 may have a cytostatic than cytocidal effect on bloodstream form *T. brucei*. An increase in cell death can observed from 48 hours post RNAi of TbGEF3, however a defect in cell cycle progression can be observed from 24 hours post RNAi of TbGEF3. This suggests that a cell cycle defect could be the cause of the cell death that was observed in Live/Dead flow cytometry.
- BigEye morphology could be seen from 0 hours post RNAi of TbGEF3 – leaky expression system of the P2T7^{Ti} vector meant that expression of BigEye morphology

could be seen in samples prior to RNAi induction. However the number BigEye morphology increased from 24 hours post RNAi of TbGEF3.

- Receptor-mediated endocytosis of Con A was compromised in bloodstream form *T. brucei* following TbGEF3 knockdown.
- Knockdown of TbGAP1, TbGAP4 and TbGEF2 does not appear to affect the growth, morphology or cellular functions of bloodstream form *T. brucei*. Further work need to be carried out to confirm the effect of TbGAP1, TbGAP4 and TbGEF2 knockdown.

Chapter 5 – Exploring the use of *T. brucei* GEF3 RNAi cell line in drug discovery

5.1 Introduction

The rise in resistance to existing drugs means that new tools to identify potent drugs against Neglected Tropical Diseases (NTDs) are of high importance (Molyneux *et al*., 2017). Field reports have identified a rise in resistance to two out of the five current drugs against Human African Trypanosomiasis (HAT) and the three current drugs against Animal African Trypanosomiasis (nagana) (Fairlamb and Horn, 2018, Giordani *et al*., 2016). These drugs are pentamidine and melarsoprol, against HAT; and diminazene aceturate, homidium and isometamidium, against nagana. All five of these drugs are taken up into the *T. brucei spp.* via *TbAT1*/P2 transporters. Resistance to these drugs have been established in *T. brucei spp.* due to loss-of-function mutations and deletion of the *TbAT1* gene that encodes the P2 transporters (Fairlamb and Horn, 2018). Additionally, deletion or rearrangement of *T. brucei* aquaglyceroporin 2 (TbAQP2) has been shown to induce resistance to pentamidine via HAPT1 transporters (Munday *et al*., 2014).

Initiatives into drug discovery against HAT and data mining approach of previously identified compounds led to the rediscovery of fexinidazole, a 5-nitroimidazole derivative that is registered as an oral treatment against late stage *T. b. gambiense* infection (Mesu *et al*., 2018, Torreele *et al*., 2010). Fexinidazole and nifurtimox are both nitroaromatic compounds, and the activation of these drugs in *T. brucei* requires reductive activation via nitroreductase (NTR). Single point mutations and deletion in NTR were shown to induce cross resistance to both nifurtimox and fexinidazole (Wyllie *et al*., 2015, Deeks, 2019). This suggests that there might be a possibility of *T. b. gambiense* undergoing mutation that could lead to resistance to the newly registered fexinidazole.

Suramin is a drug that is used to treat early stage *T. b. rhodesiense* infection in humans. As a large highly charged molecule, suramin is unable to diffuse through the cell membrane (Wiedemar *et al*., 2019). This means that suramin entry into *T. brucei spp.* occurs via a highly specific endocytic pathway that involves bloodstream stage specific invariant surface glycoprotein ISG75 and variant surface glycoproteins (Thomas *et al*., 2018, Wiedemar *et al*.,

2018). Despite suramin being used as a drug against HAT for over 50 years, there has been no reports of resistance to suramin by human infective *T. brucei spp.* (Wiedemar *et al*., 2018). However there have been limited reports of suramin resistance in animal pathogenic trypanosomes such as *T. evansi* (Wiedemar *et al*., 2018). The lack of widespread resistance to suramin in HAT suggests that drugs taken up by endocytosis mechanism may be less likely to induce resistance in parasites.

There are two main types of early drug discovery techniques that can be used to screen and identify potential compounds against *T. brucei spp.* These are the target-based screening and the phenotypic screening approaches. In the target-based screening approach, an essential target molecule within *T. brucei* is identified and studied, and compounds that are hypothesised to interact with the target molecule and inhibit its functions are tested in order to identify potential drugs. The phenotypic screening on the other hand utilises a library of compounds which are tested against *T. brucei*, and positive hits are further studied in order to identify their mechanism of action (Lage *et al*., 2018, Croston, 2017, Brown and Wobst, 2019).

It is essential during the drug discovery process to test hit compounds to prevent development of drugs for which there are existing or potential mechanisms of cross-resistance in *T. brucei*; for example any identified drug compounds that are taken up into *T. brucei spp.* via *TbAT1*/P2 transporters. However, we hypothesise that compounds that are taken up via endocytosis in *T. brucei spp.* may have reduced potential for development of resistance in parasites.

The Pathogen Box provided by Medicines for Malaria Ventures (MMV) (https://www.mmv.org/mmv-open/pathogen-box – accessed: Feb 2020; Geneva, Switzerland) consists of 400 molecules that have been shown to have inhibitory activity against pathogens causing a range of infectious diseases including: toxoplasmosis, tuberculosis, neosporosis, malaria, leishmaniasis and trypanosomiasis (Machicado *et al*., 2019, Duffy *et al*., 2017).

In Chapter 4, I identified transgenic Lister 427 bloodstream form *T. brucei* cell lines that exhibited endocytosis defects following RNAi knockdown of TbGEF3. In this chapter, a

TbGEF3 RNAi cell line will be used to develop an assay for identifying compounds in the Pathogen Box that are taken up via endocytosis in bloodstream form *T. brucei* and not by transporter proteins.

5.1.1 Aims

The aim of this chapter is to test whether transgenic Lister 427 bloodstream form *T. brucei* cell lines that have an endocytosis defect due to RNAi knockdown of TbGEF3, can be used to identify compounds that are taken up via endocytosis. The Pathogen Box open access source of compounds will be used as a proof of principle.

5.2 Methods

The following methods were used to determine drug compounds that are taken up via endocytosis:

5.2.1 Determination of IC_{50} of tetracycline

The IC_{50} value of tetracycline was identified using concentrations ranging from 1 μg/mL to 7.63 pg/mL. These concentrations were tested on bloodstream form P2T7-GEF3 *T. brucei* and Lister 427 bloodstream form wild type *T. brucei*. PrestoBlue® was used to measure parasite viability by reading fluorescence after 48 hours.

5.2.2 Determination of IC_{50} of suramin

The IC_{50} value of suramin was identified using concentrations ranging from 1 μM to 1.95 nM. These concentrations were tested on bloodstream form P2T7-GEF3 *T. brucei* and Lister 427

bloodstream form wild type *T. brucei*. PrestoBlue® was used to measure parasite viability by reading fluorescence after 48 hours.

5.2.3 Determination of IC_{50} of diminazene aceturate

The IC_{50} value of diminazene aceturate was identified using concentrations ranging from 1 μg/mL to 7.63 ng/mL. These concentrations were tested on bloodstream form P2T7-GEF3 *T. brucei* and Lister 427 bloodstream form wild type *T. brucei*. PrestoBlue® was used to measure parasite viability by reading fluorescence after 48 hours.

5.2.4 MMV Pathogen Box

Compounds from the Pathogen Box (MMV) were prepared at 10 μM and 1 μM concentration in HMI-9 media. Compounds were tested on Lister 427 bloodstream form wild type *T. brucei*. PrestoBlue® was used to measure parasite viability by reading fluorescence.

5.2.5 Determination of IC_{50} of Pathogen Box compounds

The IC_{50} value of 20 compounds that had positive activity against Lister 427 bloodstream form wild type *T. brucei* at 1 μM concentration was carried out. Concentrations ranging from 1 μM to 7.63 pM was used. These concentrations were tested on Lister 427 bloodstream form wild type *T. brucei*. PrestoBlue® was used to measure parasite viability by reading fluorescence after 48 hours.

5.3 Results

5.3.1 Identifying the IC_{50} of tetracycline, suramin and diminazene aceturate in transgenic lines of *T. brucei*

Tetracycline induced RNAi of TbGEF3 in bloodstream form *T. brucei* was shown to induce an endocytosis defect in Chapter 4. However data in that chapter also showed that tetracycline induced RNAi of TbGEF3 caused a cell cycle defect and increase in cell death. Viable cells with a partial endocytosis defect would be desirable to test for compounds that are taken up into bloodstream form *T. brucei* via endocytosis. This means that the concentration of tetracycline used in Chapter 4 to induce RNAi of TbGEF3 would not be ideal for the experiments in this chapter, since RNAi will also lead to widespread cell death. This chapter aimed to identify a suitable concentration of tetracycline that can induce endocytosis defect whilst maintaining a stable cell line.

Suramin and diminazene aceturate are drugs that are taken up via endocytosis and P2 transporters, respectively. Disruption of endocytosis in bloodstream form *T. brucei* has previously been shown to affect sensitivity to suramin. Wiedemar *et al*. (2019) identified that expression of variant surface glycoprotein (VSG^{Sur}) in bloodstream form *T. b. brucei* resulted in increased suramin resistance. Suramin strongly binds to low density lipoproteins prior to endocytosis, however the expression of VSG^{Sur} strongly impaired low density lipoprotein (LDL) endocytosis; thus causing increased drug resistance (Wiedemar *et al*., 2019). This study suggests that suramin can be used as an indicator of a defect in endocytosis, which could therefore be used to identify drugs that are taken up by endocytosis. As a drug taken up by P2 transporters into *T. brucei spp.*, diminazene aceturate sensitivity should not be directly affected by an endocytosis defect. For this reason, diminazene aceturate was used in this chapter as a control; since this drug should kill the parasites regardless of an endocytosis defect.

5.3.1.1 IC_{50} of suramin and diminazene aceturate

Sensitivity to suramin in wild type Lister 427 bloodstream form *T. brucei* and all clones of the transgenic P2T7-TbGEF3 *T. brucei* cell lines was determined in the absence of tetracycline (i.e. RNAi not induced). The half maximal effective concentration (IC_{50}) of suramin was obtained for wild type and all clones of the transgenic cell line (Table 5.1).

Figure 5.1 shows the IC_{50} curves for suramin for all of the clones from P2T7-TbGEF3 cell lines and the wild type samples.

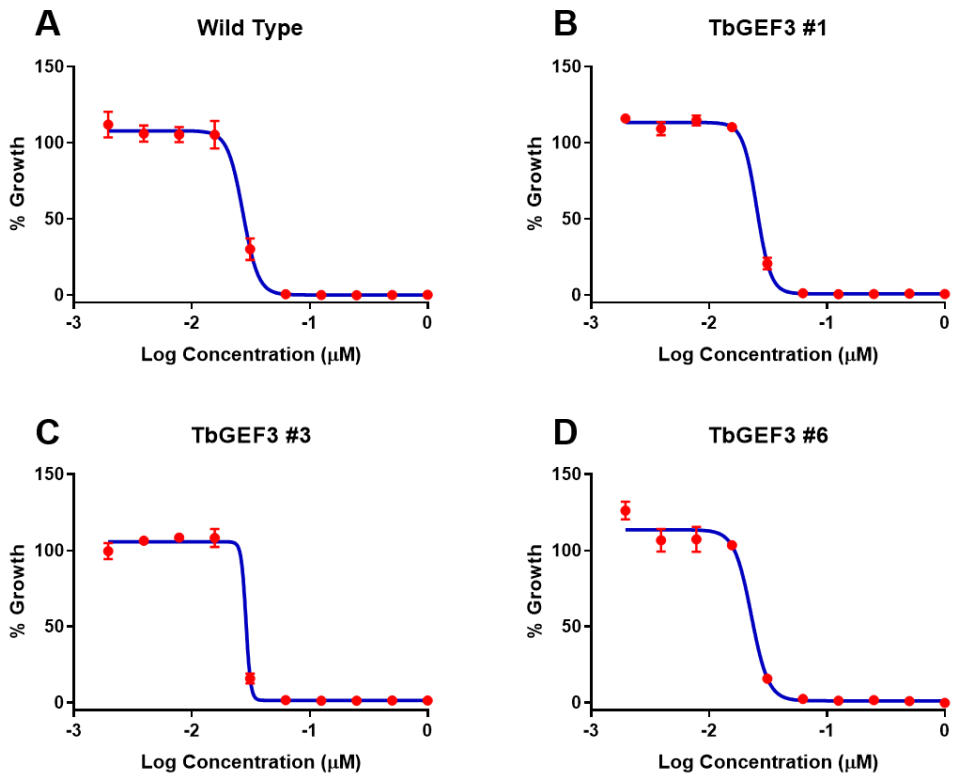

Figure 5.1. IC_{50} for suramin in transgenic* T. brucei *cell lines. *Half maximal inhibitory concentration for suramin was determined for (A) wild type* T. brucei*, (B) clone 1, (C) clone 3 and (D) clone 6 of the transgenic P2T7-TbGEF3 cell line (n = 3)*

The IC_{50} values for wild type and all clones of TbGEF3 cell line are presented in Table 5.1. The data in Table 5.1 shows that wild type, clone 1 and clone 3 from the P2T7-TbGEF3 transgenic cells had similar sensitivity to suramin. However clone 6 from the P2T7-TbGEF3 cell line had a higher sensitivity to suramin, as highlighted by the lower IC_{50} value. The 95% confidence interval could not be accurately determined. Increasing additional dilution points to determine the sensitivity of suramin in wild type and transgenic cells may provide a more accurate measurement of IC_{50} (Paolini *et al*., 2010).

Sample	**IC_{50} of suramin (nM)**
Wild type	27.12
Clone 1	25.39
Clone 3	~28.77
Clone 6	22.82

Table 5.1. IC_{50} of suramin in transgenic* T. brucei *lines. *The IC_{50} of suramin was determined for wild type bloodstream form* T. brucei *and all clones of the P2T7-TbGEF3 transgenic cell line. The IC_{50} value calculated using GraphPad Prism v.8.2.*

Diminazene aceturate sensitivity in wild type Lister 427 bloodstream form *T. brucei* was identified using 18 serial drug dilutions. The same was done for clone 6 of the P2T7-TbGEF3 transgenic cell line.

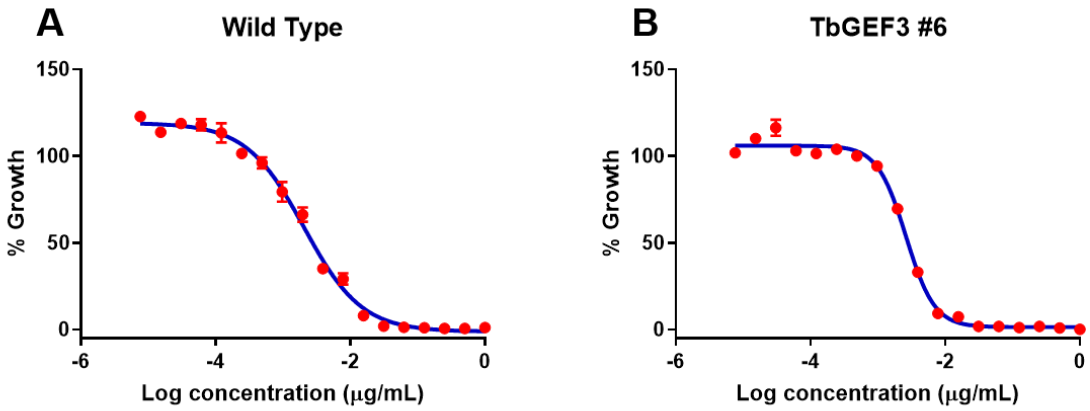

Figure 5.2. IC_{50} of diminazene aceturate in transgenic cell lines. *Data points for different concentrations of diminazene aceturate was plotted and the IC_{50} for diminazene aceturate was calculated for (A) wild type and (B) clone 6 of TbGEF3 cell line using GraphPad prism (n = 3).*

The IC_{50} of diminazene aceturate in wild type and clone 6 of the transgenic cell line was calculated, Table 5.2 shows that the IC_{50} for wild type and clone 6 of the transgenic cell line were 7.287 nM and 9.281 nM respectively.

Sample	**IC_{50} of diminazene aceturate (nM)**	**95% confidence interval (nM)**
Wild type	7.287	6.320 – 8.396
Clone 6	9.281	8.606 – 10.010

Table 5.2. IC_{50} values for diminazene aceturate in transgenic* T. brucei *cell line. *The IC_{50} value for diminazene aceturate was identified in wild type and clone 6 of the P2T7-TbGEF3 cells. IC_{50} calculated using GraphPad Prism v.8.2.*

5.3.1.2 IC_{50} of tetracycline

The sensitivity of tetracycline in wild type Lister 427 bloodstream form *T. brucei* and clone 6 of the transgenic P2T7-TbGEF3 cell line was identified in order to determine whether there were differences in sensitivity to tetracycline. The sensitivity of tetracycline in wild type and transgenic cell lines were also determined to confirm that tetracycline did not affect cell growth in wild type *T. brucei*, as demonstrated in Chapter 4 Section 4.3.3. Sensitivity to tetracycline was also identified in clone 1 and 3. This is because work described in Chapter 4 Section 4.3.3 also showed that clone 1 did not have any morphological or physiological differences post addition of tetracycline, whilst clone 3 exhibited both morphological and physiological difference from 48 hours post addition of tetracycline.

Wild type and clone 1 were used as a negative control to test sensitivity to tetracycline, since both cell samples are not expected to have any differences in parasite growth in the presence of this antibiotic.

A serial drug dilution of tetracycline was carried out and incubated with the cell samples for 48 hours. Viability of the cells was then measured using PrestoBlue® (fluorescence). Figure 5.3 shows that wild type and clone 1 of the transgenic P2T7-TbGEF3 cell line did not show sensitivity to tetracycline (Figure 5.3.A-B), whilst both clones 3 and 6 from the transgenic P2T7-TbGEF3 cell line showed a dose response curve (Figure 5.3.C-D).

The IC_{50} of tetracycline could not be calculated for wild type and clone 1 because the highest tetracycline concentration used (1 μg/mL) did not cause cell death. However clone 3 and clone 6 had an IC_{50} of 0.3959 ng/mL and 0.4132 ng/mL respectively (Table 5.3).

Sample	IC_{50} of tetracycline (ng/mL)	95% confidence interval (ng/mL)
Clone 3	0.3959	0.2850 – 0.5272
Clone 6	0.4132	0.3107 – 0.5240

Table 5.3. IC_{50} of tetracycline in transgenic* T. brucei *cell line. *Tetracycline IC_{50} was calculated in clone 3 and 6 of the P2T7-TbGEF3 cell line using GraphPad Prism v.8.2.*

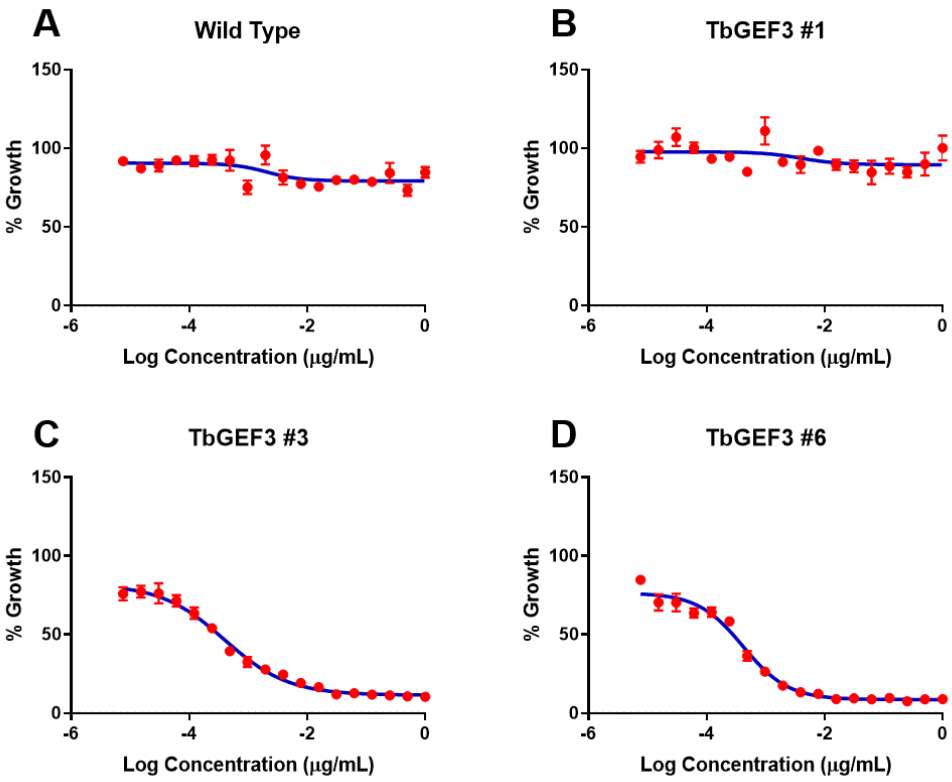

Figure 5.3. IC_{50} of tetracycline for the transgenic TbGEF3 cell lines. *IC_{50} of tetracycline was determined for (A) wild type bloodstream form* T. brucei*, as well as (B) clone 1, (C) clone 3 and (D) clone 6 of the TbGEF3 cell lines (n = 3).*

5.3.2. Identifying the potency of suramin on transgenic *T. brucei* in the presence of tetracycline

5.3.2.1 Identifying optimum tetracycline concentration

The addition of tetracycline at a high concentration was shown to affect the growth of clone 6 from the transgenic P2T7-TbGEF3 cell line in Chapter 4, which led to increased cell death from 48 hours post addition of tetracycline. However to successfully test compounds for their mechanism of uptake, a tetracycline concentration that induces endocytosis defect in the transgenic cell line without killing the parasites was needed.

The IC_{50} of tetracycline was calculated as 0.4132 ng/mL. A range of concentrations above and below the calculated IC_{50} of tetracycline was then used to identify an optimum concentration of tetracycline that can be used to induce an endocytosis defect without compromising the parasites viability. The range of tetracycline concentration tested was between 0.1 ng/mL and 0.5 ng/mL.

Similarly a range of concentrations above and below the IC_{50} of suramin was used. This was primarily done in order to avoid over-saturation of suramin in the cell samples, thus leading to increased cell death which can be interpreted as false negative results.

In the first experiment, tetracycline and suramin were added at the same time to the bloodstream form cells. The plates were incubated for 48 hours and the viability was determined using PrestoBlue®. Figure 5.4 shows the results observed after 48 hours incubation. Cells incubated in tetracycline concentrations between 0.1 ng/mL and 0.25 ng/mL had only 10 – 20% of viable cells at the lowest suramin concentration. The percentage of viable cells decreased when suramin concentration was increased, and likewise the percentage of viable cells at lower suramin concentration decreased as the concentration of tetracycline increased (Figure 5.4).

The work presented in Chapter 4 highlighted that the endocytosis defect in transgenic cell lines was evident from 24 hours post-induction of RNAi. Adding tetracycline and suramin at

the same time results in a very high death rate as the parasites are taking up suramin via endocytosis before the tetracycline-induced endocytosis defect can develop.

To ensure that cells had an endocytosis defect before the addition of suramin, the cultures were incubated at different concentrations of tetracycline for 24 hours. Suramin was then added and the plates were further incubated for 48 hours. As a control, samples of cells were incubated in medium only for the extra 24 hours. This was done in order to ensure that any changes in the results were due to the endocytosis defect and not due to the additional incubation time.

Results show that at lower concentrations of suramin, the cells incubated in the lowest concentrations of 0.1 ng/mL and 0.15 ng/mL of tetracycline had a similar percentage of viability as the control group with no tetracycline. However as the suramin concentration increased, the percentage of viable cells in the 0.1 ng/mL and 0.15 ng/mL tetracycline groups were greater than those in the control group without tetracycline (Figure 5.4). This suggests that the tetracycline was inducing a protective effect at these low concentrations. At higher tetracycline concentrations, high levels of cell death were seen regardless of the suramin concentration which will be due to the RNAi effect.

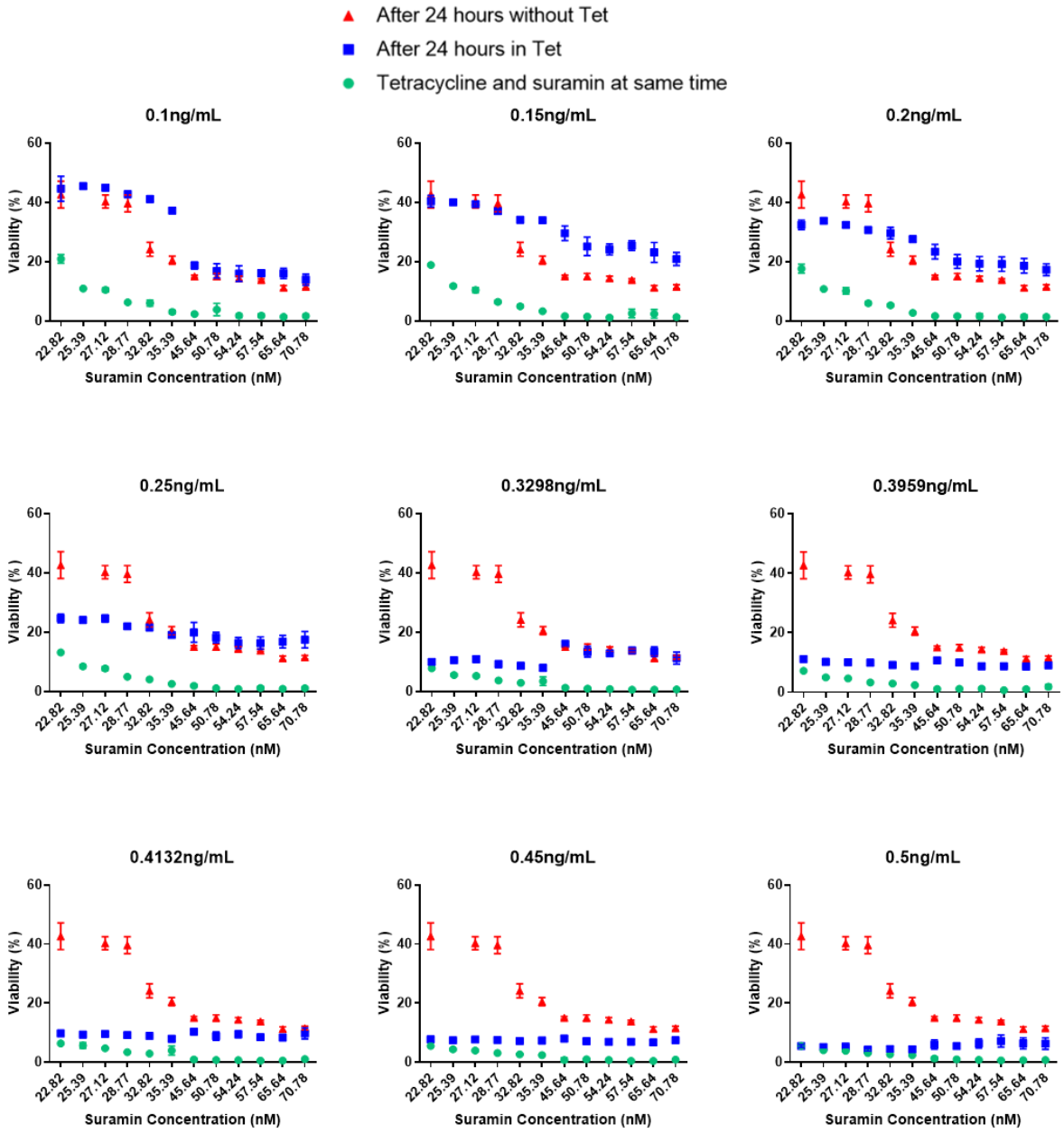

Figure 5.4. Identifying the tetracycline concentration that affects the growth of transgenic* T. brucei *cells in the presence of suramin. *Shown in green: tetracycline and suramin was added to P2T7-TbGEF3 cells at the same time. Blue: P2T7-TbGEF3 cells were incubated in tetracycline for 24 hours before addition of suramin. Red: P2T7-TbGEF3 cells were incubated without tetracycline for 24 hours before addition of suramin. The concentration of tetracycline used is labelled on each graph (n = 3).*

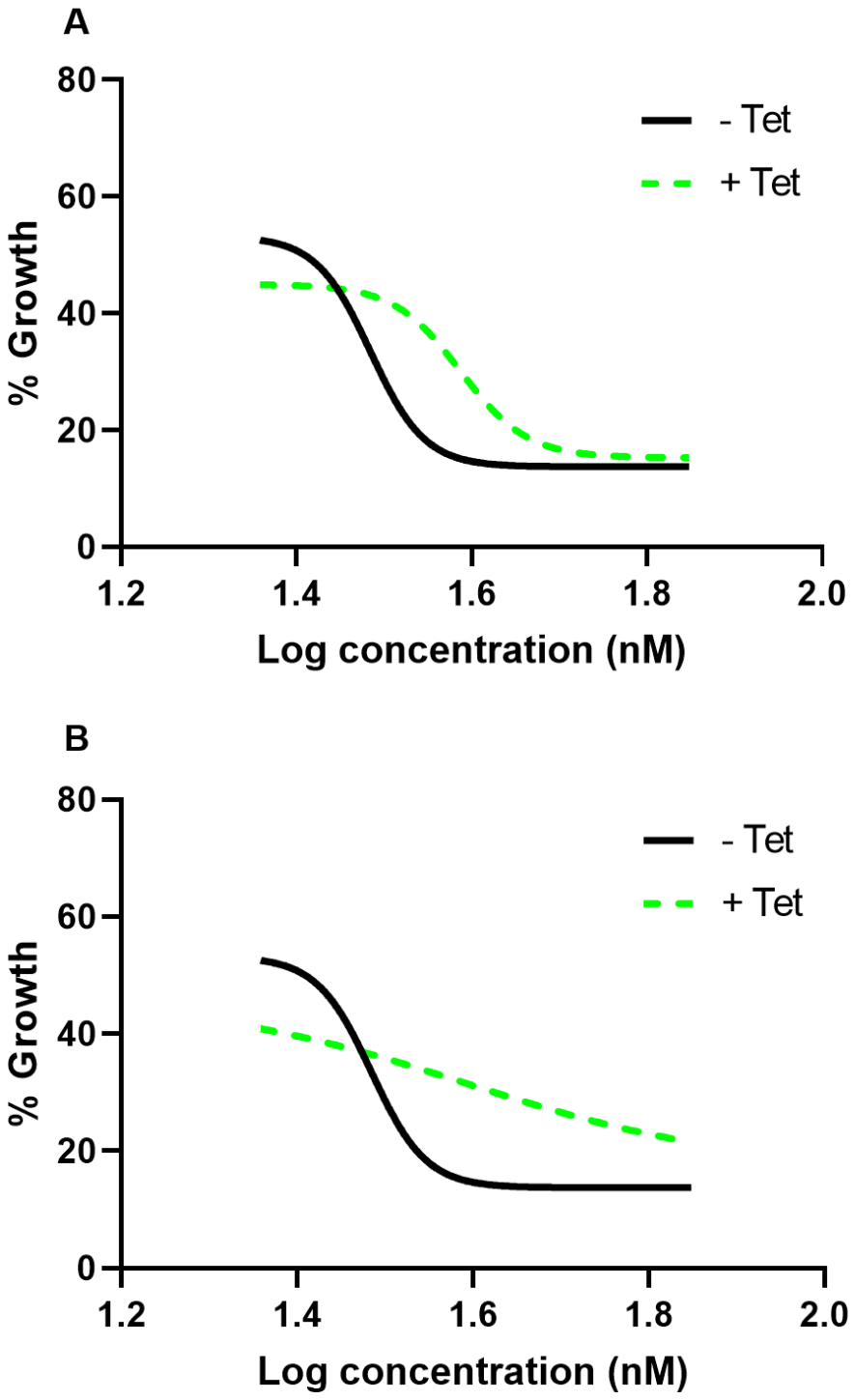

Figure 5.5. Comparison of IC_{50} for suramin in transgenic P2T7-TbGEF3 cell line incubated +/- tetracycline. *Suramin IC_{50} for samples incubated with (A) 0.1 ng/mL and (B) 0.15 ng/mL tetracycline (green) was compared to the control group (black) (n = 3).*

The IC_{50} for suramin was determined for samples with 0.1 ng/mL and 0.15 ng/mL tetracycline and compared to the IC_{50} for samples without tetracycline (Table 5.4 and Figure 5.5). The results show that the IC_{50} for samples incubated for 24 hours in 0.1 ng/mL tetracycline was higher relative to the no tetracycline sample. Samples incubated in 0.1 ng/mL tetracycline had an IC_{50} of 38.65 nM whilst the control group had an IC_{50} of 30.51 nM. The 95% confidence interval for both samples did not overlap (Table 5.4). It is likely that this is due to the induction of an endocytosis defect which reduces the uptake of suramin. One-way ANOVA multiple comparison showed that the differences in IC_{50} value compared to the control group were highly significant ($P \leq 0.0001$).

The IC_{50} for samples incubated in 0.15 ng/mL tetracycline did not produce an accurate dose response curve (Figure 5.5.B), which meant that the 95% confidence interval for IC_{50} of suramin could not be determined but the IC_{50} value was similar to that for cells incubated in 0.1 ng/mL tetracycline. (Table 5.4). Considering the findings, 0.1 ng/mL tetracycline was selected for use for further experiments in this chapter.

Sample	**IC_{50} of Suramin (nM)**	**95% Confidence Interval (nM)**
Wild type	30.51	28.69 – 32.63
0.1 ng/mL tetracycline	38.65	36.71 – 40.84
0.15 ng/mL tetracycline	39.29	ND

Table 5.4. IC_{50} of suramin with and without tetracycline in transgenic P2T7-TbGEF3 cell line. *IC_{50} for suramin was identified in samples incubated with 0.1 ng/mL and 0.15 ng/mL tetracycline for 24 hours and for control sample without tetracycline. The 95% confidence interval was also determined. One-way ANOVA multiple comparison was carried out and the statistical significance of IC_{50} shift was calculated ($P \leq 0.0001$).*

5.3.2.2 Validating the effect of tetracycline on transgenic T. brucei growth in suramin

To confirm the effects of tetracycline in P2T7-TbGEF3 transgenic cells, the experiment was repeated with a different range of concentrations of suramin.

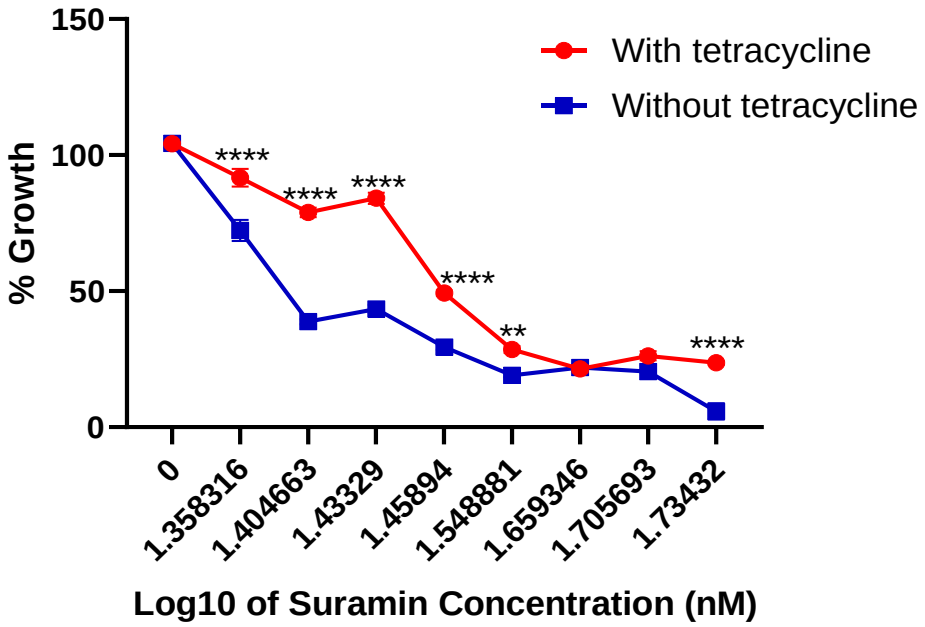

Figure 5.6. Effects of TbGEF3 RNAi on parasite sensitivity to suramin. *Bloodstream form* T. brucei *cells were grown for 24 hours with 0.1 ng/mL and without tetracycline prior to addition of different concentration of suramin (n = 6). 2-way ANOVA multiple comparisons was used for statistical analysis. **** = P ≤ 0.0001, ** = P ≤ 0.01.*

As seen in the previous experiment, there was a significant reduction in sensitivity to suramin in cells that had previously been incubated in tetracycline to induce RNAi knockdown of TbGEF3. (Figure 5.6). This relationship was observed until the concentration of suramin increased to 45.64 nM (log10 = 1.659346) at which point cell viability was very low in all samples.

5.3.2.3 Using diminazene aceturate to validate endocytosis defect in transgenic cells

In order to test whether the reduced response to suramin observed in Figure 5.5 and Figure 5.6 was due to endocytosis being affected and not due to other cellular functions being compromised, the experiment was repeated using diminazene aceturate (Figure 5.7). Diminazene aceturate is a drug that is taken up into bloodstream form *T. brucei* via *TbAT1*/P2 transporters (Gysin *et al*., 2018). I predicted that induction of TbGEF3 RNAi would not change sensitivity to diminazene aceturate, since uptake of this drug is not believed to be affected by endocytosis.

Figure 5.7 shows that cells incubated in tetracycline were more sensitive to diminazene aceturate than the control group. There is a possibility that this increase in sensitivity to diminazene aceturate in the tetracycline incubated cells may have been caused by synergy between the RNAi of TbGEF3 and either the action or uptake of the drug.

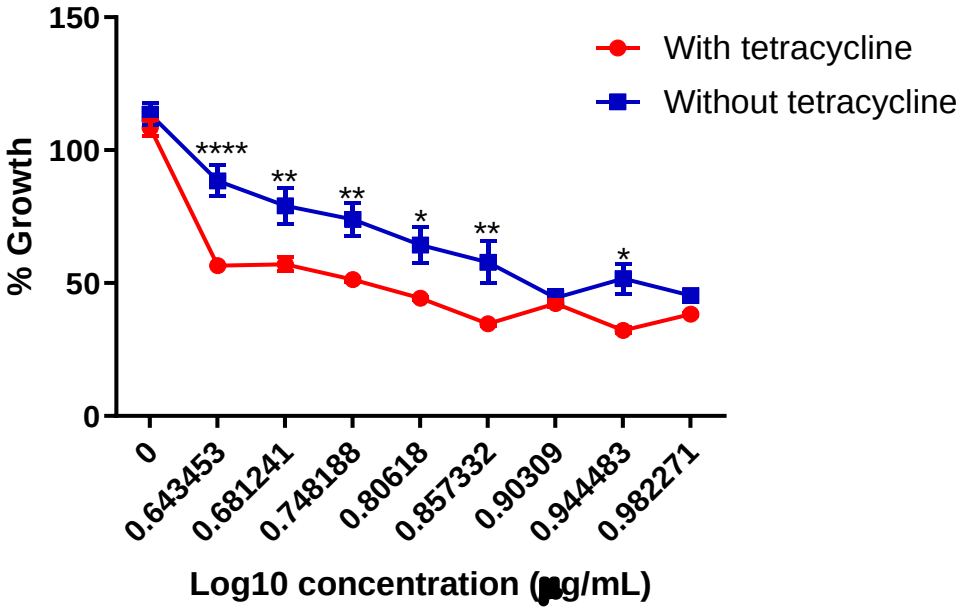

Figure 5.7. Effect of diminazene aceturate on cells before and after induction of TbGEF3 RNAi. *Different concentrations of diminazene aceturate was added to bloodstream form* T. brucei *exposed to 0.1 ng/mL tetracycline and control group (n = 6). 2-way ANOVA was used for statistical analysis. *** = P ≤ 0.0001, ** = P ≤ 0.01, * = P ≤ 0.05.*

5.3.3 Pathogen Box (MMV) screening

In Section 5.3.2 I identified an optimum concentration of tetracycline that can be used to induce a partial endocytosis defect in bloodstream form *T. brucei*, which is sufficient to reduce sensitivity to suramin without killing the cells. The next stage was to determine whether this system can be used to identify potential drug compounds that are taken up via endocytosis, using the Pathogen Box for proof of principle.

There are 400 compounds in the Pathogen Box that could have potential activity against bloodstream form *T. brucei*. Of these, sufficient quantities of 384 compounds were available for screening. The compounds were screened using wild type Lister 427 bloodstream form *T. brucei*. The compounds were screened at two different concentrations, 10 μM and 1 μM, to determine positive hits; defined as any compounds that had less than 5% parasite growth compared to an untreated control. The Pathogen Box consists of 5 plates labelled from A to E. In this chapter the plates will be referred to by numbers (1 to 5) and the compounds by their plate number and well co-ordinates (e.g. 1A11)

5.3.3.1 Pathogen Box screening at a concentration of 10 μM

Figures 5.8 to 5.12 show the results of initial screening the Pathogen Box compounds at a single concentration of 10 μM on wild type Lister 427 bloodstream form *T. brucei*. 110 compounds out of the 384 screened were shown to have reduced the percentage growth below 5% against bloodstream form *T. brucei* at 10 mM concentration.

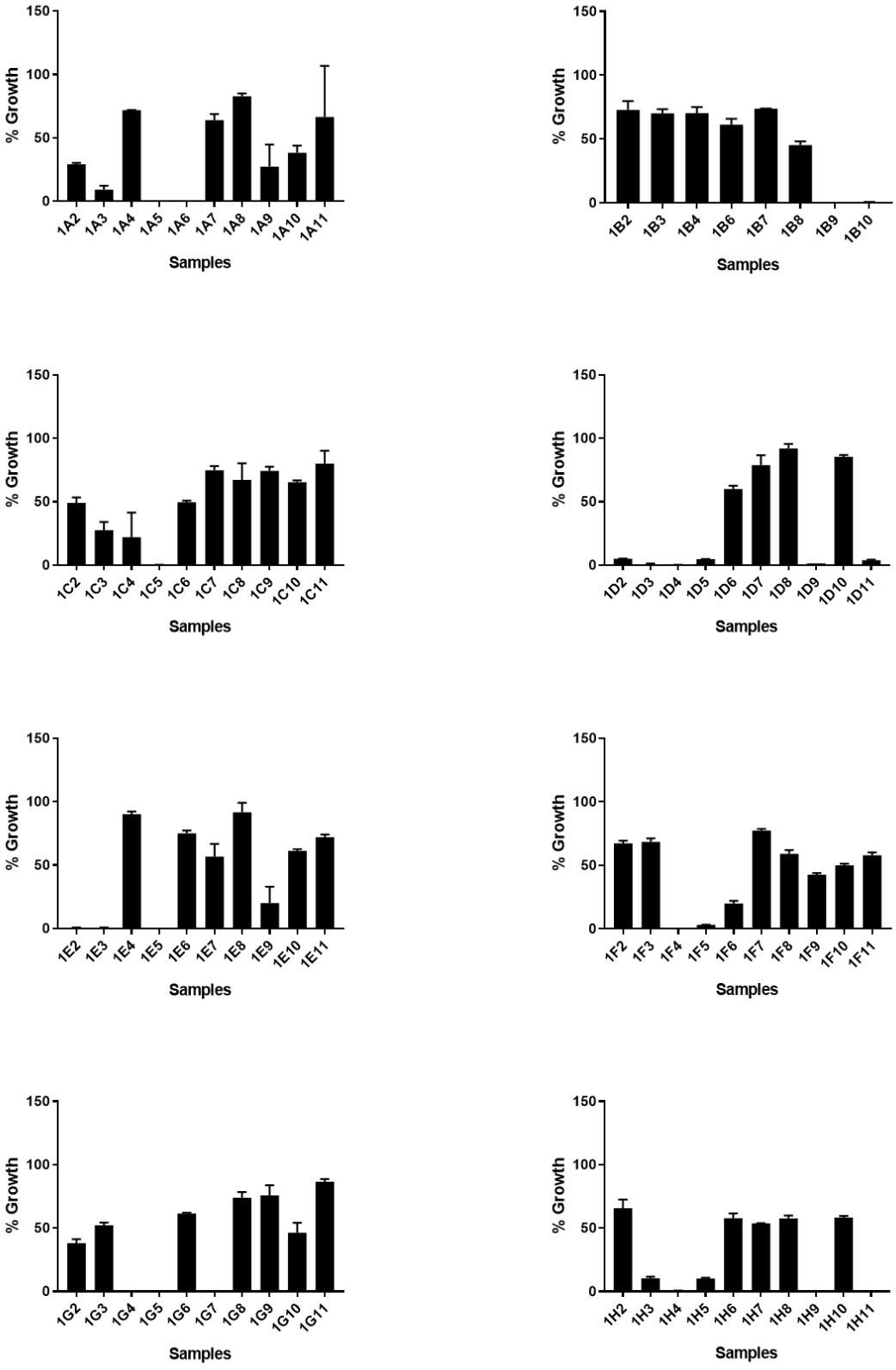

***Figure 5.8. Plate 1 of the Pathogen Box compounds screened at 10 μM Lister 427 bloodstream form* T. brucei.**

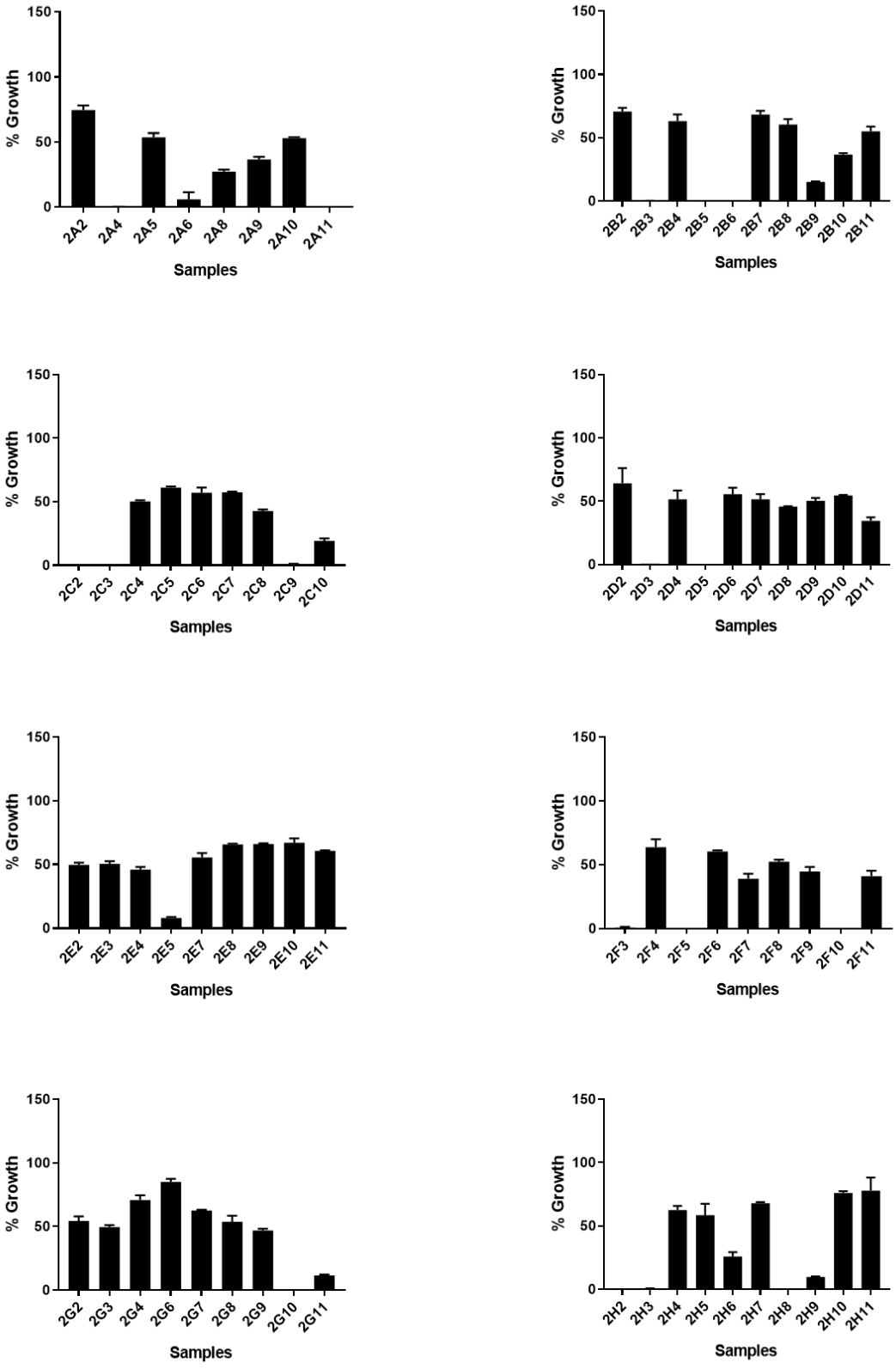

***Figure 5.9. Plate 2 of the Pathogen Box compounds screened at 10 μM on Lister 427 bloodstream form* T. brucei.**

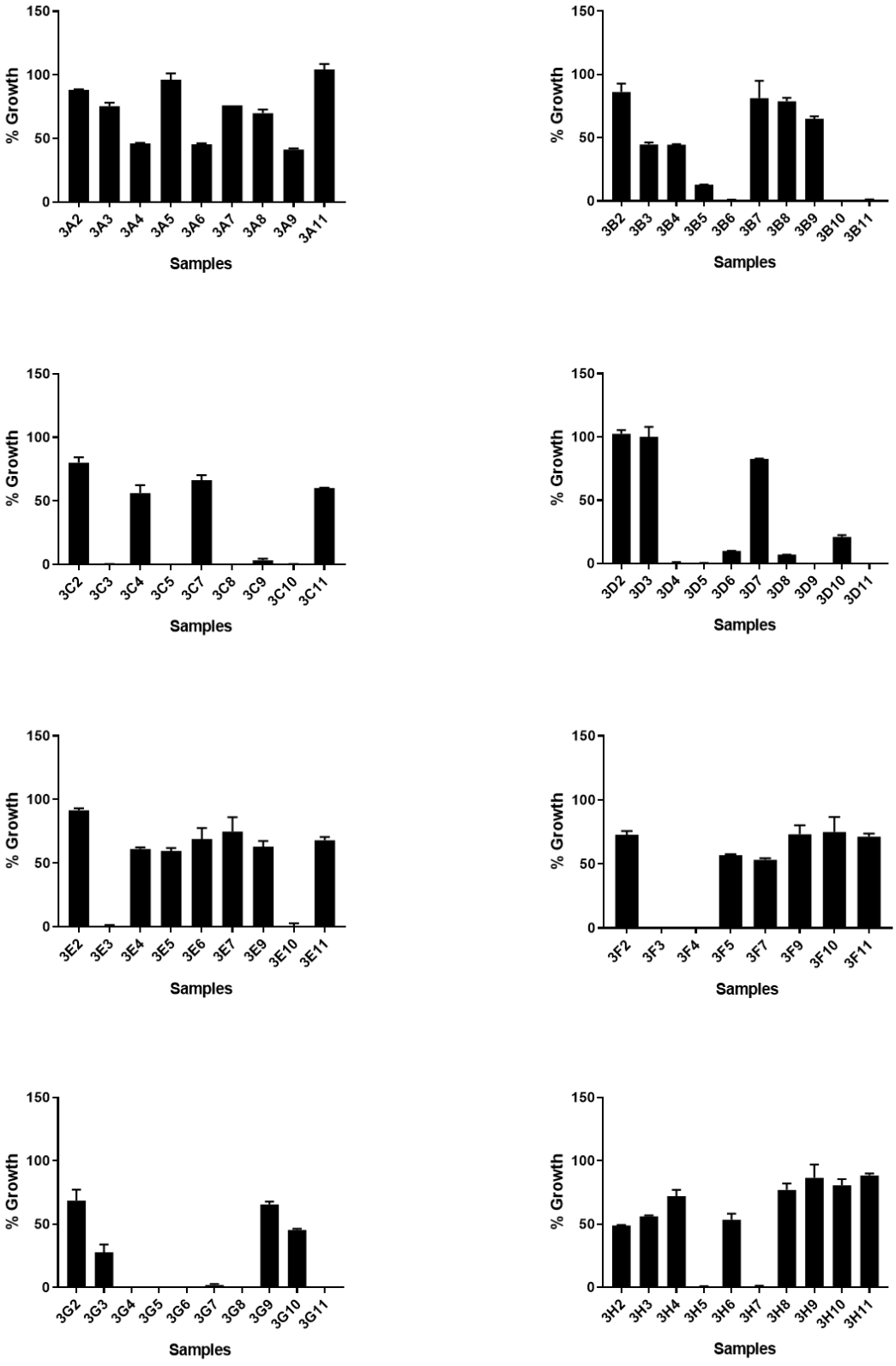

***Figure 5.10. Plate 3 of the Pathogen Box compounds screened at 10 μM on Lister 427 bloodstream form* T. brucei.**

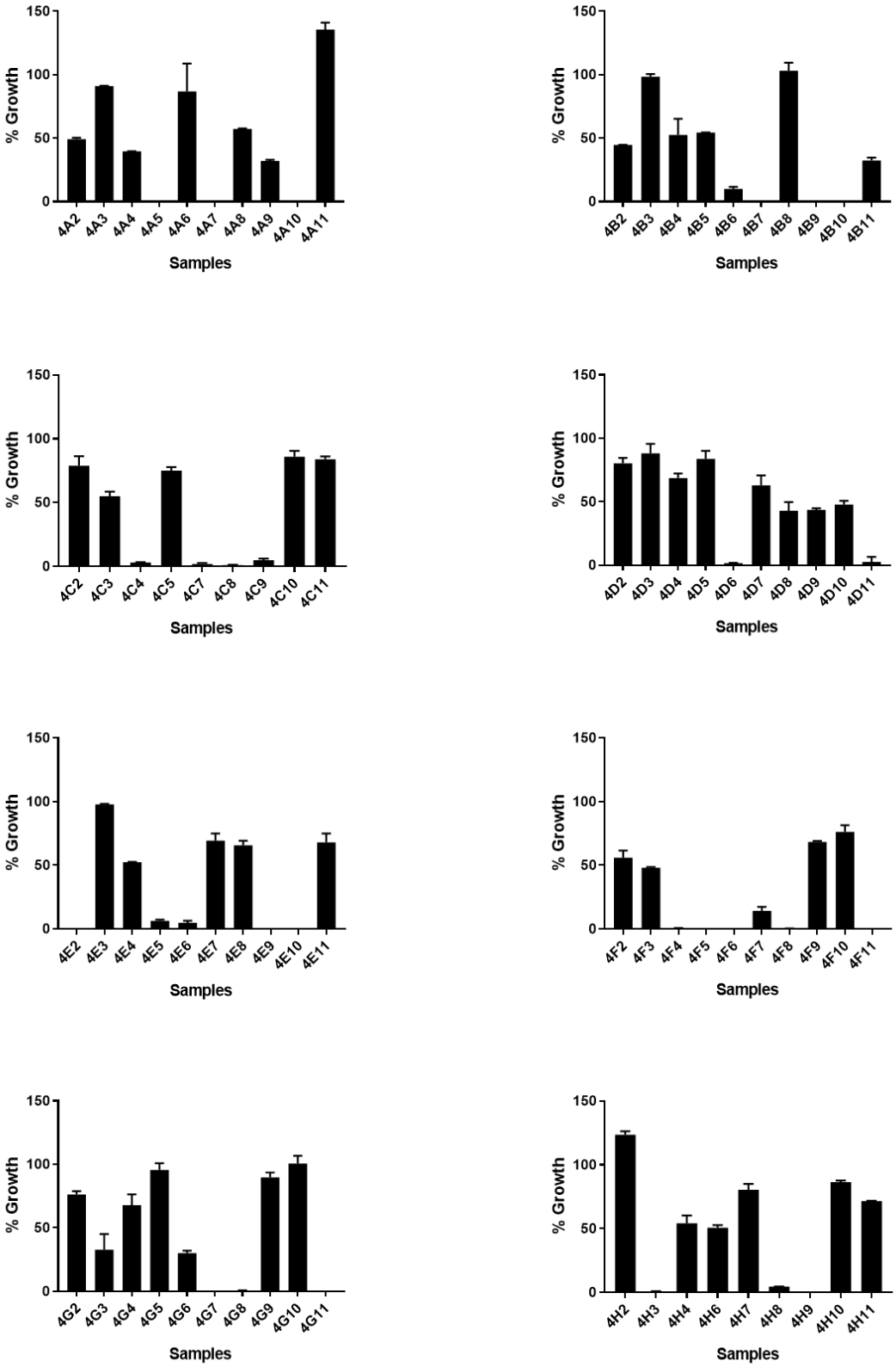

***Figure 5.11. Plate 4 of the Pathogen Box compounds screened at 10 μM on Lister 427 bloodstream form* T. brucei.**

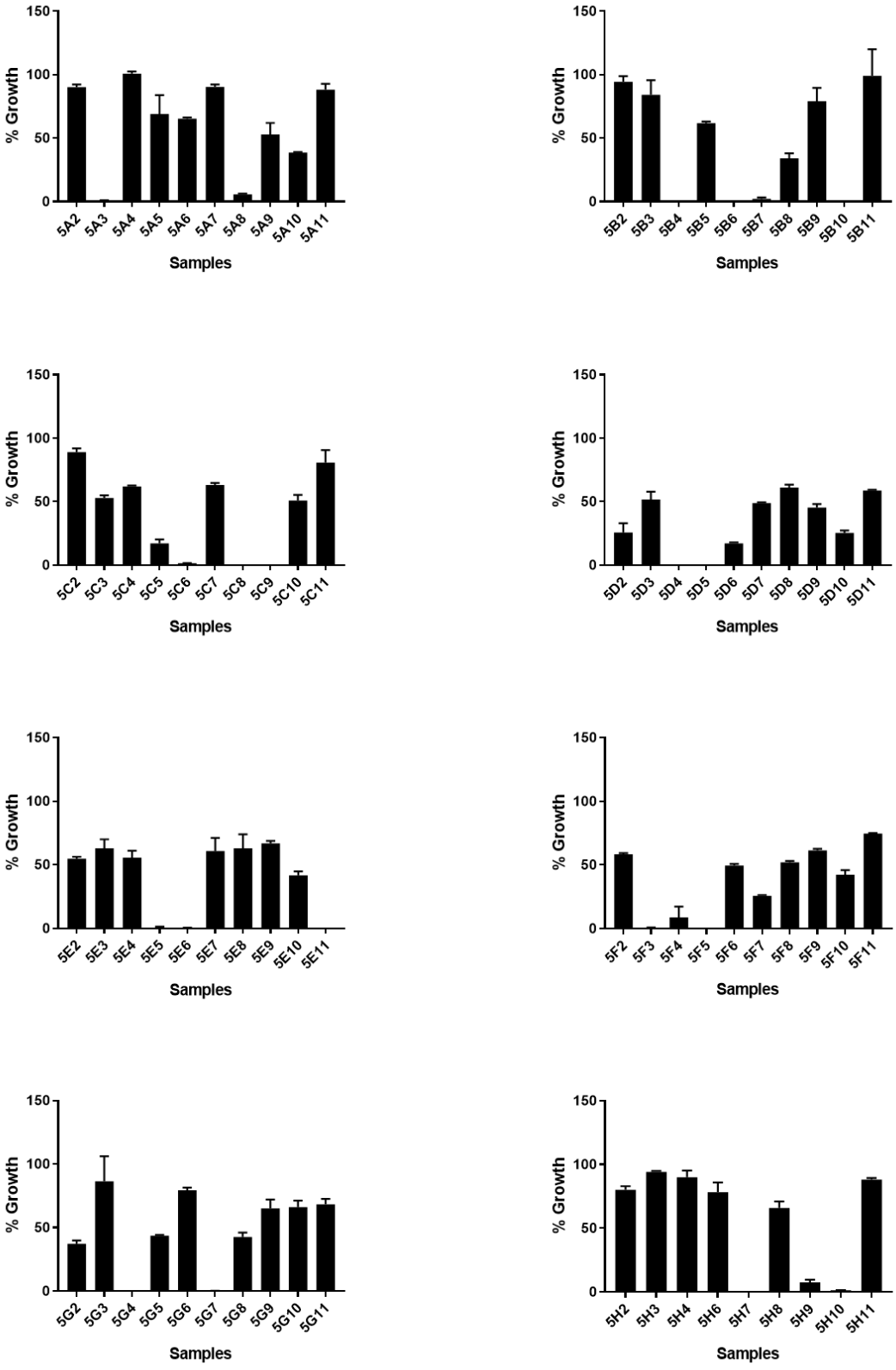

***Figure 5.12. Plate 5 of the Pathogen Box compounds screened at 10 μM on Lister 427 bloodstream form* T. brucei.**

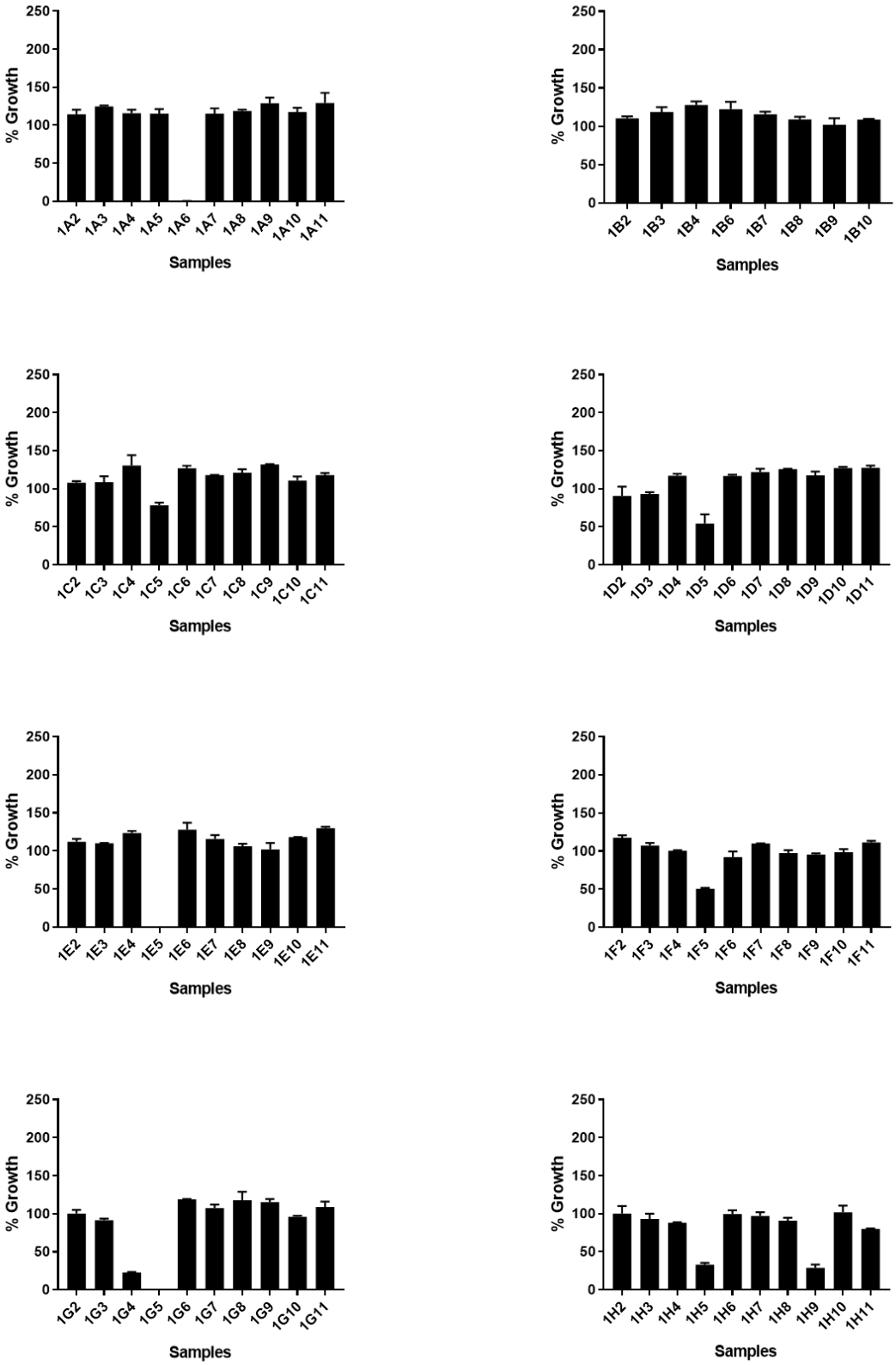

***Figure 5.13. Plate 1 of Pathogen Box compounds screened at 1 μM on Lister 427 bloodstream form* T. brucei.**

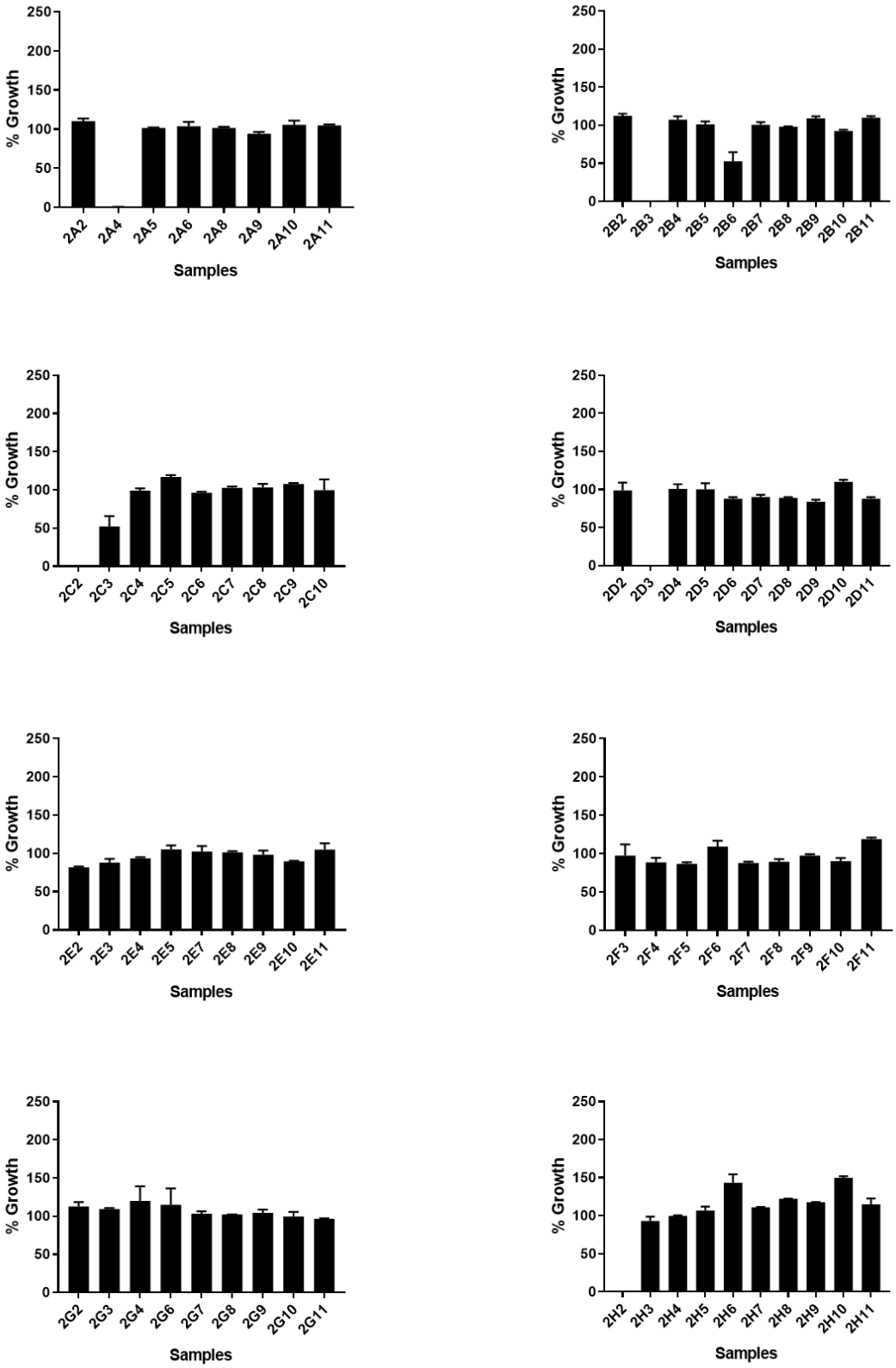

***Figure 5.14. Plate 2 of Pathogen Box compounds screened at 1 μM on Lister 427 bloodstream form* T. brucei.**

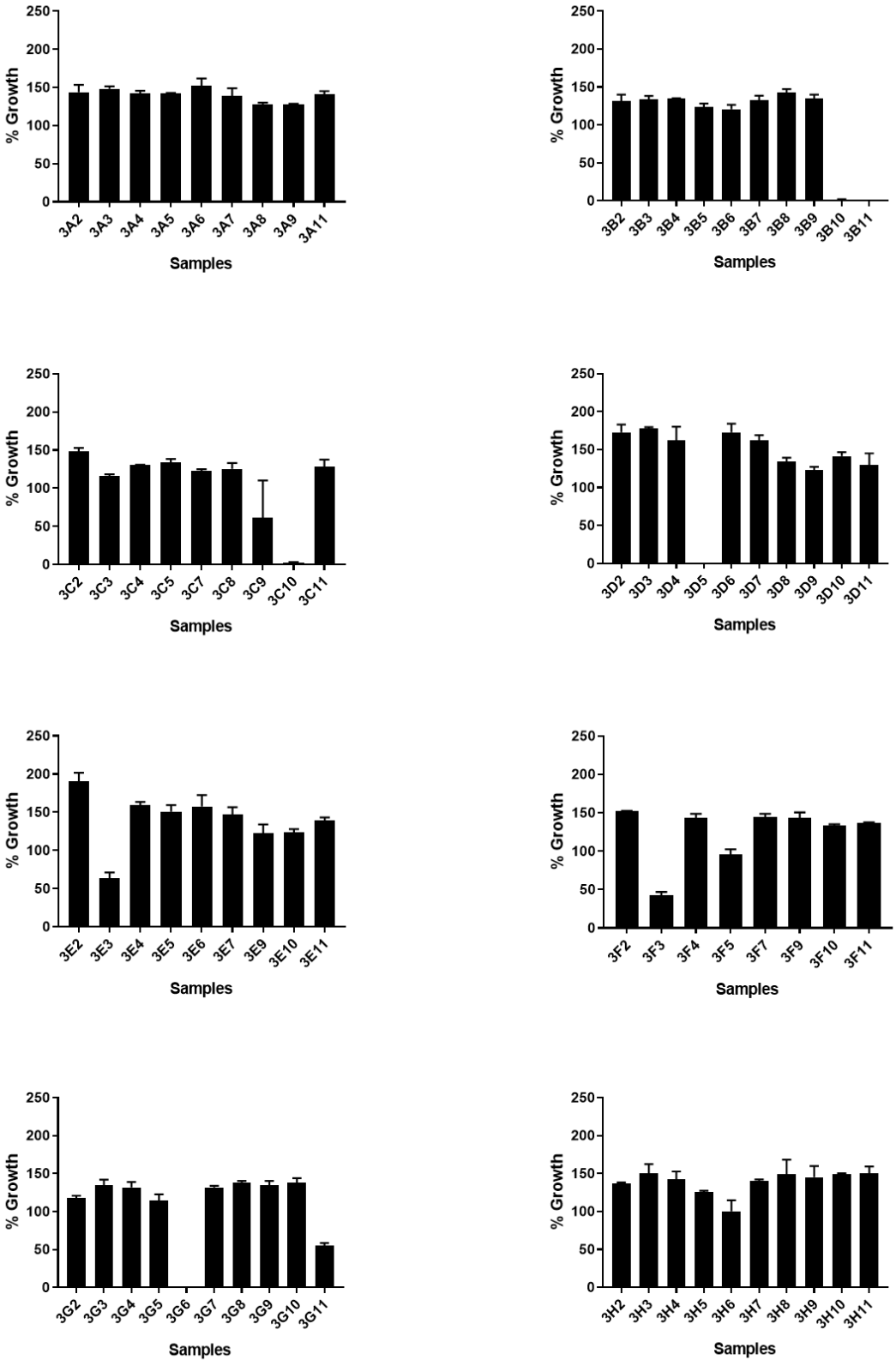

***Figure 5.15. Plate 3 of Pathogen Box compounds screened at 1 μM on Lister 427 bloodstream form* T. brucei.**

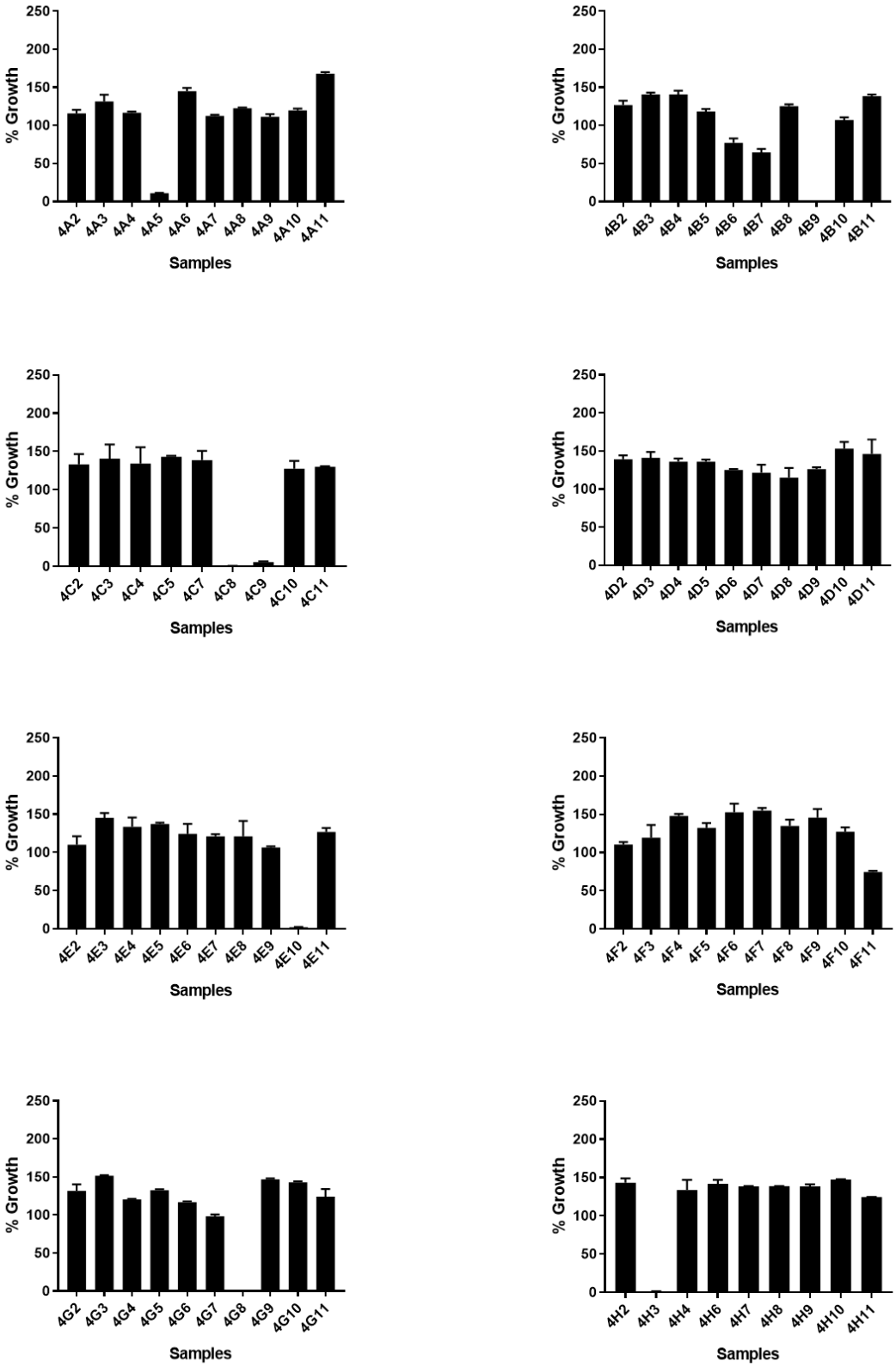

***Figure 5.16. Plate 4 of Pathogen Box compounds screened at 1 μM on Lister 427 bloodstream form* T. brucei.**

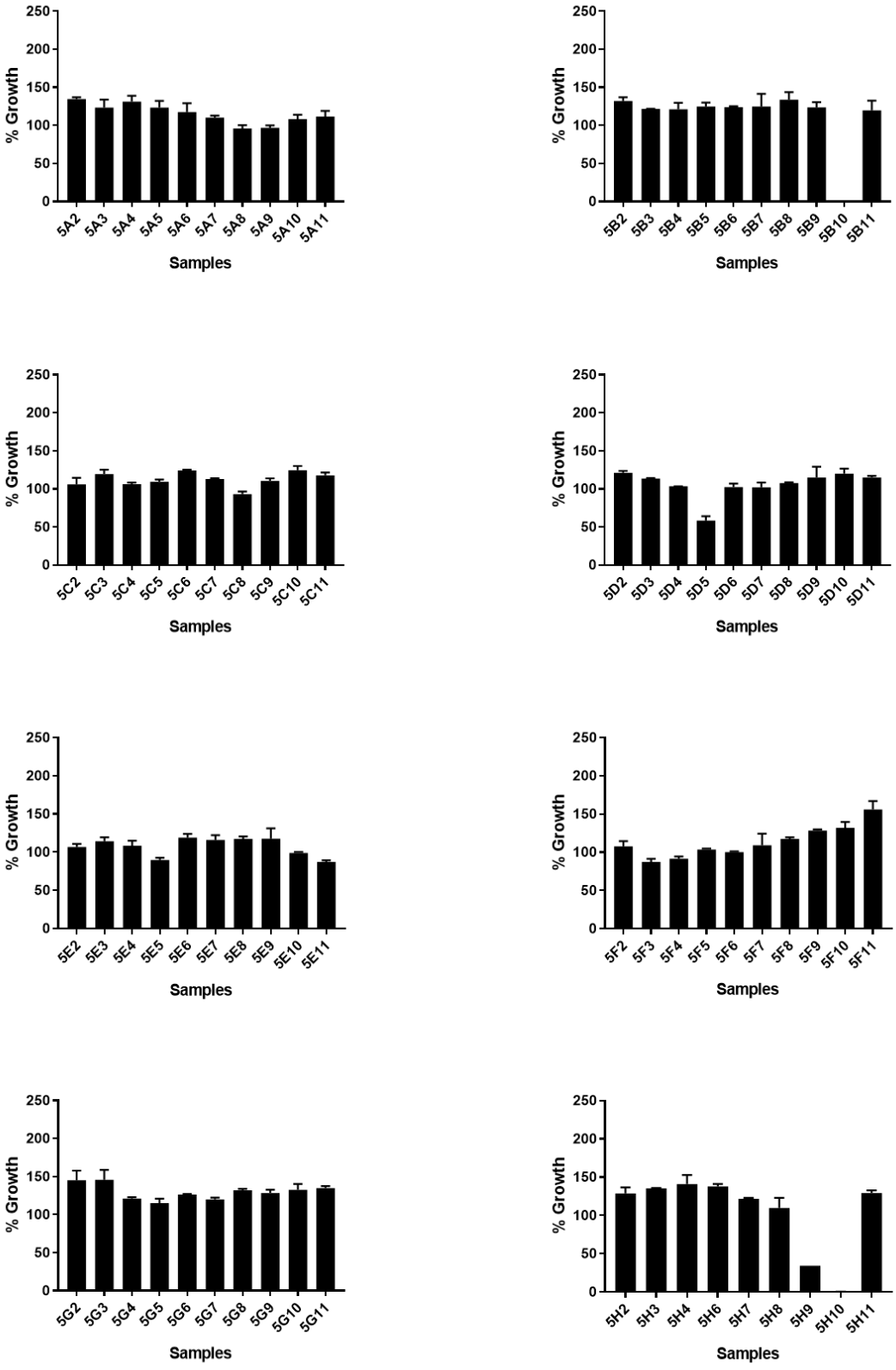

***Figure 5.17. Plate 5 of Pathogen Box compounds screened at 1 μM on Lister 427 bloodstream form* T. brucei.**

5.3.3.2 Pathogen Box screening at a concentration of 1 μM

To identify compounds that were effective against bloodstream form *T. brucei* at a lower concentration, drug screening was carried out using 1 μM of the compounds from the Pathogen Box. Figures 5.13 to 5.17 shows that 20 compounds out of the 384 compounds screened from the Pathogen Box library were effective against bloodstream form *T. brucei* (percentage growth below 5% compared to untreated control) at this lower concentration.

Of the 20 hit compounds, 19 were taken forward for further analysis. More material for compound 2A4 could not be obtained in order to carry out further experiments. A 2-fold serial drug dilution was carried out on the remaining 19 hit compounds in order to determine the IC_{50} value for bloodstream form *T. brucei*.

A lower IC_{50} signifies higher sensitivity to that particular compound, therefore measuring the IC_{50} of the positive hits will identify which compound is more effective against bloodstream form *T. brucei* (Doldán-Martelli and Míguez, 2018).

The IC_{50} value and the 95% confidence interval was obtained for each compound (Table 5.5). Out of all the positive hits, five compounds that had the lowest IC_{50} and smallest 95% confidence interval were chosen as potential drug compounds against bloodstream form *T. brucei* (Table 5.5).

Table 5.6 shows the chemical structures and pathogen screen in which these five compounds were identified. The chemical structures and pathogen screen for the other 14 positive hits are provided in the Appendix 9.

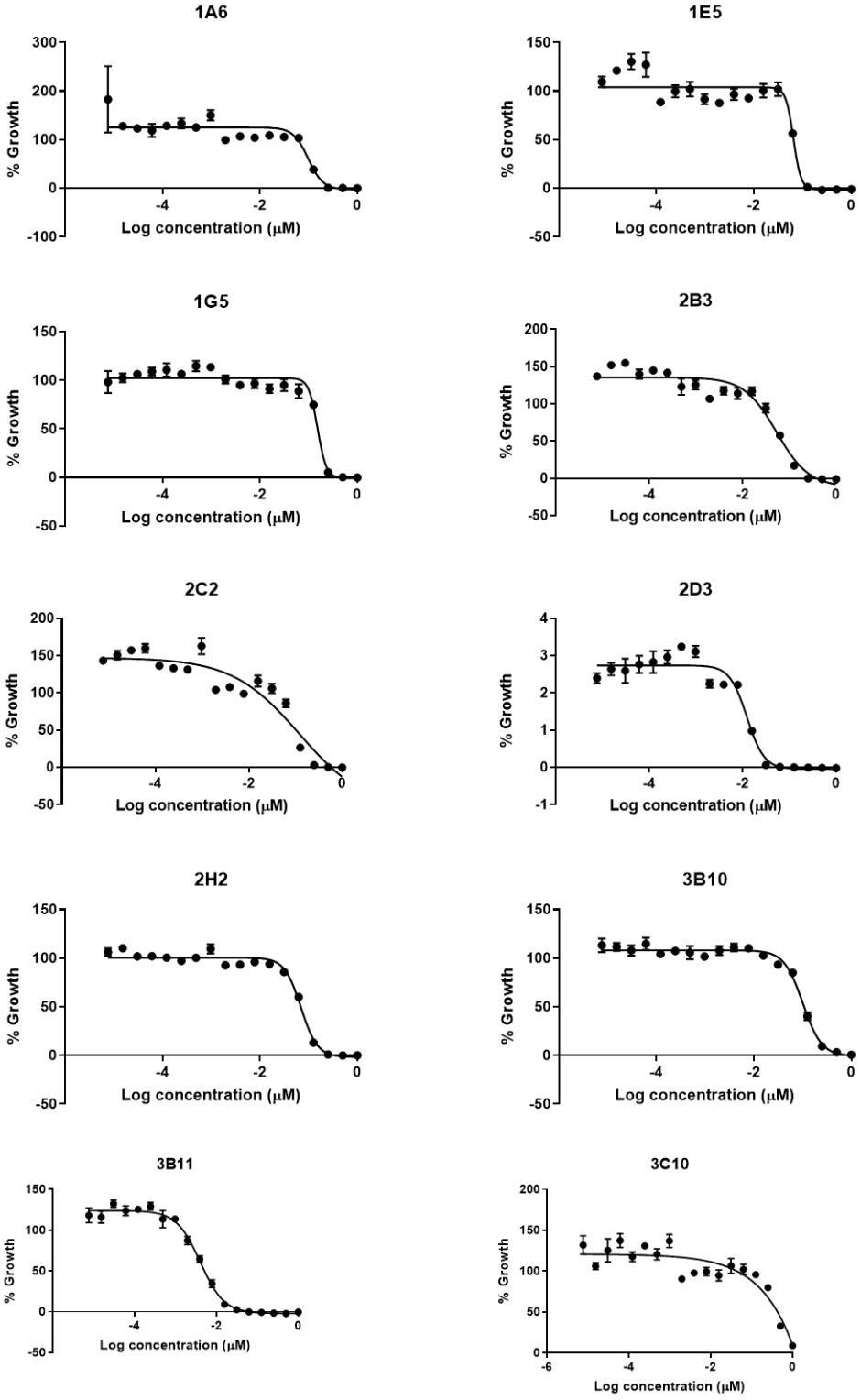

Figure 5.18. IC_{50} of positive hit compounds from Pathogen Box. *IC_{50} was calculated for positive hit compounds using Lister 427 bloodstream form* T. brucei*. Cells were incubated for 48 hours and viability was measured using fluorescence.*

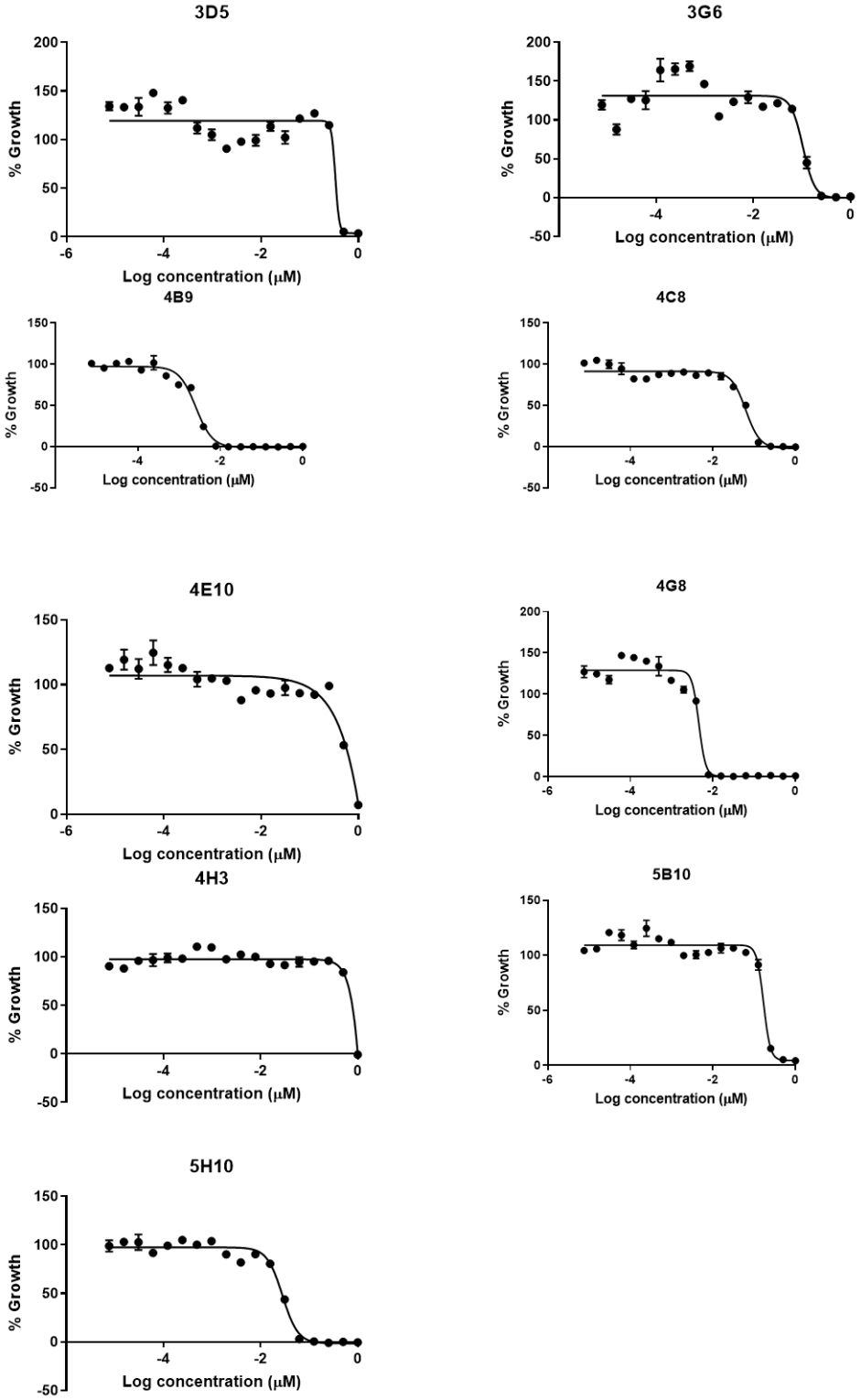

Figure 5.19. IC_{50} of positive hit compounds from Pathogen Box. *IC_{50} was calculated for positive hit compounds using Lister 427 bloodstream form* T. brucei*. Cells were incubated for 48 hours and viability was measured using fluorescence.*

Compound	IC_{50} (nM)	95% Confidence Interval (nM)
1A6	97.48	64.35 – 147.70
1E5	64.79	56.54 – 74.24
1G5	151.70	131 – 175.60
2B3	53.14	38.68 – 73
2C2	121.70	24.44 – 605.90
2D3	12.30	10.03 – 15.09
2H2	69.29	62.36 – 76.98
3B10	101.10	88.67 – 115.20
3B11	4.013	3.441 – 4.679
3C10	>1000	ND
3D5	336.30	153.10 – 739.10
3G6	104.20	81.62 – 133.10
4B9	2.546	2.256 – 2.872
4C8	62.18	53.82 – 71.83
4E10	>1000	ND
4G8	4.554	4.062 – 5.107
4H3	>1000	ND
5B10	167.50	148.60 – 188.80
5H10	28.10	24.98 – 31.61

Table 5.5. IC_{50} and 95% confidence interval for all positive hits. *2-fold serial dilution was carried out and the IC_{50} was determined for all positive hits at 1 μM. Compounds with the lowest IC_{50} and 95% confidence interval (highlighted in green box) were selected for further studies.*

Compound	Structure	Pathogen screened
2D3	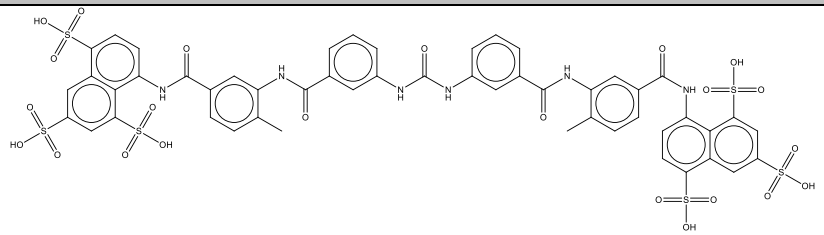	Reference compound (suramin)
3B11	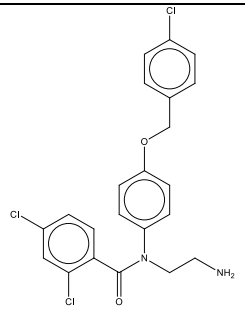	Kinetoplastids
4B9	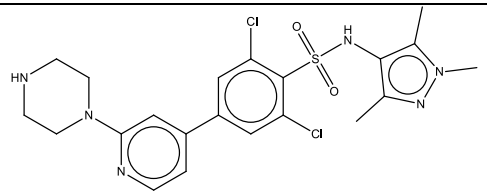	Kinetoplastids

4G8	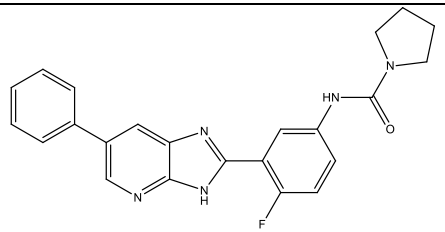	Kinetoplastids
5H10	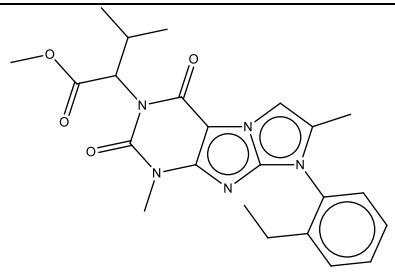	Kinetoplastids

Table 5.6. Chemical structure and pathogen screens of the positive hits. *Visualisation of the chemical structure and pathogen screens for the five positive hits with the lowest IC_{50} and 95% confidence interval. Data on chemical structure and pathogen screens are provided by Pathogen Box (MMV;* https://www.mmv.org/mmv-open/pathogen-box – accessed: Feb 2020*).*

5.3.3.3 Determining whether endocytosis uptake can be identified in hit compounds

Five compounds from Pathogen Box (2D3, 3B11, 4B9, 4G8 and 5H10) were selected that had the lowest IC_{50} values and smallest 95% confidence interval. Each compound was diluted in HMI-9 in order to obtain 9 different concentrations within the 95% confidence interval. These were added to 96 well plates containing clone 6 of the P2T7-TbGEF3 transgenic cell lines that had previously been incubated in 0.1 ng/mL tetracycline or in the absence of tetracycline for 24 hours, as for the suramin assays in section 5.3.2.2. The plates were incubated for 48 hours and fluorescence was read 3 hours post addition of PrestoBlue®.

Figure 5.20 shows that there were no statistical differences between parasite growth in cells with or without tetracycline in compounds 4G8, which suggests that compound 4G8 may be taken up into bloodstream form *T. brucei* via a transporter protein mechanism. Similar results were observed in compound 2D3, 3B11 and 5H10, however at certain concentrations there was significantly more parasite death in the tetracycline positive cells than the tetracycline negative cells, in a similar trend to the findings for diminazene aceturate. This statistically significant increase in parasite death was not uniform across all concentrations in these compounds and was present at the lower range of the diluted concentrations. Regardless of the significant increase in tetracycline positive cell death, results suggest that compounds 2D3, 3B11 and 5H10 are not taken up by endocytosis into bloodstream form *T. brucei*.

It should also be noted that although there were no significant differences between the growth of transgenic *T. brucei* cell with or without tetracycline, compounds 3B11 and 4G8 had 90 to 100% or more viable parasite present (Figure 5.20). This data suggests that the range of concentrations used were too low to have any effect on the parasite viability. These compounds therefore require re-testing at higher concentrations.

Compound 4B9 showed no significant differences in parasite growth from 0 nM to 5 nM concentration range. However, an increase in compound 4B9 concentration showed that transgenic bloodstream form *T. brucei* incubated in tetracycline had significantly higher parasite growth than the cells that were not incubated in tetracycline (Figure 5.20). The data suggests that the first 5 concentrations used were not effective at killing the parasite, and this was further shown by the percentage of viable cells – more than 100% viable cells present.

A wider concentration range is required in order to confirm whether compound 4B9 may be taken up by endocytosis.

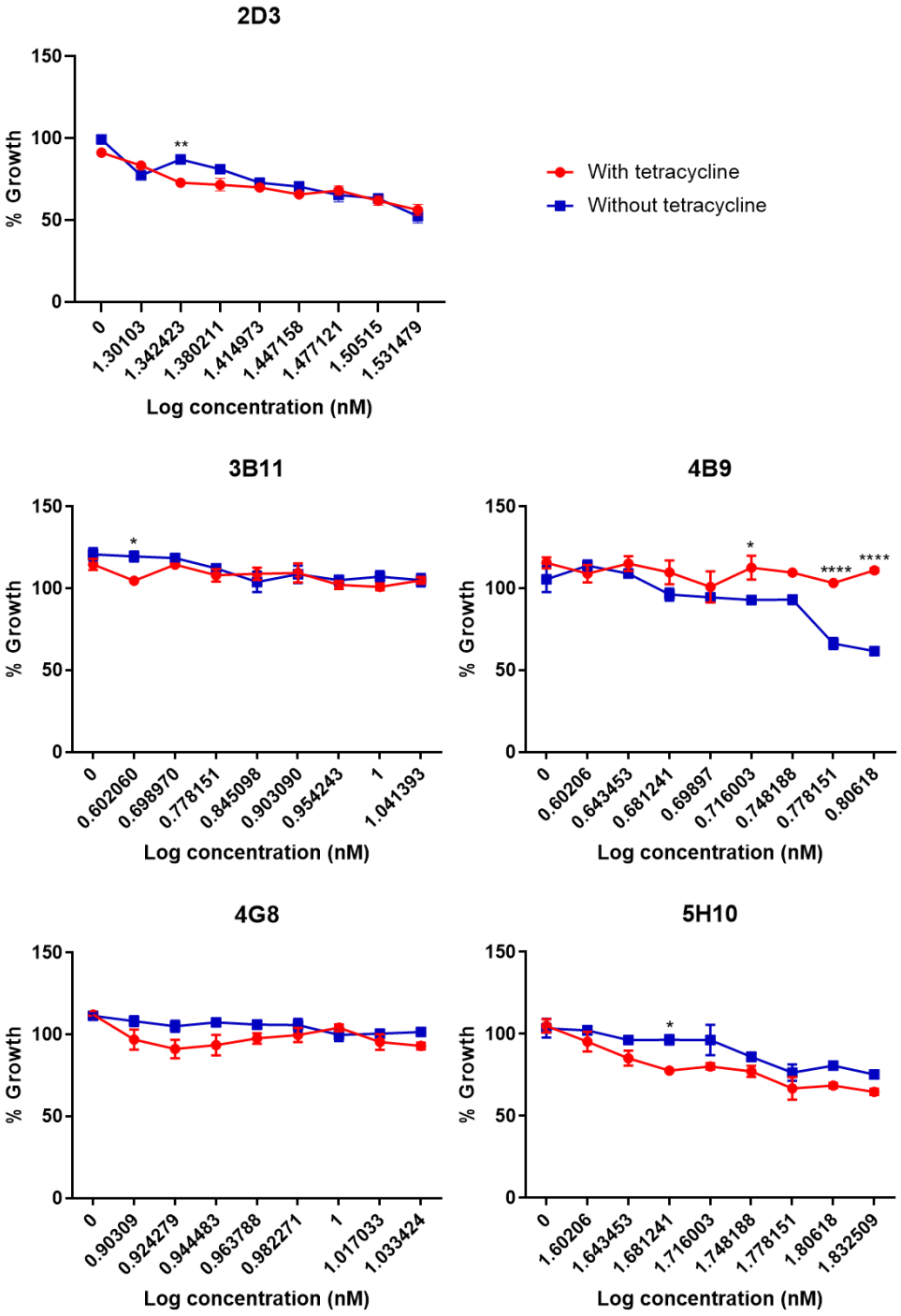

Figure 5.20. Determining the activity of selected compounds in transgenic P2T7-TbGEF3 cells. *Different concentrations of selected compounds with low IC_{50} values were added to P2T7-TbGEF3 cell lines with (red) and without (blue) tetracycline (n = 3). 2-way ANOVA multiple comparisons was used for statistical analysis. * = P ≤ 0.05, ** = P ≤ 0.01, **** = P ≤ 0.0001*

5.4 Discussion

The current drugs against Human African Trypanosomiasis (HAT) and Animal African Trypanosomiasis (nagana) are largely costly, cause severe side effects and there is emerging resistance (Thomas *et al*., 2018, Delespaux and de Koning, 2007).

The aim of this chapter was to test whether the transgenic P2T7-TbGEF3 RNAi cell lines that exhibited an endocytosis defect could be used in a novel drug discovery assay to identify compounds that are taken up via endocytosis. An optimal concentration of tetracycline was identified through a series of dilutions. The sensitivity of transgenic P2T7-TbGEF3 cell line to suramin and diminazene aceturate was also identified. Pathogen Box (MMV) compound screening at 1 μM identified 20 positive hits against bloodstream form *T. brucei* with less than 5% parasite growth after incubation for 48 hours. From the 20, 19 of these compounds were further analysed in order to identify their activity in tetracycline induced transgenic *T. brucei*.

5.4.1 Inducing a partial endocytosis defect in a TbGEF3 RNAi cell line

Endocytosis in bloodstream form *T. brucei* is a rapid process that occurs exclusively at the flagellar pocket. This process is important for immune evasion and normal cellular functions (Allen *et al*., 2003, Umaer *et al*., 2018). Disruption of endocytosis in bloodstream form *T. brucei* has been shown to decrease sensitivity to suramin (Zoltner *et al*., 2015). Reduced sensitivity to suramin was demonstrated to be due to disruption in endocytosis of low density lipoproteins (LDLs) (Wiedemar *et al*., 2019). This principle could be used in conjunction with transgenic cell lines exhibiting an endocytosis defect in order to identify compounds from drug libraries that are also taken up via endocytosis, since exposure to those compounds would theoretically not kill the parasite or have reduced sensitivity. New drug compounds that are taken up via endocytosis may have less potential to induce resistance in parasites in the future.

Indirect immunofluorescent microscopy images in chapter 4 section 4.7.1 identified the presence of abnormal morphology in bloodstream form *T. brucei* from 24 hours post RNAi of

TbGEF3 in the transgenic P2T7-TbGEF3 cell lines. Transmission Electron Microscopy images in section 4.7.2 showed that the abnormal morphology was due to enlarged flagellar pockets, establishing this morphology as the previously described BigEye morphology. Allen et at., (2003) and Price *et al*., (2007) demonstrated that bloodstream form *T. brucei* with BigEye morphology had endocytosis defect (Price *et al*., 2007b, Allen *et al*., 2003). This was further demonstrated in this thesis (section 4.9), where endocytosis of Concanavalin A (Con A) did not occur in bloodstream form *T. brucei* from 24 hours following RNAi knockdown of TbGEF3.

A concentration of 1 μg/mL of tetracycline was used to induce RNAi in the transgenic cell lines in Chapter 4. In addition to an endocytosis defect, RNAi of TbGEF3 also lead to a defect in cell cycle progression, eventually leading to increased cell death which is evident from 48 hours onwards. If RNAi cell lines were to be used in drug screening assays, I needed to identify a concentration of tetracycline which induced a partial endocytosis defect but did not cause extensive cell death. The IC_{50} (the half maximal inhibitory concentration) of tetracycline was identified in section 5.3.1. This was found to be between 0.3959 ng/mL to 0.4132 ng/mL, which is considerably less than the standard concentration (1 μg/mL) used previously (Hashimi *et al*., 2016).

Suramin was used in pilot experiments in this chapter to test if the transgenic P2T7-TbGEF3 cell lines, in the presence of the optimum concentration of tetracycline, can demonstrate reduced sensitivity to the drug, therefore suggesting a reduction in uptake by endocytosis (Wiedemar *et al*., 2019).

Diminazene aceturate, a therapeutic agent used to treat cattle with nagana (Tsegaye *et al*., 2015), was used in this chapter as a control drug. This is because diminazene aceturate is taken up into *T. brucei* via the *TbAT1*/P2 transporters, meaning that there should still be a trypanocidal effect in bloodstream form *T. brucei* cells that exhibit an endocytosis defect (Delespaux and de Koning, 2007).

Results from Figure 5.5 show that incubating P2T7-TbGEF3 transgenic cells in 0.1 ng/mL and 0.15 ng/mL tetracycline for 24 hours prior to addition of suramin had a reduced sensitivity to suramin compared to the control group. This observation correlates with the findings in chapter 4, where a BigEye morphology and endocytosis defect (shown by Con A uptake assay) was observed from 24 hours post RNAi of TbGEF3. An increase in IC_{50} of suramin in the tetracycline incubated samples further confirmed the decrease in sensitivity to suramin than compared to the control sample without tetracycline incubation.

The effect of tetracycline on suramin activity in transgenic P2T7-TbGEF3 cell line was validated using different concentrations of suramin. Diminazene aceturate was used as a control in order to ensure that the differences in suramin sensitivity were due to endocytosis being affected and not due to cellular functions being compromised. Figures 5.6 and 5.7 show that cells incubated in tetracycline had reduced sensitivity to suramin and increased sensitivity to diminazene aceturate.

A possible reason for the increased sensitivity to diminazene aceturate could be due to the bloodstream form *T. brucei* compensating for lack of endocytosis by increasing uptake of molecules via P2 transporters. Future studies are needed to identify if this is the case. Since *TbAT1*/P2 transporters are adenosine/adenine transporters, it may be possible to use fluorescent tagged adenosine/adenine and fluorescent cell imaging or flow cytometry to determine the intensity of the fluorescence. Fluorescence in normal cells will be used as a baseline, and any shift in the baseline fluorescence in the presence of endocytosis defect may provide information on P2 transporter activities; thereby identifying if bloodstream form *T. brucei* increases P2 transporter activity in the presence of an endocytosis defect (Munday *et al*., 2014, Bircsak *et al*., 2013). Interestingly Sykes *et al*., (2012) identified the IC_{50} of diminazene aceturate to be around 65.4 nM in *T. b. brucei* (Sykes *et al*., 2012). This concentration is significantly higher than the IC_{50} observed in section 5.3.1.1 (7.287 – 9.281 nM), which suggest that either the Lister 427 bloodstream form *T. brucei* and the transgenic cell lines used in the current study may be highly sensitive to diminazene aceturate.

5.4.2 Measuring parasite viability

During the work presented here, cell viability following incubation in test compounds were measured using PrestoBlue® - a resazurin based reagent that is reduced into resorufin by metabolically active cells. The reduction of resazurin into resorufin occurs due to mitochondrial enzymes present in the viable cells accepting electrons from NADPH, FADH, FMNH, NADH and cytochromes. Reduction of resazurin into resorufin causes colour change from blue to pink, this reduction also causes a shift in fluorescence which is used to assess cell viability (Al-Nasiry *et al*., 2007, Xu *et al*., 2015, Hernandez-Patlan *et al*., 2018). However Gould *et al*., (2008) proposed that using propidium iodide to assess drug action against trypanosomes may provide more accurate data than use of a resazurin based reagent. This is because resazurin based reagent are unable to distinguish between live cells and growth arrested cells, and resazurin needs to enter the cell in order to be reduced. Gould *et al*., (2008) also argued that some test compounds have the capability to reduce resazurin, therefore providing false positive results (Gould *et al*., 2008). However adding test compounds to resazurin based reagent and measuring changes in fluorescence may help identify compounds that reduce resazurin in the absence of live cells. There is also a possibility of compounds exhibiting fluorescence, thus providing a false negative reading by suggesting that there is a higher percentage of viable cells. Testing compounds without the presence of fluorescent agents may help identify any compounds that exhibit fluorescence.

Another technique that can be used to measure viability is the bioluminescence assay, which utilises *T. brucei spp.* strains expressing *Renilla luciferase* (*RLuc*) or other forms of luciferase enzyme. The expression of *RLuc* in *T. brucei spp.* does not alter their functions or viability *in vitro* or *in vivo*, therefore this assay could be used to screen drugs (Van Reet *et al*., 2013, Claes *et al*., 2009). Resazurin based assays require longer incubation period in the reagent in order to get a high signal to background reading for detection, whereas luminescence gives a much higher signal to background reading regardless of time incubated. The longer incubation period can also affect the IC_{50}/EC_{50} of the compounds that are being tested (Van Reet *et al*.,

2013). Van Reet *et al*., (2013) utilised the *RLuc* luminescence assay alongside the ATP-bioluminescence assay; an assay where bioluminescence is generated due to luciferase catalysing the transformation of luciferin to oxyluciferin in the presence of cellular ATP, thus yielding PP_i, AMP and luminescence (Van Reet *et al*., 2013, Mackey *et al*., 2006). They noted that using *RLuc* and ATP luminescence assay as a luminescence multiplex viability assay resulted in an increase in sensitivity to the assay due to two sensitive and independent viability assays being performed, as well as requiring less incubation time than the resazurin based assays (Van Reet *et al*., 2013). NanoLuc-PEST is another luciferase that could be used for bioluminescence assays. NanoLuc originates from a deep-sea shrimp and is a small and stable enzyme compared to *RLuc* (19 kDa compared to 36 kDa). Fusion of NanoLuc to PEST sequence results in reduced intracellular half-life but increase in enzymatic activity (Berry *et al*., 2018). Comparison of assay performed using NanoLuc-PEST and PrestoBlue® in *Leishmania mexicana* axenic amastigotes found a 50 to 100 fold higher signal to background ratio in assays performed using NanoLuc-PEST (Berry *et al*., 2018).

5.4.3 Pathogen Box screening

The Medicines for Malaria Ventures (MMV) foundation initially assembled a set of compounds that were active against various pathogens, including *Plasmodium falciparum*, *Schistosoma mansoni* and *Toxoplasma gondii*. This set of compounds was named the Malaria Box (Machicado *et al*., 2019, Hennessey *et al*., 2018). Extensive research using the compounds in Malaria Box has led to a compilation of screening data (Van Voorhis *et al*., 2016) that provides a wealth of information on the compounds. Data from 236 screens have shown that 135 (34%) compounds out of the 400 in the Malaria Box actively kill malaria parasite in multiple life cycle stages (Van Voorhis *et al*., 2016). In addition to compounds killing malaria, research has also found 16 compounds that are active against other protozoa, 7 compounds against helminths, and 9 compounds against bacterial and mycobacterial species (Van Voorhis *et al*., 2016). The success in generating valuable screening data from the Malaria Box led MMV to release a new

set of 400 compounds that have been shown to have inhibitory activities against toxoplasmosis, tuberculosis, neosporosis, malaria, leishmaniasis and trypanosomiasis. The set of 400 compounds were termed the Pathogen Box (Machicado *et al*., 2019, Nugraha *et al*., 2019).

Pathogen Box compounds were screened against wild type Lister 427 bloodstream form *T. brucei* in this chapter. Positive hits were confirmed as any compounds that had less than 5% parasite growth after 48 hours. A total of 20 compounds out of the 384 were identified as having activity on bloodstream form *T. brucei*. A set of 5 compounds with the lowest IC_{50} values were taken forward for further analysis. Of these, 4 compounds were identified in screens against kinetoplastids (Table 5.6); possibly explaining the low IC_{50} values observed in Table 5.5. While assays were performed 'blind', later analysis revealed that compound 2D3 is suramin. This means that the IC_{50} value and the possible uptake determination assay carried out in section 5.3.3.2 and 5.3.3.3 respectively, contradicts the results observed in section 5.3.1 and 5.3.2 using freshly prepared suramin. The IC_{50} value in Lister 427 bloodstream form *T. brucei* using a fresh batch of suramin was calculated as 27.12 nM, whilst the IC_{50} for Pathogen Box provided suramin (2D3) was 12.30 nM. Similarly data from Figure 5.6 shows that the lab prepared suramin exhibited lower sensitivity in the presence of tetracycline whilst data from Figure 5.20 shows that suramin (2D3) did not show differences in sensitivity even in the presence of tetracycline.

Several factors could have contributed to the differences in results observed, including the preparation and storage of the compounds and potential contaminants. The Pathogen Box compounds were shipped as liquid stocks from MMV and may have been exposed to freeze-thawing, whereas the suramin stock was prepared immediately upon arrival and stored in -20°C in aliquots before use in the assay. Storage of suramin, as recommended by the manufacturer is at +2°C to +8°C for short term use, whilst suramin liquid stocks should be stored at -20°C, where they will be stable for up to a month. There is a possibility that the suramin stock stored at -20°C may have become unstable or may have been contaminated,

thus affecting potency and IC_{50} values. However Otoguro *et al*., (2008) identified the IC_{50} value of suramin to be around 37 nM in *T. b. rhodesiense* (Otoguro *et al*., 2008), which is closest to the *T. b. brucei* IC_{50} value for lab prepared suramin (27.12 nM) than the equivalent value from the Pathogen Box stock (12.30 nM). Further work with new compound stocks is therefore needed to confirm the results.

Comparison of data obtained in this chapter and previous works on Pathogen Box using Lister 427 bloodstream form *T. brucei* found that the same compounds as the ones identified in this chapter were also identified as having inhibitory activities against *T. b. brucei*, however the IC_{50} values for the compounds obtained in previous data were higher than the IC_{50} values obtained in this chapter (Veale and Hoppe, 2018, Duffy *et al*., 2017). The differences in the IC_{50} observed may have been due to the methodology differences, as Veale and Hoppe, (2008) incubated their cells in resazurin based reagent for 24 hours whilst the cell in this thesis were incubated for 3 hours in a similar resazurin based reagent (Veale and Hoppe, 2018). There could also be a possibility that the low IC_{50} values observed in this chapter were due to contamination in the Pathogen Box stocks prepared; this also coincides with the low IC_{50} value observed for compound 2D3 (suramin). Future work is required using new suramin stocks and Pathogen Box compounds in order to confirm the results found in this chapter.

5.5 Conclusions

The main findings of this chapter are as follows:

- Transgenic P2T7-TbGEF3 cell lines incubated in 0.1 ng/mL tetracycline for 24 hours to induce RNAi had significantly reduced sensitivity to suramin compared to cells grown in the absence of tetracycline.
- Transgenic P2T7-TbGEF3 cell lines incubated in tetracycline for 24 hours had increased sensitivity to diminazene aceturate compared to cells grown in the absence of tetracycline.
- Pathogen Box, screening identified that 20 compounds out of 384 had inhibitory activities (viability below 5%) against *T. brucei*. Out of the 20 compounds, 5 of them had IC_{50} values below 30 nM.

P2T7-TbGEF3 transgenic cells (with and without tetracycline incubation) had increased sensitivity to compound 2D3 from the Pathogen Box (suramin) than freshly prepared suramin but the latter matched previously published IC_{50} values.

Chapter 6 – Discussion

6.1 General Discussion

In this thesis I studied ARF regulating proteins in bloodstream form *T. brucei* as potential drug targets. Human ARF regulators and their orthologues in bloodstream form *T. brucei* were identified and RNAi constructs were generated. RNAi constructs for knockdown of two GEFs and two GAPs were successfully transfected into bloodstream form *T. brucei*, and the effects of tetracycline inducible RNAi were analysed. Tetracycline induced RNAi of TbGEF3 was shown to be essential for viability in bloodstream form *T. brucei*, with knockdown resulting in an endocytosis defect

6.1.1 Why study *T. brucei* drug targets?

Previous control initiatives and surveillance of HAT resulted in a sharp decrease in the number of recorded HAT cases (Legros *et al*., 2002, Franco *et al*., 2014). However the number of cases always saw a re-emergence when the initiatives were withdrawn (Simarro *et al*., 2008, Kennedy, 2019). The current WHO target for HAT, as highlighted during the London Declaration on Neglected Tropical Diseases, is to reduce the number of *T. b. gambiense* case to less than 1 new case/10,000 population at risk globally by 2020 and for zero cases by 2030. In 2016, the number of recorded HAT cases had dropped to 2,184; suggesting that elimination of HAT by 2030 may be possible and within the set milestones by the WHO (Rock *et al*., 2015, Kennedy, 2019, Franco *et al*., 2018).

Since the number of HAT cases per year are based on the recorded data, there is a possibility that the actual number of HAT cases may be significantly higher due to high levels of unreporting in regions of instability, which may hamper elimination efforts (Legros *et al*., 2002, Chappuis *et al*., 2005). There is also a risk that non-human infectious *T. b. brucei* may evolve to gain serum-resistance associated (SRA)-like proteins, making them infectious to humans. This was observed by Szempruch *et al*., (2016) who noted that SRA can be transferred from

T. b. rhodesiense to T*. b. brucei* via membranous nanotubes originating from flagellar membrane (Szempruch *et al*., 2016).

The majority of drugs against HAT were discovered several decades ago, with each drug being stage- or species-specific. The rise in resistance to the drugs against HAT, as well as the high cost and severe side effects led to new initiatives into drug discovery (Baker and Welburn, 2018). Through collaborative efforts of Drugs for Neglected Diseases initiative (DNDi) and Sanofi, a new drug against HAT was developed. This drug, fexinidazole, has recently been registered for use as an oral treatment against late stage *T. b. gambiense* infection (Mesu *et al*., 2018, Pollastri, 2018, Chappuis, 2018). However studies by Wyllie *et al*., (2015) have shown that there is scope for *T. brucei spp.* developing resistance to fexinidazole due to mutations in nitroreductase (Wyllie *et al*., 2015). The DNDi strategy for developing new drugs against HAT focuses on developing safe, effective and practical drug against second stage HAT, and very simple treatment for first stage HAT.

Control initiatives against African Trypanosomiasis have primarily been focused on HAT; whilst nagana is still a prevalent veterinary disease which renders a quarter of Africa unsuitable for livestock farming (Giordani *et al*., 2019, Meyer *et al*., 2018, Morrison *et al*., 2016). Nagana kills three million animals per years in sub-Saharan Africa, leading to huge socioeconomic burden costing billions of US dollars on people living in nagana endemic countries, especially those in poorer countries (Morrison *et al*., 2016, Giordani *et al*., 2019). The current drugs against nagana are toxic, animal specific and there are resistant strains of parasites emerging, thus providing opportunities for transmission and re-infection (Giordani *et al*., 2016).

Research into novel drug targets against *T. brucei ssp.*, the causative agent of African Trypanosomiasis is still urgently need. Such research led to a family of GTPase proteins called ADP-ribosylation factors (ARFs). These proteins have been shown previously to have important roles in *T. brucei*. Several ARFs and ARLs are essential for *T. brucei* viability, with RNAi leading to increased cell death, lethal phenotypes (Figure 6.1) and decreased cell division (Price *et al*., 2007b, Price *et al*., 2005b, Price *et al*., 2005a).

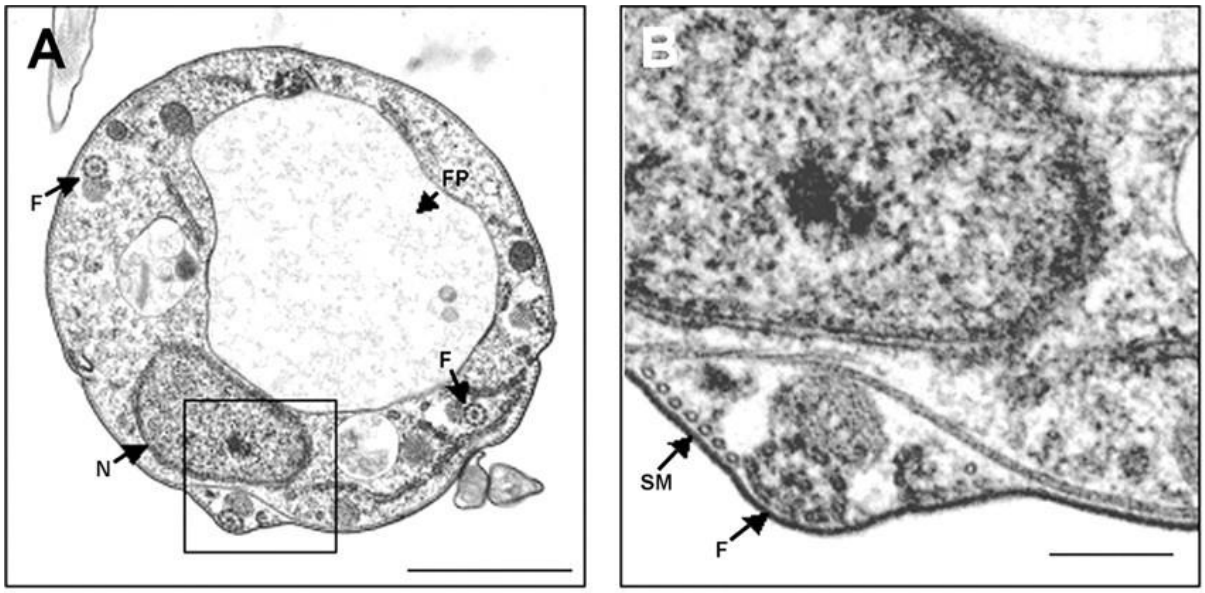

***Figure 6.1. Electron Micrograph of lethal phenotype in bloodstream form* T. brucei.** *Price et al (2007) identified that RNAi of ARF1 lead to (A) lethal phenotype. B is the enlarged (3.75 times) view of the boxed area in A. F, flagellum; FP, flagellar pocket; N. nucleus; SM, subpellicular microtubules. Bar: A is 1 μm and B is 0.2 μm. Adapted from (Price et al., 2007b).*

Despite previous studies showing ARF1 and several ARLs to be potential drug targets in bloodstream form *T. brucei*, the human and *T. brucei* proteins have a high level of sequence identity, especially at the GDP/GTP binding sites, which is required for activation and inactivation of these small GTPase proteins (Price *et al*., 2007b, Price *et al*., 2005b). This would mean that targeting *T. brucei* ARF/ARL functions via inhibitors binding to the highly conserved sites, may lead to binding of the inhibitors to the human proteins. Several of the members of the ARF family of proteins are known to be essential in a range of eukaryotes. For example, gene knockdown of ARL2 in a mouse model was shown to cause aggressive proliferation of breast cancer tumours, whilst knockdown of ARF1 in mice was shown to be lethal for embryogenesis and no viable pups were born (Beghin *et al*., 2009, Hayakawa *et al*., 2014).

The functions of ARF are regulated by two types of regulatory proteins: guanine nucleotide exchange factors (GEFs) and GTPase activating proteins (GAPs), activating and inactivating by binding of GTP or hydrolysis of GTP respectively (Bhatt *et al*., 2016, Sztul *et al*., 2019). ARF/ARLs, the ARF GEFs and GAPs are highly divergent overall at the protein sequence level (Xu and Scheres, 2005, Mandiyan *et al*., 1999); meaning that the functions of ARF/ARLs could be targeted by targeting their regulators.

I hypothesised that ARF GEFs are more likely to be essential in bloodstream form *T. brucei* than the ARF GAPs. This is because GEFs are required for the activation of ARF/ARLs: knockdown of the GEFs could lead to a decrease in the level of active ARF proteins; thus potentially having a similar effect as ARF RNAi (Bhatt *et al*., 2016, Sztul *et al*., 2019). This thesis aimed to identify ARF regulating proteins that are present in bloodstream form *T. brucei*; and generate and use RNAi expressing cell lines to identify which ARF regulating proteins are essential for *T. brucei* viability. Finally, studies were performed to evaluate if transgenic cell lines with an endocytosis defect could be used in drug discovery to predict the mechanism of hit compound uptake.

6.1.2 ARF GEFs and GAPs are conserved at the catalytic domains

Protein BLAST search using human GEF and GAP sequences identified four *T. brucei* GAPs and three *T. brucei* GEFs. The level of similarities between the human and *T. brucei* ARF regulators was determined using bioinformatics tools. Multiple sequence alignment showed that the identified *T. brucei* ARF regulators were very diverse at the amino acid sequence level, except for their catalytic Sec7 and ARFGAP domains. Out of the three identified *T. brucei* GEFs, TbGEF3 appears to share the lowest sequence identity with other ARF GEFs, even at the conserved binding motifs found in the catalytic Sec7 domain. All four identified *T. brucei* GAPs shared a similar Cys_4 zinc finger motives of $CX_2CX_{16}CX_2C$ with the human orthologues. Targeting the catalytic domain in GEFs and GAPs using specific chemical inhibitors such as brefeldin A has the potential of disrupting ARF functions by preventing their activation or

inactivation (Jackson and Casanova, 2000). The high level of amino acid sequence similarities in TbGAPs and TbGEF2 suggest that these *T. brucei* ARF regulators may not be ideal drug targets against *T. brucei* (Ilari *et al*., 2018). The lower level of sequence identity at the Sec7 domain seen in TbGEF3 suggests that specific inhibition of this protein by small molecules may be possible.

Domain analysis revealed that the identified *T. brucei* ARF regulators only had their respective catalytic domains present, lacking other protein-protein interaction domains that were present in most subfamilies of human ARF regulators. The *T. brucei* GEFs had similar domain composition to the high molecular weight ARFGEF and GBF subfamilies of human GEFs, suggesting that these regulators may have similar mechanisms of interaction with the ARFs. Interestingly the identified *T. brucei* GEFs had a molecular weight of above 100 kDa, a criterion that is used to classify high molecular vs low molecular weight GEFs in humans (Shinotsuka *et al*., 2002b). This suggests that the *T. brucei* GEFs may be true orthologues of the ARFGEF and GBF subfamilies. The *T. brucei* GAPs were similar in domain composition to the ARFGAP and SMAP subfamilies, lacking any protein-protein interaction domains. Like the *T. brucei* GEFs, this similarities amongst GAPs suggest that they may share a similar mechanism of interaction with ARFs.

No previous data on *T. brucei* GEF and GAP structures exist, which meant that the protein structures in Chapter 3 were predicted using Phyre2 predictive software and pre-existing templates of homologous structures (Kelley *et al*., 2015). The predicted structures of *T. brucei* GEFs and GAPs matched the description of Sec7 and ARFGAP domains as stated in previous studies (Mandiyan *et al*., 1999, Mossessova *et al*., 1998). This was expected since the catalytic domains have been shown to be highly conserved at the amino acid sequence level across all species (Pocognoni *et al*., 2018, Arakel *et al*., 2020). Structural alignment showed that the predicted *T. brucei* GEF Sec7 domains were structurally similar to CTYH1 and CYTH2 but not CYTH3 (which was later identified as CYTH3 PH complex), or to the other human ARF GEFs. Although the Sec7 domain has been reported to be highly conserved at the amino acid level,

the differences in structural similarities suggest that a high level of amino acid sequence identity may not necessarily equate to secondary structure similarity. The potential differences in secondary structure of the Sec7 domain could be exploited in drug design. The ARFGAP domains in both human and *T. brucei* GAPs were shown to be relatively similar structurally, however unlike the *T. brucei* GEFs, the ARF GAPs did not all show similarity to one particular subfamily of proteins in humans. Each of the *T. brucei* GAPs was shown to be structurally similar to a different ARF GAP subfamily. This suggests that there may be a higher secondary structure diversity amongst the *T. brucei* ARF GAPs that could be taken into consideration when designing specific inhibitor molecules.

6.1.3 TbGEF3 is essential for viability in *T. brucei*

Tetracycline induced RNAi knockdown of *T. brucei* GEFs and GAPs in Chapter 4 showed that TbGEF3 is essential for bloodstream form *T. brucei* viability. A decrease in cell growth, increase in cells with BigEye morphology and defect in cell cycle progression was observed from 24 hours post RNAi of TbGEF3, with increased cell death occurring from 48 hours post RNAi. The BigEye phenotype suggests that TbGEF3 may be implicated in endocytic pathways. This was further confirmed when endocytosis assay in section 4.3.7 showed that uptake of Con A was compromised from 24 hours post RNAi of TbGEF3. Data from Chapter 5 further shows that TbGEF3 is required for endocytosis since sensitivity to suramin decreased in cells following the induction of TbGEF3 RNAi.

The RNAi effect of TbGEF3 data from Chapter 4 and the low level of amino acid sequence identity at the ARF binding regions of the Sec7 domain shown in Chapter 3 suggests that TbGEF3 is the most promising of the 4 studied proteins as a novel drug target against *T. brucei*. An ideal drug target is defined by several rules that identify and prioritise drug targets, and TbGEF3 meets the 3 main rules for drug targets against parasites. These rules are: 1) the drug target should be sufficiently different from the host or be absent in host for specific targeting – TbGEF3 has low level of overall amino acid sequence identity and at the essential ARF binding

sites. 2) the drug target should be essential for the host-stage parasite – RNAi knockdown of TbGEF3 led to cell cycle defect and increased death in bloodstream form *T. brucei*. 3) the target should be 'druggable' – inhibitors have previously been designed to target the catalytic Sec7 domain of ARF GEFs (Ilari *et al*., 2018, Kandoi *et al*., 2015).

Previous work by Demmel *et al*., (2016) have shown that reductions in phosphatidylinositol (4,5)-bisphosphate via knockdown of TbPIPKA, located at the neck of flagellar pocket, led to an enlarged flagellar pocket and endocytosis defect (Demmel *et al*., 2016). This is similar to the observed phenotype following RNAi of TbGEF3. Since phosphatidylinositol (4,5)-bisphosphate is required for the interactions of GEFs to ARF/ARLs (Meissner *et al*., 2018), it could be hypothesised that the results observed by Demmel *et al*., (2016) may have been due to lack of *T. brucei* GEFs (TbGEF3) interacting with ARF/ARLs; thus further highlighting the potential use of TbGEF3 as a novel drug target

RNAi of TbGAP1, TbGAP4 and TbGEF2 did not affect the cellular functions or morphology in bloodstream form *T. brucei*, suggesting that these ARF regulators may not be essential for bloodstream form *T. brucei* viability. However, measuring the changes in gene expression across all clones in all of the ARF regulator cell lines is needed to provide information on whether RNAi knockdown was sufficient, thus confirming whether TbGAP1, TbGAP4 and TbGEF2 are truly not essential in the cells.

6.2 Future work

The work done in this thesis identified *T. brucei* ARF regulators and the effect of tetracycline induced RNAi knockdown of these regulators in bloodstream form *T. brucei*. Further work is now required in order to develop a clear understanding of the ARF regulators and their functions within bloodstream form *T. brucei*. Proposed work is described below.

6.2.1 Identification of ARF regulator structures

The structures of the identified ARFs were predicted in this thesis using Phyre2 software (described in Chapter 3). However, this prediction software uses homologous templates in order to predict secondary structures. This meant that the predicted structures in Chapter 3 were of the highly conserved Sec7 and ARFGAP domains, and not the overall structure of the GEFs and GAPs. Identifying the three-dimensional structure of ARF regulators may provide a better understanding of their subcellular functions.

Mandiyan *et al*., (1999) and Mossessova *et al*., (1998) described the catalytic domains of ARF GAPs and GEFs using X-ray crystallography (Mandiyan *et al*., 1999, Mossessova *et al*., 1998). The first step of X-ray crystallography requires a crystal of the protein of interest. This is usually the limiting factor since crystallization of proteins are not uniform and require specific conditions depending on their tertiary and quaternary structures present, as well as amino acids present that may affect polarity (Smyth and Martin, 2000). Once the crystals have been obtained, a beam of X-ray is used to strike the crystals. Some of the X-ray beam is scattered when the beam hits the protein present in the crystal. The diffraction (scatter) of the X-ray beam is used to determine the structure of the protein (Smyth and Martin, 2000).

Prior to X-ray crystallography, the protein of interest needs to be expressed and purified. A technique that can be used to purify *T. brucei* proteins is the overexpression of histidine tagged (His-tagged) protein of interest in *E. coli*. The His-tagged proteins can then be isolated using nickel-nitrilotriacetic acid (Ni-NTA) agarose and purified for X-ray crystallography (Wang *et al*., 2017). The same technique could be used to express and purify the identified ARF GEFs and GAPs, however purification of the entire length of GEFs have been shown to be difficult due to the size of these ARF regulators being approximately 2000 amino acids in length. Therefore expression and purification of the essential function retaining fragments (Sec7 catalytic domain) may be more feasible (Richardson *et al*., 2012).

6.2.2 Identifying ARF and ARF-regulator interactions

With the current data it is difficult to determine which ARFs and ARLs are regulated by each of the *T. brucei* GEFs and GAPs. Protein-protein interaction studies may give a wealth of information regarding the ARF regulator interactions, localisation and associated cellular pathways the regulators might be implicated in. A mutated version of *E. coli* biotin ligase (BirA*) could be used to determine the interactions of *T. brucei* GEFs and GAPs. In *E. coli*, the BirA is required for the regulation of acetyl-CoA carboxylase through biotinylation. The BirA* binds biotin and ATP, this generates reactive bioAMP, these bioAMP covalently interact with primary amines present in proximity to BirA* fused proteins. The biotinylated proteins can then be isolated via streptavidin affinity purification and identified through mass spectrometry (Khan *et al*., 2018, Oostdyk *et al*., 2019). The use of BirA* in *T. brucei* was successfully demonstrated by Morriswood *et al*., (2013), therefore the *T. brucei* GEFs and GAPs could be expressed as BirA* fused proteins in future studies (Morriswood *et al*., 2013).

The Yeast 2 Hybrid (Y2H) protein-protein interaction technique has been used widely and could be applied to study specific interactions of *T. brucei* GEFs and GAPs. The Y2H utilises two interacting proteins, the protein of interest – “bait”, and a predicted protein that interacts with the protein of interest – “prey”. The bait is fused to DNA binding domain (DBD), whilst the prey is fused to the activation domain (AD) of a transcription factor. The hypothetical binding of prey to bait results in the reconstitution of the transcription factor and expression of a reporter gene (Erffelinck *et al*., 2018, Brückner *et al*., 2009). Y2H technique was used in Lister 427 bloodstream form *T. brucei* with N-terminal fused GAL4 on both BDB and AD, positive interactions were determined using selective medium (quadruple drop-out medium) and colour change (Singh *et al*., 2014). Other protein-protein interaction techniques include split luciferase assay, a technique where luciferase is split and the inactive C-terminal and N-terminal of the luciferase is fused to protein of interest and hypothetical interacting protein. The C-terminus and N-terminus luciferase fuse together when the protein of interest binds to the hypothetical interacting protein, thus producing a detectable bioluminescence signal (Hatzios *et al*., 2012).

6.2.3 Different systems of gene targeting

The P2T7^{Ti} vector was used for the RNAi system in this thesis to induce knockdown of *T. brucei* GEFs and GAPs. However the P2T7Ti vector is known to cause leaky expression in uninduced cells (LaCount *et al*., 2002). This would mean that *T. brucei* transfected with an essential ARF regulator could have been killed prior to being induced (e.g. GEF1), thus this particular gene transfection would then be determined as unsuccessful. Other methods of targeting genes of interest have been studied in *T. brucei*, which include the p*Tb*FIX vectors consists of two transcription units and eliminated the need for pre-existing transgenic cell lines (Niemirowicz *et al*., 2018). There is also the *glmS* ribozyme based inducible gene expression system which worked as effectively as the conventional RNAi system but without the leaky expression (Cruz-Bustos *et al*., 2018).

The clustered regularly interspaced short palindromic repeats (CRISPR) is a gene editing technique that has gained popularity over the last 5 years. CRISPR utilises an RNA guided DNA endonuclease, Cas-9, and a synthetic guide RNA (gRNA) (Beneke *et al*., 2017). The gRNA matches the target DNA sequence, which facilitates endonuclease activity on target DNA sequence. In order to cut the target DNA, the DNA sequence must lie at the protospacer adjacent motif (PAM), which is at the 3' end of the gRNA (Figure 6.2) (Rico et al., 2018, Redman et al., 2016). Vasquez *et al*., (2018) demonstrated the use of CRISPR/Cas-9 in *T. brucei.* They inserted a C-terminal GFP tag to the suppressor of clathrin deficient 6 (SCD6) without changing the UTRs, and targeted two different genes both individually and at the same time. This gene editing was done without the use of selective markers, thus demonstrating the robustness of the CRISPR/Cas-9 system (Vasquez *et al*., 2018).

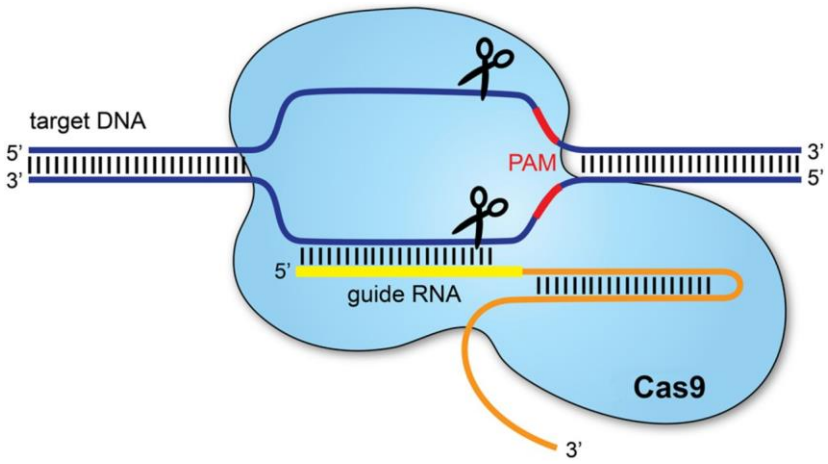

Figure 6.2. The CRISPR/Cas-9 gene editing system. *CRISPR/Cas-9 gene editing system showing the guide RNA that has the same sequence as the target DNA. Target DNA is cleaved at the 3' end of the guide RNA termed protospacer adjacent motif (PAM) (Redman et al., 2016).*

6.2.4 Effects of TbGEF3 RNAi on *T. brucei* in a mouse infection model

The experiments in this thesis were carried out in in vitro culture in order to observe the effect of RNAi of TbGEF3 in bloodstream form *T. brucei*. However carrying out an RNAi experiment *in vivo* might provide additional information to further validate TbGEF3 as a novel drug target against *T. brucei*. This is because bloodstream form *T. brucei* interacting with the host environment, especially the host's immune system greatly influences the subcellular functions. Immune evasion by bloodstream form *T. brucei* heavily relies on internalisation of variant surface glycoproteins (VSGs) via endocytosis (Natesan *et al*., 2011). Knockdown of TbGEF3 has been shown to induce an endocytosis defect in bloodstream form *T. brucei in vitro*, therefore it could be hypothesised that the knockdown of TbGEF3 *in vivo* may lead to a rapid decrease in parasitaemia due to lack of VSG internalisation and cell cycle defect, leading to greater levels of parasites being killed by the host immune system. *In vivo* effect of TbGEF3 knockdown could be studied in rodent models. Taking inspiration from a study by Price *et al*., (2010), parasitaemia could be measured using tail-cut blood samples of infected rodents at

different time points following induction of RNAi in transgenic P2T7-TbGEF3 cells by the addition of doxycycline to drinking water (Price *et al*., 2010a).

6.2.5 Screening inhibitors against TbGEF3 using compound libraries

Several studies have identified specific inhibitors of ARF GEFs, which then have effects on ARF functions. The most well-known inhibitor is Brefeldin A (BFA). BFA is a hydrophobic lactone produced by fungi, which inhibits ARF GEF function by binding to the interface between ARF and GEF (Myers and Casanova, 2008, Ohashi *et al*., 2012). Screening for compounds similar to BFA led to the discovery of AMF-26, a BFA-like inhibitor that was shown to inhibit the functions of GBF1 (Ohashi *et al*., 2012). Similar screening also identified LM11, a compound that has inhibitory functions on ARFGEF1 and CYTH subfamily (Viaud *et al*., 2007). GEF assay screening identified a compound that has inhibitory functions against IQSEC and CYTH subfamilies; this inhibitor was named NAV-2729 (Yoo *et al*., 2016). Another inhibitor of CYTH subfamily is SecinH3, discovered during in vitro screening using RNA aptamer (Hafner *et al*., 2006). Golgicide A is an inhibitor that targets GBF1 present in the Golgi. Treatment of Vero cells (a African green monkey kidney epithelial line) with Golgicide A caused Golgi and trans-Golgi network dispersal (Saenz *et al*., 2009).

Protein-protein interaction assays such as the ones described in section 6.2.2 can be used using TbGEF3 and these inhibitors of ARF GEFs in order to determine if existing inhibitors could potentially be used to target TbGEF3, as well as to study the inhibition mechanism in TbGEF3. However since many of these inhibitors are known to inhibit human ARF GEFs, they are not suitable as potential therapeutic agents against *T. brucei*. The chemical structures and the mode of interactions of these molecules might help identify or design novel inhibitors that can be used to inhibit the functions of TbGEF3 in bloodstream form *T. brucei*.

6.3 Conclusion

The work carried out in this thesis identified 4 putative orthologues of human ARF GAPs and 3 putative orthologues of human ARF GEFs in *T. brucei*. Through RNAi induced gene knockdown, TbGEF3 was identified as an essential ARF regulator in bloodstream form *T. brucei*. Further analysis on TbGEF3 led to the conclusion that TbGEF3 may be promising as a novel drug target against *T. brucei*. Additional work will need to be carried out in order to understand the specific functions of TbGEF3 as the molecular level; and to further validate TbGEF3 as a drug target. The data in this thesis shows a promising step into identifying ARF regulators as novel drug targets against *T. brucei*.

References

ACOSTA-SERRANO, A., COLE, R. N., MEHLERT, A., LEE, M. G., FERGUSON, M. A. & ENGLUND, P. T. 1999. The procyclin repertoire of Trypanosoma brucei. Identification and structural characterization of the Glu-Pro-rich polypeptides. *J Biol Chem,* 274**,** 29763-71.

ACOSTA-SERRANO, A., VASSELLA, E., LINIGER, M., KUNZ RENGGLI, C., BRUN, R., RODITI, I. & ENGLUND, P. T. 2001. The surface coat of procyclic Trypanosoma brucei: programmed expression and proteolytic cleavage of procyclin in the tsetse fly. *Proc Natl Acad Sci U S A,* 98**,** 1513-8.

AGARWAL, S., RASTOGI, R., GUPTA, D., PATEL, N., RAJE, M. & MUKHOPADHYAY, A. 2013. Clathrin-mediated hemoglobin endocytosis is essential for survival of Leishmania. *Biochim Biophys Acta,* 1833**,** 1065-1077.

AHMED, H. A., MACLEOD, E. T., WELBURN, S. C. & PICOZZI, K. 2015. Development of Real Time PCR to Study Experimental Mixed Infections of T. congolense Savannah and T. b. brucei in Glossina morsitans morsitans. *PLoS One,* 10**,** e0117147.

AL-NASIRY, S., GEUSENS, N., HANSSENS, M., LUYTEN, C. & PIJNENBORG, R. 2007. The use of Alamar Blue assay for quantitative analysis of viability, migration and invasion of choriocarcinoma cells. *Human Reproduction,* 22**,** 1304-1309.

ALBISETTI, A., FLORIMOND, C., LANDREIN, N., VIDILASERIS, K., EGGENSPIELER, M., LESIGANG, J., DONG, G., ROBINSON, D. R. & BONHIVERS, M. 2017. Interaction between the flagellar pocket collar and the hook complex via a novel microtubule-binding protein in Trypanosoma brucei. *PLoS Pathog,* 13**,** e1006710.

ALBISETTI, A., WIESE, S., SCHNEIDER, A. & NIEMANN, M. 2015. A component of the mitochondrial outer membrane proteome of T. brucei probably contains covalent bound fatty acids. *Exp Parasitol,* 155**,** 49-57.

ALCANTARA, C. D. L., VIDAL, J. C., DE SOUZA, W. & CUNHA-E-SILVA, N. L. 2017. The cytostome–cytopharynx complex of Trypanosoma cruzi epimastigotes disassembles during cell division. *Journal of Cell Science,* 130**,** 164-176.

ALCANTARA, C. L., VIDAL, J. C., DE SOUZA, W. & CUNHA-E-SILVA, N. L. 2014. The three-dimensional structure of the cytostome-cytopharynx complex of Trypanosoma cruzi epimastigotes. *Journal of Cell Science,* 127**,** 2227-2237.

ALIBU, V. P., STORM, L., HAILE, S., CLAYTON, C. & HORN, D. 2005. A doubly inducible system for RNA interference and rapid RNAi plasmid construction in Trypanosoma brucei. *Mol Biochem Parasitol,* 139**,** 75-82.

ALLEN, C. L., GOULDING, D. & FIELD, M. C. 2003. Clathrin-mediated endocytosis is essential in Trypanosoma brucei. *EMBO J,* 22**,** 4991-5002.

AMOR, J. C., HORTON, J. R., ZHU, X., WANG, Y., SULLARDS, C., RINGE, D., CHENG, X. & KAHN, R. A. 2001. Structures of yeast ARF2 and ARL1: distinct roles for the N terminus in the structure and function of ARF family GTPases. *J Biol Chem,* 276**,** 42477-84.

ANDERS, N. & JURGENS, G. 2008. Large ARF guanine nucleotide exchange factors in membrane trafficking. *Cell Mol Life Sci,* 65**,** 3433-45.

ANENE, B., ONAH, D. & NAWA, Y. 2001. Drug resistance in pathogenic African trypanosomes: what hopes for the future? *Veterinary Parasitology,* 96**,** 83-100.

ANTONNY, B., HUBER, I., PARIS, S., CHABRE, M. & CASSEL, D. 1997. Activation of ADP-ribosylation factor 1 GTPase-activating protein by phosphatidylcholine-derived diacylglycerols. *J Biol Chem,* 272**,** 30848-51.

ARAKEL, E. C., HURANOVA, M., ESTRADA, A. F., RAU, E.-M., SPANG, A. & SCHWAPPACH, B. 2020. Dissection of GTPase-activating proteins reveals functional asymmetry in the COPI coat of budding yeast. *Journal of Cell Science,* 132**,** jcs232124.

ARAKEL, E. C. & SCHWAPPACH, B. 2018. Formation of COPI-coated vesicles at a glance. *J Cell Sci,* 131**,** jcs209890.

ASLETT, M., AURRECOECHEA, C., BERRIMAN, M., BRESTELLI, J., BRUNK, B. P., CARRINGTON, M., DEPLEDGE, D. P., FISCHER, S., GAJRIA, B., GAO, X., GARDNER, M. J., GINGLE, A., GRANT, G., HARB, O. S., HEIGES, M., HERTZ-FOWLER, C., HOUSTON, R., INNAMORATO, F., IODICE, J.,

KISSINGER, J. C., KRAEMER, E., LI, W., LOGAN, F. J., MILLER, J. A., MITRA, S., MYLER, P. J., NAYAK, V., PENNINGTON, C., PHAN, I., PINNEY, D. F., RAMASAMY, G., ROGERS, M. B., ROOS, D. S., ROSS, C., SIVAM, D., SMITH, D. F., SRINIVASAMOORTHY, G., STOECKERT, C. J., JR., SUBRAMANIAN, S., THIBODEAU, R., TIVEY, A., TREATMAN, C., VELARDE, G. & WANG, H. 2010. TriTrypDB: a functional genomic resource for the Trypanosomatidae. *Nucleic Acids Res,* 38**,** D457-62.

BABOKHOV, P., SANYAOLU, A. O., OYIBO, W. A., FAGBENRO-BEYIOKU, A. F. & IRIEMENAM, N. C. 2013. A current analysis of chemotherapy strategies for the treatment of human African trypanosomiasis. *Pathogens and Global Health,* 107**,** 242-252.

BACCHI, C. J. 2009. Chemotherapy of human african trypanosomiasis. *Interdiscip Perspect Infect Dis,* 2009**,** 195040.

BAI, M., GAD, H., TURACCHIO, G., COCUCCI, E., YANG, J. S., LI, J., BEZNOUSSENKO, G. V., NIE, Z., LUO, R., FU, L., COLLAWN, J. F., KIRCHHAUSEN, T., LUINI, A. & HSU, V. W. 2011. ARFGAP1 promotes AP-2-dependent endocytosis. *Nat Cell Biol,* 13**,** 559-67.

BAI, M., PANG, X., LOU, J., ZHOU, Q., ZHANG, K., MA, J., LI, J., SUN, F. & HSU, V. W. 2012. Mechanistic insights into regulated cargo binding by ACAP1 protein. *Journal of Biological Chemistry,* 287**,** 28675-28685.

BAKER, C. H. & WELBURN, S. C. 2018. The long wait for a new drug for human African trypanosomiasis. *Trends in Parasitology,* 34**,** 818-827.

BAKER, N., DE KONING, H. P., MASER, P. & HORN, D. 2013. Drug resistance in African trypanosomiasis: the melarsoprol and pentamidine story. *Trends Parasitol,* 29**,** 110-8.

BALCH, W. E., KAHN, R. A. & SCHWANINGER, R. 1992. ADP-ribosylation factor is required for vesicular trafficking between the endoplasmic reticulum and the cis-Golgi compartment. *J Biol Chem,* 267**,** 13053-61.

BARRETT, M. P., BOYKIN, D. W., BRUN, R. & TIDWELL, R. R. 2007. Human African trypanosomiasis: pharmacological re-engagement with a neglected disease. *Br J Pharmacol,* 152**,** 1155-71.

BARRETT, M. P., BURCHMORE, R. J., STICH, A., LAZZARI, J. O., FRASCH, A. C., CAZZULO, J. J. & KRISHNA, S. 2003. The trypanosomiases. *The Lancet,* 362**,** 1469-80.

BARRY, J. D., GRAHAM, S. V., FOTHERINGHAM, M., GRAHAM, V. S., KOBRYN, K. & WYMER, B. 1998. VSG gene control and infectivity strategy of metacyclic stage Trypanosoma brucei. *Mol Biochem Parasitol,* 91**,** 93-105.

BART, J. M., CORDON-OBRAS, C., VIDAL, I., REED, J., PEREZ-PASTRANA, E., CUEVAS, L., FIELD, M. C., CARRINGTON, M. & NAVARRO, M. 2015. Localization of serum resistance-associated protein in Trypanosoma brucei rhodesiense and transgenic Trypanosoma brucei brucei. *Cell Microbiol,* 17**,** 1523-35.

BATISTA, J. S., RODRIGUES, C. M., GARCÍA, H. A., BEZERRA, F. S., OLINDA, R. G., TEIXEIRA, M. M. & SOTO-BLANCO, B. 2011. Association of Trypanosoma vivax in extracellular sites with central nervous system lesions and changes in cerebrospinal fluid in experimentally infected goats. *Veterinary Research,* 42**,** 63.

BECHEVA, Z. R., GABROVSKA, K. I. & GODJEVARGOVA, T. I. 2018. Comparison between direct and indirect immunofluorescence method for determination of somatic cell count. *Chemical Papers,* 72**,** 1861-1867.

BECK, R., ADOLF, F., WEIMER, C., BRUEGGER, B. & WIELAND, F. T. 2009. ArfGAP1 Activity and COPI Vesicle Biogenesis. *Traffic,* 10**,** 307-315.

BECKER, M., AITCHESON, N., BYLES, E., WICKSTEAD, B., LOUIS, E. & RUDENKO, G. 2004. Isolation of the repertoire of VSG expression site containing telomeres of Trypanosoma brucei 427 using transformation-associated recombination in yeast. *Genome Research,* 14**,** 2319-2329.

BEGHIN, A., BELIN, S., SLEIMAN, R. H., BRUNET MANQUAT, S., GODDARD, S., TABONE, E., JORDHEIM, L. P., TREILLEUX, I., POUPON, M.-F., DIAZ, J.-J. & DUMONTET, C. 2009. ADP Ribosylation Factor Like 2 (Arl2) Regulates Breast Tumor Aggressivity in Immunodeficient Mice. *PloS One,* 4**,** e7478.

BENABDI, S., PEUROIS, F., NAWROTEK, A., CHIKIREDDY, J., CANEQUE, T., YAMORI, T., SHIINA, I., OHASHI, Y., DAN, S., RODRIGUEZ, R., CHERFILS, J. & ZEGHOUF, M. 2017. Family-wide Analysis

of the Inhibition of Arf Guanine Nucleotide Exchange Factors with Small Molecules: Evidence of Unique Inhibitory Profiles. *Biochemistry,* 56**,** 5125-5133.

BENEKE, T., MADDEN, R., MAKIN, L., VALLI, J., SUNTER, J. & GLUENZ, E. 2017. A CRISPR Cas9 high-throughput genome editing toolkit for kinetoplastids. *Royal Society Open Science,* 4**,** 170095.

BENZ, C., DONDELINGER, F., MCKEAN, P. G. & URBANIAK, M. D. 2017. Cell cycle synchronisation of Trypanosoma brucei by centrifugal counter-flow elutriation reveals the timing of nuclear and kinetoplast DNA replication. *Scientific Reports,* 7**,** 17599.

BERAUD-DUFOUR, S., ROBINEAU, S., CHARDIN, P., PARIS, S., CHABRE, M., CHERFILS, J. & ANTONNY, B. 1998. A glutamic finger in the guanine nucleotide exchange factor ARNO displaces Mg2+ and the beta-phosphate to destabilize GDP on ARF1. *EMBO J,* 17**,** 3651-9.

BERBEROF, M., PEREZ-MORGA, D. & PAYS, E. 2001. A receptor-like flagellar pocket glycoprotein specific to Trypanosoma brucei gambiense. *Mol Biochem Parasitol,* 113**,** 127-38.

BERRIMAN, M., GHEDIN, E., HERTZ-FOWLER, C., BLANDIN, G., RENAULD, H., BARTHOLOMEU, D. C., LENNARD, N. J., CALER, E., HAMLIN, N. E., HAAS, B., BOHME, U., HANNICK, L., ASLETT, M. A., SHALLOM, J., MARCELLO, L., HOU, L., WICKSTEAD, B., ALSMARK, U. C., ARROWSMITH, C., ATKIN, R. J., BARRON, A. J., BRINGAUD, F., BROOKS, K., CARRINGTON, M., CHEREVACH, I., CHILLINGWORTH, T. J., CHURCHER, C., CLARK, L. N., CORTON, C. H., CRONIN, A., DAVIES, R. M., DOGGETT, J., DJIKENG, A., FELDBLYUM, T., FIELD, M. C., FRASER, A., GOODHEAD, I., HANCE, Z., HARPER, D., HARRIS, B. R., HAUSER, H., HOSTETLER, J., IVENS, A., JAGELS, K., JOHNSON, D., JOHNSON, J., JONES, K., KERHORNOU, A. X., KOO, H., LARKE, N., LANDFEAR, S., LARKIN, C., LEECH, V., LINE, A., LORD, A., MACLEOD, A., MOONEY, P. J., MOULE, S., MARTIN, D. M., MORGAN, G. W., MUNGALL, K., NORBERTCZAK, H., ORMOND, D., PAI, G., PEACOCK, C. S., PETERSON, J., QUAIL, M. A., RABBINOWITSCH, E., RAJANDREAM, M. A., REITTER, C., SALZBERG, S. L., SANDERS, M., SCHOBEL, S., SHARP, S., SIMMONDS, M., SIMPSON, A. J., TALLON, L., TURNER, C. M., TAIT, A., TIVEY, A. R., VAN AKEN, S., WALKER, D., WANLESS, D., WANG, S., WHITE, B., WHITE, O., WHITEHEAD, S., WOODWARD, J., WORTMAN, J., ADAMS, M. D.,

EMBLEY, T. M., GULL, K., ULLU, E., BARRY, J. D., FAIRLAMB, A. H., OPPERDOES, F., BARRELL, B. G., DONELSON, J. E., HALL, N., FRASER, C. M., *et al*. 2005. The genome of the African trypanosome Trypanosoma brucei. *Science,* 309**,** 416-22.

BERRY, S. L., HAMEED, H., THOMASON, A., MACIEJ-HULME, M. L., SAIF ABOU-AKKADA, S., HORROCKS, P. & PRICE, H. P. 2018. Development of NanoLuc-PEST expressing Leishmania mexicana as a new drug discovery tool for axenic- and intramacrophage-based assays. *PLoS Negl Trop Dis,* 12**,** e0006639.

BHAMIDIPATI, A., LEWIS, S. A. & COWAN, N. J. 2000. ADP ribosylation factor-like protein 2 (Arl2) regulates the interaction of tubulin-folding cofactor D with native tubulin. *J Cell Biol,* 149**,** 1087-96.

BHATT, J. M., VIKTOROVA, E. G., BUSBY, T., WYROZUMSKA, P., NEWMAN, L. E., LIN, H., LEE, E., WRIGHT, J., BELOV, G. A. & KAHN, R. A. 2016. Oligomerization of the Sec7 domain Arf guanine nucleotide exchange factor GBF1 is dispensable for Golgi localization and function but regulates degradation. *Am J Physiol Cell Physiol*.

BIRCSAK, K. M., GIBSON, C. J., ROBEY, R. W. & ALEKSUNES, L. M. 2013. Assessment of drug transporter function using fluorescent cell imaging. *Current Protocols in Toxicology,* 57**,** 23.6.1-23.6.

BISSER, S., LUMBALA, C., NGUERTOUM, E., KANDE, V., FLEVAUD, L., VATUNGA, G., BOELAERT, M., BÜSCHER, P., JOSENANDO, T. & BESSELL, P. R. 2016. Sensitivity and specificity of a prototype rapid diagnostic test for the detection of Trypanosoma brucei gambiense infection: a multi-centric prospective study. *PLoS Negl Trop Dis,* 10**,** e0004608.

BOAL, F. & STEPHENS, D. J. 2010. Specific functions of BIG1 and BIG2 in endomembrane organization. *PLoS One,* 5**,** e9898.

BOELAERT, M., MUKENDI, D., BOTTIEAU, E., LILO, J. R. K., VERDONCK, K., MINIKULU, L., BARBÉ, B., GILLET, P., YANSOUNI, C. P. & CHAPPUIS, F. 2018. A phase III diagnostic accuracy study of a rapid diagnostic test for diagnosis of second-stage human African trypanosomiasis in the Democratic Republic of the Congo. *EBioMedicine,* 27**,** 11-17.

BONNET, J., BOUDOT, C. & COURTIOUX, B. 2015. Overview of the Diagnostic Methods Used in the Field for Human African Trypanosomiasis: What Could Change in the Next Years? *BioMed research international,* 2015**,** 583262-583262.

BORK, P. 1993. Hundreds of ankyrin-like repeats in functionally diverse proteins: mobile modules that cross phyla horizontally? *Proteins: Structure, Function, and Bioinformatics,* 17**,** 363-374.

BREIDBACH, T., NGAZOA, E. & STEVERDING, D. 2002. Trypanosoma brucei: in vitro slender-to-stumpy differentiation of culture-adapted, monomorphic bloodstream forms. *Exp Parasitol,* 101**,** 223-30.

BREMS, S., GUILBRIDE, D. L., GUNDLESDODJIR-PLANCK, D., BUSOLD, C., LUU, V. D., SCHANNE, M., HOHEISEL, J. & CLAYTON, C. 2005. The transcriptomes of Trypanosoma brucei Lister 427 and TREU927 bloodstream and procyclic trypomastigotes. *Mol Biochem Parasitol,* 139**,** 163-72.

BRIDGES, D. J., PITT, A. R., HANRAHAN, O., BRENNAN, K., VOORHEIS, H. P., HERZYK, P., DE KONING, H. P. & BURCHMORE, R. J. 2008. Characterisation of the plasma membrane subproteome of bloodstream form Trypanosoma brucei. *Proteomics,* 8**,** 83-99.

BROWN, D. G. & WOBST, H. J. 2019. Opportunities and Challenges in Phenotypic Screening for Neurodegenerative Disease Research. *Journal of Medicinal Chemistry*.

BRÜCKNER, A., POLGE, C., LENTZE, N., AUERBACH, D. & SCHLATTNER, U. 2009. Yeast two-hybrid, a powerful tool for systems biology. *International Journal of Molecular Sciences,* 10**,** 2763-2788.

BRUHN, D. F., WYLLIE, S., RODRÍGUEZ-CORTÉS, A., CARRILLO, A. K., GUY, R. K., FAIRLAMB, A. H. & LEE, R. E. 2015. Pentacyclic nitrofurans that rapidly kill nifurtimox-resistant trypanosomes. *Journal of Antimicrobial Chemotherapy,* 71**,** 956-963.

BURD, C. G., STROCHLIC, T. I. & GANGI SETTY, S. R. 2004. Arf-like GTPases: not so Arf-like after all. *Trends Cell Biol,* 14**,** 687-94.

BÜSCHER, P., CECCHI, G., JAMONNEAU, V. & PRIOTTO, G. 2017. Human african trypanosomiasis. *The Lancet,* 390**,** 2397-2409.

BÜSCHER, P., GONZATTI, M. I., HÉBERT, L., INOUE, N., PASCUCCI, I., SCHNAUFER, A., SUGANUMA, K., TOURATIER, L. & VAN REET, N. 2019. Equine trypanosomosis: enigmas and diagnostic challenges. *Parasites & Vectors,* 12**,** 234.

CALJON, G., VAN REET, N., DE TREZ, C., VERMEERSCH, M., PÉREZ-MORGA, D. & VAN DEN ABBEELE, J. 2016. The Dermis as a Delivery Site of Trypanosoma brucei for Tsetse Flies. *PLoS Pathog,* 12**,** e1005744.

CAMPA, F. & RANDAZZO, P. A. 2008. Arf GTPase-activating proteins and their potential role in cell migration and invasion. *Cell Adh Migr,* 2**,** 258-62.

CAMPA, F., YOON, H.-Y., HA, V. L., SZENTPETERY, Z., BALLA, T. & RANDAZZO, P. A. 2009. A PH domain in the Arf GTPase-activating protein (GAP) ARAP1 binds phosphatidylinositol 3, 4, 5-trisphosphate and regulates Arf GAP activity independently of recruitment to the plasma membranes. *Journal of Biological Chemistry,* 284**,** 28069-28083.

CAO, H. & SHOCKEY, J. M. 2012. Comparison of TaqMan and SYBR Green qPCR methods for quantitative gene expression in tung tree tissues. *Journal of Agricultural and Food Chemistry,* 60**,** 12296-12303.

CAPEWELL, P., CLUCAS, C., DEJESUS, E., KIEFT, R., HAJDUK, S., VEITCH, N., STEKETEE, P. C., COOPER, A., WEIR, W. & MACLEOD, A. 2013. The TgsGP gene is essential for resistance to human serum in Trypanosoma brucei gambiense. *PLoS Pathog,* 9**,** e1003686.

CAPEWELL, P., CREN-TRAVAILLÉ, C., MARCHESI, F., JOHNSTON, P., CLUCAS, C., BENSON, R. A., GORMAN, T.-A., CALVO-ALVAREZ, E., CROUZOLS, A., JOUVION, G., JAMONNEAU, V., WEIR, W., STEVENSON, M. L., O'NEILL, K., COOPER, A., SWAR, N.-R. K., BUCHETON, B., NGOYI, D. M., GARSIDE, P., ROTUREAU, B. & MACLEOD, A. 2016. The skin is a significant but overlooked anatomical reservoir for vector-borne African trypanosomes. *eLife,* 5**,** e17716.

CAPEWELL, P., VEITCH, N. J., TURNER, C. M., RAPER, J., BERRIMAN, M., HAJDUK, S. L. & MACLEOD, A. 2011. Differences between Trypanosoma brucei gambiense groups 1 and 2 in their resistance to killing by trypanolytic factor 1. *PLoS Negl Trop Dis,* 5**,** e1287.

CASAS-SÁNCHEZ, A., PERALLY, S., RAMASWAMY, R., HAINES, L. R., ROSE, C., YUNTA, C., AGUILERA-FLORES, M., LEHANE, M. J., ALMEIDA, I. C., BOULANGER, M. J. & ACOSTA-SERRANO, A. 2018. The crystal structure and localization of Trypanosoma brucei invariant surface glycoproteins suggest a more permissive VSG coat in the tsetse-transmitted metacyclic stage. *bioRxiv*, 477737.

CASTILLO-ACOSTA, V. M., BALZARINI, J. & GONZÁLEZ-PACANOWSKA, D. 2017. Surface Glycans: A Therapeutic Opportunity for Kinetoplastid Diseases. *Trends in Parasitology,* 33**,** 775-787.

CAYLA, M., ROJAS, F., SILVESTER, E., VENTER, F. & MATTHEWS, K. R. 2019. African trypanosomes. *Parasites & Vectors,* 12**,** 190.

CHAN, K. C., LU, L., SUN, F. & FAN, J. 2017. Molecular details of the PH domain of ACAP1BAR-PH protein binding to PIP-containing membrane. *The Journal of Physical Chemistry B,* 121**,** 3586-3596.

CHAPPUIS, F. 2018. Oral fexinidazole for human African trypanosomiasis. *The Lancet,* 391**,** 100-102.

CHAPPUIS, F., LOUTAN, L., SIMARRO, P., LEJON, V. & BUSCHER, P. 2005. Options for field diagnosis of human african trypanosomiasis. *Clin Microbiol Rev,* 18**,** 133-46.

CHARDIN, P. & MCCORMICK, F. 1999. Brefeldin A: the advantage of being uncompetitive. *Cell,* 97**,** 153-5.

CHATTOPADHYAY, A., JONES, N. G., NIETLISPACH, D., NIELSEN, P. R., VOORHEIS, H. P., MOTT, H. R. & CARRINGTON, M. 2005. Structure of the C-terminal domain from Trypanosoma brucei variant surface glycoprotein MITat1.2. *J Biol Chem,* 280**,** 7228-35.

CHECCHI, F., FUNK, S., CHANDRAMOHAN, D., HAYDON, D. T. & CHAPPUIS, F. 2015. Updated estimate of the duration of the meningo-encephalitic stage in gambiense human African trypanosomiasis. *BMC Res Notes,* 8**,** 292.

CHEN, F., MACKEY, A. J., STOECKERT JR, C. J. & ROOS, D. S. 2006. OrthoMCL-DB: querying a comprehensive multi-species collection of ortholog groups. *Nucleic Acids Res,* 34**,** D363-D368.

CHOW, Y. T., CHEN, S., WANG, R., LIU, C., KONG, C.-W., LI, R. A., CHENG, S. H. & SUN, D. 2016. Single cell transfection through precise microinjection with quantitatively controlled injection volumes. *Scientific Reports,* 6**,** 24127.

CHUN, J., SHAPOVALOVA, Z., DEJGAARD, S. Y., PRESLEY, J. F. & MELANCON, P. 2008. Characterization of class I and II ADP-ribosylation factors (Arfs) in live cells: GDP-bound class II Arfs associate with the ER-Golgi intermediate compartment independently of GBF1. *Mol Biol Cell,* 19**,** 3488-500.

CLAES, F., VODNALA, S. K., VAN REET, N., BOUCHER, N., LUNDEN-MIGUEL, H., BALTZ, T., GODDEERIS, B. M., BÜSCHER, P. & ROTTENBERG, M. E. 2009. Bioluminescent Imaging of Trypanosoma brucei Shows Preferential Testis Dissemination Which May Hamper Drug Efficacy in Sleeping Sickness. *PLoS Negl Trop Dis,* 3**,** e486.

CORDON-OBRAS, C., RODRIGUEZ, Y. F., FERNANDEZ-MARTINEZ, A., CANO, J., NDONG-MABALE, N., NCOGO-ADA, P., NDONGO-ASUMU, P., APARICIO, P., NAVARRO, M., BENITO, A. & BART, J. M. 2015. Molecular evidence of a Trypanosoma brucei gambiense sylvatic cycle in the human african trypanosomiasis foci of Equatorial Guinea. *Front Microbiol,* 6**,** 765.

CROSTON, G. E. 2017. The utility of target-based discovery. Taylor & Francis.

CROWLEY, L. C., SCOTT, A. P., MARFELL, B. J., BOUGHABA, J. A., CHOJNOWSKI, G. & WATERHOUSE, N. J. 2016. Measuring cell death by propidium iodide uptake and flow cytometry. *Cold Spring Harbor Protocols,* 2016**,** pdb. prot087163.

CROZIER, T. W. M., TINTI, M., WHEELER, R. J., LY, T., FERGUSON, M. A. J. & LAMOND, A. I. 2018. Proteomic Analysis of the Cell Cycle of Procylic Form Trypanosoma brucei. *Molecular & Cellular Proteomics,* 17**,** 1184-1195.

CRUZ-BUSTOS, T., RAMAKRISHNAN, S., CORDEIRO, C. D., AHMED, M. A. & DOCAMPO, R. 2018. A Riboswitch-based Inducible Gene Expression System for Trypanosoma brucei. *Journal of Eukaryotic Microbiology,* 65**,** 412-421.

CUKIERMAN, E., HUBER, I., ROTMAN, M. & CASSEL, D. 1995. The ARF1 GTPase-activating protein: zinc finger motif and Golgi complex localization. *Science,* 270**,** 1999-2002.

CURRIER, R. B., COOPER, A., BURRELL-SAWARD, H., MACLEOD, A. & ALSFORD, S. 2018. Decoding the network of Trypanosoma brucei proteins that determines sensitivity to apolipoprotein-L1. *PLoS Pathog,* 14**,** e1006855.

DASCHER, C. & BALCH, W. E. 1994. Dominant inhibitory mutants of ARF1 block endoplasmic reticulum to Golgi transport and trigger disassembly of the Golgi apparatus. *J Biol Chem,* 269**,** 1437-48.

DE CLARE BRONSVOORT, B. M., VON WISSMANN, B., FÈVRE, E. M., HANDEL, I. G., PICOZZI, K. & WELBURN, S. C. 2010. No gold standard estimation of the sensitivity and specificity of two molecular diagnostic protocols for Trypanosoma brucei spp. in Western Kenya. *PLoS One,* 5**,** e8628.

DE GAUDENZI, J. G., NOÉ, G., CAMPO, V. A., FRASCH, A. C. & CASSOLA, A. 2011. Gene expression regulation in trypanosomatids. *Essays In Biochemistry,* 51**,** 31-46.

DE SILVA RODRIGUES, J. H., STEIN, J., STRAUSS, M., RIVAROLA, H. W., UEDA-NAKAMURA, T., NAKAMURA, C. V. & DUSZENKO, M. 2016. Clomipramine kills Trypanosoma brucei by apoptosis. *International Journal of Medical Microbiology,* 306**,** 196-205.

DEAN, S., MARCHETTI, R., KIRK, K. & MATTHEWS, K. R. 2009. A surface transporter family conveys the trypanosome differentiation signal. *Nature,* 459**,** 213-7.

DEAN, S., SUNTER, J. D. & WHEELER, R. J. 2017. TrypTag. org: a trypanosome genome-wide protein localisation resource. *Trends in Parasitology,* 33**,** 80-82.

DEEKS, E. D. 2019. Fexinidazole: First Global Approval. *Drugs,* 79**,** 215-220.

DELESPAUX, V. & DE KONING, H. P. 2007. Drugs and drug resistance in African trypanosomiasis. *Drug resistance updates,* 10**,** 30-50.

DEMMEL, L., SCHMIDT, K., LUCAST, L., HAVLICEK, K., ZANKEL, A., KOESTLER, T., REITHOFER, V., DE CAMILLI, P. & WARREN, G. 2016. The endocytic activity of the flagellar pocket in Trypanosoma brucei is regulated by an adjacent phosphatidylinositol phosphate kinase. *J Cell Sci,* 129**,** 2285.

DEY, P. 2018. Flow Cytometry: Basic Principles, Procedure and Applications in Pathology. *Basic and Advanced Laboratory Techniques in Histopathology and Cytology.* Springer.

DING, S.-W., HAN, Q., WANG, J. & LI, W.-X. 2018. Antiviral RNA interference in mammals. *Current Opinion in Immunology,* 54**,** 109-114.

DOLDÁN-MARTELLI, V. & MÍGUEZ, D. G. 2018. Drug treatment efficiency depends on the initial state of activation in nonlinear pathways. *Scientific Reports,* 8**,** 12495-12495.

DONALDSON, J. G. 2000. Filling in the GAPs in the ADP-ribosylation factor story. *Proc Natl Acad Sci U S A,* 97**,** 3792-4.

DONALDSON, J. G. & JACKSON, C. L. 2000. Regulators and effectors of the ARF GTPases. *Curr Opin Cell Biol,* 12**,** 475-82.

DONALDSON, J. G. & JACKSON, C. L. 2011. ARF family G proteins and their regulators: roles in membrane transport, development and disease. *Nature Reviews Molecular Cell Biology,* 12**,** 362-375.

DRAIN, J., BISHOP, J. R. & HAJDUK, S. L. 2001. Haptoglobin-related protein mediates trypanosome lytic factor binding to trypanosomes. *J Biol Chem,* 276**,** 30254-60.

DUFFY, S., SYKES, M. L., JONES, A. J., SHELPER, T. B., SIMPSON, M., LANG, R., POULSEN, S.-A., SLEEBS, B. E. & AVERY, V. M. 2017. Screening the Medicines for Malaria Venture Pathogen Box across multiple pathogens reclassifies starting points for open-source drug discovery. *Antimicrobial agents and chemotherapy,* 61**,** e00379-17.

DURAND-DUBIEF, M. & BASTIN, P. 2003. TbAGO1, an argonaute protein required for RNA interference, is involved in mitosis and chromosome segregation in Trypanosoma brucei. *BMC biology,* 1**,** 2-2.

EAST, M. P. & KAHN, R. A. 2011. Models for the functions of Arf GAPs. *Semin Cell Dev Biol,* 22**,** 3-9.

ENGSTLER, M., PFOHL, T., HERMINGHAUS, S., BOSHART, M., WIEGERTJES, G., HEDDERGOTT, N. & OVERATH, P. 2007. Hydrodynamic flow-mediated protein sorting on the cell surface of trypanosomes. *Cell,* 131**,** 505-15.

ENGSTLER, M., THILO, L., WEISE, F., GRUNFELDER, C. G., SCHWARZ, H., BOSHART, M. & OVERATH, P. 2004. Kinetics of endocytosis and recycling of the GPI-anchored variant surface glycoprotein in Trypanosoma brucei. *J Cell Sci,* 117**,** 1105-15.

ENOMOTO, K. & GILL, D. 1980. Cholera toxin activation of adenylate cyclase. Roles of nucleoside triphosphates and a macromolecular factor in the ADP ribosylation of the GTP-dependent regulatory component. *Journal of Biological Chemistry,* 255**,** 1252-1258.

ERFFELINCK, M.-L., RIBEIRO, B., PERASSOLO, M., PAUWELS, L., POLLIER, J., STORME, V. & GOOSSENS, A. 2018. A user-friendly platform for yeast two-hybrid library screening using next generation sequencing. *PloS One,* 13**,** e0201270.

FAIRLAMB, A. H. 2003. Chemotherapy of human African trypanosomiasis: current and future prospects. *Trends Parasitol,* 19**,** 488-94.

FAIRLAMB, A. H. & HORN, D. 2018. Melarsoprol resistance in African trypanosomiasis. *Trends in Parasitology,* 34**,** 481-492.

FENN, K. & MATTHEWS, K. R. 2007. The cell biology of Trypanosoma brucei differentiation. *Curr Opin Microbiol,* 10**,** 539-46.

FEVRE, E. M., WISSMANN, B. V., WELBURN, S. C. & LUTUMBA, P. 2008. The burden of human African trypanosomiasis. *PLoS Negl Trop Dis,* 2**,** e333.

FIELD, M. C. 2005. Signalling the genome: the Ras-like small GTPase family of trypanosomatids. *Trends in Parasitology,* 21**,** 447-450.

FIELD, M. C. & CARRINGTON, M. 2009. The trypanosome flagellar pocket. *Nat Rev Microbiol,* 7**,** 775-86.

FILARDY, A. A., GUIMARÃES-PINTO, K., NUNES, M. P., ZUKERAM, K., FLIESS, L., PEREIRA, L., OLIVEIRA NASCIMENTO, D., CONDE, L. & MORROT, A. 2018. Human Kinetoplastid Protozoan Infections: Where Are We Going Next? *Front Immunol,* 9**,** 1493.

FIRE, A., XU, S., MONTGOMERY, M. K., KOSTAS, S. A., DRIVER, S. E. & MELLO, C. C. 1998. Potent and specific genetic interference by double-stranded RNA in Caenorhabditis elegans. *nature,* 391**,** 806.

FRANCO, J. R., CECCHI, G., PRIOTTO, G., PAONE, M., DIARRA, A., GROUT, L., SIMARRO, P. P., ZHAO, W. & ARGAW, D. 2018. Monitoring the elimination of human African trypanosomiasis: Update to 2016. *PLoS Negl Trop Dis,* 12**,** e0006890-e0006890.

FRANCO, J. R., SIMARRO, P. P., DIARRA, A. & JANNIN, J. G. 2014. Epidemiology of human African trypanosomiasis. *Clin Epidemiol,* 6**,** 257-75.

FRIGERIO, G., GRIMSEY, N., DALE, M., MAJOUL, I. & DUDEN, R. 2007. Two human ARFGAPs associated with COP-I-coated vesicles. *Traffic,* 8**,** 1644-1655.

GARCHITORENA, A., SOKOLOW, S., ROCHE, B., NGONGHALA, C., JOCQUE, M., LUND, A., BARRY, M., MORDECAI, E., DAILY, G. & JONES, J. 2017. Disease ecology, health and the environment: a framework to account for ecological and socio-economic drivers in the control of neglected tropical diseases. *Philosophical Transactions of the Royal Society B: Biological Sciences,* 372**,** 20160128.

GASHAW, I., ELLINGHAUS, P., SOMMER, A. & ASADULLAH, K. 2011. What makes a good drug target? *Drug Discov Today,* 16**,** 1037-43.

GEERTS, S., HOLMES, P. H., EISLER, M. C. & DIALL, O. 2001. African bovine trypanosomiasis: the problem of drug resistance. *Trends in Parasitology,* 17**,** 25-28.

GEYER, M. & WITTINGHOFER, A. 1997. GEFs, GAPs, GDIs and effectors: taking a closer (3D) look at the regulation of Ras-related GTP-binding proteins. *Curr Opin Struct Biol,* 7**,** 786-92.

GIBSON, W., BACKHOUSE, T. & GRIFFITHS, A. 2002. The human serum resistance associated gene is ubiquitous and conserved in Trypanosoma brucei rhodesiense throughout East Africa. *Infect Genet Evol,* 1**,** 207-14.

GIBSON, W., NEMETSCHKE, L. & NDUNG'U, J. 2010. Conserved sequence of the TgsGP gene in Group 1 Trypanosoma brucei gambiense. *Infect Genet Evol,* 10**,** 453-8.

GIDEON, P., JOHN, J., FRECH, M., LAUTWEIN, A., CLARK, R., SCHEFFLER, J. E. & WITTINGHOFER, A. 1992. Mutational and kinetic analyses of the GTPase-activating protein (GAP)-p21 interaction: the C-terminal domain of GAP is not sufficient for full activity. *Mol Cell Biol,* 12**,** 2050-6.

GIORDANI, F., KHALAF, A. I., GILLINGWATER, K., MUNDAY, J. C., DE KONING, H. P., SUCKLING, C. J., BARRETT, M. P. & SCOTT, F. J. 2019. Novel Minor Groove Binders cure animal African trypanosomiasis in an in vivo mouse model. *Journal of Medicinal Chemistry,* 62**,** 3021-3035.

GIORDANI, F., MORRISON, L. J., ROWAN, T. G., DE KONING, H. P. & BARRETT, M. P. 2016. The animal trypanosomiases and their chemotherapy: a review. *Parasitology,* 143**,** 1862-1889.

GOATER, T. M., GOATER, C. P. & ESCH, G. W. 2013. *Parasitism: the diversity and ecology of animal parasites*, Cambridge University Press.

GOLDBERG, J. 1998. Structural basis for activation of ARF GTPase: mechanisms of guanine nucleotide exchange and GTP-myristoyl switching. *Cell,* 95**,** 237-48.

GOLDBERG, J. 1999. Structural and functional analysis of the ARF1-ARFGAP complex reveals a role for coatomer in GTP hydrolysis. *Cell,* 96**,** 893-902.

GOULD, M. K., VU, X. L., SEEBECK, T. & DE KONING, H. P. 2008. Propidium iodide-based methods for monitoring drug action in the kinetoplastidae: comparison with the Alamar Blue assay. *Anal Biochem,* 382**,** 87-93.

GRANDGENETT, P. M., OTSU, K., WILSON, H. R., WILSON, M. E. & DONELSON, J. E. 2007. A function for a specific zinc metalloprotease of African trypanosomes. *PLoS Pathog,* 3**,** 1432-45.

GU, F. & GRUENBERG, J. 2000. ARF1 regulates pH-dependent COP functions in the early endocytic pathway. *J Biol Chem,* 275**,** 8154-60.

GUADALUPE, P.-M., CARLOS, M.-H., VIRIDIANA, P.-A., JESUS, V.-M., RAFAEL, C.-G., VICTORIANO, R.-D. & VICTOR, G. 2018. Control of morphology and virulence by ADP-ribosylation factors (Arf) in Mucor circinelloides. *Current Genetics*.

GUBLER, D. J. 1998. Resurgent vector-borne diseases as a global health problem. *Emerg Infect Dis,* 4**,** 442-50.

GYSIN, M., BRAISSANT, O., GILLINGWATER, K., BRUN, R., MÄSER, P. & WENZLER, T. 2018. Isothermal microcalorimetry–A quantitative method to monitor Trypanosoma congolense growth and growth inhibition by trypanocidal drugs in real time. *International Journal for Parasitology: Drugs and Drug Resistance,* 8**,** 159-164.

HAFNER, M., SCHMITZ, A., GRUNE, I., SRIVATSAN, S. G., PAUL, B., KOLANUS, W., QUAST, T., KREMMER, E., BAUER, I. & FAMULOK, M. 2006. Inhibition of cytohesins by SecinH3 leads to hepatic insulin resistance. *Nature,* 444**,** 941-4.

HAMMARTON, T. C. 2007. Cell cycle regulation in Trypanosoma brucei. *Mol Biochem Parasitol,* 153**,** 1-8.

HAMMARTON, T. C., CLARK, J., DOUGLAS, F., BOSHART, M. & MOTTRAM, J. C. 2003. Stage-specific differences in cell cycle control in Trypanosoma brucei revealed by RNA interference of a mitotic cyclin. *J Biol Chem,* 278**,** 22877-86.

HANCK, T., STRICKER, R., SEDEHIZADE, F. & REISER, G. 2004. Identification of gene structure and subcellular localization of human centaurin alpha 2, and p42IP4, a family of two highly homologous, Ins 1,3,4,5-P4-/PtdIns 3,4,5-P3-binding, adapter proteins. *J Neurochem,* 88**,** 326-36.

HANZAL-BAYER, M., LINARI, M. & WITTINGHOFER, A. 2005. Properties of the interaction of Arf-like protein 2 with PDEdelta. *J Mol Biol,* 350**,** 1074-82.

HARDWICK, R. J., MENARD, A., SIRONI, M., MILET, J., GARCIA, A., SESE, C., YANG, F., FU, B., COURTIN, D. & HOLLOX, E. J. 2014. Haptoglobin (HP) and Haptoglobin-related protein (HPR) copy number variation, natural selection, and trypanosomiasis. *Hum Genet,* 133**,** 69-83.

HASEGAWA, J., TSUJITA, K., TAKENAWA, T. & ITOH, T. 2012. ARAP1 regulates the ring size of circular dorsal ruffles through Arf1 and Arf5. *Mol Biol Cell,* 23**,** 2481-9.

HASHIMI, H., KALTENBRUNNER, S., ZÍKOVÁ, A. & LUKEŠ, J. 2016. Trypanosome Mitochondrial Translation and Tetracycline: No Sweat about Tet. *PLoS Pathog,* 12**,** e1005492-e1005492.

HATZIOS, S. K., RINGGAARD, S., DAVIS, B. M. & WALDOR, M. K. 2012. Studies of Dynamic Protein-Protein Interactions in Bacteria Using Renilla Luciferase Complementation Are Undermined by Nonspecific Enzyme Inhibition. *PloS One,* 7**,** e43175.

HAYAKAWA, N., OGOH, H., SUMIYOSHI, M., MATSUI, Y., NISHIKAWA, S., MIYAMOTO, K., MAEDE, Y., KIYONARI, H., SUZUKI, M. & WATANABE, T. 2014. The ADP-ribosylation factor 1 gene is indispensable for mouse embryonic development after implantation. *Biochem Biophys Res Commun,* 453**,** 748-53.

HELLER, L. C., UGEN, K. & HELLER, R. 2005. Electroporation for targeted gene transfer. *Expert Opin Drug Deliv,* 2**,** 255-68.

HEMSWORTH, G. R., PRICE, H. P., SMITH, D. F. & WILSON, K. S. 2013. Crystal structure of the small GTPase Arl6/BBS3 from Trypanosoma brucei. *Protein Sci,* 22**,** 196-203.

HENNESSEY, K. M., ROGIERS, I. C., SHIH, H.-W., HULVERSON, M. A., CHOI, R., MCCLOSKEY, M. C., WHITMAN, G. R., BARRETT, L. K., MERRITT, E. A. & PAREDEZ, A. R. 2018. Screening of the Pathogen Box for inhibitors with dual efficacy against Giardia lamblia and Cryptosporidium parvum. *PLoS Negl Trop Dis,* 12**,** e0006673.

HERNANDEZ-PATLAN, D., SOLIS-CRUZ, B., MÉNDEZ-ALBORES, A., LATORRE, J., HERNANDEZ-VELASCO, X., TELLEZ, G. & LÓPEZ-ARELLANO, R. 2018. Comparison of PrestoBlue® and plating method to evaluate antimicrobial activity of ascorbic acid, boric acid and curcumin in an in vitro gastrointestinal model. *Journal of Applied Microbiology,* 124**,** 423-430.

HERTZ-FOWLER, C., FIGUEIREDO, L. M., QUAIL, M. A., BECKER, M., JACKSON, A., BASON, N., BROOKS, K., CHURCHER, C., FAHKRO, S. & GOODHEAD, I. 2008. Telomeric expression sites are highly conserved in Trypanosoma brucei. *PLoS One,* 3**,** e3527.

HIGGINS, M. K., TKACHENKO, O., BROWN, A., REED, J., RAPER, J. & CARRINGTON, M. 2013. Structure of the trypanosome haptoglobin-hemoglobin receptor and implications for nutrient uptake and innate immunity. *Proc Natl Acad Sci U S A,* 110**,** 1905-10.

HOEFEN, R. J. & BERK, B. C. 2006. The multifunctional GIT family of proteins. *J Cell Sci,* 119**,** 1469-1475.

HOLMES, P. 2014. First WHO Meeting of Stakeholders on Elimination of Gambiense Human African Trypanosomiasis. *PLoS Negl Trop Dis,* 8**,** e3244.

HONG, Y. & KINOSHITA, T. 2009. Trypanosome glycosylphosphatidylinositol biosynthesis. *Korean J Parasitol,* 47**,** 197-204.

HOSOI, N., SHIBASAKI, K., HOSONO, M., KONNO, A., SHINODA, Y., KIYONARI, H., INOUE, K., AIZAWA, S., MURAMATSU, S., ISHIZAKI, Y., HIRAI, H., FURUICHI, T. & SADAKATA, T. 2018. Deletion of class II ARF causes essential tremors through Nav1.6 traffic impairment. *bioRxiv***,** 357160.

HSU, J. W., CHEN, K. J. & LEE, F. J. 2015. Snf1/AMP-activated protein kinase activates Arf3p to promote invasive yeast growth via a non-canonical GEF domain. *Nat Commun,* 6**,** 7840.

HU, H., GOURGUECHON, S., WANG, C. C. & LI, Z. 2016. The G1 Cyclin-dependent Kinase CRK1 in Trypanosoma brucei Regulates Anterograde Protein Transport by Phosphorylating the COPII Subunit Sec31. *Journal of Biological Chemistry,* 291**,** 15527-15539.

HUBER, I., CUKIERMAN, E., ROTMAN, M. & CASSEL, D. 2002. ARF GTPase-activating protein 1. *Methods Mol Biol,* 189**,** 199-206.

HUSSEIN, H. A., GENEIX, C., PETITJEAN, M., BORREL, A., FLATTERS, D. & CAMPROUX, A.-C. 2017. Global vision of druggability issues: applications and perspectives. *Drug Discov Today,* 22**,** 404-415.

IBRAHIM, H. M., AL-SALABI, M. I., EL SABBAGH, N., QUASHIE, N. B., ALKHALDI, A. A., ESCALE, R., SMITH, T. K., VIAL, H. J. & DE KONING, H. P. 2011. Symmetrical choline-derived dications display strong anti-kinetoplastid activity. *J Antimicrob Chemother,* 66**,** 111-25.

ILARI, A., GENOVESE, I., FIORILLO, F., BATTISTA, T., DE IONNA, I., FIORILLO, A. & COLOTTI, G. 2018. Toward a Drug Against All Kinetoplastids: From LeishBox to Specific and Potent Trypanothione Reductase Inhibitors. *Molecular Pharmaceutics,* 15**,** 3069-3078.

JACKSON, A. P., GOYARD, S., XIA, D., FOTH, B. J., SANDERS, M., WASTLING, J. M., MINOPRIO, P. & BERRIMAN, M. 2015. Global Gene Expression Profiling through the Complete Life Cycle of Trypanosoma vivax. *PLoS Negl Trop Dis,* 9**,** e0003975.

JACKSON, C. L. & BOUVET, S. 2014. Arfs at a Glance. *Journal of Cell Science,* 127**,** 4103-4109.

JACKSON, C. L. & CASANOVA, J. E. 2000. Turning on ARF: the Sec7 family of guanine-nucleotide-exchange factors. *Trends Cell Biol,* 10**,** 60-7.

JACOBS, R. T., NARE, B., WRING, S. A., ORR, M. D., CHEN, D., SLIGAR, J. M., JENKS, M. X., NOE, R. A., BOWLING, T. S. & MERCER, L. T. 2011. SCYX-7158, an orally-active benzoxaborole for the treatment of stage 2 human African trypanosomiasis. *PLoS Negl Trop Dis,* 5**,** e1151.

JAKOB, M., HOFFMANN, A., AMODEO, S., PEITSCH, C., ZUBER, B. & OCHSENREITER, T. 2016. Mitochondrial growth during the cell cycle of Trypanosoma brucei bloodstream forms. *Scientific Reports,* 6**,** 36565.

JEFFRIES, T. R., MORGAN, G. W. & FIELD, M. C. 2001. A developmentally regulated rab11 homologue in Trypanosoma brucei is involved in recycling processes. *J Cell Sci,* 114**,** 2617-26.

JIAN, X., GRUSCHUS, J. M., SZTUL, E. & RANDAZZO, P. A. 2012. The pleckstrin homology (PH) domain of the Arf exchange factor Brag2 is an allosteric binding site. *Journal of Biological Chemistry,* 287**,** 24273-24283.

JIN, H. & NACHURY, M. V. 2009. The BBSome. *Current Biology,* 19**,** R472-R473.

JIN, H., WHITE, S. R., SHIDA, T., SCHULZ, S., AGUIAR, M., GYGI, S. P., BAZAN, J. F. & NACHURY, M. V. 2010. The conserved Bardet-Biedl syndrome proteins assemble a coat that traffics membrane proteins to cilia. *Cell,* 141**,** 1208-1219.

JONES, A. J. & AVERY, V. M. 2015. Future treatment options for human African trypanosomiasis. *Expert Review of Anti-infective Therapy,* 13**,** 1429-1432.

JONES, N. G., THOMAS, E. B., BROWN, E., DICKENS, N. J., HAMMARTON, T. C. & MOTTRAM, J. C. 2014. Regulators of Trypanosoma brucei Cell Cycle Progression and Differentiation Identified Using a Kinome-Wide RNAi Screen. *PLoS Pathog,* 10**,** e1003886.

KAHN, R., VOLPICELLI-DALEY, L., BOWZARD, B., SHRIVASTAVA-RANJAN, P., LI, Y., ZHOU, C. & CUNNINGHAM, L. 2005. Arf family GTPases: roles in membrane traffic and microtubule dynamics. *Biochem Soc Trans,* 33**,** 1269-1272.

KAHN, R. A., BRUFORD, E., INOUE, H., LOGSDON, J. M., JR., NIE, Z., PREMONT, R. T., RANDAZZO, P. A., SATAKE, M., THEIBERT, A. B., ZAPP, M. L. & CASSEL, D. 2008. Consensus nomenclature for the human ArfGAP domain-containing proteins. *J Cell Biol,* 182**,** 1039-44.

KAHN, R. A. & GILMAN, A. G. 1984. Purification of a protein cofactor required for ADP-ribosylation of the stimulatory regulatory component of adenylate cyclase by cholera toxin. *J Biol Chem,* 259**,** 6228-34.

KAHN, R. A. & GILMAN, A. G. 1986. The protein cofactor necessary for ADP-ribosylation of Gs by cholera toxin is itself a GTP binding protein. *Journal of Biological Chemistry,* 261**,** 7906-7911.

KAHN, R. A., KERN, F. G., CLARK, J., GELMANN, E. P. & RULKA, C. 1991. Human ADP-ribosylation factors. A functionally conserved family of GTP-binding proteins. *J Biol Chem,* 266**,** 2606-14.

KAHN, R. A. & LAMBRIGHT, D. G. 2015. A PH domain with dual phospholipid binding sites regulates the ARF GAP, ASAP1. *Structure,* 23**,** 1971-1973.

KALB, L. C., ANTUNES FREDERICO, Y. C., BATISTA, C. M., EGER, I., FRAGOSO, S. P. & SOARES, M. J. 2014. Clathrin expression in Trypanosoma cruzi. *BMC Cell Biology,* 15**,** 23.

KAM, J. L., MIURA, K., JACKSON, T. R., GRUSCHUS, J., ROLLER, P., STAUFFER, S., CLARK, J., ANEJA, R. & RANDAZZO, P. A. 2000. Phosphoinositide-dependent activation of the ADP-ribosylation factor GTPase-activating protein ASAP1. Evidence for the pleckstrin homology domain functioning as an allosteric site. *J Biol Chem,* 275**,** 9653-63.

KAMIMURA, K., SUDA, T., ZHANG, G. & LIU, D. 2011. Advances in Gene Delivery Systems. *Pharmaceutical Medicine,* 25**,** 293-306.

KANDOI, G., ACENCIO, M. L. & LEMKE, N. 2015. Prediction of druggable proteins using machine learning and systems biology: a mini-review. *Frontiers in Physiology,* 6**,** 366.

KANSIIME, F., ADIBAKU, S., WAMBOGA, C., IDI, F., KATO, C. D., YAMUAH, L., VAILLANT, M., KIOY, D., OLLIARO, P. & MATOVU, E. 2018. A multicentre, randomised, non-inferiority clinical trial comparing a nifurtimox-eflornithine combination to standard eflornithine monotherapy for

late stage Trypanosoma brucei gambiense human African trypanosomiasis in Uganda. *Parasites & vectors,* 11**,** 105-105.

KAUFER, A., ELLIS, J., STARK, D. & BARRATT, J. 2017. The evolution of trypanosomatid taxonomy. *Parasites & vectors,* 10**,** 287.

KEATING, J., YUKICH, J. O., SUTHERLAND, C. S., WOODS, G. & TEDIOSI, F. 2015. Human African trypanosomiasis prevention, treatment and control costs: a systematic review. *Acta Tropica,* 150**,** 4-13.

KELLEY, L. A., MEZULIS, S., YATES, C. M., WASS, M. N. & STERNBERG, M. J. 2015. The Phyre2 web portal for protein modeling, prediction and analysis. *Nature Protocols,* 10**,** 845.

KENNEDY, P. G. 2004. Human African trypanosomiasis of the CNS: current issues and challenges. *J Clin Invest,* 113**,** 496-504.

KENNEDY, P. G. 2008. The continuing problem of human African trypanosomiasis (sleeping sickness). *Ann Neurol,* 64**,** 116-26.

KENNEDY, P. G. 2013. Clinical features, diagnosis, and treatment of human African trypanosomiasis (sleeping sickness). *The Lancet Neurology,* 12**,** 186-194.

KENNEDY, P. G. 2019. Update on human African trypanosomiasis (sleeping sickness). *Journal of Neurology***,** 1-4.

KENNEDY, P. G. E. & RODGERS, J. 2019. Clinical and Neuropathogenetic Aspects of Human African Trypanosomiasis. *Frontiers in Immunology,* 10**,** 39-39.

KHAN, AMIR R. & MÉNÉTREY, J. 2013. Structural Biology of Arf and Rab GTPases' Effector Recruitment and Specificity. *Structure,* 21**,** 1284-1297.

KHAN, M., YOUN, J.-Y., GINGRAS, A.-C., SUBRAMANIAM, R. & DESVEAUX, D. 2018. In planta proximity dependent biotin identification (BioID). *Scientific Reports,* 8**,** 9212.

KIEFT, R., CAPEWELL, P., TURNER, C. M., VEITCH, N. J., MACLEOD, A. & HAJDUK, S. 2010. Mechanism of Trypanosoma brucei gambiense (group 1) resistance to human trypanosome lytic factor. *Proc Natl Acad Sci U S A,* 107**,** 16137-41.

KIM, S., KO, J., SHIN, H., LEE, J.-R., LIM, C., HAN, J.-H., ALTROCK, W. D., GARNER, C. C., GUNDELFINGER, E. D. & PREMONT, R. T. 2003. The GIT family of proteins forms multimers and associates with the presynaptic cytomatrix protein Piccolo. *Journal of Biological Chemistry,* 278**,** 6291-6300.

KIMUDA, M. P., NOYES, H., MULINDWA, J., ENYARU, J., ALIBU, V. P., SIDIBE, I., MUMBA NGOYI, D., HERTZ-FOWLER, C., MACLEOD, A., TASTAN BISHOP, Ö., MATOVU, E. & TRYPANO, G. E. N. R. G. A. M. O. T. H. A. C. 2018. No evidence for association between APOL1 kidney disease risk alleles and Human African Trypanosomiasis in two Ugandan populations. *PLoS Negl Trop Dis* [Online], 12.

KIRCHHAUSEN, T. 2000. Three ways to make a vesicle. *Nature Reviews Molecular Cell Biology,* 1**,** 187.

KOHL, K., ZANGGER, H., ROSSI, M., ISORCE, N., LYE, L. F., OWENS, K. L., BEVERLEY, S. M., MAYER, A. & FASEL, N. 2018. Importance of polyphosphate in the Leishmania life cycle. *Microb Cell,* 5**,** 371-384.

KOLEV, N. G., RAMSDELL, T. K. & TSCHUDI, C. 2018. Temperature shift activates bloodstream VSG expression site promoters in Trypanosoma brucei. *Molecular and Biochemical Parasitology,* 226**,** 20-23.

KOLEV, N. G., TSCHUDI, C. & ULLU, E. 2011. RNA interference in protozoan parasites: achievements and challenges. *Eukaryot Cell,* 10**,** 1156-63.

KON, S., TANABE, K., WATANABE, T., SABE, H. & SATAKE, M. 2008. Clathrin dependent endocytosis of E-cadherin is regulated by the Arf6GAP isoform SMAP1. *Experimental Cell Research,* 314**,** 1415-1428.

KÖTTING, C. & GERWERT, K. 2004. Time-resolved FTIR studies provide activation free energy, activation enthalpy and activation entropy for GTPase reactions. *Chemical physics,* 307**,** 227-232.

KUANG, J., YAN, X., GENDERS, A. J., GRANATA, C. & BISHOP, D. J. 2018. An overview of technical considerations when using quantitative real-time PCR analysis of gene expression in human exercise research. *PLoS One,* 13**,** e0196438.

LACOUNT, D. J., BARRETT, B. & DONELSON, J. E. 2002. Trypanosoma brucei FLA1 is required for flagellum attachment and cytokinesis. *J Biol Chem,* 277**,** 17580-8.

LACOUNT, D. J., BRUSE, S., HILL, K. L. & DONELSON, J. E. 2000. Double-stranded RNA interference in Trypanosoma brucei using head-to-head promoters. *Mol Biochem Parasitol,* 111**,** 67-76.

LACOUNT, D. J. & DONELSON, J. E. 2001. RNA Interference in African Trypanosomes. *Protist,* 152**,** 103-111.

LAGE, O. M., RAMOS, M. C., CALISTO, R., ALMEIDA, E., VASCONCELOS, V. & VICENTE, F. 2018. Current Screening Methodologies in Drug Discovery for Selected Human Diseases. *Marine Drugs,* 16**,** 279.

LAMA, R., SANDHU, R., ZHONG, B., LI, B. & SU, B. 2012. Identification of selective tubulin inhibitors as potential anti-trypanosomal agents. *Bioorganic & medicinal chemistry letters,* 22**,** 5508-5516.

LANGOUSIS, G. & HILL, K. L. 2014. Motility and more: the flagellum of Trypanosoma brucei. *Nature Reviews Microbiology,* 12**,** 505.

LE, K., LI, C. C., YE, G., MOSS, J. & VAUGHAN, M. 2013. Arf guanine nucleotide-exchange factors BIG1 and BIG2 regulate nonmuscle myosin IIA activity by anchoring myosin phosphatase complex. *Proc Natl Acad Sci U S A,* 110**,** E3162-70.

LECORDIER, L., VANHOLLEBEKE, B., POELVOORDE, P., TEBABI, P., PATURIAUX-HANOCQ, F., ANDRIS, F., LINS, L. & PAYS, E. 2009. C-terminal mutants of apolipoprotein L-I efficiently kill both Trypanosoma brucei brucei and Trypanosoma brucei rhodesiense. *PLoS Pathog,* 5**,** e1000685.

LEE, D. M., RODRIGUES, F. F., YU, C. G., SWAN, M. & HARRIS, T. J. 2015. PH domain-Arf G protein interactions localize the Arf-GEF Steppke for cleavage furrow regulation in Drosophila. *PLoS One,* 10**,** e0142562.

LEE, M. H., MIN, M. K., LEE, Y. J., JIN, J. B., SHIN, D. H., KIM, D. H., LEE, K. H. & HWANG, I. 2002. ADP-ribosylation factor 1 of Arabidopsis plays a critical role in intracellular trafficking and maintenance of endoplasmic reticulum morphology in Arabidopsis. *Plant Physiol,* 129**,** 1507-20.

LEGROS, D., OLLIVIER, G., GASTELLU-ETCHEGORRY, M., PAQUET, C., BURRI, C., JANNIN, J. & BUSCHER, P. 2002. Treatment of human African trypanosomiasis--present situation and needs for research and development. *The Lancet Infectious Diseases,* 2**,** 437-40.

LEONE, M., CELLITTI, J. & PELLECCHIA, M. 2009. The Sam domain of the lipid phosphatase Ship2 adopts a common model to interact with Arap3-Sam and EphA2-Sam. *BMC structural biology,* 9**,** 59.

LETUNIC, I. & BORK, P. 2017. 20 years of the SMART protein domain annotation resource. *Nucleic Acids Res,* 46**,** D493-D496.

LETUNIC, I., DOERKS, T. & BORK, P. 2015. SMART: recent updates, new developments and status in 2015. *Nucleic Acids Res,* 43**,** D257-60.

LI, H., ADAMIK, R., PACHECO-RODRIGUEZ, G., MOSS, J. & VAUGHAN, M. 2003. Protein kinase A-anchoring (AKAP) domains in brefeldin A-inhibited guanine nucleotide-exchange protein 2 (BIG2). *Proc Natl Acad Sci U S A,* 100**,** 1627-1632.

LI, Y., KELLY, W. G., LOGSDON JR, J. M., SCHURKO, A. M., HARFE, B. D., HILL-HARFE, K. L. & KAHN, R. A. 2004. Functional genomic analysis of the ADP-ribosylation factor family of GTPases: phylogeny among diverse eukaryotes and function in C. elegans. *The FASEB Journal,* 18**,** 1834-1850.

LIN, C. Y., HUANG, P. H., LIAO, W. L., CHENG, H. J., HUANG, C. F., KUO, J. C., PATTON, W. A., MASSENBURG, D., MOSS, J. & LEE, F. J. 2000. ARL4, an ARF-like protein that is developmentally regulated and localized to nuclei and nucleoli. *J Biol Chem,* 275**,** 37815-23.

LINIGER, M., URWYLER, S., STUDER, E., OBERLE, M., RENGGLI, C. K. & RODITI, I. 2004. Role of the N-terminal domains of EP and GPEET procyclins in membrane targeting and the establishment of midgut infections by Trypanosoma brucei. *Mol Biochem Parasitol,* 137**,** 247-51.

LIU, J., QIAO, X., DU, D. & LEE, M. G. 2000. Receptor-mediated endocytosis in the procyclic form of Trypanosoma brucei. *J Biol Chem,* 275**,** 12032-40.

LIU, Y., KAHN, R. A. & PRESTEGARD, J. H. 2009. Structure and membrane interaction of myristoylated ARF1. *Structure,* 17**,** 79-87.

LIVAK, K. J. & SCHMITTGEN, T. D. 2001. Analysis of relative gene expression data using real-time quantitative PCR and the 2− ΔΔCT method. *Methods,* 25**,** 402-408.

LU, L., HORSTMANN, H., NG, C. & HONG, W. 2001. Regulation of Golgi structure and function by ARF-like protein 1 (Arl1). *J Cell Sci,* 114**,** 4543-55.

LUO, R., JENKINS, L. M. M., RANDAZZO, P. A. & GRUSCHUS, J. 2008. Dynamic interaction between Arf GAP and PH domains of ASAP1 in the regulation of GAP activity. *Cellular signalling,* 20**,** 1968-1977.

MACHICADO, C., SOTO, M. P., TIMOTEO, O., VAISBERG, A., PAJUELO, M., ORTIZ, P. & MARCOS, L. A. 2019. Screening the Pathogen Box for identification of new chemical agents with anti-Fasciola hepatica activity. *Antimicrobial agents and chemotherapy,* 63**,** e02373-18.

MACKEY, Z. B., BACA, A. M., MALLARI, J. P., APSEL, B., SHELAT, A., HANSELL, E. J., CHIANG, P. K., WOLFF, B., GUY, K. R. & WILLIAMS, J. 2006. Discovery of trypanocidal compounds by whole cell HTS of Trypanosoma brucei. *Chemical Biology & Drug Design,* 67**,** 355-363.

MAJEKODUNMI, A. O., FAJINMI, A., DONGKUM, C., PICOZZI, K., THRUSFIELD, M. V. & WELBURN, S. C. 2013. A longitudinal survey of African animal trypanosomiasis in domestic cattle on the Jos Plateau, Nigeria: prevalence, distribution and risk factors. *Parasites & vectors,* 6**,** 239.

MALVY, D. & CHAPPUIS, F. 2011. Sleeping sickness. *Clinical Microbiology and Infection,* 17**,** 986-995.

MANDIYAN, V., ANDREEV, J., SCHLESSINGER, J. & HUBBARD, S. R. 1999. Crystal structure of the ARF-GAP domain and ankyrin repeats of PYK2-associated protein beta. *EMBO J,* 18**,** 6890-8.

MANSOUR, S. J., SKAUG, J., ZHAO, X. H., GIORDANO, J., SCHERER, S. W. & MELANCON, P. 1999. p200 ARF-GEP1: a Golgi-localized guanine nucleotide exchange protein whose Sec7 domain is targeted by the drug brefeldin A. *Proc Natl Acad Sci U S A,* 96**,** 7968-73.

MÄSER, P., WITTLIN, S., ROTTMANN, M., WENZLER, T., KAISER, M. & BRUN, R. 2012. Antiparasitic agents: new drugs on the horizon. *Current Opinion in Pharmacology,* 12**,** 562-566.

MASLOV, D. A., VOTYPKA, J., YURCHENKO, V. & LUKES, J. 2013. Diversity and phylogeny of insect trypanosomatids: all that is hidden shall be revealed. *Trends Parasitol,* 29**,** 43-52.

MAYER, B. J. 2001. SH3 domains: complexity in moderation. *Journal of Cell Science,* 114**,** 1253-1263.

MAYER, G., BLIND, M., NAGEL, W., BOHM, T., KNORR, T., JACKSON, C. L., KOLANUS, W. & FAMULOK, M. 2001. Controlling small guanine-nucleotide-exchange factor function through cytoplasmic RNA intramers. *Proc Natl Acad Sci U S A,* 98**,** 4961-5.

MAZAKI, Y., NISHIMURA, Y. & SABE, H. 2012. GBF1 bears a novel phosphatidylinositol-phosphate binding module, BP3K, to link PI3Kγ activity with Arf1 activation involved in GPCR-mediated neutrophil chemotaxis and superoxide production. *Mol Biol Cell,* 23**,** 2457-67.

MCINTOSH, J. R., MORPHEW, M. K. & GIDDINGS, T. H. 2017. Electron microscopy of fission yeast. *Cold Spring Harbor Protocols,* 2017**,** pdb. top079822.

MEISSNER, J. M., BHATT, J. M., LEE, E., STYERS, M. L., IVANOVA, A. A., KAHN, R. A. & SZTUL, E. 2018. The ARF guanine nucleotide exchange factor GBF1 is targeted to Golgi membranes through a PIP-binding domain. *J Cell Sci,* 131**,** jcs210245.

MESU, V. K. B. K., KALONJI, W. M., BARDONNEAU, C., MORDT, O. V., BLESSON, S., SIMON, F., DELHOMME, S., BERNHARD, S., KUZIENA, W. & LUBAKI, J.-P. F. 2018. Oral fexinidazole for late-stage African Trypanosoma brucei gambiense trypanosomiasis: a pivotal multicentre, randomised, non-inferiority trial. *The Lancet,* 391**,** 144-154.

MEYER, A., HOLT, H. R., OUMAROU, F., CHILONGO, K., GILBERT, W., FAURON, A., MUMBA, C. & GUITIAN, J. 2018. Integrated cost-benefit analysis of tsetse control and herd productivity to inform control programs for animal African trypanosomiasis. *Parasites & Vectors,* 11**,** 154.

MILLERIOUX, Y., MAZET, M., BOUYSSOU, G., ALLMANN, S., KIEMA, T. R., BERTIAUX, E., FOUILLEN, L., THAPA, C., BIRAN, M., PLAZOLLES, N., DITTRICH-DOMERGUE, F., CROUZOLS, A., WIERENGA, R. K., ROTUREAU, B., MOREAU, P. & BRINGAUD, F. 2018. De novo biosynthesis of sterols and fatty acids in the Trypanosoma brucei procyclic form: Carbon source preferences and metabolic flux redistributions. *PLoS Pathog,* 14**,** e1007116.

MILNE, K. G., PRESCOTT, A. R. & FERGUSON, M. A. 1998. Transformation of monomorphic Trypanosoma brucei bloodstream form trypomastigotes into procyclic forms at 37 C by

removing glucose from the culture medium. *Molecular and Biochemical Parasitology,* 94**,** 99-112.

MITASHI, P., HASKER, E., MBO, F., VAN GEERTRUYDEN, J. P., KASWA, M., LUMBALA, C., BOELAERT, M. & LUTUMBA, P. 2015. Integration of diagnosis and treatment of sleeping sickness in primary healthcare facilities in the Democratic Republic of the Congo. *Trop Med Int Health,* 20**,** 98-105.

MIURA, K., JACQUES, K. M., STAUFFER, S., KUBOSAKI, A., ZHU, K., HIRSCH, D. S., RESAU, J., ZHENG, Y. & RANDAZZO, P. A. 2002. ARAP1: a point of convergence for Arf and Rho signaling. *Molecular cell,* 9**,** 109-119.

MOHAN, K., PAI, S., RAO, R., SRIPATHI, H. & PRABHU, S. 2008. Techniques of immunofluorescence and their significance. *Indian Journal of Dermatology, Venereology, and Leprology,* 74**,** 415.

MOLINA-PORTELA MDEL, P., LUGLI, E. B., RECIO-PINTO, E. & RAPER, J. 2005. Trypanosome lytic factor, a subclass of high-density lipoprotein, forms cation-selective pores in membranes. *Mol Biochem Parasitol,* 144**,** 218-26.

MOLINA-PORTELA, M. P., SAMANOVIC, M. & RAPER, J. 2008. Distinct roles of apolipoprotein components within the trypanosome lytic factor complex revealed in a novel transgenic mouse model. *J Exp Med,* 205**,** 1721-8.

MOLINA PORTELA, M. P., RAPER, J. & TOMLINSON, S. 2000. An investigation into the mechanism of trypanosome lysis by human serum factors. *Mol Biochem Parasitol,* 110**,** 273-82.

MOLINARI, J. & MORENO, S. A. 2018. Trypanosoma brucei Plimmer & Bradford, 1899 is a synonym of T. evansi (Steel, 1885) according to current knowledge and by application of nomenclature rules. *Systematic Parasitology,* 95**,** 249-256.

MOLYNEUX, D. H., SAVIOLI, L. & ENGELS, D. 2017. Neglected tropical diseases: progress towards addressing the chronic pandemic. *The Lancet,* 389**,** 312-325.

MONTI, L., WANG, S. C., OUKOLOFF, K., SMITH III, A. B., BRUNDEN, K. R., CAFFREY, C. R. & BALLATORE, C. 2018. Brain-Penetrant Triazolopyrimidine and Phenylpyrimidine Microtubule Stabilizers as Potential Leads to Treat Human African Trypanosomiasis. *ChemMedChem,* 13**,** 1751-1754.

MORENO, C. J. G., TEMPORÃO, A., TORRES, T. & SOUSA SILVA, M. 2019. Trypanosoma brucei Interaction with Host: Mechanism of VSG Release as Target for Drug Discovery for African Trypanosomiasis. *International Journal of Molecular Sciences,* 20**,** 1484.

MORGAN, C., LEWIS, P. D., HOPKINS, L., BURNELL, S., KYNASTON, H. & DOAK, S. H. 2015. Increased expression of ARF GTPases in prostate cancer tissue. *Springerplus,* 4**,** 342.

MORGAN, G. W., ALLEN, C. L., JEFFRIES, T. R., HOLLINSHEAD, M. & FIELD, M. C. 2001. Developmental and morphological regulation of clathrin-mediated endocytosis in Trypanosoma brucei. *J Cell Sci,* 114**,** 2605-15.

MORRISON, L. J., VEZZA, L., ROWAN, T. & HOPE, J. C. 2016. Animal African trypanosomiasis: time to increase focus on clinically relevant parasite and host species. *Trends in Parasitology,* 32**,** 599-607.

MORRISWOOD, B., HAVLICEK, K., DEMMEL, L., YAVUZ, S., SEALEY-CARDONA, M., VIDILASERIS, K., ANRATHER, D., KOSTAN, J., DJINOVIC-CARUGO, K., ROUX, K. J. & WARREN, G. 2013. Novel bilobe components in Trypanosoma brucei identified using proximity-dependent biotinylation. *Eukaryot Cell,* 12**,** 356-367.

MOSS, J. & VAUGHAN, M. 1995. Structure and function of ARF proteins: activators of cholera toxin and critical components of intracellular vesicular transport processes. *J Biol Chem,* 270**,** 12327-30.

MOSSESSOVA, E., CORPINA, R. A. & GOLDBERG, J. 2003. Crystal structure of ARF1*Sec7 complexed with Brefeldin A and its implications for the guanine nucleotide exchange mechanism. *Mol Cell,* 12**,** 1403-11.

MOSSESSOVA, E., GULBIS, J. M. & GOLDBERG, J. 1998. Structure of the guanine nucleotide exchange factor Sec7 domain of human arno and analysis of the interaction with ARF GTPase. *Cell,* 92**,** 415-423.

MOURATOU, B., BIOU, V., JOUBERT, A., COHEN, J., SHIELDS, D. J., GELDNER, N., JÜRGENS, G., MELANÇON, P. & CHERFILS, J. 2005. The domain architecture of large guanine nucleotide exchange factors for the small GTP-binding protein Arf. *BMC genomics,* 6**,** 20.

MUCHIRI, M. W., NDUNG'U, K., KIBUGU, J. K., THUITA, J. K., GITONGA, P. K., NGAE, G. N., MDACHI, R. E. & KAGIRA, J. M. 2015. Comparative pathogenicity of Trypanosoma brucei rhodesiense strains in Swiss white mice and Mastomys natalensis rats. *Acta Tropica,* 150**,** 23-8.

MUDOGO, C. N., WERNER, S. F., MOGK, S., BETZEL, C. & DUSZENKO, M. 2018. The conserved hypothetical protein Tb427.10.13790 is required for cytokinesis in Trypanosoma brucei. *Acta Tropica,* 188**,** 34-40.

MÜLLER, J. & HEMPHILL, A. 2016. Drug target identification in protozoan parasites. *Expert Opinion on Drug Discovery,* 11**,** 815-824.

MUNDAY, J. C., EZE, A. A., BAKER, N., GLOVER, L., CLUCAS, C., AGUINAGA ANDRÉS, D., NATTO, M. J., TEKA, I. A., MCDONALD, J., LEE, R. S., GRAF, F. E., LUDIN, P., BURCHMORE, R. J. S., TURNER, C. M. R., TAIT, A., MACLEOD, A., MÄSER, P., BARRETT, M. P., HORN, D. & DE KONING, H. P. 2014. Trypanosoma brucei aquaglyceroporin 2 is a high-affinity transporter for pentamidine and melaminophenyl arsenic drugs and the main genetic determinant of resistance to these drugs. *Journal of Antimicrobial Chemotherapy,* 69**,** 651-663.

MUNRO, S. 2005. The Arf-like GTPase Arl1 and its role in membrane traffic. *Biochem Soc Trans,* 33**,** 601-5.

MUTHAMILARASAN, M., MANGU, V. R., ZANDKARIMI, H., PRASAD, M. & BAISAKH, N. 2016. Structure, organization and evolution of ADP-ribosylation factors in rice and foxtail millet, and their expression in rice. *Scientific Reports,* 6**,** 24008.

MYERS, K. R. & CASANOVA, J. E. 2008. Regulation of actin cytoskeleton dynamics by Arf-family GTPases. *Trends Cell Biol,* 18**,** 184-92.

N'DJETCHI, M. K., ILBOUDO, H., KOFFI, M., KABORÉ, J., KABORÉ, J. W., KABA, D., COURTIN, F., COULIBALY, B., FAURET, P. & KOUAKOU, L. 2017. The study of trypanosome species circulating in domestic animals in two human African trypanosomiasis foci of Cote d'Ivoire identifies pigs and cattle as potential reservoirs of Trypanosoma brucei gambiense. *PLoS Negl Trop Dis,* 11**,** e0005993.

NATESAN, S. K. A., BLACK, A., MATTHEWS, K. R., MOTTRAM, J. C. & FIELD, M. C. 2011. Trypanosoma brucei brucei: endocytic recycling is important for mouse infectivity. *Exp Parasitol,* 127**,** 777-783.

NEUMANN, E., SCHAEFER-RIDDER, M., WANG, Y. & HOFSCHNEIDER, P. H. 1982. Gene transfer into mouse lyoma cells by electroporation in high electric fields. *EMBO J,* 1**,** 841-845.

NGÔ, H., TSCHUDI, C., GULL, K. & ULLU, E. 1998. Double-stranded RNA induces mRNA degradation in Trypanosoma brucei. *Proc Natl Acad Sci U S A,* 95**,** 14687-14692.

NIE, Z., FEI, J., PREMONT, R. T. & RANDAZZO, P. A. 2005. The Arf GAPs AGAP1 and AGAP2 distinguish between the adaptor protein complexes AP-1 and AP-3. *J Cell Sci,* 118**,** 3555-3566.

NIE, Z., HIRSCH, D. S. & RANDAZZO, P. A. 2003. Arf and its many interactors. *Curr Opin Cell Biol,* 15**,** 396-404.

NIE, Z., STANLEY, K. T., STAUFFER, S., JACQUES, K. M., HIRSCH, D. S., TAKEI, J. & RANDAZZO, P. A. 2002. AGAP1, an endosome-associated, phosphoinositide-dependent ADP-ribosylation factor GTPase-activating protein that affects actin cytoskeleton. *Journal of Biological Chemistry,* 277**,** 48965-48975.

NIELSEN, E., CHEUNG, A. Y. & UEDA, T. 2008. The Regulatory RAB and ARF GTPases for Vesicular Trafficking. *Plant Physiology,* 147**,** 1516-1526.

NIEMIROWICZ, G. T., CAZZULO, J. J., ÁLVAREZ, V. E. & BOUVIER, L. A. 2018. Simplified inducible system for Trypanosoma brucei. *PLoS One,* 13**,** e0205527.

NJAMNSHI, A. K., GETTINBY, G. & KENNEDY, P. G. 2017. The challenging problem of disease staging in human African trypanosomiasis (sleeping sickness): a new approach to a circular question. *Transactions of The Royal Society of Tropical Medicine and Hygiene,* 111**,** 199-203.

NJIRU, Z. K., MBAE, C. K. & MBURUGU, G. N. 2017. Loop-mediated isothermal amplification test for Trypanosoma gambiense group 1 with stem primers: a molecular xenomonitoring test for sleeping sickness. *Journal of Tropical Medicine,* 2017.

NOK, A. J. 2003. Arsenicals (melarsoprol), pentamidine and suramin in the treatment of human African trypanosomiasis. *Parasitol Res,* 90**,** 71-9.

NUGRAHA, A. B., TUVSHINTULGA, B., GUSWANTO, A., TAYEBWA, D. S., RIZK, M. A., GANTUYA, S., EL-SABER BATIHA, G., BESHBISHY, A. M., SIVAKUMAR, T., YOKOYAMA, N. & IGARASHI, I. 2019. Screening the Medicines for Malaria Venture Pathogen Box against piroplasm parasites. *International Journal for Parasitology: Drugs and Drug Resistance,* 10**,** 84-90.

ODELL, I. D. & COOK, D. 2013. Immunofluorescence techniques. *The Journal of Investigative Dermatology,* 133**,** e4.

OHASHI, Y., IIJIMA, H., YAMAOTSU, N., YAMAZAKI, K., SATO, S., OKAMURA, M., SUGIMOTO, K., DAN, S., HIRONO, S. & YAMORI, T. 2012. AMF-26, a novel inhibitor of the Golgi system, targeting ADP-ribosylation factor 1 (Arf1) with potential for cancer therapy. *J Biol Chem,* 287**,** 3885-97.

OLI, M. W., COTLIN, L. F., SHIFLETT, A. M. & HAJDUK, S. L. 2006. Serum resistance-associated protein blocks lysosomal targeting of trypanosome lytic factor in Trypanosoma brucei. *Eukaryot Cell,* 5**,** 132-9.

OOSTDYK, L. T., SHANK, L., JIVIDEN, K., DWORAK, N., SHERMAN, N. E. & PASCHAL, B. M. 2019. Towards improving proximity labeling by the biotin ligase BirA. *Methods,* 157**,** 66-79.

OTOGURO, K., ISHIYAMA, A., NAMATAME, M., NISHIHARA, A., FURUSAWA, T., MASUMA, R., SHIOMI, K., TAKAHASHI, Y., YAMADA, H. & ŌMURA, S. 2008. Selective and potent in vitro antitrypanosomal activities of ten microbial metabolites. *Journal of Antibiotics,* 61**,** 372.

OVERATH, P. & ENGSTLER, M. 2004. Endocytosis, membrane recycling and sorting of GPI-anchored proteins: Trypanosoma brucei as a model system. *Molecular Microbiology,* 53**,** 735-744.

PADILLA, P. I., PACHECO-RODRIGUEZ, G., MOSS, J. & VAUGHAN, M. 2004. Nuclear localization and molecular partners of BIG1, a brefeldin A-inhibited guanine nucleotide-exchange protein for ADP-ribosylation factors. *Proc Natl Acad Sci U S A,* 101**,** 2752-7.

PADOVANI, D., FOLLY-KLAN, M., LABARDE, A., BOULAKIRBA, S., CAMPANACCI, V., FRANCO, M., ZEGHOUF, M. & CHERFILS, J. 2014. EFA6 controls Arf1 and Arf6 activation through a negative feedback loop. *Proc Natl Acad Sci U S A,* 111**,** 12378-12383.

PADOVANI, D., ZEGHOUF, M., TRAVERSO, J. A., GIGLIONE, C. & CHERFILS, J. 2013. High yield production of myristoylated Arf6 small GTPase by recombinant N-myristoyl transferase. *Small GTPases,* 4**,** 3-8.

PADUCH, M., JELEN, F. & OTLEWSKI, J. 2001. Structure of small G proteins and their regulators. *Acta Biochim Pol,* 48**,** 829-50.

PAI, E. F. 1998. The alpha and beta of turning on a molecular switch.

PANETHYMITAKI, C., BOWYER, P. W., PRICE, H. P., LEATHERBARROW, R. J., BROWN, K. A. & SMITH, D. F. 2006. Characterization and selective inhibition of myristoyl-CoA: protein N-myristoyltransferase from Trypanosoma brucei and Leishmania major. *Biochemical Journal,* 396**,** 277-285.

PANG, L., WANG, J., ZHAO, L., WANG, C. & ZHAN, H. 2019. A Novel Protein Subcellular Localization Method With CNN-XGBoost Model for Alzheimer's Disease. *Front Genet,* 9.

PANINA, Y., GERMOND, A., MASUI, S. & WATANABE, T. M. 2018. Validation of common housekeeping genes as reference for qpcr gene expression analysis during iPS reprogramming process. *Scientific Reports,* 8**,** 8716.

PAOLINI, G. V., LYONS, R. A. & LAFLIN, P. 2010. How desirable are your IC50s? A way to enhance screening-based decision making. *Journal of Biomolecular Screening,* 15**,** 1183-1193.

PARK, S. Y. & GUO, X. 2014. Adaptor protein complexes and intracellular transport. *Bioscience reports,* 34**,** e00123.

PARNIS, A., RAWET, M., REGEV, L., BARKAN, B., ROTMAN, M., GAITNER, M. & CASSEL, D. 2006. Golgi localization determinants in ArfGAP1 and in new tissue-specific ArfGAP1 isoforms. *J Biol Chem,* 281**,** 3785-92.

PASQUALATO, S., MENETREY, J., FRANCO, M. & CHERFILS, J. 2001. The structural GDP/GTP cycle of human Arf6. *EMBO Rep,* 2**,** 234-8.

PASQUALATO, S., RENAULT, L. & CHERFILS, J. 2002. Arf, Arl, Arp and Sar proteins: a family of GTP-binding proteins with a structural device for 'front-back' communication. *EMBO Rep,* 3**,** 1035-41.

PATRICK, K. L., SHI, H., KOLEV, N. G., ERSFELD, K., TSCHUDI, C. & ULLU, E. 2009. Distinct and overlapping roles for two Dicer-like proteins in the RNA interference pathways of the ancient eukaryote Trypanosoma brucei. *Proc Natl Acad Sci U S A,* 106**,** 17933-17938.

PAYS, E., COQUELET, H., PAYS, A., TEBABI, P. & STEINERT, M. 1989. Trypanosoma brucei: posttranscriptional control of the variable surface glycoprotein gene expression site. *Mol Cell Biol,* 9**,** 4018-21.

PAYS, E. & VANHOLLEBEKE, B. 2009. Human innate immunity against African trypanosomes. *Curr Opin Immunol,* 21**,** 493-8.

PEACOCK, L., BAILEY, M., CARRINGTON, M. & GIBSON, W. 2014. Meiosis and haploid gametes in the pathogen Trypanosoma brucei. *Current Biology,* 24**,** 181-186.

PERRY, J. A., SINCLAIR-DAVIS, A. N., MCALLASTER, M. R. & DE GRAFFENRIED, C. L. 2018. TbSmee1 regulates hook complex morphology and the rate of flagellar pocket uptake in Trypanosoma brucei. *Mol Microbiol,* 107**,** 344-362.

PEUROIS, F., PEYROCHE, G. & CHERFILS, J. 2019. Small GTPase peripheral binding to membranes: molecular determinants and supramolecular organization. *Biochem Soc Trans,* 47**,** 13-22.

PEYROCHE, A., ANTONNY, B., ROBINEAU, S., ACKER, J., CHERFILS, J. & JACKSON, C. L. 1999. Brefeldin A acts to stabilize an abortive ARF-GDP-Sec7 domain protein complex: involvement of specific residues of the Sec7 domain. *Mol Cell,* 3**,** 275-85.

PINEDA, E., THONNUS, M., MAZET, M., MOURIER, A., CAHOREAU, E., KULYK, H., DUPUY, J.-W., BIRAN, M., MASANTE, C., ALLMANN, S., RIVIÈRE, L., ROTUREAU, B., PORTAIS, J.-C. & BRINGAUD, F. 2018. Glycerol supports growth of the Trypanosoma brucei bloodstream forms in the absence

of glucose: Analysis of metabolic adaptations on glycerol-rich conditions. *PLoS Pathog,* 14**,** e1007412-e1007412.

PIPERAKI, E.-T. & TASSIOS, P. 2016. Parasitic infections: their position and impact in the postindustrial world. *Clinical Microbiology and Infection,* 22**,** 469-470.

POCOGNONI, C. A., VIKTOROVA, E. G., WRIGHT, J., MEISSNER, J. M., SAGER, G., LEE, E., BELOV, G. A. & SZTUL, E. 2018. Highly conserved motifs within the large Sec7 ARF guanine nucleotide exchange factor GBF1 target it to the Golgi and are critical for GBF1 activity. *Am J Physiol Cell Physiol,* 314**,** C675-c689.

PODLIPAEV, S. 2001. The more insect trypanosomatids under study-the more diverse Trypanosomatidae appears. *Int J Parasitol,* 31**,** 648-52.

POLLASTRI, M. P. 2018. Fexinidazole: A New Drug for African Sleeping Sickness on the Horizon. *Trends in Parasitology,* 34**,** 178-179.

POON, S., PEACOCK, L., GIBSON, W., GULL, K. & KELLY, S. 2012. A modular and optimized single marker system for generating Trypanosoma brucei cell lines expressing T7 RNA polymerase and the tetracycline repressor. *Open Biology,* 2**,** 110037.

PRESLEY, J. F., WARD, T. H., PFEIFER, A. C., SIGGIA, E. D., PHAIR, R. D. & LIPPINCOTT-SCHWARTZ, J. 2002. Dissection of COPI and Arf1 dynamics in vivo and role in Golgi membrane transport. *Nature,* 417**,** 187-93.

PRICE, H. P., GOULDING, D. & SMITH, D. F. 2005a. ARL1 has an essential role in Trypanosoma brucei. *Biochem Soc Trans,* 33**,** 643-5.

PRICE, H. P., GÜTHER, M. L. S., FERGUSON, M. A. J. & SMITH, D. F. 2010a. Myristoyl-CoA:protein N-myristoyltransferase depletion in trypanosomes causes avirulence and endocytic defects. *Molecular and Biochemical Parasitology,* 169**,** 55-58.

PRICE, H. P., HODGKINSON, M. R., WRIGHT, M. H., TATE, E. W., SMITH, B. A., CARRINGTON, M., STARK, M. & SMITH, D. F. 2012. A role for the vesicle-associated tubulin binding protein ARL6 (BBS3) in flagellum extension in Trypanosoma brucei. *Biochim Biophys Acta,* 1823**,** 1178-91.

PRICE, H. P., PANETHYMITAKI, C., GOULDING, D. & SMITH, D. F. 2005b. Functional analysis of TbARL1, an N-myristoylated Golgi protein essential for viability in bloodstream trypanosomes. *J Cell Sci,* 118**,** 831-41.

PRICE, H. P., PELTAN, A., STARK, M. & SMITH, D. F. 2010b. The small GTPase ARL2 is required for cytokinesis in Trypanosoma brucei. *Mol Biochem Parasitol,* 173**,** 123-31.

PRICE, H. P., STARK, M., SMITH, B. & SMITH, D. F. 2007a. TbARF1 influences lysosomal function but not endocytosis in procyclic stage Trypanosoma brucei. *Mol Biochem Parasitol,* 155**,** 123-7.

PRICE, H. P., STARK, M. & SMITH, D. F. 2007b. Trypanosoma brucei ARF1 plays a central role in endocytosis and golgi-lysosome trafficking. *Mol Biol Cell,* 18**,** 864-73.

QIAO, X., CHUANG, B. F., JIN, Y., MURANJAN, M., HUNG, C. H., LEE, P. T. & LEE, M. G. 2006. Sorting signals required for trafficking of the cysteine-rich acidic repetitive transmembrane protein in Trypanosoma brucei. *Eukaryot Cell,* 5**,** 1229-42.

QUINTANA, J. F., PINO, R. C. D., YAMADA, K. & ZHANG, N. 2018. Adaptation and Therapeutic Exploitation of the Plasma Membrane of African Trypanosomes. *Genes,* 9**,** 368.

RAAIJMAKERS, J. H., DENEUBOURG, L., REHMANN, H., DE KONING, J., ZHANG, Z., KRUGMANN, S., ERNEUX, C. & BOS, J. L. 2007. The PI3K effector Arap3 interacts with the PI (3, 4, 5) P3 phosphatase SHIP2 in a SAM domain-dependent manner. *Cellular signalling,* 19**,** 1249-1257.

RAHIMZADEH, M., SADEGHIZADEH, M., NAJAFI, F., ARAB, S. & MOBASHERI, H. 2016. Impact of heat shock step on bacterial transformation efficiency. *Molecular biology research communications,* 5**,** 257-261.

RALSTON, K. S., KABUTUTU, Z. P., MELEHANI, J. H., OBERHOLZER, M. & HILL, K. L. 2009. The Trypanosoma brucei flagellum: moving parasites in new directions. *Annual review of microbiology,* 63**,** 335-362.

RAMEY-BUTLER, K., ULLU, E., KOLEV, N. G. & TSCHUDI, C. 2015. Synchronous expression of individual metacyclic variant surface glycoprotein genes in Trypanosoma brucei. *Molecular and Biochemical Parasitology,* 200**,** 1-4.

RANDAZZO, P. A., ANDRADE, J., MIURA, K., BROWN, M. T., LONG, Y. Q., STAUFFER, S., ROLLER, P. & COOPER, J. A. 2000. The Arf GTPase-activating protein ASAP1 regulates the actin cytoskeleton. *Proc Natl Acad Sci U S A,* 97**,** 4011-6.

RANDAZZO, P. A. & KAHN, R. A. 1994. GTP hydrolysis by ADP-ribosylation factor is dependent on both an ADP-ribosylation factor GTPase-activating protein and acid phospholipids. *J Biol Chem,* 269**,** 10758-63.

RAPER, J., NUSSENZWEIG, V. & TOMLINSON, S. 1996. The main lytic factor of Trypanosoma brucei brucei in normal human serum is not high density lipoprotein. *J Exp Med,* 183**,** 1023-9.

RAPER, J., PORTELA, M. P., LUGLI, E., FREVERT, U. & TOMLINSON, S. 2001. Trypanosome lytic factors: novel mediators of human innate immunity. *Curr Opin Microbiol,* 4**,** 402-8.

RASTOGI, R., VERMA, J. K., KAPOOR, A., LANGSLEY, G. & MUKHOPADHYAY, A. 2016. Rab5 Isoforms Specifically Regulate Different Modes of Endocytosis in Leishmania. *J Biol Chem,* 291**,** 14732-46.

REDMAN, M., KING, A., WATSON, C. & KING, D. 2016. What is CRISPR/Cas9? *Archives of Disease in Childhood - Education & Practice Edition,* 101**,** 213-215.

REDMOND, S., VADIVELU, J. & FIELD, M. C. 2003. RNAit: an automated web-based tool for the selection of RNAi targets in Trypanosoma brucei. *Molecular and Biochemical Parasitology,* 128**,** 115-118.

RICHARDSON, B. C. & FROMME, J. C. 2012. Autoregulation of Sec7 Arf-GEF activity and localization by positive feedback. *Small GTPases,* 3**,** 240-3.

RICHARDSON, B. C., MCDONOLD, C. M. & FROMME, J. C. 2012. The Sec7 Arf-GEF is recruited to the trans-Golgi network by positive feedback. *Dev Cell,* 22**,** 799-810.

RICO, E., JEACOCK, L., KOVÁŘOVÁ, J. & HORN, D. 2018. Inducible high-efficiency CRISPR-Cas9-targeted gene editing and precision base editing in African trypanosomes. *Scientific Reports,* 8**,** 7960.

RIEGER, A. M., HALL, B. E., SCHANG, L. M. & BARREDA, D. R. 2010. Conventional apoptosis assays using propidium iodide generate a significant number of false positives that prevent accurate assessment of cell death. *Journal of Immunological Methods,* 358**,** 81-92.

ROBINSON, C. R. & KANAMARLAPUDI, V. 2017. ADAP2. *Encyclopedia of Signaling Molecules*, 1-6.

ROCK, K. S., TORR, S. J., LUMBALA, C. & KEELING, M. J. 2015. Quantitative evaluation of the strategy to eliminate human African trypanosomiasis in the Democratic Republic of Congo. *Parasites & Vectors,* 8, 532.

RODITI, I., SCHWARZ, H., PEARSON, T. W., BEECROFT, R. P., LIU, M. K., RICHARDSON, J. P., BUHRING, H. J., PLEISS, J., BULOW, R., WILLIAMS, R. O. & *ET AL*. 1989. Procyclin gene expression and loss of the variant surface glycoprotein during differentiation of Trypanosoma brucei. *J Cell Biol,* 108, 737-46.

ROJAS, F. & MATTHEWS, K. R. 2019. Quorum sensing in African trypanosomes. *Curr Opin Immunol,* 52, 124-129.

ROTH, M. G. 1999. Snapshots of ARF1: implications for mechanisms of activation and inactivation. *Cell,* 97, 149-52.

ROTUREAU, B., SUBOTA, I., BUISSON, J. & BASTIN, P. 2012. A new asymmetric division contributes to the continuous production of infective trypanosomes in the tsetse fly. *Development,* 139, 1842-50.

ROY, N. S., YOHE, M. E., RANDAZZO, P. A. & GRUSCHUS, J. M. 2016. Allosteric properties of PH domains in Arf regulatory proteins. *Cell Logist,* 6, e1181700.

SAENZ, J. B., SUN, W. J., CHANG, J. W., LI, J., BURSULAYA, B., GRAY, N. S. & HASLAM, D. B. 2009. Golgicide A reveals essential roles for GBF1 in Golgi assembly and function. *Nat Chem Biol,* 5, 157-65.

SALASSA, B. N. & ROMANO, P. S. 2018. Autophagy: A necessary process during the Trypanosoma cruzi life-cycle. *Virulence*, 1-10.

SANTY, L. C. & CASANOVA, J. E. 2002. GTPase Signaling: Bridging the GAP between ARF and Rho. *Current Biology,* 12, R360-R362.

SAURABH, S., VIDYARTHI, A. S. & PRASAD, D. 2014. RNA interference: concept to reality in crop improvement. *Planta,* 239, 543-564.

SCHEFFZEK, K. & AHMADIAN, M. R. 2005. GTPase activating proteins: structural and functional insights 18 years after discovery. *Cell Mol Life Sci,* 62**,** 3014-38.

SCHEFFZEK, K., AHMADIAN, M. R., KABSCH, W., WIESMULLER, L., LAUTWEIN, A., SCHMITZ, F. & WITTINGHOFER, A. 1997. The Ras-RasGAP complex: structural basis for GTPase activation and its loss in oncogenic Ras mutants. *Science,* 277**,** 333-8.

SCHLACHT, A., MOWBREY, K., ELIAS, M., KAHN, R. A. & DACKS, J. B. 2013. Ancient Complexity, Opisthokont Plasticity, and Discovery of the 11th Subfamily of Arf GAP Proteins. *Traffic,* 14**,** 636-649.

SCHMIDT, A. & HALL, A. 2002. Guanine nucleotide exchange factors for Rho GTPases: turning on the switch. *Genes Dev,* 16**,** 1587-609.

SCHMIDT, R. S., MACÊDO, J. P., STEINMANN, M. E., SALGADO, A. G., BÜTIKOFER, P., SIGEL, E., RENTSCH, D. & MÄSER, P. 2018. Transporters of Trypanosoma brucei—phylogeny, physiology, pharmacology. *The FEBS Journal,* 285**,** 1012-1023.

SCHORB, M., GAECHTER, L., AVINOAM, O., SIECKMANN, F., CLARKE, M., BEBEACUA, C., BYKOV, Y. S., SONNEN, A. F. P., LIHL, R. & BRIGGS, J. A. G. 2017. New hardware and workflows for semi-automated correlative cryo-fluorescence and cryo-electron microscopy/tomography. *Journal of Structural Biology,* 197**,** 83-93.

SCHULTZ, J., BORK, P., PONTING, C. P. & HOFMANN, K. 1997. SAM as a protein interaction domain involved in developmental regulation. *Protein Sci,* 6**,** 249-253.

SCHULTZ, J., MILPETZ, F., BORK, P. & PONTING, C. P. 1998. SMART, a simple modular architecture research tool: identification of signaling domains. *Proc Natl Acad Sci U S A,* 95**,** 5857-64.

SEGELETZ, S., DANGLOT, L., GALLI, T. & HOFLACK, B. 2018. ARAP1 Bridges Actin Dynamics and AP-3-Dependent Membrane Traffic in Bone-Digesting Osteoclasts. *iScience,* 6**,** 199-211.

SERBZHINSKIY, D. A., CLIFTON, M. C., SANKARAN, B., STAKER, B. L., EDWARDS, T. E. & MYLER, P. J. 2015. Structure of an ADP-ribosylation factor, ARF1, from Entamoeba histolytica bound to Mg(2+)-GDP. *Acta Crystallogr F Struct Biol Commun,* 71**,** 594-9.

SHARER, J. D. & KAHN, R. A. 1999. The ARF-like 2 (ARL2)-binding protein, BART. Purification, cloning, and initial characterization. *J Biol Chem,* 274**,** 27553-61.

SHARER, J. D., SHERN, J. F., VAN VALKENBURGH, H., WALLACE, D. C. & KAHN, R. A. 2002. ARL2 and BART enter mitochondria and bind the adenine nucleotide transporter. *Mol Biol Cell,* 13**,** 71-83.

SHARMA, M., MARWAHA, R. R. & DWIVEDI, D. 2019. Emerging Roles of Arf-Like GTP-Binding Proteins: From Membrane Trafficking to Cytoskeleton Dynamics and Beyond. *Proceedings of the Indian National Science Academy,* 85**,** 189-212.

SHARMA, R., GLUENZ, E., PEACOCK, L., GIBSON, W., GULL, K. & CARRINGTON, M. 2009. The heart of darkness: growth and form of Trypanosoma brucei in the tsetse fly. *Trends in Parasitology,* 25**,** 517-524.

SHI, A., LIU, O., KOENIG, S., BANERJEE, R., CHEN, C. C.-H., EIMER, S. & GRANT, B. D. 2012. RAB-10-GTPase–mediated regulation of endosomal phosphatidylinositol-4, 5-bisphosphate. *Proc Natl Acad Sci U S A,* 109**,** E2306-E2315.

SHI, H., CHAMOND, N., DJIKENG, A., TSCHUDI, C. & ULLU, E. 2009. RNA interference in Trypanosoma brucei: role of the n-terminal RGG domain and the polyribosome association of argonaute. *J Biol Chem,* 284**,** 36511-20.

SHI, H., DJIKENG, A., TSCHUDI, C. & ULLU, E. 2004. Argonaute protein in the early divergent eukaryote Trypanosoma brucei: control of small interfering RNA accumulation and retroposon transcript abundance. *Molecular and cellular biology,* 24**,** 420-427.

SHI, H., TSCHUDI, C. & ULLU, E. 2006. An unusual Dicer-like1 protein fuels the RNA interference pathway in Trypanosoma brucei. *RNA,* 12**,** 2063-2072.

SHIBA, Y., LUO, R., HINSHAW, J. E., SZUL, T., HAYASHI, R., SZTUL, E., NAGASHIMA, K., BAXA, U. & RANDAZZO, P. A. 2011. ArfGAP1 promotes COPI vesicle formation by facilitating coatomer polymerization. *Cell Logist,* 1**,** 139-154.

SHIMOGAWA, M. M., SAADA, E. A., VASHISHT, A. A., BARSHOP, W. D., WOHLSCHLEGEL, J. A. & HILL, K. L. 2015. Cell Surface Proteomics Provides Insight into Stage-Specific Remodeling of the Host-Parasite Interface in Trypanosoma brucei. *Molecular & Cellular Proteomics,* 14**,** 1977-1988.

SHINOTSUKA, C., WAGURI, S., WAKASUGI, M., UCHIYAMA, Y. & NAKAYAMA, K. 2002a. Dominant-negative mutant of BIG2, an ARF–guanine nucleotide exchange factor, specifically affects membrane trafficking from the trans-Golgi network through inhibiting membrane association of AP-1 and GGA coat proteins. *Biochemical and biophysical research communications,* 294**,** 254-260.

SHINOTSUKA, C., YOSHIDA, Y., KAWAMOTO, K., TAKATSU, H. & NAKAYAMA, K. 2002b. Overexpression of an ADP-ribosylation factor-guanine nucleotide exchange factor, BIG2, uncouples brefeldin A-induced adaptor protein-1 coat dissociation and membrane tubulation. *Journal of Biological Chemistry,* 277**,** 9468-9473.

SHOUBRIDGE, C., TARPEY, P. S., ABIDI, F., RAMSDEN, S. L., RUJIRABANJERD, S., MURPHY, J. A., BOYLE, J., SHAW, M., GARDNER, A., PROOS, A., PUUSEPP, H., RAYMOND, F. L., SCHWARTZ, C. E., STEVENSON, R. E., TURNER, G., FIELD, M., WALIKONIS, R. S., HARVEY, R. J., HACKETT, A., FUTREAL, P. A., STRATTON, M. R. & GECZ, J. 2010. Mutations in the guanine nucleotide exchange factor gene IQSEC2 cause nonsyndromic intellectual disability. *Nat Genet,* 42**,** 486-8.

SIEGEL, T. N., HEKSTRA, D. R., WANG, X., DEWELL, S. & CROSS, G. A. 2010. Genome-wide analysis of mRNA abundance in two life-cycle stages of Trypanosoma brucei and identification of splicing and polyadenylation sites. *Nucleic Acids Res,* 38**,** 4946-57.

SILVESTER, E., IVENS, A. & MATTHEWS, K. R. 2018. A gene expression comparison of Trypanosoma brucei and Trypanosoma congolense in the bloodstream of the mammalian host reveals species-specific adaptations to density-dependent development. *PLoS Negl Trop Dis,* 12**,** e0006863-e0006863.

SILVESTER, E., MCWILLIAM, K. R. & MATTHEWS, K. R. 2017. The Cytological Events and Molecular Control of Life Cycle Development of Trypanosoma brucei in the Mammalian Bloodstream. *Pathogens,* 6**,** 29.

SIMARRO, P. P., DIARRA, A., RUIZ POSTIGO, J. A., FRANCO, J. R. & JANNIN, J. G. 2011. The human African trypanosomiasis control and surveillance programme of the World Health Organization 2000-2009: the way forward. *PLoS Negl Trop Dis,* 5**,** e1007.

SIMARRO, P. P., JANNIN, J. & CATTAND, P. 2008. Eliminating human African trypanosomiasis: where do we stand and what comes next? *PLoS Med,* 5**,** e55.

SIMPSON, A. G., GILL, E. E., CALLAHAN, H. A., LITAKER, R. W. & ROGER, A. J. 2004. Early evolution within kinetoplastids (euglenozoa), and the late emergence of trypanosomatids. *Protist,* 155**,** 407-22.

SIMPSON, A. G., STEVENS, J. R. & LUKES, J. 2006. The evolution and diversity of kinetoplastid flagellates. *Trends Parasitol,* 22**,** 168-74.

SINGH, A., MINIA, I., DROLL, D., FADDA, A., CLAYTON, C. & ERBEN, E. 2014. Trypanosome MKT1 and the RNA-binding protein ZC3H11: interactions and potential roles in post-transcriptional regulatory networks. *Nucleic Acids Res,* 42**,** 4652-4668.

SMITH, A. B., ESKO, J. D. & HAJDUK, S. L. 1995. Killing of trypanosomes by the human haptoglobin-related protein. *Science,* 268**,** 284-6.

SMITH, D. F., PEACOCK, C. S. & CRUZ, A. K. 2007. Comparative genomics: from genotype to disease phenotype in the leishmaniases. *Int J Parasitol,* 37**,** 1173-86.

SMITH, D. H., PEPIN, J. & STICH, A. H. 1998. Human African trypanosomiasis: an emerging public health crisis. *Br Med Bull,* 54**,** 341-55.

SMYTH, M. S. & MARTIN, J. H. 2000. x ray crystallography. *Molecular Pathology,* 53**,** 8-14.

SOMEYA, A., SATA, M., TAKEDA, K., PACHECO-RODRIGUEZ, G., FERRANS, V. J., MOSS, J. & VAUGHAN, M. 2001. ARF-GEP(100), a guanine nucleotide-exchange protein for ADP-ribosylation factor 6. *Proc Natl Acad Sci U S A,* 98**,** 2413-8.

SONG, J., BAKER, N., ROTHERT, M., HENKE, B., JEACOCK, L., HORN, D. & BEITZ, E. 2016. Pentamidine Is Not a Permeant but a Nanomolar Inhibitor of the Trypanosoma brucei Aquaglyceroporin-2. *PLoS Pathog,* 12**,** e1005436.

SOTO, A. M. & DRAPER, D. 2012. White gels: an easy way to preserve methylene blue stained gels. *Anal Biochem,* 421**,** 345-6.

SPINKS, D., SMITH, V., THOMPSON, S., ROBINSON, D. A., LUKSCH, T., SMITH, A., TORRIE, L. S., MCELROY, S., STOJANOVSKI, L., NORVAL, S., COLLIE, I. T., HALLYBURTON, I., RAO, B., BRAND, S., BRENK, R., FREARSON, J. A., READ, K. D., WYATT, P. G. & GILBERT, I. H. 2015. Development of Small-Molecule Trypanosoma brucei N-Myristoyltransferase Inhibitors: Discovery and Optimisation of a Novel Binding Mode. *ChemMedChem,* 10**,** 1821-1836.

STAMNES, M. A. & ROTHMAN, J. E. 1993. The binding of AP-1 clathrin adaptor particles to Golgi membranes requires ADP-ribosylation factor, a small GTP-binding protein. *Cell,* 73**,** 999-1005.

STANNE, T. M. & RUDENKO, G. 2010. Active VSG expression sites in Trypanosoma brucei are depleted of nucleosomes. *Eukaryot Cell,* 9**,** 136-47.

STEKETEE, P. C., VINCENT, I. M., ACHCAR, F., GIORDANI, F., KIM, D.-H., CREEK, D. J., FREUND, Y., JACOBS, R., RATTIGAN, K., HORN, D., FIELD, M. C., MACLEOD, A. & BARRETT, M. P. 2018. Benzoxaborole treatment perturbs S-adenosyl-L-methionine metabolism in Trypanosoma brucei. *PLoS Negl Trop Dis,* 12**,** e0006450-e0006450.

STEPHENS, N. A. & HAJDUK, S. L. 2011. Endosomal localization of the serum resistance-associated protein in African trypanosomes confers human infectivity. *Eukaryot Cell,* 10**,** 1023-33.

STIJLEMANS, B., CALJON, G., VAN DEN ABBEELE, J., VAN GINDERACHTER, J. A., MAGEZ, S. & DE TREZ, C. 2016. Immune Evasion Strategies of Trypanosoma brucei within the Mammalian Host: Progression to Pathogenicity. *Frontiers in Immunology,* 7**,** 233-233.

STOCKMAR, I., FEDDERSEN, H., CRAMER, K., GRUBER, S., JUNG, K., BRAMKAMP, M. & SHIN, J. Y. 2018. Optimization of sample preparation and green color imaging using the mNeonGreen

fluorescent protein in bacterial cells for photoactivated localization microscopy. *Scientific Reports,* 8**,** 10137.

STRICKER, R. & REISER, G. 2014. Functions of the neuron-specific protein ADAP1 (centaurin-α1) in neuronal differentiation and neurodegenerative diseases, with an overview of structural and biochemical properties of ADAP1. *Biological chemistry,* 395**,** 1321-1340.

STUART, K., BRUN, R., CROFT, S., FAIRLAMB, A., GÜRTLER, R. E., MCKERROW, J., REED, S. & TARLETON, R. 2008. Kinetoplastids: related protozoan pathogens, different diseases. *Journal of Clinical Investigation,* 118**,** 1301-1310.

SUGAR, I. P. & NEUMANN, E. 1984. Stochastic model for electric field-induced membrane pores. Electroporation. *Biophys Chem,* 19**,** 211-25.

SVEC, D., TICHOPAD, A., NOVOSADOVA, V., PFAFFL, M. W. & KUBISTA, M. 2015. How good is a PCR efficiency estimate: Recommendations for precise and robust qPCR efficiency assessments. *Biomolecular Detection and Quantification,* 3**,** 9-16.

SYKES, M. L., BAELL, J. B., KAISER, M., CHATELAIN, E., MOAWAD, S. R., GANAME, D., IOSET, J. R. & AVERY, V. M. 2012. Identification of compounds with anti-proliferative activity against Trypanosoma brucei brucei strain 427 by a whole cell viability based HTS campaign. *PLoS Negl Trop Dis,* 6**,** e1896.

SYMULA, R. E., BEADELL, J. S., SISTROM, M., AGBEBAKUN, K., BALMER, O., GIBSON, W., AKSOY, S. & CACCONE, A. 2012. Trypanosoma brucei gambiense group 1 is distinguished by a unique amino acid substitution in the HpHb receptor implicated in human serum resistance. *PLoS Negl Trop Dis,* 6**,** e1728.

SZEMPRUCH, A. J., SYKES, S. E., KIEFT, R., DENNISON, L., BECKER, A. C., GARTRELL, A., MARTIN, W. J., NAKAYASU, E. S., ALMEIDA, I. C., HAJDUK, S. L. & HARRINGTON, J. M. 2016. Extracellular Vesicles from Trypanosoma brucei Mediate Virulence Factor Transfer and Cause Host Anemia. *Cell,* 164**,** 246-257.

SZTUL, E., CHEN, P.-W., CASANOVA, J. E., CHERFILS, J., DACKS, J. B., LAMBRIGHT, D. G., LEE, F.-J. S., RANDAZZO, P. A., SANTY, L. C. & SCHÜRMANN, A. 2019. ARF GTPases and their GEFs and GAPs: concepts and challenges. *Molecular biology of the cell,* 30**,** 1249-1271.

SZUL, T., GRABSKI, R., LYONS, S., MOROHASHI, Y., SHESTOPAL, S., LOWE, M. & SZTUL, E. 2007. Dissecting the role of the ARF guanine nucleotide exchange factor GBF1 in Golgi biogenesis and protein trafficking. *Journal of Cell Science,* 120**,** 3929-3940.

TAKEUCHI, M., UEDA, T., YAHARA, N. & NAKANO, A. 2002. Arf1 GTPase plays roles in the protein traffic between the endoplasmic reticulum and the Golgi apparatus in tobacco and Arabidopsis cultured cells. *Plant J,* 31**,** 499-515.

TAMKUN, J. W., KAHN, R. A., KISSINGER, M., BRIZUELA, B. J., RULKA, C., SCOTT, M. P. & KENNISON, J. A. 1991. The arflike gene encodes an essential GTP-binding protein in Drosophila. *Proc Natl Acad Sci U S A,* 88**,** 3120-4.

TANABE, K., TORII, T., NATSUME, W., BRAESCH-ANDERSEN, S., WATANABE, T. & SATAKE, M. 2005. A novel GTPase-activating protein for ARF6 directly interacts with clathrin and regulates clathrin-dependent endocytosis. *Mol Biol Cell,* 16**,** 1617-28.

TETLEY, L., TURNER, C. M., BARRY, J. D., CROWE, J. S. & VICKERMAN, K. 1987. Onset of expression of the variant surface glycoproteins of Trypanosoma brucei in the tsetse fly studied using immunoelectron microscopy. *J Cell Sci,* 87 (Pt 2)**,** 363-72.

TETLEY, L. & VICKERMAN, K. 1985. Differentiation in Trypanosoma brucei: host-parasite cell junctions and their persistence during acquisition of the variable antigen coat. *J Cell Sci,* 74**,** 1-19.

THOMAS, J. A., BAKER, N., HUTCHINSON, S., DOMINICUS, C., TRENAMAN, A., GLOVER, L., ALSFORD, S. & HORN, D. 2018. Insights into antitrypanosomal drug mode-of-action from cytology-based profiling. *PLoS Negl Trop Dis,* 12**,** e0006980.

THORNTON, B. & BASU, C. 2011. Real-time PCR (qPCR) primer design using free online software. *Biochem Mol Biol Educ,* 39**,** 145-54.

THUL, P. J., ÅKESSON, L., WIKING, M., MAHDESSIAN, D., GELADAKI, A., BLAL, H. A., ALM, T., ASPLUND, A., BJÖRK, L. & BRECKELS, L. M. 2017. A subcellular map of the human proteome. *Science,* 356**,** eaal3321.

TIENGWE, C., MURATORE, K. A. & BANGS, J. D. 2016. Surface proteins, ERAD and antigenic variation in Trypanosoma brucei. *Cellular Microbiology,* 18**,** 1673-1688.

TORREELE, E., TRUNZ, B. B., TWEATS, D., KAISER, M., BRUN, R., MAZUE, G., BRAY, M. A. & PECOUL, B. 2010. Fexinidazole–a new oral nitroimidazole drug candidate entering clinical development for the treatment of sleeping sickness. *PLoS Negl Trop Dis,* 4**,** e923.

TSEGAYE, B., DAGNACHEW, S. & TEREFE, G. 2015. Review on drug resistant animal trypanosomes in africa and overseas. *African J Basic Appl Sci,* 7**,** 73-83.

TU, X. & WANG, C. C. 2005. Pairwise knockdowns of cdc2-related kinases (CRKs) in Trypanosoma brucei identified the CRKs for G1/S and G2/M transitions and demonstrated distinctive cytokinetic regulations between two developmental stages of the organism. *Eukaryotic Cell,* 4**,** 755-764.

UHLEN, M., OKSVOLD, P., FAGERBERG, L., LUNDBERG, E., JONASSON, K., FORSBERG, M., ZWAHLEN, M., KAMPF, C., WESTER, K. & HOBER, S. 2010. Towards a knowledge-based human protein atlas. *Nature Biotechnology,* 28**,** 1248.

UMAER, K., BUSH, P. J. & BANGS, J. D. 2018. Rab11 mediates selective recycling and endocytic trafficking in Trypanosoma brucei. *Traffic,* 19**,** 406-420.

UMEAKUANA, P. U., GIBSON, W., EZEOKONKWO, R. C. & ANENE, B. M. 2019. Identification of Trypanosoma brucei gambiense in naturally infected dogs in Nigeria. *Parasites & Vectors,* 12**,** 420.

URWYLER, S., STUDER, E., RENGGLI, C. K. & RODITI, I. 2007. A family of stage-specific alanine-rich proteins on the surface of epimastigote forms of Trypanosoma brucei. *Mol Microbiol,* 63**,** 218-28.

UZUREAU, P., UZUREAU, S., LECORDIER, L., FONTAINE, F., TEBABI, P., HOMBLE, F., GRELARD, A., ZHENDRE, V., NOLAN, D. P., LINS, L., CROWET, J. M., PAYS, A., FELU, C., POELVOORDE, P.,

VANHOLLEBEKE, B., MOESTRUP, S. K., LYNGSO, J., PEDERSEN, J. S., MOTTRAM, J. C., DUFOURC, E. J., PEREZ-MORGA, D. & PAYS, E. 2013. Mechanism of Trypanosoma brucei gambiense resistance to human serum. *Nature,* 501**,** 430-4.

VAN REET, N., PYANA, P., ROGÉ, S., CLAES, F. & BÜSCHER, P. 2013. Luminescent multiplex viability assay for Trypanosoma brucei gambiense. *Parasites & Vectors,* 6**,** 207.

VAN VOORHIS, W. C., ADAMS, J. H., ADELFIO, R., AHYONG, V., AKABAS, M. H., ALANO, P., ALDAY, A., ALEMÁN RESTO, Y., ALSIBAEE, A., ALZUALDE, A., ANDREWS, K. T., AVERY, S. V., AVERY, V. M., AYONG, L., BAKER, M., BAKER, S., BEN MAMOUN, C., BHATIA, S., BICKLE, Q., BOUNAADJA, L., BOWLING, T., BOSCH, J., BOUCHER, L. E., BOYOM, F. F., BREA, J., BRENNAN, M., BURTON, A., CAFFREY, C. R., CAMARDA, G., CARRASQUILLA, M., CARTER, D., BELEN CASSERA, M., CHIH-CHIEN CHENG, K., CHINDAUDOMSATE, W., CHUBB, A., COLON, B. L., COLÓN-LÓPEZ, D. D., CORBETT, Y., CROWTHER, G. J., COWAN, N., D'ALESSANDRO, S., LE DANG, N., DELVES, M., DERISI, J. L., DU, A. Y., DUFFY, S., ABD EL-SALAM EL-SAYED, S., FERDIG, M. T., FERNÁNDEZ ROBLEDO, J. A., FIDOCK, D. A., FLORENT, I., FOKOU, P. V. T., GALSTIAN, A., GAMO, F. J., GOKOOL, S., GOLD, B., GOLUB, T., GOLDGOF, G. M., GUHA, R., GUIGUEMDE, W. A., GURAL, N., GUY, R. K., HANSEN, M. A. E., HANSON, K. K., HEMPHILL, A., HOOFT VAN HUIJSDUIJNEN, R., HORII, T., HORROCKS, P., HUGHES, T. B., HUSTON, C., IGARASHI, I., INGRAM-SIEBER, K., ITOE, M. A., JADHAV, A., NARANUNTARAT JENSEN, A., JENSEN, L. T., JIANG, R. H. Y., KAISER, A., KEISER, J., KETAS, T., KICKA, S., KIM, S., KIRK, K., KUMAR, V. P., KYLE, D. E., LAFUENTE, M. J., LANDFEAR, S., LEE, N., LEE, S., LEHANE, A. M., LI, F., LITTLE, D., LIU, L., LLINÁS, M., LOZA, M. I., LUBAR, A., LUCANTONI, L., LUCET, I., MAES, L., MANCAMA, D., *et al*. 2016. Open Source Drug Discovery with the Malaria Box Compound Collection for Neglected Diseases and Beyond. *PLoS Pathog,* 12**,** e1005763.

VANHAMME, L., LECORDIER, L. & PAYS, E. 2001. Control and function of the bloodstream variant surface glycoprotein expression sites in Trypanosoma brucei. *Int J Parasitol,* 31**,** 523-31.

VANHAMME, L. & PAYS, E. 2004. The trypanosome lytic factor of human serum and the molecular basis of sleeping sickness. *Int J Parasitol,* 34**,** 887-98.

VANHOLLEBEKE, B. & PAYS, E. 2010. The trypanolytic factor of human serum: many ways to enter the parasite, a single way to kill. *Molecular Microbiology,* 76**,** 806-814.

VASQUEZ, J.-J., WEDEL, C., COSENTINO, R. O. & SIEGEL, T. N. 2018. Exploiting CRISPR-Cas9 technology to investigate individual histone modifications. *Nucleic Acids Res,* 46**,** e106-e106.

VASSELLA, E., OBERLE, M., URWYLER, S., RENGGLI, C. K., STUDER, E., HEMPHILL, A., FRAGOSO, C., BÜTIKOFER, P., BRUN, R. & RODITI, I. 2009. Major Surface Glycoproteins of Insect Forms of Trypanosoma brucei Are Not Essential for Cyclical Transmission by Tsetse. *PLoS One,* 4**,** e4493.

VASSELLA, E., REUNER, B., YUTZY, B. & BOSHART, M. 1997. Differentiation of African trypanosomes is controlled by a density sensing mechanism which signals cell cycle arrest via the cAMP pathway. *J Cell Sci,* 110 (Pt 21)**,** 2661-71.

VEALE, C. G. L. & HOPPE, H. C. 2018. Screening of the Pathogen Box reveals new starting points for anti-trypanosomal drug discovery. *MedChemComm,* 9**,** 2037-2044.

VETTER, I. R. & WITTINGHOFER, A. 2001. The guanine nucleotide-binding switch in three dimensions. *Science,* 294**,** 1299-304.

VIAUD, J., ZEGHOUF, M., BARELLI, H., ZEEH, J.-C., PADILLA, A., GUIBERT, B., CHARDIN, P., ROYER, C. A., CHERFILS, J. & CHAVANIEU, A. 2007. Structure-based discovery of an inhibitor of Arf activation by Sec7 domains through targeting of protein-protein complexes. *Proc Natl Acad Sci U S A,* 104**,** 10370-10375.

VICKERMAN, K. 1985. Developmental cycles and biology of pathogenic trypanosomes. *Br Med Bull,* 41**,** 105-14.

WANG, D.-S., SHAW, R., WINKELMANN, J. C. & SHAW, G. 1994. Binding of PH domains of β-adrenergic-receptor kinase and β-spectrin to WD40/β-transducin repeat containing regions of the β-subunit of trimeric G-proteins. *Biochemical and biophysical research communications,* 203**,** 29-35.

WANG, X., INAOKA, D. K., SHIBA, T., BALOGUN, E. O., ALLMANN, S., WATANABE, Y. I., BOSHART, M., KITA, K. & HARADA, S. 2017. Expression, purification, and crystallization of type 1 isocitrate dehydrogenase from Trypanosoma brucei brucei. *Protein Expr Purif,* 138**,** 56-62.

WEBB, D. J., MAYHEW, M. W., KOVALENKO, M., SCHROEDER, M. J., JEFFERY, E. D., WHITMORE, L., SHABANOWITZ, J., HUNT, D. F. & HORWITZ, A. F. 2006. Identification of phosphorylation sites in GIT1. *Journal of Cell Science,* 119**,** 2847-2850.

WIEDEMAR, N., GRAF, F. E., ZWYER, M., NDOMBA, E., KUNZ RENGGLI, C., CAL, M., SCHMIDT, R. S., WENZLER, T. & MÄSER, P. 2018. Beyond immune escape: a variant surface glycoprotein causes suramin resistance in Trypanosoma brucei. *Molecular Microbiology,* 107**,** 57-67.

WIEDEMAR, N., ZWYER, M., ZOLTNER, M., CAL, M., FIELD, M. C. & MÄSER, P. 2019. Expression of a specific variant surface glycoprotein has a major impact on suramin sensitivity and endocytosis in Trypanosoma brucei. *FASEB BioAdvances,* 0.

WIENS, C. J., TONG, Y., ESMAIL, M. A., OH, E., GERDES, J. M., WANG, J., TEMPEL, W., RATTNER, J. B., KATSANIS, N. & PARK, H.-W. 2010. Bardet-Biedl syndrome-associated small GTPase ARL6 (BBS3) functions at or near the ciliary gate and modulates Wnt signaling. *Journal of Biological Chemistry,* 285**,** 16218-16230.

WINGFIELD, JENNA L., LECHTRECK, K.-F. & LORENTZEN, E. 2018. Trafficking of ciliary membrane proteins by the intraflagellar transport/BBSome machinery. *Essays In Biochemistry***,** EBC20180030.

WIRTZ, E., LEAL, S., OCHATT, C. & CROSS, G. A. 1999. A tightly regulated inducible expression system for conditional gene knock-outs and dominant-negative genetics in Trypanosoma brucei. *Mol Biochem Parasitol,* 99**,** 89-101.

WYLLIE, S., FOTH, B. J., KELNER, A., SOKOLOVA, A. Y., BERRIMAN, M. & FAIRLAMB, A. H. 2015. Nitroheterocyclic drug resistance mechanisms in Trypanosoma brucei. *Journal of Antimicrobial Chemotherapy,* 71**,** 625-634.

XIE, X., TANG, S.-C., CAI, Y., PI, W., DENG, L., WU, G., CHAVANIEU, A. & TENG, Y. 2016. Suppression of breast cancer metastasis through the inactivation of ADP-ribosylation factor 1. *Oncotarget,* 7**,** 58111.

XONG, H. V., VANHAMME, L., CHAMEKH, M., CHIMFWEMBE, C. E., VAN DEN ABBEELE, J., PAYS, A., VAN MEIRVENNE, N., HAMERS, R., DE BAETSELIER, P. & PAYS, E. 1998. A VSG expression site-associated gene confers resistance to human serum in Trypanosoma rhodesiense. *Cell,* 95**,** 839-46.

XU, J. & SCHERES, B. 2005. Dissection of Arabidopsis ADP-RIBOSYLATION FACTOR 1 function in epidermal cell polarity. *Plant Cell,* 17**,** 525-36.

XU, M., MCCANNA, D. J. & SIVAK, J. G. 2015. Use of the viability reagent PrestoBlue in comparison with alamarBlue and MTT to assess the viability of human corneal epithelial cells. *Journal of Pharmacological and Toxicological Methods,* 71**,** 1-7.

YAMAJI, R., ADAMIK, R., TAKEDA, K., TOGAWA, A., PACHECO-RODRIGUEZ, G., FERRANS, V. J., MOSS, J. & VAUGHAN, M. 2000. Identification and localization of two brefeldin A-inhibited guanine nucleotide-exchange proteins for ADP-ribosylation factors in a macromolecular complex. *Proc Natl Acad Sci U S A,* 97**,** 2567-72.

YOO, J. H., SHI, D. S., GROSSMANN, A. H., SORENSEN, L. K., TONG, Z., MLEYNEK, T. M., ROGERS, A., ZHU, W., RICHARDS, J. R., WINTER, J. M., ZHU, J., DUNN, C., BAJJI, A., SHENDEROVICH, M., MUELLER, A. L., WOODMAN, S. E., HARBOUR, J. W., THOMAS, K. R., ODELBERG, S. J., OSTANIN, K. & LI, D. Y. 2016. ARF6 Is an Actionable Node that Orchestrates Oncogenic GNAQ Signaling in Uveal Melanoma. *Cancer cell,* 29**,** 889-904.

YORIMITSU, T., SATO, K. & TAKEUCHI, M. 2014. Molecular mechanisms of Sar/Arf GTPases in vesicular trafficking in yeast and plants. *Front Plant Sci,* 5**,** 411.

YU, C.-J. & LEE, F.-J. S. 2017. Multiple activities of Arl1 GTPase in the trans-Golgi network. *Journal of Cell Science,* 130**,** 1691-1699.

YUN, O., PRIOTTO, G., TONG, J., FLEVAUD, L. & CHAPPUIS, F. 2010. NECT is next: implementing the new drug combination therapy for Trypanosoma brucei gambiense sleeping sickness. *PLoS Negl Trop Dis,* 4**,** e720.

ZHANG, Q., CALAFAT, J., JANSSEN, H. & GREENBERG, S. 1999. ARF6 is required for growth factor- and rac-mediated membrane ruffling in macrophages at a stage distal to rac membrane targeting. *Mol Cell Biol,* 19**,** 8158-68.

ZHANG, Q., COX, D., TSENG, C. C., DONALDSON, J. G. & GREENBERG, S. 1998. A requirement for ARF6 in Fcgamma receptor-mediated phagocytosis in macrophages. *J Biol Chem,* 273**,** 19977-81.

ZHANG, X., AN, T., PHAM, K. T. M., LUN, Z.-R. & LI, Z. 2019. Functional Analyses of Cytokinesis Regulators in Bloodstream Stage Trypanosoma brucei Parasites Identify Functions and Regulations Specific to the Life Cycle Stage. *mSphere,* 4**,** e00199-19.

ZHANG, Y., CHEN, X., GUEYDAN, C. & HAN, J. 2018. Plasma membrane changes during programmed cell deaths. *Cell research,* 28**,** 9-21.

ZHAO, X., CLAUDE, A., CHUN, J., SHIELDS, D. J., PRESLEY, J. F. & MELANÇON, P. 2006. GBF1, a cis-Golgi and VTCs-localized ARF-GEF, is implicated in ER-to-Golgi protein traffic. *Journal of Cell Science,* 119**,** 3743-3753.

ZIMMERMANN, H., SUBOTA, I., BATRAM, C., KRAMER, S., JANZEN, C. J., JONES, N. G. & ENGSTLER, M. 2017. A quorum sensing-independent path to stumpy development in Trypanosoma brucei. *PLoS Pathog,* 13**,** e1006324.

ZOLTNER, M., LEUNG, K. F., ALSFORD, S., HORN, D. & FIELD, M. C. 2015. Modulation of the Surface Proteome through Multiple Ubiquitylation Pathways in African Trypanosomes. *PLoS Pathog,* 11**,** e1005236-e1005236.

Appendix 1

List of identified human ARF GAPs and their localisation. Data obtained from NCBI database and The Human Protein Atlas (www.proteinatlas.org).

Accession number	Gene Identified	Aliases	Localisation	Function
Q9NP61	ADP-ribosylation factor GTPase-activating protein 3	ARFGAP3, ARFGAP1	Cytosol and Golgi apparatus	GTPase-activating protein (GAP) for ADP ribosylation factor 1 (ARF1). Hydrolysis of ARF1-bound GTP may lead to dissociation of coatomer from Golgi-derived membranes to allow fusion with target membranes.
Q8N6T3	ADP-ribosylation factor GTPase-activating protein 1	**ARFGAP1,** ARF1GAP	Golgi apparatus, vesicles and nuclear membrane	GTPase-activating protein (GAP) for the ADP ribosylation factor 1 (ARF1). Involved in membrane trafficking and /or vesicle transport. Required for the dissociation of coat proteins from Golgi-derived membranes and vesicles
Q8N6H7	ADP-ribosylation factor GTPase-activating protein 2	ARFGAP2 ZNF289 Nbla10535	Golgi apparatus	GTPase-activating protein (GAP) for ADP ribosylation factor 1 (ARF1). Implicated in coatomer-mediated protein transport between the Golgi complex and the endoplasmic reticulum. Hydrolysis of ARF1-bound GTP may lead to dissociation of coatomer from Golgi-derived

				membranes to allow fusion with target membranes.
O75689	Arf-GAP with dual PH domain-containing protein 1	**ADAP1** CENTA1	Plasma membrane and cytosol	GTPase-activating protein for the ADP ribosylation factor family (Probable). Binds phosphatidylinositol 3,4,5-trisphosphate (PtdInsP3) and inositol 1,3,4,5-tetrakisphosphate (InsP4)
Q9NPF8	Arf-GAP with dual PH domain-containing protein 2	**ADAP2** CENTA2	Data not available	GTPase-activating protein for the ADP ribosylation factor family (Potential). Binds phosphatidylinositol 3,4,5-trisphosphate (PtdInsP3) and inositol 1,3,4,5-tetrakisphosphate (InsP4).
Q8IYB5	Stromal membrane-associated protein 1	SMAP1	Plasma membrane, cytosol and golgi apparatus	GTPase activating protein that acts on ARF6. Plays a role in clathrin-dependent endocytosis. May play a role in erythropoiesis
Q8WU79	Stromal membrane-associated protein 2	**SMAP2** SMAP1L	Data not available	GTPase activating protein that acts on ARF1. Can also activate ARF6 (in vitro). May play a role in clathrin-dependent retrograde transport from early endosomes to the trans-Golgi network.
Q9Y2X7	ARF GTPase-	**GIT1**	Focal adhesion	May serve as a scaffold to bring together molecules to form signaling

	activating protein GIT1		sites and cytosol	modules controlling vesicle trafficking, adhesion and cytoskeletal organization. Increases the speed of cell migration, as well as the size and rate of formation of protrusions, possibly by targeting PAK1 to adhesions and the leading edge of lamellipodia. Sequesters inactive non-tyrosine-phosphorylated paxillin in cytoplasmic complexes. Involved in the regulation of cytokinesis.
Q14161	ARF GTPase-activating protein GIT2	**GIT2,** KIAA0148	Microtubules	GTPase-activating protein for the ADP ribosylation factor family.
Q9ULH1	Arf-GAP with SH3 domain, ANK repeat and PH domain-containing protein 1	**ASAP1,** DDEF1, KIAA1249	Plasma membrane, centrosome and cytosol	Possesses phosphatidylinositol 4,5-bisphosphate-dependent GTPase-activating protein activity for ARF1 (ADP ribosylation factor 1) and ARF5 and a lesser activity towards ARF6. May coordinate membrane trafficking with cell growth or actin cytoskeleton remodeling by binding to both SRC and PIP2. May function as a signal transduction protein involved in the differentiation of fibroblasts into

				adipocytes and possibly other cell types (By similarity). Plays a role in ciliogenesis.
O43150	Arf-GAP with SH3 domain, ANK repeat and PH domain-containing protein 2	**ASAP2,** DDEF2, KIAA0400	Cytosol	Activates the small GTPases ARF1, ARF5 and ARF6. Regulates the formation of post-Golgi vesicles and modulates constitutive secretion. Modulates phagocytosis mediated by Fc gamma receptor and ARF6. Modulates PXN recruitment to focal contacts and cell migration.
Q8TDY4	Arf-GAP with SH3 domain, ANK repeat and PH domain-containing protein 3	**ASAP3,** DDEFL1, UPLC1	Vesicles and nucleoplasm	Promotes cell proliferation.
Q15027	Arf-GAP with coiled-coil, ANK repeat and PH domain-containing protein 1	**ACAP1,** CENTB1, KIAA0050	Golgi apparatus	GTPase-activating protein (GAP) for ADP ribosylation factor 6 (ARF6) required for clathrin-dependent export of proteins from recycling endosomes to trans-Golgi network and cell surface. Required for regulated export of ITGB1 from recycling endosomes to the cell

				surface and ITGB1-dependent cell migration.
Q15057	Arf-GAP with coiled-coil, ANK repeat and PH domain-containing protein 2	**ACAP2,** CENTB2, KIAA0041	Endosomes	GTPase-activating protein (GAP) for ADP ribosylation factor 6 (ARF6).
Q96P50	Arf-GAP with coiled-coil, ANK repeat and PH domain-containing protein 3	**ACAP3,** CENTB5, KIAA1716	Nucleoplasm and Golgi apparatus	GTPase-activating protein for the ADP ribosylation factor family.
Q9UPQ3	Arf-GAP with GTPase, ANK repeat and PH domain-containing protein 1	**AGAP1,** CENTG2, KIAA1099	Data not available	GTPase-activating protein for ARF1 and, to a lesser extent, ARF5. Directly and specifically regulates the adapter protein 3 (AP-3)-dependent trafficking of proteins in the endosomal-lysosomal system.
Q99490	Arf-GAP with GTPase,	**AGAP2,** CENTG1, KIAA0167	Nucleoli, mitochondria and nucleus	GTPase-activating protein (GAP) for ARF1 and ARF5.

	ANK repeat and PH domain-containing protein 2			
Q96P47	Arf-GAP with GTPase, ANK repeat and PH domain-containing protein 3	**AGAP3,** CENTG3	Data not available	GTPase-activating protein for the ADP ribosylation factor family (Potential). GTPase which may be involved in the degradation of expanded polyglutamine proteins through the ubiquitin-proteasome pathway.
Q96P64	Arf-GAP with GTPase, ANK repeat and PH domain-containing protein 4	**AGAP4,** AGAP8, CTGLF1, CTGLF5, MRIP2	Data not available	Putative GTPase-activating protein.
Q5VTM2	Arf-GAP with GTPase, ANK repeat and PH domain-	**AGAP9,** CTGLF6	Data not available	Putative GTPase-activating protein.

	containing protein 9			
Q5VW22	Arf-GAP with GTPase, ANK repeat and PH domain-containing protein 6	**AGAP6,** CTGLF3	Data not available	Putative GTPase-activating protein.
Q8TF27	Arf-GAP with GTPase, ANK repeat and PH domain-containing protein 11	**AGAP11,** KIAA1975	Data not available	Putative GTPase-activating protein.
A6NIR3	Arf-GAP with GTPase, ANK repeat and PH domain-containing protein 5	**AGAP5,** CTGLF2	Data not available	Putative GTPase-activating protein.

Q96P48	Arf-GAP with Rho-GAP domain, ANK repeat and PH domain-containing protein 1	**ARAP1,** CENTD2, KIAA0782	Nucleoplasm, plasma membrane, vesicles and cytosol	Phosphatidylinositol 3,4,5-trisphosphate-dependent GTPase-activating protein that modulates actin cytoskeleton remodeling by regulating ARF and RHO family members. Is activated by phosphatidylinositol 3,4,5-trisphosphate (PtdIns(3,4,5)P3) binding. Can be activated by phosphatidylinositol 3,4-bisphosphate (PtdIns(3,4,5)P2) binding, albeit with lower efficiency. Has a preference for ARF1 and ARF5 (By similarity).
Q8WZ64	Arf-GAP with Rho-GAP domain, ANK repeat and PH domain-containing protein 2	**ARAP2,** CENTD1, KIAA0580	Focal adhesion sites and actin filaments	Phosphatidylinositol 3,4,5-trisphosphate-dependent GTPase-activating protein that modulates actin cytoskeleton remodeling by regulating ARF and RHO family members. Is activated by phosphatidylinositol 3,4,5-trisphosphate (PtdIns(3,4,5)P3) binding. Can be activated by phosphatidylinositol 3,4-bisphosphate (PtdIns(3,4,5)P2) binding, albeit with lower efficiency (By similarity).

Q8WWN8	Arf-GAP with Rho-GAP domain, ANK repeat and PH domain-containing protein 3	**ARAP3,** CENTD3	Data not available	Phosphatidylinositol 3,4,5-trisphosphate-dependent GTPase-activating protein that modulates actin cytoskeleton remodeling by regulating ARF and RHO family members. Is activated by phosphatidylinositol 3,4,5-trisphosphate (PtdIns(3,4,5)P3) binding. Can be activated by phosphatidylinositol 3,4-bisphosphate (PtdIns(3,4,5)P2) binding, albeit with lower efficiency. Acts on ARF6, RAC1, RHOA and CDC42. Plays a role in the internalization of anthrax toxin.

Appendix 2

List of identified human ARF GEFs and their localisation. Data obtained from NCBI database and The Human Protein Atlas (www.proteinatlas.org).

Accession number	**Gene Identified**	**Aliases**	**Localisation**	**Function**
Q15438	Cytohesin-1	**CYTH1**, D17S811E, PSCD1	Nucleus and nucleoli	Promotes guanine-nucleotide exchange on ARF1, ARF5 and ARF6. Plays an important role in membrane trafficking, during junctional remodelling and epithelial polarization, through regulation of ARF6 activity.
Q99418	Cytohesin-2	**CYTH2**, ARNO, PSCD2, PSCD2L	Cytosol, golgi apparatus and plasma membrane	GEF, promotes guanine nucleotide exchange on ARF1, ARF3 and AF6. Reqruits ARF6 to plasma membrane
O43739	Cytohesin-3	**CYTH2**, ARNO3, GRP1, PSCD3	Cytosol and nucleoplasm	Promotes guanine-nucleotide exchange on ARF1 and ARF6. Promotes the activation of ARF factors through replacement of GDP with GTP. Play a role in the epithelial polarization

Q9UIA0	Cytohesin-4	**CYTH4,** CYT4, PSCD4	Data not available	Promotes guanine-nucleotide exchange on ARF1 and ARF5
Q92538	Golgi-specific brefeldin A-resistance guanine nucleotide exchange factor 1	**GBF1**, KIAA0248	Golgi apparatus	Trafficking in the early secretory pathway; GEF activity initiates the coating of nascent vesicles via the localized generation of activated ARFs. Involved in the recruitment of the COPI coat complex to the endoplasmic reticulum exit sites (ERES), and the endoplasmic reticulum-Golgi intermediate (ERGIC). Has GEF activity towards ARF1
Q9Y6D5	Brefeldin A-inhibited guanine nucleotide-exchange protein 2	**ARFGEF2,** ARFGEP2, BIG2	Golgi apparatus	Promotes guanine-nucleotide exchange on ARF1 and ARF3 and to a lower extent on ARF5 and ARF6. Regulation of Golgi vesicular transport. Required for the integrity of the endosomal compartment. Involved in trafficking from the trans-Golgi network (TGN) to endosomes and is required

				for membrane association of the AP-1 complex and GGA1.
Q9Y6D6	Brefeldin A-inhibited guanine nucleotide-exchange protein 1	**ARFGEF1,** ARFGEP1, BIG1	Golgi apparatus, nucleoplasm and cytosol	Promotes guanine-nucleotide exchange on ARF1 and ARF3. Involved in vesicular trafficking. Required for the maintenance of Golgi structure; the function may be independent of its GEF activity. Required for the maturaion of integrin beta-1 in the Golgi. Involved in the establishment and persistence of cell polarity during directed cell movement in wound healing.
A5PKW4	PH and SEC7 domain-containing protein 1	**PSD,** EFA6, EFA6A, KIAA2011, PSD1, TYL	Nucleoplasm, plasma membrane and cytosol	Guanine nucleotide exchange factor for ARF6. Induces cytoskeletal remodeling.
Q8NDX1	PH and SEC7 domain-containing protein 4	**PSD4,** EFA6B, TIC	Data not available	Guanine nucleotide exchange factor for ARF6 and ARL14/ARF7. Through ARL14 activation, controls the movement of MHC class

				II-containing vesicles along the actin cytoskeleton in dendritic cells. Involved in membrane recycling. Interacts with several phosphatidylinositol phosphate species, including phosphatidylinositol 3,4-bisphosphate, phosphatidylinositol 3,5-bisphosphate and phosphatidylinositol 4,5-bisphosphate.
Q9BQI7	PH and SEC7 domain-containing protein 2	**PSD2,** EFA6C	Data not available	
Q9NYI0	PH and SEC7 domain-containing protein 3	**PSD3,** EFA6D, EFA6R, HCA67, KIAA0942	Nucleus and vesicles	Guanine nucleotide exchange factor for ARF6.

Q5JU85	IQ motif and SEC7 domain-containing protein 2	**IQSEC2,** KIAA0522	Vesicles	Is a guanine nucleotide exchange factor for the ARF GTP-binding proteins
Q6DN90	IQ motif and SEC7 domain-containing protein 1	**IQSEC1**, ARFGEP100, BRAG2, KIAA0763	Nucleoli and vesicles	Guanine nucleotide exchange factor for ARF1 and ARF6. Guanine nucleotide exchange factor activity is enhanced by lipid binding. Accelerates GTP binding by ARFs of all three classes. Guanine nucleotide exchange protein for ARF6, mediating internalisation of beta-1 integrin.
Q9UPP2	IQ motif and SEC7 domain-containing protein 3	I**QSEC3**, KIAA1110	No data available	Acts as a guanine nucleotide exchange factor (GEF) for ARF1.

Appendix 3

Amino acid sequence alignment for TbGAP1 (OG5127251) in other kinetoplastids

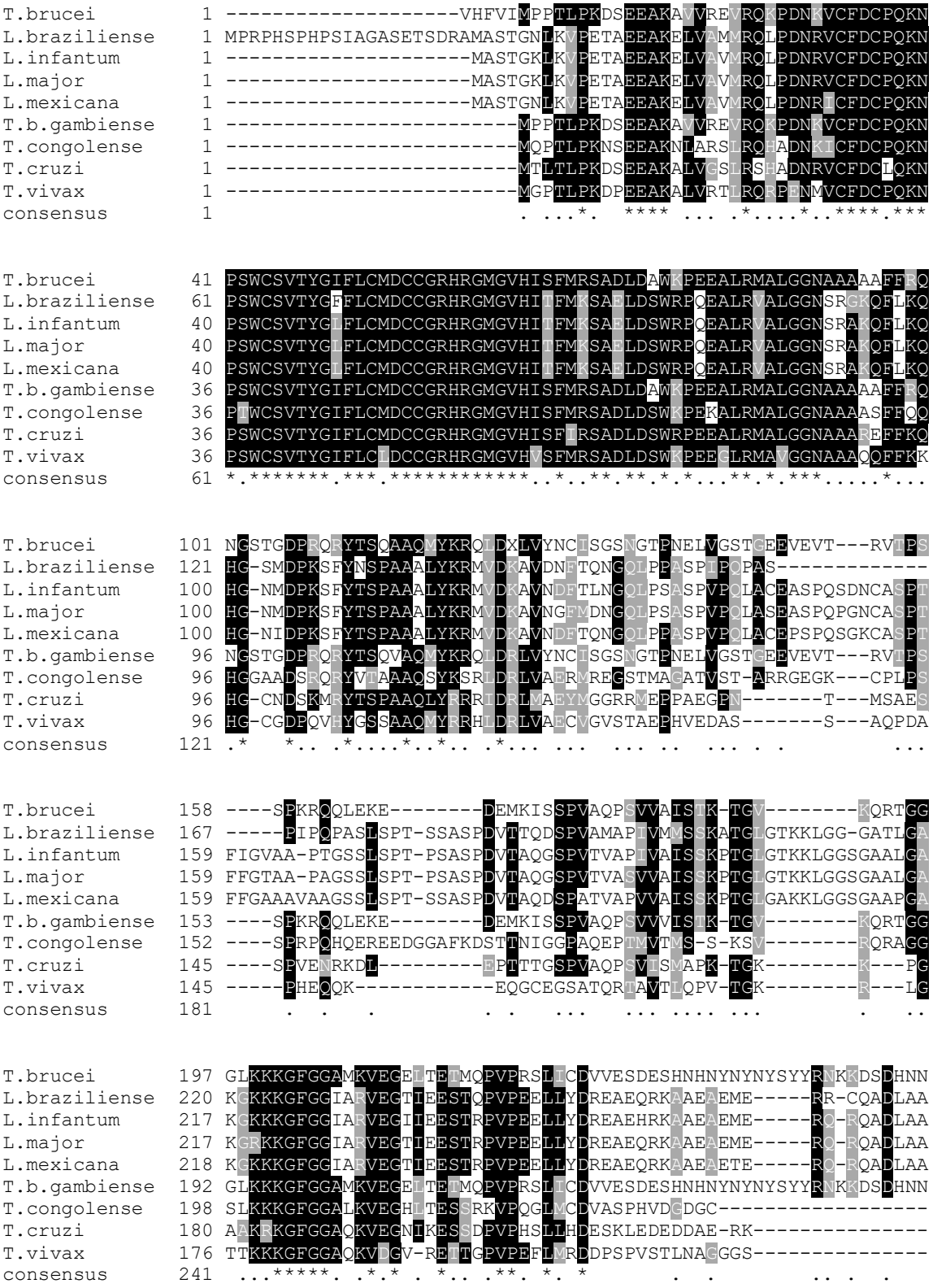

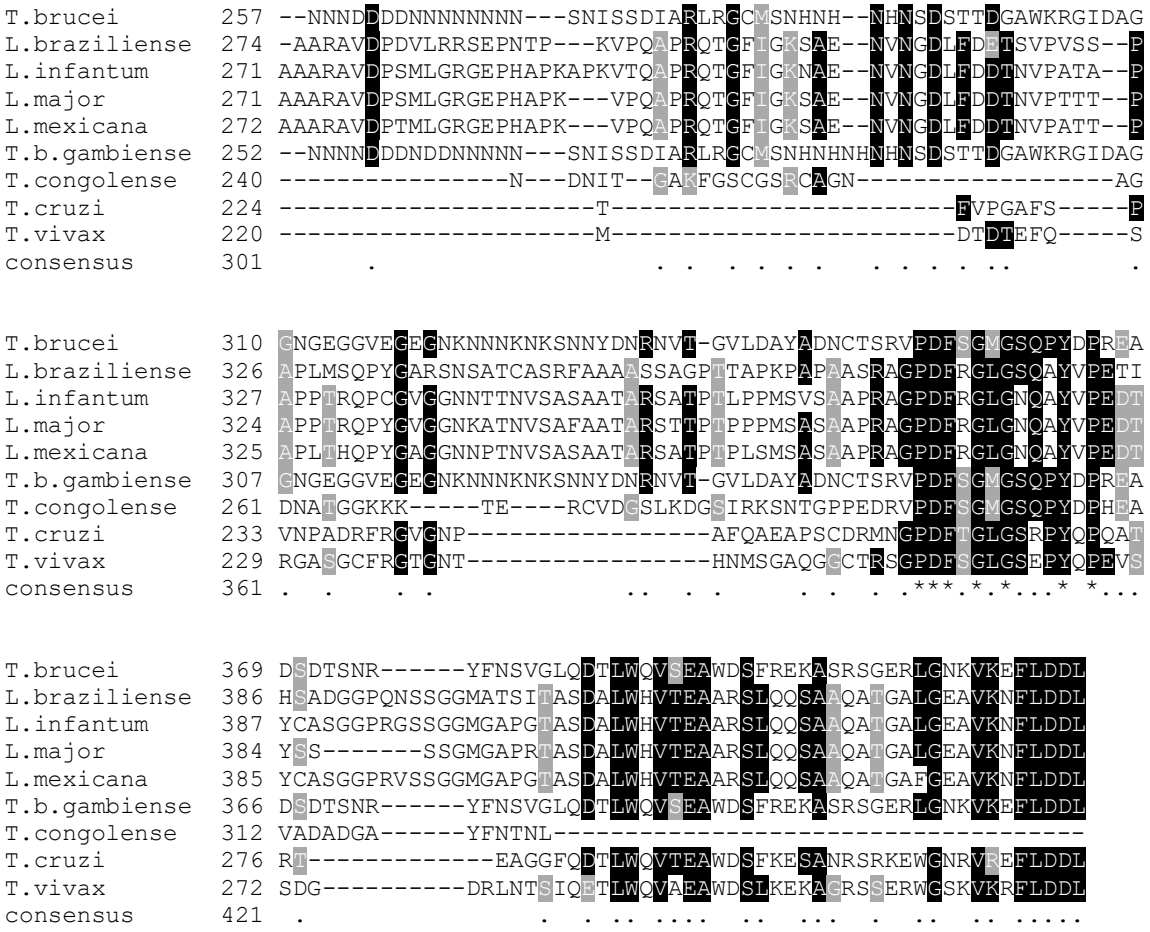
T.brucei 257 --NNNDDDDNNNNNNNNN---SNISSDIARLRGCMSNHNH--NHNSDSTTDGAWKRGIDAG
L.braziliense 274 -AARAVDPDVLRRSEPNTP---KVPQAPRQTGFIGKSAE--NVNGDLFDETSVPVSS--P
L.infantum 271 AAARAVDPSMLGRGEPHAPKAPKVTQAPRQTGFIGKNAE--NVNGDLFDDTNVPATA--P
L.major 271 AAARAVDPSMLGRGEPHAPK---VPQAPRQTGFIGKSAE--NVNGDLFDDTNVPTTT--P
L.mexicana 272 AAARAVDPTMLGRGEPHAPK---VPQAPRQTGFIGKSAE--NVNGDLFDDTNVPATT--P
T.b.gambiense 252 --NNNNDDDNDDNNNNN---SNISSDIARLRGCMSNHNHNHNHNSDSTTDGAWKRGIDAG
T.congolense 240 ----------------N---DNIT--CAKFGSCGSRCAGN----------------AG
T.cruzi 224 ----------------------T----------------------FVPGAFS-----P
T.vivax 220 ----------------------M----------------------DTDTEFQ-----S
consensus 301 . . . .
T.brucei 310 GNGEGGVEGEGNKNNNKNKSNNYDNRNVT-GVLDAYADNCTSRVPDFSGMGSQPYDPRPA
L.braziliense 326 APLMSQPYGARSNSATCASRFAAAASSAGPTTAPKPAPAASRAGPDFRGLGSQAYVPETI
L.infantum 327 APPTRQPCGVGGNNTTNVSASAATARSATPTLPPMSVSAAPRAGPDFRGLGNQAYVPEDT
L.major 324 APPTRQPYGVGGNKATNVSAFAATARSTTPTPPPMSASAAPRAGPDFRGLGNQAYVPEDT
L.mexicana 325 APLTHQPYGAGGNNPTNVSASAATARSATPTPLSMSASAAPRAGPDFRGLGNQAYVPEDT
T.b.gambiense 307 GNGEGGVEGEGNKNNNKNKSNNYDNRNVT-GVLDAYADNCTSRVPDFSGMGSQPYDPRPA
T.congolense 261 DNATGGKKK-----TE----RCVDGSLKDGSIRKSNTGPPEDRVPDFSGMGSQPYDPHPA
T.cruzi 233 VNPADRFRGVGNP----------------AFQAEAPSCDRMNGPDFTGLGSRPYQPQAT
T.vivax 229 RGASGCFRGTGNT----------------HNMSGAQGGCTRSGPDFSGLGSEPYQPEVS
consensus 361 . . . .***.*.*...* *...
T.brucei 369 DSDTSNR------YFNSVGLQDTLWQVSEAWDSFREKASRSGERLGNKVKEFLDDL
L.braziliense 386 HSADGGPQNSSGGMATSITASDALWHVTEAARSLQQSAAQATGALGEAVKNFLDDL
L.infantum 387 YCASGGPRGSSGGMGAPGTASDALWHVTEAARSLQQSAAQATGALGEAVKNFLDDL
L.major 384 YSS-------SSGMGAPRTASDALWHVTEAARSLQQSAAQATGALGEAVKNFLDDL
L.mexicana 385 YCASGGPRVSSGGMGAPGTASDALWHVTEAARSLQQSAAQATGAFGEAVKNFLDDL
T.b.gambiense 366 DSDTSNR------YFNSVGLQDTLWQVSEAWDSFREKASRSGERLGNKVKEFLDDL
T.congolense 312 VADADGA------YFNTNL----------
T.cruzi 276 RT----------EAGGFQDTLWQVTEAWDSFKESANRSRKEWGNRVREFLDDL
T.vivax 272 SDG----------DRLNTSIQETLWQVAEAWDSLKEKAGRSSERWGSKVKRFLDDL
consensus 421 . . ..

Appendix 4

Amino acid alignment of TbGAP2 (OG5_127190) orthologues in other kinetoplastids

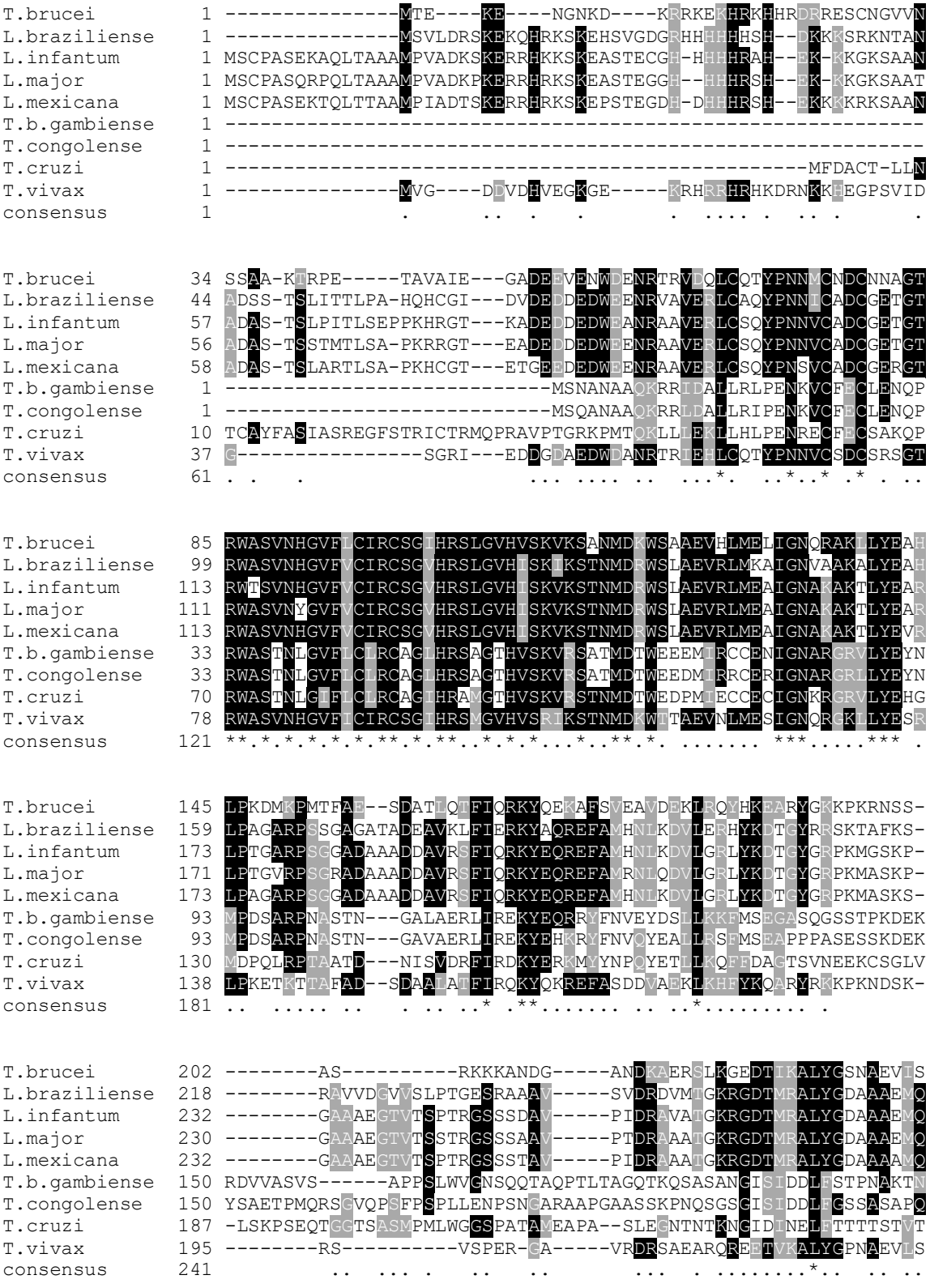

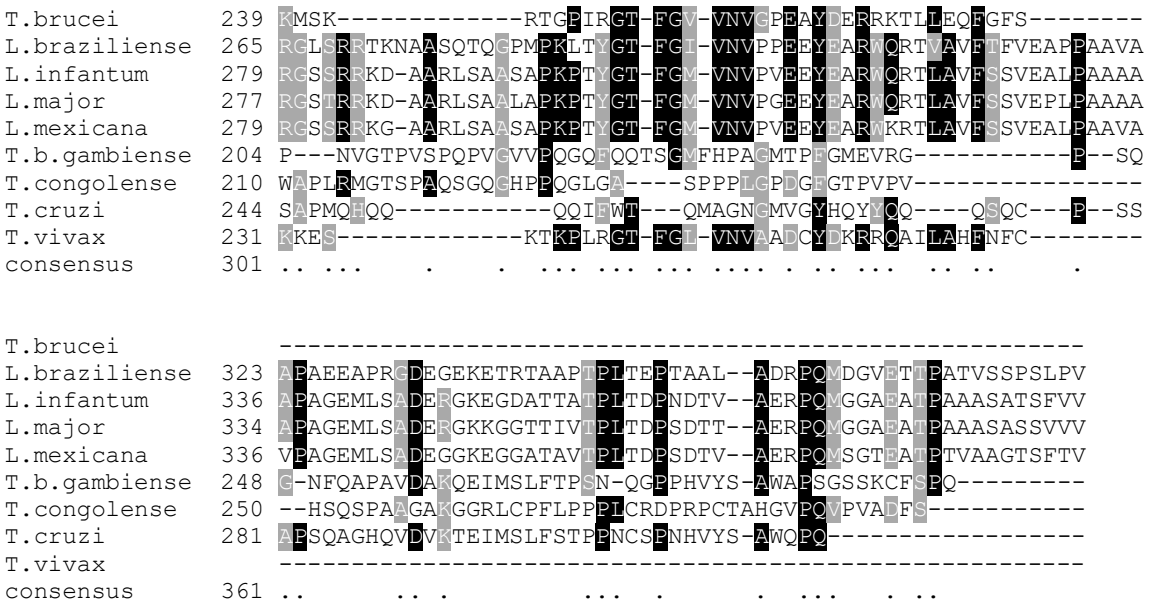
T.brucei 239 KMSK----------RTGEIRGT-FGV-VNVGPEAYDERRKTLLEQFGFS--------
L.braziliense 265 RGLSRRTKNAASQTQGPMPKLTYGT-FGI-VNVPPEEYEARWQRTVAVFTFVEAPPAAVA
L.infantum 279 RGSSRRKD-AARLSAASAPKPTYGT-FGM-VNVPVEEYEARWQRTLAVFSSVEALPAAAA
L.major 277 RGSTRRKD-AARLSAALAPKPTYGT-FGM-VNVPGEEYEARWQRTLAVFSSVEPLPAAAA
L.mexicana 279 RGSSRRKG-AARLSAASAPKPTYGT-FGM-VNVPVEEYEARWKRTLAVFSSVEALPAAVA
T.b.gambiense 204 P---NVGTPVSPQPVGVVPQGQFQQTSGMFHPAGMTPFGMEVRG----------P--SQ
T.congolense 210 WAPLRMGTSPAQSGQGHPPQGLGA----SPPPLGPDGFGTPVPV----------------
T.cruzi 244 SAPMQHQQ----------QQIFWT---QMAGNGMVGYHQYYQQ----QSQC---P--SS
T.vivax 231 KKES----------KTKPLRGT-FGL-VNVAADCYDKRRQAILAHFNFC--------
consensus 301 .. ..
T.brucei ----------
L.braziliense 323 APAEEAPRGDEGEKETRTAAPTPITEPTAAL--ADRPQMDGVETTPATVSSPSLPV
L.infantum 336 APAGEMLSADERGKEGDATTATPITDPNDTV--AERPQMGGAEATPAAASATSFVV
L.major 334 APAGEMLSADERGKKGGTTIVTPITDPSDTT--AERPQMGGAEATPAAASASSVVV
L.mexicana 336 VPAGEMLSADEGGKEGGATAVTPITDPSDTV--AERPQMSGTEATPTVAAGTSFTV
T.b.gambiense 248 G-NFQAPAVDAKQEIMSLFTPSN-QGPPHVYS-AWAPSGSSKCFSPQ---------
T.congolense 250 --HSQSPAAGAKGGRLCPFLPPPICRDPRPCTAHGVPQVPVADFS----------
T.cruzi 281 APSQAGHQVDVKTEIMSLFSTPPNCSPNHVYS-AWQPQ----------
T.vivax ----------
consensus 361 .. ..

Appendix 5

Amino acid sequence alignment for TbGAP3 (OG5_127813) in other kinetoplastids

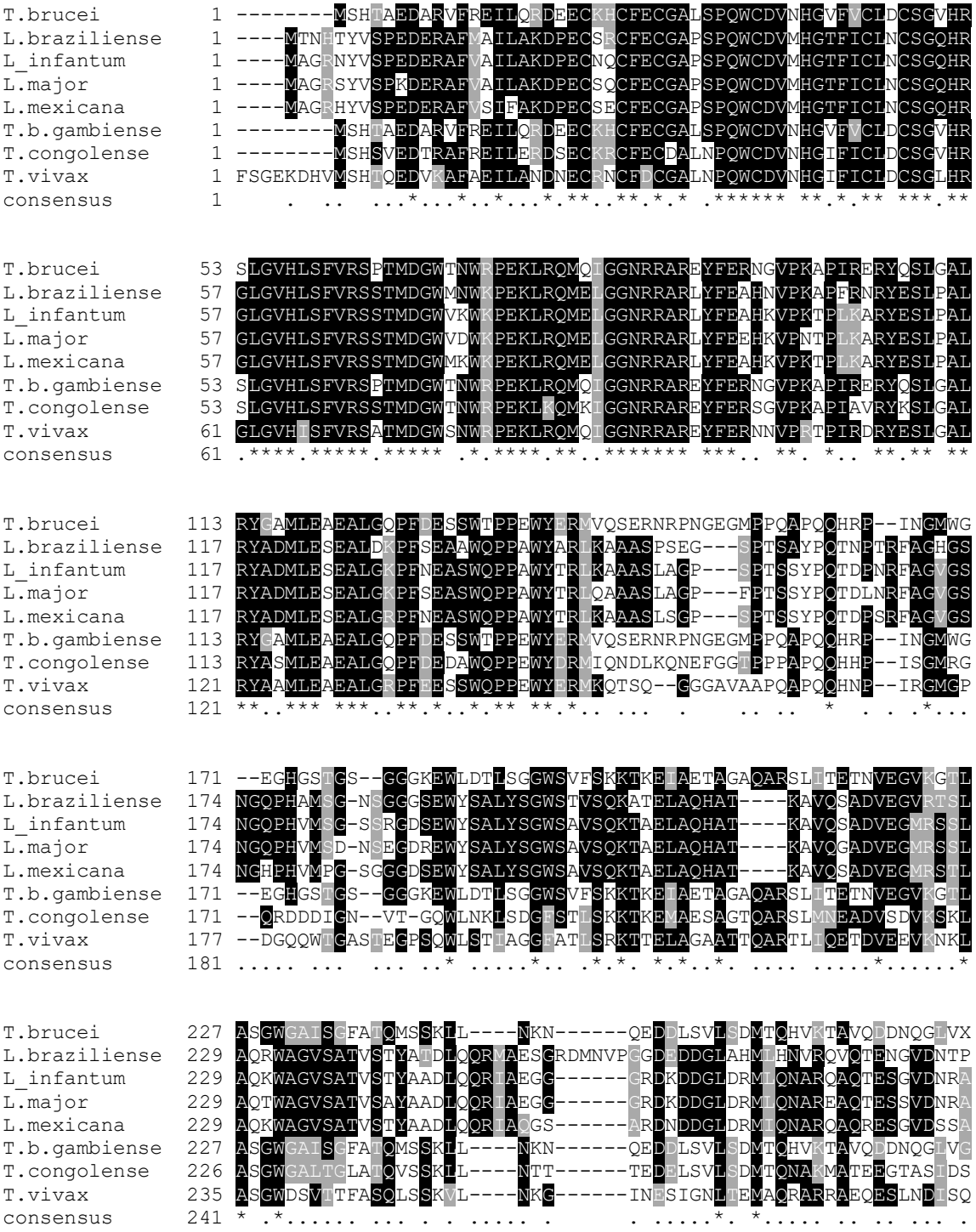

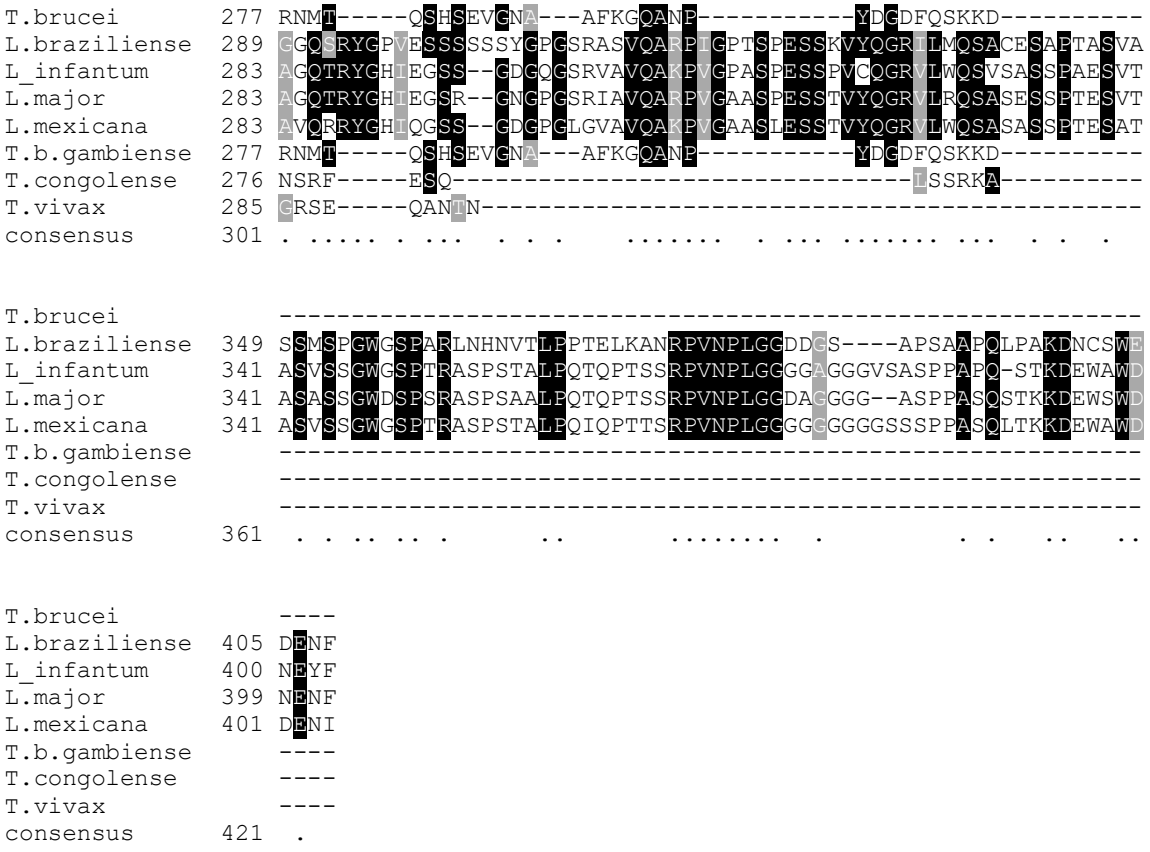
T.brucei 277 RNMT-----QSHSEVGNA---AFKGQANP-----------YDGDFQSKKD----------
L.braziliense 289 GGQSRYGPVESSSSSSYGPGSRASVQARPIGPTSPESSKVYQGRILMQSACESAETASVA
L_infantum 283 AGQTRYGHIEGSS--GDGQGSRVAVQAKPVGPASPESSPVCQGRVLWQSVSASSEAESVT
L.major 283 AGQTRYGHIEGSR--GNGPGSRIAVQARPVGAASPESSTVYQGRVLRQSASESSETESVT
L.mexicana 283 AVQRRYGHIQGSS--GDGPGLGVAVQAKPVGAASLESSTVYQGRVLWQSASASSETESAT
T.b.gambiense 277 RNMT-----QSHSEVGNA---AFKGQANP-----------YDGDFQSKKD----------
T.congolense 276 NSRF-----ESQ-------------------------------LSSRKA----------
T.vivax 285 GRSE-----QANTN---
consensus 301 . ...
T.brucei --
L.braziliense 349 SSMSPGWGSPARLNHNVTLPPTELKANRPVNPLGGDDGS----APSAAPQLPAKDNCSWE
L_infantum 341 ASVSSGWGSPTRASPSTALPQTQPTSSRPVNPLGGGAGGGVSASPPAPQ-STKDEWAWD
L.major 341 ASASSGWDSPSRASPSAALPQTQPTSSRPVNPLGGDAGGGG--ASPPASQSTKKDEWSWD
L.mexicana 341 ASVSSGWGSPTRASPSTALPQIQPTTSRPVNPLGGGGGGGGGSSSPPASQLTKKDEWAWD
T.b.gambiense --
T.congolense --
T.vivax --
consensus 361 . . ..
T.brucei ----
L.braziliense 405 DENF
L_infantum 400 NEYF
L.major 399 NENF
L.mexicana 401 DENI
T.b.gambiense ----
T.congolense ----
T.vivax ----
consensus 421 .

Appendix 6

Amino acid sequence alignment of TbGEF1 (OG5_150051) in other kinetoplastids

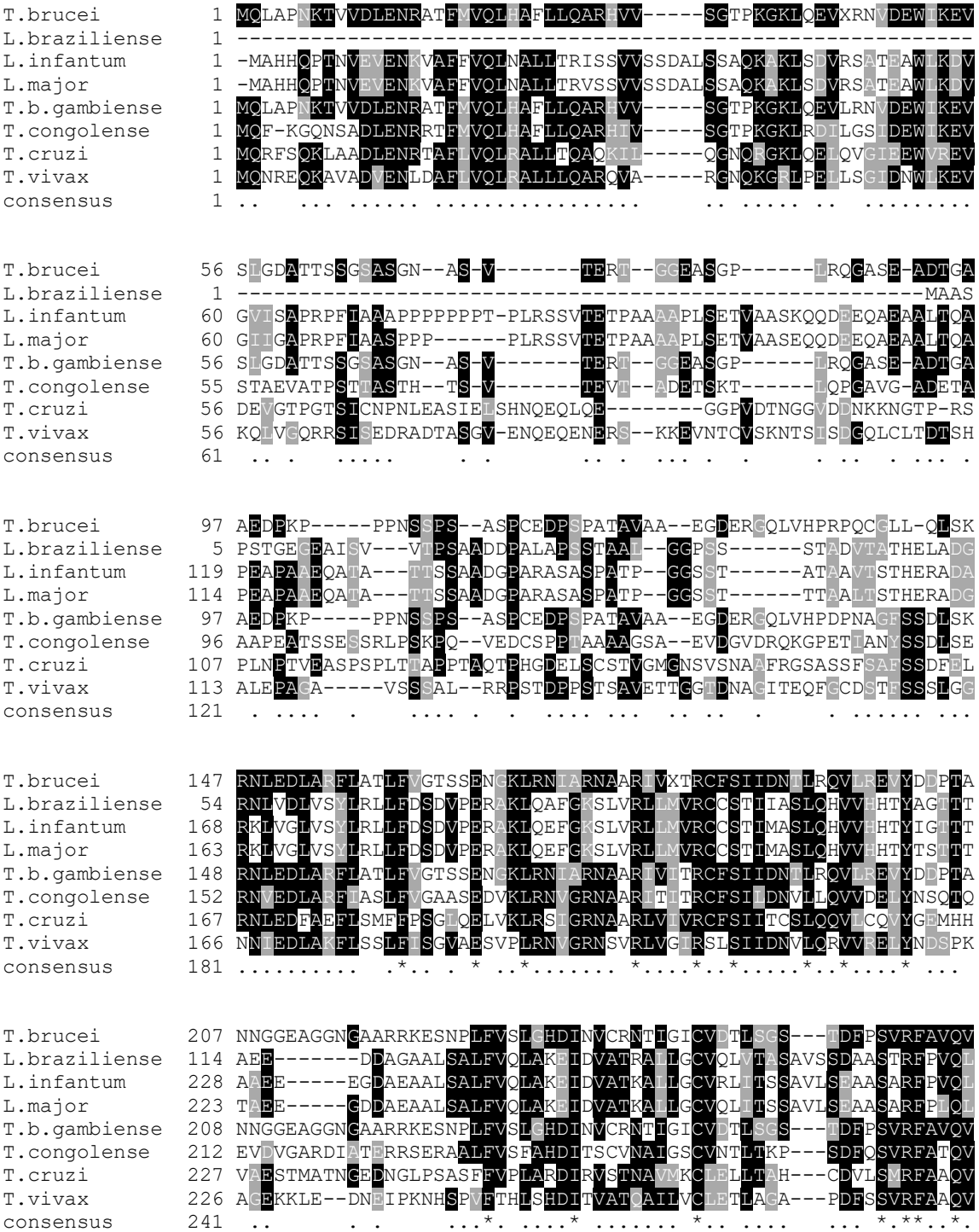

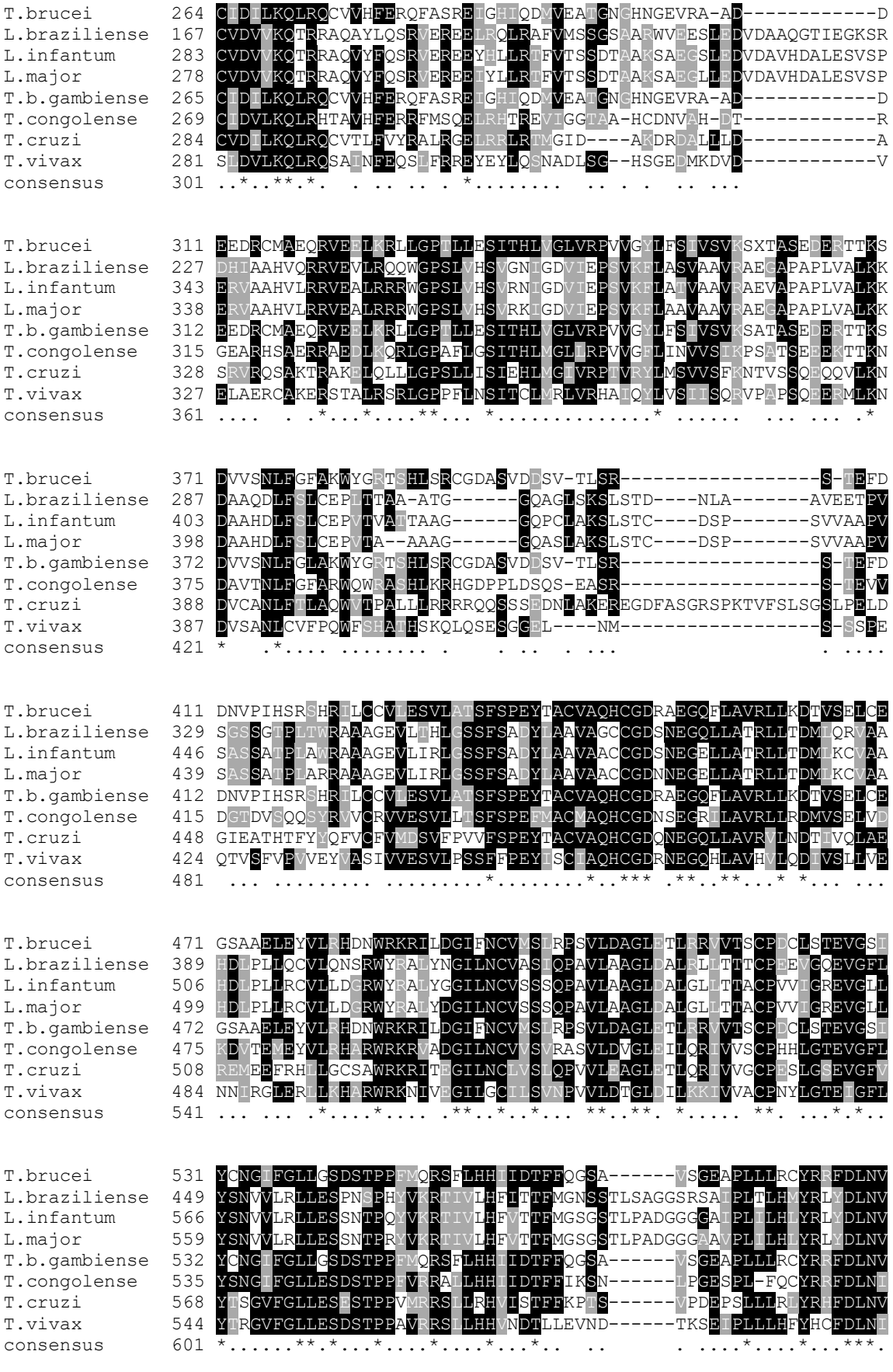

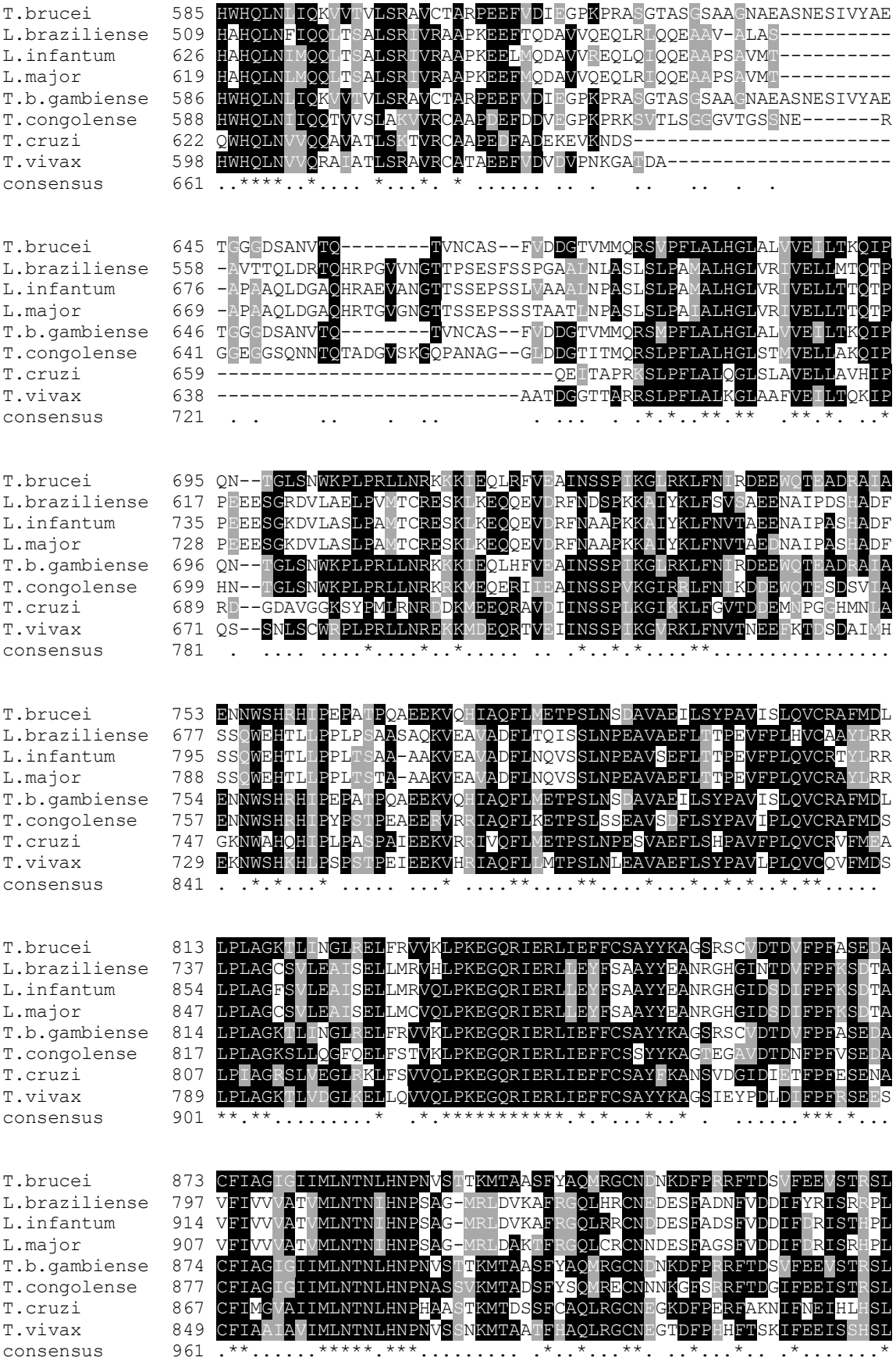
T.brucei 585 HWHQLNLIQKVVTVLSRAVCTARPEEFVDIEGPKPRASGTASGSAAGNAEASNESIVYAE
L.braziliense 509 HAHQLNFIQQLTSALSRIVRAAPKEEETQDAVVQEQLRLQQEAAV-ALAS----------
L.infantum 626 HAHQLNIMQQLTSALSRIVRAAPKEELMQDAVVREQLQLQQEAAPSAVMT----------
L.major 619 HAHQLNLMQQLTSALSRIVRAAPKEEFMQDAVVQEQLRLQQEAAPSAVMT----------
T.b.gambiense 586 HWHQLNLIQKVVTVLSRAVCTARPEEFVDIEGPKPRASGTASGSAAGNAEASNESIVYAE
T.congolense 588 HWHQLNIIQQTVVSLAKVVRCAAPDEEDDVEGPKPRKSVTLSGGGVTGSSNE-------R
T.cruzi 622 QWHQLNVVQQAVATLSKTVRCAAPEDFADEKEVKNDS----------
T.vivax 598 HWHQLNVVQRAIATLSRAVRCATAEEFVDVDVPNKGATDA----------
consensus 661 ..****..*.... *...*. * ....
T.brucei 645 TGGGDSANVTQ--------TVNCAS--FVDDGTVMMQRSVPFLALHGLALVVEILTKQIP
L.braziliense 558 -AVTTQLDRTQHRPGVVNGTTPSESFSSPGAAINLASLSLPAMALHGLVRIVELLMTQTP
L.infantum 676 -APAAQLDGAQHRAEVANGTTSSEPSSLVAAAINPASLSLPAMALHGLVRIVELLTTQTP
L.major 669 -APAAQLDGAQHRTGVGNGTTSSEPSSSTAATINPASLSLPAIALHGLVRIVELLTTQTP
T.b.gambiense 646 TGGGDSANVTQ--------TVNCAS--FVDDGTVMMQRSMPFLALHGLALVVEILTKQIP
T.congolense 641 GGEGGSQNNTQTADGVSKGQPANAG--GLDDGTITMQRSLPFLALHGLSTMVELLAKQIP
T.cruzi 659 ----------QETAPRKSLPFLALQGLSLAVELLAVHIP
T.vivax 638 ----------AATDGGTTARRSLPFLALKGLAAFVEILTQKIP
consensus 721 . . ..*.*..**.** .**.*. ..*
T.brucei 695 QN--TGLSNWKPLPRLLNRKKKIEQLRFVEAINSSPIKGLRKLFNIRDEEWQTEADRAIA
L.braziliense 617 PEEESGRDVLAELPVMTCRESKLKEQQEVDRFNDSPKKAIYKLFSVSAEENAIPDSHADF
L.infantum 735 PEEESGKDVLASLPAMTCRESKLKEQQEVDRFNAAPKKAIYKLFNVTAEENAIPASHADF
L.major 728 PEEESGKDVLASLPAMTCRESKLKEQQEVDRFNAAPKKAIYKLFNVTAEDNAIPASHADF
T.b.gambiense 696 QN--TGLSNWKPLPRLLNRKKKIEQLHFVEAINSSPIKGLRKLFNIRDEEWQTEADRAIA
T.congolense 699 HN--TGLSNWKPLPRLLNRKRKMEQERIIEAINSSPVKGIRRLFNIKDDEWQTESDSVIA
T.cruzi 689 RD--GDAVGGKSYPMLRNRDDKMEEQRAVDIINSSPLKGIKKLFGVTDDEMNPGGHMNLA
T.vivax 671 QS--SNLSCWRPLPRLLNREKKMDEQRTVEIINSSPIKGVRKLFNVTNEEFKTDSDAIMH
consensus 781 . ...*....*..*..... .. .*..*.*....**.....
T.brucei 753 ENNWSHRHIPEPATPQAEEKVQHIAQFLMETPSLNSDAVAEILSYPAVISLQVCRAFMDL
L.braziliense 677 SSQWEHTLLPPLPSAASAQKVEAVADFLTQISSLNPEAVAEFLTTPEVFPLHVCAAYLRR
L.infantum 795 SSQWEHTLLPPLTSAA-AAKVEAVADFLNQVSSLNPEAVSEFLTTPEVFPLQVCRTYLRR
L.major 788 SSQWEHTLLPPLTSTA-AAKVEAVADFLNQVSSLNPEAVAEFLTTPEVFPLQVCRAYLRR
T.b.gambiense 754 ENNWSHRHIPEPATPQAEEKVQHIAQFLMETPSLNSDAVAEILSYPAVISLQVCRAFMDL
T.congolense 757 ENNWSHRHIPYPSTPEAEERVRRIAQFLKETPSLSSEAVSDFLSYPAVIPLQVCRAFMDS
T.cruzi 747 GKNWAHQHIPLPASPAIEEKVRRIVQFLMETPSLNPESVAEFLSHPAVFPLQVCRVFMEA
T.vivax 729 EKNWSHKHLPSPSTPEIEEKVHRIAQFLLMTPSLNLEAVAEFLSYPAVLPLQVCQVFMDS
consensus 841 . .*.*...* ....* ....**....**....*...*..*.*..*.**.....
T.brucei 813 LPLAGKTLINGLRELFRVVKLPKEGQRIERLIEFFCSAYYKAGSRSCVDTDVFPFASELA
L.braziliense 737 LPLAGCSVLEAISELLMRVHLPKEGQRIERLIEYFSAAYYEANRGHGINTDVFPFKSLTA
L.infantum 854 LPLAGFSVLEAISELLMRVQLPKEGQRIERLIEYFSAAYYEANRGHGIDSDIFPFKSDTA
L.major 847 LPLAGCSVLEAISELLMCVQLPKEGQRIERLIEYFSAAYYEANRGHGIDSDIFPFKSDTA
T.b.gambiense 814 LPLAGKTLINGLRELFRVVKLPKEGQRIERLIEFFCSAYYKAGSRSCVDTDVFPFASELA
T.congolense 817 LPLAGKSLLQGFQELFSTVKLPKEGQRIERLIEFFCSSYYKAGTEGAVDTDNFPFVSELA
T.cruzi 807 LPLAGRSLVEGLRKLFSVVQLPKEGQRIERLIEFFCSAYFKANSVDGIDIETFPFESENA
T.vivax 789 LPLAGKTLVDGLKELLQVVQLPKEGQRIERLIEFFCSAYYKAGSIEYPDLDIFPFRSEES
consensus 901 **.**.........* .*.**********.*.*...*..* . ...***.*...
T.brucei 873 CFIAGIGIIMLNTNLHNPNVSTTKMTAASFYAQMRGCNDNKDFPRRFTDSVFEEVSTRSL
L.braziliense 797 VFIVVVATVMLNTNIHNPSAG-MRLDVKAFRQQLHRCNEDESFADNFVDDIFYRISRRPL
L.infantum 914 VFIVVVATVMLNTNIHNPSAG-MRLDVKAFRQQLRRCNDDESFADSFVDDIFDRISTRPL
L.major 907 VFIVVVATVMLNTNIHNPSAG-MRLDAKTFRQQLCRCNNDESFAGSFVDDIFDRISRRPL
T.b.gambiense 874 CFIAGIGIIMLNTNLHNPNVSTTKMTAASFYAQMRGCNDNKDFPRRFTDSVFEEVSTRSL
T.congolense 877 CFIAGIGIIMLNTNLHNPNASSVKMTADSFYSQMRECNNNKGFSRRFTDGIFEEISTRSL
T.cruzi 867 CFIMGVAIIMLNTNLHNPHAASTKMTDSSFCAQLRGCNEGKDFPERFAKNIFNEIHLRSL
T.vivax 849 CFIAAIAVIMLNTNLHNPNVSSNKMTAAFFAQLRGCNEGTDFPHHFTSKIFEEISSRSL
consensus 961 .**......*****.***......... .*..*...**. ..*...*.. .*.......*

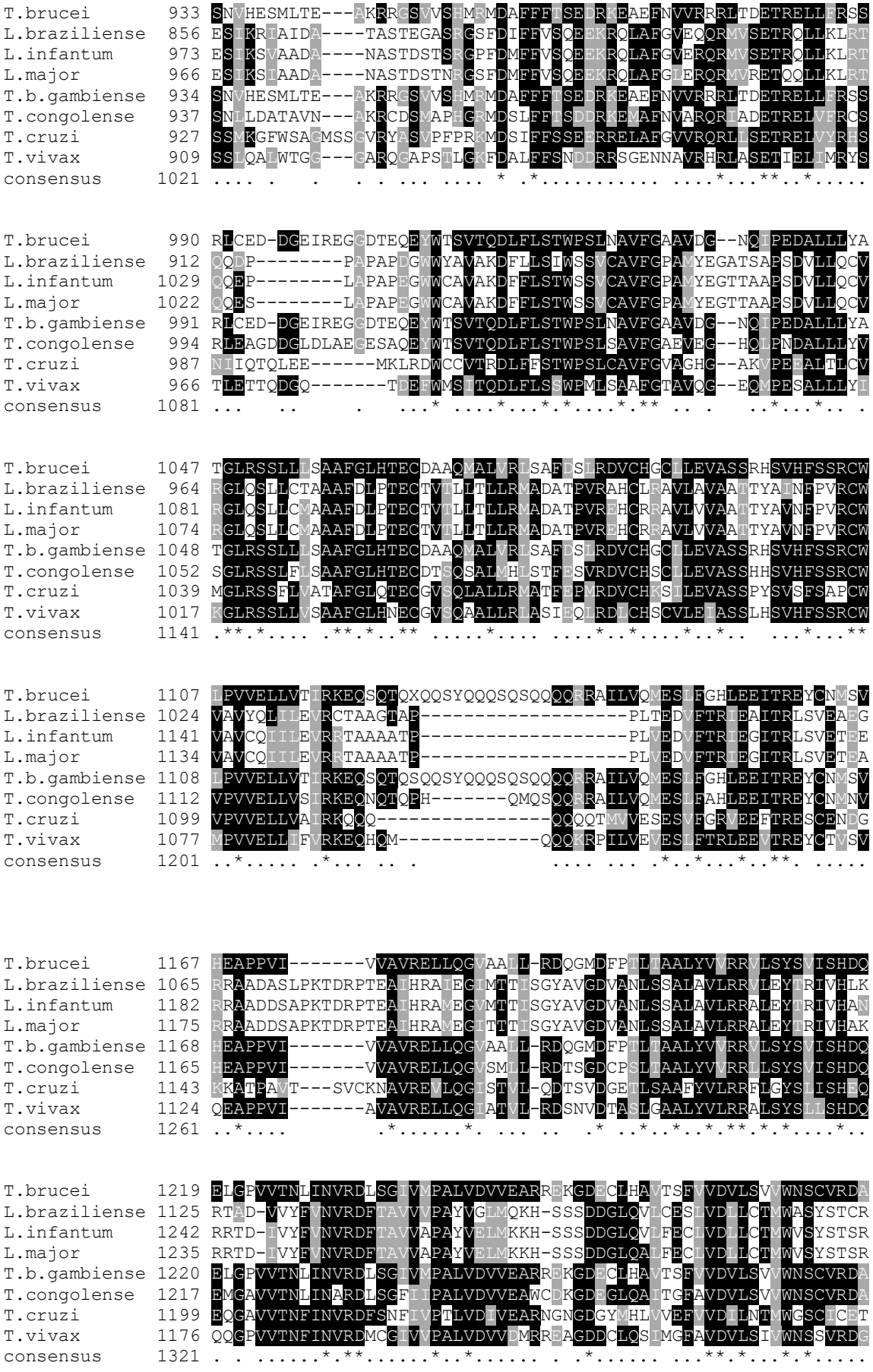
T.brucei 933 SNVHESMLTE---AKRRGSVVSHMRMDAFFFTSEDRKEAEFNVVRRRLTDETRELLFRSS
L.braziliense 856 ESIKRIAIDA----TASTEGASFGSFDIFFVSQEEKRQLAFGVEQQRMVSETRQLLKLRT
L.infantum 973 ESIKSVAADA----NASTDSTSFGPFDMFFVSQEEKRQLAFGVERQRMVSETRQLLKLRT
L.major 966 ESIKSIAADA----NASTDSTNFGSFDMFFVSQEEKRQLAFGLERQRMVRETQQLLKLRT
T.b.gambiense 934 SNVHESMLTE---AKRRGSVVSFMRMDAFFFTSEDRKEAEFNVVRRRLTDETRELLFRSS
T.congolense 937 SNLLDATAVN---AKRCDSMAPFGRMDSLFFISDDRKEMAFNVARQRIADETRELVFRCS
T.cruzi 927 SSMKGFWSAGMSSGVRYASVPFPRRMDSIFFSSEERRELAFGVVRQRLLSETRELVYRFS
T.vivax 909 SSLQALWTGG---GARQGAPSILGRFDALFFSNDDRRSGENNAVRHRLASETIELIMRYS
consensus 1021 .... * .*.......... ....*...**..*.....
T.brucei 990 RLCED-DGEIREGGDTEQEYWTSVTQDLFLSTWPSLNAVFGAAVDG--NQIPEDALLLYA
L.braziliense 912 QQDP--------PAPAPDGWWYAVAKDFLLSIWSSVCAVFGPAMYEGATSAPSDVLLQCV
L.infantum 1029 QQEP--------LAPAPEGWWCAVAKDFFLSTWSSVCAVFGPAMYEGTTAAPSDVLLQCV
L.major 1022 QQES--------LAPAPEGWWCAVAKDFFLSTWSSVCAVFGPAMYEGTTAAPSDVLLQCV
T.b.gambiense 991 RLCED-DGEIREGGDTEQEYWTSVTQDLFLSTWPSLNAVFGAAVDG--NQIPEDALLLYA
T.congolense 994 RLEAGDDGLDLAEGESAQEYWTSVTQDLFLSTWPSLSAVFGAEVEG--HQLPNDALLLYV
T.cruzi 987 NIIQTQLEE------MKLRDWCCVTRDLFFSTWPSLCAVFGVAGHG--AKVPEEALTLCV
T.vivax 966 TLETTQDGQ-------TDEFWMSITQDLFLSSWPMLSAAFGTAVQG--EQMPESALLLYI
consensus 1081 ... .* ....*...*.*....*.** .. . ..*...*.. .
T.brucei 1047 TGLRSSLLLSAAFGLHTECDAAQMALVRLSAFDSLRDVCHGCLLEVASSRHSVHFSSRCW
L.braziliense 964 RGLQSLLCTAAAFDLPTECTVTLLTLLRMADATPVRAHCLRAVLAVAATTYAINFPVRCW
L.infantum 1081 RGLQSLLCMAAAFDLPTECTVTLLTLLRMADATPVREHCRRAVLVVAATTYAVNFPVRCW
L.major 1074 RGLQSLLCMAAAFDLPTECTVTLLTLLRMADATPVREHCRRAVLVVAATTYAVNFPVRCW
T.b.gambiense 1048 TGLRSSLLLSAAFGLHTECDAAQMALVRLSAFDSLRDVCHGCLLEVASSRHSVHFSSRCW
T.congolense 1052 SGLRSSLFLSAAFGLHTECDTSQSALMHLSTFESVRDVCHSCLLEVASSHHSVHFSSRCW
T.cruzi 1039 MGLRSSFLVATAFGLQTECGVSQLALLRMATFEPMRDVCHKSILEVASSPYSVSFSAPCW
T.vivax 1017 KGLRSSLLVSAAFGLHNECGVSQAALLRLASIEQLRDLCHSCVLEIASSLHSVHFSSRCW
consensus 1141 .**.*.... .**.*..** .....*.... ....*..*....*..*.. ...*...**
T.brucei 1107 LPVVELLVTIRKEQSQTQXQQSYQQQSQSQQQQRRAILVQMESLFGHLEEITREYCNMSV
L.braziliense 1024 VAVYQLILEVRCTAAGTAP-------------------PLTEDVFTRIEAITRLSVEAFG
L.infantum 1141 VAVCQIILEVRRTAAAATP-------------------PLVEDVFTRIEGITRLSVETTE
L.major 1134 VAVCQIILEVRRTAAAATP-------------------PLVEDVFTRIEGITRLSVETEA
T.b.gambiense 1108 LPVVELLVTIRKEQSQTQSQQSYQQQSQSQQQQRRAILVQMESLFGHLEEITREYCNMSV
T.congolense 1112 VPVVELLVSIRKEQNQTQPH-------QMQSQQRRAILVQMESLFAHLEEITREYCNMNV
T.cruzi 1099 VPVVELLVAIRKQQQ----------------QQQQTMVVESESVFGRVEEFTRESCENDG
T.vivax 1077 MPVVELLIFVRKEQHQM------------QQQKRPILVEVESLFTRLEEVTREYCTVSV
consensus 1201 ..*..... .*... .. . .*..*...*..**. .....
T.brucei 1167 HEAPPVI-------VVAVRELLQGVAALL-RDQGMDFPTLTAALYVVRRVLSYSVISHDQ
L.braziliense 1065 RRAADASLPKTDRPTEAIHRAIEGIMTTISGYAVGDVANLSSALAVLRRVLEYTRIVHLK
L.infantum 1182 RRAADDSAPKTDRPTEAIHRAVEGVMTTISGYAVGDVANLSSALAVLRRALEYTRIVHAN
L.major 1175 RRAADDSAPKTDRPTEAIHRAVEGITTTISGYAVGDVANLSSALAVLRRALEYTRIVHAK
T.b.gambiense 1168 HEAPPVI-------VVAVRELLQGVAALL-RDQGMDFPTLTAALYVVRRVLSYSVISHDQ
T.congolense 1165 HEAPPVI-------VVAVRELLQGVSMLL-RDTSGDCPSLTAALYVVRRLLSYSVISHDQ
T.cruzi 1143 KKATPAVT---SVCKNAVREVLQGISTVL-QDTSVDGELLSAAFYVLRRFLGYSIISHHQ
T.vivax 1124 QEAPPVI-------AVAVRELLQGIATVL-RDSNVDTASLGAALYVLRRALSYSLISHDQ
consensus 1261 ..*.... .*.....*. ... .. .* ..*..*..*.**.*.*....*..
T.brucei 1219 ELGPVVTNLINVRDLSGIVMPALVDVVEARREKGDECLHAVTSFVVDVLSVVWNSCVRDA
L.braziliense 1125 RTAD-VVYFVNVRDFTAVVPAYVGLMQKH-SSSDDGLQVLCESLVDLLCTMWASYSTCR
L.infantum 1242 RRTD-IVYFVNVRDFTAVVAPAYVELMKKH-SSSDDGLQVLFECLVDLLCTMWVSYSTSR
L.major 1235 RRTD-IVYFVNVRDFTAVVAPAYVELMKKH-SSSDDGLQALFECLVDLLCTMWVSYSTSR
T.b.gambiense 1220 ELGPVVTNLINVRDLSGIVMPALVDVVEARREKGDECLHAVTSFVVDVLSVVWNSCVRDA
T.congolense 1217 EMGAVVTNLINARDLSGFIIPALVDVVEAWCDKGDEGLQAITGFAVDVLSVVWNSCVRDA
T.cruzi 1199 EQGAVVTNFINVRDFSNFIVPTLVDIVEARNGNGDGYMHLVVEFVVDILNTMWGSCICET
T.vivax 1176 QQGPVVTNFINVRDMCGIVVPALVDVVTMRREAGDDCLQSIMGFAVDVLSIVWNSSVRDG
consensus 1321 . . ..*.**......*..*..... . .*..... ...**.*...*.*.....

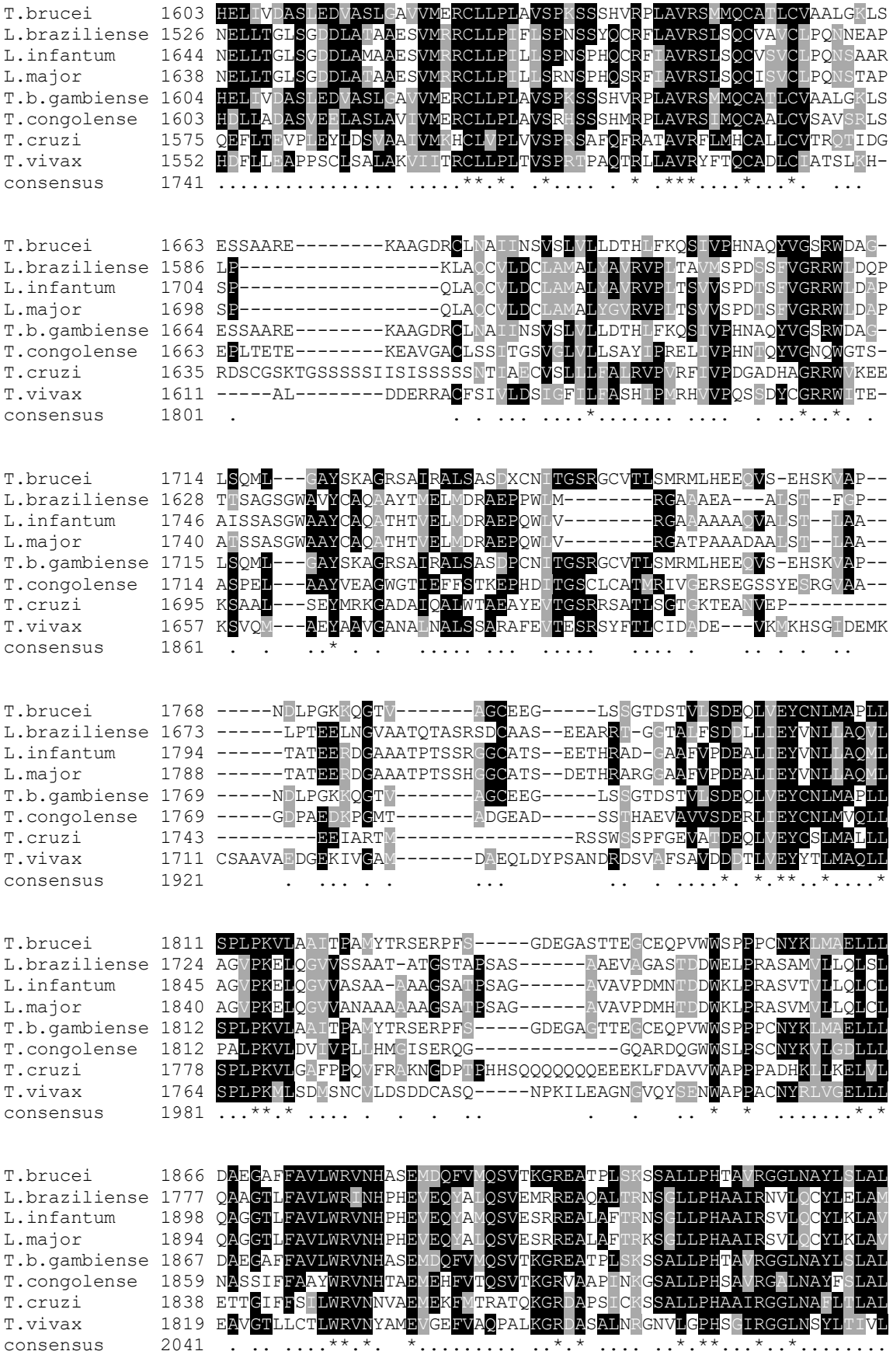
T.brucei 1603
L.braziliense 1526
L.infantum 1644
L.major 1638
T.b.gambiense 1604
T.congolense 1603
T.cruzi 1575
T.vivax 1552
consensus 1741
T.brucei 1663
L.braziliense 1586
L.infantum 1704
L.major 1698
T.b.gambiense 1664
T.congolense 1663
T.cruzi 1635
T.vivax 1611
consensus 1801
T.brucei 1714
L.braziliense 1628
L.infantum 1746
L.major 1740
T.b.gambiense 1715
T.congolense 1714
T.cruzi 1695
T.vivax 1657
consensus 1861
T.brucei 1768
L.braziliense 1673
L.infantum 1794
L.major 1788
T.b.gambiense 1769
T.congolense 1769
T.cruzi 1743
T.vivax 1711
consensus 1921
T.brucei 1811
L.braziliense 1724
L.infantum 1845
L.major 1840
T.b.gambiense 1812
T.congolense 1812
T.cruzi 1778
T.vivax 1764
consensus 1981
T.brucei 1866
L.braziliense 1777
L.infantum 1898
L.major 1894
T.b.gambiense 1867
T.congolense 1859
T.cruzi 1838
T.vivax 1819
consensus 2041

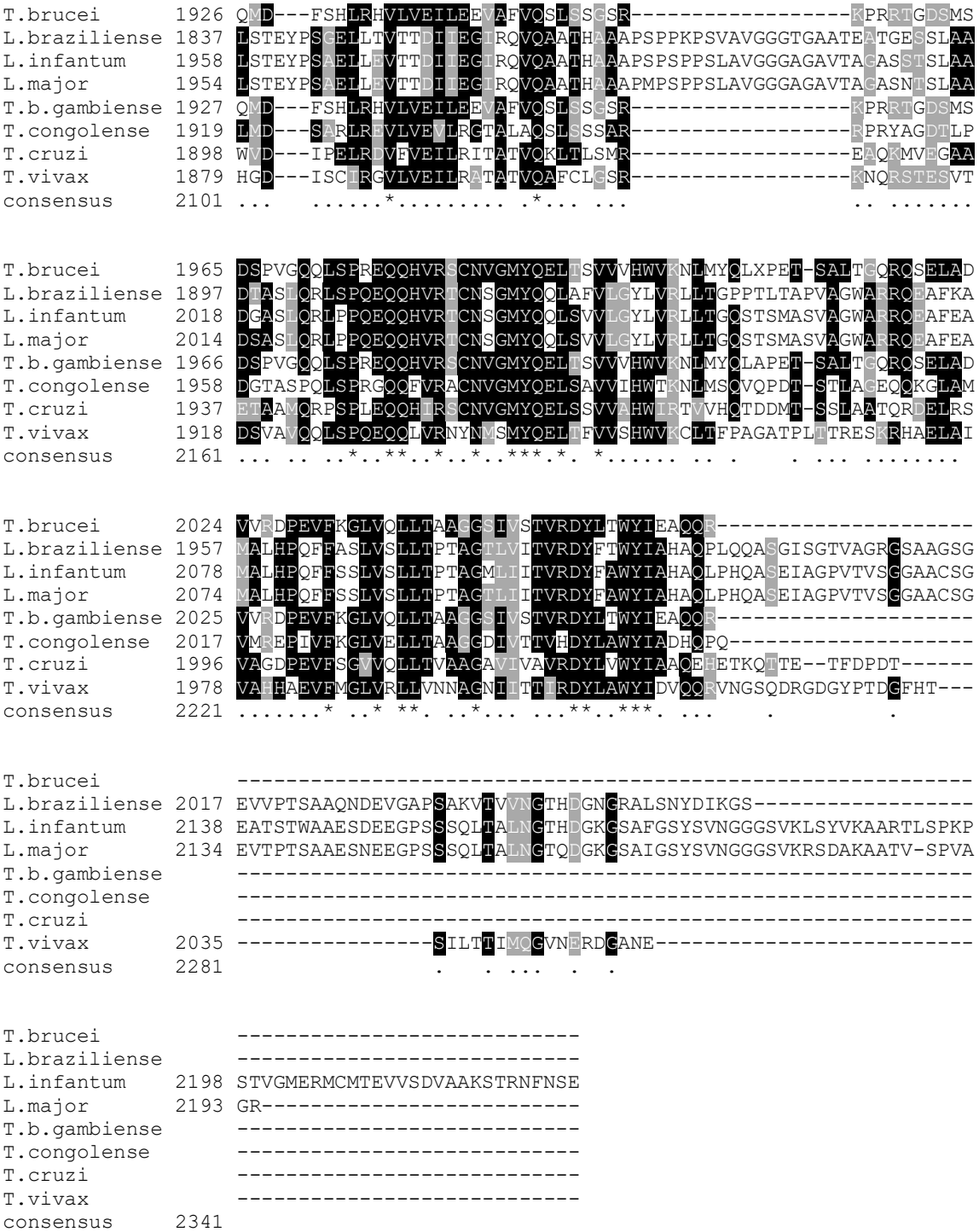
T.brucei 1926
L.braziliense 1837
L.infantum 1958
L.major 1954
T.b.gambiense 1927
T.congolense 1919
T.cruzi 1898
T.vivax 1879
consensus 2101
T.brucei 1965
L.braziliense 1897
L.infantum 2018
L.major 2014
T.b.gambiense 1966
T.congolense 1958
T.cruzi 1937
T.vivax 1918
consensus 2161
T.brucei 2024
L.braziliense 1957
L.infantum 2078
L.major 2074
T.b.gambiense 2025
T.congolense 2017
T.cruzi 1996
T.vivax 1978
consensus 2221
T.brucei
L.braziliense 2017
L.infantum 2138
L.major 2134
T.b.gambiense
T.congolense
T.cruzi
T.vivax 2035
consensus 2281
T.brucei
L.braziliense
L.infantum 2198
L.major 2193
T.b.gambiense
T.congolense
T.cruzi
T.vivax
consensus 2341

Appendix 7

Amino acid sequence of TbGEF2 (OG5_150255) in other kinetoplastids

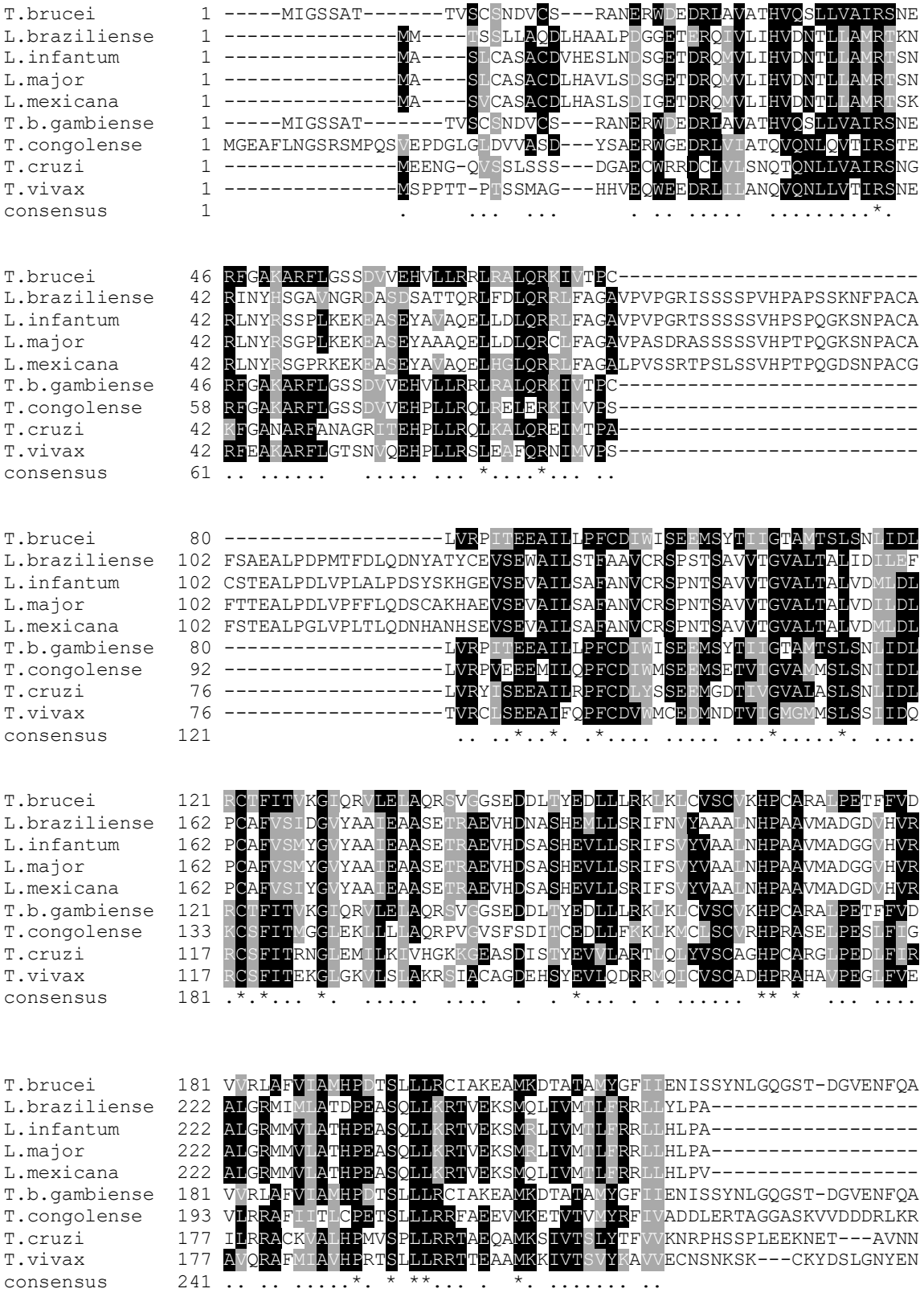

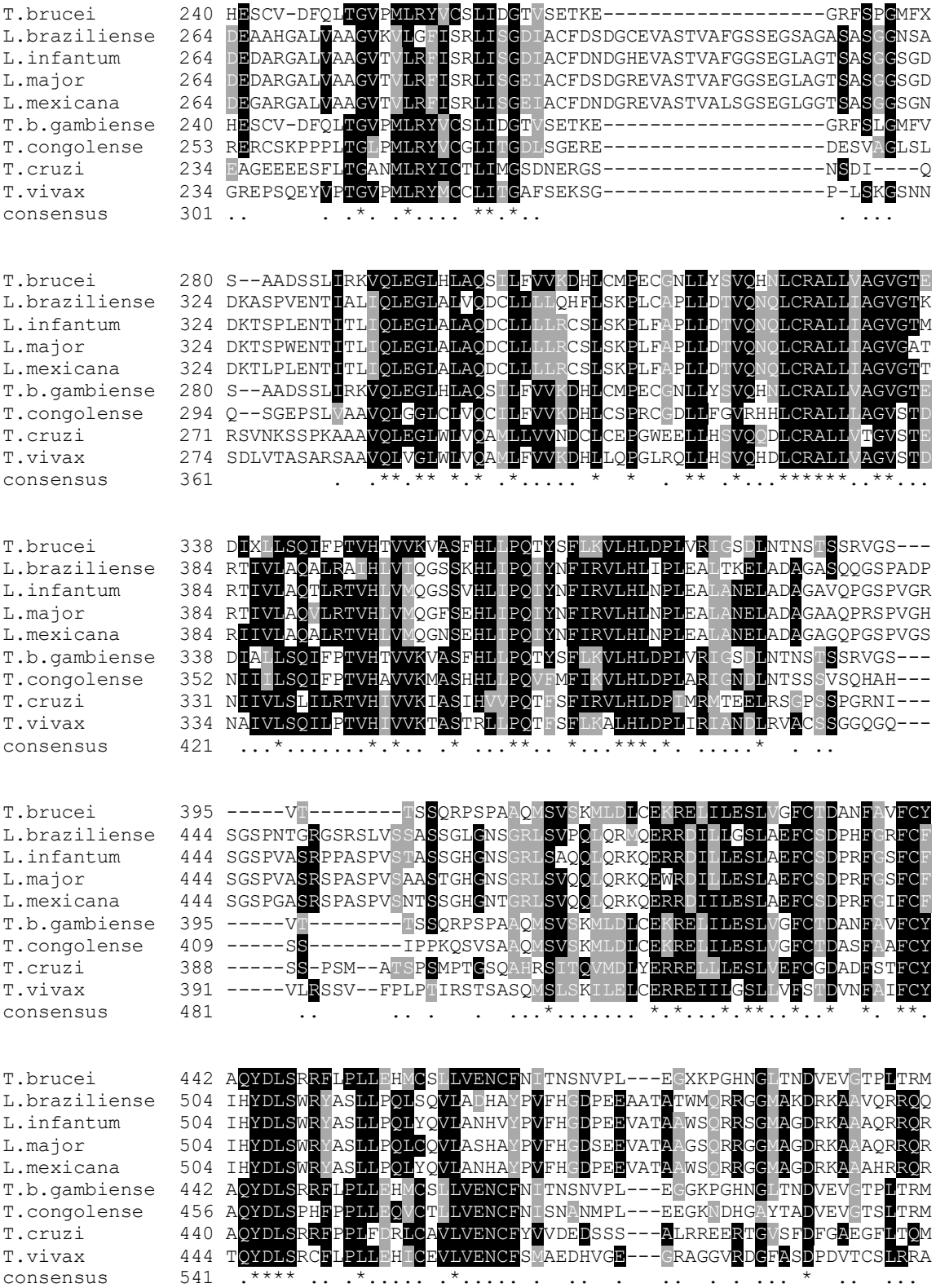

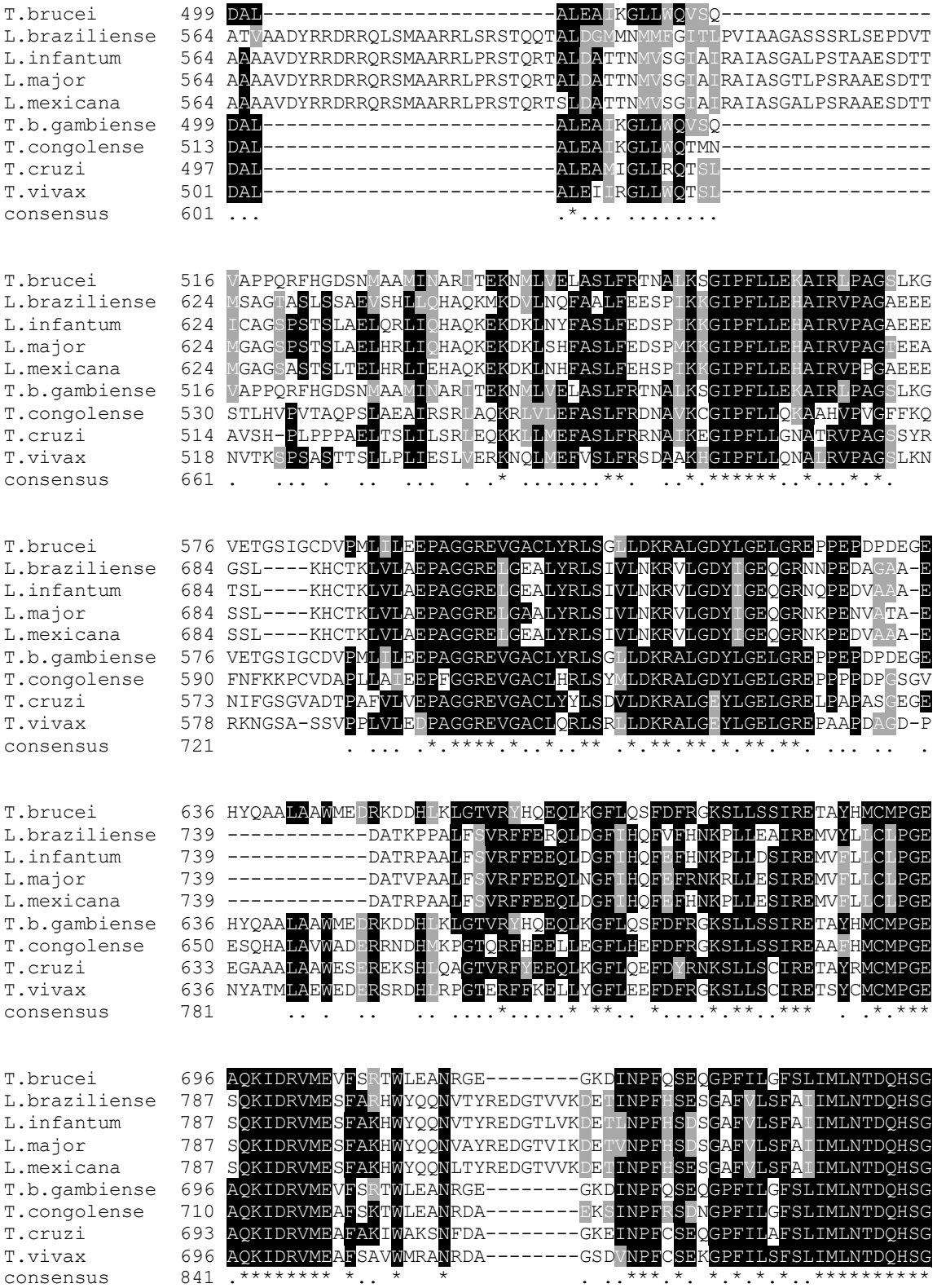
T.brucei 499 DAL----------ALEAIKGLLWQVSQ----------
L.braziliense 564 ATVAADYRRDRRQLSMAARRLSRSTQQTALDGMMNMMFGITLPVIAAGASSSRLSEPDVT
L.infantum 564 AAAAVDYRRDRRQRSMAARRLPRSTQRTALDATTNMVSGIAIRAIASGALPSTAAESDTT
L.major 564 AAAAVDYRRDRRQRSMAARRLPRSTQRTALDATTNMVSGIAIRAIASGTLPSRAAESDTT
L.mexicana 564 AAAAVDYRRDRRQRSMAARRLPRSTQRTSLDATTNMVSGIAIRAIASGALPSRAAESDTT
T.b.gambiense 499 DAL----------ALEAIKGLLWQVSQ----------
T.congolense 513 DAL----------ALEAIKGLLWQTMN----------
T.cruzi 497 DAL----------ALEAMIGLLRQTSL----------
T.vivax 501 DAL----------ALEIIRGLLWQTSL----------
consensus 601 ... .*... ....
T.brucei 516 VAPPQRFHGDSNMAAMINARITEKNMLVELASLFRTNALKSGIPFLLEKAIRLPAGSLKG
L.braziliense 624 MSAGTASLSSAEVSHLLQHAQKMKDVLNQFAALFEESPIKKGIPFLLEHAIRVPAGAEEE
L.infantum 624 ICAGSPSTSLAELQRLIQHAQKEKDKLNYFASLFEDSPIKKGIPFLLEHAIRVPAGAEEE
L.major 624 MGAGSPSTSLAELHRLIQHAQKEKDKLSHFASLFEDSPMKKGIPFLLEHAIRVPAGTEEA
L.mexicana 624 MGAGSASTSLTELHRLIEHAQKEKDKLNHFASLFEHSPIKKGIPFLLEHAIRVPPGAEEE
T.b.gambiense 516 VAPPQRFHGDSNMAAMINARITEKNMLVELASLFRTNALKSGIPFLLEKAIRLPAGSLKG
T.congolense 530 STLHVPVTAQPSLAEAIRSRLAQKRLVLEFASLFRDNAVKCGIPFLLQKAAHVPVGFFKQ
T.cruzi 514 AVSH-PLPPPAELTSLILSRLEQKKLMEFASLFRRNAIKEGIPFLLGNATRVPAGSSYR
T.vivax 518 NVTKSPSASTTSLLPLIESLVERKNQLMEFVSLFRSDAAKHGIPFLLQNAIRVPAGSLKN
consensus 661 . ...* ....**. ..*.******..*...*.*.
T.brucei 576 VETGSIGCDVPMLILEEPAGGREVGACLYRLSGLLDKRALGDYLGELGREPPEPDPDEGE
L.braziliense 684 GSL----KHCTKLVLAEPAGGREIGEALYRLSIVLNKRVLGDYIGEQGRNNPEDAGAA-E
L.infantum 684 TSL----KHCTKLVLAEPAGGREIGEALYRLSIVLNKRVLGDYIGEQGRNQPEDVAAA-E
L.major 684 SSL----KHCTKLVLAEPAGGREIGAALYRLSIVLNKRVLGDYIGEQGRNKPENVATA-E
L.mexicana 684 SSL----KHCTKLVLAEPAGGREIGEALYRLSIVLNKRVLGDYIGEQGRNKPEDVAAA-E
T.b.gambiense 576 VETGSIGCDVPMLILEEPAGGREVGACLYRLSGLLDKRALGDYLGELGREPPEPDPDEGE
T.congolense 590 FNFKKPCVDAPLLAIEEPFGGREVGACLHRLSYMLDKRALGDYLGELGREPPPPDPGSGV
T.cruzi 573 NIFGSGVADTPAFVLVEPAGGREVGACLYYLSDVLDKRALGEYLGELGRELPAPASGEGE
T.vivax 578 RKNGSA-SSVPPLVLEDPAGGREVGACLQRLSRLLDKRALGEYLGELGREPAAPDAGD-P
consensus 721 . ... .*.****.*..*..** .*.**.**.*.**.**. ... .. .
T.brucei 636 HYQAALAAWMEDRKDDHLKLGTVRYHQEQLKGFLQSFDFRGKSLLSSIRETAYHMCMPGE
L.braziliense 739 ------------DATKPPALFSVRFFERQLDGFTHQFVFHNKPLLEAIREMVYLLCLPGE
L.infantum 739 ------------DATRPAALFSVRFFEEQLDGFIHQFEFHNKPLLDSIREMVFLLCLPGE
L.major 739 ------------DATVPAALFSVRFFEEQLNGFIHQFEFRNKRLLESIREMVFLLCLPGE
L.mexicana 739 ------------DATRPAALFSVRFFEEQLDGFIHQFEFHNKPLLESIREMVFLLCLPGE
T.b.gambiense 636 HYQAALAAWMEDRKDDHLKLGTVRYHQEQLKGFLQSFDFRGKSLLSSIRETAYHMCMPGE
T.congolense 650 ESQHALAVWADERRNDHMKPGTQRFHEELLEGFLHEFDFRGKSLLSSIREAAFHMCMPGE
T.cruzi 633 EGAAALAAWESEREKSHLQAGTVRFYEEQLKGFLQEFDYRNKSLLSCIRETAYRMCMPGE
T.vivax 636 NYATMLAEWEDERSRDHLRPGTERFFKELLYGFLEEFDFRGKSLLSCIRETSYCMCMPGE
consensus 781 .. . .*.....* **.. *....*.**..*** . .*.***
T.brucei 696 AQKIDRVMEVFSRTWLEANRGE--------GKDINPFQSEQGPFILGFSLIMLNTDQHSG
L.braziliense 787 SQKIDRVMESFARHWYQQNVTYREDGTVVKDETINPFHSESGAFVLSFAIIMLNTDQHSG
L.infantum 787 SQKIDRVMESFAKHWYQQNVTYREDGTLVKDETLNPFHSDSGAFVLSFAIIMLNTDQHSG
L.major 787 SQKIDRVMESFAKHWYQQNVAYREDGTVIKDETVNPFHSDSGAFVLSFAIIMLNTDQHSG
L.mexicana 787 SQKIDRVMESFAKHWYQQNLTYREDGTVVKDETINPFHSESGAFVLSFAIIMLNTDQHSG
T.b.gambiense 696 AQKIDRVMEVFSRTWLEANRGE--------GKDINPFQSEQGPFILGFSLIMLNTDQHSG
T.congolense 710 AQKIDRVMEAFSKTWLEANRDA--------EKSINPFRSDNGPFILGFSLIMLNTDQHSG
T.cruzi 693 AQKIDRVMEAFAKIWAKSNFDA--------GKEINPFCSEQGPFILAFSLIMLNTDQHSG
T.vivax 696 AQKIDRVMEAFSAVWMRANRDA--------GSDVNPFCSEKGPFILSFSLIMLNTDQHSG
consensus 841 .******** *.. * * . ..***.*. *.*.*.*..**********

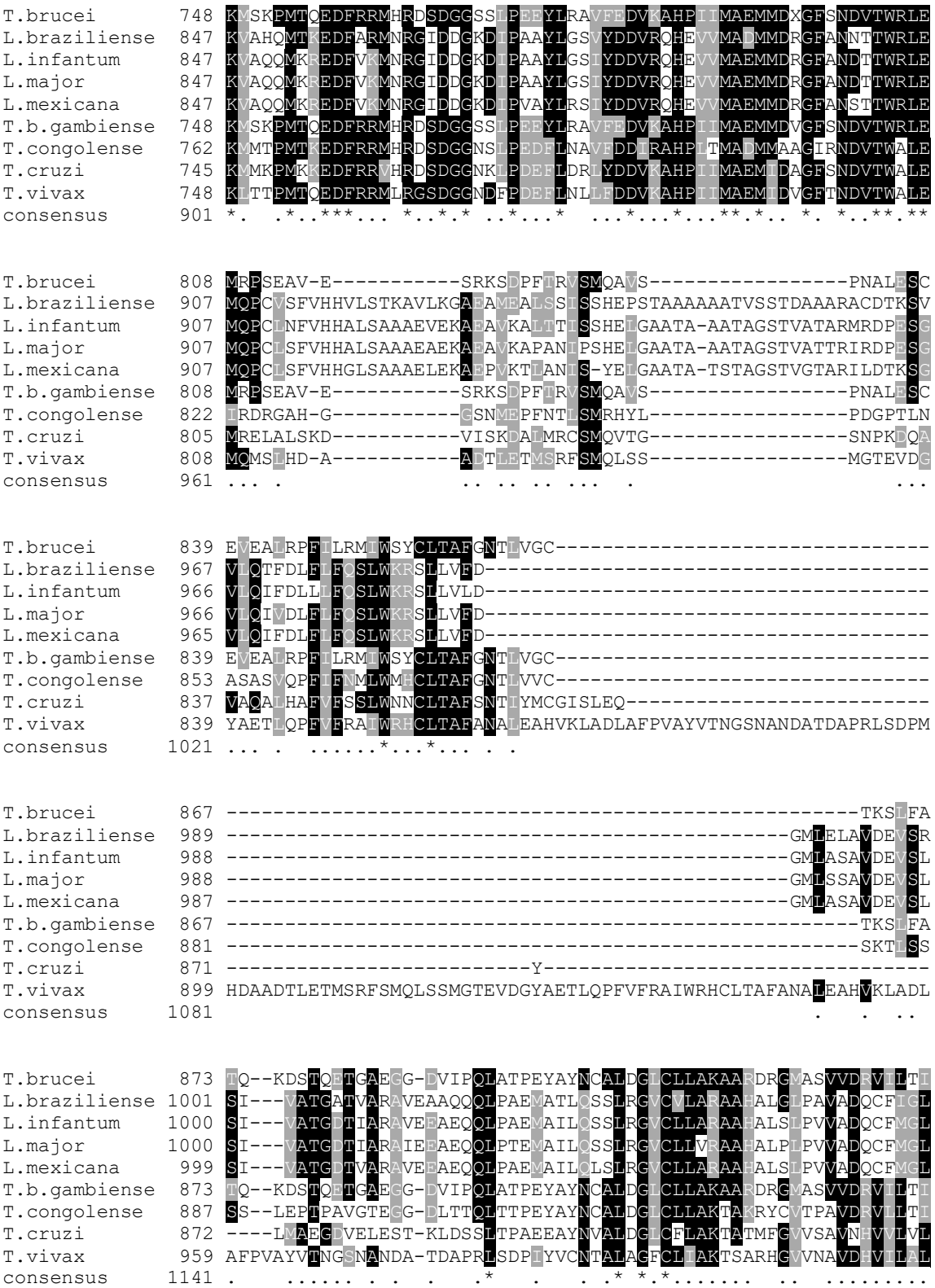
T.brucei 748
L.braziliense 847
L.infantum 847
L.major 847
L.mexicana 847
T.b.gambiense 748
T.congolense 762
T.cruzi 745
T.vivax 748
consensus 901
T.brucei 808
L.braziliense 907
L.infantum 907
L.major 907
L.mexicana 907
T.b.gambiense 808
T.congolense 822
T.cruzi 805
T.vivax 808
consensus 961
T.brucei 839
L.braziliense 967
L.infantum 966
L.major 966
L.mexicana 965
T.b.gambiense 839
T.congolense 853
T.cruzi 837
T.vivax 839
consensus 1021
T.brucei 867
L.braziliense 989
L.infantum 988
L.major 988
L.mexicana 987
T.b.gambiense 867
T.congolense 881
T.cruzi 871
T.vivax 899
consensus 1081
T.brucei 873
L.braziliense 1001
L.infantum 1000
L.major 1000
L.mexicana 999
T.b.gambiense 873
T.congolense 887
T.cruzi 872
T.vivax 959
consensus 1141

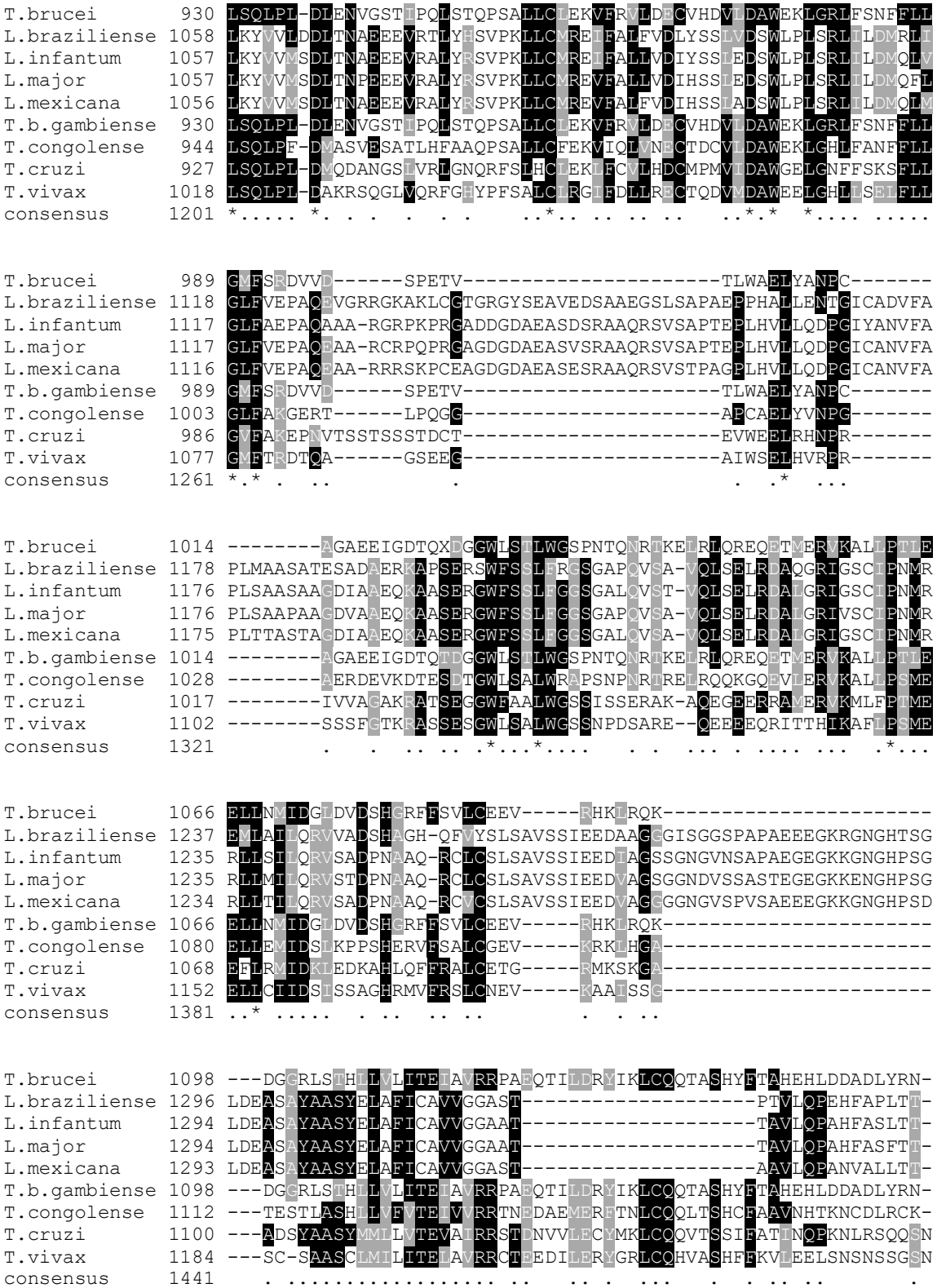

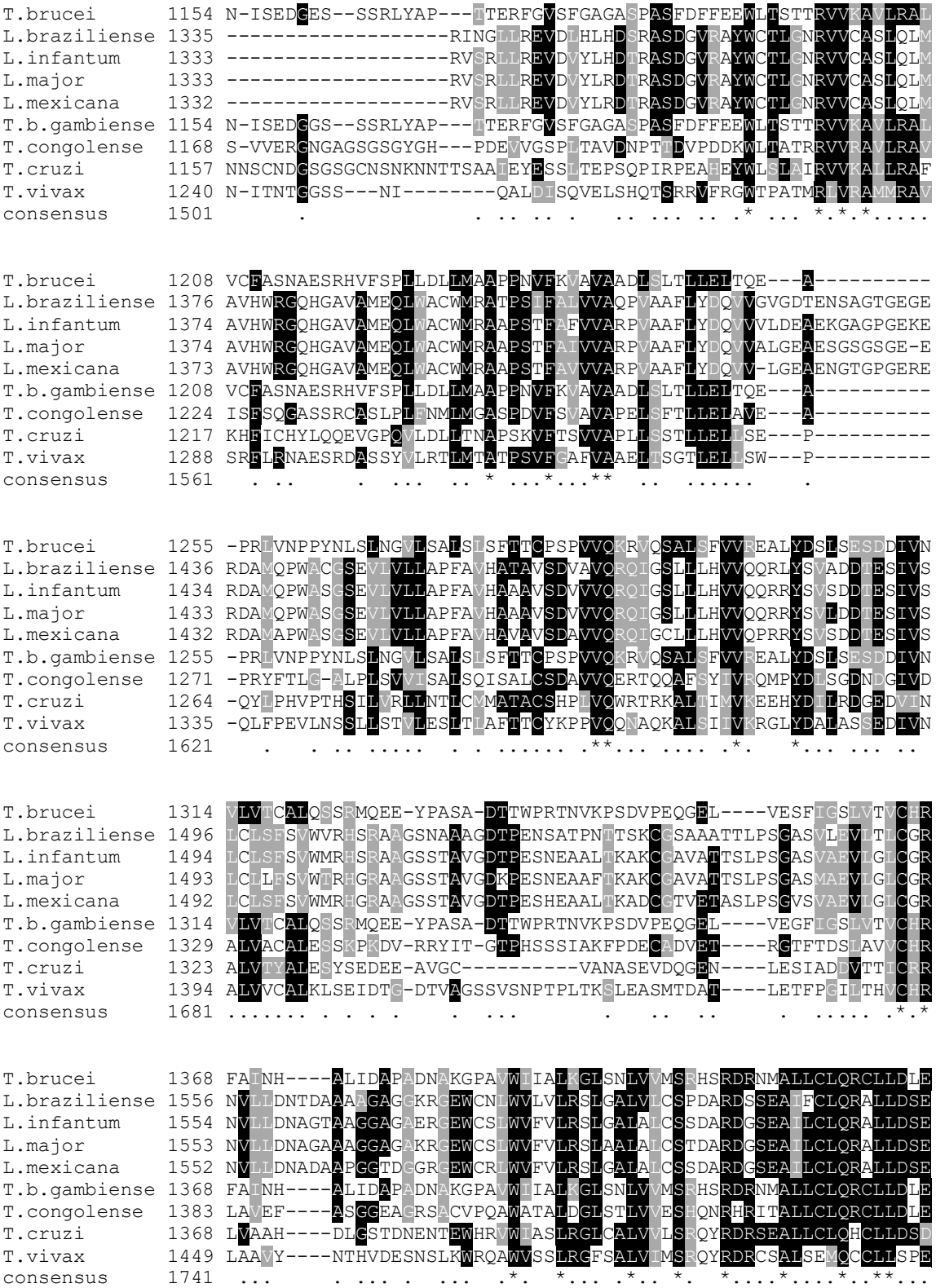
T.brucei 1154 N-ISEDGES--SSRLYAP---TTERFGVSFGAGASPASFDFFEEWLTSTTRVVKAVLRAL
L.braziliense 1335 ----------RINGLLREVDLHLHDSRASDGVRAYWCTLGNRVVCASLQLM
L.infantum 1333 ----------RVSRLLREVDVYLHDIRASDGVRAYWCTLGNRVVCASLQLM
L.major 1333 ----------RVSRLLREVDVYLRDIRASDGVRAYWCTLGNRVVCASLQLM
L.mexicana 1332 ----------RVSRLLREVDVYLRDIRASDGVRAYWCTLGNRVVCASLQLM
T.b.gambiense 1154 N-ISEDGGS--SSRLYAP---TTERFGVSFGAGASPASFDFFEEWLTSTTRVVKAVLRAL
T.congolense 1168 S-VVERGNGAGSGSGYGH---PDEVVGSPLTAVDNPTTDVPDDKWLTATRRVVRAVLRAV
T.cruzi 1157 NNSCNDGSGSGCNSNKNNTTSAAIEYESSLTEPSQPIRPEAHEYWLSLAIRVVKALLRAF
T.vivax 1240 N-ITNTGGSS---NI--------QALDISQVELSHQTSRRVFRGWTPATMRLVRAMMRAV
consensus 1501 . . ..* ... *.*.*.....
T.brucei 1208 VCFASNAESRHVFSPLLDLLMAAPPNVFKVAVAADLSLTLLELTQE---A----------
L.braziliense 1376 AVHWRGQHGAVAMEQLWACWMRATPSIFAIVVAQPVAAFLYDQVVGVGDTENSAGTGEGE
L.infantum 1374 AVHWRGQHGAVAMEQLWACWMRAAPSTFAFVVARPVAAFLYDQVVVLDEAEKGAGPGEKE
L.major 1374 AVHWRGQHGAVAMEQLWACWMRAAPSTFAIVVARPVAAFLYDQVVALGEAESGSGSGE-E
L.mexicana 1373 AVHWRGQHGAVAMEQLWACWMRAAPSTFAVVVARPVAAFLYDQVV-LGEAENGTGPGERE
T.b.gambiense 1208 VCFASNAESRHVFSPLLDLLMAAPPNVFKVAVAADLSLTLLELTQE---A----------
T.congolense 1224 ISFSQGASSRCASLPLFNMLMGASPDVFSVAVAPELSFTLLELAVE---A----------
T.cruzi 1217 KHFICHYLQQEVGPQVLDLLTNAPSKVFTSVVAPLLSSTLLELLSE---P----------
T.vivax 1288 SRFLRNAESRDASSYVLRTLMTATPSVFCAFVAAELISGTLELLSW---P----------
consensus 1561 . .. . * ...*...** .. ..
T.brucei 1255 -PRLVNPPYNLSLNGVLSALSLSFTTCPSPVVQKRVQSALSFVVREALYDSLSESDDIVN
L.braziliense 1436 RDAMQPWACGSEVLVLLAPFAVHATAVSDVAVQRQIGSLLLHVVQQRLYSVADDIESIVS
L.infantum 1434 RDAMQPWASGSEVLVLLAPFAVHAAAVSDVVVQRQIGSLLLHVVQQRRYSVSDDIESIVS
L.major 1433 RDAMQPWASGSEVLVLLAPFAVHAAAVSDVVVQRQIGSLLLHVVQQRRYSVLDDIESIVS
L.mexicana 1432 RDAMAPWASGSEVLVLLAPFAVHAVAVSDAVVQRQIGCLLLHVVQPRRYSVSDDIESIVS
T.b.gambiense 1255 -PRLVNPPYNLSLNGVLSALSLSFTTCPSPVVQKRVQSALSFVVREALYDSLSESDDIVN
T.congolense 1271 -PRYFTLG-ALPLSVVISALSQISALCSDAVVQERTQQAFSYTVRQMPYDLSGDNLGIVD
T.cruzi 1264 -QYLPHVPTHSILVRLLNTLCMMATACSHPLVQWRTRKALTIMVKEEHYDILRDGEDVIN
T.vivax 1335 -QLFPEVLNSSLLSTVLESLTLAFTTCGYKPPVQQNAQKALSIIVKRGLYDALASSEDIVN
consensus 1621 . . ..**... .... .*. *... ... ..
T.brucei 1314 VLVTCALQSSRMQEE-YPASA-DTTWPRTNVKPSDVPEQGEL----VESFIGSLVTVCHR
L.braziliense 1496 LCLSFSVWVRHSRAAGSNAAGDTPENSATPNLTSKCGSAAATTLPSGASVLEVLTLCGR
L.infantum 1494 LCLSFSVWMRHSRAAGSSTAVGDTPESNEAALLKAKCGAVATTSLPSGASVAEVLGLCGR
L.major 1493 LCLLFSVWTRHGRAAGSSTAVGDKPESNEAAFLKAKCGAVATTSLPSGASMAEVLGLCGR
L.mexicana 1492 LCLSFSVWMRHGRAAGSSTAVGDTPESHEAALLKADCGTVETASLPSGVSVAEVLGLCGR
T.b.gambiense 1314 VLVTCALQSSRMQEE-YPASA-DTTWPRTNVKPSDVPEQGEL----VEGFIGSLVTVCHR
T.congolense 1329 ALVACALESSKPKDV-RRYIT-GTPHSSSIAKFPDECADVET----RGTFTDSLAVVCHR
T.cruzi 1323 ALVTYALESYSEDEE-AVGC----------VANASEVDQGEN----LESIADDVTTICRR
T.vivax 1394 ALVVCALKLSEIDTG-DTVAGSSVSNPTPLTKSLEASMTDAT----LETFPGILTHVCHR
consensus 1681 ....*.*
T.brucei 1368 FAINH----ALIDAPADNAKGPAVWTIALKGLSNLVVMSRHSRDRNMALLCLQRCLLDLE
L.braziliense 1556 NVLLDNTDAAAAGAGGKRGEWCNLWVLVLRSLGALVLCSPDARDSSEAIFCLQRALLDSE
L.infantum 1554 NVLLDNAGTAAGGAGAERGEWCSLWVFVLRSLGALALCSSDARDGSEAILCLQRALLDSE
L.major 1553 NVLLDNAGAAAGGAGAKRGEWCSLWVFVLRSLAALALCSTDARDGSEAILCLQRALLDSE
L.mexicana 1552 NVLLDNADAAPGGTDGGRGEWCRLWVFVLRSLGALALCSSDARDGSEAILCLQRALLDSE
T.b.gambiense 1368 FAINH----ALIDAPADNAKGPAVWTIALKGLSNLVVMSRHSRDRNMALLCLQRCLLDLE
T.congolense 1383 LAVEF----ASGGEAGRSACVPQAWATALDGLSTLVVESHQNRHRITALLCLQRCLLDLE
T.cruzi 1368 LVAAH----DLGSTDNENTEWHRVWTASLRGLCALVVLSRQYRDRSEALLCLQHCLLDSD
T.vivax 1449 LAAVY----NTHVDESNSLKWRQAWVSSLRGFSALVIMSRQYRDRCSALSEMQCCLISPE
consensus 1741 ... .*. *... .*.. *. *....*....*..**...

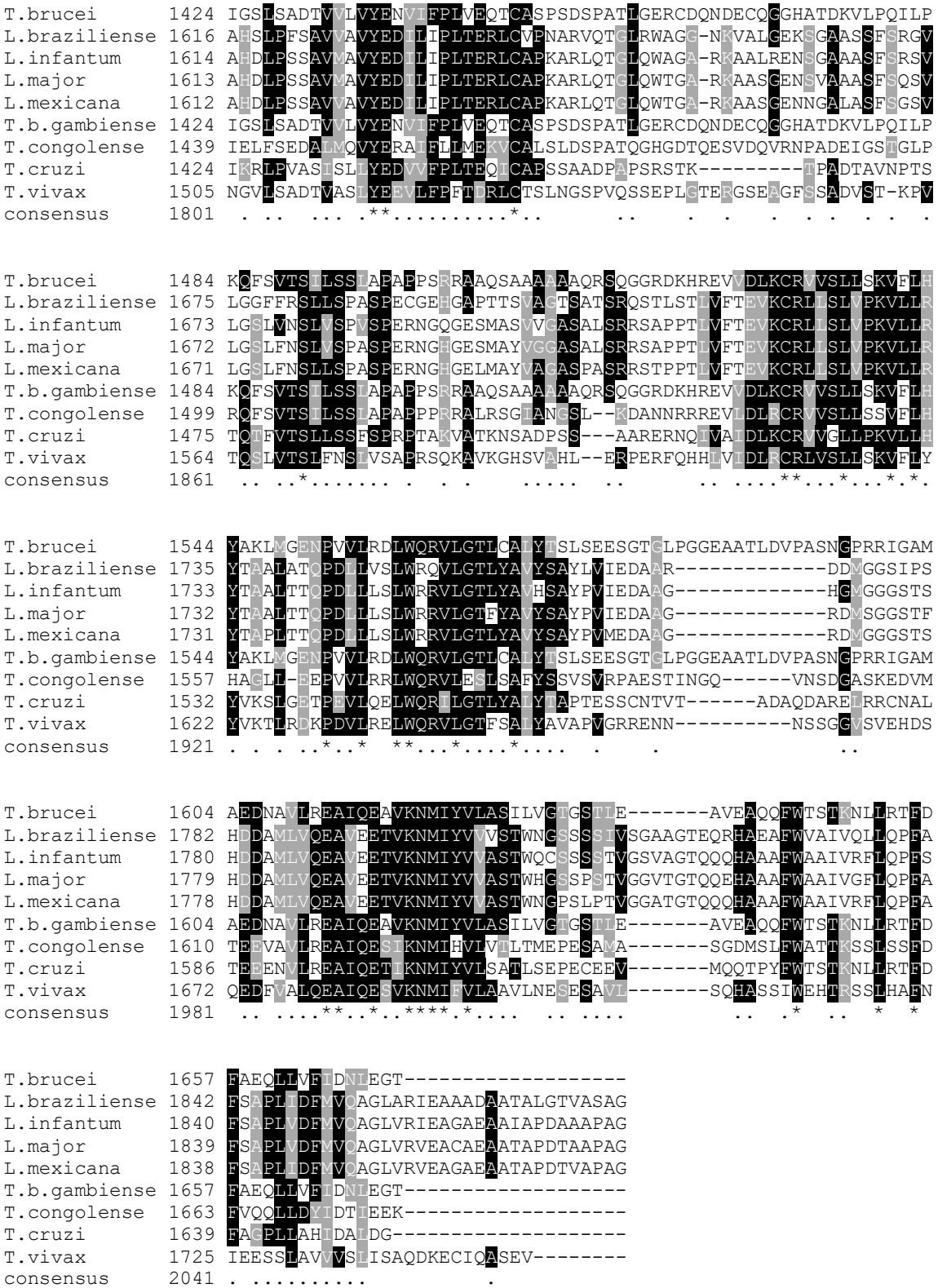
T.brucei 1424 IGSLSADTVVLVYENVIFPLVEQTCASPSDSPATLGERCDQNDECQGGHATDKVLPQILP
L.braziliense 1616 AHSLPFSAVVAVYEDILIPLTERLCVPNARVQTGLRWAGG-NKVALGEKSGAASSFSRGV
L.infantum 1614 AHDLPSSAVMAVYEDILIPLTERLCAPKARLQTGLQWAGA-RKAALRENSGAAASFSRSV
L.major 1613 AHDLPSSAVMAVYEDILIPLTERLCAPKARLQTGLQWTGA-RKAASGENSVAAASFSQSV
L.mexicana 1612 AHDLPSSAVVAVYEDILIPLTERLCAPKARLQTGLQWTGA-RKAASGENNGALASFSGSV
T.b.gambiense 1424 IGSLSADTVVLVYENVIFPLVEQTCASPSDSPATLGERCDQNDECQGGHATDKVLPQILP
T.congolense 1439 IELFSEDALMQVYERAIFLLMEKVCALSLDSPATQGHGDTQESVDQVRNPADEIGSIGLP
T.cruzi 1424 IKRLPVASISLLYEDVVFPLTEQICAPSSAADPAPSRSTK---------TPADTAVNPTS
T.vivax 1505 NGVLSADTVASLYEEVLFPFTIRLCTSLNGSPVQSSEPLGTERGSEAGFSSADVST-KPV
consensus 1801 . .. .**.........*.. .. . .
T.brucei 1484 KQFSVTSILSSLAPAPPSRRAAQSAAAAAAQRSQGGRDKHREVVDLKCRVVSLLSKVFLH
L.braziliense 1675 LGGFFRSLLSPASPECGEHGAPTTSVAGTSATSRQSTLSTLVFTEVKCRLLSLVPKVLLR
L.infantum 1673 LGSLVNSLVSPVSPERNGQGESMASVVGASALSRRSAPPTLVFTEVKCRLLSLVPKVLLR
L.major 1672 LGSLFNSLVSPASPERNGHGESMAYVGGASALSRRSAPPTLVFTEVKCRLLSLVPKVLLR
L.mexicana 1671 LGSLFNSLLSPASPERNGHGELMAYVAGASPASRRSTPPTLVFTEVKCRLLSLVPKVLLR
T.b.gambiense 1484 KQFSVTSILSSLAPAPPSRRAAQSAAAAAAQRSQGGRDKHREVVDLKCRVVSLLSKVFLH
T.congolense 1499 RQFSVTSILSSLAPAPPPRRALRSGIANGSL--KDANNRRREVLDLRCRVVSLLSSVFLH
T.cruzi 1475 TQTFVTSLLSSFSPRPTAKVATKNSADPSS---AARERNQIVAIDLKCRVVGLLPKVLLH
T.vivax 1564 TQSLVTSLFNSLVSAPRSQKAVKGHSVAHL--ERPERFQHHLVIDLRCRLVSLLSKVFLY
consensus 1861 .. ..*..... . . . .**...*...*.*.
T.brucei 1544 YAKLMGENPVVLRDLWQRVLGTLCALYISLSEESGTGLPGGEAATLDVPASNGPRRIGAM
L.braziliense 1735 YTAALATQPDLLVSLWRQVLGTLYAVYSAYLVIEDAAR-------------DDMGGSIPS
L.infantum 1733 YTAALTTQPDLLLSLWRRVLGTLYAVHSAYPVIEDAAG-------------HGMGGGSTS
L.major 1732 YTAALTTQPDLLLSLWRRVLGTFYAVYSAYPVIEDAAG-------------RDMSGGSTF
L.mexicana 1731 YTAPLTTQPDLLLSLWRRVLGTLYAVYSAYPVMEDAAG-------------RDMGGGSTS
T.b.gambiense 1544 YAKLMGENPVVLRDLWQRVLGTLCALYTSLSEESGTGLPGGEAATLDVPASNGPRRIGAM
T.congolense 1557 HAGLL-EEPVVLRRLWQRVLESLSAEYSSVSVRPAESTINGQ------VNSDGASKEDVM
T.cruzi 1532 YVKSLGETPEVLQELWQRILGTLYALYIAPTESSCNTVT------ADAQDAREIRRCNAL
T.vivax 1622 YVKTLRDKPDVLRELWQRVLGTFSALYAVAPVGRRENN----------NSSGGVSVEHDS
consensus 1921 . . . ..*..* **...*....*.... . . ..
T.brucei 1604 AEDNAVLREAIQEAVKNMIYVLASILVGIGSTLE-------AVEAQQFWTSTKNLLRTED
L.braziliense 1782 HDDAMLVQEAVEETVKNMIYVVVSTWNGSSSSIVSGAAGTEQRHAEAFWVAIVQLLQPEA
L.infantum 1780 HDDAMLVQEAVEETVKNMIYVVASTWQCSSSTVGSVAGTQQQHAAAFWAAIVRFLQPES
L.major 1779 HDDAMLVQEAVEETVKNMIYVVASTWHGSSPSTVGGVTGTQQEHAAAFWAAIVGFLQPEA
L.mexicana 1778 HDDAMLVQEAVEETVKNMIYVVASTWNGPSLPTVGGATGTQQQHAAAFWAAIVRFLQPEA
T.b.gambiense 1604 AEDNAVLREAIQEAVKNMIYVLASILVGIGSTLE-------AVEAQQFWTSTKNLLRTED
T.congolense 1610 TEEVAVLREAIQESIKNMIHVIVLLTMEPESAMA-------SGDMSLFWATTKSSLSSED
T.cruzi 1586 TEEENVLREAIQETIKNMIYVLSATLSEPECEEV-------MQQTPYFWTSTKNLLRTED
T.vivax 1672 QEDFVALQEAIQESVKNMIHVLAAVLNESESAVL-------SQHASSIWEHTRSSLHAEN
consensus 1981 .. ....**..*..****.*.... .. ..* .. * *
T.brucei 1657 FAEQLLVFIDNLEGT--------------------
L.braziliense 1842 FSAPLIDFMVQAGLARIEAAADAATALGTVASAG
L.infantum 1840 FSAPLVDFMVQAGLVRIEAGAEAAIAPDAAAPAG
L.major 1839 FSAPLVDFMVQAGLVRVEACAEAATAPDTAAPAG
L.mexicana 1838 FSAPLIDFMVQAGLVRVEAGAEAATAPDTVAPAG
T.b.gambiense 1657 FAEQLLVFIDNLEGT--------------------
T.congolense 1663 FVQQLLDYIDTIEEK--------------------
T.cruzi 1639 FAGPLLAHIDALDG--------------------
T.vivax 1725 IEESSLAVVVSLISAQDKECIQASEV--------
consensus 2041 . ...

Appendix 8

Amino acid sequence of TbGEF3 (OG5_154690) in other kinetoplastids

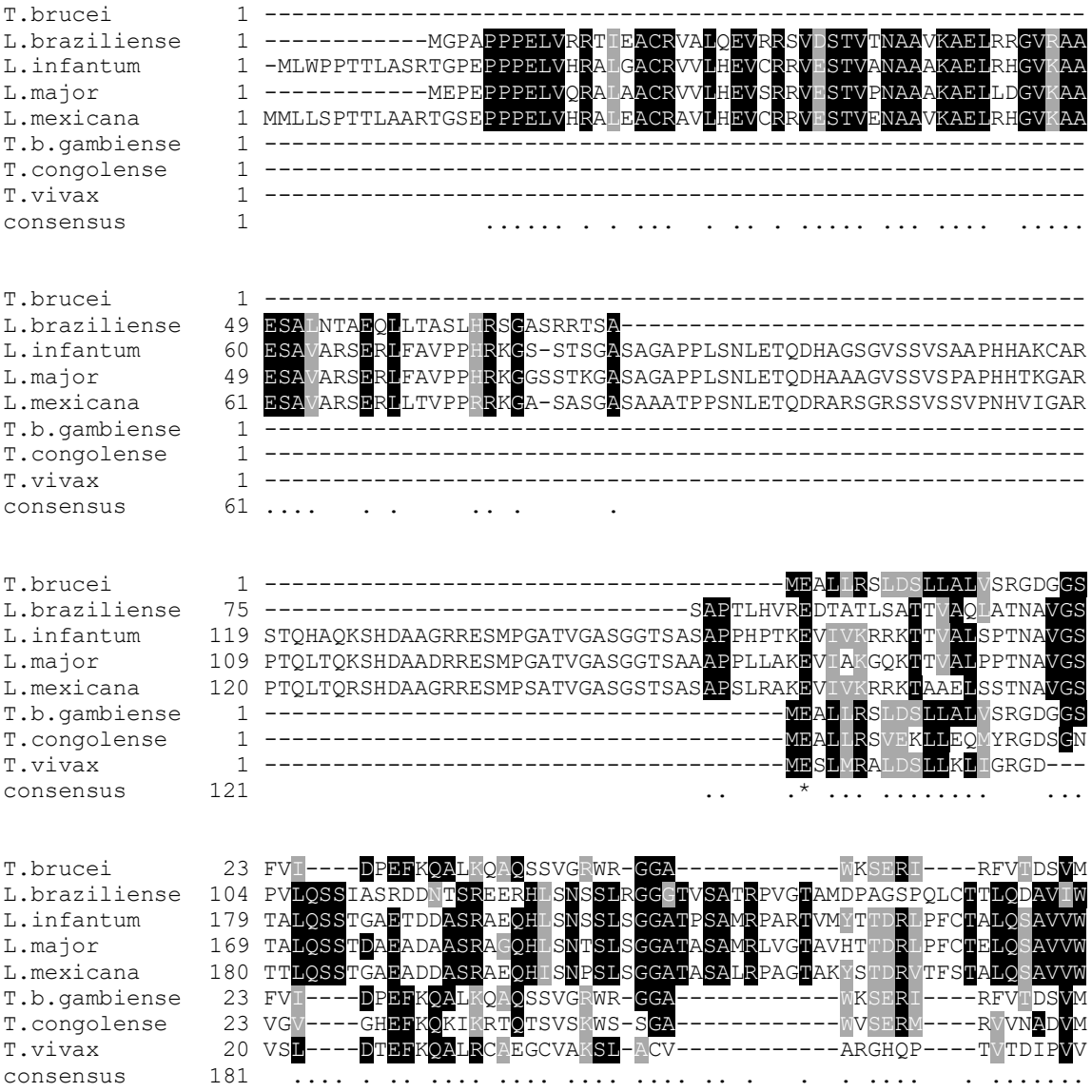

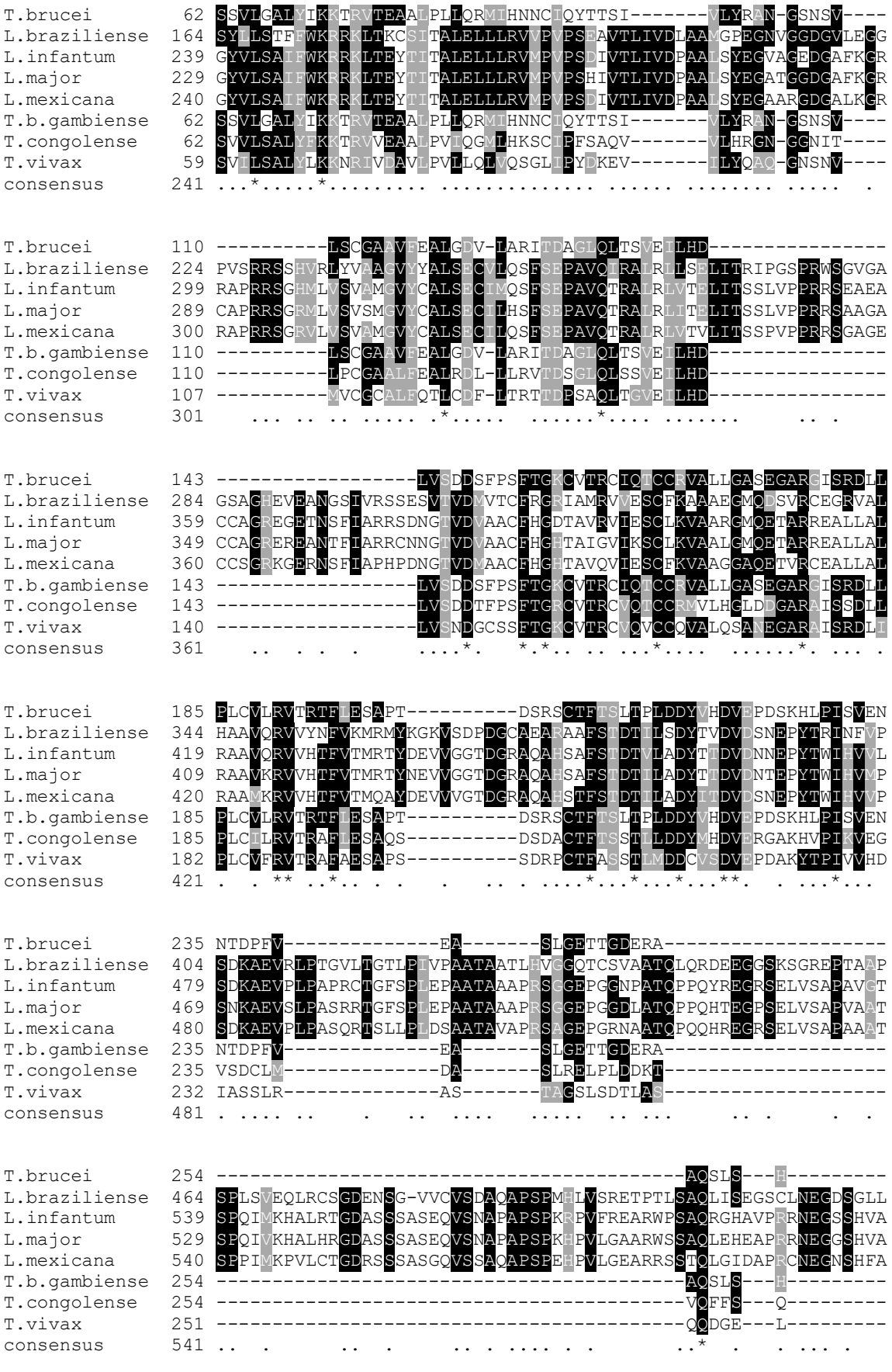

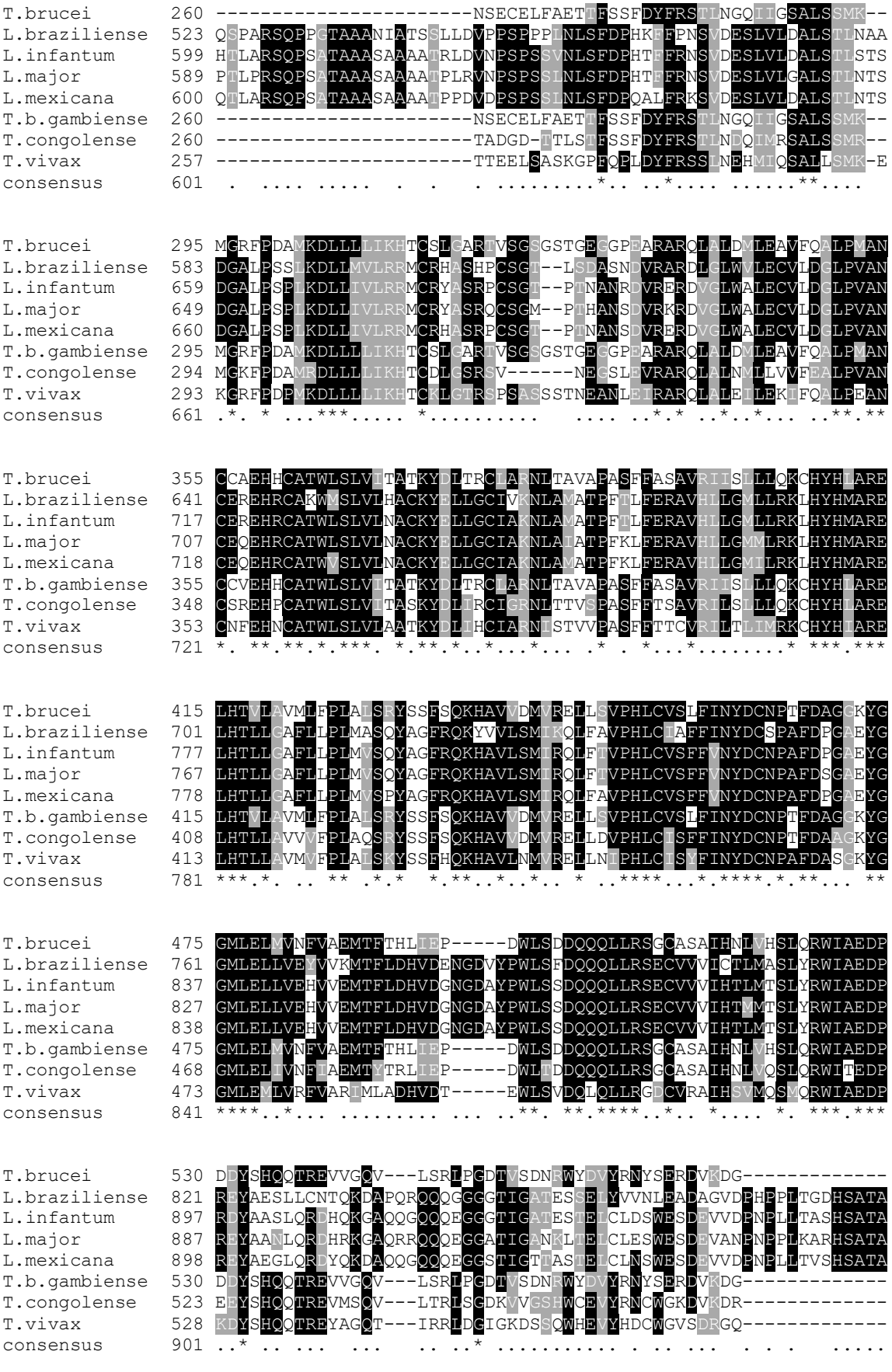

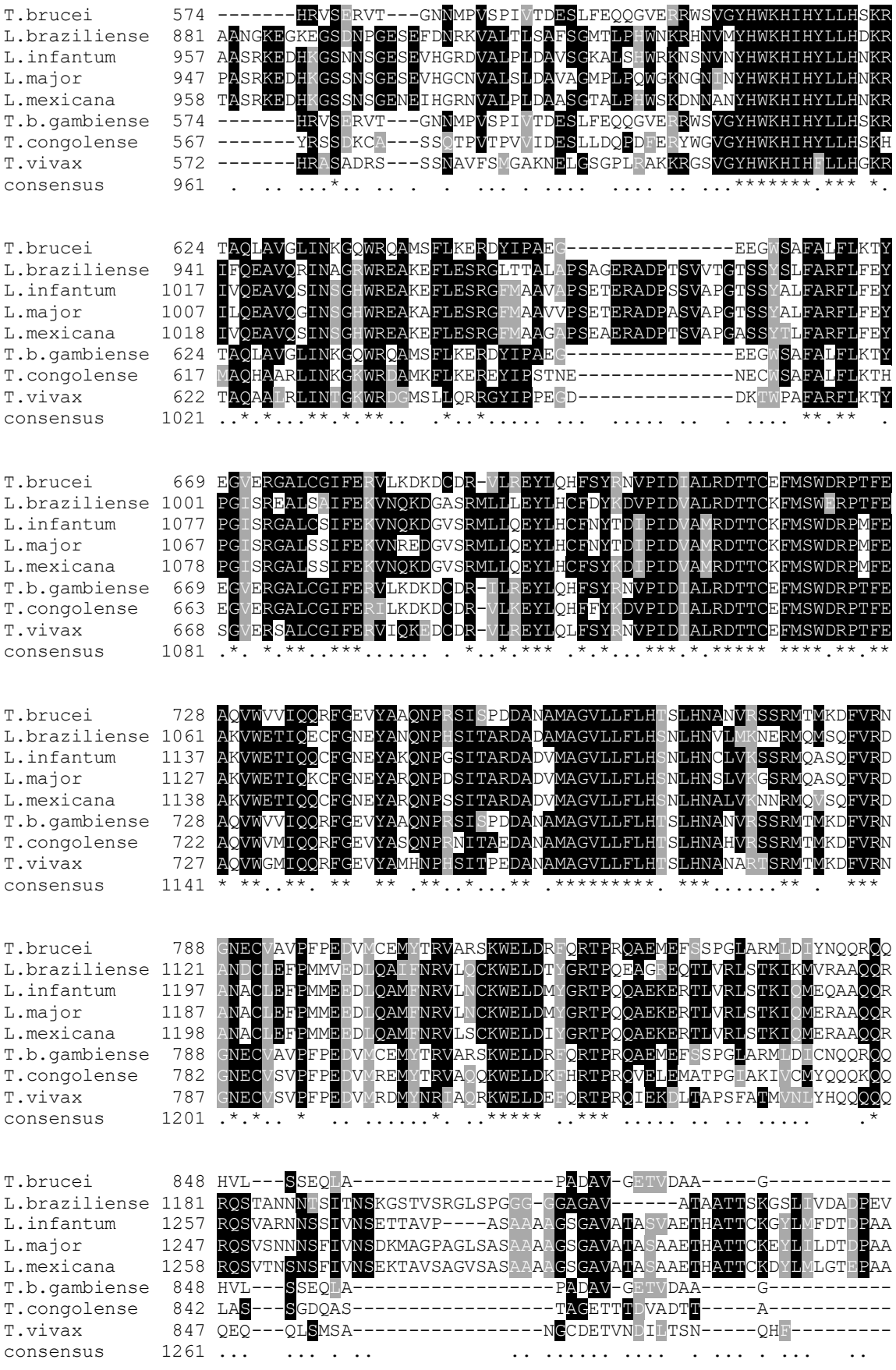
T.brucei 574 -------HRVSERVT---GNNMPVSPIVTDESLFEQQGVERRWSVGYHWKHIHYLLHSKR
L.braziliense 881 AANGKEGKEGSDNPGESEFDNRKVALTLSAFSGMTLPHWNKRHNVMYHWKHIHYLLHDKR
L.infantum 957 AASRKEDHKGSNNSGESEVHGRDVALPLDAVSGKALSHWRKNSNVNYHWKHIHYLLHNKR
L.major 947 PASRKEDHKGSSNSGESEVHGCNVALSLDAVAGMPLPQWGKNGNINYHWKHIHYLLHNKR
L.mexicana 958 TASRKEDHKGSSNSGENEIHGRNVALPLDAASGTALPHWSKDNNANYHWKHIHYLLHNKR
T.b.gambiense 574 -------HRVSERVT---GNNMPVSPIVTDESLFEQQGVERRWSVGYHWKHIHYLLHSKR
T.congolense 567 -------YRSSDKCA---SSQTPVTPVVIDESLLDQPDFERYWGVGYHWKHIHYLLHSKH
T.vivax 572 -------HRASADRS---SSNAVFSMGAKNELGSGPLRAKKRGSVGYHWKHIHFLLHGKR
consensus 961 . .. ...*.. .. . .*******.*** *.
T.brucei 624 TAQLAVGLINKGQWRQAMSFLKERDYIPAEG---------------EEGWSAFALFLKTY
L.braziliense 941 IFQEAVQRINAGRWREAKEFLESRGLTTALAPSAGERADPTSVVTGTSSYSLFARFLFEY
L.infantum 1017 IVQEAVQSINSGHWREAKEFLESRGFMAAVAPSETERADPSSVAPGTSSYALFARFLFEY
L.major 1007 ILQEAVQGINSGHWREAKAFLESRGFMAAVVPSETERADPASVAPGTSSYALFARFLFEY
L.mexicana 1018 IVQEAVQSINSGHWREAKEFLESRGFMAAGAPSEAERADPTSVAPGASSYTLFARFLFEY
T.b.gambiense 624 TAQLAVGLINKGQWRQAMSFLKERDYIPAEG---------------EEGWSAFALFLKTY
T.congolense 617 MAQHAARLINKGKWRDAMKFLKEREYIPSTNE--------------NECWSAFALFLKTH
T.vivax 622 TAQAALRLINTGKWRDGMSLLQRRGYIPPEGD--------------DKTWPAFARFLKTY
consensus 1021 ..*.*...**.*.**.. .*..*..... ... . **.** .
T.brucei 669 EGVERGALCGIFERVLKDKDCDR-VLREYLQHFSYRNVPIDIALRDTTCEFMSWDRPTFE
L.braziliense 1001 PGISREALSAIFEKVNQKDGASRMLLLEYLHCFDYKDVPIDVALRDTTCKFMSWERPTFE
L.infantum 1077 PGISRGALCSIFEKVNQKDGVSRMLLQEYLHCFNYTDIPIDVAMRDTTCKFMSWDRPMFE
L.major 1067 PGISRGALSSIFEKVNREDGVSRMLLQEYLHCFNYTDIPIDVAMRDTTCKFMSWDRPMFE
L.mexicana 1078 PGISRGALSSIFEKVNQKDGVSRMLLQEYLHCFSYKDIPIDVAMRDTTCKFMSWDRPMFE
T.b.gambiense 669 EGVERGALCGIFERVLKDKDCDR-ILREYLQHFSYRNVPIDIALRDTTCEFMSWDRPTFE
T.congolense 663 EGVERGALCGIFERILKDKDCDR-VLKEYLQHFFYKDVPIDIALRDTTCEFMSWDRPTFE
T.vivax 668 SGVERSALCGIFERVIQKEDCDR-VLREYLQLFSYRNVPIDIALRDTTCEFMSWDRPTFE
consensus 1081 .*. *.**..***..... . *..*.*** .*.*...***.*.***** ****.**.**
T.brucei 728 AQVWVVIQQRFGEVYAAQNPRSISPDDANAMAGVLLFLHTSLHNANVRSSRMTMKDFVRN
L.braziliense 1061 AKVWETIQECFGNEYANQNPHSITARDADAMAGVLLFLHSNLHNVLMKNERMQMSQFVRD
L.infantum 1137 AKVWETIQQCFGNEYAKQNPGSITARDADVMAGVLLFLHSNLHNCLVKSSRMQASQFVRD
L.major 1127 AKVWETIQKCFGNEYARQNPDSITARDADVMAGVLLFLHSNLHNSLVKGSRMQASQFVRD
L.mexicana 1138 AKVWETIQQCFGNEYARQNPSSITARDADVMAGVLLFLHSNLHNALVKNNRMQMSQFVRD
T.b.gambiense 728 AQVWVVIQQRFGEVYAAQNPRSISPDDANAMAGVLLFLHTSLHNANVRSSRMTMKDFVRN
T.congolense 722 AQVWVMIQQRFGEVYASQNPRNITAEDANAMAGVLLFLHTSLHNAHVRSSRMTMKDFVRN
T.vivax 727 AQVWGMIQQRFGEVYAMHNPHSITPEDANAMAGVLLFLHTSLHNANARTSRMTMKDFVRN
consensus 1141 * **..**. ** ** .**..*...** .********. ***......** . ***
T.brucei 788 GNECVAVPFPEDVMCEMYTRVARSKWELDRFQRTPRQAEMEFSSPGLARMIDIYNQQRQQ
L.braziliense 1121 ANDCLEFPMMVEDLQAIFNRVLQCKWELDTYGRTPQEAGREQTLVRLSTKIKMVRAAQQR
L.infantum 1197 ANACLEFPMMEEDLQAMFNRVLNCKWELDMYGRTPQQAEKERTLVRLSTKIQMEQAAQQR
L.major 1187 ANACLEFPMMEEDLQAMFNRVLNCKWELDMYGRTPQQAEKERTLVRLSTKIQMERAAQQR
L.mexicana 1198 ANACLEFPMMEEDLQAMFNRVLSCKWELDIYGRTPQQAEKERTLVRLSTKIQMERAAQQR
T.b.gambiense 788 GNECVAVPFPEDVMCEMYTRVARSKWELDRFQRTPRQAEMEFSSPGLARMIDICNQQRQQ
T.congolense 782 GNECVSVPFPEDVMREMYTRVAQQKWELDKFHRTPRQVELEMATPGIAKIVCMYQQQKQQ
T.vivax 787 GNECVSVPFPEDVMRDMYNRIAQRKWELDEFQRTPRQIEKDLTAPSFATMVNLYHQQQQQ
consensus 1201 .*.*.. * .. ..*. ..***** ..*** ....*
T.brucei 848 HVL---SSEQLA------------------PADAV-GETVDAA-----G----------
L.braziliense 1181 RQSTANNNTSITNSKGSTVSRGLSPGGG-GGAGAV------ATAATTSKGSLIVDADPEV
L.infantum 1257 RQSVARNNSSIVNSETTAVP----ASAAAAGSGAVATASVAETHATTCKGYLMFDTDPAA
L.major 1247 RQSVSNNNSFIVNSDKMAGPAGLSASAAAAGSGAVATASAAETHATTCKEYLILDTDPAA
L.mexicana 1258 RQSVTNSNSFIVNSEKTAVSAGVSASAAAAGSGAVATASAAETHATTCKDYLMLGTEPAA
T.b.gambiense 848 HVL---SSEQLA------------------PADAV-GETVDAA-----G----------
T.congolense 842 LAS---SGDQAS------------------TAGETTTDVADTT-----A----------
T.vivax 847 QEQ---QLSMSA------------------NGCDETVNDILTSN-----QHF---------
consensus 1261 ... ...

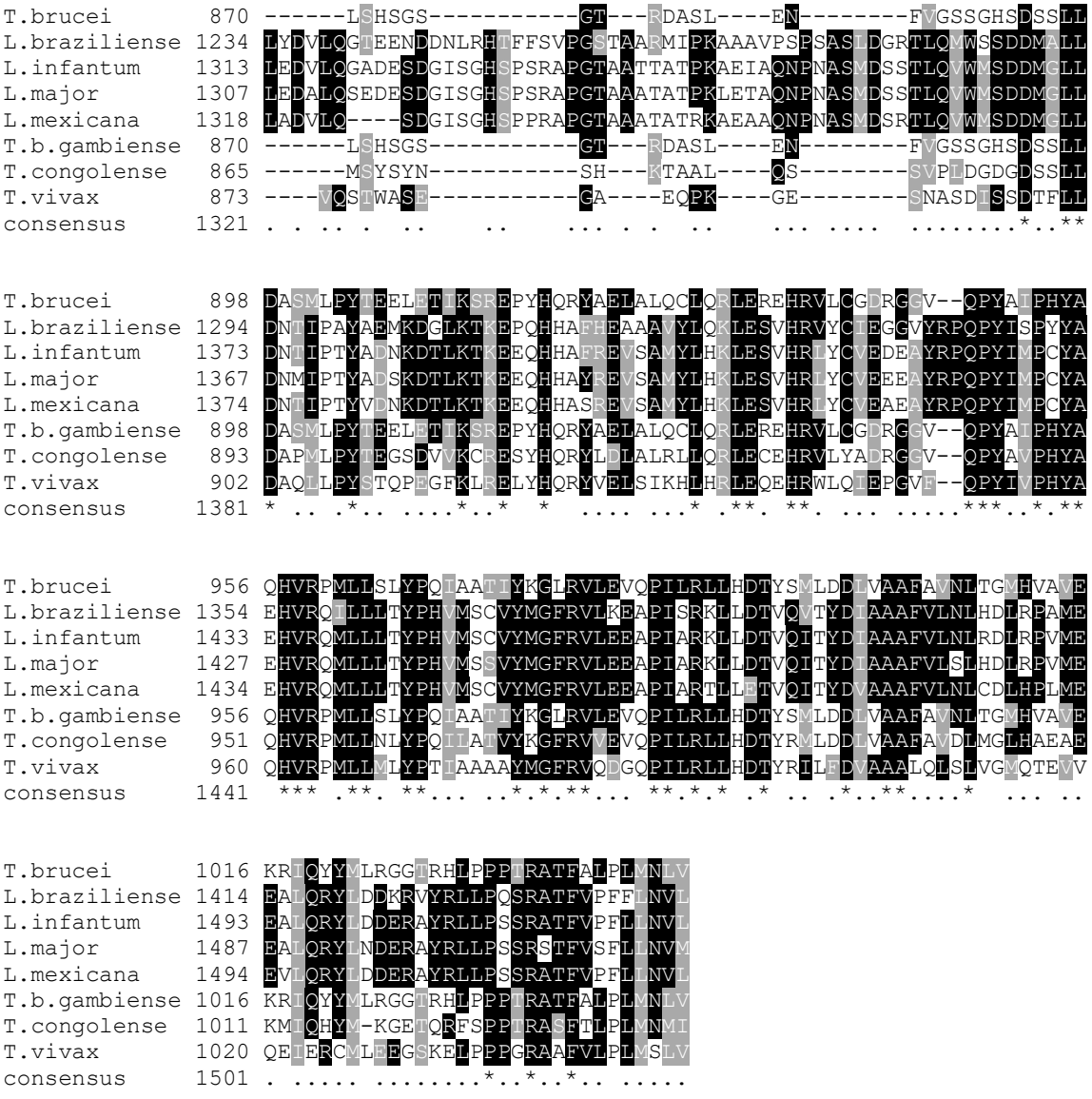
T.brucei 870
L.braziliense 1234
L.infantum 1313
L.major 1307
L.mexicana 1318
T.b.gambiense 870
T.congolense 865
T.vivax 873
consensus 1321
T.brucei 898
L.braziliense 1294
L.infantum 1373
L.major 1367
L.mexicana 1374
T.b.gambiense 898
T.congolense 893
T.vivax 902
consensus 1381
T.brucei 956
L.braziliense 1354
L.infantum 1433
L.major 1427
L.mexicana 1434
T.b.gambiense 956
T.congolense 951
T.vivax 960
consensus 1441
T.brucei 1016
L.braziliense 1414
L.infantum 1493
L.major 1487
L.mexicana 1494
T.b.gambiense 1016
T.congolense 1011
T.vivax 1020
consensus 1501

Appendix 9

List of compounds, their structure and the pathogen screened for that showed inhibitory effect in bloodstream form T. brucei at 1 μM. Data obtained from Pathogen Box (www.pathogenbox.org/)

Compound	Structure	Pathogen screened
1A6	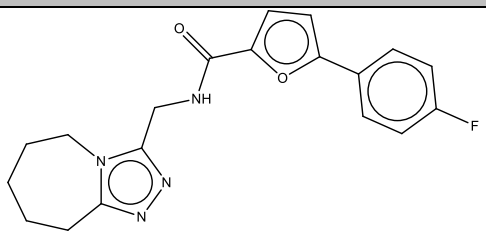	Kinetoplastids
1E5	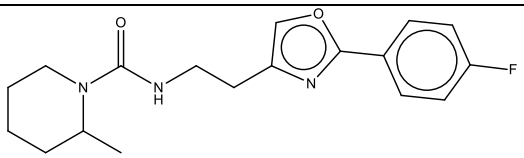	Kinetoplastids
1G5	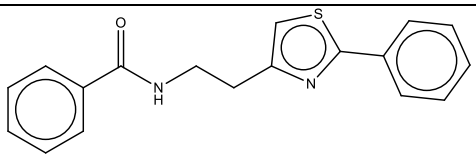	Kinetoplastids
2B3	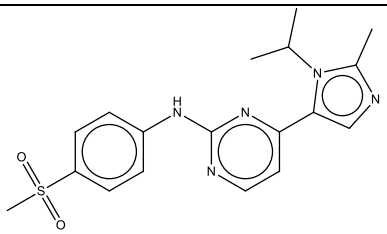	Kinetoplastids
2C2	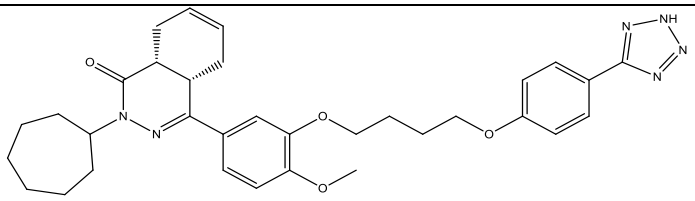	Kinetoplastids
2D3	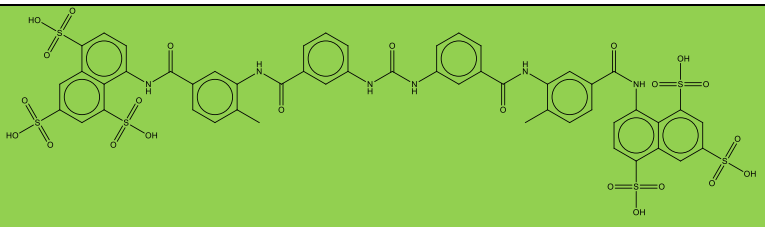	Reference compound

2H2	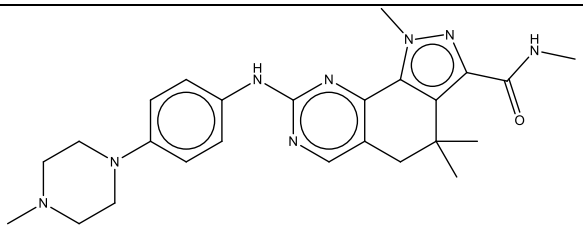	Kinetoplastids
3B10	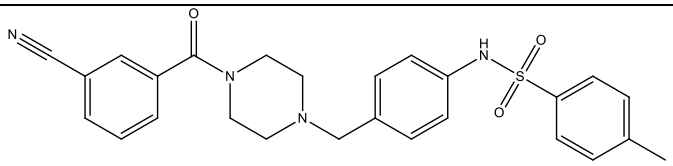	Kinetoplastids
3B11	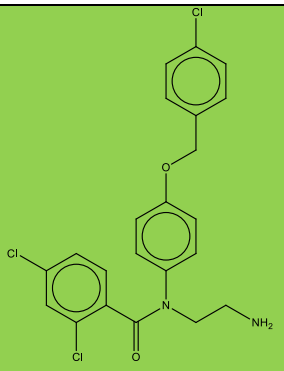	Kinetoplastids
3C10	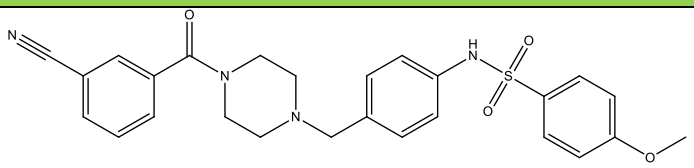	Kinetoplastids
3D5	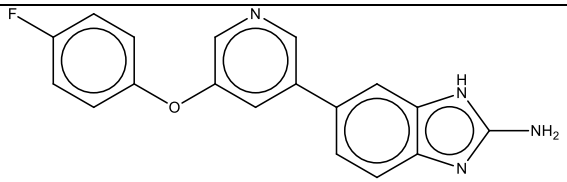	Tuberculosis
3G6	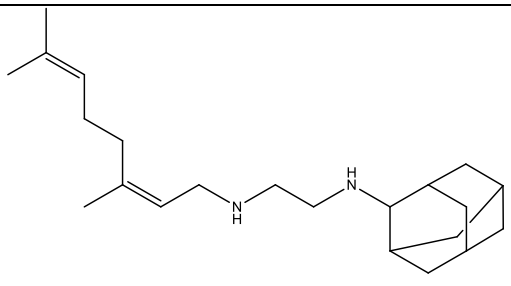	Tuberculosis
4B9	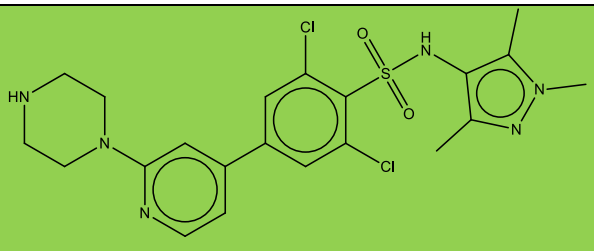	Kinetoplastids

4C8	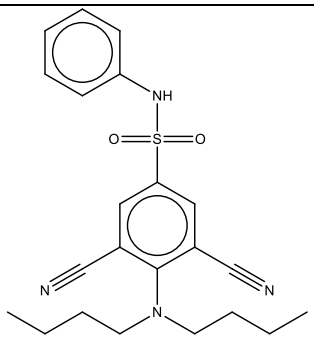	Kinetoplastids
4E10	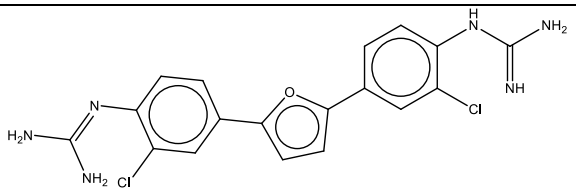	Kinetoplastids
4G8	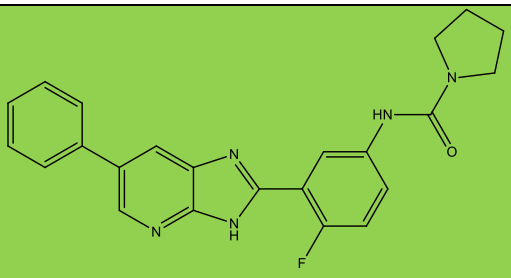	Kinetoplastids
4H3	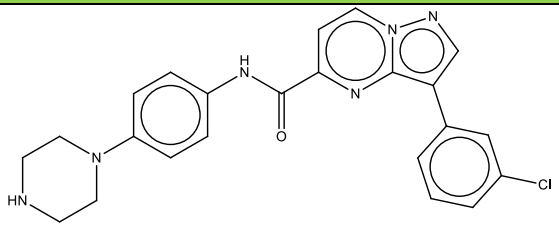	Malaria
5B10	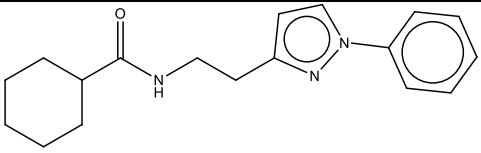	Kinetoplastids
5H10	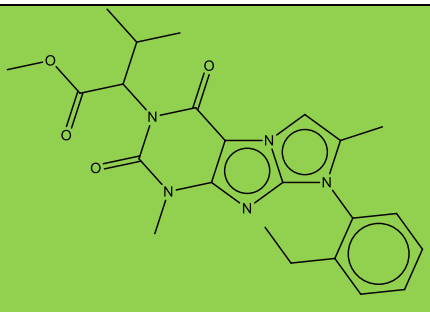	Kinetoplastids